Evaluating the capabilities of some constitutive models in reproducing the experimental behaviour of stiff clay subjected to tunnelling stress paths

by

Monica Valls-Marquez

A thesis submitted to
The University of Birmingham
for the degree of
DOCTOR OF PHILOSOPHY

Department of Civil Engineering
School of Engineering
The University of Birmingham
June 2009

UNIVERSITY OF
BIRMINGHAM

University of Birmingham Research Archive

e-theses repository

This unpublished thesis/dissertation is copyright of the author and/or third parties. The intellectual property rights of the author or third parties in respect of this work are as defined by The Copyright Designs and Patents Act 1988 or as modified by any successor legislation.

Any use made of information contained in this thesis/dissertation must be in accordance with that legislation and must be properly acknowledged. Further distribution or reproduction in any format is prohibited without the permission of the copyright holder.

Abstract

Accurate prediction of soil behaviour around tunnel excavations is vital for the assessment of its effects on existing infrastructures and services, both underground and surface, and evaluation of risks to enable safe designs.

This thesis evaluates the capabilities of four constitutive models in reproducing the intrinsic experimental behaviour of stiff clay when subjected to tunnelling-induced stress paths.

Relevant stress paths have been determined from 2D and 3D finite element analysis using PLAXIS.

Reconstituted Speswhite Kaolin clay specimens have been prepared from slurry, their properties investigated in detail, and tested using state-of-the-art stress path equipment and on-sample instrumentation.

The soil model testing software SM2D has been used to compare the models' predictions to the experimental measurements.

The results have shown that there are yet many limitations in terms of accurately simulating the response of overconsolidated clay when subjected to extension, essential in tunnelling problems. Also the only model considered that has features to account for small-strain behaviour has been found to be too crude in its current state to be applied to complex geotechnical problems without further reflection. Some suggestions for improvement have been given.

The results presented should help in making a more informed selection of models for design purposes.

This has been a long journey that I can only fully enjoy right now

I want to dedicate this work to my parents

Joan i Elena

who gave me the opportunity to have a good education

and most specially to

Andreu

for his love, patience, encouragement

and all the sacrifices we have done together to achieve this

Acknowledgements

This research wouldn't have been possible without the encouragement and advice from my three supervisors Dr. David Chapman, Prof. Andrew Chan and Dr. Gurmel Ghataora and without the financial support provided by the Civil Engineering Department and the EPSRC.

I really appreciate as well the understanding and support received from Prof. Chris Rogers when things were going wrong in the laboratory due to the limited facilities at the time.

I would like to say thank you as well to one of the laboratory technicians, Bruce Read, for being always ready to help with a smile on his face. It has been a pleasure working with him.

The time spent at the University of Birmingham wouldn't have been the same without the time shared with all the other researchers in rooms F59A and F59B, the ones that were already there when I started and those who arrived soon before I left.

Thanks as well to Julia Fabrega and Nahia Gil, for the lunch times and for listening to me when I most needed.

Having got all the unimaginable problems in the laboratory I would like to very specially thank Karl Snelling from GDS Instruments and Chris Russell from Geolabs Ltd for being always at the other end of the phone offering unconditional help and advice.

Last but not least, thanks to two people who I got to know on the train during my daily commuting from Leamington Spa to Birmingham University, Rodrigo Agerri and Graham Worth, who listened to me and shared interesting experiences from their own times as PhD students.

LIST OF CONTENTS

List of Symbols
List of Figures
List of Tables

Page

CHAPTER 1: Project Introduction. Development of aims and objectives
1.1. General……... 1
1.2. Aims and objectives of the research…….. 5
1.3. Thesis layout…….. 7

CHAPTER 2: Literature review
2.1. Introduction…… 8
2.2. PART I: Understanding and modelling tunnel excavations…….. 8
2.2.1. Finite element analysis (FEA)…….. 8
2.2.2. Constitutive soil models……... 10
2.2.2.1. Original Cam-Clay…….. 12
2.2.2.2. Modified Cam-Clay……. 15
2.2.2.3. S-CLAY1……. 16
2.2.2.4. Small-strain stiffness……... 17
2.2.2.5. Multi-surface kinematic hardening…… 21
2.2.2.6. Recent application …….. 22
2.2.3. Tunnelling induced stress paths…… 25
2.3. PART II: Triaxial and stress path testing……... 38
2.3.1. Preparation of K_0-consolidated reconstituted samples……. 38
2.3.2. Sample disturbance……... 39
2.3.3. Natural versus reconstituted soil behaviour……. 42
2.3.4. Triaxial testing…….. 42
2.3.5. Stress path testing……. 44
2.3.6. On-sample strain instrumentation and small-strain stiffness…… 44
2.3.6.1. Hall Effect devices…….. 45
2.3.6.2. LVDT´s……... 46
2.3.7. Some parameters for Speswhite Kaolin clay…… 46
2.4. Key findings and justification for current research…… 48

CHAPTER 3: Methodology
3.1. Introduction…… 50
3.2. Context and preliminary calculations…… 51
3.3. Finite element analysis……... 51
3.3.1. Description of the analyses……... 52
3.3.1.1. Variables…….. 53
3.3.1.2. Nomenclature used for the analyses……. 58
3.3.1.3. Geometry details……... 59
3.3.1.3.1. 1-layer 2D single and twin tunnels…….. 60
3.3.1.3.2. 3-layer 2D single tunnel……... 61

3.3.1.3.3. 1-layer 3D single tunnel…….. 61
3.3.1.4. Stress measurement points…….. 62
3.3.1.5. Parameters…… 64
3.3.1.6. Sensitivity analyses…….. 65
3.4. Selection of soil for testing…….... 67
3.5. Preparation of reconstituted specimens……. 68
3.5.1. Equipment…… 68
3.5.1.1. Consolidation Device A…….... 68
3.5.1.2. Consolidation Device B…… 70
3.5.2. Preparing the slurry…….... 71
3.5.3. Load sequence…….. 71
3.5.4. Extrusion and trimming of samples…….. 72
3.5.5. Study of the characteristics of the reconstituted samples……. 72
3.5.5.1. Stage 1 - Preliminary investigation…….. 73
3.5.5.2. Stage 2 - Secondary investigation…… 76
3.5.5.3. Stage 3 - Measurement of *u* during K_0-consolidation…….. 77
3.5.5.4. Stage 4 - Modifications to Device A…… 78
3.6. Triaxial and Stress path testing…….. 79
3.6.1. Equipment……. 79
3.6.1.1. Large stress path equipment……. 79
3.6.1.2. Standard Stress Path equipment - STDTTS and GDSLAB……. 80
3.6.1.2.1. Zero pressure datum and calibration of standard components…… 82
3.6.1.2.2. Extension kit……. 82
3.6.1.2.3. On-sample instrumentation…….. 83
3.6.1.3. Conventional triaxial equipment – WINHOST…… 86
3.6.2. Critical state tests…….. 87
3.6.2.1. Consolidated undrained tests under compression ……..……. 91
3.6.2.2. Consoliadated undrained tests under extension ……..……. 92
3.6.2.3. Consolidated drained tests under compression ……..……. 94
3.6.2.4. Isotropic consolidation tests……. 94
3.6.2.5. K_0-consolidation and related tests…… 95
3.6.3. Definition of simplified tunnel induced stress paths and their simulation in the laboratory…… 97
3.7. Soil model testing and evaluation using SM2D……. 105
3.7.1. Selection of models……... 106
3.7.2. Evaluation of the small-strain parameters…… 111
3.7.3. Simulation of conventional triaxial tests…….. 116
3.7.4. Simulation of tunnelling induced stress path tests…… 119

CHAPTER 4: Finite element analysis
4.1. Introduction…… 120
4.2. Results…… 120
4.2.1. 1-layer 2D single tunnel…… 120
4.2.2. 3-layer 2D single tunnel…… 125
4.2.3. 1-layer 2D twin tunnels…… 126

4.2.4. Sensitivity analyses…….. 130
4.2.5. 1-layer 3D single tunnel…… 137
4.3. Discussion…….. 143
4.3.1. 2D……. 143
4.3.1.1. Single tunnel……. 143
4.3.1.2. Twin tunnels……. 149
4.3.2. 3D……. 150
4.4. Summary…… 152

CHAPTER 5: Study of the characteristics of the reconstituted samples
5.1. Introduction…… 153
5.2. Index tests and determination of *Gs*……... 153
5.3. Stage 1 - Preliminary investigation…… 154
5.3.1. e - σ_v' relationship……. 154
5.3.2. c_u - *IL* relationship……... 156
5.3.3. c_u - $\sigma_{v\,max}'$ relationship…… 157
5.3.4. w - $\sigma_{v\,max}'$ relationship…….. 158
5.3.5. UU tests……... 158
5.3.6. p' measurements in the triaxial cells……... 159
5.3.7. Shortcomings from Stage 1……. 159
5.4. Stage 2 - Secondary investigation…….. 165
5.4.1. Variation of w along the samples´ length……... 165
5.4.2. Alternative method for the measurement of c_u……... 167
5.4.3. Evaluating the reasons for the low p' measured values…….. 168
5.5. Stage 3 - Pore water pressure measurements during K_0-consolidation……. 169
5.6. Stage 4 - Modifications to Device A……. 171
5.7. Implications of the findings……... 174
5.8. Summary…… 177

CHAPTER 6: Laboratory tests Part I: Critical state framework for Speswhite Kaolin clay
6.1. Introduction…… 178
6.2. Results…… 178
6.2.1. Isotropically consolidated undrained and drained tests under compression…….... 178
6.2.2. Isotropically consolidated undrained tests under extension …….. 181
6.2.3. Isotropic consolidation tests…… 183
6.2.4. K_0-consolidation and related tests …….. 184
6.3. Discussion…….. 189
6.4. Summary…… 199

CHAPTER 7: Laboratory tests Part II: Stress path testing
7.1. Introduction…… 200
7.2. Initial soil conditions…….. 200
7.3. Definition of tunnel induced stress paths for laboratory simulation…….. 202
7.4. Results…… 205
7.4.1. Crown of single tunnel. K_o<1 (Tests SP1 and SP1-c)…….. 205

7.4.2. Springline of twin tunnels. K_o<1 (Tests SP2, SP2B and SP2C)……... 208
7.4.3. Crown of single tunnel. K_o>1 (Test SP3)……. 209
7.4.4. Springline of twin tunnels. K_o>1 (Test SP4)…… 209
7.5. Determination of the small-strain parameters ……... 209
7.5.1. Shear response…….. 210
7.5.2. Volumetric response……. 212
7.6. Discussion…….. 212
7.6.1. Stress path testing……. 213
7.6.2. Variation in soil stiffness and evaluation of the Jardine et al. (1991) parameters…… 223
7.7. Summary…… 228

CHAPTER 8: Evaluation of soil constitutive model performance for conventional triaxial testing
8.1. Introduction…… 229
8.2. Results using parameters deduced from experimental work……. 229
8.2.1. Normally isotropic consolidated Kaolin sheared in compression…… 229
8.2.2. Lightly isotropic overconsolidated Kaolin sheared in compression……. 230
8.2.3. Normally isotropic consolidated Kaolin sheared in extension……. 231
8.2.4. Lightly isotropic overconsolidated Kaolin sheared in extension…….. 233
8.2.5. Heavily isotropic overconsolidated Kaolin sheared in extension……. 234
8.2.6. Normally K_0-consolidated Kaolin sheared in compression…….. 235
8.2.7. Normally K_0-consolidated Kaolin sheared in extension……... 237
8.3. Parametric study: Optimal choice of parameters……... 239
8.3.1. Sensitivity analysis I……. 239
8.3.2. Sensitivity analysis II…… 250
8.4. Discussion…….. 266
8.5. Summary…… 275

CHAPTER 9: Evaluation of soil constitutive model performance for tunnelling induced stress path testing
9.1. Introduction…… 276
9.2. Results…… 276
9.2.1. Crown of single tunnel. K_o<1 (Test SP1)……. 276
9.2.2. Springline of twin tunnels. K_o<1 (Test SP2)…… 278
9.2.3. Crown of single tunnel. K_o>1 (Test SP3)……. 281
9.3. Discussion…….. 283
9.4. Summary…… 292

CHAPTER 10: Conclusions and suggestions for future research
10.1. Introduction…….. 293
10.2. Total stress paths due to tunneling……... 293
10.3. Reconstituted samples…….. 294
10.4. Critical state parameters for Speswhite Kaolin clay……..... 295
10.5. Reproducing tunnelling-induced total stress paths in the laboratory……... 296

10.6. Evaluation of the capabilities of the Modified Cam-Clay, Al-Tabbaa, S-CLAY1 and small-strain Jardine models……. 297
10.7. Suggestions for future research…… 300

REFERENCES

APPENDIXES
APPENDIX A: Chapter 3 - Additional Information
APPENDIX B: Chapter 5 - Tap water analysis
APPENDIX C: Chapter 5 - Additional Figures
APPENDIX D: Chapter 7 - Additional Figures
APPENDIX E: Chapter 8 - Additional Figures
APPENDIX F: Complete list of laboratory experiments

LIST OF SYMBOLS

α	Parameter for the shear response in the Jardine et al. (1986) and Jardine et al. (1991) models
α_s	Initial inclination of the yield surface in the S-CLAY1 model
A	Skempton´s parameter
A_{ss}	Parameter for the shear response in the Jardine et al. (1986) model
B	Skempton´s parameter
B_{ss}	Parameter for the shear response in the Jardine et al. (1986) model
β_{PL}	Tunnel convergence factor in PLAXIS
β	Relative effectiveness of rotational hardening in the S-CLAY1 model
c'	Cohesion
$c_{c'ic}$	Cohesion for isotropically consolidated specimens sheared in compression
$c_{c'0}$	Cohesion for K_0-consolidated specimens sheared in compression
$c_{c'}$	Cohesion for specimens sheared in compression
$c_{e'ic}$	Cohesion for isotropically consolidated specimens sheared in extension
$c_{e'0}$	Cohesion for K_0-consolidated specimens sheared in extension
$c_{e'}$	Cohesion for specimens sheared in extension
C1	Parameter for the shear response in the Jardine et al. (1991) model
C2	Parameter for the shear response in the Jardine et al. (1991) model
C3	Parameter for the shear response in the Jardine et al. (1991) model
C4	Parameter for the volumetric response in the Jardine et al. (1991) model
C5	Parameter for the volumetric response in the Jardine et al. (1991) model
C6	Parameter for the volumetric response in the Jardine et al. (1991) model
C_{ss}	Parameter for the shear response in the Jardine et al. (1986) model
c_u	Undrained shear strength
δ	Parameter for the volumetric response in the Jardine et al. (1991) model
d	Plate equivalent thickness for lining simulation in PLAXIS
D_0	Initial specimen diameter
ΔBV	Change in back pressure
ΔH	Change in height
e	Void ratio
e_0	Initial void ratio
ε_1	Major principal strain
ε_2	Intermediate principal strain
ε_3	Minor principal strain
ε_a	Axial strain
ε_s	Shear strain
ε_s^e	Elastic component of the shear strain
ε_s^p	Plastic component of the shear strain
ε_v	Volumetric Strain
ε_v^e	Elastic component of the volumetric strain
ε_v^p	Plastic component of the volumetric strain
E	Young modulus
E_{50}	Young modulus at 50 % strain
E_{sec}	Secant Young Modulus
E_u	Undrained Young modulus
$E_{u\ sec}$	Undrained secant Young modulus
EA	Lining axial stiffness
EI	Lining flexural rigidity
E_{oed}	Young modulus from oedometer results
ϕ'	Friction angle
$\phi_{c'ic}$	Friction angle for isotropically consolidated specimens sheared in compression

$\phi_c'_0$	Friction angle for K_0-consolidated specimens sheared in compression
ϕ_c'	Friction angle for specimens sheared in compression
$\phi_e'_{ic}$	Friction angle for isotropically consolidated specimens sheared in extension
$\phi_e'_0$	Friction angle for K_0-consolidated specimens sheared in extension
ϕ_e'	Friction angle for specimens sheared in extension
G	Shear modulus
G_{sec}	Secant shear modulus
G_t	Tangential shear modulus
g	Gravity
γ	Parameter for the shear response in the Jardine et al. (1986) and Jardine et al. (1991) models
Γ	Specific volume on the critical state line at $p' = 1kN/m^2$
γ_{sat}	Saturated soil density
γ_{unsat}	Unsaturated soil density
η	Parameter for the volumetric response in the Jardine et al. (1991) model
H_0	Initial specimen height
h_f	Distance from the cone apex to the soil surface (Fall cone test)
H_s	Equivalent height of solid particles
η_s	Stress ratio in the S-CLAY1 model
i_f	Depth of penetration of the cone (Fall cone test)
i_y	Trough width parameter
IL	Liquidity index
κ	Slope of the loading-unloading lines in the v - lnp′ space
κ_{ic}	Slope of the loading-unloading lines in the v - lnp′ space for isotropically consolidated specimens
κ_0	Slope of the loading-unloading lines in the v - lnp′ space for K_0-consolidated specimens
κ^*	Slope of the loading-unloading lines in the lnv - lnp′ space
κ_{ic}^*	Slope of the loading-unloading lines in the lnv - lnp′ space for isotropically consolidated specimens
κ_0^*	Slope of the loading-unloading lines in the lnv - lnp′ space for K_0-consolidated specimens
K	Bulk modulus
K_{sec}	Secant bulk modulus
K_t	Tangential bulk modulus
K_0	Coefficient of earth pressure at rest
K_0^{nc}	Coefficient of earth pressure at rest for normally consolidated states
K_0^{oc}	Coefficient of earth pressure at rest for overconsolidated states
k_f	Constant depending on the cone angle (Fall cone test)
K_x	Horizontal soil permeability
K_y	Vertical soil permeability
λ	Slope of the normal consolidation line in the v - lnp′ space
λ_{ic}	Slope of the normal consolidation line in the v - lnp′ space for isotropically consolidated specimens
λ_0	Slope of the normal consolidation line in the v - lnp′ space for K_0-consolidated specimens
λ^*	Slope of the normal consolidation line in the lnv - lnp′ space
λ_{ic}^*	Slope of the normal consolidation line in the lnv - lnp′ space for isotropically consolidated specimens
λ_0^*	Slope of the normal consolidation line in the lnv - lnp′ space for K_0-consolidated specimens
λ_{cc}	Unloading parameter in the Convergence-confinement method
λ_{cs}	Slope of the critical state line in the a v -lnp' space
LL	Liquid limit
M	Slope of the critical state line projected in the q - p′ space
Mc_{ic}	Slope of the critical state line for isotropically consolidated specimens sheared in compression
Mc_0	Slope of the critical state line for K_0-consolidated specimens sheared in compression

Me_{ic}	Slope of the critical state line for isotropically consolidated specimens sheared in extension
Me_0	Slope of the critical state line for K_0-consolidated specimens sheared in extension
m	Level of stiffness dependency in the Hardening model
m_f	Mass of the falling cone (Fall cone test)
μ_s	Absolute effectiveness of rotational hardening in the S-CLAY1 model
N	Specific volume of the isotropically normally consolidated soil at $p' = 1kN/m^2$
N_0	Specific volume of the one-dimensionally normally consolidated soil at $p' = 1kN/m^2$
p	Mean total stress = $(\sigma_1 + 2 \cdot \sigma_3) / 3$
p'	Mean effective stress = $(\sigma_1' + 2 \cdot \sigma_3') / 3$
p_0'	Initial p'
p_c'	Preconsolidation pressure
PL	Plastic limit
q	Deviator stress = $\sigma_v - \sigma_h$
q*	Deviator stress = $\sigma_1 - \sigma_3$
θ	At-rest rebound parameter for the determination of K_0^{oc}
RVALU	Ratio of the size of the yield surface to that of the bounding surface in the Al-Tabbaa (1987) model
s	Mean total stress = $\sigma_1 + \sigma_3$
s'	Mean effective stress = $\sigma_1' + \sigma_3'$
σ_1	Major principal stress
σ_2	Intermediate principal stress
σ_3	Minor principal stress
σ_h	Total horizontal stress
σ_h'	Effective horizontal stress
σ_v	Total vertical stress
σ_v'	Effective vertical stress
σ_x	Total horizontal stress in PLAXIS
σ_x'	Effective horizontal stress in PLAXIS
σ_y	Total vertical stress in PLAXIS
σ_y'	Effective vertical stress in PLAXIS
t	Shear total stress = $\sigma_1 - \sigma_3$
υ	Poisson´s ratio
υ_l	Lining Poisson´s ratio
υ_u	Undrained Poisson´s ratio
υ_{ur}	Poisson´s ratio during unloading-reloading cycles
u	Pore water pressure
v	Specific volume
Vl	Volume loss at the tunnel level
Vs	Volume of the settlement trough
W	Magnitude of the ground settlement due to tunnelling
w	Moisture content
w_i	Initial moisture content
w_f	Final moisture content
w_l	Lining weight
W_{max}	Maximum surface ground settlement due to tunnelling
XIVAL	Exponent in the hardening function in the Al-Tabbaa (1987) model
ψ	Dilatancy
Z_0	Depth from the ground surface to the tunnel axis

LIST OF FIGURES

Figure		Page
	CHAPTER 2. Literature review	
2.1	Two-dimensional and three-dimensional movement idealisation around tunnelling operations (after Mair and Taylor, 1997).	9
2.2	Some trends in the evolution of constitutive models for clays	12
2.3	Original Cam-Clay yielding surface	13
2.4	Modified Cam-Clay yielding surface	16
2.5	Yielding envelope for the S-CLAY1 model (Wheeler et al., 2003)	16
2.6	Phases of soil behaviour according to Jardine et al. (1991)	18
2.7	Curve fitting to strain-stiffness data (after Jardine et al. 1986)	19
2.8	Al-Tabbaa (1987) multi-surface kinematic envelopes	21
2.9	Effect of non-linear stiffness at small strains on the predicted surface settlement trough (Addenbrooke et al., 1997). J4 refers to the Jardine et al. (1991) model.	23
2.10	Normalised stiffness-strain curve predictions of the Al-Tabbaa model for the triaxial compression paths (test data from Jardine, 1985) (Grammatikopoulou, 2004)	24
2.11	Normalised stiffness-strain curve predictions of the Al-Tabbaa model for the triaxial extension paths (test data from Jardine, 1985) (Grammatikopoulou, 2004)	24
2.12	Total and effective stress paths during finite element analysis: (a) Crown, (b) Springline, (c) Invert (after Mair, 1979)	27
2.13	Stress paths for typical elements in soil due to tunnelling (Ng and Lo, 1985)	28
2.14	Schematic diagram with idealised stress paths due to undrained excavation of a single tunnel (Dasari, 1996)	29
2.15	Stress paths around a tunnel for different cross section shapes: (a) $K_0 = 1$, (b) $K_0 = 2$ (after Barla, 1999)	30
2.16	Stress changes at the tunnel crown and sidewalls during construction from elastic analyses for (a) $K_0 = 1$ and (b) $K_0 = 2$ (Barla, 1999)	31
2.17	Stress changes at the tunnel crown and sidewalls during construction from elasto-plastic analyses for (a) $K_0 = 1$ and (b) $K_0 = 2$ (Barla, 1999)	31
2.18	Stress paths proposed for laboratory testing reproducing expected conditions at (a) tunnel crown and (b) tunnel sidewalls (Barla, 1999)	32
2.19	Effective stress paths around an unlined tunnel up to $\lambda = 100$ % using the CJS elasto-plastic model (Bernat et al. 1999) (Each point along the stress paths represents an increment of 10 % of deconfinement)	33
2.20	Stress paths at different locations for the driving of a NATM tunnel in London Clay; $K_0 = 1.5$ (after Tang et al., 2000)	34

Figure		Page
2.21	Magnitude and orientation of principal stresses at fixed points in the tunnel roof and wall for a given initial initial stress (Eberhardt, 2001)	35
2.22	Stress paths of vertical versus horizontal stress on the tunnel centreline during volume loss (Jacobsz, 2002)	36
2.23	Vertical stress profile on tunnel centreline at different volume loss values (Jacobsz, 2002)	36
2.24	Horizontal stress profile on tunnel centreline at different volume loss values (Jacobsz, 2002)	37
2.25	Typical variation of stiffness with strain, strain range relevant to various geotechnical problems and application of different equipment for its measurement (PLAXIS Manuals (after Atkinson and Sallfors (1991))	45
	CHAPTER 3. Methodology	
3.1	Flow diagram describing the project methodology	50
3.2	Tunnel coordinate system (after Yeates, 1985)	52
3.3	Application to 2D finite element analysis of the principle of Convergence-confinement method (Panet and Guenot, 1982)	56
3.4	Geometry and mesh used for the 1-layer 2D analyses of a single tunnel in PLAXIS	60
3.5	Geometry and mesh used for the 1-layer 2D analyses of twin tunnels in PLAXIS	61
3.6	Geometry and mesh used for the 3-layer 2D analyses of a single tunnel in PLAXIS	61
3.7	Geometry and mesh used for the 1-layer 3D analyses of a single tunnel in PLAXIS	62
3.8	Positive coordinate system (including shear stresses) in PLAXIS	63
3.9	Measurement stress points in the PLAXIS 3D analyses	64
3.10	Scaled front elevation and plan views of consolidation Device A	69
3.11	Consolidation Device A	70
3.12	Sequence of preparation of the drainage layers in consolidation Device A, from the placement of the wet filter paper and metallic mesh, to the smooth compaction of the layer prior to pouring the slurry into the tube	70
3.13	Consolidation Device B: (a) Pump, hydraulic jacks and rig, (b) Detail of the compressed air pump	71
3.14	(a) Sample extrusion and (b) Trimming kit	72
3.15	(a) Hand vane measurement of c_u and (b) Picture showing the code, date and use of the different parts of the extruded sample: “T” (top of the sample), “B” (base of the sample), “HV” (part used for c_u determination by the hand vane), “1”, “2” and “3” (parts used for moisture content determination)	75

Figure		Page
3.16	(a) Pore water pressure measurements at three positions equally spaced along the consolidation Device A (Upper, Intermediate and Bottom) during K_0-consolidation in tests F01, F02, F03 and F04, and details of (b) the push-in sealed connections and (c) the filter	78
3.17	Adapted 100 mm inner diameter consolidation device	79
3.18	Standard Stress Path equipment: (a) Equipment overview; (b) Stress Path Bishop and Wesley-type cell, (c) From top to bottom: RS232, ±2.5 mm LVDT's signal amplifier and 8-channel data-logger, (d) Standard pressure/volume controllers	81
3.19	50 mm extension caps: (a) Detail of the gap between the puller cap and the vylastic sleeve in the Wykeham Farrance device , (b) Wykeham Farrance and GDS kits, left and right respectively	83
3.20	(a) ±2.5 mm range LVDT axial and radial small-strain measurement device, (b) Detail of the radial arrangement	85
3.21	(a) ±3 mm range Hall Effect device, (b) Detail of the radial arrangement	85
3.22	(a) Conventional triaxial equipment and (b) Automatic volume change measuring apparatus	87
3.23	Fuse wire technique arrangement	88
3.24	Location of the inner bubble in a kinematic hardening model with (B,B′) and without creep (A,A′) during K_0-consolidation	102
3.25	Location of the inner bubble in a kinematic hardening model when approaching the same point through different consolidation paths	103
3.26	Location of the inner bubble in a kinematic hardening model when allowing for some creep (a) at the end of different consolidation paths. (b) represents the ideal final state after long creep	103
3.27	Geometrical relationship for the determination of the shear parameters *C1*, *C2* and *C3* (after Jardine et al., 1986)	115

CHAPTER 4. Finite element analysis

4.1	Stress paths at the crown and springlines of a single tunnel under K_0 conditions below (blue), equal to (red) and above "1" (green) using the Linear Elastic model. Only the excavation of the cavity has been considered as well as the progressive relaxation of the stresses controlled by the *ΣMstage* parameter	121
4.2	Stress paths at the crown and springlines of a single tunnel in terms of σ_y - σ_x under K_0 conditions below (blue), equal to (red) and above "1" (green) using the Elastic, Mohr-Coulomb, Hardening and Jardine et al. (1991)+Mohr-Coulomb models. Both the excavation of the cavity and the placement of the lining have been considered	122
4.3	Typical settlement troughs and total displacements obtained during 2D PLAXIS elastic analyses: (a) $K_0<1$, (b) $K_0>1$	123

Figure		Page
4.4	Comparison of stress paths at the crown and springlines of a single tunnel under K_0 conditions below (blue) and above "1" (green) using the Elastic model for both 'dry' and 'wet' conditions	124
4.5	Stress paths at the crown and springlines of a single tunnel under K_0 conditions below (blue) and above "1" (green) using the Elastic and Mohr-Coulomb models and a 3-layer soil geometry	125
4.6	Stress paths at the springline between twin tunnels separated by a distance of 2.0 d between centrelines for K_0 conditions below (blue), equal to (red) and above "1" (green)	126
4.7	Stress paths at the springline between twin tunnels separated by a distance of 2.5 d between centrelines for K_0 conditions below (blue), equal to (red) and above "1" (green)	127
4.8	Stress paths at the springline between twin tunnels separated by a distance of 3.0 d between centrelines for K_0 conditions below (blue), equal to (red) and above "1" (green)	128
4.9	Calculated vertical transverse surface settlement troughs above twin tunnels separated 2.0 d between centrelines considering K_0<1 conditions and using the Elastic, Mohr-Coulomb and Hardening constitutive models	129
4.10	Calculated vertical transverse surface settlement trough above twin tunnels separated 2.5 d between centrelines considering K_0<1 conditions and using the Elastic, Mohr-Coulomb and Hardening constitutive models	129
4.11	Calculated vertical transversal surface settlement trough above twin tunnels separated 3.0 d between centrelines considering K_0<1 conditions and using the Elastic, Mohr-Coulomb and Hardening constitutive models	130
4.12	Sensitivity analysis with respect to the Mohr-Coulomb parameters, the lining properties and the mesh coarseness when K_0 = 1	131
4.13	Sensitivity analysis with respect to the lining properties when K_0<1	133
4.14	Sensitivity analysis with respect to the lining properties when K_0>1	134
4.15	Sensitivity analysis with respect to c', ϕ' and ψ when using the Hardening model under K_0>1 conditions	135
4.16	Surface settlement trough above a single tunnel when using the Hardening model for various K_0 values	136
4.17	Occurrence of plastic points for increasing values of K_0 when using the Hardening model	136
4.18	Surface settlement trough above a single tunnel when using the Hardening model and K_0 = 1.52 for various m values	136
4.19	3D-changes in σ_v, σ_x and σ_z at the measurement section points (a) A* and (b) B* with respect to the position of the tunnel face using the Elastic, Mohr-Coulomb and Hardening models when K_0<1	137
4.20	3D-changes in σ_v, σ_x and σ_z at the measurement section points (a) A* and (b) B* with respect to the position of the tunnel face using the Mohr-Coulomb model when K_0 = 1	138

Figure		Page
4.21	3D-changes in σ_v, σ_x and σ_z at the measurement section points (a) A* and (b) B* with respect to the position of the tunnel face using the Mohr-Coulomb model when K_0>1	139
4.22	Stress paths at point A* and B* in terms of σ_x and σ_y using the Elastic, Mohr-Coulomb and Hardening models for K_0 below, equal to and above "1"	140
4.23	(a) Longitudinal total displacements, (b) Vertical and horizontal-x displacements on the x = -2.5 m plane, (c) Transverse surface settlement trough and deformed tunnel contour and (d) 3D surface settlement trough for K_0 below, equal to and above "1" using the Mohr-Coulomb criterion	141
4.24	Idealised mechanisms occurring during a cavity unloading in PLAXIS for (a) Normally consolidated soil (K_0<1) and (b) Overconsolidated soil (K_0>1)	145

CHAPTER 5. Study of the characteristics of the reconstituted samples

(NOTE: Some of the Figures corresponding to this chapter are shown in Appendix C)

5.1	Void ratio change with σ_v' during the K_0-consolidation of Speswhite Kaolin slurry under different conditions	155
5.2	Detail of the void ratio change during the K_0-consolidation for σ_v' below 150 kPa	155
5.3	Laboratory consolidation curves during the different loading steps in the preparation of sample IN 1.8 using the square root of the time fitting method (British Standard 1377-5:1990)	156
5.4	c_u - IL relationship for reconstituted Speswhite Kaolin samples with an initial w equal to 1.5 LL, c_u being measured by a hand vane	157
5.5	c_u - $\sigma_{v'max}$ relationship for reconstituted Speswhite Kaolin samples with an initial w equal to 1.5 LL, c_u being measured by a hand vane	157
5.6	w - $\sigma_{v'max}$ relationship for one-dimensionally consolidated	158
5.7	Mode of failure for specimen UU2	159
5.8	Concave fabric created in the soil during one-dimensional consolidation	160
5.9	Moisture content distribution along Speswhite Kaolin samples after one-dimensional consolidation	166
5.10	Visual inspection of one of the samples showing differences in w along its length	166
5.11	Fall-cone test results for sample 'c_uw': (a) Moisture content, cone penetration and c_u distributions along the sample length, (b) Discrete c_u - w relationship	168
5.12	Pore water pressure measurements at three points equally spaced along the consolidation device (Upper, Intermediate and Bottom) during K_0-consolidation in tests (a) F01, (b) F02, (c) F03 and (d) F04	167
5.13	Internal fabric from top (a) to base (e) in the sample A100-1 K_0-consolidated in the 100 mm inner diameter modified Device A	173

Figure		Page
5.14	Void ratio change with σ_v' during the K_0-consolidationof sample A100-1 compared to data in Figure 5.1	174
5.15	Theoretical and real stress history of the K_0-consolidated specimens	175

CHAPTER 6. Laboratory tests Part I: Critical state framework for Speswhite Kaolin clay

6.1	Failure envelope for the isotropically consolidated specimens sheared in compression	179
6.2	q - ε_a relationship for specimens sheared in compression in undrained conditions	179
6.3	u -*Time* measurements during undrained shearing in compression	180
6.4	Modes of failure for the specimens sheared undrained in compression	180
6.5	Typical pore water pressure response during B-check	181
6.6	Failure envelope for the isotropically consolidated specimens sheared in extension	182
6.7	q - ε_a relationship for specimens sheared in extension in undrained conditions	182
6.8	u - *Time* measurements during undrained shearing in extension	182
6.9	Modes of failure for the specimens sheared undrained in extension	183
6.10	Definition of the normally consolidated and unloading-reloading lines based on tests NCL1 and NCL2	183
6.11	One-dimensional consolidation during test Ko1 using on-sample LVDT's	185
6.12	One-dimensional consolidation during test Ko2 using on-sample LVDT's	185
6.13	One-dimensional consolidation during test Ko3 using on-sample LVDT's	185
6.14	Results from the stress paths performed after the one-dimensional consolidation in test Ko3	186
6.15	Proposed stress path for the simulation of K_0-consolidation during test KoAL1	186
6.16	Results from test KoAL1	186
6.17	One-dimensional consolidation (using the specimen volume change option) and undrained shearing in compression during tests Ko4 and Ko5	187
6.18	One-dimensional consolidation (using the Hall Effect device) and undrained shearing in extension during test Ko6	187
6.19	(a) Radial Hall Effect device measurements during test Ko6, (b) Detail of the radial strain during the B-check stage and (c) Detail of the radial strain during the K_0-consolidation stage	188
6.20	One-dimensional normal consolidation lines in the v - lnp' plane obtained during tests Ko4, Ko5 and Ko6	188
6.21	Pore water pressure changes with time during undrained shearing in tests Ko4, Ko5 and Ko6	189

Figure		Page
6.22	Modes of failure for various K_0-consolidated specimens	189
6.23	Correlations between the load cell, radial and axial deformations and the pore water pressure readings during test Ko1. The vertical columns relate the same observed behaviour between the different plots	194
6.24	Difference between the radial strains measured by the on-sample Hall Effect device and those calculated based on the external LVDT during undrained shearing in test Ko6	197
6.25	Critical state line in the v - lnp' plane	198
6.26	π-plane representation of the laboratory data for compression and extension triaxial states	199

CHAPTER 7. Laboratory tests Part II: Stress path testing

(NOTE: Some of the Figures corresponding to this chapter are shown in Appendix D)

7.1	Failure envelopes in compression and extension for the Speswhite Kaolin clay based on the experimental data presented in Chapter 6	181
7.2	Total and effective experimental stress paths during tests SP1 and SP1-c	205
7.3	Tests SP1 and SP1-c. q - ε_s relationship during the K_0-consolidation stage	206
7.4	Tests SP1 and SP1-c. p' - ε_v relationship during the K_0-consolidation stage	206
7.5	Tests SP1 and SP1-c. Variation in ε_a with time measured by the two axial on-sample Hall Effect devices	206
7.6	Tests SP1 and SP1-c. Variation in ε_r with time measured by the radial on-sample Hall Effect device	206
7.7	Tests SP1 and SP1-c. q - ε_a relationship during PART 1	206
7.8	Tests SP1 and SP1-c. Variation in u with time during PART 1	206
7.9	Tests SP1 and SP1-c. Comparison between the axial deformation registered by both axial Hall Effect devices during PART 1	207
7.10	Tests SP1 and SP1-c. Variation in ε_a with time during PART 2 measured by the two axial on-sample Hall Effect devices	207
7.11	Tests SP1 and SP1-c. Variation in ε_r with time during PART 2 measured by the radial on-sample Hall Effect device	207
7.12	Tests SP1 and SP1-c. q - ε_a relationship during PART 2	207
7.13	Tests SP1 and SP1-c. Variation in u with time during PART 2	207
7.14	Tests SP1 and SP1-c. Comparison between the axial deformation registered by both axial Hall Effect devices during PART 2	208
7.15	Test SP2. Variation in specimen area during K_0-consolidation as measured by both internal and external instrumentation	213

Figure		Page
7.16	Tests SP2 and Ko6. Calculated $\sigma_{v'}$ - $\sigma_{h'}$ variation during K_0-consolidation based on both internal and external specimen area measurements	213
7.17	Test SP2C. Variation in ε_a during PART 2-overnight under constant stress undrained conditions	219
7.18	Test SP2C. Variation in ε_r during PART 2-overnight under constant stress undrained conditions	219
7.19	Test SP2C. Variation in u during PART 2-overnight under constant stress undrained conditions	219
7.20	Fitting of experimental K_0-OCR data during tests SP3 and SP4	221

CHAPTER 8. Evaluation of soil constitutive model performance for conventional triaxial testing

(NOTE: Some of the Figures corresponding to this chapter are shown in Appendix E)

8.1	Measured versus predicted q - p' relationship during test USc7	230
8.2	Measured versus predicted q - ε_a relationship during test USc7	230
8.3	Measured versus predicted u - ε_a relationship during test USc7	230
8.4	Measured versus predicted E_{sec} - ε_a relationship during test USc7	230
8.5	Measured versus predicted q - p' relationship during test USc9	231
8.6	Measured versus predicted q - ε_a relationship during test USc9	231
8.7	Measured versus predicted u - ε_a relationship during test USc9	231
8.8	Measured versus predicted E_{sec} - ε_a relationship during test USc9	231
8.9	Measured versus predicted q - p' relationship during test USe3	232
8.10	Measured versus predicted q - ε_a relationship during test USe3	232
8.11	Measured versus predicted u - ε_a relationship during test USe3	232
8.12	Measured versus predicted E_{sec} - ε_a relationship during test USe3	232
8.13	Measured versus predicted q - p' relationship during test USe5	232
8.14	Measured versus predicted q - ε_a relationship during test USe5	232
8.15	Measured versus predicted u - ε_a relationship during test USe5	234
8.16	Measured versus predicted E_{sec} - ε_a relationship during test USe5	234
8.17	Measured versus predicted q - p' relationship during test USe6	235
8.18	Measured versus predicted q - ε_a relationship during test USe6	235
8.19	Measured versus predicted u - ε_a relationship during test USe6	235
8.20	Measured versus predicted E_{sec} - ε_a relationship during test USe6	235

Figure		Page
8.21	Measured versus predicted q - p' relationship during test Ko5	236
8.22	Measured versus predicted q - ε_a relationship during test Ko5	236
8.23	Measured versus predicted u - ε_a relationship during test Ko5	237
8.24	Measured versus predicted E_{sec} - ε_a relationship during test Ko5	237
8.25	Measured versus predicted q - p' relationship during test Ko6	238
8.26	Measured versus predicted q - ε_a relationship during test Ko6	238
8.27	Measured versus predicted u - ε_a relationship during test Ko6	238
8.28	Measured versus predicted E_{sec} - ε_a relationship during test Ko6	239
8.29	Sensitivity of the Al-Tabbaa model to κ_{ic}* in terms of the q - p' behaviour during test USe5	240
8.30	Sensitivity of the Al-Tabbaa model to κ_{ic}* in terms of the q - ε_a behaviour during test USe5	240
8.31	Sensitivity of the Al-Tabbaa model to κ_{ic}* in terms of the u - ε_a behaviour during test USe5	240
8.32	Sensitivity of the Al-Tabbaa model to κ_{ic}* in terms of the E_{sec} - ε_a behaviour during test USe5	240
8.33	Sensitivity of the Al-Tabbaa model to *RVALU* in terms of the q - p' behaviour during test USe5	241
8.34	Sensitivity of the Al-Tabbaa model to *RVALU* in terms of the q - ε_a behaviour during test USe5	241
8.35	Sensitivity of the Al-Tabbaa model to *RVALU* in terms of the u - ε_a behaviour during test USe5	241
8.36	Sensitivity of the Al-Tabbaa model to *RVALU* in terms of the E_{sec} - ε_a behaviour during test USe5	241
8.37	Sensitivity of the Al-Tabbaa model to *XIVAL* in terms of the q - p' behaviour during test USe5	242
8.38	Sensitivity of the Al-Tabbaa model to *XIVAL* in terms of the q - ε_a behaviour during test USe5	242
8.39	Sensitivity of the Al-Tabbaa model to *XIVAL* in terms of the u - ε_a behaviour during test USe5	242
8.40	Sensitivity of the Al-Tabbaa model to *XIVAL* in terms of the E_{sec} - ε_a behaviour during test USe5	242
8.41	Sensitivity of the Modified Cam-Clay model to κ_{ic} in terms of the q - p' behaviour during test USc7	243
8.42	Sensitivity of the Modified Cam-Clay model to κ_{ic} in terms of the q - ε_a behaviour during test USc7	243
8.43	Sensitivity of the Modified Cam-Clay model to κ_{ic} in terms of the u - ε_a behaviour during test USc7	243

Figure		Page
8.44	Sensitivity of the Modified Cam-Clay model to κ_{ic} in terms of the E_{sec} - ε_a behaviour during test USc7	243
8.45	Sensitivity of the Modified Cam-Clay model to υ in terms of the q - p' behaviour during test USc7	244
8.46	Sensitivity of the Modified Cam-Clay model to υ in terms of the q - ε_a behaviour during test USc7	244
8.47	Sensitivity of the Modified Cam-Clay model to υ in terms of the u - ε_a behaviour during test USc7	244
8.48	Sensitivity of the Modified Cam-Clay model to υ in terms of the E_{sec} - ε_a behaviour during test USc7	244
8.49	Sensitivity of the Al-Tabbaa model to κ_{ic}* in terms of the q - p' behaviour during test USc7	245
8.50	Sensitivity of the Al-Tabbaa model to κ_{ic}* in terms of the q - ε_a behaviour during test USc7	245
8.51	Sensitivity of the Al-Tabbaa model to κ_{ic}* in terms of the u - ε_a behaviour during test USc7	245
8.52	Sensitivity of the Al-Tabbaa model to κ_{ic}* in terms of the E_{sec} - ε_a behaviour during test USc7	245
8.53	Sensitivity of the Al-Tabbaa model to *RVALU* in terms of the q - p' behaviour during test USc7	246
8.54	Sensitivity of the Al-Tabbaa model to *RVALU* in terms of the q - ε_a behaviour during test USc7	246
8.55	Sensitivity of the Al-Tabbaa model to *RVALU* in terms of the u - ε_a behaviour during test USc7	246
8.56	Sensitivity of the Al-Tabbaa model to *RVALU* in terms of the E_{sec} - ε_a behaviour during test USc7	246
8.57	Sensitivity of the Al-Tabbaa model to *XIVAL* in terms of the q - p' behaviour during test USc7	247
8.58	Sensitivity of the Al-Tabbaa model to *XIVAL* in terms of the q - ε_a behaviour during test USc7	247
8.59	Sensitivity of the Al-Tabbaa model to *XIVAL* in terms of the u - ε_a behaviour during test USc7	247
8.60	Sensitivity of the Al-Tabbaa model to *XIVAL* in terms of the E_{sec} - ε_a behaviour during test USc7	247
8.61	Sensitivity of the S-CLAY1 model to κ_0 in terms of the q - p' behaviour during test Ko6	248
8.62	Sensitivity of the S-CLAY1 model to κ_0 in terms of the q - ε_a behaviour during test Ko6	248
8.63	Sensitivity of the S-CLAY1 model to κ_0 in terms of the u - ε_a behaviour during test Ko6	248

Figure		Page
8.64	Sensitivity of the S-CLAY1 model to κ_0 in terms of the E_{sec} - ε_a behaviour during test Ko6	248
8.65	Sensitivity of the S-CLAY1 model to β in terms of the q - p' behaviour during test Ko6	249
8.66	Sensitivity of the S-CLAY1 model to β in terms of the q - ε_a behaviour during test Ko6	249
8.67	Sensitivity of the S-CLAY1 model to β in terms of the u - ε_a behaviour during test Ko5	249
8.68	Sensitivity of the S-CLAY1 model to β in terms of the E_{sec} - ε_a behaviour during test Ko5	249
8.69	Sensitivity of the Al-Tabbaa model to κ_{ic}* in terms of the q - p' behaviour during test USc9	250
8.70	Sensitivity of the Al-Tabbaa model to κ_{ic}* in terms of the q - ε_a behaviour during test USc9	250
8.71	Sensitivity of the Al-Tabbaa model to κ_{ic}* in terms of the u - ε_a behaviour during test USc9	250
8.72	Sensitivity of the Al-Tabbaa model to κ_{ic}* in terms of the E_{sec} - ε_a behaviour during test USc9	250
8.73	Sensitivity of the Al-Tabbaa model to *RVALU* in terms of the q - p' behaviour during test USc9	251
8.74	Sensitivity of the Al-Tabbaa model to *RVALU* in terms of the q - ε_a behaviour during test USc9	251
8.75	Sensitivity of the Al-Tabbaa model to *RVALU* in terms of the u - ε_a behaviour during test USc9	251
8.76	Sensitivity of the Al-Tabbaa model to *RVALU* in terms of the E_{sec} - ε_a behaviour during test USc9	251
8.77	Sensitivity of the Al-Tabbaa model to XIVAL in terms of the q - p' behaviour during test USc9	252
8.78	Sensitivity of the Al-Tabbaa model to *XIVAL* in terms of the q - ε_a behaviour during test USc9	252
8.79	Sensitivity of the Al-Tabbaa model to *XIVAL* in terms of the u - ε_a behaviour during test USc9	252
8.80	Sensitivity of the Al-Tabbaa model to *XIVAL* in terms of the E_{sec} - ε_a behaviour during test USc9	252
8.81	Sensitivity of the Al-Tabbaa model to κ_{ic}* in terms of the q - p' behaviour during test USe3	253
8.82	Sensitivity of the Al-Tabbaa model to κ_{ic}* in terms of the q - ε_a behaviour during test USe3	253
8.83	Sensitivity of the Al-Tabbaa model to κ_{ic}* in terms of the u - ε_a behaviour during test USe3	253

Figure		Page
8.84	Sensitivity of the Al-Tabbaa model to κ_{ic}* in terms of the E_{sec} - ε_a behaviour during test USe3	253
8.85	Sensitivity of the Al-Tabbaa model to *RVALU* in terms of the q - p' behaviour during test USe3	254
8.86	Sensitivity of the Al-Tabbaa model to *RVALU* in terms of the q - ε_a behaviour during test USe3	254
8.87	Sensitivity of the Al-Tabbaa model to *RVALU* in terms of the u - ε_a behaviour during test USe3	254
8.88	Sensitivity of the Al-Tabbaa model to *RVALU* in terms of the E_{sec} - ε_a behaviour during test USe3	254
8.89	Sensitivity of the Al-Tabbaa model to XIVAL in terms of the q - p' behaviour during test USe3	255
8.90	Sensitivity of the Al-Tabbaa model to *XIVAL* in terms of the q - ε_a behaviour during test USe3	255
8.91	Sensitivity of the Al-Tabbaa model to *XIVAL* in terms of the u - ε_a behaviour during test USe3	255
8.92	Sensitivity of the Al-Tabbaa model to *XIVAL* in terms of the E_{sec} - ε_a behaviour during test USe3	255
8.93	Sensitivity of the Al-Tabbaa model to κ_{ic}* in terms of the q - p' behaviour during test USe6	256
8.94	Sensitivity of the Al-Tabbaa model to κ_{ic}* in terms of the q - ε_a behaviour during test USe6	256
8.95	Sensitivity of the Al-Tabbaa model to κ_{ic}* in terms of the u - ε_a behaviour during test USe6	256
8.96	Sensitivity of the Al-Tabbaa model to κ_{ic}* in terms of the E_{sec} - ε_a behaviour during test USe6	256
8.97	Sensitivity of the Al-Tabbaa model to *RVALU* in terms of the q - p' behaviour during test USe6	257
8.98	Sensitivity of the Al-Tabbaa model to *RVALU* in terms of the q - ε_a behaviour during test USe6	257
8.99	Sensitivity of the Al-Tabbaa model to *RVALU* in terms of the u - ε_a behaviour during test USe6	257
8.100	Sensitivity of the Al-Tabbaa model to *RVALU* in terms of the E_{sec} - ε_a behaviour during test USe6	257
8.101	Sensitivity of the Al-Tabbaa model to XIVAL in terms of the q - p' behaviour during test USe6	258
8.102	Sensitivity of the Al-Tabbaa model to *XIVAL* in terms of the q - ε_a behaviour during test USe6	258
8.103	Sensitivity of the Al-Tabbaa model to *XIVAL* in terms of the u - ε_a behaviour during test USe6	258

Figure		Page
8.104	Sensitivity of the Al-Tabbaa model to *XIVAL* in terms of the E_{sec} - ε_a behaviour during test USe6	258
8.105	Sensitivity of the Modified Cam-Clay model to κ_0 in terms of the q - p' behaviour during test Ko5	259
8.106	Sensitivity of the Modified Cam-Clay model to κ_0 in terms of the q - ε_a behaviour during test Ko5	259
8.107	Sensitivity of the Modified Cam-Clay model to κ_0 in terms of the u - ε_a behaviour during test Ko5	259
8.108	Sensitivity of the Modified Cam-Clay model to κ_0 in terms of the E_{sec} - ε_a behaviour during test Ko5	259
8.109	Sensitivity of the Modified Cam-Clay model to υ in terms of the q - p' behaviour during test Ko5	260
8.110	Sensitivity of the Modified Cam-Clay model to υ in terms of the q - ε_a behaviour during test Ko5	260
8.111	Sensitivity of the Modified Cam-Clay model to υ in terms of the u - ε_a behaviour during test Ko5	260
8.112	Sensitivity of the Modified Cam-Clay model to υ in terms of the E_{sec} - ε_a behaviour during test Ko5	260
8.113	Sensitivity of the Al-Tabbaa model to κ_0* in terms of the q - p' behaviour during test Ko5	261
8.114	Sensitivity of the Al-Tabbaa model to κ_0* in terms of the q - ε_a behaviour during test Ko5	261
8.115	Sensitivity of the Al-Tabbaa model to κ_0* in terms of the u - ε_a behaviour during test Ko5	261
8.116	Sensitivity of the Al-Tabbaa model to κ_0* in terms of the E_{sec} - ε_a behaviour during test Ko5	261
8.117	Sensitivity of the Al-Tabbaa model to *RVALU* in terms of the q - p' behaviour during test Ko5	262
8.118	Sensitivity of the Al-Tabbaa model to *RVALU* in terms of the q - ε_a behaviour during test Ko5	262
8.119	Sensitivity of the Al-Tabbaa model to *RVALU* in terms of the u - ε_a behaviour during test Ko5	262
8.120	Sensitivity of the Al-Tabbaa model to *RVALU* in terms of the E_{sec} - ε_a behaviour during test Ko5	262
8.121	Sensitivity of the Al-Tabbaa model to *XIVAL* in terms of the q - p' behaviour during test Ko5	263
8.122	Sensitivity of the Al-Tabbaa model to *XIVAL* in terms of the q - ε_a behaviour during test Ko5	263
8.123	Sensitivity of the Al-Tabbaa model to *XIVAL* in terms of the u - ε_a behaviour during test Ko5	263

Figure		Page
8.124	Sensitivity of the Al-Tabbaa model to *XIVAL* in terms of the E_{sec} - ε_a behaviour during test Ko5	263
8.125	Sensitivity of the S-CLAY1 model to κ_0 in terms of the q - p' behaviour during test Ko5	264
8.126	Sensitivity of the S-CLAY1 model to κ_0 in terms of the q - ε_a behaviour during test Ko5	264
8.127	Sensitivity of the S-CLAY1 model to κ_0 in terms of the u - ε_a behaviour during test Ko5	264
8.128	Sensitivity of the S-CLAY1 model to κ_0 in terms of the E_{sec} - ε_a behaviour during test Ko5	264
8.129	Sensitivity of the S-CLAY1 model to β in terms of the q - p' behaviour during test Ko5	265
8.130	Sensitivity of the S-CLAY1 model to β in terms of the q - ε_a behaviour during test Ko5	265
8.131	Sensitivity of the S-CLAY1 model to β in terms of the u - ε_a behaviour during test Ko5	265
8.132	Sensitivity of the S-CLAY1 model to β in terms of the E_{sec} - ε_a behaviour during test Ko5	265
8.133	Al-Tabbaa predictions using SM2D for the behaviour of Speswhite Kaolin clay in test Ko5: (a,b,c) Using preconsolidation pressures of 1240, 280, 300, 388 and 400 kPa for analyses controlling p'_{max}; (d,e,f) Using the same preconsolidation pressures but for analyses controlling $\varepsilon_{a\,max}$	269
8.134	Modified Cam Clay predictions using SM2D for the behaviour of Speswhite Kaolin clay in test Ko5: (a,b,c) Increasing κ (0.032, 0.034, 0.036, 0.038, 0.040) for the analysis based on p'_{max}; (d,e,f) Increasing κ (0.032, 0.034, 0.036, 0.038, 0.040) for the analysis based on $\varepsilon_{a\,max}$	270

CHAPTER 9. Evaluation of soil constitutive model performance for tunnelling induced stress path testing

9.1	Measured versus predicted q - ε_a relationship during test SP1	276
9.2	Measured versus predicted q - ε_a relationship during undrained shearing in test SP1	277
9.3	Measured versus predicted q - p' relationship during test SP1	277
9.4	Measured versus predicted q - p, p' relationship during undrained shearing in test SP1	278
9.5	Measured versus predicted q - ε_a relationship during test SP2	279
9.6	Measured versus predicted q - ε_a relationship during undrained shearing in test SP2	279
9.7	Measured versus predicted q - p' relationship during test SP2	280

Figure		Page
9.8	Measured versus predicted q - p, p' relationship during undrained shearing in test SP2	280
9.9	Measured versus predicted q - ε_a relationship during test SP3	281
9.10	Measured versus predicted q - ε_a relationship during undrained shearing in test SP3	282
9.11	Measured versus predicted q - p' relationship during test SP3	282
9.12	Measured versus predicted q - p, p' relationship during undrained shearing in test SP3	283
9.13	Measured versus predicted q - p, p' relationship during undrained shearing in test SP1 using shear and volumetric test-specific parameters from Table 7.5	286
9.14	Movement of the inner bubble and the bounding surface in the Al-Tabbaa model during test SP1	287
9.15	Movement of the inner bubble and the bounding surface in the Al-Tabbaa model during test SP2	288
9.16	Movement of the inner bubble and the bounding surface in the Al-Tabbaa model during test SP3	289
9.17	Measured versus predicted E_{sec} - ε_a relationship during undrained shearing in test SP1 for the Al-Tabbaa, MCC and S-CLAY1 models	290
9.18	Measured versus predicted E_{sec} - ε_a relationship during undrained shearing in test SP2 for the Al-Tabbaa, MCC and S-CLAY1 models	290
9.19	Measured versus predicted E_{sec} - ε_a relationship during undrained shearing in test SP1 for the Jardine model	291
9.20	Measured versus predicted E_{sec} - ε_a relationship during undrained shearing in test SP2 for the Jardine model	291

LIST OF TABLES

Table		Page
	CHAPTER 2. Literature review	
2.1	Stress changes during tunnel excavation (after Mair, 1979)	26
2.2	Factors involved in the variation of p' during specimen preparation	41
2.3	Variability in the "rate of axial stress" and "rate of axial strain" values during drained and undrained shearing in triaxial testing	43
2.4	Variability in *PL* and *LL* values for Kaolin clays	47
2.5	K_0 values for Speswhite Kaolin clay reported by previous authors	47
2.6	Summary of some critical state parameters in the published literature for Speswhite Kaolin clay	48
	CHAPTER 3. Methodology	
3.1	List of PLAXIS analyses	59
3.2	Coordinates for the stress measurement points in PLAXIS	63
3.3	Soil parameters used for the different PLAXIS analyses	65
3.4	Parameters values used for the sensitivity analyses of the PLAXIS models	66
3.5	Measurements of conductivity for de-ionized water (DI), tap water no running for a long period of time (TNR) and running tap water (TR). Units are in mg/l TDS	74
3.6	Details for the first group (IN i) of samples	74
3.7	Details for the group of specimens prepared for unconsolidated undrained triaxial testing	75
3.8	Samples prepared during Stage 2: details and aims of the tests	76
3.9	Initial specifications for the consolidated undrained tests under compression	92
3.10	Initial specifications for the consolidated undrained tests under extension	92
3.11	Initial specifications for the K_0-consolidation tests	96
3.12	Some published values of rate of tunnel advance in London Clay	99
3.13	List of stress path tests	99
3.14	Initial specifications for the specimens used for the tunnelling induced stress path tests	105
3.15	Constitutive models used for SM2D simulation of conventional triaxial tests	116

Table		Page
	CHAPTER 4. Finite element analysis	
4.1	Total 2D stress path trends predicted at points above the tunnel crown and at the springlines for K_0 conditions below, equal to and above "1"	144
	CHAPTER 5. Study of the characteristics of the reconstituted samples	
5.1	Index tests and G_s results	154
5.2	Results from the unconsolidated undrained tests	158
5.3	Scanner Electron Microscope images of a horizontal cross-section C1A close to the base of sample C1	161
5.4	Scanner Electron Microscope images of the vertical cross-section C1B close to the base of sample C1	163
5.5	Scanner Electron Microscope images of a horizontal cross-section C1C close to the top of sample C1	164
	CHAPTER 6. Laboratory tests Part I: Critical state framework for Speswhite Kaolin clay	
6.1	Results from the isotropically consolidated undrained and drained tests under compression	178
6.2	Results from the isotropically consolidated undrained tests under extension	181
6.3	Results from the isotropic consolidation tests	183
6.4	Results from the K_0-consolidation and related tests	184
6.5	Critical state parameters in compression for isotropically consolidated specimens	190
6.6	Critical state parameters in extension for isotropically consolidated specimens	191
6.7	Normal consolidation line and swelling line parameters	192
6.8	K_0-consolidation line parameters	195
6.9	Critical state line parameters	198
	CHAPTER 7. Laboratory tests Part II: Stress path testing	
7.1	Change in vertical and horizontal total stress magnitudes aimed during tests SP1, SP1-c, SP2, SP2B, SP2C, SP3 and SP4	203
7.2	Summary of laboratory data during tests SP1 and SP1-c	208
7.3	Classification of tests into Groups 1, 2 and 3 according to the methodology in Section 3.7.2	210
7.4	Shear response during stress path testing: Curve fitting method, variation in shear modulus and Jardine et al. (1991) fitting accuracy	211

Table		Page
7.5	Jardine et al. (1991) shear parameters obtained from experimental data	211
7.6	Volumetric response during stress path testing: Curve fitting method, variation in bulk modulus and Jardine et al. (1991) fitting accuracy	212
7.7	Jardine et al. (1991) volumetric parameters obtained from experimental data	212
7.8	Differences between GDSLAB-calculated data (external transducers) and user-calculated data (internal transducers) at the end of PART 1 in tests SP2 and SP2C	214
7.9	Differences observed between tests SP2 and SP2C due to strain rates used during testing	218
7.10	Variability in computed K_0 values during K_0-consolidation in the triaxial cell	218
	CHAPTER 8. Evaluation of soil constitutive model performance for conventional triaxial testing	
8.1	Soil parameters and initial state data for test USc7	229
8.2	Soil parameters and initial state data for test USc9	230
8.3	Soil parameters and initial state data for test USe3	232
8.4	Soil parameters and initial state data for test USe5	233
8.5	Soil parameters and initial state data for test USe6	234
8.6	Soil parameters and initial state data for test Ko5	236
8.7	Soil parameters and initial state data for test Ko6	237
	CHAPTER 9. Evaluation of soil constitutive model performance for tunnelling induced stress path testing	
9.1	Soil parameters for test SP1	276
9.2	Soil parameters for test SP2	278
9.3	Soil parameters for test SP3	281

Chapter 1: PROJECT INTRODUCTION.

DEVELOPMENT OF AIMS AND OBJECTIVES

1.1. GENERAL

Tunnelling has received increased attention in the last two decades due to major underground schemes taking place all over the world. Part of this interest has been materialised in the form of extensive research in a wide variety of tunnelling aspects. One of these aspects is the prediction of soil movements so that their effect on adjacent structures and services can be evaluated before construction. The knowledge gained allows assessing the potential risks and performing safe and cost-effective designs.

At the moment, typical approaches to movements due to tunnelling in 'soft' ground at the design stage range from well known empirical methods to the use of numerical analyses. The former are still widely used for the simplest situations because of their simplicity and as a preliminary calculation, but the accuracy of the results has been reported to be limited. As a result of this, a lot of effort has been put into the development of other techniques such as the finite element and finite differences methods, improving the numerical codes and computational power as well as developing more user-friendly versions. Numerical approaches allow the simulation of the various aspects of tunnel construction (i.e. surrounding soil, initial stresses and groundwater conditions, tunnel shape and construction sequence, type of support and ground treatments) so that the broader picture can be studied and more complex situations analysed.

In parallel to the numerical improvements, there has been much effort devoted to the development of constitutive soil models, each of them capturing specific patterns of observed experimental behaviour.

Despite the sophisticated constitutive relationships and modelling techniques available, it is obvious from the published literature that:

- The predictions at the present time are not as good as expected (e.g. the width of the surface settlement trough tend to be very often overpredicted, the settlements tend to be underestimated, 3D results are not always better than 2D results (Eisenstein, 1986; Franzius et al., 2005; Brinkgreve et al., 2006).
- Both research institutions and industry not only use the latest constitutive models but also the simplest ones as part of their analysis (Viggiani et al., 2005; Karakus and Fowell, 2005; Lee et al., 2006). The reasons for this being: (1) the theory behind the basic models is more widely understood, (2) the parameters required by the more advanced models are not easily obtained from conventional in-situ and laboratory testing, and (3) very often the level of detail given by

the authors of the more advanced constitutive models is not enough for these to be conveniently used.

The result of this is that:

- 80% of the numerical analyses published in the field of tunnelling correspond to Class-C (after-event, according to terminology by Lambe, 1973) analyses (Negro and Queiroz, 2000). These aim at providing recommendations for future predictions based on the findings from sensitivity analyses that compare the numerical results with available field data. Examples of recommendations to date include: using a reduced K_0 value close to the tunnel perimeter (Addenbrooke, 1996; Potts and Zdravkovic, 2001), and using non-linear elastic anisotropic constitutive models (Addenbrooke, 1996; Masin and Herle, 2005). Unfortunately, what works for one case does not necessarily work when applied to another situation, therefore it is still not possible to use with confidence the proposed recommendations for Class-A (before-event) analyses.
- Almost half of the studies presented only study one tunnelling aspect, commonly the surface settlements (Negro and Queiroz, 2000).
- At the moment numerical modelling is mainly used at the design stage in order to establish the ultimate limit states and observe mechanisms of behaviour.
- Significant human expertise is still required in order to compensate for the deficiencies in the numerical and/or empirical methods available.

In addition to the limitations inherent to the numerical method used (e.g. necessary simplifications of the real tunnelling problem), the constitutive models used in the analyses are partially to blame for all the issues above. In particular, a large number of them are not good at simulating the soil stress-strain response during unloading stress paths, which are very important to underground excavations.

It was consequently clear at the beginning of this project that there was a large scope for further improvement in this field and that perhaps, some of the advances that had been made to date should be reconsidered.

As Eisenstein (1986) stated, "the success of relating the stress changes to realistic displacements depends on the ability of the numerical model to incorporate the complex relationships which exist between stresses and strains in soils". It is precisely this ability that was intended to be evaluated during the present project, with particular application to tunnelling. This, which constitutes the aim of this research, has been done with particular emphasis on the models′ abilities during unloading states (i.e. extension) in addition to other most commonly investigated issues such as the effect of K_0, the effect of anisotropy (induced anisotropy in this case) and small-strain non-linearity.

Four constitutive models have been selected for this independent evaluation. These are: the Modified Cam-Clay model (Roscoe and Burland, 1968), the Jardine et al. (1991) small-strain stiffness model, the Al-Tabbaa (1987) multi-surface kinematic hardening model and the S-CLAY1 rotational hardening model (Wheeler et al., 2003). The S-CLAY1 model is relatively new and its validity has not been extensively shown to date. The Jardine et al. (1991) model has assumed significant relevance within the engineering community since the improvements in laboratory techniques allowed the observation of soil behaviour at small-strain level and highlighted the need for models that could simulate this aspect. However, there is perhaps not enough transparency in the published literature in terms of how to obtain the model parameters. The present study has intended to provide some guidance on this as well as evaluating the advantages, if any, of using this model over the others, the only one out of the four that addresses small-strain behaviour.

It should be noted that it was never intended to either propose modifications to the current formulation of these models or formulating any new numerical model. This may be done at a later stage by making use of the present results.

The originality of this thesis comes primarily from the way that stress path testing, finite element analysis (FEA) and the evaluation of constitutive modelling have been combined. Typically, in the field of tunnelling, the evaluation of the performance of constitutive models is done by comparing back-analysis calculations of tunnelling problems with real field data. Most generally, the same people/institution formulating the model compares the model predictions with measurements taken during triaxial testing. In the present study, the evaluation of the models has been carried out by comparing experimental observations on stiff Speswhite Kaolin clay specimens reconstituted from slurry subjected to both conventional triaxial testing and tunnelling-induced stress paths with the constitutive models' predictions using the soil testing software SM2D produced by Chan (see for example Zienkiewicz et al, 1999) at the University of Birmingham. One of the advantages of using SM2D is the fact that it is not affected by variables such as the geometry selected, the mesh coarseness or the boundary conditions.

The conceptual idea behind this thesis is simple: if a given constitutive model is not capable of closely reproducing the soil behaviour observed in the laboratory under these representative but simplified stress paths, it is unlikely that the model will be able to accurately reproduce the behaviour of the natural ground in more complex numerical analyses when the tunnelling construction is modelled as a whole. This may only be possible if some 'alterations' are introduced during the numerical analyses.

It was noticed, when reviewing the published literature, that there are only a limited number of publications that describe the type of stress paths expected to be found around single tunnels. None have been found with regards to twin tunnels. The results are generally presented in terms of strains and not in terms of stresses. The few publications available are normally based on simplified

idealizations, numerical analyses or, more rarely, from physical modelling. It should be noted however that if real data had been available for the project, the stress paths would have quite likely been too complicated to be reproduced in a triaxial cell.

The stress paths to be reproduced in the laboratory were therefore defined from FEA using the software PLAXIS v.8.2 and PLAXIS 3D Tunnel. The initial intention was using some previous analyses carried out with ABAQUS at the University of Birmingham by Hunt (2004). Unfortunately this option had to be abandoned soon after the start of the investigation because of the incompatibility of the files from different software versions. The constitutive models used in PLAXIS were those available as part of the software at the time (i.e. Linear Elastic, Mohr-Coulomb and Hardening). Additionally, the pre-yield small-strain Jardine et al. (1991) model plus Mohr-Coulomb for large strains was introduced as a dynamic link library prepared, and kindly supplied, by Dr. Rouainia at the University of Newcastle.

Despite this thesis being concerned with the overall poor predictions of ground deformations due to tunnelling, the present project has focused particularly on the mechanics of soil behaviour in the neighbourhood of the tunnel in order to limit the extent of the investigation. Close to the surface the strains are smaller hence properly simulating the small strain behaviour may be more critical. Close to the tunnel perimeter however, all the strain range is potentially important, from small elastic strains to plastic strains.

The stress paths selected did therefore correspond to those determined at points above the crown and to the side of the springline of single deep circular tunnels and at a point in between side-by-side twin tunnels. The author is aware that the stress paths occurring during tunnelling are very much dependent on the particular conditions of each project. It is therefore clearly stated herein that the analyses carried out have been more qualitative than quantitative and have mainly tried to capture the essential trends of stress mobilisation during tunnelling at the selected locations.

Stress path testing is rarely used to simulate tunnelling-induced stress paths. The only relevant case found is that by Barla (1999), who reproduced tunnelling induced stress paths obtained from FEA using triaxial apparatus in order to study the effect of tunnelling in swelling ground.

Despite the obvious limitations in the use of triaxial type equipment for such a purpose (i.e. the stress paths run in the laboratory should necessarily be a simplified version of the stress paths found in tunnelling projects), it was hoped for the present investigation that the stress paths selected would capture many features and hence provide an interesting insight into the behaviour of soils affected by underground excavations. In the present study, in comparison with the work by Barla (1999) who used isotropically consolidated specimens, all the specimens subjected to tunnelling stress paths were initially K_0-consolidated. This was believed to be more representative of the general stress states commonly encountered in nature, which are very rarely isotropic.

In the present research a lot of effort has been devoted to the experimental part, aiming at the production of high quality results using state-of-the-art equipment. The reproduction of the selected stress paths in the laboratory was initially intended to be performed using a large stress path cell (capable of performing tests on 200 mm diameter x 400 mm long specimens) that had been donated to the Civil Engineering Department in Birmingham by Advantica (British Gas Research Centre) some years before the present project started. Most of the time at the beginning of the project was spent on putting this equipment together because of its very poor initial general state. However, after approximately three months, the system proved to be in a too bad condition to be repaired in a sensible period of time. This caused a change in direction and as a result conventional triaxial cells and a GDS-Wykeham Farrance computer-controlled Standard Stress Path equipment were used instead.

Apart from obtaining relevant stress paths with PLAXIS and reproducing them in the laboratory, other objectives were set up in order to successfully achieve the aim of this research. The first was bringing the GDS-Wykeham Farrance Standard Stress Path system available in the soils laboratory to the necessary state-of-the-art before undertaking the scheduled tests. A considerable amount of time was required for this. Also, and despite not being the original intention, there was a considerable amount of time invested in studying the properties of the reconstituted samples after a few observations were made into the limitations of the consolidation apparatus. The author considered this to be important for (1) proper planning of the laboratory experiments, (2) allowing a proper interpretation of the findings made during the present investigation, and (3) increasing the knowledge in this sense for future research. Finally, the critical state parameters for the particular Speswhite Kaolin clay being used were established since some of them had not been previously investigated at the University of Birmingham (e.g. soil strength under extension).

1.2. AIMS AND OBJECTIVES OF THE RESEARCH

Four different main areas of investigation will be found in this thesis: tunnelling, finite element analysis, advanced laboratory testing and evaluation of constitutive soil models, with the main aim and objectives being as follows:

Aim:

This research aims to provide an independent evaluation of the performance of four selected soil constitutive models in reproducing the intrinsic behaviour of a stiff clay during conventional triaxial testing and, more particularly, when subjected to simplified tunnelling-induced stress paths. This should help in making a more informed selection of models when carrying out a tunnel analysis.

Objectives:

1. Obtaining general stress paths at specific points around single and twin tunnels based on a series of finite element analyses carried out using PLAXIS and also on the review of previous published work.
2. Performing an in-depth study into the issues involved in the preparation of reconstituted samples made from slurry.
3. Bringing the Standard Stress Path system available in the soils laboratory closer to the current state-of-the-art with the final objective of being able to perform some tests and measurements that had never been undertaken before at the University of Birmingham (e.g. extension tests and the use of on-sample instrumentation).
4. Finding critical state parameters for the Speswhite Kaolin clay used for this research by running a series of 'conventional' triaxial tests.
5. Identifying the limitations in reproducing the stress paths encountered in Objective 1 in triaxial-type cells, defining suitable stress paths that are representative of some of the main stress changes during tunnelling, and reproducing these in the Stress Path cell.
6. Simulating some of the conventional (Objective 4) and the tunnelling stress path tests (Objective 5) in SM2D using the four selected constitutive models.

The time devoted to each of these objectives was affected considerably by the limited facilities and reduced experience in the soils laboratory with regard to this particular application and also by the general poor state of the laboratory due to relocation taking place a short time before the beginning of this project. Due to the latter, the laboratory required a general refurbishment that took more than six months. The main improvement achieved during this time with application to the present study was the installation of a temperature control system in the room where the stress path tests were undertaken. A lot of time had to be invested in order to make the equipment fully operational. The author got actively involved in the various repositioning of equipment in the laboratory, reconnection of supplies (e.g. water, compressed air), dealing with suppliers and purchasing of new parts in order to bring the stress path cell as close to the state-of-the-art as possible within the budget available.

Due to the various events stated, the available time was shorter than initially planned for the reproduction of the tunnelling induced stress paths in the laboratory and for the evaluation of the selected soil constitutive models. Care was taken, however, to ensure that the minimum number of tests required to obtain representative information from which to evaluate the performance of the different constitutive models were conducted. On the other hand, the author believes that the improvements made in the laboratory and the detailed study of the characteristics of the one-dimensionally consolidated samples from slurry were worth the effort. The first because the upgrade of the equipment and knowledge gained will give future researchers in the Department better

conditions to start their own work; the second because it will help future researchers be more aware of the issues likely to occur during the preparation of reconstituted samples so that they can make more informed decisions.

The author has been very thorough and open in expressing not only the successes, but also the limitations observed and the problems experienced during the present investigation because these often tend not to be included in the published literature thus reducing the chances of continuous improvement.

Some of the findings made during this research regarding the characteristics of reconstituted samples have been previously published (Valls-Marquez et al., 2008).

1.3. THESIS LAYOUT

This thesis has been divided into ten chapters organized as follows:

Chapter 2: A detailed description of the methodology followed for each of the parts into which the project has been divided.

Chapter 3: A review of the previous published literature in the field.

Chapter 4: An identification of the stress paths induced during excavation and tunnel support placement at various points around single and twin tunnels using PLAXIS.

Chapter 5: A study into the characteristics of the reconstituted Speswhite Kaolin clay samples.

Chapter 6: A presentation of the results obtained from conventional triaxial testing for the identification of the critical state parameters for Speswhite Kaolin clay.

Chapter 7: A study of the Speswhite Kaolin clay behaviour in the laboratory when subjected to a series of simplified stress paths defined based on the results obtained in Chapter 4 along with the determination of small-strain parameters.

Chapter 8: An evaluation of the performance of the selected constitutive soil models in reproducing the observed soil behaviour during conventional triaxial testing.

Chapter 9: An evaluation of the performance of the selected constitutive soil models in reproducing the observed soil behaviour during tunnelling induced stress path testing.

Chapter 10: Conclusions and suggestions for future research.

It should be noted that because of the layout of the present investigation, in which each chapter depends of the outcome from the previous chapters, individual discussions have been presented at the end of each chapter from Chapter 4 onwards.

Chapter 2: LITERATURE REVIEW

2.1. INTRODUCTION

The information presented in this chapter is part of a review into the previous, as well as contemporary, literature in the fields that form the basis for the present investigation. Throughout this chapter the author wants to guide the reader through some of the main findings up to date as well as issues/limitations identified that motivated this research as briefly introduced in Chapter 1.

This chapter is divided in two parts as follows:

PART I: Understanding and modelling tunnel excavations

PART II: Triaxial and stress path testing

Part I provides the background and guidance for pursuing Objective 1 and ultimately the aim of the research, both specified in Chapter 1. Part II has the same purpose but with respect to Objectives 2 to 5.

2.2. PART I: UNDERSTANDING AND MODELLING TUNNEL EXCAVATIONS

Section 2.2.1 presents the finite element method as one of the available approaches for studying tunnelling problems by associating specific constitutive models to the in-situ ground. A large number of constitutive models exist nowadays for soils and rocks. There are various schools of thought, each of them focusing on specific aspects of soil behaviour. Some of the up to date trends in modelling clay behaviour are briefly presented in Section 2.2.2 followed by a comprehensive presentation of the constitutive models that will be evaluated during the present research. Section 2.2.3 presents some of the findings up to date in terms of stress paths followed by soil elements in close proximity to tunnel openings.

2.2.1. Finite Element Analysis (FEA)

The engineering processes involved in the planning, design and construction of a tunnel are improving but simultaneously becoming more challenging as the urban space for tunnel construction reduces and the technical improvements encourage engineers to attempt more complex and sophisticated designs. If something goes wrong during execution, the effects can be devastating, especially in highly populated areas. Even when construction is conducted to very high standards it is never a completely risk-free activity. New and O'Reilly (1991), Lake et al. (1992), Bracegirdle and Mair (1996), Mair and Taylor (1997) and many others have studied the effects of tunnelling on surface structures and worked towards producing risk classifications. The main reason why tunnels are very complex constructions technically is the fact that they are completely assembled in a very uncertain

medium: the natural ground, whose properties can vary at all scales. This means that any initial prediction into the soil-support behaviour based on preliminary site investigations will inevitably be only approximate (Clough and Leca, 1989).

Engineers started using FEA for rock tunnelling problems in the early 1970s, but the application of these to soil tunnelling is more recent (Ghaboussi et al., 1979). There are two approaches regarding the geometry of the problem as described by Taylor (1998) (Figure 2.1). The two-dimensional approach is commonly used when the tunnel excavation has passed the measurement section hence a plane strain model can be used as an approximate representation of the problem. In this case the movement vectors would approximately develop in the plane perpendicular to the tunnel axis. Three-dimensional analyses are generally used when considering the face stability during excavation and when modelling in detail the construction process. The vector movements in this case would develop above and towards the tunnel heading.

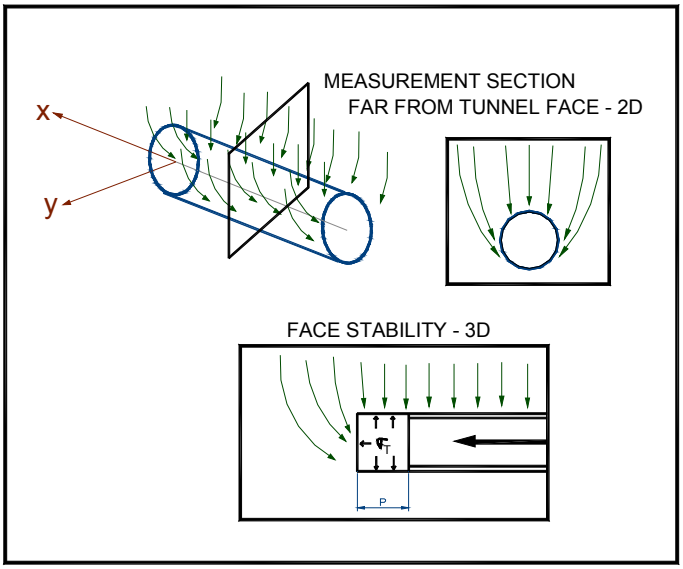

Figure 2.1. Two-dimensional and three-dimensional movement idealisation around tunnelling operations (after Mair and Taylor, 1997). σ_t is the pressure applied at the tunnel heading and P is the unsupported tunnel length

Since the 1970s, most of the FEA have been carried out in two dimensions (2D), which according to some authors (Mair and Taylor, 1997) leads to a poor prediction of the movements when compared to field observations, and tend to assume one unique homogeneous and isotropic stratum (Cooper, 2001). Many authors have stated that since a cylindrical body (or any other shape used) is being bored into the ground, the approach should be three-dimensional if the modelling is to be accurate (Attewell et al., 1986; Clough and Leca, 1989; New and O'Reilly, 1991; Taylor, 1998). Clough and Leca (1989)

identified many reasons that at that time they believed were impeding the fast development of the finite element methods:

- Full three-dimensional FEA was difficult to justify despite increased computer power and cost reductions.
- Multiple analyses would often be required due to variations in alignment and geological variability.
- Typical ground investigations would produce a scarce data base.
- None of the available constitutive soil models at that time was able to simulate all aspects of soil behaviour important to tunnelling.
- Many of the parameters influencing the analysis were difficult to determine.

At the present time, three-dimensional analyses are more routinely used in industry than previously, but continue being mainly a research tool. The predictions obtained from 3D analyses however have been found not to be essentially better than those from two-dimensional modelling (Negro and Queiroz, 2000, Franzius et al., 2005) or better than empirical solutions (Selby, 1988; Rankin, 1988). Excluding the ´natural´ uncertainty described above inherent to the soil and the restricted amount of ground investigation, which will be always the case, recent publications seem to indicate that the success achieved during Class-A predictions by improving the numerical codes and computational power is still limited. The capacity for predicting the soil behaviour during tunnelling is not satisfactory hence the need for human expertise in order to compensate for such deficiencies.

By reviewing more than 60 case histories from 1980 to 2000, Negro and Queiroz (2000) stated that no correlation was possible between the quality of the predictions and the features of the numerical code, constitutive relationships, soil type, construction method or type of study (i.e. before, during or after event).

2.2.2. Constitutive Soil Models

In the past four decades, a lot of effort has been devoted to the development of constitutive soil models based on experimental observations on soil behaviour. However, the previous observations seem to indicate that the constitutive models used in FEA, even the most sophisticated, are at least partially to blame for the inaccurate predictions of soil behaviour during tunnelling. Comparing predictions with in-situ measurements, commonly surface settlement profiles, it is frequently reported (Eisenstein, 1986; Addenbrooke, 1996; Potts and Zdravkovic, 2001; Lee and Ng, 2002; Masin and Herle, 2005; Brinkgreve et al., 2006) that:

- There is a tendency to predict wider and shallower settlements than the real ones.
- Anisotropy, non-linear stiffness at small strains and different stiffness at least for loading and unloading paths are required to achieve relatively realistic predictions.

- Very simple models with long elastic ranges and constant stiffness tend to predict heave of the soil for K_0 conditions above unity, but this also occurs sometimes when using more sophisticated models (e.g. Stallebrass and Taylor, 1997) as reported by Masin and Herle, 2005).

In addition to the classic stress-strain models (Mohr-Coulomb and Drucker-Prager for effective stresses and Tresca and Von Mises for total stresses), which are still widely used due to their simplicity (Viggiani et al., 2005; Karakus and Fowell, 2005; Lee et al., 2006), a large number of constitutive models are available nowadays for the study of clay behaviour. Some of these are based on the Cam-Clay models developed at Cambridge University after the formulation of the Critical State Soil Mechanics framework. Each subsequent model has been formulated with the aim of either correcting mistakes identified in previous versions or in order to account for a limited amount of additional observed patterns in soil behaviour. As previously stated, the complexity of the models seems to have increased with time, but the predictions are not necessarily much better. Figure 2.2 shows in a simplified way some of the trends in the evolution of constitutive models for clays up to date, which include those that triggered the formulation of the models that will be evaluated during the present research. It should be noted that Figure 2.2 was never intended to be an exhaustive list of all the existing types of models. The classical models before the critical state framework was published will not be reviewed herein. This is primarily because these models will be only used in the present study for preliminary assessments and the complete formulation and details of them are easily accessible in numerous publications (e.g. Potts and Zdravkovic, 1999 and engineering text books). There are various models that belong to each of the different categories specified in Figure 2.2. Essentially, only the models that will be evaluated during the present investigation have been reviewed in depth and are presented in this chapter. Further details and the reasons for this particular selection are given in Section 3.7.1.

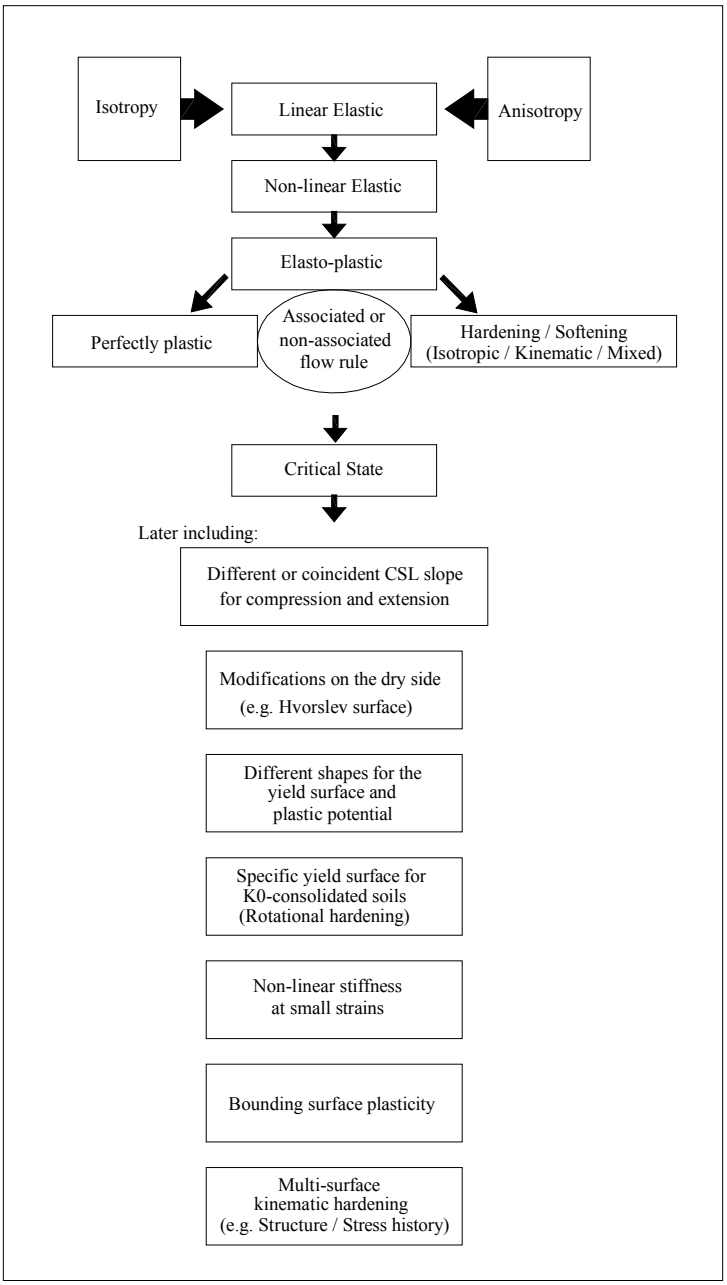

Figure 2.2. Some trends in the evolution of constitutive models for clays

2.2.2.1. Original Cam-Clay

The Original Cam-Clay model was the first critical state model to be formulated based on triaxial tests results. This associated isotropic elasto-plastic model was developed by Roscoe and Schofield (1963) and has been the basis for many other more advanced models. This model was intended to amalgamate most of the features identified for normally consolidated and lightly overconsolidated

clays within the critical state framework. The yielding surfaces are asymmetrical elliptic in shape as that illustrated in Figure 2.3. Equation 2.1 describes the shape of the yielding curves and the associated flow rule is defined by Equation 2.2.

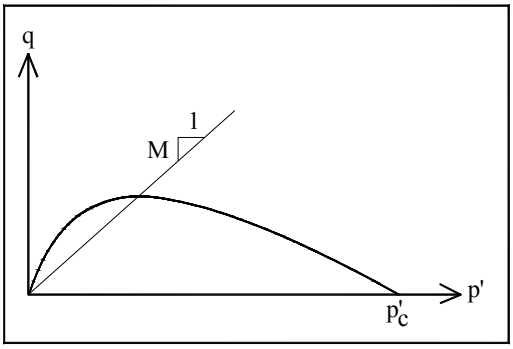

Figure 2.3. Original Cam-Clay yielding surface

M corresponds to the slope (or stress ratio) of the critical state line projected on the q - p' space and p_c' represents the pre-consolidation pressure.

$$q'+M \cdot p' \cdot \ln\left(\frac{p'}{p_c'}\right)=0 \qquad \text{[Eq.2.1]}$$

$$\frac{d\varepsilon_v^p}{d\varepsilon_s^p}=M-\frac{q'}{p'} \qquad \text{[Eq.2.2]}$$

The Original Cam-Clay assumes isotropic strain hardening for normally consolidated and lightly overconsolidated clays, with the size of the yielding surface being controlled by p_c' and only related to changes in volume according to the hardening rule in Equation 2.3 **(**i.e. isotropic volumetric hardening). On the dry side, the model assumes isotropic strain softening giving rise to predictions for heavily overconsolidated clays that are not very accurate. Dilatancy is also linked to the plastic volumetric strain, which induces compressive ($\Delta\varepsilon_v^p > 0$) and dilatant ($\Delta\varepsilon_v^p < 0$) behaviour in the wet and dry sides of the critical state respectively.

$$d\varepsilon_v^p=\frac{\lambda-\kappa}{v}\cdot\frac{dp_c'}{p_c'} \qquad \text{[Eq.2.3]}$$

The behaviour within the yield surface is isotropic elastic as defined by Equation 2.4 therefore assumes that the bulk and shear components are explicitly decoupled.

$$\begin{bmatrix} \delta\varepsilon_v^e \\ \delta\varepsilon_s^e \end{bmatrix} = \begin{bmatrix} \frac{1}{K'} & 0 \\ 0 & \frac{1}{3G'} \end{bmatrix} \cdot \begin{bmatrix} \delta p' \\ \delta q \end{bmatrix} \qquad \text{[Eq.2.4]}$$

The elastic behaviour is also stated to be non-linear in this model. This refers to the fact that K varies with p'. For the volumetric response, using the idealised v - lnp' relationship for volumetric change in clay, the following relationship can be derived:

$$d\varepsilon_v^e = \frac{\kappa}{vp'} dp' \qquad \text{[Eq.2.5]}$$

therefore:

$$K' = \frac{vp'}{\kappa} \qquad \text{[Eq.2.6]}$$

The original formulation of the Cam-Clay models did not give specifications for the shear response (i.e. G was infinite). Subsequently, different proposals have been used in order to avoid numerical problems and to better reproduce the observed soil behaviour. Commonly, these consist of one of the following two options:

Option 1: The Poisson ratio is considered to be constant and therefore G varies with p' according to Equation 2.7 using the ratio of G / K.

$$G = \frac{vp'}{\kappa} \cdot \frac{3}{2} \cdot \frac{(1-2\upsilon)}{(1+\upsilon)} \qquad \text{[Eq.2.7]}$$

It should be noted that according to this, G is implicitly dependent on p' therefore decoupling between bulk and shear behaviour does not strictly apply.

Option 2: G is considered to be constant therefore the Poisson ratio depends on p' (since $K=K(p')$) according to Equation 2.8.

$$\upsilon = \frac{3K - 2G}{6K + 2G} \qquad \text{[Eq.2.8]}$$

These two options have been found to have some limitations. Option 1 has been found not to be energy conservative for some elastic paths (Zytinski et al., 1978) and Option 2 does not agree with experimental observations (e.g. non-linearity in the small-strain range) and may give rise to negative Poisson ratios. The only alternative to this seems to be abandoning the idea of pure elastic behaviour for soil (Stallebrass, 1990). The elastic behaviour described above implies that:

- During undrained shearing the volume does not change (i.e. water and soil particles incompressible) therefore $K_u = \infty$, $\nu_u = 0.5$ and G can be constant or dependent on p'. If the latter, then G will also be constant since for an undrained path p' is constant.

- During drained shearing p' varies hence K is not constant. G can be again defined as being constant or dependent on p'.
- $G_u = G'$ since the shear modulus is independent of the volumetric change hence drainage conditions.

The Original Cam-Clay model therefore requires the following 5 parameters: λ, κ, M, υ and N. Additional specifications need to be given with regard to the preconsolidation pressure p_c' and the current soil state (e.g. current void ratio).

The Original Cam-Clay has been found to have some problems in its application. Some of these problems can be briefly described as follows:

- The model singularity at the isotropic compression state (p_c' point in Figure 2.3), which introduces numerical and theoretical difficulties (e.g. isotropic stress changes inducing shear strains under associated plasticity).
- The use of a unique M for compression and extension when experimental observations have shown this to be smaller for extension states (refer to Section 2.3.7).
- The overestimation of the soil strength for stress states on the dry side of the critical.
- The prediction of stress paths different than the experimental during K_0-consolidation when controlling the zero lateral strain condition due to the shape of the yield surface. Only the isotropic consolidation case can be properly reproduced.

2.2.2.2. Modified Cam-Clay

The Modified Cam-Clay was developed by Roscoe and Burland (1968). This model has mainly the same features than the Original Cam-Clay, but the shape of the yield surface is different. In the Modified Cam-Clay the yielding surfaces are elliptical in shape, as illustrated in Figure 2.4, therefore although most of the limitations previously stated for the original Cam-Clay model are still deficiencies in this modified version, the singularity at the isotropic compression state was eliminated. The equation for the Modified Cam-Clay yielding curves are of the type:

$$\frac{q'^2}{p'^2} + M^2 \cdot \left(1 - \frac{p_c'}{p'}\right) = 0 \qquad \text{[Eq.2.9]}$$

The flow rule is defined by Equation 2.10.

$$\frac{d\varepsilon_v^p}{d\varepsilon_s^p} = \frac{M^2 - \upsilon^2}{2\upsilon} \qquad \text{[Eq.2.10]}$$

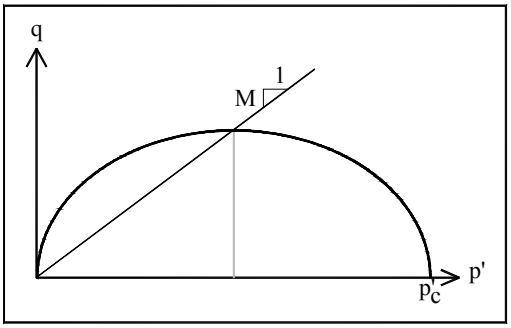

Figure 2.4. Modified Cam-Clay yielding surface

2.2.2.3. S-CLAY1

Various modifications to the classic critical state models have been published. One particular case are the constitutive models that consider, based on recent experimental observations, a yield surface rotated towards the K_0-line (or any other stress ratio q/p' (η) being followed during consolidation) (Figure 2.5). One recent model belonging to this group is the S-CLAY1 model proposed by Wheeler et al. (2003) at the University of Glasgow, which was validated against a series of drained triaxial stress paths on normally and lightly overconsolidated soft Otaniemi clay from Finland.

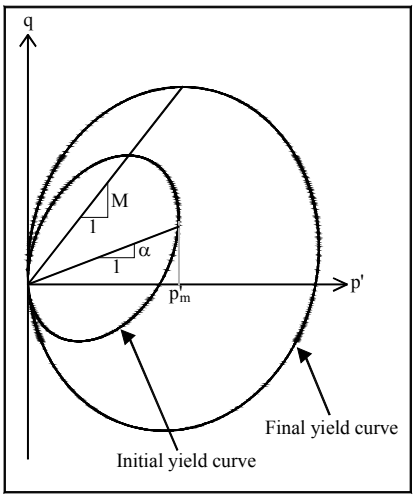

Figure 2.5. Yielding envelope for the S-CLAY1 model (Wheeler et al., 2003)

The soil behaviour inside the yield surface is equal to that in the Cam-Clay models, with G varying with p'. In this model, an initial yield surface with an associated flow rule and potentially created by the cross-anisotropy developed during deposition (inherent anisotropy), will rotate and expand due to additional straining according to two different hardening laws (induced anisotropy). The first describes the change in size and is only related to plastic volumetric strains. The second, known as rotational

hardening, describes the change in inclination of the yield surface and depends on both shear and volumetric plastic strains. The S-CLAY1 model is presented by its authors as an anisotropic model, but the concept refers solely to the anisotropy of plastic behaviour created due to further straining. Since the model deals with further development or erasure of anisotropy, it assumes isotropic elasticity inside the yield surface, rather than elastic anisotropy for simplicity. The S-CLAY1 model requires 6 parameters: κ, υ, λ, M, μ (absolute effectiveness of rotational hardening), β (relative effectiveness of rotational hardening). Additionally, the model requires the initial state of the soil described by: *OCR* (overconsolidation ratio) or *POP* (pre-overburden pressure defined as the difference between the vertical preconsolidation pressure and the in-situ vertical effective stress), e_0 (initial void ratio) and α (initial inclination of the yield surface, being a measure of the degree of plastic anisotropy in the soil). From the *OCR* value (or *POP*) the model calculates p'_m, which defines the size of the initial yield surface. The rotational hardening law includes η and $\chi_v(\eta)$ and $\chi_s(\eta)$ which are the target values towards which the plastic volumetric and shear strains tend to drag the value of α during straining. The determination of the initial α, β and μ corresponding to K_0-consolidation can be estimated using the following relationships:

$$\alpha = \frac{\eta^2 + 3\eta - M^2}{3} \qquad \text{[Eq.2.11]}$$

with the stress ratio η calculated as: $$\eta = \frac{q}{p'} = \frac{3\cdot(1-K_0)}{1+2K_0} \qquad \text{[Eq.2.12]}$$

$$\beta = \frac{3\cdot\left(4M^2 - 4\eta^2 - 3\eta\right)}{8\cdot\left(\eta^2 - M^2 + 2\eta\right)} \qquad \text{[Eq.2.13]}$$

$$\frac{10}{\lambda} \le \mu \le \frac{15}{\lambda} \qquad \text{[Eq.2.14]}$$

The S-CLAY1 was stated to be mostly suitable for problems not involving unloading where large plastic strains dominate therefore would not be particularly suited for tunnelling problems. However, two aspects made this model of particular interest for the present project: (1) The fact that it tackles specifically the effects of consolidation other than isotropic (e.g. K_0-consolidation) on soil response and (2) The fact that the performance of the model during subsequent undrained stress paths has not been demonstrated so far. The present project can therefore help evaluating the importance of incorporating this new type of yield surface.

2.2.2.4. Small-strain stiffness

The Jardine et al. (1986) and Jardine et al. (1991) models belong to this category. These models are non-linear elastic pre-yield models. The Jardine et al. (1986) model was, as described by Potts and

Zdravkovic (1999), one of the earliest models specifically developed to deal with the concept of non-linear small-strain behaviour of soils that has been relatively recently discovered thanks to the improvements in laboratory instrumentation. The theory behind these models assumes four phases of behaviour being exhibited along a certain single stress path that moves towards failure. These different phases occur within zones defined by surfaces as schematically illustrated in Figure 2.6.

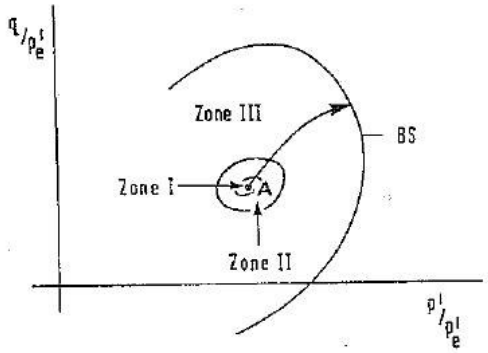

Figure 2.6. Phases of soil behaviour according to Jardine et al. (1991)

The first phase of behaviour, in Zone I, conventionally occurring within a very small zone, would be truly linear elastic. Phase two, in Zone II, would be non-linear with the stiffness being dependent on stress history. Phase three, in Zone III, would be plastic therefore involving the development of irrecoverable strains. Both phases two and three would exhibit a significant and rapid loss of stiffness, therefore this 4-phase concept assumes both elastic and inelastic non-linearity. Finally, phase four would correspond to that when the soil reaches the bounding surface. At this point dilation or contraction would occur and the stiffness would be greatly reduced. The surfaces that limit the extent of the linear and the non-linear elastic regions are considered to be kinematic moving towards the outer yield surface. These concepts fit into the framework of LER (Linear Elastic Region) where the soil behaviour is linear elastic / SSR (Small Strain Region) where the stress-strain behaviour is non-linear, very stiff and fully recoverable and kinematic regions developed by Jardine (1985) and Skinner (1975) respectively.

The small-strain models focus on phase two and give mathematical relationships that describe the variation of soil stiffness in this particular zone. When used for numerical analysis, constant stiffness (i.e. linear elastic behaviour) is considered for strains below Zone II. For strains beyond Zone II a convenient yield criterion (conventionally a classical elasto-plastic model such as Mohr-Coulomb) must be specified.

Jardine et al. (1986) proposed a simple mathematical expression to describe the shape of the undrained secant Young modulus ($E_{u\ sec}$) - axial strain (ε_a) relationship empirically observed during

undrained triaxial tests. The expression, given by Equation 2.15, corresponds to that of a period logarithmic function.

$$\frac{E_{u\sec}}{c_u} = A_{ss} + B_{ss} \cdot \cos\left[\alpha\left(\log\frac{\varepsilon_a}{C_{ss}}\right)^{\gamma}\right] \qquad \text{[Eq.2.15]}$$

The authors gave some indications on how to obtain the non-linear parameters from laboratory data. It basically consists of obtaining A_{ss}, B_{ss} and C_{ss} graphically (Figure 2.7) and calculating α and γ using Equations 2.16 and 2.17 respectively.

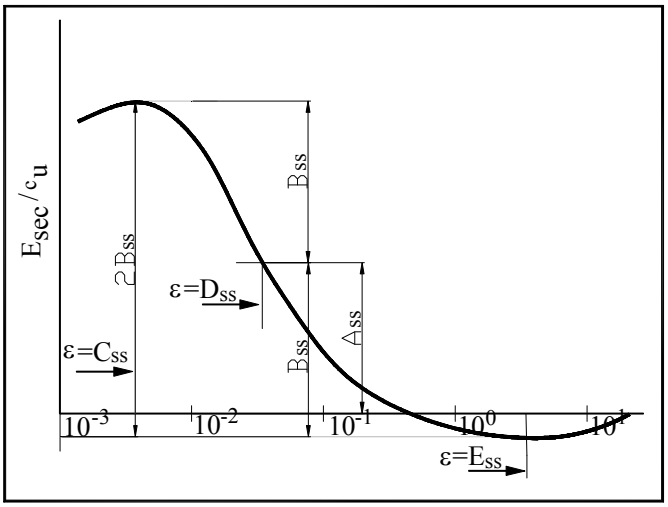

Figure 2.7. Curve fitting to strain-stiffness data (after Jardine et al. 1986)

$$\alpha = \frac{\frac{\pi}{2}}{\left[\log\left(\frac{D_{ss}}{C_{ss}}\right)\right]^{\gamma}} \qquad \text{[Eq.2.16]}$$

$$\gamma = \frac{\log 2}{\log\cdot\left[\frac{\log\left(\frac{E_{ss}}{C_{ss}}\right)}{\log\left(\frac{D_{ss}}{C_{ss}}\right)}\right]} \qquad \text{[Eq.2.17]}$$

As previously stated, Equation 2.15 is only valid over a range of axial strain between ε_{min} and ε_{max}. Equation 2.15 can be rewritten in terms of the tangent modulus instead of the secant modulus by differentiation as given by Equation 2.18.

$$\frac{E_t}{c_u} = A_{ss} + B_{ss} \cdot \cos\left(\alpha \cdot \left(\log\left(\frac{\varepsilon_a}{C_{ss}}\right)^{\gamma}\right)\right) - \frac{B_{ss}\alpha\gamma \cdot \log\left(\frac{\varepsilon_a}{C_{ss}}\right)^{\gamma-1}}{2.303} \cdot \sin\left(\alpha \cdot \log\left(\frac{\varepsilon_a}{C_{ss}}\right)^{\gamma}\right) \qquad \text{[Eq.2.18]}$$

Some time later, Jardine et al. (1991) extended the model in order to account for the non-linearity of both the shear and the volumetric soil response. Equations 2.19 and 2.20 were proposed for the variation of the shear and bulk moduli respectively, where *C1, C2, C3, C4, C5, C6,* α, γ, δ and η are material constants and ε_s and ε_v are given by Equations 2.21 and 2.22 respectively for triaxial states. The $\varepsilon_{s,min}$, $\varepsilon_{s\ max}$, $\varepsilon_{v,min}$ and $\varepsilon_{v,max}$ limits are also selected so that outside this range the moduli vary only with p' and not with strain. Experimental evidence has not been given for Equation 2.20.

$$\frac{3G_{\sec}}{p'} = C1 + C2 \cdot \cos\left[\alpha \cdot \left(\log\cdot\left(\frac{\varepsilon_s}{\sqrt{3} \cdot C3}\right)\right)^{\gamma}\right] \qquad \text{[Eq.2.19]}$$

$$\frac{K_{\sec}}{p'} = C4 + C5 \cdot \cos\left[\delta \cdot \left(\log\cdot\left(\frac{|\varepsilon_v|}{C6}\right)\right)^{\eta}\right] \qquad \text{[Eq.2.20]}$$

$$\varepsilon_s = \frac{2}{3} \cdot (\varepsilon_1 - \varepsilon_3) = \varepsilon_1 - \frac{\varepsilon_v}{3} \qquad \text{[Eq.2.21]}$$

$$\varepsilon_v = (\varepsilon_1 + 2 \cdot \varepsilon_3) \qquad \text{[Eq.2.22]}$$

Equation 2.19 can also be written as in Equation 2.24 accounting for the relationship in Equation 2.23:

$$\varepsilon_s = \sqrt{3} \cdot \varepsilon_a \qquad \text{(valid for triaxial undrained tests)} \qquad \text{[Eq.2.23]}$$

$$\frac{3G_{\sec}}{p'} = C1 + C2 \cdot \cos\left[\alpha\left(\log\cdot\left(\frac{\varepsilon_a}{C3}\right)\right)^{\gamma}\right] \qquad \text{[Eq.2.24]}$$

Equations 2.19 and 2.20 can be differentiated to obtain the following tangential expressions.

$$\frac{3G_t}{p'} = C1 + \left[C2 \cdot \cos\left(\alpha \cdot \left(\log\left(\frac{\varepsilon_d}{\sqrt{3} \cdot C3}\right)\right)^{\gamma}\right)\right] - \left[C2 \cdot \frac{1}{\ln(10)} \cdot \alpha \cdot \gamma \cdot \left(\log\left(\frac{\varepsilon_d}{\sqrt{3} \cdot C3}\right)\right)^{\gamma-1} \cdot \sin\left(\alpha \cdot \left(\log\left(\frac{\varepsilon_d}{\sqrt{3} \cdot C3}\right)\right)^{\gamma}\right)\right]$$

[Eq.2.25]

$$\frac{K_t}{p'} = C4 + \left[C5 \cdot \cos\left(\delta \cdot \left(\log\left(\frac{|\varepsilon_v|}{C6}\right)\right)^{\eta}\right)\right] - \left[C5 \cdot \frac{1}{\ln(10)} \cdot \delta \cdot \eta \cdot \left(\log\left(\frac{|\varepsilon_v|}{C6}\right)\right)^{\eta-1} \cdot \sin\left(\delta \cdot \left(\log\left(\frac{|\varepsilon_v|}{C6}\right)\right)^{\eta}\right)\right]$$

[Eq.2.26]

2.2.2.5. Multi-surface kinematic hardening

There are a variety of multi-surface kinematic hardening models, also known as 'bubble' models. Some of them use the critical state formulation as the basic framework. The proposed modifications intend to improve the limitations observed in the bounding surface plasticity concept (Dafalias, 1975), mainly with respect to the likely elasto-plastic behaviour of the soil during unloading. The model proposed by Al-Tabbaa (1987), which was intended to account for some aspects of soil behaviour that were inadequately described by other models (e.g. hysteretic non-linear behaviour with accumulation of permanent strains during closed stress cycles, and a failure envelope for overconsolidated soils), is the simplest within this category. It was formulated based on results from tests on Speswhite Kaolin clay. This model involves an outer Modified Cam-Clay bounding surface (not considered a conventional yield because elasto-plastic behaviour can occur inside) and a single inner yield surface (bubble) with associated plasticity of the same shape that the bounding surface (Figure 2.8). In the Al-Tabbaa model the yield surface can expand or contract and translate (mixed hardening) within the bounding surface maintaining the ratio of the size of the yield surface to that of the bounding surface. The bounding surface can also expand or contract but not translate (isotropic hardening).

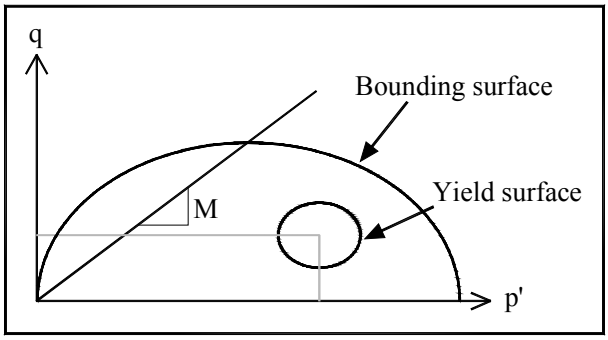

Figure 2.8. Al-Tabbaa (1987) multi-surface kinematic envelopes

Both surfaces require a plastic potential and a hardening rule. To establish the movement of the inner bubble within the bounding surface, a translation rule and mapping functions are also required. Within the kinematic bubble, the model considers non-linear isotropic elasticity in the sense that the bulk modulus is described as in Equation 2.27, where κ^* is the slope of the unloading-reloading lines on the lnv - lnp' plane (instead of using the v - lnp' plane as in the Cam-Clay models). The shear modulus is also considered to vary with p' (i.e. υ is constant). The model does not have a specific empirical expression for the observed small-strain curves as the Jardine´s models.

$$K = \frac{p'}{\kappa^*} \qquad \text{[Eq.2.27]}$$

Outside the inner bubble and within the bounding surface progressive plastic deformations occur resulting in a non-linear stress-strain behaviour during both loading and unloading. The model uses therefore non-linear plasticity to describe the pre-yield behaviour in comparison to the non-linear elasticity used by the Jardine models. The kinematic hardening model requires 6 soil constants: λ^* (slope of the ICL in the *lnv* - *lnp'* plane), κ^*, *M*, *RVALU* (ratio of the size of the yield surface to that of the bounding surface), *XIVAL* (exponent in the hardening function) and υ plus one additional parameter that defines the initial stress conditions of the soil and fixes the model in the *lnv* - *lnp'* space (e.g. *N*). As for the Cam-Clay models, *M* is considered to be the same for extension and compression, but this model theoretically improves the prediction of the overconsolidated response due to the definition of the hardening rule.

This model has been more recently extended by other authors. Examples of this are Stallebrass and Taylor (1997) and Rouainia and Wood (2000) who included the effect of recent stress history and the effects of structure in natural soils respectively.

The complete formulation for the model can be found in Al-Tabbaa (1987). Further guidance can be found in Grammatikopoulou (2004) (e.g. implementation in FEA and extensions from triaxial to general stress space).

2.2.2.6. Recent application

Although there is a trend towards using more sophisticated constitutive models, the more `basic´ Original and Modified Cam-Clay critical sate models are still used for the study of all sorts of geotechnical problems. One example of this for tunnels is Mair et al. (1992).

Linear elasticity and the elastic-plastic Mohr-Coulomb are also widely used nowadays for geotechnical problems including tunnel excavations (e.g. Urciuoli et al., 1996; Viggiani et al., 2005; Karakus and Fowell, 2005; Lee et al., 2006).

The Jardine et al. (1986) and Jardine et al. (1991) models have been extensively used for tunnelling problems. Examples of this are Addenbrooke et al. (1997), Potts and Zdravkovic (1999), Hassal and Rouainia (2004) and Hunt (2004). In those cases where the predictions of the small-strain models are compared to those from more conventional models, the authors normally report on significant improvements (e.g. the surface settlement trough deepens). However, from the present author's point of view, these are still far from the in-situ measurements (e.g. Figure 2.9).

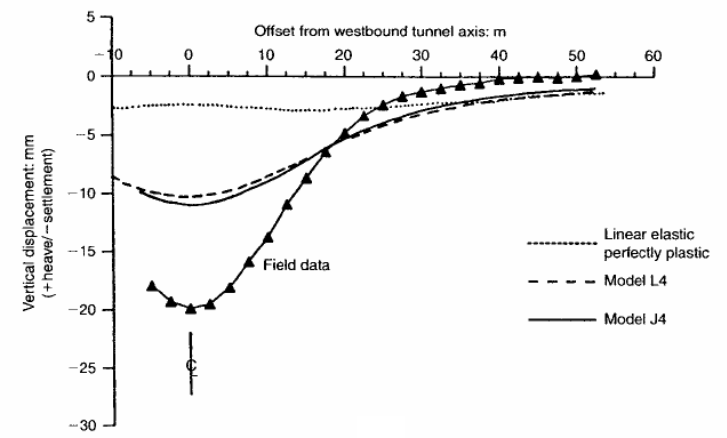

Figure 2.9. Effect of non-linear stiffness at small strains on the predicted surface settlement trough (Addenbrooke et al., 1997). J4 refers to the Jardine et al. (1991) model.

In the Jardine et al. (1986) paper the authors run a series of analyses in order to illustrate the capacity of the model in comparison to that of linear elasticity for various boundary value problems. The authors highlighted the limitations of the elastic approach (which are well known) and the advantages of their model. However, this study did not compare the models' simulations with real data so the quality of the predictions was not truly validated. Jardine et al. (1991) presented their model and showed the accuracy of this in predicting ground movements for six major projects. The authors provide a plot that shows how far the predictions and measurements were from the prediction = measurement line. Each project is represented by one unique point and details on how the predictions were made are not given. The information given by this chart can be therefore used as an indication but little more than this. The predictions were reasonable, but not exceptionally good. The authors report on non-linear small-strain analyses having been run for all sorts of engineering problems and all sorts of geologies from weak rock to very soft clays (half in the London Clay). Franzius et al. (2005) used the Jardine et al. (1991) model (although the authors refer to this as being the Jardine et al., 1986) to simulate the response of London Clay during tunnel construction. The prediction of settlements was quite poor and this could not be significantly improved by adding a realistic degree of anisotropy and/or using 3D FEA instead of 2D. This was particularly true for high K_0 values (e.g. 1.5).

Most of the studies into the application of the kinematic hardening models for tunnelling and other geotechnical problems have been focused not on the Al-Tabbaa model but on models that are an extension of this (e.g. Masin and Herle, 2005; Rouainia et al., 2005). Grammatikopoulou (2004) proposed modifications for both the Al-Tabbaa (1987) (e.g. reformulating the hardening modulus) and the Stallebrass (1990) models and evaluated the ability of the various models in simulating the soil

response observed during previously available laboratory tests on overconsolidated clays. For the analyses, the models were implemented in the Imperial College Finite Element Program (ICFEP). Relevant observations by Grammatikopoulou (2004) for the Al-Tabbaa model included:

- Non-smooth elasto-plastic transition when the stress state reaches the kinematic yield surface due to the hardening modulus assumed in the model. This was more obvious for compression than for extension paths (Figures 2.10 and 2.11) respectively where the number accompanying the ´LR´ prefix represents the OCR)
- For low OCR (e.g. 1.5) during compression paths the stiffness is largely underpredicted (Figure 2.10). The same occurs for extension paths but for high OCR (e.g. above 3) (Figure 2.11). This was related to the relative direction from the current stress path to the previous stress path.
- The model does not have good capabilities for modelling the effect of recent stress history and stress path direction after creep.

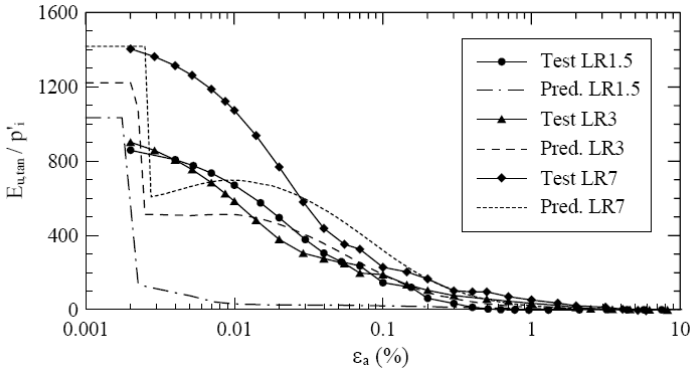

Figure 2.10. Normalised stiffness-strain curve predictions of the Al-Tabbaa model for the triaxial compression paths (test data from Jardine, 1985) (Grammatikopoulou, 2004)

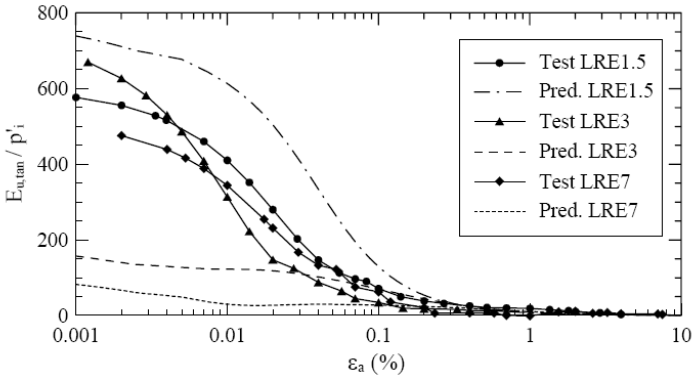

Figure 2.11. Normalised stiffness-strain curve predictions of the Al-Tabbaa model for the triaxial extension paths (test data from Jardine, 1985) (Grammatikopoulou, 2004)

The author also evaluated the performance of the models for two boundary problems. One of these consisted of single and twin tunnel constructions in overconsolidated London Clay. In this case also the Jardine et al. (1991) model was used for comparison. The constitutive model used to model the behaviour of the London Clay was varied (Al-Tabbaa, 1987; Jardine et al., 1991 and others), but the behaviour of the other soil layers (Alluvium and Terrace Gravel) was always simulated using isotropic linear elasticity and Jardine et al. (1991) respectively. As a result of this, the prediction cannot be attributed to one of the models in particular and hence the individual performance of each constitutive model is less clear. The author reported however on the performance of the Al-Tabbaa (1987) and Jardine et al. (1991) models (this would strictly refer to the contribution of the model when attributed to the London Clay):

- The Al-Tabbaa model predictions of surface settlement being very similar whatever configuration of the kinematic surface was used at the end of the geological history.
- The Al-Tabbaa model being significantly influenced by the K_0 profile assumed.
- The Jardine model being also significantly influenced by the K_0 profile assumed, but to a lesser extent.

The S-CLAY1 model is more recent and, to the author's knowledge, it has not been used yet for tunnelling problems in particular. The predictions of this model have been investigated by Karstunen et al. (2006) for embankments on soft clay and the trends compared to those from other better established models (e.g. Modified Cam-Clay, Soft-Soil model in PLAXIS). Additional research is still required for other types of geotechnical boundary value problems as well as further validation against real field data.

2.2.3. Tunnelling Induced Stress Paths

It has been noted from the published literature that excluding a few cases regarding the sort of stress paths that are experienced by the ground during the construction of bored single tunnels (Mair, 1979; Myrianthis, 1981; Ng and Lo, 1985; Lee and Rowe, 1989; Dasari, 1996; Addenbrooke, 1996; Barla, 1999, Bernat et al., 1999; Tang et al., 2000; Eberhardt, 2001 and Jacobsz, 2002) and their reproduction in the laboratory (Barla, 1999) it is clear that most of the studies carried out to date are mainly concerned with strains. This has been related to the difficulties that exist in measuring stresses on site during construction. Some of these difficulties have been reported by Hartkorn (1997). Furthermore, as far as the author is concerned, no work has been published on stress paths at different points around twin tunnels. The previous listed references are briefly reviewed below.

Mair (1979) compared the results from centrifuge model testing and FEA. Initial K_0 values were less than unity at the springlines and invert and just greater than unity at the tunnel crown. The author gave total and effective stress paths for soil elements near the crown, springing and invert as illustrated in Figure 2.12. It should be noted that in Figure 2.12, q (i.e. q^* in the figure) is defined as σ_1 - σ_3 therefore it is always positive.

Such stress paths were reported to induce the stress changes in Table 2.1 at different points around the tunnel.

Table 2.1. Stress changes during tunnel excavation (after Mair, 1979)

Location		**Crow**					**Springline**					**Invert**				
Stress		σ_v	σ_h	p	p'	q	σ_v	σ_h	p	p'	q	σ_v	σ_h	p	p'	q
(a) After tunnel cutting (Elastic)		++	--	0	0	++	--	++	0	0	++	--	++	--	0	--
(b) Due to reducing support	(i) Elastic	--	++	0	0	-+	++	--	0	0	-+	--	++	0	0	-+
	(ii) Yielded	--	--	--	++	0	--	--	--	++	0	--	--	--	++	0

NOTES: ++: Continuous increase; --: Continuous decrease; -+: Decrease followed by increase; 0: Zero or small change

Based on these results, during stage (a) σ_v increased at the crown and decreased at the springline and invert. σ_h behaved in the opposite way. During stage (b) the authors reported an elastic response of the soil with stress-arching occurring as for the contraction of an axisymmetric cavity (the circumferential stresses increasing as the radial stresses decreased). Due to this, the crown and invert experienced extension paths and the springing element underwent compression. The three elements crown, springing and invert experienced particularly simple stress paths because the directions of the principal axis remained unchanged. All of the surrounding soil elements experienced rotation of the axes.

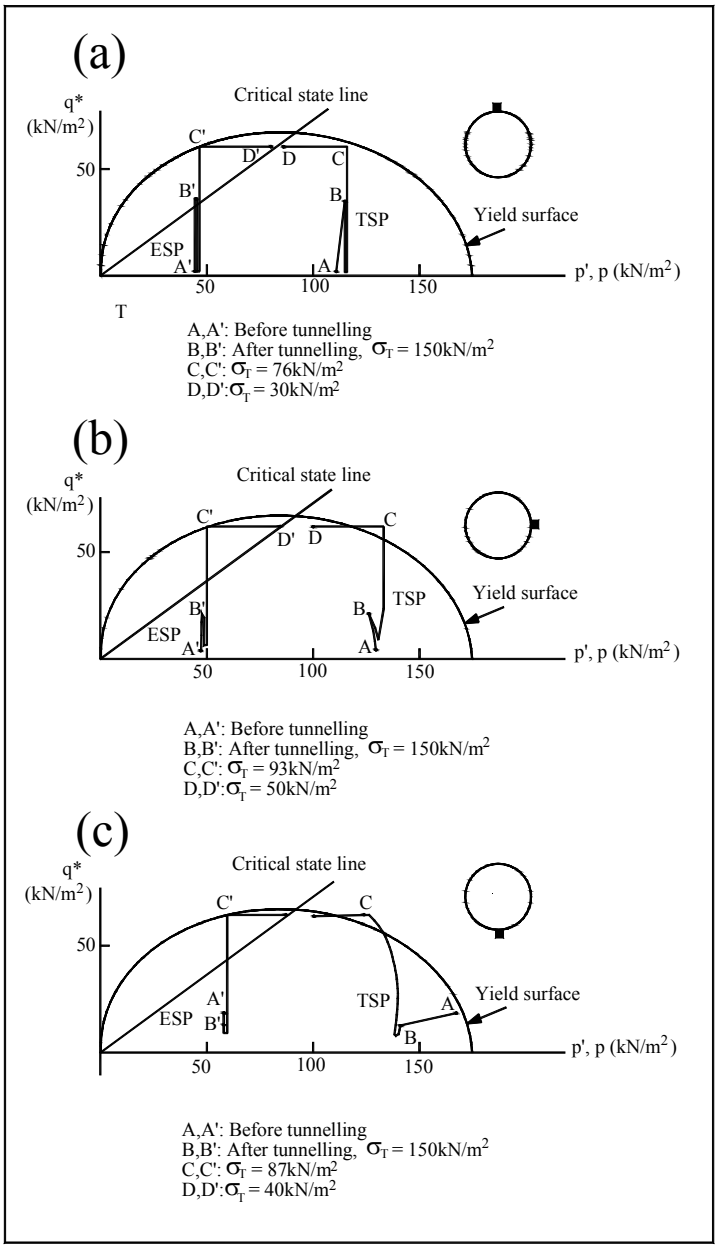

Figure 2.12. Total and effective stress paths during finite element analysis: (a) Crown, (b) Springline, (c) Invert (after Mair, 1979)

Myrianthis (1981) described the stress paths occurring at the tunnel axis and soffit levels using elasto-plastic equations for the excavation of a shield-driven 4.15 m diameter circular tunnel in overconsolidated stiff fissured clay at a depth of 29.3 m ($K_0 \cong 1.7$). The author reported horizontal stresses decreasing by a larger amount than the increase in vertical stress at the tunnel axis (i.e. K_0 decreasing), and a large decrease in vertical stress accompanied by minor changes in horizontal stress (i.e. K_0 increasing) at the tunnel soffit. The author also reported uplifts at the tunnel soffit and a

reduction and increase in horizontal and vertical lining diameters respectively based on in-situ measurements presented by Attewell and Farmer (1974).

Ng and Lo (1985) performed an elastoplastic FEA (the software used is not specified in their paper) simulating the excavation process of a single tunnel and found the stress paths at the crown (point B), springline (point A) and at a point situated at 45 ^{o} between the last two (point C) (Figure 2.13). The authors do not give any details about the modelling performed, which makes it impossible to gain a complete understanding and hence make an easy assessment of their results.

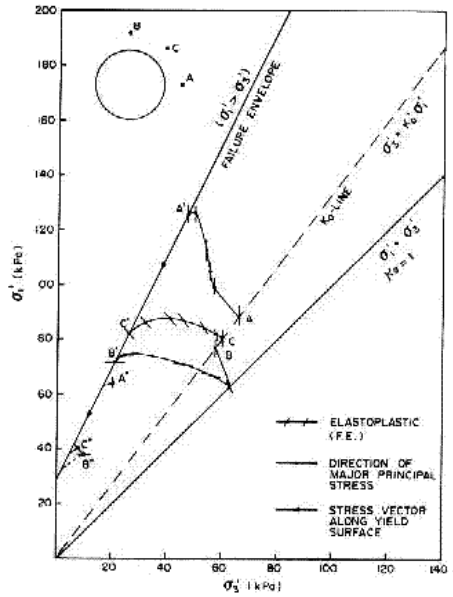

Figure 2.13. Stress paths for typical elements in soil due to tunnelling (Ng and Lo, 1985)

Considering an initial field stress state where σ_3 is horizontal and σ_1 is the vertical stress (i.e. K_0<1) and according to Figure 2.13, at point A the excavation induced a reduction in the radial stress σ_3 and an increase in the tangential stress σ_1. The stress path reached failure at A´, but further yielding of the element occurred along the failure envelope until the soil came into contact with the lining when the stress redistribution moved to A″. At the crown, the excavation produced a decrease in σ_1 and a small initial increase in σ_3, but as the decrease in σ_1 was very fast, the stress tensor rotated 90 ^{o} and σ_1 became σ_3 and σ_3 became σ_1. As for point A, the element failed at B´ and yielding continued until the lining was placed when the stress state was represented by point B″. Similar behaviour was found for point C, but with a rotation of the stress tensor of about 45 ^{o}.

Lee and Rowe (1989) have a section dedicated to the "stress paths in tunnel excavation". These authors stated that the stress paths are very much dependent on the soil element position and on the construction procedure. According to the authors, at the springline the excavation induces a reduction in radial stress and an increase in tangential stress, hence the stress path rises to failure. Near the crown, the excavation produces a reduction in radial stress and a small increase in the tangential stress at an early stage. The reduction of the radial stress is fast and a point is reached when the vertical stress becomes the minor stress and the horizontal stress becomes the major principal stress so the principal directions rotate 90 degrees. The authors referred to previous work by Lo and Rowe (1984) and Ng and Lo (1986). Both papers concluded that the stress paths above and below the tunnel correspond to triaxial extension and that the strength and deformation profile in these regions can be estimated from triaxial extension tests. The authors also concluded that near the springline the stress path is intermediate between compression and extension and so the modulus and strength parameters in this area should lie between compression and extension values.

Dasari (1996) gave idealised stress paths at the crown, springlines and invert elements (Figure 2.14) due to undrained excavation of a single tunnel in an overconsolidated soil. A Cam-Clay type yielding surface was considered in this case. The stress paths presented in Figure 2.14 indicate the same sort of behaviour occurring at the crown and invert, involving a reduction in q (i.e. vertical extension) and a complete opposite behaviour at the springlines with q increasing due to the soil being subjected to vertical compression and horizontal extension.

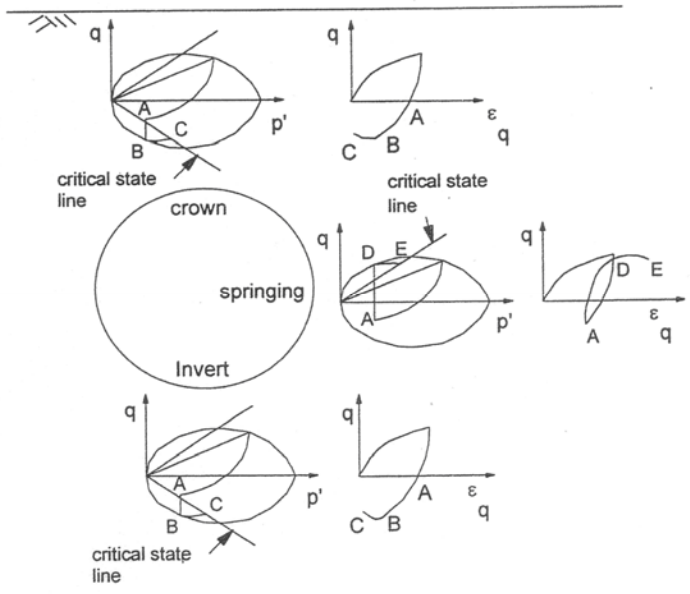

Figure 2.14. Schematic diagram with idealised stress paths due to undrained excavation of a single tunnel (Dasari, 1996)

Addenbrooke (1996) performed two-dimensional undrained FEA of single tunnels excavated in stiff London Clay using the software ICFEP and various pre-yield models (isotropic linear elastic, anisotropic linear elastic and non-linear small-strain stiffness models) with perfect plasticity. Two values of K_0 were considered for the study, 1.5 and 0.5. The most relevant findings for the present research are as follows:

- For K_0 above unity the yielding zone extended above and below the tunnel
- For K_0 below unity the yielding zone extended to the side of the tunnel.
- The K_0 value changed during the excavation process for both linear and non-linear elastic models. For K_0 above unity, K_0 decreased at the tunnel sides and increased at the crown and invert. For K_0 below unity, K_0 decreased (almost constant) at the springlines and increased again at the tunnel crown and invert.

For K_0 above unity and during tunnel excavation, the author reported on extension paths leading to yield at the crown and compression paths at the springline with principal stress rotation. When the lining was applied, the crown would move away from the yield surface. In addition to these, the author also reported an increase and decrease in the tunnel vertical and horizontal diameters respectively for K_0 above unity and opposite for the K_0 below unity case.

Barla (1999) reproduced tunnel induced stress paths in the laboratory using 'undisturbed' stiff Italian Caneva Clay samples aiming to study the swelling behaviour of argillaceous rocks. In order to obtain representative stress paths, the author performed (1) 2D plane strain isotropic linear elastic analysis using the Phase^2 FE Code for values of K_0 equal to 1 and 2 and (2) Elastic and elasto-plastic 2D and 3D analyses using FLAC and FLAC3D together with the boundary element code Examine3D. The points for study were elements situated 1 m away from the tunnel opening at the crown and springline. The installation of tunnel support was not considered during the analyses. The results obtained from Phase^2 FE Code are illustrated in Figure 2.15.

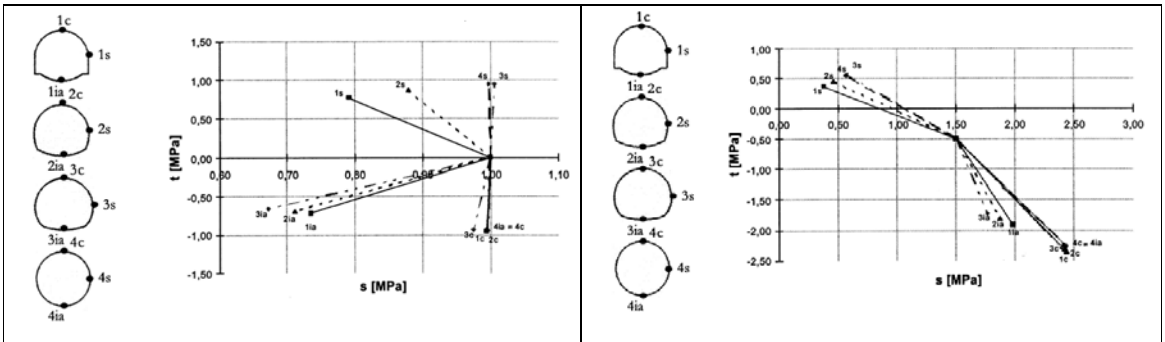

Figure 2.15. Stress paths around a tunnel for different cross section shapes: (a) K_0= 1, (b) K_0= 2 (after Barla, 1999)

The results obtained at a certain measurement section using FLAC, FLAC3D and Examine3D with elastic and elasto-plastic models are presented in Figures 2.16 and 2.17 respectively. From all the results, the author defined the stress paths illustrated in Figure 2.18 for reproduction in the laboratory, which basically resemble those obtained for the elastic solution.

The author correlated the swelling behaviour of the tunnel to a decrease in the mean normal stress. According to this, and based on the results obtained, the author stated that swelling was more likely to occur for $K_0 = 2$ conditions and at the sidewalls. However, the author reproduced $K_0 = 1$ conditions during subsequent stress path testing, presumably in order to avoid K_0-consolidation in the triaxial cell.

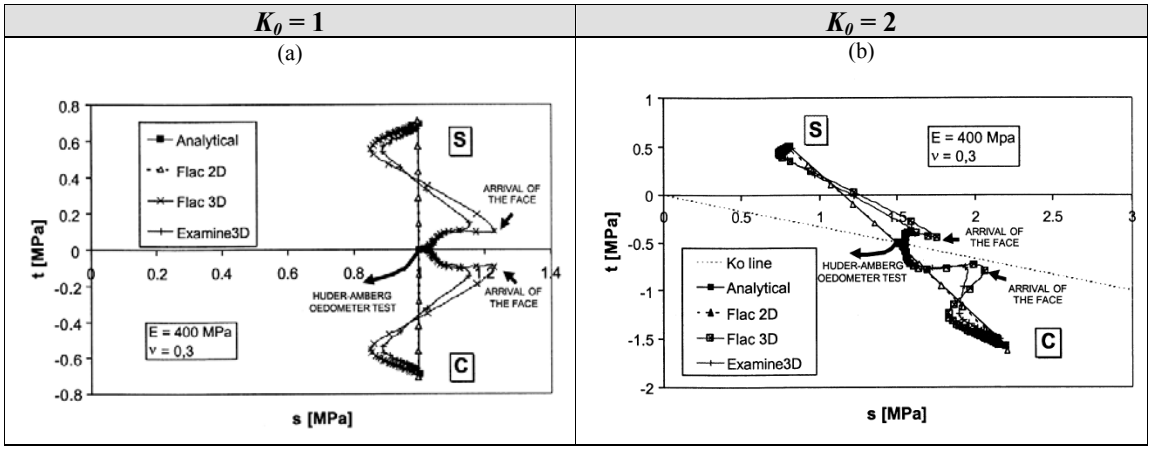

Figure 2.16. Stress changes at the tunnel crown and sidewalls during construction from elastic analyses for (a) $K_0 = 1$ and (b) $K_0 = 2$ (Barla, 1999)

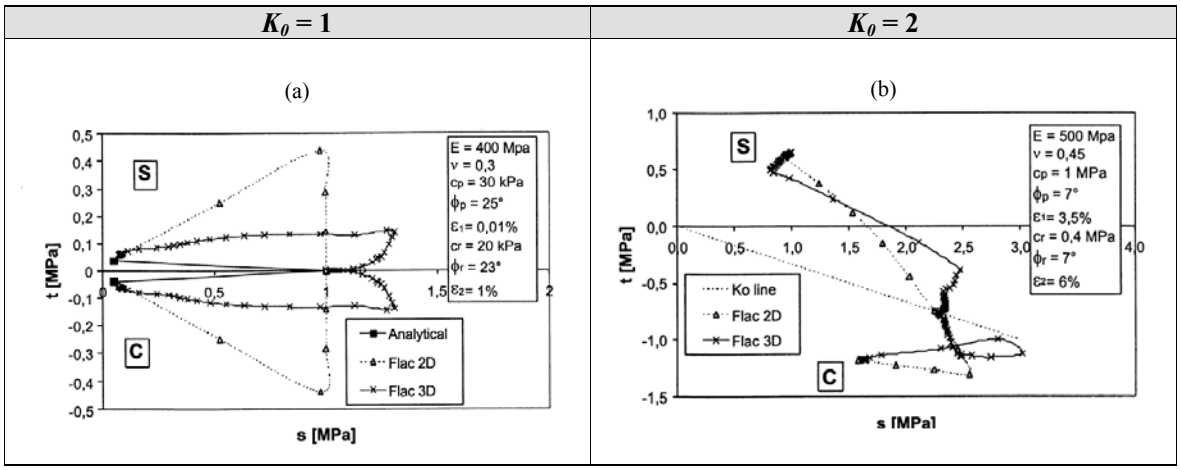

Figure 2.17. Stress changes at the tunnel crown and sidewalls during construction from elasto-plastic analyses for (a) $K_0 = 1$ and (b) $K_0 = 2$ (Barla, 1999)

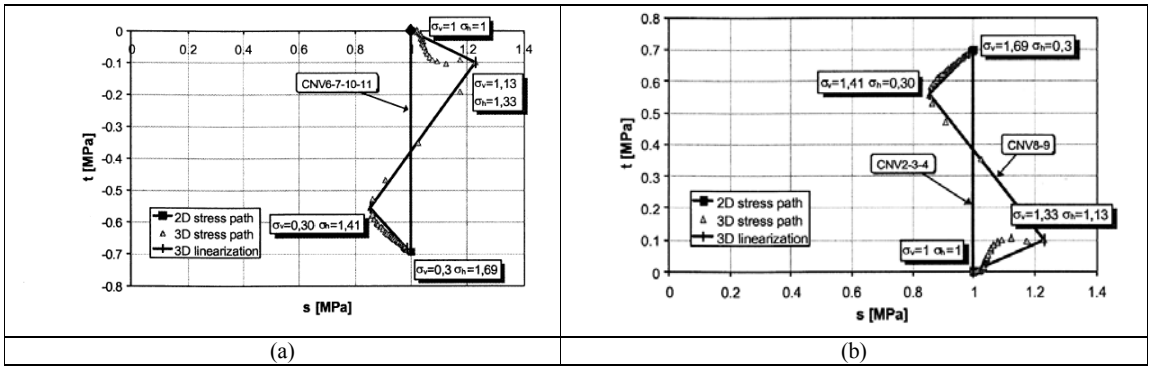

(a) (b)

Figure 2.18. Stress paths proposed for laboratory testing reproducing expected conditions at (a) tunnel crown and (b) tunnel sidewalls (Barla, 1999)

The author considered the initial state stress of the soil being unknown and assumed an isotropic state for simplicity, which was achieved in the laboratory by performing isotropic consolidation. This certainly ignored the previous stress history of the soil.

Bernat et al. (1999) presented their work assessing an elasto-plastic numerical soft soil tunnelling model (CJS) in CESAR-LCPC using field data on the Lyon-Vaise metro works and also preformed an initial general analysis to better understand the different stress paths occurring around the tunnel. The tunnel was of 3 m radius and an overburden thickness of 12 m. The soil was homogeneous. The initial stress of state was considered to be located at the K_0-line. The excavation process in CESAR was simulated using the deconfinement factor λ_{cc} (see Section 3.3.1.1) and plane strain. Relevant results for the present study include (Figure 2.19):

- Crown and invert: The excavation produced a decrease in vertical stress, following an elastic stress unloading path to the isotropic state where the principal directions were inverted (for λ_{cc} close to 50 %). The vertical stress continued decreasing and the path reached failure.
- At the haunches, excavation produced horizontal unloading which lead to a plastic state (for λ_{cc} close to 30 %). The path then followed the plastic criterion for each model.
- For points allocated at 45 ^{o}, rotation of the principal directions occurred in such a way that the minor principal stress took the radial direction.

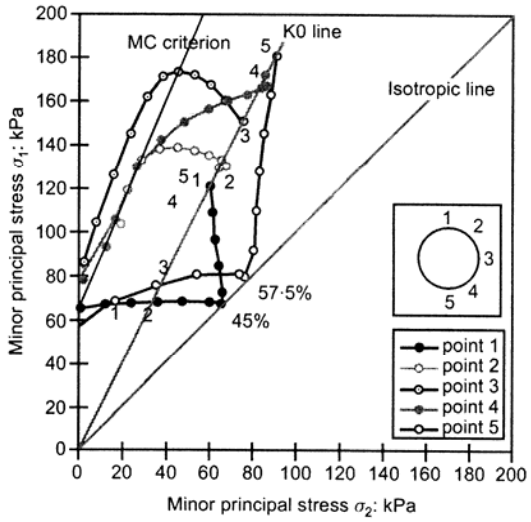

Figure 2.19. Effective stress paths around an unlined tunnel up to λ = 100 % using the CJS elasto-plastic model (Bernat et al. 1999) (Each point along the stress paths represents an increment of 10 % of deconfinement)

Tang et al. (2000) used ABAQUS to perform a three-dimensional simulation of a NATM tunnelling construction (with two stages of excavation) in overconsolidated London Clay at 20 m depth using an elasto-plastic coupled-consolidation model. The constitutive model adopted was the Drucker-Prager failure criterion. The tunnel considered was of oval shape being about 8 m high and 9 m wide. The authors presented the stress paths occurring at some representative points (crown, right and left springline, right and left shoulder and invert) around the unsupported tunnel during the excavation process. The resulting stress paths (Figure 2.20) were, as for any other investigation, conditioned by the particular excavation process assumed during the analysis, but the general trends indicate a decrease in q at the crown and invert (which fails under extension) and an increase in q at the springlines (which fails under compression). The complexity of the predicted stress paths when the analysis tries to capture many of the features of the real construction process (e.g. considering the various construction stages of a NATM tunnel) is evident from Figure 2.20.

The authors summarized some of their findings as follows:

- The non-symmetrical excavation sequence gave rise to non-symmetrical stress paths.
- Rotation of stresses was pronounced at the springlines and left shoulder.
- For high values of K_0, the soil at the invert and right shoulder reached failure during the excavation process.

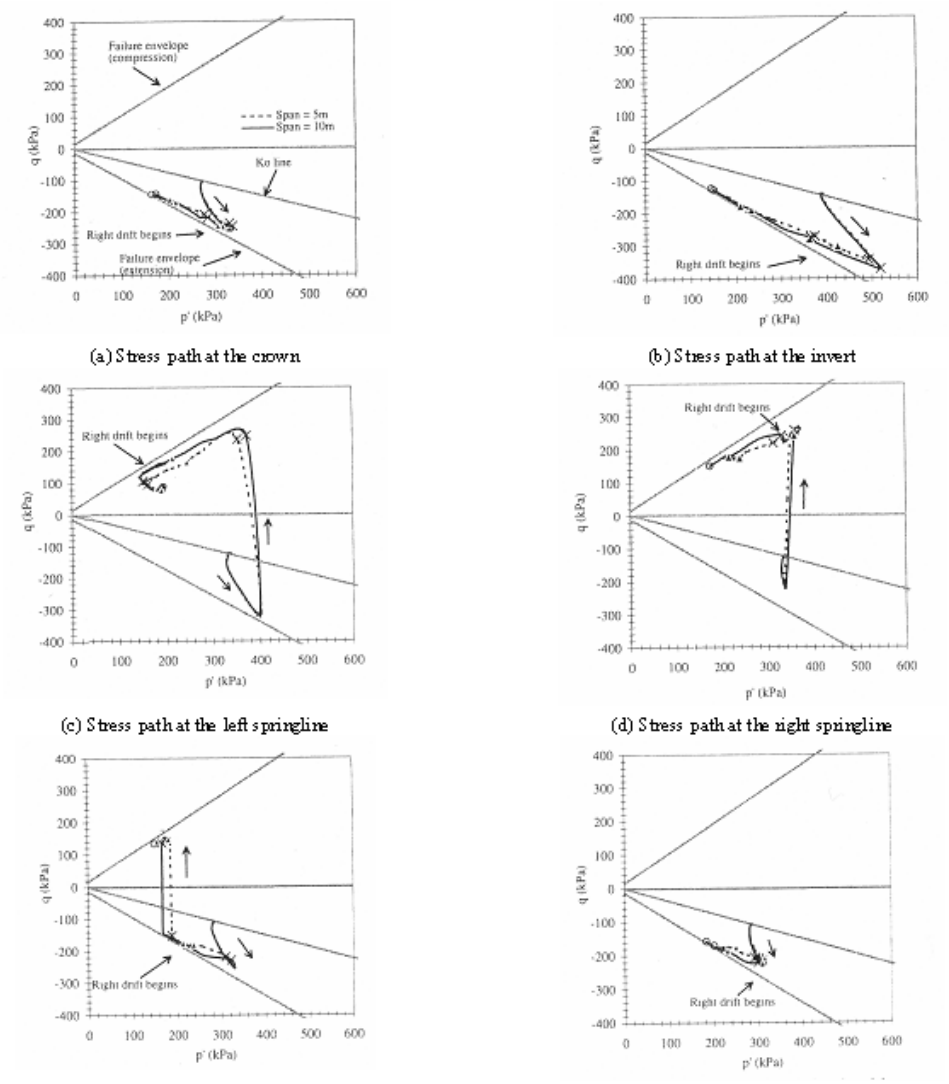

Figure 2.20. Stress paths at different locations for the driving of a NATM tunnel in London Clay; K_0 = 1.5 (after Tang et al., 2000)

Eberhardt (2001) performed interesting numerical research on the three-dimensional rotation and changes in magnitude of the stress tensor in the proximity of the tunnel boundary rather than considering plane strain conditions. Although the study was based in rock, the basics of stress redistributions can also be extrapolated for soils. The author used various three-dimensional finite element models using the code Visage in order to take into account different initial field stresses. Case III for example, corresponded to a stress situation where σ_3 is initially vertical, σ_1 is initially horizontal perpendicular to the tunnel axis and σ_2 is parallel to the tunnel axis, so $K_0 > 1$. Figure 2.21 shows the author's findings in terms of the principal stress magnitudes and orientations at the tunnel roof and walls assuming linear elasticity. Instead of the increase in σ_1 observed at the tunnel roof once the face had passed the measuring point, a large decrease was observed when using elasto-plasticity. The authors did not comment extensively on this observation.

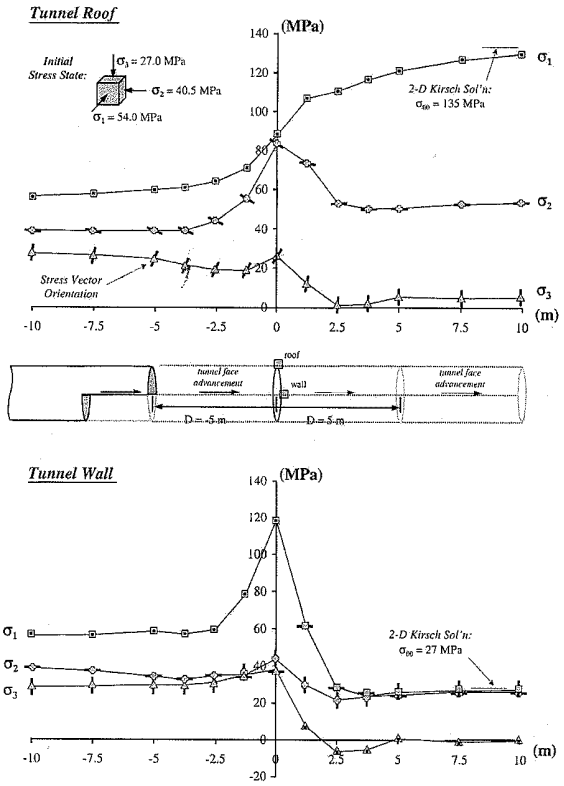

Figure 2.21. Magnitude and orientation of principal stresses at fixed points in the tunnel roof and wall for a given initial initial stress (Eberhardt, 2001)

Jacobsz (2002) used miniature Entran (EPL) surface-mountable stainless steel pressure sensors in the centrifuge in order to measure changes in vertical and horizontal total stress due to the progressive contraction of a single tunnel excavated in fine dense sand and for various values of volume loss. The measurement points were located directly above the tunnel centreline. The author anticipated that the

stress measurements would be realistic mainly in a qualitative sense (e.g. showing general trends) and only to some extent quantitatively. The coefficient of earth pressure at rest was below unity. The most relevant results for the present investigation are illustrated in Figures 2.22, 2.23 and 2.24. These indicate that during excavation of the tunnel the vertical stress decreased with volume loss and the horizontal stress increased with the exception of those points very close to the tunnel perimeter at which the soil reached failure because $\sigma_v \approx 0$ and so σ_h also decreased very fast. The author reported on a reduction in shear and mean normal stresses for all the stress paths as volume loss increased.

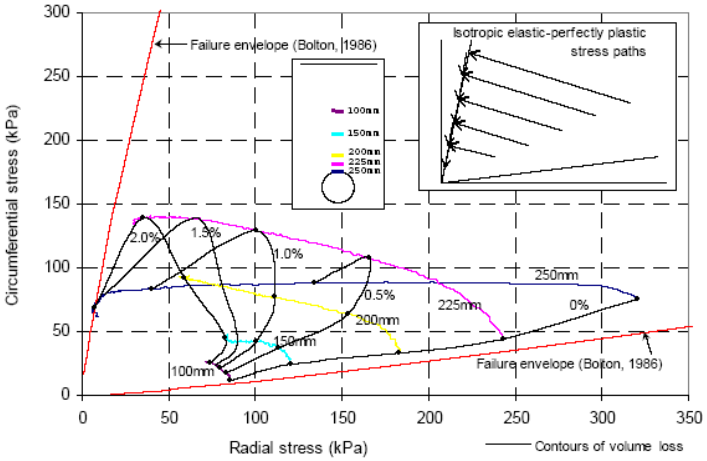

Figure 2.22. Stress paths of vertical versus horizontal stress on the tunnel centreline during volume loss (Jacobsz, 2002)

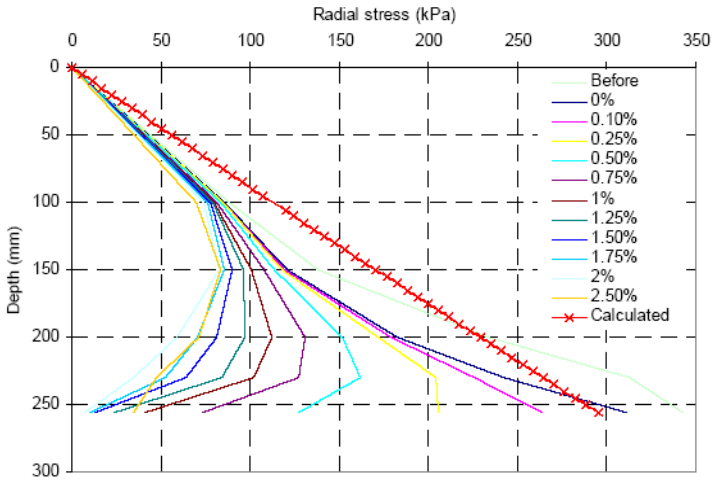

Figure 2.23. Vertical stress profile on tunnel centreline at different volume loss values (Jacobsz, 2002)

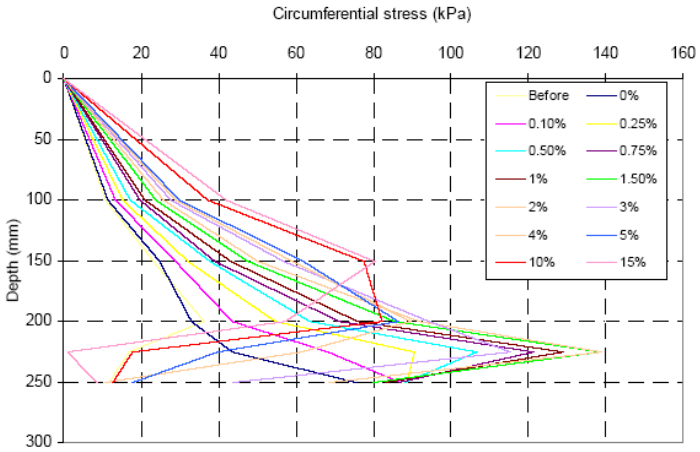

Figure 2.24. Horizontal stress profile on tunnel centreline at different volume loss values (Jacobsz, 2002)

Many similarities can be observed in the results just presented. The most relevant of these can be summarised as follows:

- At the crown of the tunnel, the vertical stress decreases and the horizontal stress increases hence the soil is subjected to extension. The opposite occurs at the springlines therefore these are subjected to compression.
- The K_0 value varies during excavation. It increases at the crown and reduces at the springlines.
- The magnitude of the increment/decrease of stress (both vertical and horizontal) seems to be related to the K_0 value. For example, σ_h' at the springline decreases less when $K_0<1$ than when $K_0>1$.
- The vertical and horizontal diameters of the tunnel increase and decrease respectively for K_0 above unity and opposite for the K_0 below unity, therefore inducing ovalisation.
- Uplifts are commonly predicted when $K_0>1$.

2.3. PART II: TRIAXIAL AND STRESS PATH TESTING

This section presents previous experimental experiences when testing reconstituted specimens in triaxial and stress path equipment such as the preparation of the specimens themselves, disturbances to which the specimens are subjected to, differences in behaviour between natural and reconstituted specimens, rates of stress and strain for testing, the concept of small-strain stiffness and the use of on-sample instrumentation. This all has helped at taking more informed decisions during the present study. Some parameters encountered for the Speswhite Kaolin clay by previous authors are also presented in Section 2.3.7. These will be used in order to either validate or question the parameters established during the present research.

2.3.1 Preparation of K_0-consolidated Reconstituted Samples

Specimens for laboratory testing range from natural and remoulded to those reconstituted from slurry. Natural specimens trimmed from high quality "undisturbed" in-situ samples are theoretically believed to maintain the stress history of the area and depth of interest and tested under this assumption. In reality however, some disturbances always occur hence a prudent view must be taken regarding the "undisturbed″ status. Reconstituted samples are conventionally prepared by mixing dry soil with water and subjecting this to one-dimensional consolidation up to the in-situ stress level. Burland (1990) commented, however, that when using natural soil, this should be mixed without previous drying and, if possible, with water of the same origin. Fearon and Coop (2000) used a natural soil without drying it initially. When using commercially processed soil (e.g. Speswhite Kaolin clay), the condition of not drying the soil does not apply and typically de-aired water is used for mixing. Jardine et al. (1984) and Hau (2003) both used distilled water. In terms of the required initial moisture content (w) Al-Tabbaa (1987) worked with Speswhite Kaolin clay and used a moisture content equal to 120 %. The author did not specify the liquid limit (LL) of the soil. According to Burland (1990), the slurry should have a water content between 1.0 and 1.5 times the LL. Hird and Hajj (1995) used a value of 1.5 times the LL. Powrie et al. (1998) used a water content of 100 %, but the authors did not specify the LL and PL for the Speswhite Kaolin being used. Fannin (1986), Kim (1996) and Hau (2003) used an initial water content of about twice the LL. Fearon and Coop (2000) investigated which way of preparing the slurry was the most convenient in terms of similitude with natural specimens. A natural clay was disaggregated and the particles mixed with water using three different preparation methods aiming to observe different behaviours depending on the remaining fabric and mixing effort. The procedure involving mixing the soil with a water content of around 1.0 to 1.5 times the LL, leaving it overnight and using a mechanical mixer for about two hours, was found to give similar response to the one for the undisturbed specimens and also showed a microstructure close to that of the natural material.

One-dimensional consolidation represents an approximation to the real geological formation of a soil and has been found to be a convenient way to prepare the samples due to its relative repeatability and hence smaller variability in properties when compared to natural samples.

The consolidation techniques used by many authors were reviewed at the beginning of this project. This includes, amongst others, the work presented by Jardine et al. (1984), Al-Tabbaa (1987), Atkinson et al. (1990), Garga and Khan (1991), Hird and Hajj (1995), Rampello et al. (1997), Powrie et al. (1998), Siddique et al. (1999), Anandarajah and Zhao (2000), Hau (2003) and Prashant and Penumadu (2005). The basic idea behind all these methods is always the same, but the materials used for the consolidation devices and the way the load is applied differs from one to another. The K_0-consolidation to the required stress state can be carried out either completely in an external consolidation device or partially in the consolidation device and partially in the triaxial cell. The choice basically depends on the equipment available, the stress levels and the proposed testing programme.

A common procedure consists on consolidating a body of soil with dimensions bigger than those of the triaxial specimen and then trimming it of to the required specimen size (usually 38 mm, 50 mm or 100 mm diameter). Al-Tabbaa (1987) used an unusual way of consolidating the slurry in which the consolidation was carried out within the triaxial cell. Some issues related to this unusual preparation procedure are the friction between the clay and the rubber membrane for triaxial testing (already in place), which Al-Tabbaa alleviated by using silicon oil and the potential cavitation in the bottom drainage line when removing the loads. The author did not comment on the latter. Advantages include minimum equipment and space required, no pushing required when extruding the sample and nil exposure of the specimens to atmosphere during preparation.

2.3.2. Sample Disturbance

Various papers report on the disturbances experienced by a given soil during in-situ sampling and preparation for testing as well as on the potential effects of these (e.g. La Rochelle et al., 1980; Baldi et al., 1988; Clayton et al., 1992; Hight et al., 1992; Hird and Hajj, 1995; Siddique et al., 1999 and Doran et al., 2000). For example Hight et al., (1992) found that different sampling methods give rise to different initial bounding surfaces and p' values, the former due to the strains imposed during sampling. In addition to this, the level of disturbance would be related to the contraction of the bounding surface. The worse the quality of the specimen, the smaller the bounding surface. Hird and Hajj (1995) found the effects of sampling disturbances, in terms of effective stress, stiffness and strength, to be more significant for normally consolidated clays than for overconsolidated clays.

Reconstituted samples in the laboratory are subjected to similar disturbances during preparation. However, a review into related published literature indicated that generally a detailed description of the consolidation devices and their limitations are missing as these are not usually the main focus of

the work. Assuming the case where the soil is under an anisotropic stress state at the last moment in the consolidation device, 'perfect' release of total stresses will imply changes in q (q becomes zero), and therefore also in p', depending on the soil properties until the pore water pressure (u) reaches equilibrium again. For clay, which undergoes undrained behaviour, this should not theoretically involve any volumetric change if the sample is indeed fully saturated, although the sample may tend to expand during the release of total stress (Garga and Khan, 1991). The expected p' due to 'perfect' release can be estimated by using Equation 2.28 (Skempton, 1954),

$$\Delta u = B \cdot \left[\Delta\sigma_h + A \cdot \left(\Delta\sigma_v - \Delta\sigma_h\right)\right] \qquad \text{[Eq.2.28]}$$

where A and B are the Skempton's pore water pressure coefficients, and σ_v and σ_h are the vertical and radial total stresses respectively. This method is not straightforward however due to soil anisotropy and the fact that A is not a constant (although usually considered as 1/3 corresponding to the elastic situation) but depends on the sample overconsolidation ratio (OCR) and stress path followed (Atkinson and Bransby, 1978).

Additional changes in p' are introduced by means of disturbances applied to the soil during extrusion and preparation of specimens for triaxial testing. Depending on the disturbance type and soil state, p' can be further decreased or increased (Baldi et al., 1988) and some of the factors can give rise to volumetric changes (e.g. those involving water suction). Hird and Hajj (1999) used the Stress History and Normalised Soil Engineering Properties Method (SHANSEP) in order to, according to the theory, leave the sample free of the effects of its own disturbance. Coatsworth and Hobbs (1984) introduced SHANSEP as a possible way of avoiding the effects of sample disturbance. This method consists of reconsolidating the specimens to the field overconsolidation ratio but at higher stress levels based on the observation that cohesive soils with the same overconsolidation ratio but different maximum past pressures exhibit very similar strength and stress-strain characteristics when normalised with respect to the maximum past pressure (Ladd and Foott, 1974).

According to Baldi et al. (1988), who reviewed the state-of-the-art in triaxial testing methods at that time, disturbances to p' can be less severe in the case of stiff clays compared to other soils (this agrees with previous discussed comments by Hight et al. (1992) and Hird and Hajj (1995). Baldi et al. (1988) commented on the factors that can potentially take part in the modification of p' from the value expected after a 'perfect' process. These have been classified and further developed in Table 2.2 according to the following groups:

(a) Factors occurring outside the triaxial cell.

(b) Factors occurring inside the triaxial cell.

Table 2.2. Factors involved in the variation of p' during specimen preparation

Outside the triaxial cell	Inside the triaxial cell
Stresses applied to the sample during extrusion, trimming and handling, which depend on the procedures used. Strains during extrusion have two origins: (1) Displacements caused by pushing the extruder piston or the tube into the soil (depending on technique used) and (2) shear strains imposed between the outside of the sample and the inside of the tube (Siddique et al., 1999).	Amount of water available to the sample or demanded from the specimen in the following: (1) Filter paper (2) Membrane (3) Porous stones and pore pressure and back-pressure lines. The latter is controlled by the technique used when setting up the specimen in the triaxial cell, including the selection of the porous stones coarseness.
Atmospheric humidity and temperature: Specimen getting wet or drying out.	Additional stresses applied during specimen installation in the triaxial cell.
Size of the specimen.	Time elapsed between setting up the specimen in the triaxial cell and the application of the all-round confining pressure.
Saturation level in the specimen.	
Storage time and conditions (if applicable).	

Since the removal of total stresses during extrusion leaves the specimen under negative u (suction), and standard pressure transducers cannot properly read high negative values (cavitation occurs at values of -100 kPa or less), u must be made positive by applying an all-round pressure in the triaxial cell. If the test stress range permits, pressures above 300 kPa are encouraged to help air in the system go into solution (BS EN ISO 1377-8: 1990). The initial negative reading made by the pressure transducer is, however, difficult to avoid if the specimen is placed in the triaxial cell in the standard way. As soon as the specimen is placed on the base platen, the soil will suck water from the water lines (pore water pressure and back-pressure) through the porous stones and the pressure transducers will give readings which are generally difficult to interpret. In order to avoid this, some techniques have been introduced in the literature such as the use of coarse porous stones with a cavity behind left dry (Berre, 1982; Lo Presti et al., 1999) or high air entry value porous stones (Bishop and Henkel, 1962; Berre, 1982) and the fuse wire technique (Baldi et al., 1988). The latter consists of a thin wire loop placed between the specimen and the porous stones in order to avoid the specimen initially interacting with the water in the system. When a cell pressure is applied in the cell, the wire is embedded into the soil and a measurement of the u response can be made in the positive range. This avoids the properties at the ends of the specimen being modified by water coming into the soil and also possible cavitation of the system. The air trapped in the zone where the wire is placed partially dissolves into the pore water, partially compresses and partially escapes through the membrane. This method does not work well for soft soils as the wire embeds into the specimen even for a cell pressure equal to zero due to its own weight and specimen handling.

2.3.3. Natural versus Reconstituted Soil Behaviour

Natural soils have, in general, some degree of internal structure and this has been found to affect the strength of the soil when compared to reconstituted specimens (Burland, 1990; Ng, 1999; Fearon and Coop, 2000). In this respect, Burland (1990) introduced an important distinction between the behaviour exhibited by reconstituted and natural specimens, and presented ways for normalisation of the results obtained from both materials. The properties linked to the former were defined as the "intrinsic properties". According to the author "the term intrinsic refers to the basic, or inherent, properties of a given soil prepared in a specified manner and which are independent of its natural state" which potentially differs from the natural properties.

2.3.4. Triaxial Testing

The triaxial apparatus has been used for many years for the understanding of soil behaviour under various stress and drainage conditions. Bishop and Henkel (1962) (and later editions) is the 'classic' book for triaxial testing procedures giving a detailed description of this apparatus, performance, applications, associated errors and methods to take into account, preparation of specimens and analysis of results. However, since then, the triaxial equipment has been further developed and it is the Bishop and Wesley (1975) hydraulic type (developed at Imperial College in London) in its various commercial versions that is extensively used (Jardine et al., 1984; Cuccovillo and Coop, 1997 and Powrie et al., 1998). Bishop and Wesley (1975) describe their cell as a simple form of triaxial apparatus in which the stress paths encountered during engineering practice could be more closely approximated than in conventional equipment. In the Bishop and Wesley (1975) cell the pressure/volume controllers control the axial, cell and back pressures. The axial strain and u are measured via external linear transducers and the whole system is computer-controlled by means of a software that very frequently allows for graphical visualization during testing and has capabilities for final reporting. The software for this is also being continuously developed and at the moment it is capable of performing complex stress paths in addition to the standard triaxial tests (unconsolidated undrained, consolidated undrained and consolidated drained). For example, K_0-modules allow computer-controlled zero lateral strains for one-dimensional consolidation, which proved to be difficult to achieve by manual control in the first triaxial apparatus. The computer-controlled hydraulic triaxial equipment was described by Menzies (1988). In addition to the basic Bishop and Wesley (1975) cell, other complementary elements have been designed that allow particular actions to be carried out. Examples of these are the extension caps, which make possible the reproduction of tensile states, of particular interest in tunnelling, and on-sample instrumentation for the measurement of small strains (Section 2.3.6).

An extensive review of more up-to-date procedures and techniques available due to developments in the triaxial equipment and a better understanding of soil behaviour through the years was given by

Baldi et al. (1988). Having a similar piece of work including more up-to-date developments would be beneficial.

Some of the limitations of the triaxial cells in terms of the ability of the equipment to recreate rotation of the principal stresses have been recently overcome by the appearance of the hollow cylinder apparatus. This topic is however well outside the scope of the present research.

During drained and undrained shearing in consolidated undrained and consolidated drained triaxial tests, the rate of axial strain or alternatively the rate of axial stress must be selected. Some scatter in values exists in the literature and no reason is usually given for why one is used in preference to another. Apparently it is more a matter of experience. Table 2.3 compiles some of the values found in different published papers and standards.

Table 2.3. Variability in the "rate of axial stress" and "rate of axial strain" values during drained and undrained shearing in triaxial testing

			Rate of axial stress		Rate of axial strain		
Author(s) and year	**Soil(s)**	**Sample diameter**	**Drained**	**Undrained**	**Drained**	**Undrained**	**Aim of the study**
BS 1377-8:1990	General	38 mm to 100 mm	-	-	-	0.05 mm/min to 4 mm/min	Determination of the undrained effective strength during compressive U-U tests
BS 1377-8:1990	General	38 mm to 100 mm	-	-	0.001 mm/min to 0.5 mm/min	0.001 mm/min to 0.5 mm/min	Determination of the drained shear strength during compressive C-U and C-D tests
Jardine et al. (1984)	North Sea clay	38 mm	-	-	-	4.5 %/day	Measurement of soil stiffness
Ng and Lo (1985)	Silty clay and varved clay (Canada)	-	-	-	0.1 %/hour	1 %/hour	Measurement of parameters relevant to tunnelling
Al-Tabbaa (1987)	Speswhite Kaolin	38 mm	-	-	0.1 %/hour The author comments on other author's rates working with Kaolin: Airey (1987): 0.08 %/hour Loudon (1967): 0.1 – 0.4 %/hour Amerasinghe (1973): 0.2 %/hour	0.1 %/hour	Stress-strain behaviour of Speswhite Kaolin clay
Rossato et al. (1992)	Speswhite Kaolin mixed with fine quartz sand and industrial quartz silt	-	-	-	-	5 %/day	To demonstrate the advantages of mixing Kaolin clay with some other components to closely reproduce the behaviour of "destructured" natural clays
Hird and Hajj (1995)	Speswhite Kaolin	-	-	2 kPa/hour	-	-	Simulation of tube sampling effects
Cuccovillo and Coop (1997)	Kaolin	-	-	-	-	0.03 %/hour	General testing and application of LVDT´s
Ng (1999)	Gault Clay	-	1 to 1.5 kPa/hour	5 to 10 kPa/hour	-	-	Stress paths during diaphragm wall construction
Fearon and Coop (2000)	Argille Scagliose (Italy)	-	1 kPa/hour	-	-	-	Comparison of behaviour between differently prepared samples

			Rate of axial stress		Rate of axial strain		
Author(s) and year	**Soil(s)**	**Sample diameter**	**Drained**	**Undrained**	**Drained**	**Undrained**	**Aim of the study**
Sivakumar et al. (2001)	Belfast Upper Boulder Clay	105 mm	-	-	0.033 %/hour	-	$K_{0(unloading)}$ – OCR relationship
Hau (2003)	Speswhite Kaolin	-	5 kPa/hour (isotropic tests) 3 kPa/hour (one-dimensional compression)	-	0.1 %/hour	-	Repeated loading of thinly surfaced pavements The author gives some references using the same rates: Al-Tabbaa (1989), Atkinson (1987) and Stallebrass (1990)

2.3.5. Stress Path Testing

The stress path method was first described by Lambe (1967). This consists of estimating the stress path (or field strain, or both) for the problem being analysed and reproducing this in the triaxial cell. The soil strain, *u* and strength will depend on the stress path followed. The objective of this was to aid engineering judgment rather than replacing it. The developments achieved in triaxial testing equipment (e.g. Menzies, 1988), and above all those related to the independent control of the different variables, are allowing with time more complex and realistic stress paths to be simulated. These tests are commercially very expensive because suitably trained personnel are required and the tests take a long time to be run. In addition to this, and in order for these tests to be representative and of real use, good quality specimens are required and realistic stress paths have to be followed. Defining stress paths associated with specific construction work (commonly involving various stages) is a very complex task and can certainly only be approximate. At least general trends should be picked up.

There are no specifications or standards on how to proceed when carrying out tests that involve extension states (to negative vertical stresses) or complex stress paths.

2.3.6. On-sample Strain Instrumentation and Small-Strain Stiffness

Many authors pointed out the need for simple but reliable methods to measure the shear-strain behaviour of soils (e.g. Jardine et al., 1984; Coatsworth and Hobbs, 1984 and Costa-Filho, 1985) and experience with local strain instrumentation placed on the central portion of the specimen in order to avoid errors attributed to external instrumentation such as the compliance of the loading system, bedding errors between the specimen and the end platens, compression of system components and imperfect connection between the load cell and the top cap. This observation became very relevant when in the early 80´s it was discovered that at small-strain level some soils can be as brittle as rocks and their stiffness is not constant but varies with strain (Figure 2.25).

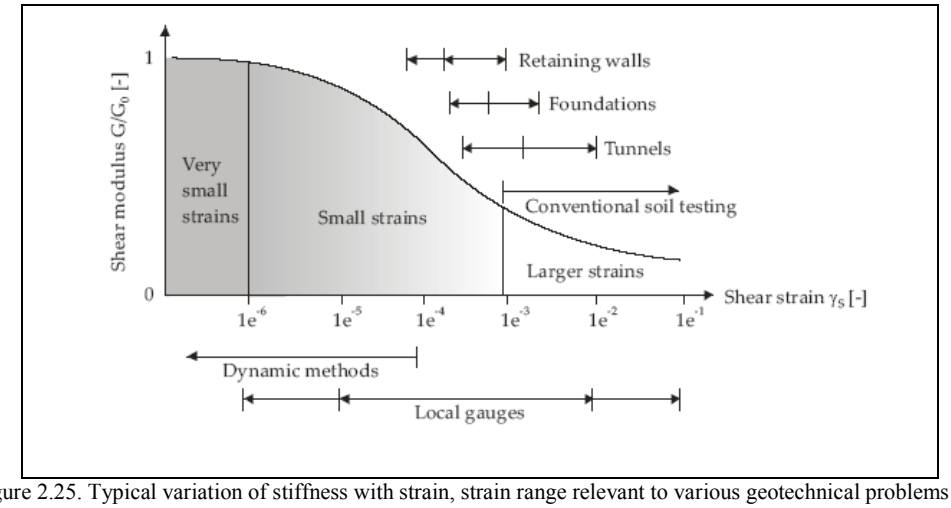

Figure 2.25. Typical variation of stiffness with strain, strain range relevant to various geotechnical problems and application of different equipment for its measurement (PLAXIS Manuals after Atkinson and Sallfors, 1991)

Over the last twenty years various internal devices and arrangements have been tested and used at different research centres and introduced in published papers with details of their capabilities. Some examples of these are: Electrolytic Liquid Levels (Cooke and Price, 1974; Burland and Symes, 1982; Jardine et al., 1984), Axial Strain Inclinometers (Burland et al., 1996), Hall Effects Devices (Clayton and Khatrush, 1986), LVDT´s (Costa-Filho, 1985; Cuccovillo and Coop, 1997; Clayton and Heymann, 2001), Local Deformation Transducers (LDT´s) (Hoque and Tatsuoka, 2004) and Bender Elements (Viggiani and Atkinson, 1995; Callisto and Rampello, 2002; Clayton et al., 2004). This chapter is concerned with the Hall Effect devices and the LVDT´s only.

2.3.6.1. Hall Effect devices

Clayton and Khatrush (1986) introduced for the first time the Hall Effect local strain measurement system based on the Hall voltage (given this name after the work by Hall, 1879) as an easy to build and reliable device capable to measure strains down to 0.002 %. The device comprised two main parts: one semiconductor chip and two magnets. The relative movement between both parts created the required effect between the flowing current through the chip and the magnetic field giving rise to an output voltage across the semiconductor plate, which is known as the Hall voltage. The difficulty was to create a sensor-magnet system able to give an output that was linear with respect to the variable to be measured, but the authors found an appropriate design by modifying the gap distance between the two magnets and the distance between the magnets and the face of the semiconductor. This device is commercially available nowadays for the measurement of both axial and radial strains.

2.3.6.2. LVDT's

Linear variable differential transformers (LVDT's) of variable range, accuracy and sensitivity can be used instead of semiconductor - magnet systems in order to measure axial and radial strains with a similar support aluminium system to fix it to the specimen. Cuccovillo and Coop (1997) produced a technical note about the use of internal LVDT's with the same triaxial equipment as the one that will be used for the present research. The authors used 60 mm diameter Kaolin specimens with an overconsolidation ratio of 3.9 and with LVDT's of 10 mm range to cover the complete stress-strain curve. However it is important to note that only axial LVDT´s were used in this case (i.e. radial transducers were not set up). Clayton and Heymann (2001) also used LVDT´s for axial measurements only. Reported accuracies and resolutions vary considerably and are improving with time. LVDT's are commercially available nowadays to measure both axial and radial strains.

2.3.7. Some Parameters for Speswhite Kaolin Clay

A large amount of the research undertaken in the United Kingdom on natural clay behaviour uses London Clay, hence the large amount of data available on this material. The London Clay formation constitutes the idealised ground context for the present investigation, but Speswhite Kaolin clay has been used during testing due to natural London Clay not being available when starting the project. A large number of publications exist as well on the behaviour of this commercially processed material, extensively used in the UK for research purposes. However, the literature tends not to be sufficiently precise when indicating the name of the soil and/or the providence of this hence making it difficult to proceed to a direct comparison of results. Sometimes not even the *LL* and *PL* values are given with potential effects over the soil's plasticity as shown in Table 2.4.

In terms of the Speswhite Kaolin specific gravity (G_s), Kim (1996) gave a value of $G_s = 2.61$ based on various previous authors' investigations. The same value was given by Rossato et al. (1992). Prashant and Penumadu (2005) reported on a value of 2.63. A value of 2.60 has been reported by other authors such as Gue (1984), Atkinson et al. (1990) and Al-Tabbaa (1987).

K_0 values reported by previous authors working with Speswhite Kaolin clay have been summarised in Table 2.5.

The K_0 value is commonly related to the friction angle ϕ' by Equation 2.29 proposed by Jacky (1948).

$$K_0 = 1 - \sin\phi' \qquad \text{[Eq.2.29]}$$

Table 2.4. Variability in *PL* and *LL* values for Kaolin clays

Author(s)	Name used for the soil	Reference to other authors	*LL*	*PL*
Gue (1984)	Speswhite Kaolin	-	65	34
		Martins (1983)	62	32
		Steenfelt (1981)	69	38
Fannin (1986)	Speswhite Kaolin	-	62	31
Atkinson et al. (1990)	Kaolin	-	65	35
Rossato et al. (1992)	Speshite Kaolin	-	63	33
Doroudian and Vucetic (1995)	Kaolinite Clay	-	53	32
Hird and Hajj (1995)	Speswhite Kaolin	-	72	40
Kim (1996)	Speswhite Kaolin	Steenfelt et al. (1981)	65 (Based on various authors' investigations)	34 (Based on various authors' investigations)
		Clegg (1981)		
		Martins (1983)		
		Airey (1984)		
		Elmes (1985)		
		Al-Tabbaa (1987)		
		Santa Maria (1988)		
		Smith (1993)		
Cuccovillo and Coop (1997)	Kaolin	-	-	-
Stallebrass and Taylor (1997)	Speswhite Kaolin	-	-	-
Powrie et al. (1998)	Speswhite Kaolin	-	-	-
Hagiwara et al. (1999)	Speswhite Kaolin	-	65	35
Hau (2003)	Speswhite Kaolin	-	63	31
		Atkinson (1987)	65	35
		Al-Tabbaa (1987)	69	38
		Martin and Houlsby (2000)	65	34
Prashant and Penumadu (2005)	Kaolin clay	-	65	30

Table 2.5. K_0 values for Speswhite Kaolin clay reported by previous authors

Author(s)	K_0
Fannin (1986)	(0.59 – 0.69) - Average 0.64
Elmes (1985)	0.82
Atkinson et al. (1987)	0.66
Al-Tabbaa (1987)	0.69±0.02

During unloading, and according to Equation 2.30 previously suggested by Schmidt (1966) and more recently validated by Mayne and Kulhawy (1982), Al-Tabbaa (1987) suggested a value of θ (at-rest rebound parameter of the soil depending on the clay mineralogy) equal to 0.464 for Speswhite Kaolin clay. By reviewing other authors' findings (e.g. Meyerhof, 1976; Schmertmann, 1975) it can be concluded that θ is generally in the range 0.4 to 0.5.

$$K_0^{oc}(unloading) = K_0^{nc}(loading) \cdot OCR^{\theta} = 0.69 \cdot OCR^{0.464} \qquad \text{[Eq.2.30]}$$

The overconsolidation ratio (OCR) in Equation 2.30 is defined as:

$$OCR = \frac{\sigma'_{v\max}}{\sigma'_v} \qquad \text{[Eq.2.31]}$$

Various relevant critical state and consolidation parameters reported by previous authors working with Speswhite Kaolin clay have been summarised in Table 2.6.

Table 2.6. Summary of some critical state parameters in the published literature for Speswhite Kaolin clay

	Isotropically consolidated specimens			
Author(s)	Mc_{ic}	$\phi c'_{ic}$	Me_{ic}	$\phi e'_{ic}$
Elmes (1985)	0.82	21.14	-	-
Fannin (1986)	0.88	22.56	-	-
Atkinson et al. (1987)	0.95	24.21	0.80	27.49
Smith (1993)	0.80	20.67	-	-

	K_0-consolidated specimens			
Author(s)	Mc_0	$\phi c'_0$	Me_0	$\phi e'_0$
Atkinson et al. (1987)	0.85	22	0.85	29
Al-Tabbaa (1987)	0.90	23	0.68	22.55

Author(s)	λ_{ic}	λ_0	κ_{ic}	N	N_0	Γ_{ic}	Γ_0
Elmes (1985)	0.140	-	0.030	3.00	-	2.87	-
Fannin (1986)	0.247	-	0.040	-	-	3.51	-
Atkinson et al. (1987)	0.190	0.19	-	3.29	3.23	3.16	3.14
Al-Tabbaa (1987)	0.187	-	0.028	3.20±0.03	3.13±0.03	3.00	-
Smith (1993)	0.174	-	0.050	-	-	3.34	-

2.4. KEY FINDINGS AND JUSTIFICATION FOR CURRENT RESEARCH

The key findings from Parts I and II that justify the current research are as follows:

- There has been and there still is at the moment a lot of effort put into the development of both numerical software and constitutive soil models for the study of all sorts of geotechnical problems, one of these being tunnelling.
- Data regarding the sort of stress paths occurring in the ground during excavation is very scarce. Measuring stresses in-situ is very complex and most of the publications in the field of tunnelling are concerned with deformations and the effect of these on nearby structures rather than with stresses. However, the stress changes presented in the few publications available show significant similarities.
- All sorts of constitutive models are being used for the study of underground excavations when in fact the improvements made for overconsolidated soils and in particular during unloading stress paths are limited. Some constitutive models are, however, very often presented in the literature as certainly improving the predictions of soil behaviour during tunnelling. Despite the various lines of thought in this respect, it is obvious from the literature that the quality of the predictions in tunnelling problems is still very limited using the available models in either 2D and 3D analyses.

- Various authors have evaluated either quantitatively or qualitatively the success of various constitutive models for tunnelling problems. This is normally done by comparing numerical predictions with field observations on surface settlement troughs. No publications have been found that compare predictions of the models with tunnel-specific laboratory stress path testing.
- One topic with a considerable impact at the moment on the geotechnical community, and hence in the way modelling and laboratory testing are approached, is the non-linear stress-strain response of soils at small strains.
- Examining the behaviour of soils at small and very small strains requires highly sophisticated equipment in the laboratory. Many types of these exist worldwide and have been in general reported to be successful with no obvious setbacks.
- Although a choice of standards exists for carrying out traditional triaxial testing, there is not a unified method when performing more state-of-the-art tests.
- The disturbance of natural soil when sampling in-situ is widely recognised, but issues surrounding the preparation of reconstituted samples in the laboratory are not always acknowledged by experimental engineers.

These key findings have motivated the present research and have conditioned the development of the project methodology in Chapter 3.

Chapter 3: METHODOLOGY

3.1. INTRODUCTION

The methodology presented in this chapter was based on the information presented in Chapter 2 and further developed according to the observations made, and knowledge gained, during the present investigation. This methodology, schematically illustrated in Figure 3.1, has provided the means for achieving the aims and objectives listed in Chapter 1.

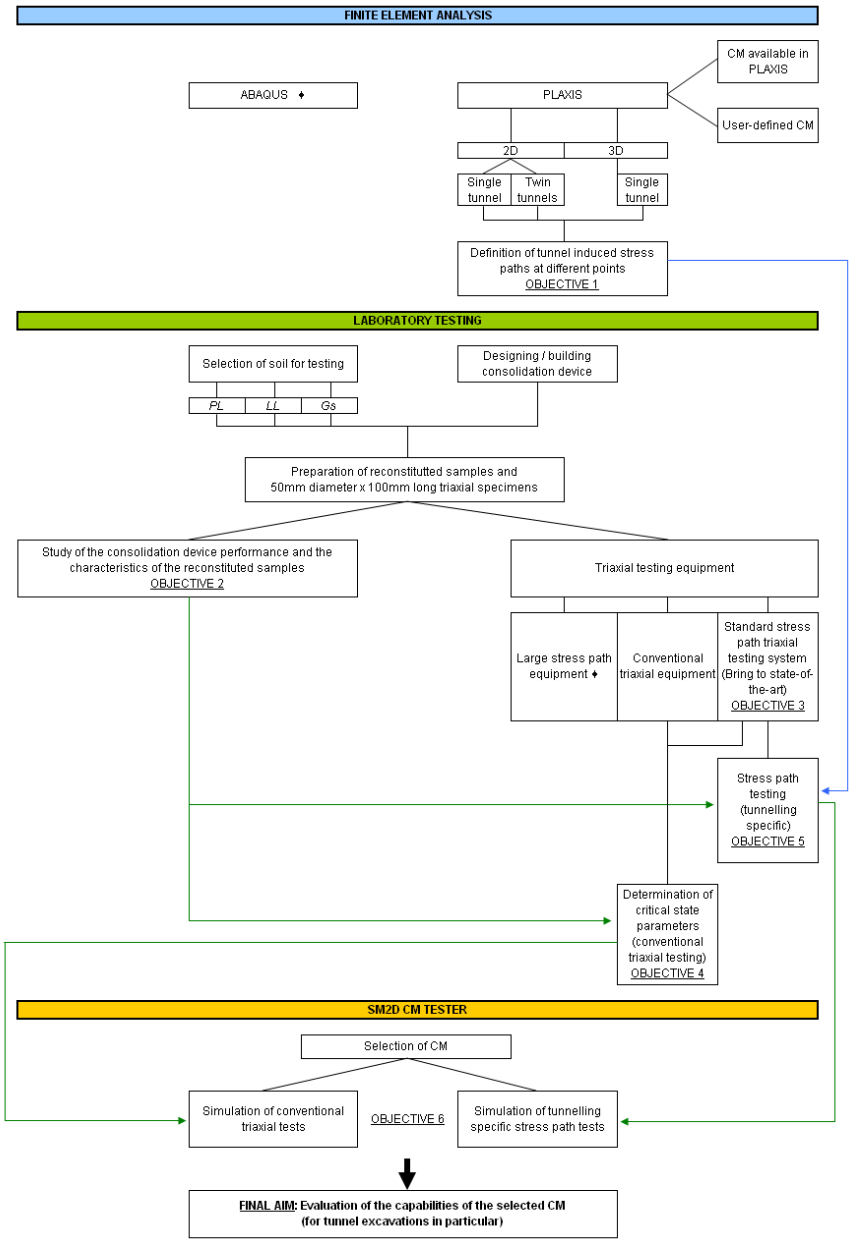

Figure 3.1. Flow diagram describing the project methodology. CM: Constitutive model.

♦ Parts of the study only partially completed

3.2. CONTEXT AND PRELIMINARY CALCULATIONS

The present research does not focus on a particular case study. However, the extent of the investigation was limited from the beginning to a particular idealized field context. This consisted of a single circular tunnel (8 to 10 m diameter), or same size twin parallel circular tunnels, being excavated in greenfield stiff overconsolidated London Clay at a depth of about 30 m. Hydrostatic pore water pressures would be considered. There were not strict specifications with respect to the position of the groundwater level. The method of excavation and sequence of construction were not fixed either. The specified K_0 value was 1.5 based on a review on reported values for London Clay (e.g. Mott MacDonald, 1991 (1.0 to 1.5); Augarde et al., 1995 (1.0), Hight and Higgins, 1995 (1.5 upper bound for tunnels at 10 - 30m depth); Tang et al., 2000 (1.0 to 2.0, used 1.5 for their analysis)).

The Empirical Method, first introduced by Martos (1958) and later validated by many authors (Schmidt, 1969; Peck, 1969; O'Reilly and New, 1982; Attewell, 1978; Attewell et al., 1986; Rankin, 1988), was used as a preliminary calculation in order to get an appreciation for the order of magnitude of the greenfield short-term soil surface and sub-surface vertical strains induced during the excavation of a single tunnel with the above characteristics. Since instrumentation for laboratory on-sample deformation measurements were, at the time, still to be bought in order to perform some of the proposed tests, these calculations were also useful for approximately identifying the requirements in terms of equipment accuracy and resolution. Further details are given in Appendix A – Section A.1 together with the results obtained and a brief discussion.

3.3. FINITE ELEMENT ANALYSIS

As stated in Chapter 1, the initial project proposal considered using stress data from the tunnel analyses run by Hunt (2004) using ABAQUS. Although this option was closely examined, and all the necessary arrangements made, all the trials failed because of incompatibilities between the old and new versions of ABAQUS.

Due to the fact that this PhD was not intended to be finite element based, the more user-friendly PLAXIS 2D v.8.2 and PLAXIS 3D Tunnel were finally adopted for the determination of stress paths around tunnel excavations despite lacking the flexibility of ABAQUS by being a bit of a "black-box" software. It was hoped that PLAXIS would still be able to provide some relevant data and clear trends that could then be compared to previous published work in order to propose some representative stress paths for reproduction in the laboratory. PLAXIS was available in the Department and has been (and is) extensively used in research and industry.

It should be noted that the coordinate system used in PLAXIS does not coincide with the criterion illustrated in Figure 3.2 widely used for tunnelling problems.

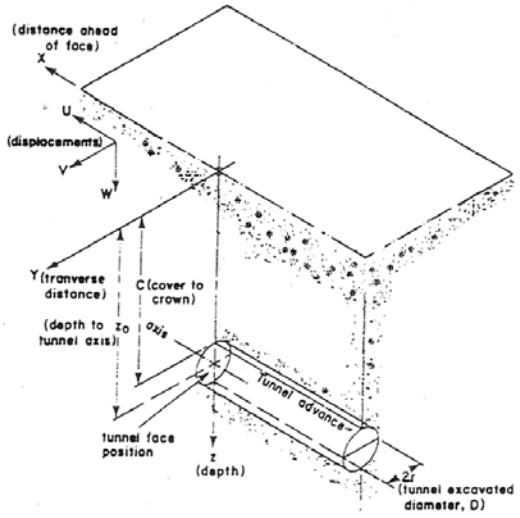

Figure 3.2. Tunnel coordinate system (after Yeates, 1985)

In PLAXIS, *y* corresponds to the vertical dimension being zero at the base of the geometry and positive upwards, *x* is the horizontal dimension being positive to the right and, for the 3D case, *z* corresponds to the out-of-plane direction being zero at the front plane of the mesh. For reference only, the coordinates of the measurement stress points were given according to both criteria, but all the results from the FEA were based on the PLAXIS coordinate system. For the analysis of the results, compression states were considered positive and extension states negative (i.e. opposite to the PLAXIS convention).

The results are presented and discussed in Chapter 4.

3.3.1. Description of the Analyses

Forty-eight 2D analyses were carried out, hence assuming plain strain conditions. From these, twenty-seven were twin tunnel analyses. The 3D effects of an advancing tunnel imply 3D arching (Lunardi, 2000; Lee et al., 2006), rotation of the stresses and a short-term longitudinal and transverse settlement trough (pre-convergence) developing with time and with the advance of the tunnel before reaching plane strain conditions far behind the tunnel face. Since the 3D analyses require longer computational times, only five were performed for the present study and all of them were for single tunnel excavations. The construction sequence reproduced in PLAXIS was kept as simple as possible given the objective of this part of the project (i.e. obtaining stress paths that can be later reproduced in triaxial-type equipment). More complex analyses would result in overcomplicated stress paths (e.g. Tang et al., 2000 in Section 2.2.3).

All the analyses considered undrained conditions in order to simulate the short-term behaviour of the soil during tunnel excavation in clay.

The calculated stress paths were presented in terms of changes in total stresses at each selected point for study. σ_x and σ_y were used for the 2D plane strain analyses and σ_x, σ_y and σ_z for the 3D analyses. In the 2D approach, σ_z would vary during the analyses according to the constitutive model law being used. For example in a linear Elastic undrained case ($\nu_u = 0.5$) it would be calculated using Equation 3.2 from the generalised 3D Hooke's law:

$$d\varepsilon_z = \frac{1}{E_u} \cdot \left[d\sigma_z - \nu_u \cdot \left(d\sigma_x + d\sigma_y \right) \right] \qquad \text{[Eq.3.1]}$$

$$d\varepsilon_z = 0 \quad \text{in plane strain}$$

$$\text{hence:} \qquad d\sigma_z = \nu_u \cdot \left(d\sigma_x + d\sigma_y \right) = \frac{d\sigma_x + d\sigma_y}{2} \qquad \text{[Eq.3.2]}$$

Since both compression and extension states are being studied, q has been defined as σ_y - σ_x instead of σ_1 - σ_3 so that q is negative for extension.

3.3.1.1. Variables

The variables for each of the analysis were:

i) Number of tunnels (single or twin):

When twin tunnels were considered, the second was supposed to be excavated right after the first one therefore not allowing for long-term consolidation between both.

ii) Number of soil layers (1 or 3):

One layer of clay, in which the soil density, the permeability and the K_0 value did not vary with depth, was used as a default for simplicity. Franzius et al. (2005) stated that since it is the value of K_0 at tunnel depth that has the major influence on the soil behaviour, the simplification of using a constant K_0 with depth is unlikely to have major influence on the results. However, in an attempt to reproduce more realistic conditions (e.g. soil having variable properties with depth), some three-layer 2D analyses of single tunnels were also run. The different layers did not represent different types of soil but were used as to account for a density increasing with depth and permeability, K_0 and OCR decreasing with depth. K_0 was calculated using the selected OCR values for each stratum and the relationship proposed by Schmidt (1966), discussed earlier in Section 2.3.7 (Equation 2.30), using a θ value equal to 0.5 (Meyerhof, 1976). In these analyses, the increment of the Young's modulus with depth was selected in such a way that E was uniformly increasing between the different layers.

iii) Geometry modelled (complete or half):

Since the geometry of the model may have some effects on the results of the analyses, two different geometries were investigated to see their impact on the stress paths. The full geometry was modeled in the 1-layer single tunnel and twin tunnels analyses. Only half of the geometry, considering symmetry, was modeled in the 2D analyses of single tunnels involving 3-layers and in all the 3D analyses.

iv) Constitutive soil model:

For each analysis one of the following soil stress-strain relationships was used: Linear Elastic, Mohr-Coulomb, Hardening (HS) (Schanz et al., 1999), all three being available in the PLAXIS library, or the Jardine et al. (1991) model for the small-strain range together with Mohr-Coulomb for large strains introduced in PLAXIS as a private user dynamic link library (DLL) developed by Dr Rouainia at Newcastle University. All these models are commonly used for the study of tunnel excavations (Section 2.2.2.6).

v) K_0 value less than, equal or greater than unity

It was considered of interest to extend the idealized K_0 ground conditions previously stated in Section 3.2 to two additional cases since the coefficient of earth pressure at rest seems to have a high repercussion in the prediction of settlements (Addenbrooke, 1996; Guedes and Santos, 2000; Franzius et al., 2005). The following values were used (also within the typical range for London Clay):

For a normally consolidated soil:

- K_0 less than unity: This value, also referred as K_0^{nc}, was calculated using Equation 2.30 for a friction angle of 24 ^{o}, hence $K_0 = 0.593$.

For an overconsolidated soil:

- $K_0 = 1.0$
- $K_0 = 1.5$

Out of the four constitutive models introduced in (iv), only the Hardening soil model relates the K_0 parameter to the concept of overconsolidation using Equation 3.3.

$$K_0^{oc} = K_0^{nc} \cdot OCR - \frac{\nu_{ur}}{1-\nu_{ur}} \cdot (OCR - 1) \qquad \text{[Eq.3.3]}$$

where K_0^{nc} and K_0^{oc} are the coefficients of earth pressure at rest for normally consolidated and overconsolidated states respectively and ν_{ur} is the Poisson's ratio during unloading-reloading cycles.

vi) The groundwater level:

Situated either at the ground surface (referred in here as 'wet' conditions) or at the base of the geometry well below the tunnel invert (referred in here as 'dry' conditions). 'Wet' conditions

were only considered for some of the 2D analyses on single tunnels. As stated earlier, the analyses were all undrained. Assuming the undrained concept in the 'dry' setting requires further explanation. In this case PLAXIS considers constant volume conditions even for a soil that is not saturated. PLAXIS uses the unsaturated unit weight to calculate the initial stresses, but generates excess pore water pressures (u) above the groundwater level under the conditions of constant volume. This is because the program considers that although being unsaturated the soil still has some water that responds to changes in stress. So strictly speaking the soil is not dry. The only way to get rid of this effect in PLAXIS is by considering the analysis as drained, but then it would be a completely different problem than that intended to study. The author understands this as a shortcoming in the use of PLAXIS.

vii) Shield or NATM tunnelling:

There are two methods in PLAXIS 2D to study the excavation of a tunnel: the "contraction" method and the "β_{PL}-method". The former is most suited for the analysis of shield tunnels, and the latter is applicable for the study of NATM tunnels (or 'sprayed concrete lined tunnels' (SCL) for 'soft' ground). In a 2D analysis, and in the case of a shield tunnel, the sequence of construction in PLAXIS consists of a first stage in which the tunnel is excavated and the support (simulated using 5-node beam elements) is placed (all in once), and a second stage in which a contraction (indicated as a percentage of the excavated area) is applied as a way of simulating the volume loss. In this case there is little stress redistribution around the tunnel.

For NATM tunnels in the 2D case, the procedure is different. To start with, although for the present study the opening was considered to be circular and the support was applied all at once, the lining can be formed by independent segments and so the tunnel shape can be non-circular. Using the NATM option, the first construction stage consists of the excavation of the cavity and it is not until the second construction stage that the lining is applied. When defining the first stage, the so called "β_{PL}-method" is used which simulates the arching effect around the opening and hence the allowance for soil relaxation before placing the support. In NATM tunnels, some time is allowed for the soil to relax with the objective of getting smaller final pressures on the lining. This is based on the observation in practice that stress redistribution occurs transferring the weight of the soil above the crown around the sides. The "β_{PL}-method" in PLAXIS is therefore a version of the convergence-confinement method by Peck (1969) in which $\lambda_{cc} = 1\text{-}\beta_{PL}$. The convergence-confinement method, most suitable for tunnels excavated without a shield (e.g. NATM tunnels), is one of the various ways of accounting for the 3D effects of tunnelling when performing 2D plane strain numerical analyses. Karakus (2007) used several of the currently available methods in this respect for a tunnelling problem and concluded that the best predictions were achieved using the convergence-confinement method together with the use of beam elements to model the tunnel support. The time of placement of

the tunnel support once the excavation is finished is the main factor controlling the short-term movements in the surrounding ground. Figure 3.3 illustrates the general idea of this method consisting of allowing a reduction of the initial stress imposed by the soil on the tunnel boundary up to some point and then the installation of the lining. According to this method, the radial stress applied by the soil on the tunnel boundary (σ_r) is given by Equation 3.4:

$$\sigma_r = (1 - \lambda_{cc}) \cdot \sigma_0 = \sigma_0 - \lambda_{cc} \cdot \sigma_0 \qquad \text{[Eq.3.4]}$$

where:

σ_0 : Initial total ground stress before tunnelling (kN/m^2)

σ_r : Radial stress applied by the soil on the tunnel boundary (kN/m^2)

λ_{cc} : Unloading parameter ($0 < \lambda cc < 1$) (-)

$\lambda_{cc} \cdot \sigma_0$: Represents the stress removed from the soil prior to installation of the tunnel lining

$(1 - \lambda_{cc}) \cdot \sigma_0$: Value of the final (short-term) stress applying to the lining.

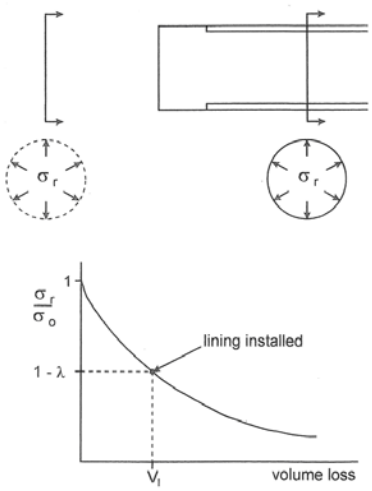

Figure 3.3. Application to 2D finite element analysis of the principle of Convergence-confinement method (Panet and Guenot, 1982)

The Convergence-confinement method is the most used procedure (about two thirds of the cases) (Negro and Queiroz, 2000) in comparison to others such as the Volume loss control method (Addenbrooke et al., 1997), the Progressive softening (Swoboda, 1979) and the Gap method based on the Gap parameter (Rowe et al., 1983).

The way of introducing the β_{PL} value into the PLAXIS analysis is by performing an unfinished calculation stage controlling the parameter *ΣMstage* (*ΣMstage* = 1-β_{PL} = λ_{cc}). *ΣMstage* gives the percentage of a construction stage that has been completed. Hence when running a

"standard" analysis, it is generally zero at the beginning of the stage and unity at the end. If *ΣMstage* is fixed below unity by the user for the first construction stage (i.e. excavation of the cavity), then this stage will be unfinished and the soil will be only allowed to relax partially. If *ΣMstage* is fixed to unity for the stage corresponding to the excavation of the tunnel, since the lining is not still in place, the soil would eventually collapse. For a back-analysis, the β_{PL} value should be estimated by running a full 3D calculation and then, by trial and error, estimating β_{PL} such that, for example, the 2D lining forces match the 3D results. For the present investigation, as only trends in stress paths are investigated, this procedure has not been required. The effect of using different β_{PL} values was investigated using various *ΣMstage* values for the excavation stage of a single tunnel (see viii below) considering elastic behaviour for the soil. For the rest of the analysis a value of $\beta_{PL} = 0.6$ ($\Sigma Mstage = 0.4$) was used.

The problem of having the tunnel collapsing during the excavation stage in a 2D analysis if *ΣMstage* is equal to unity, does not occur in a 3D analysis of NATM tunnels in PLAXIS because the possible collapse of any unsupported section is prevented by the supported section behind and the still un-excavated soil in front of it. Therefore the consideration of a β_{PL} value is not necessary in a 3D analysis.

Although the construction sequence proposed in PLAXIS for the study of shield tunnels is probably a convenient way to model the process numerically because of the way PLAXIS operates, after some initial simulations it was found to be a long way from the real sequence of events that would happen in practice. For example, in PLAXIS the lining is in place before the contraction occurs. Evaluating the implications of this was not possible since real data were not available. As a result, all the analyses performed in this project, either 2D or 3D, are of the NATM type where the relationship between the stress paths and the induced mechanisms in the soil during tunnel construction were found to be more easily correlated. For further details on the NATM method the reader can refer for example to Whittaker and Frith (1990), New and Bowers (1994) and Mair and Taylor (1997).

Using this technique for the analyses was found sensible also when referring to the idealized field context previously introduced in Section 3.2. As stated by Burland et al. (2001) "NATM is a technique particularly well suited to London Clay because this ground is sufficiently strong and impermeable to remain temporarily stable without support". Karakus and Fowell (2005) have recently reported a stand up time of at least 18 hours based on the results reported by Dean and Basset (1995). Powell and Clayton (2007) also reported a relatively high stand-up time for London Clay implying that relatively large cross-sectional areas can be constructed without problems, sometimes simplifying the excavation sequence by using full-face construction. The same NATM construction sequence concept was used for the 2D twin

tunnels (first applied to the left-hand tunnel and then afterwards to the right-hand tunnel) without allowing for consolidation in between, and also for the 3D analyses of single tunnels with respect to the 2D planes. In the 3D case, however, the sequence of construction in the *z* direction introduced new variables to the problem (e.g. the length of the unsupported tunnel slices) that may well have some effect on the stress paths as well as on the ground movements (e.g. related to the volume loss). The sequence used for this investigation will be described in Section 3.3.1.3.3 together with the description of the geometry in the 3D case.

viii) Modelling involving excavation and placement of lining or only excavation:
Some 2D analyses considered only the excavation of the tunnel and not the placement of the lining in order to isolate the stress path characteristics exclusively due to the removal of the soil elements. The following *ΣMstage* values were used: 0.3, 0.5 and 0.7.

ix) Distance between twin tunnel centrelines:
This distance was considered as 2.0, 2.5 or 3.0 times the tunnel diameter (*d*) in order to investigate the effect of the distance between the first and second excavated tunnels on the stress paths and surface settlements. The reason for doing this comes from previous observations by Peck (1969); Cording and Hansmire (1975); Attewell et al. (1986); Rankin (1988); Ghaboussi and Ranken (1977); Leca (1989); Whittaker and Frith (1990); New and O'Reilly (1991); Addenbrooke and Potts (1996); Mair and Taylor (1997); Cooper (2001); Cooper et al. (2002); Kim (2004) and Chapman et al. (2004), who in summary reported greater deformations and volume losses for the second tunnel resulting in asymmetrical surface settlement troughs more noticeable for centre-line spacings smaller than 2.0 *d*.

It should be noted that although the objective here was the definition of stress paths and not the evaluation of the accuracy in predicting settlements, bending moments and others (note that field data were not available for comparison), some characteristics of the surface settlement troughs, as well as the occurrence of plastic zones, were illustrated in order to evaluate the validity of the predicted stress paths.

3.3.1.2. Nomenclature used for the analyses

Each analysis was coded using a sequence of letters and numbers which made reference to the variables involved as indicated below and thus uniquely described the characteristics of each analysis:

S, T:	Single tunnel, Twin tunnel
1L, 3L:	One-layer, Three-layers
C, H:	Complete geometry, Half geometry
-1, 1, +1:	K_0 less than unity 1, K_0 equal to 1, K_0 greater than 1
EL, MC, HR, J:	Elastic, Mohr-Coulomb, Hardening, Jardine et al. (1991)+Mohr-Coulomb

DRY, WET:	'Dry' conditions, 'Wet' conditions
2D, 3D:	Two-dimensional analysis, Three-dimensional analysis
e:	Only excavation (no lining)
2d, 25d, 3d:	Distances of 2.0, 2.5 and 3.0 times the tunnel diameter between twin tunnel centrelines

As an example, "S1LC1ELDRY_N2D_e" would mean "Single tunnel, 1-layer, Complete geometry, $K_0 = 1$, Elastic, Dry conditions, NATM tunnel, two-dimensional analysis, only excavation". Table 3.1 summarizes the analysis performed.

Table 3.1. List of PLAXIS analyses

2D Single NATM tunnel			
1. S1LC-1ELDRY_N2D	**7.** S1LC-1HRDRY_N2D	**13.** S1LC-1ELWET_N2D	**19.** S1LC-1ELDRY_N2D_e
2. S1LC1ELDRY_N2D	**8.** S1LC1HRDRY_N2D	**14.** S1LC+1ELWET_N2D	**20.** S1LC1ELDRY_N2D_e
3. S1LC+1ELDRY_N2D	**9.** S1LC+1HRDRY_N2D	**15.** S3LH-1ELDRY_N2D	**21.** S1LC+1ELDRY_N2D_e
4. S1LC-1MCDRY_N2D	**10.** S1LC-1JDRY_N2D	**16.** S3LH+1ELDRY_N2D	
5. S1LC1MCDRY_N2D	**11.** S1LC1JDRY_N2D	**17.** S3LH-1MCDRY_N2D	
6. S1LC+1MCDRY_N2D	**12.** S1LC+1JDRY_N2D	**18.** S3LH+1MCDRY_N2D	
2D Twin NATM tunnels			**3D Single NATM tunnel**
22. T1LC-1ELDRY_N2D_2d	**31.** T1LC-1ELDRY_N2D_25d	**40.** T1LC-1ELDRY_N2D_3d	**49.** S1LH-1ELDRY_N3D
23. T1LC1ELDRY_N2D_2d	**32.** T1LC1ELDRY_N2D_25d	**41.** T1LC1ELDRY_N2D_3d	**50.** S1LH-1MCDRY_N3D
24. T1LC+1ELDRY_N2D_2d	**33.** T1LC+1ELDRY_N2D_25d	**42.** T1LC+1ELDRY_N2D_3d	**51.** S1LH-1HRDRY_N3D
25. T1LC-1MCDRY_N2D_2d	**34.** T1LC-1MCDRY_N2D_25d	**43.** T1LC-1MCDRY_N2D_3d	**52.** S1LH1MCDRY_N3D
26. T1LC1MCDRY_N2D_2d	**35.** T1LC1MCDRY_N2D_25d	**44.** T1LC1MCDRY_N2D_3d	**53.** S1LH+1MCDRY_N3D
27. T1LC+1MCDRY_N2D_2d	**36.** T1LC+1MCDRY_N2D_25d	**45.** T1LC+1MCDRY_N2D_3d	
28. T1LC-1HRDRY_N2D_2d	**37.** T1LC-1HRDRY_N2D_25d	**46.** T1LC-1HRDRY_N2D_3d	
29. T1LC1HRDRY_N2D_2d	**38.** T1LC1HRDRY_N2D_25d	**47.** T1LC1HRDRY_N2D_3d	
30. T1LC+1HRDRY_N2D_2d	**39.** T1LC+1HRDRY_N2D_25d	**48.** T1LC+1HRDRY_N2D_3d	

3.3.1.3. Geometry details

For the 2D analyses (x-y planes) a medium coarse mesh refined at the tunnel(s) perimeter(s) was used and formed by 15-node triangular elements involving twelve Gauss stress points each. For the 3D analyses, this mesh was extended over the z-direction by copying the 2D model cross-section onto user-defined spaced z-planes. Under these conditions, the 15-node elements include six stress points each. The dimensions of the geometry were chosen to eliminate (or at least minimise) boundary effects. "Standard fixities" were used at the boundaries for both 2D and 3D analyses. In the 2D case, this implies $u_x = 0$ for vertical geometry lines and $u_x = u_y = 0$ for horizontal geometry lines. In three-dimensions the front plane, the rear plane and any point fixed in the x and y direction are fixed in the z-direction.

The diameter of the tunnels was always 10 m. The lining was simulated using structural plate elements of equivalent thickness calculated using Equation 3.5:

$$d = \sqrt{12 \cdot \frac{EI}{EA}} \qquad \text{[Eq.3.5]}$$

where *EI* is the flexural rigidity and *EA* the axial stiffness assuming an elastic behaviour for the lining. The following sections describe the geometry for each analysis and the coordinates for the measurement stress points.

3.3.1.3.1. 1-layer 2D single and twin tunnels – For the 1-layer 2D analyses, a 50 m high and 200 m wide geometry was used. A 10 m diameter tunnel was modelled at a depth of 30 m (from ground surface level to the tunnel axis), situated at the centre of the rectangular geometry (Figure 3.4). When modelling the twin tunnels, the same conditions applied with both tunnels being situated symmetrically into the geometry and considering distances of 2.0 *d*, 2.5 *d* and 3.0 *d* between the tunnel centrelines (see Figure 3.5 illustrating the 2.5 *d* case).

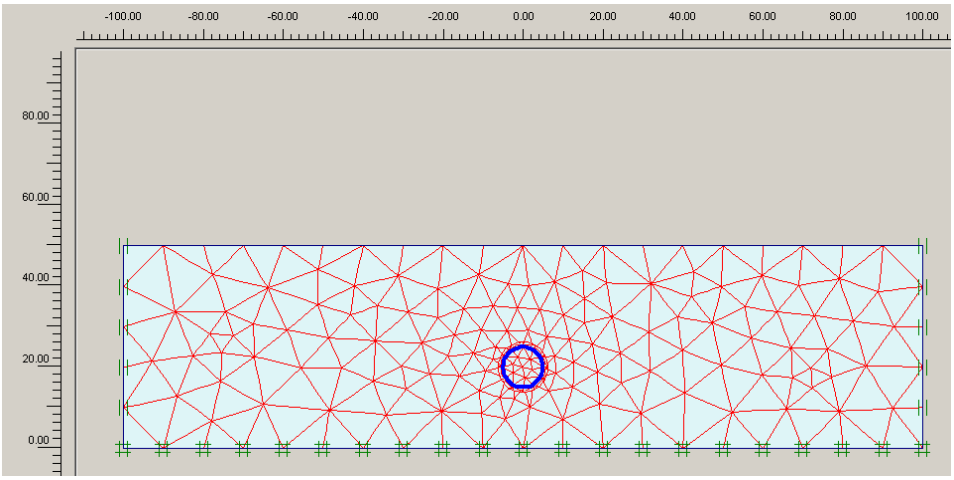

Figure 3.4. Geometry and mesh used for the 1-layer 2D analyses of a single tunnel in PLAXIS

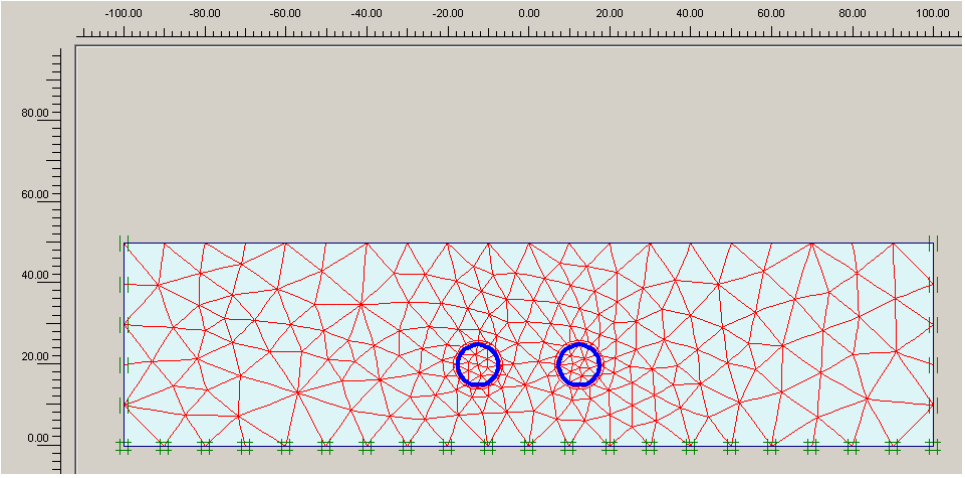

Figure 3.5. Geometry and mesh used for the 1-layer 2D analyses of twin tunnels in PLAXIS.
The distance between the tunnel centrelines is 2.5 *d* in this example, *d* being the tunnel diameter

3.3.1.3.2. 3-layer 2D single tunnel – For the 3-layer 2D analyses, only the right hand half of the geometry was modelled and this consisted of a 60 m x 100 m mesh divided into three soil layers (top, middle and base) of equal thickness. The axis of the 10 m diameter tunnel was situated at a depth of 30 m (Figure 3.6).

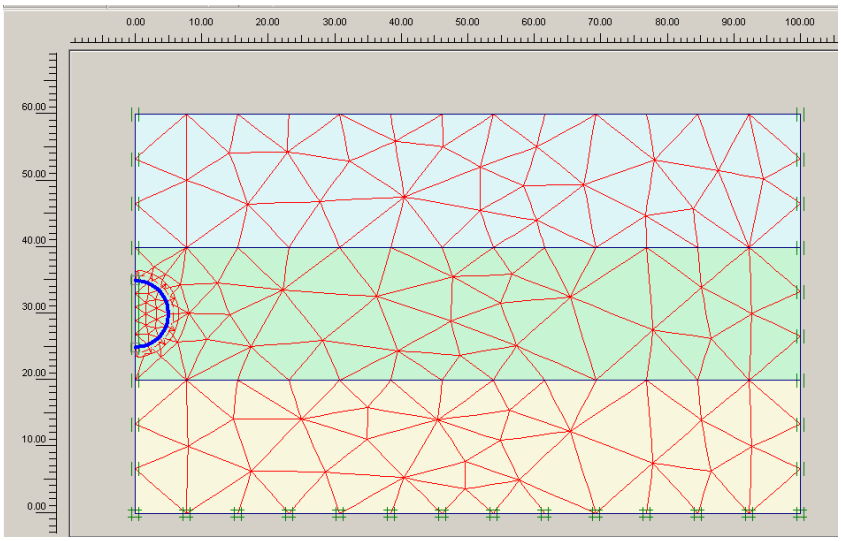

Figure 3.6. Geometry and mesh used for the 3-layer 2D analyses of a single tunnel in PLAXIS

3.3.1.3.3. 1-layer 3D single tunnel – Half of the geometry was simulated in this case. The ground was represented by a 100 m x 60 m x 60 m (*x, y* and *z* respectively) block (see Figure 3.7). The right-hand side of a 10 m diameter circular tunnel was simulated with its centre at 30 m depth from the ground

surface level. In the *z* dimension, 16 planes (coded from A to P) were defined including the front and rear planes, the first thirteen spaced at 2.5 m and the last three spaced at 10 m.

The tunnel excavation was considered to extend over the first 30 m (from z-plane A to z-plane M). The spacing of 2.5 m between z-planes along its length represented each of the slices in which the tunnel construction sequence was divided (i.e. 12 in total). The construction process was divided into 24 stages and consisted of the excavation of the first slice (first stage), the placement of the lining on that slice (second stage), the excavation of the second slice (third stage) and so on. For the purposes of this study, support was not provided to the open face of the tunnel in any of the 3D analyses.

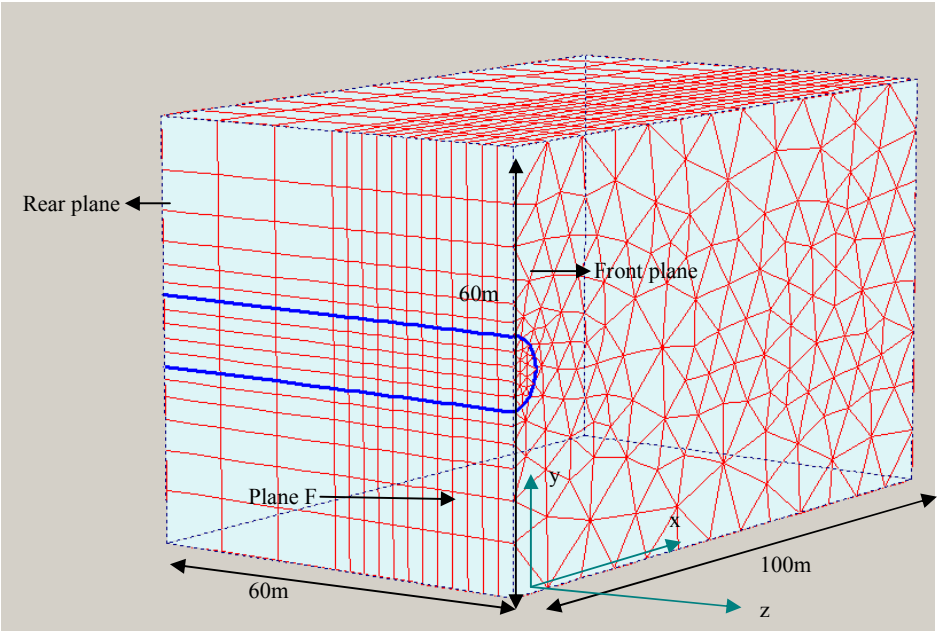

Figure 3.7. Geometry and mesh used for the 1-layer 3D analyses of a single tunnel in PLAXIS

3.3.1.4. Stress measurement points

The selected points in the ground in order to study the stress changes during the tunnelling operations in two-dimensions were:

i) Single tunnel

-Point A above the tunnel crown

-Point B to the side of the springline

ii) Twin tunnels

-Point C in between both tunnels at springline level

The coordinates for these points are shown in Table 3.2.

Table 3.2. Coordinates for the stress measurement points in PLAXIS

Stress point	Criterion	1-layer Single	3-layer Single	1-layer Twin 1 *d*	1-layer Twin 1.5 *d*	1-layer Twin 2 *d*
A	x,y PLAXIS	(0.144, 30.832)	(0.179, 39.502)	-	-	-
	y,z Figure 3.2	(0.144, 19.168)	(0.179, 20.498)			
B	x,y PLAXIS	(8.352, 19.933)	(7.678, 29.965)	-	-	-
	y,z Figure 3.2	(8.352, 30.067)	(7.678, 30.035)			
C	x,y PLAXIS	-	-	(0.451, 20.134)	(-1.671, 20.123)	(0.032, 19.647)
	y,z Figure 3.2			(0.451, 29.866)	(-1.671, 29.877)	(0.032, 30.353)

Due to the dimensions of the elements used in the FEA and the particular aspects of each geometry (i.e. modelling of only half or the whole geometry; variable distances between twin tunnels), the PLAXIS stress points A, B and C were selected for each analysis as similar as possible to allow proper comparison of the results, but some differences were unavoidable. Theoretically, shear stresses would not be expected at points situated on the vertical axis above the tunnel centreline, but due to the geometry of the finite element mesh and the coordinates of points A, some could be taking place. The shear stresses are also expected to be smaller at the springlines that at other points (e.g. points situated at 45 ^{o} from the vertical), but these are more likely than at the tunnel crown due to the deformation mechanisms occurring around the tunnel during excavation. The occurrence of shear stresses was noted for every analysis in Table 3.1 and for every measurement stress point according to the PLAXIS sign criterion illustrated in Figure 3.8.

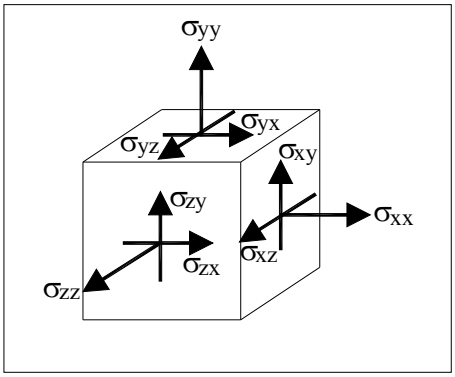

Figure 3.8. Positive coordinate system (including shear stresses) in PLAXIS

For the 3D analyses of a single tunnel excavation, two points A* (above the tunnel crown) and B* (to the side of the springline) were also investigated. In this case the measurement section was fixed at a distance of 15 m behind the front section (z-plane G in Figure 3.9). According to the construction sequence earlier explained, six slices of the tunnel would then be excavated (and supported) before reaching the instrumented section and six slices afterwards. As in the 2D case, due to the geometry of

the elements in the mesh, the stress points could well be situated slightly in front or behind the z = -15 m plane and could also be experiencing small shear stresses.

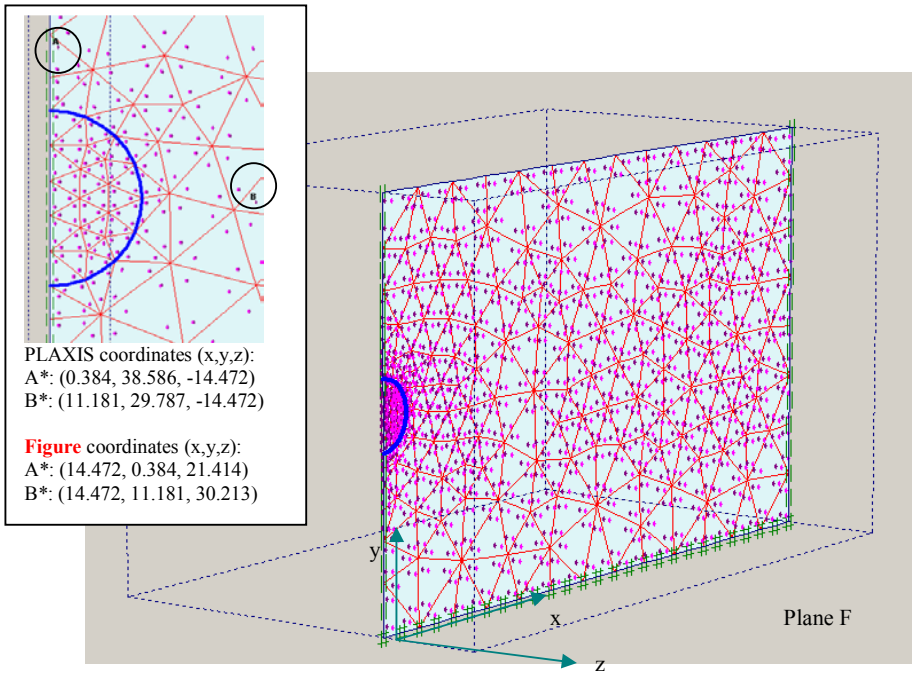

Figure 3.9. Measurement stress points in the PLAXIS 3D analyses

3.3.1.5. Parameters

For the lining, elastic behaviour was assumed and the following parameters were used and kept constant for all the analyses:

EA:	Axial stiffness:	4.4 x 10^7 kN/m
EI:	Flexural rigidity:	4.5 x 10^5 kNm^2/m
d:	Plate thickness:	0.35 m
w_l:	Weight:	30 kN/m/m
ν_l:	Poisson's ratio:	0.15

The soil parameters used for the different analyses are summarised in Table 3.3 for the 1-Layer and the 3-Layer geometries and are specified for each constitutive soil model. The selection of the parameters was arbitrary, but sensible values were used based on those reported for London Clay. The parameters used for the small-strain pre-yield Jardine et al. (1991) model were taken from Potts and Zdravkovic (2001) for a stiff clay and were therefore likely to be not "equivalent" to those used for the other constitutive models in PLAXIS. This was not crucial for the present study since only trends in behaviour were investigated. However, and in order to better appreciate the differences between the

various soil parameters and evaluate their effects in the predicted soil behaviour, a simple triaxial undrained tests was reproduced in PLAXIS. The results are shown in Appendix A – Section A.2. The differences were considered interesting on their own as part of the stress path sensitivity evaluation.

Table 3.3. Soil parameters used for the different PLAXIS analyses

1-LAYER ANALYSES							
γ_{unsat}: 16 kN/m^3		γ_{sat}: 19 kN/m^3		$K_x = K_y = 1{\cdot}10^{-6}$ m/day			
Elastic		Mohr-Coulomb		Hardening		Jardine et al. (1991) + Mohr-Coulomb	
E	400000 kPa	E	400000 kPa	E_{50}	400000 kPa	$C1$	862
E_Δ	5000 kPa/m	E_Δ	5000 kPa/m	E_{oed}	300000 kPa	$C2$	862
ν	0.3	c'	5 kPa	E_{ur}	1200000 kPa	$C3$	0.0005
		c'_Δ	0	m	0.4	α	1.348
		ν	0.3	c'	5 kPa	γ	0.58
		ϕ'	24^o	c_Δ	0	$\varepsilon_{d,min}$	0.0121
		ψ	0°	ϕ'	24^o	$\varepsilon_{d,max}$	0.866
				ψ	0°	G_{min}	1000
				ν_{ur}	0.2	$C4$	375
				p_{ref}	100 kPa	$C5$	315
				K_0^{nc}	0.593	$C6$	0.0008
				R_f	0.82	δ	1.462
						λ	0.77
						$\varepsilon_{v,min}$	0.004
						$\varepsilon_{v,max}$	0.2
						K_{min}	1000
						c'	5
						ν	0.3
						ϕ'	24
						ψ	0

3-LAYER ANALYSES											
Top layer				Middle layer				Base layer			
γ_{unsat}	15 kN/m^3			γ_{unsat}	16 kN/m^3			γ_{unsat}	17 kN/m^3		
γ_{sat}	18 kN/m^3			γ_{sat}	19 kN/m^3			γ_{sat}	20 kN/m^3		
$K_x = K_y$	$1{\cdot}10^{-5}$ m/day			$K_x = K_y$	$1{\cdot}10^{-6}$ m/day			$K_x = K_y$	$1{\cdot}10^{-7}$ m/day		
K_0	0.840 (K_0<1) or 1.450 (K_0>1)			K_0	0.730 (K_0<1) or 1.180 (K_0>1)			K_0	0.593 (K_0<1) or 0.840		
Elastic		Mohr-Coulomb		Elastic		Mohr-Coulomb		Elastic		Mohr-Coulomb	
E	300000 kPa	E	300000 kPa	E	400000 kPa	E	400000 kPa	E	500000 kPa	E	500000 kPa
E_Δ	5000 kPa/m	E_Δ	5000 kPa/m	E_Δ	5000 kPa/m	E_Δ	5000 kPa/m	E_Δ	5000 kPa/m	E_Δ	5000 kPa/m
ν	0.3	c'	5 kPa	ν	0.3	c'	5 kPa	ν	0.3	c'	5 kPa
		c'_Δ	0			c'_Δ	0			c'_Δ	0
		ν	0.3			ν	0.3			ν	0.3
		ϕ'	24°			ϕ'	24°			ϕ'	24°
		ψ	0°			ψ	0°			ψ	0°

3.3.1.6. Sensitivity analyses

The geometry and model characteristics in "S1LC1MCDRY_N2D" ($K_0 = 1$) were used to perform sensitivity analyses for the stress paths defined in terms of total stresses with respect to the soil and lining parameters, as well as the mesh coarseness. It should be noted that because of time constraints and also due to the similarities in the stress path trends observed using the different constitutive models, only the soil parameters in the Mohr-Coulomb failure criterion were investigated. The effect

of varying the mesh coarseness was studied in terms of the settlements predicted at the ground surface since the same stress measurement points could not be selected given the differences among the various meshes. The effects of varying the lining parameters *EA*, *EI* and weight w_l were further investigated for K_0-conditions less than and greater than unity (using the analyses S1LC+1MCDRY_N2D and S1LC-1MCDRY_N2D). The effect that varying c', ϕ' and ψ had on the stress paths at the crown and springline, as well as the effect of the coefficient of earth pressure at rest on the predicted surface settlement trough in PLAXIS using S1LC+1HRDRY_N2D as the reference analysis were also investigated. For the latter, reference was made to the occurrence of plastic points. It should be noted that when studying the effect of varying ϕ' using the Hardening model, the OCR had to be modified when calculating the initial stresses in order to keep K_0 around 1.5 (Equation 3.3) since K_0^{nc} depends on ϕ' according to Equation 2.29. Additionally, the analysis S1LC+1HRDRY_N2D was re-run for various *m* values for an initial soil stress condition corresponding to $K_0 = 1.52$. The parameter *m* dictates the level of stiffness dependency on stress level in such a way that the smaller the value of *m* the slower the variation of stiffness with stress. The results were illustrated in terms of the surface settlement profile. The parameters investigated in each case and the values used are summarised in Table 3.4. A sensitivity analysis for the 3D models was not carried out due to the computing time required.

Table 3.4. Parameters values used for the sensitivity analyses of the PLAXIS models

Parameter			Values used for the sensitivity analysis
S1LC1MCDRY_N2D (K_0=1)			
E	kPa	Soil Young modulus	10000 / 100000 / 400000 / 700000 / 4000000
c'	kPa	Soil cohesion	5 / 10 / 15 / 20
ϕ'	Degrees	Soil friction angle	20 / 22 / 24 / 30
ν_s	-	Soil Poisson´s ratio	0.25 / 0.30 / 0.35
E_Δ	kPa	Increment of *E* with depth	0 / 1000 / 5000 / 10000
c'_Δ	kPa	Increment of *c'* with depth	0 / 0.5 / 1.0
ψ	Degrees	Dilatancy angle	0 / 2 / 5 / 20
EA *EI* *d*	kN/m kNm²/m m	Lining axial stiffness and flexural rigidity	(1) EA=4.400E+06 / EI=4.500E+04 / d=0.350 (2) EA=4.400E+07 / EI=4.500E+05 / d=0.350 (3) EA=4.400E+08 / EI=4.500E+06 / d=0.350 (4) EA=8.600E+07 / EI=4.500E+05 / d=0.251 (5) EA=4.400E+07 / EI=7.500E+05 / d=0.452
w_l	kN/m/m	Lining weight	10 / 20 / 30 / 40
ν_l	-	Lining Poisson´s ratio	0.12 / 0.15 / 0.18 / 0.21
Mesh	-	Mesh coarseness	Very coarse / Coarse / Medium / Fine / Very fine
S1LC-1MCDRY_N2D (K_0<1) and S1LC+1MCDRY_N2D (K_0>1)			
EA *EI* *d*	kN/m kNm²/m m	Lining axial stiffness and flexural rigidity	(1) EA=4.400E+06 / EI=4.500E+04 / d=0.350 (2) EA=4.400E+07 / EI=4.500E+05 / d=0.350 (3) EA=4.400E+08 / EI=4.500E+06 / d=0.350 (4) EA=8.600E+07 / EI=4.500E+05 / d=0.251 (5) EA=4.400E+07 / EI=7.500E+05 / d=0.452
S1LC+1HRDRY_N2D (K_0>1)			
c'	kPa	Soil cohesion	5 / 10 / 15 / 20

Parameter			Values used for the sensitivity analysis
ϕ'	Degrees	Soil friction angle	(1) 20 (OCR=3.11 to have K_0=1.519) (2) 22 (OCR=3.38 to have K_0=1.519) (3) 24 (OCR=3.70 to have K_0=1.520) (4) 30 (OCR=5.10 to have K_0=1.525)
ψ	Degrees	Dilatancy angle	0 / 2 / 5 / 20
K_0 (OCR)	-	Coefficient of earth pressure at test and corresponding OCR	(1) K_0=1.005, OCR=2.200 (2) K_0=1.101, OCR=2.480 (3) K_0=1.201, OCR=2.770 (4) K_0=1.300, OCR=3.060 (5) K_0=1.400, OCR=3.350 (6) K_0=1.520, OCR=3.700
m	-	Parameter controlling the stress dependency of the soil stiffness	(1) K_0=1.520, m=0 (constant stiffness) (2) K_0=1.520, m=0.2 (2) K_0=1.520, m=0.4 (3) K_0=1.520, m=0.6 (4) K_0=1.520, m=0.8 (5) K_0=1.520, m=1.0 (linear stiffness with stress)

3.4. SELECTION OF SOIL FOR TESTING

Considering the context introduced in Section 3.2, the initial idea was to form reconstituted or remoulded samples from London clay, but the supply of this material was not possible at that time. Due to this, processed Kaolin clay was selected for the study, which would eventually help in improving repeatability throughout the project. Kaolinite mineral is known to be of a very common occurrence in soils of engineering interest (Mitchell and Soga, 2005). The samples were prepared by one-dimensional consolidation from slurry. Further details on their preparation are given in Section 3.5. Two types of Kaolin clay are commonly used in the Soils Laboratory at the University of Birmingham: (1) English China clay PURAFLO 50 supplied by WBB Minerals in Sandbach (Cheshire, UK) and (2) Speswhite Kaolin clay supplied by Witchem Ltd in Newcastle (Staffordshire, UK). The Speswhite Kaolin clay was finally chosen for the current project since other researchers into the field of tunnelling in the Department had been using this material and comparison of results would be easier if this was required. Three Index tests (*LL* and *PL*) were carried out for each of the two Kaolin clays in accordance with British Standard 1377-2:1990 and an average taken. For the Liquid Limit test the cone penetrometer method was used. This allowed observing a comparison of the *LL* and *PL* results for the different Kaolin clays to the published literature. Two specific gravity (*Gs*) tests were also carried out for the Speswhite Kaolin clay in accordance with the British Standard 1377-2:1990 and an average value was taken. The results for these tests can be found in Section 5.2.

3.5. PREPARATION OF RECONSTITUTED SAMPLES

3.5.1. Equipment

3.5.1.1. Consolidation Device A

A new device was designed and built for preparing K_0-consolidated samples from slurry based on the review of previous experiences worldwide. The final prototype was a modified version of a previous technique used at the University of Birmingham by Burns (2006) originally based on the work by Atkinson et al. (1990). This device is referred to as Device A in this thesis. For the design, and in order to reduce costs and manufacturing time, all the resources in terms of materials, machinery and space available in the laboratory were investigated. Even so, at least six months were required to have the device made and fully working.

Consolidation devices can be described as having two distinct parts: the consolidation chamber and the pressure system. The pressure system in Device A consisted of a vertical rod with a rigid smooth stainless steel piston at one of the extremes and horizontal plates attached to the former to allow for the application of dead weights. The main body of the consolidation chamber comprised an acrylic transparent tube (so that the soil could be seen at all times) of 50 mm internal diameter held vertically by three horizontal discs and three vertical rods. The use of larger diameter tubes was also considered, but there were obvious limitations in terms of the maximum vertical effective stress that could be applied using weights alone. The length of the transparent acrylic tube was long enough to have samples longer than 150 mm at the end of the consolidation process and for all the maximum values of the vertical effective stress likely to be applied. This would permit the formation of a specimen from the less disturbed central part of the sample and using the remaining material for determination of w and undrained shear strength (c_u) as required. An outline drawing of the device is shown in Figure 3.10 and a typical set up is illustrated in Figure 3.11. An acrylic tube of length 360 mm was found to be appropriate for sample preparation. Dial gauges were used for measuring the settlement during consolidation, and a scaled tape was attached to the tube as a secondary check. The minimum readable settlement in the dial gauges was 0.002 mm. Drainage was allowed both in the upward and downward directions by placing plastic ballotini balls (2.5 mm diameter), wet Whatman No. 52 hardened filter paper folded into a cup shape and metallic meshes at both ends (Figure 3.12), and excess water was allowed to drain out of the chamber during the process. For this project a steel frame was built to allow fours samples to be prepared at the same time.

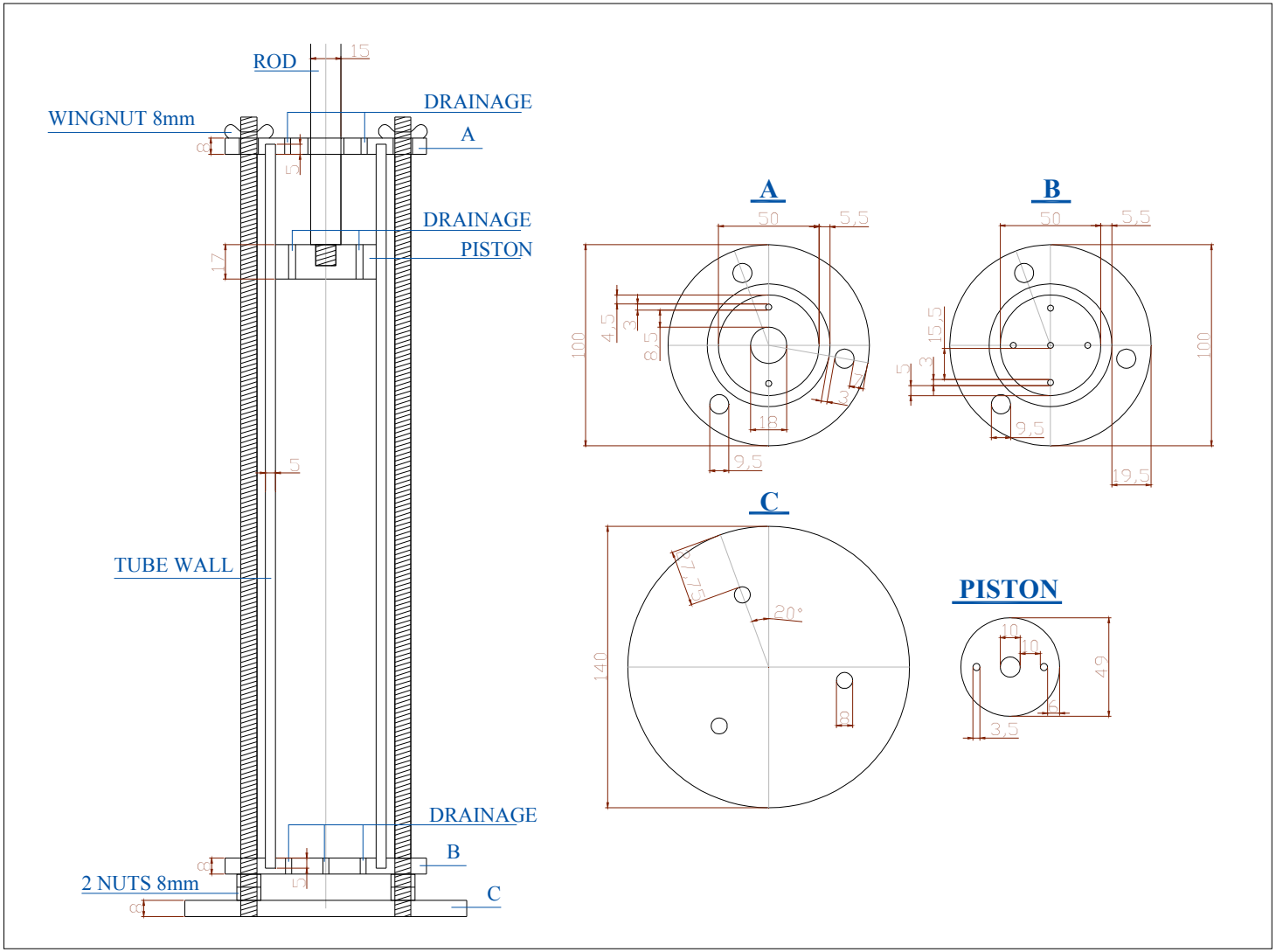

Figure 3.10. Scaled front elevation and plan views of consolidation Device A. (units are in mm)

Figure 3.11. Consolidation Device A

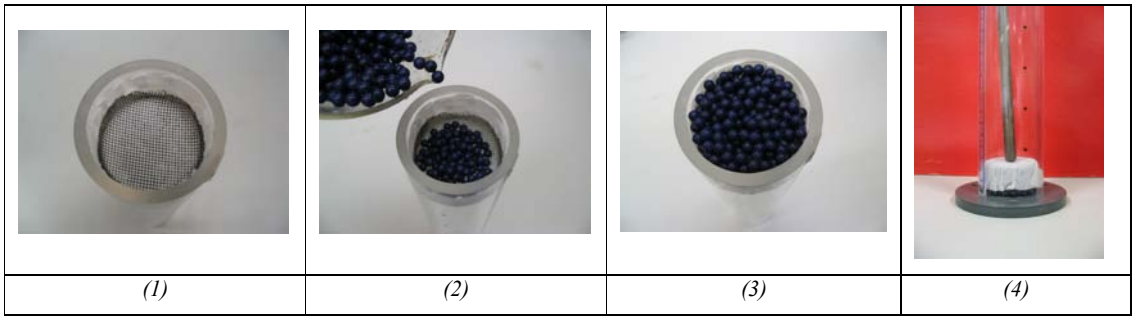

(1)	(2)	(3)	(4)

Figure 3.12. Sequence of preparation of the drainage layers in consolidation Device A, from the placement of the wet filter paper and metallic mesh, to the smooth compaction of the layer prior to pouring the slurry into the tube

3.5.1.2. Consolidation Device B

According to the initial results using the consolidation Device A, large vertical stresses were required in order to obtain firm to stiff samples. These high stresses could not safely be achieved in Device A, therefore the suitability of another consolidation device, developed by Liaki (2006), was investigated. In this case the consolidation chamber would remain the same, but the pressure system would use compressed air and three hydraulic jacks instead (Figure 3.13). Unfortunately, the preliminary tests demonstrated that without many modifications to the system the equipment was not suitable for the purpose. Although there were conversations with the supplier to design an improved system, it was apparent that this could not be purchased and commissioned in time for the current project.

Fortunately, later results using Device A (Section 5.3.7) demonstrated that the required undrained shear strength for the samples could be reached using Device A simply by taking additional safety precautions.

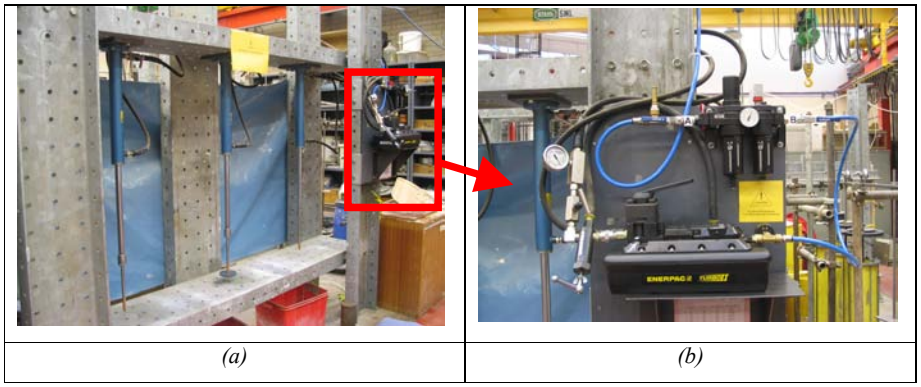

(a) (b)

Figure 3.13. Consolidation Device B: (a) Pump, hydraulic jacks and rig, (b) Detail of the compressed air pump

3.5.2. Preparing the Slurry

For each sample, 550 g of dry Speswhite Kaolin clay was mixed with enough water to form a slurry with a *w* of 1.5 times the soil *LL* in a mechanical mixer for 1.5 hours according to conventional practice (Section 2.3.1). The prepared saturated mixture, was then carefully poured into the consolidation chamber to an initial height of 295 mm trying not to trap any air. Some stirring was carried out to avoid big air bubbles and any possible predetermined arrangement of the soil particles within the soil. Under these conditions the initial void ratio (e_0) and the equivalent height of solid particles (*Hs*) were calculated as 2.535 and 83.451 respectively according to BS 1377-5:1990.

3.5.3. Load Sequence

The initial load applied to the slurry always corresponded to the weight of the rod plus the piston (just under 16 kPa) which were greased with WD-40 at the beginning of each sample preparation to reduce friction. The sequence of weights used varied according to the maximum vertical effective stress required and the ultimate purpose of each sample. Every load step was held for a minimum of 48 hours and a maximum of 72 hours to ensure that primary consolidation was complete. This was corroborated for the first thirteen samples and for every load step using the compression readings and the square root of time method according to British Standard 1377-5:1990 until at least primary consolidation was attained. The samples were left in the consolidation device until they were required for testing.

3.5.4. Extrusion and Trimming of Samples

After consolidating the soil to the required maximum vertical effective stress, the samples were removed from the consolidation chamber using a piston extruder. The samples were then trimmed with a very thin saw and a split mould (Figure 3.14). When extruded, care was taken to push in the same direction as during consolidation (i.e. from top to bottom). An exception to this was the first group of samples being prepared (samples "INi" in Section 3.5.5.1). The same orientation was also used afterwards in the triaxial cells.

(a)

(b)

Figure 3.14. (a) Sample extrusion and (b) Trimming kit

3.5.5. Study of the Characteristics of the Reconstituted Samples

The study of the characteristics of the K_0-consolidated samples was divided into four different stages:

1) Stage 1:
   Preliminary investigation. Presenting the initial results and the shortcomings observed
2) Stage 2:
   A more in depth investigation to evaluate the significance of the observations made during Stage 1.
3) Stage 3:
   A study into the distribution of stresses inside the consolidation Device A
4) Stage 4:
   Some subtle variations to Device A in order to observe the effects on the prepared specimens

The results from this part of the study are presented and discussed in Chapter 5.

It should be noted in here that the main aims of this part of the project were to: (1) Understand the limitations, if any, inherent to the use of the Device A, which is not very different from others used

worldwide and (2) gain a better understanding of the characteristics of the prepared samples using this particular device in order to take the necessary actions during subsequent testing. The results have been reported so that future researchers can make more informed decisions when it comes to designing consolidation devices to prepare reconstituted samples. However, although a few changes considered to be of interest were made to Device A and the effects on the prepared samples reported, it was well beyond the scope of this research to develop a 'more suitable' design. In fact the author believes that each particular design, together with the method of trimming the samples, has its own effect on the prepared specimens, so the concept of being 'more suitable' is only relative. The important point was considered to be the identification of the particular characteristics of the samples prepared in Device A for the present study in such a way that the limitations observed would not be considered limitations any more, but these would provide the possibility to do appropriate amendments during subsequent testing.
The following sections describe the procedure followed for each of the stages above.

3.5.5.1. Stage 1 – Preliminary investigation

The first group of samples was prepared with the following objectives:

i) Testing the performance of the consolidation device

ii) Study the repeatability of the samples in terms of the void ratio (e)

iii) Observing the effect, if any, of using different types of water (tap, de-ionized, de-ionized de-aired) in terms of void ratio changes and the relationships between liquidity index c_u - (IL), c_u - maximum vertical effective stress ($\sigma_{v'max}$) and w - $\sigma_{v'max}$. Most of the ions in the tap water supplied by Severn Trent Water in the area would have been removed during de-ionization, as well as the organic matter. For five random days over a period of two months, three samples were taken from each water: de-ionized, tap water not having been running for at least 6 hours, and the same tap water but after this having been used normally in order to perform conductivity tests using a pre-calibrated Hanna HI 9033 portable multi-range with an accuracy of ±1 % of the reading taken. These tests were used as an indirect method for comparing the amount of ions present in the waters and its variability over time. The results are compiled in Table 3.5 expressed in terms of the total dissolved ions (TDS). It can be observed that the ion concentration in the tap water with an average value of 61.6 mg/l TDS is almost 24 times higher that that of the de-ionized water with an average concentration of 2.6 mg/l TDS. A table showing the average composition of the tap water in the University area was supplied by Severn Trent Water and has been included in Appendix B for information.

Table 3.5. Measurements of conductivity for de-ionized water (DI), tap water no running for a long period of time (TNR) and running tap water (TR). Units are in mg/l TDS

	Day 1			Day 2			Day 3			Day 4			Day 5		
	DI	TNR	TR	DI	TNR	TR	DI	TNR	TR	DI	TNR	TR	DI	TNR	TR
Sample 1	2.35	64.10	63.50	3.60	63.75	61.70	2.35	61.10	58.15	2.30	61.70	60.95	2.40	62.40	60.35
Sample 2	2.35	64.10	63.50	3.70	63.85	61.80	2.35	61.30	57.95	2.30	60.30	60.75	2.40	60.95	60.50
Sample 3	2.30	64.20	63.60	3.65	64.40	61.80	2.35	61.05	58.00	2.35	60.20	60.70	2.40	60.90	60.60

iv) Evaluating which $\sigma_v'_{max}$ was required in order to prepare firm to stiff samples (c_u = 75 to 100 kPa)

v) Performing various types of triaxial tests on some 100 mm long trimmed specimens in order to learn about the performance of the available triaxial equipment.

The details of each of these samples are listed in Table 3.6.

Table 3.6. Details for the first group (IN i) of samples

Sample Code	$\sigma_v'_{max}$ (kPa)	Water type
IN 1.1	301	Tap
IN 1.2	450	Tap
IN 1.3	620	Tap
IN 1.4	770	Tap
IN 1.5	1017	Tap
IN 1.6	903	Tap
IN 1.7	1114	Tap
IN 1.8	620	Tap
IN 1.9	804	Tap
IN 2.1	639	De-ionized
IN 2.3	639	De-ionized de-aired
IN 2.4 (*)	639	Tap

NOTES: (*) This sample is the only one that was allowed to swell back after reaching the maximum vertical effective stress

During extrusion of these samples, c_u was measured at the top with a 12.7 mm hand vane. From one to three (depending on the final length of the sample) sub-samples from the remaining soil (close to the base) were taken for determination of w. If required, a specimen was also trimmed from the centre for triaxial testing. Figure 3.15 illustrates the measurement of c_u and a picture taken of one extruded sample indicating the use given to the different parts.

As a result of some improvements made to the supply of de-ionized water in the laboratory, and the outcome from point iii) above, de-ionized water was used for all the specimens prepared for the project after this initial group had been tested. The objective of this was keeping the soil-water chemical interactions as constant as possible (e.g. cation exchange, flocculation) as these may condition the fabric

created during consolidation therefore influencing the engineering properties of the soil (Mitchell and Soga, 2005).

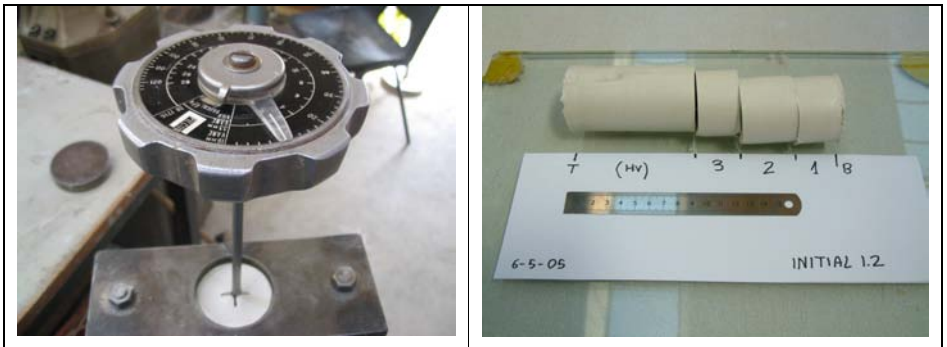

(a) (b)

Figure 3.15. (a) Hand vane measurement of c_u and (b) Picture showing the code, date and use of the different parts of the extruded sample: "T" (top of the sample), "B" (base of the sample), "HV" (part used for c_u determination by the hand vane), "1", "2" and "3" (parts used for moisture content determination)

A second group of samples was prepared in order to perform unconsolidated undrained triaxial tests on the 100 mm long specimens trimmed from the middle part and then corroborate the c_u values measured using the hand vane. In this way it could be deduced whether the maximum possible pressure in consolidation Device A was enough or whether other equipment would be required. Particulars of these specimens are described in Table 3.7.

Table 3.7. Details for the group of specimens prepared for unconsolidated undrained triaxial testing

Specimen Code	$\sigma_{v'max}$ (kPa)	Water type
UU2	757	De-ionized
UU3	1065	De-ionized
UU4	404	De-ionized
UU6	1065	De-ionized

The first three samples, UU2, UU3 and UU4, were tested using conventional triaxial equipment (Section 3.6.1.3), and the GDS Standard Stress Path equipment (Section 3.6.1.2) was used for testing the sample UU6. The tests were carried out in accordance with British Standard 1377-7:1990 (including membrane correction) with the exception of UU2 for which the initial p' was measured (refer to Section 3.6.2). All these tests were strain controlled at a rate of 0.066 mm/min and there was no measurement of u. The moisture content of the sample after failure was only measured for UU2.

The initial p' measurement in the triaxial cells for sample UU2 was compared to the p' value predicted by Skempton's (1954) (Equation 2.28) using sensible values for A as indicated by Skempton

and Bjerrun (1957) and Atkinson and Bransby (1978) equal to 1/3, 1/2 and 2/3 and $B = 1$. This was also later done for all the specimens used for the present project.

3.5.5.2. Stage 2 – Secondary investigation

Based on Stage 1, some shortcomings were identified and a more detailed follow-up investigation was carried out to account for the significance of these observations. Other samples were therefore prepared. The maximum vertical effective stress to which they were consolidated and the individual objectives are detailed in Table 3.8.

Table 3.8. Samples prepared during Stage 2: details and aims of the tests

Sample code	$\sigma_{v'max}$	e after consolidation	Aim of the test
w1	138	1.552	Evaluating the variation in moisture content along the sample
w2	202	1.457	
c_uw	404	1.361	Measuring the moisture content variation along the sample and corresponding undrained shear strength calculated by using the Fall-cone method (Hansbo, 1957 and 1994)
C1 (Subsamples C1A, C1B and C1C)	358	1.379	Observing the arrangement of the clay particles within the sample using a Scanning Electron microscope (SEM)

The methodology followed for each test was as follows:

i) Samples "w1" and "w2"

These two samples were consolidated to vertical effective stresses of 138 and 202 kPa respectively to observe the distribution of w along their length by dividing them into 7 sections.

ii) Sample "c_uw"

This sample was prepared in order to use an alternative technique for estimating c_u along the length of the samples. This testing method, developed by the Geotechnical Commission of the Swedish State Railways, is based on the use of a cone penetrometer and known as the fall-cone test (Hansbo, 1957 and 1994). The theory, based on experimental results, proposes that the c_u of clay can be calculated according to Equation 3.6.

$$c_u = \frac{K_{cp} \cdot m_{cp} \cdot g}{{i_{cp}}^2} \cdot \left(1 + \frac{h_{cp}}{i_{cp}}\right) \qquad \text{[Eq.3.6]}$$

where K_{cp} is a constant whose magnitude depends on the cone angle, and is equal to 1 for a 30° cone, m_{cp} is the mass of the falling cone, g is the acceleration of gravity, and i_{cp} is the depth of penetration of the falling cone from a distance h_{cp} between the cone apex and the soil surface (zero in this case). The relationship is quadratic and so it is only appropriate for cone penetrations between approximately 4 and 20 mm. An average value of c_u, from where the 100 mm specimen would be trimmed (i.e. the central part), could then be calculated and compared with both the hand vane and the triaxial results for samples consolidated at the same $\sigma_{v\,max}'$.

During the extrusion of sample "c_uw", the cone penetrometer was dropped at 5 different positions on the surface of sections of material cut every 1 cm along the sample length. The moisture content of each of the discs was also determined.

iii) Sample "C1"

This sample was consolidated in Device A up to a maximum vertical effective stress of 358 kPa in order to study the potential arrangement of the clay particles. From this sample, three dry subsamples with undisturbed surfaces were taken to be studied in the Scanning Electron Microscope (SEM) as follows:

C1A: Horizontal cross-section close to the base of the sample.

C1B: Vertical cross-section close to the base of the sample.

C1C: Horizontal cross-section close to the top of the sample.

"C1" was considered as being representative of all the previous observations made by visual inspection on other samples.

3.5.5.3. Stage 3 – Measurement of u during K_0-consolidation

From the results obtained during Stages 1 and 2, it was found necessary to gain a better understanding of the stress distribution in the soil during the one-dimensional consolidation of the slurry when using consolidation Device A. The consolidation chamber was modified slightly in order to measure u at three different positions along its height. At these positions, situated at 90 mm (1/4), 180 mm (1/2) and 270 mm (3/4) (upper (U), intermediate (I) and base (B) points respectively) from the top of the acrylic cylinder, push-in connections were placed that joined 4 mm outer diameter pipes full of water to three calibrated 1000 kPa range pressure transducers (Figure 3.16). Silicon was used around the connections to improve the seal. On the wall of the tube, between each pressure line and the clay, filter paper was placed to stop the clay from being washed away during consolidation.

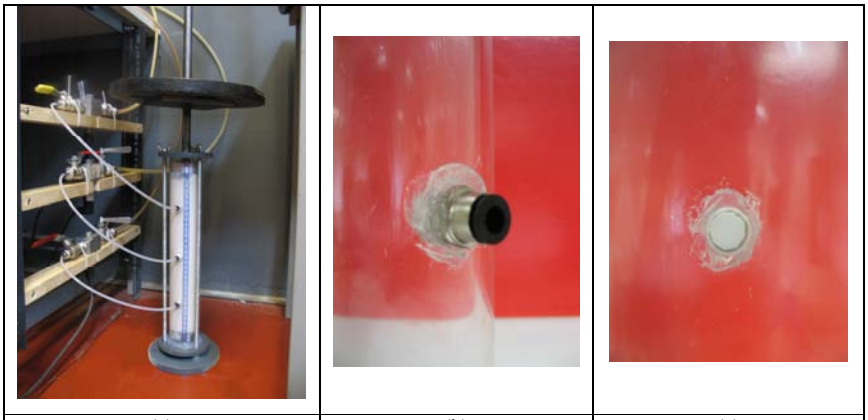

(a) (b) (c)

Figure 3.16. (a) Pore water pressure measurements at three positions equally spaced along the consolidation Device A (Upper, Intermediate and Bottom) during K_0-consolidation in tests F01, F02, F03 and F04, and details of (b) the push-in sealed connections and (c) the filter

The *u* measurements were logged at one minute intervals during between 30 and 210 hours depending on the test. The vertical stress was increased in four stages (20, 61, 143 and 358 kPa). Two tests, F01 and F02, were carried out without letting the pore water pressure dissipate between successive steps, assuming a short term undrained behaviour for the clay. This was done to gain an understanding of the *u* distribution along the height of the samples. Only after the last loading stage, was the soil allowed to drain, either only one-way (upwards) in test F01 or two-way in test F02. In order to delay the drainage during the application of the dead weights, the base of the cylinder was sealed and the top filter paper and ballotini balls were substituted by a rigid plastic disc wrapped in filter paper to simulate similar friction effects, but reducing the possibilities for drainage. For test F02 the base drainage was only closed during loading and then opened during the drainage stage. Two additional tests, coded F03 and F04, reproducing the drainage conditions explained in Section 3.5.1.1 were also performed.

At the end of test F03, *w* was measured along the sample by dividing it into 8 sections of soil, two of them containing positions I and B. c_u values were estimated for each of the moisture contents based on the results from sample "c_uw" (Section 3.5.5.2). Based on the final percentage of $\sigma_v'_{max}$ and *w* measured at positions I and B, the percentage of vertical effective stress applied at the other positions was calculated using the *w* data available. From these calculations, approximate relationships between $\sigma_v'_{max}$, c_u and *w* for individual locations along the sample were given.

3.5.5.4. Stage 4 – Modifications to Device A

Based on the observations made when using the consolidation Device A, some modifications were introduced to this device in order to observe the effect on the prepared samples. Some of these attempts were made close to the beginning of the project with the aim of adopting such modifications,

if found successful, for the rest of the project to maintain repeatability. These were intended not to introduce large variations to the Device A and consisted on trying to reduce the friction by using various coating-type techniques on the 50 mm diameter acrylic tube (e.g. WD-40 was used for the preparation of a specimen coded INWD).

Further modifications were made later on in the project. Since these investigations required significant variations into the design of Device A, they were planned to be performed towards the end of the project (only if time allowed) with the objective of improving the knowledge in this respect. This late modification consisted of using a larger diameter tube (i.e. 100 mm instead of 50 mm). A larger consolidation device, but with identical characteristics to those of Device A, had to be built for this purpose (Figure 3.17). Two samples, coded A100-1 and A100-2, were prepared to a $\sigma_{v'max}$ = 195 kPa.

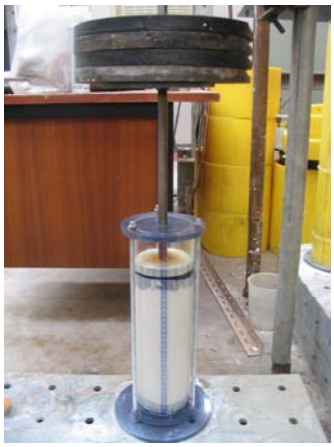

Figure 3.17. Adapted 100 mm inner diameter consolidation device

The changes in void ratio with σ_{v}' during one-dimensional consolidation for samples A100-1 and A100-2 were compared to that of sample C1 (Section 3.5.5.2). Samples A100-1 and A100-2 were inspected visually for the existence of more or less developed forms of clay orientation than in sample C1. The observations were then discussed.

3.6. TRIAXIAL AND STRESS PATH TESTING

3.6.1. Equipment

3.6.1.1. Large stress path equipment

The initial project planning (see also Chapter 1) included setting up a large stress path equipment that had been acquired some years before the present project started. Unfortunately this proved to be too deteriorated to be repaired in a sensible period of time therefore other equipment was used instead

as explained in the following sections. Additional details about this equipment can be found in Appendix A – Section A.3.

3.6.1.2. Standard Stress Path equipment - STDTTS and GDSLAB

Most of the laboratory tests carried out during this project were performed in a computer-controlled Standard Stress Path Triaxial Testing System manufactured partially by GDS and partially by Wykeham Farrance. The equipment had only been used in the Department by a previous researcher and on a very different field hence virtually no guidance on its use was provided. Starting from scratch and learning the state-of-the-art techniques related to this type of equipment, as well as updating the system to be able to perform the required tests, proved to be a slow process. The system is illustrated in Figure 3.18 and consists of the following main parts:

i) A Bishop and Wesley-type cell with a maximum working pressure of 1700 kPa including a 5 kN submersible load cell with pedestals for performing tests on 38 and 50 mm diameter specimens.

ii) Three GDS standard 3 MPa/200 cc pressure/volume controllers for:
(1) The cell pressure (CP);
(2) The back pressure (BP) and measurement of the specimen volume change;
(3) The application of the deviator stress to the sample by controlling the lower chamber volume (LC) in the movable base pedestal activated by a diaphragm and a guided piston.
The pressure and volume change resolutions for these controllers are 1 kPa and 1 mm^3 respectively. The pressure is provided hydraulically.

iii) One ±25 mm range external linear displacement transducer.

iv) One 1700 kPa range pressure transducer for the measurement of u.

v) One GDS 8-channel 16bit serial pad for data acquisition of the external displacement transducer, pore water pressure transducer and the load cell above, and any other additional transducers required.

vi) One GDS RS232 one-to-four serial pad convertor for the three pressure/volume controllers and the 8-channel data-logger.

vii) One water tank and de-airing pump system.

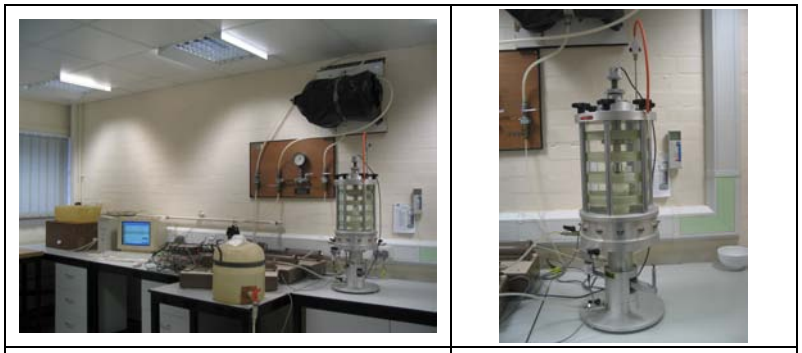

(a) (b)

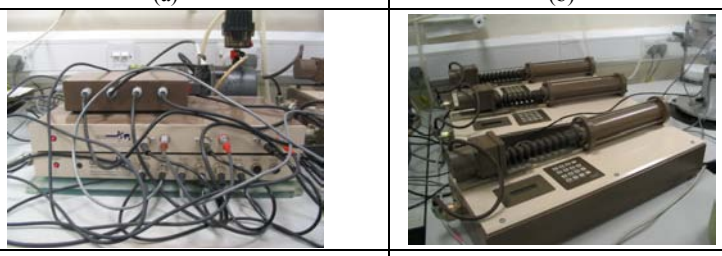

(c) (d)

Figure 3.18. Standard Stress Path equipment: (a) Equipment overview; (b) Stress Path Bishop and Wesley-type cell, (c) From top to bottom: RS232, ±2.5 mm LVDT's signal amplifier (see Section 3.6.1.2.3) and 8-channel data-logger, (d) Standard pressure/volume controllers

The original software available at the start of the project was the Standard Triaxial Testing System (STDTTS) supplied by GDS. After some time getting used to the system and many failed tests, it was realized that due to errors in this software it was not capable of reaching the residual strength when the specimens were sheared undrained, but only the peak strength could be achieved. This relatively old software was also not capable of performing some computer-controlled tests such as K_0-consolidation and no upgrade was available. The new GDSLAB software had to be installed. Only a few modules were purchased as follows:

i) Standard Saturation and Consolidation Module:
   - B-check
   - Saturation ramps of CP and BP
   - Isotropic consolidation

ii) Standard Triaxial Testing Module:
   - Unconsolidated-undrained
   - Consolidated-undrained with pore water pressure measurement
   - Consolidated-drained with pore water pressure measurement

iii) Advanced Loading Module with independent control (constant, ramp, cycle) of:
- Axial stress, axial strain or axial load
- CP
- BP
- Low frequency cyclic loading

iv) Stress Path Module:
- Linear stress paths using either q - p or t - s stress invariants

v) K_0-Module using either a direct measurement of the radial deformation (on-sample instrumentation) or an indirect measurement using the back volume.

For all the tests performed using this equipment, the BP was connected to the top of the sample and u was measured at the base.

The room where the equipment was situated was temperature controlled with a maximum variation of $\pm 2\ ^{o}C$ in spring/summer and $\pm 1\ ^{o}C$ in autumn/winter.

3.6.1.2.1. Zero pressure datum and calibration of standard components – When using the GDS computer-controlled Stress Path equipment, a zero pressure datum has to be fixed in order to ensure that all the pressure controllers measure consistently and from the same reference level. The procedure used for this is described in detail in Appendix A – Section A.4 together with details on the calibration of the different Stress Path cell standard components.

3.6.1.2.2. Extension kit – Extension tests had never been performed at the University of Birmingham before this project. In order to perform this type of test, two extension caps (puller and receiver), with the corresponding vylastic sleeve and connections to the cell are required. The receiver extension cap lies on top of the specimen and contains the line to the back-pressure. The puller extension cap is attached to the load cell. It has a sort of "V" shape pointing downwards with a flat base and contains a connection to a valve at the top of the cell that opens to atmosphere. The objective of the vylastic sleeve is to seal both caps together for the application of tensile stresses by creating a vacuum between them using the bleed valve that connects to the puller cap. The Wykeham Farrance extension caps available at the time did not have the best design to allow a proper seal and the application of high negative deviator stresses. After considering different options and checking with other users for appropriate performance, it was decided to buy a new set from GDS. The connections to the cell had to be adapted before they could be used. Figure 3.19 illustrates the two kits.

(a) (b)

Figure 3.19. 50 mm extension caps: (a) Detail of the gap between the puller cap and the vylastic sleeve in the Wykeham Farrance device , (b) Wykeham Farrance and GDS kits, left and right respectively

3.6.1.2.3. On-sample instrumentation – For a more accurate measurement of soil strains and for the evaluation of stiffness changes at small-strain range, using on-sample instrumentation was a requirement. Both high resolution linear LVDT´s (either ±2.5 mm or ±5.0 mm range) and the Hall Effect device were investigated and the suitability of each of them was carefully considered. Some enquiries were also made with regards to the acquisition of Bender Elements, but this option was rejected due to budget limitations. Based on its better accuracy (0.1 % of the full range output (FRO): 0.005 mm), robustness and the experience of third parties (personal communications), the ±2.5 mm range GDS LVDT's was purchased. The only foreseen difficulty in using such small range LVDT's was their initial positioning so that the LVDT's would not get out of range during the duration of the tests. These LVDT's were calibrated by the manufacturer. The complete small-strain system consists of three LVDT´s, two for measuring axial deformations and one for the measurement of the radial deformation, a stainless steel mounting calliper and a signal amplifier that connects to the GDS 8-channel data-logger mentioned in Section 3.6.1.2. To gain access to the cell for these transducers, a 12-access ring was also purchased (Figure 3.18b). The LVDT cables presented some initial problems because of their thickness and rigidity. The problem was conveyed to GDS and after approximately one year they manufactured a more flexible alternative. The cables were changed to this new version, which reduced the maximum allowable working pressure (from 3600 kPa to 1700 kPa), but facilitated the setting up. The reduction in allowable working pressure was not a constraint as this was also the maximum working pressure for the stress path cell. The mounting calliper consists of a circular frame to support the radial LVDT and two mounting blocks to hold the axial LVDT´s. The three parts were bonded to the membrane using silicon rubber compound 555-588 from RS Component International on the pads, and fixed to the specimen by pins. Silicon sealant was also placed all around the pins to

avoid any leakage from the specimen due to the pinning of the membrane. Some initial problems were also encountered with the mounting calliper. In summary, it can be said that the relative dimensions of the 50 mm diameter specimen, the different parts of the calliper and the LVDT´s were not the most appropriate to enable everything to be set up without risk of interaction during specimen deformation if using the LVDT´s over the middle 1/3 of the specimens (common approach). This meant that the measurements were taken over the mid ½ of the specimen. The arrangement for the device is illustrated in Figure 3.20. The initial positioning for the three LVDT's was selected individually for each test working out the expected positive movements (i.e. gauge getting shorter or specimen diameter decreasing) and negative movements (i.e. gauge extending or specimen diameter increasing) for each part of the test in order to have the LVDT's within their linear range when reaching the point at which the small-strain soil behaviour needs to be measured.

Due to a series of unexpected problems and the poor general performance of the radial LVDT (see Section 6.2.4), a ±3 mm range Hall Effect device prototype made of titanium (the conventional model is made of aluminium) was kindly supplied by GDS towards the end of the investigation to try to sort out the problems experienced and help achieve the project objectives. Although this device is lighter and easier to put in place (especially for soft specimens) compared to the LVDT's, they are not as robust and their accuracy is 0.8 % of FRO. The device resolution can be, as for the LVDT's, more than 10 times better than the accuracy. In order to fix the Hall Effect kit to the specimen, the mounting radial calliper and the vertical gauges were glued to the membrane and pinned to the specimen in the same way as for the LVDT's. The axial Hall Effect devices were placed over the middle 50 mm of each specimen as for the LVDT's. Figure 3.21 illustrates the Hall Effect device in place. The arrangement of the Hall Effect device presents less potential friction issues than the LVDT as the chip and magnet slide one against each other (see Figure 3.21b). Potential misalignments due to the weight of the LVDT's are also minimized with the Hall Effect device.

(a) (b)

Figure 3.20. (a) ±2.5 mm range LVDT axial and radial small-strain measurement device, (b) Detail of the radial arrangement

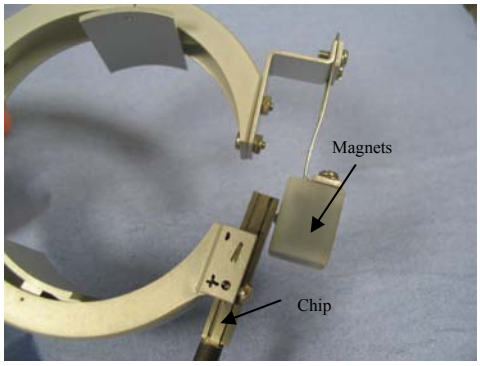

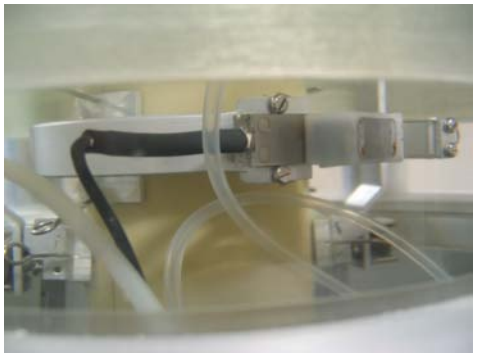

(a) (b)

Figure 3.21. (a) ±3 mm range Hall Effect device, (b) Detail of the radial arrangement

3.6.1.3. Conventional triaxial equipment – WINHOST

Since only one GDS Standard Stress Path device was available to run all the required tests and this required of some improvements, and there was not much experience in its use, a conventional triaxial equipment, with a 100 mm diameter cell, was initially used to perform some of the tests. Although it was useful to learn on and practice with, the poor state of maintenance of the equipment introduced more problems than advantages as will be seen later. In this equipment, illustrated in Figure 3.22, the cell and back pressures were provided by compressed air with a maximum working pressure of approximately 690 kPa and measured using 1000 kPa range pressure transducers. The back-pressure was applied at both the top and the base of the specimen and u was measured at the base. When pressures above 690 kPa were required, a constant pressure system with an interface oil/water (Pressure Test 1700 by ELE International) was used. The axial load was applied by a 50 kN Wykeham Farrance TRITECH digital load frame capable of running strain controlled tests at rates from 0.00001 to 5.99999 mm/min, this rate being corroborated by using an external linear ±25 mm transducer. The axial load was measured by a load ring with a dial gauge of 12 mm travel and 0.0002 mm divisions, calibrated by using a 50 kN Instron tension/compression machine in compression mode. Generally, this gauge was substituted by a ±10 mm range linear strain transducer in order to have a continuous record of the readings. The linear strain transducers were calibrated using a Wykeham Farrance calibration device with precision micrometer, and the pressure transducers were calibrated against the compressed air system in the laboratory. The sample volume change was measured by a WF17044 automatic volume change unit with a capacity of 100 ml and an accuracy better than ±0.05 ml connected to the BP line. All the data were logged using the Wykeham Farrance AT2000 16-channel data-logger using the WinHOST software. One of the reasons for not performing a large number of tests in this equipment was the fact that the data-logger only had a capacity of storing 1024 readings and so manual intervention was required for long tests, with the inevitable loss of some data. An independent water tank and de-airing pump system was available for this equipment.

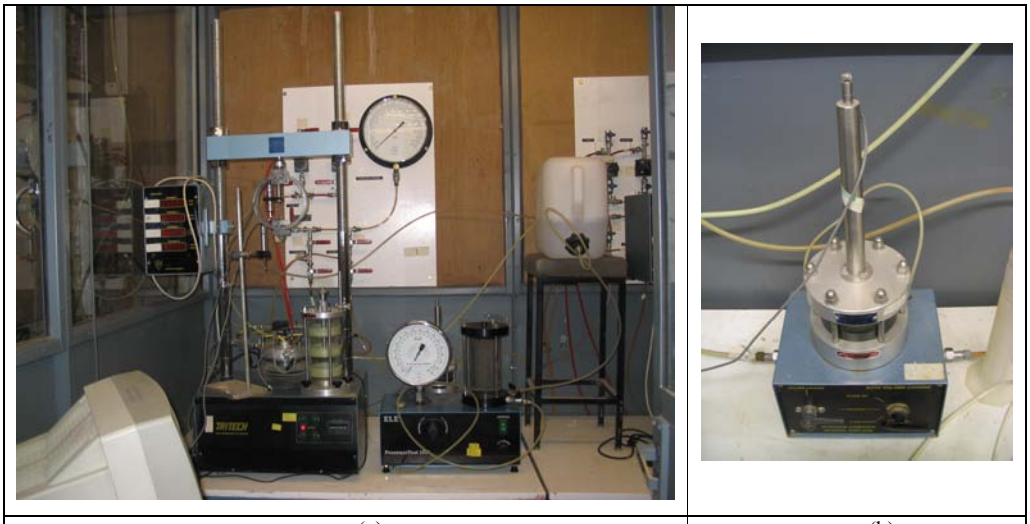

(a) (b)

Figure 3.22. (a) Conventional triaxial equipment and (b) Automatic volume change measuring apparatus

3.6.2. Critical State Tests

Despite the large amount of data available on Speswhite Kaolin clays, it was considered more appropriate (and accurate) to obtain specific critical state parameters for the particular soil in our laboratory instead of taking an average from published data. It should be noted, however, that the main objective of this part of the project was to obtain the necessary soil parameters for the subsequent parts of the project rather than actually performing a very extensive test programme to learn about the behaviour of Speswhite Kaolin, which is sufficiently well known. On the other hand, the proposal of performing some representative conventional triaxial tests was found to fit in well with an easy-to-complex strategy for learning due to the limited experience of using the stress path cell in the Department. These tests were carried out using either the conventional triaxial cell or the stress path equipment (the former was only used for some initial consolidated undrained tests whilst learning how to use the stress path equipment and whilst obtaining the required parts). The target parameters were as follows:

i) Effective cohesion for compression and extension states for both isotropically ($c_c'_{ic}$, $c_e'_{ic}$) and K_0-consolidated specimens ($c_c'_0$, $c_e'_0$)

ii) Mohr-Coulomb friction angles for compression and extension estates for both isotropically ($\phi_c'_{ic}$, $\phi_e'_{ic}$) and K_0-consolidated specimens ($\phi_c'_0$, $\phi_e'_0$)

iii) Drained Poisson's ratio (ν)

iv) Coefficient of earth pressure at rest (K_0)

v) Slope of the critical state line in a q - p' plane for compression and extension for both isotropically (Mc_{ic}, Me_{ic}) and K_0-consolidated specimens (Mc_0, Me_0)

vi) Slope of the isotropic consolidation line (ICL) in a v - lnp' plane (λ_{ic})

vii) Slope of the one-dimensional consolidation line in a v - lnp' plane (λ_0)

viii) Slope of the unloading-reloading (swelling) lines in a v - lnp' plane for isotropically consolidated specimens (κ_{ic})

ix) Specific volume of isotropically normally consolidated specimens at $p' = 1$ kN/m^2 (N_{ic})

x) Specific volume of K_0-consolidated specimens at $p' = 1$ kN/m^2 (N_0)

xi) Slope of the critical state line in a v - lnp' plane (λ_{cs})

xii) Specific volume of specimens on the critical state line at $p' = 1$ kN/m^2 (Γ)

On some occasions the symbols have been cut down for simplicity (e.g. M instead of Mc_0 *or* c_c' instead of $c_c'_0$ where the context is explicit). The results are presented and discussed in Chapter 6.

The sign criterion used for presenting the results was as follows: compressive stresses and strains positive, extension stresses and related strains negative.

This section describes in detail the tests performed and the procedures followed. The tests were carried out according to the British Standard 1377-8:1990 when using the conventional triaxial equipment. When the stress path cell was used, the procedure was conducted according to the same British Standard, but adapted in order to account for the more modern equipment and the availability of new techniques. As there are no British Standards for all the tests (e.g. extension tests), a review of the state-of-the-art in triaxial testing was also conducted and put into practice. For example, the fuse wire technique (Section 2.3.2) was used, after it came to the attention of the author, in order to reduce specimen disturbance (i.e. swelling). Figure 3.23 shows the wire arrangement used.

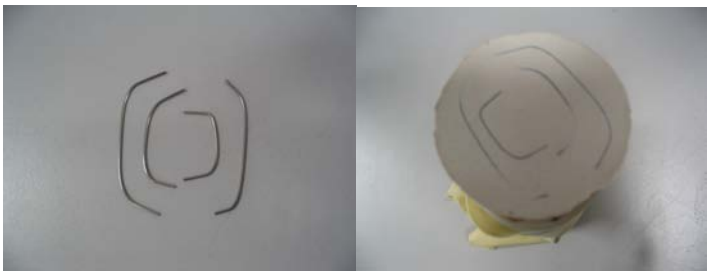

Figure 3.23. Fuse wire technique arrangement

The first stages of each test were identical and included setting up the specimen and the overall system, a B-check and an initial mean effective stress (p') measurement. Only when the extension caps and/or the on-sample instrumentation were used was some variation from this general procedure required, and this will be explained in the appropriate sections. The setting up of the specimen and system when using the Stress Path equipment is described below as it is a particular application of the British Standard 1377-8:1990.

General specimen and system set up:

1) Just after the extrusion of each sample from the consolidation device, a specimen was trimmed from the central-upper part and two sub-samples were taken from each of the remaining ends for moisture content determination.
2) De-aired water was used from a tank left under a vacuum pressure of -750 mmHg overnight the day before the test.
3) The volumes of water available in the three pressure/volume controllers (CP, BP and LC) were checked before starting any test, as well as the position of the lower chamber piston and the external displacement transducer.
4) The porous stones were submerged in de-ionised water, boiled for 30 minutes to remove any trapped air and then allowed to cool down to room temperature before using them.
5) The membrane was initially checked for fissures/holes by filling it with water and then leaving it slightly moistened before use.
6) The BP line was connected to the pore water pressure port to flush the system and remove any trapped air. This was continued until the water coming out from the base pedestal of the cell had no observable bubbles. Then the valve to the pore water pressure port was closed.
7) One porous stone was slid over the base pedestal trying not to trap air.
8) One filter paper was soaked in water, wrapped in absorbent paper to remove any excess water to prevent changes in *w* and then placed on top of the porous stone.
9) Non-corrosive wires (fuse wire technique) were carefully placed on top of the filter paper.
10) The specimen was placed, and correctly oriented, so that it was gently standing on top of the wires.
11) The moistened membrane was placed around the specimen using a stretcher.
12) Two rubber o-rings were placed to hold the membrane to the base pedestal.
13) Wires were also placed on top of the specimen.
14) Another moistened filter paper was placed on top of the wires.
15) A saturated porous stone was placed on top of the filter paper.
16) The BP line, if required for the specific test, was connected to the BP port and flushed to remove any trapped air.
17) The required top cap (standard-blind or standard with BP line) was slid on top of the porous stone. If the BP was required, then water was allowed to initially drip while sliding on the porous stone to avoid any trapped air bubbles. Once the top cap was in place, the valve to the BP was closed.
18) Two rubber o-rings were placed to hold the membrane tight to the top cap.
19) A thin coat of silicon grease was smeared on the edge of the loading piston.

20) The cell was put in place and checked for specimen/load cell alignment.
21) The load cell was fixed at an appropriate position according to the individual test conditions (generally close, but not touching the top cap for isotropic conditions) and in good agreement to the position of the lower chamber piston that was already connected to the lower chamber pressure/volume controller full of water (the valve was open).
22) The cell was tightened into place and the bleed valve at the top left open (the extension vacuum valve should be closed at all times during the setting up).
23) The cell was then filled with de-aired water using the CP port until it just came out of the bleed valve at the top of the cell. At this point, the valve to the CP was closed followed by the bleed valve at the top of the cell.
24) The cell pressure/volume controller was then connected to the CP port on the cell ensuring that no air was trapped in the pipe. At that point, when opening the valve, the cell pressure/volume controller measured about 3 kPa (also the BP would measure this due to the zero pressure datum). The CP controller was then set up to target a pressure equal to 0 kPa (according to the zero pressure datum this would mean that a 0 kPa pressure would be applied at the middle of the specimen or reference level).
25) At this point, both the lower chamber controller and the load cell were zeroed (Section 3.6.1.2.1 and Appendix A – Section A.4).

For the B-check and initial p' measurement in the conventional and the Stress Path equipments, the following procedure was adopted:

Checking for saturation (B-check) and initial p' measurement

Once the specimen and controllers had been properly set up, the former was checked for saturation and its initial p' was measured. The general procedure (i.e. not to be applied when using the extension caps), under initial isotropic conditions inside the cell and considering that the specimen is saturated (or close to saturation) at the end of the K_0-consolidation, consisted of increasing the CP, using increments of equal magnitude, and observing the u response until it reached a constant value. The first CP increment was always left overnight to remove any pressure gradient within the specimen. The Skempton's coefficient B (Equation 2.28) was calculated for each step as the ratio between the increment in u and the increment in CP. p' was calculated for each step as the difference between the mean stress (p) and the final u. The initial u (i.e. when CP = 0) would be 'hidden' by the effect of the fuse wire technique and the limited performance of the pore water pressure transducer in measuring negative pressures. The trend observed during the different steps was an increment in both B and p'. The number of steps and the values for the pressure varied from test to test, but generally the

CP was increased first from 0 to 300 kPa and then in increments of 100 kPa until reaching a B value ≥ 0.96. This condition in *B* was generally attained with the exception of a few cases, but *B* was always above 0.92. The BP was always set up above 300 kPa to ensure that any remaining air in the system was in solution

3.6.2.1. Consolidated undrained tests under compression

Ten consolidated undrained tests were required in order to determine $c_c'_{ic}$, $\phi_c'_{ic}$ and Mc_{ic} due to the poor state and performance of the conventional triaxial equipment. The results were then compared to the results given by other researchers. Some initial specifications for these tests are given in Table 3.9. All except two specimens were isotropically consolidated before shearing and only one of them was allowed to swell back (i.e. lightly overconsolidated). During isotropic consolidation and swelling, the specimen cross-sectional area was corrected over time by using the volume change in the specimen as indicated by Equations 3.7 and 3.8.

Axial deformation (mm): $$\Delta H = H_0 - \left(H_0 \cdot \left(\frac{V_0 + \Delta BV}{V_0} \right)^{\frac{1}{3}} \right) \qquad \text{[Eq.3.7]}$$

Specimen area (mm^2): $$\left(\frac{\left(\pi \cdot \left(\frac{D_0}{2} \right)^2 \cdot H_0 \right) - \Delta BV}{H_0 - \Delta H} \right) \qquad \text{[Eq.3.8]}$$

where H_0 and D_0 are the initial specimen length and diameter respectively and ΔBV is the back volume change.

After consolidation, some manual intervention was required to fix the load cell piston onto the specimen. In order to do this, the valve to the back-pressure line was closed, the CP was fixed as a target pressure and the lower chamber controller was set up to increase around 10 to 15 kPa above the CP. The latter made the load cell piston come closer to the specimen until a force of about 0.01 to 0.02 kN (i.e. 5 - 10 kPa) was registered by the load cell. This was considered as the seating pressure and the load cell was then re-zeroed. The external linear strain transducer was also zeroed at that point. The undrained shearing stage was strain controlled at a rate of 0.0016 mm/min (based on Al-Tabbaa, 1987 and also within the range specified by BS 1377-8:1990 – refer to Table 2.3) in order to register both peak and residual strengths. The axial strain was measured by the external linear transducer and the radial strain calculated from this and the no volume change condition in Equation 3.8. The mode of failure was recorded for all tests. *w* was determined at the end of tests USc7 to USc11. The fuse wire technique was not used for specimens USc2 to USc6.

Table 3.9. Initial specifications for the consolidated undrained tests under compression

Specimen code	$\sigma_v'_{max}$ in the consolidation Device A (kPa)	e after consolidation in Device A	NC/LOC (*) in the triaxial equipment	Equipment used for testing
USc2	756	1.211	NC	Conventional triaxial
USc3	756	1.199	NC ([1])	Conventional triaxial
USc4	756	1.211	NC	Conventional triaxial
USc5	756	1.193	NC	Conventional triaxial
USc6	756	1.157	NC	Conventional triaxial
USc7	756	1.157	NC	Stress Path
USc8	756	1.187	NC	Stress Path
USc9	756	1.163	LOC	Stress Path
USc10	353	1.385	NC	Stress Path
USc11	870	1.169	NC ([1])	Stress Path

NOTES: NC, LOC: Normally consolidated and lightly overconsolidated before shearing respectively
([1]): Specimens that were sheared without further consolidation in the triaxial equipment

3.6.2.2. Consolidated undrained tests under extension

Five specimens were tested in the stress path equipment in order to determine $c_e'_{ic}$, $\phi_e'_{ic}$ and Me_{ic}. The results were then compared to the results presented by other researchers. All the specimens were isotropically consolidated before shearing and only two of them were allowed to swell back (i.e. one lightly and one heavily overconsolidated). Some initial specifications for these tests are given in Table 3.10.

Table 3.10. Initial specifications for the consolidated undrained tests under extension

Specimen code	$\sigma_v'_{max}$ in the consolidation device A (kPa)	e after consolidation in Device A	NC / LOC / H C (*)
USe1	643	1.217	NC
USe2	467	1.301	NC
USe3	467	1.331	NC
USe4	467	1.313	NC
USe5	467	1.295	LOC
USe6	643	1.205	HOC

NOTES: NC, LOC, HOC: Normally consolidated, lightly overconsolidated and heavily overconsolidated before shearing respectively

Since the extension caps were used for these tests, some test procedures introduced in Sections 3.6.2 (for the initial stages) and 3.6.2.1 (for isotropic consolidation and shearing) were different as described below:

General specimen and system set up

Instead of the standard top cap and load cell piston, the receiver extension cap was placed on top of the specimen and the pulling extension cap was attached to the load cell. Both caps were carefully cleaned and the vylastic sleeve was placed on the receiver cap. A very thin smear of silicon grease was spread on all contact surfaces between the sleeve and the extension caps. The tube going from the pulling cap to the vacuum valve at the top of the cell (open at this stage) was emptied and all the connections checked to ensure a perfect seal. If pressurized water gets into this pipe during the process, a perfect seal between the two caps and the sleeve would not be possible, thus preventing negative deviator stresses being applied. Once a proper alignment had been ensured whilst adjusting the cell, the load cell was lowered until the pulling cap was very close to the receiver cap.

B-check, initial p' measurement and isotropic consolidation

It was learned during the first experiences that during these stages the perfect initial alignment between the pulling and receiver caps could be easily lost making it difficult, if not impossible, to establish a good seal between them later on. The distance between both caps was therefore optimised to reduce this effect yet maintaining isotropic conditions thorough these initial stages. The procedure finally selected was as follows:

1) The extension pulling cap was kept only 1 to 2 mm away from the receiver cap while having the tube to atmosphere empty and the valve to atmosphere open. Once in position, the valve to atmosphere was closed. The cell was then filled with water and the system set up to the initial conditions as explained in Section 3.6.2.
2) By leaving the CP targeting 0 kPa, the lower chamber pressure was slightly increased until a value of about 0.01 to 0.02 kN could be read by the load cell. The load cell was then zeroed. Although at this point some seal occurs between the extension caps and the elastic sleeve (i.e. some tension can be applied to the specimen), it is better to create the vacuum (i.e. it will be stronger) at a later stage when the CP is higher so as to have a larger differential between the CP value and the atmospheric pressure.
3) The B-check was carried out at this time by increasing the CP (as described in Section 3.6.2). The Advanced Loading Module in GDSLAB was used during this stage for tests USe4 to Use6 after observing tension stresses occurring during test USe3. The CP was therefore increased at a rate of 200 kPa/30 min (i.e. slow enough for the system to keep the deviator stress equal to zero at all times).

4) Once the Skempton´s *B* value was ensured to be ≥ 0.92, generally for CP equal or above 500 kPa, the Advanced Loading Module was stopped. The CP was then manually set up to target its last value and the valve to atmosphere was finally opened. If a good seal had been obtained, the CP would not drop at all and no water should come out of the vacuum line. The valve to atmosphere should be closed after this and before attempting to perform the remaining test stages.

5) For the isotropic consolidation stage, the Advanced Loading Module was also used in order to ensure zero deviator stress at all times. The CP was slowly increased to the required value (or the BP decreased) using a rate of 100 kPa/60 min to avoid stressing the specimen unnecessarily when opening the valve to the BP at the beginning of the consolidation. The same procedure, but with CP decreasing, was used if a swelling stage was required. As the specimen is docked in this situation, the change in area is calculated by using Equation 3.8 and the change in height is measured by the external transducer.

Undrained shearing

The undrained shearing stage was strain controlled at a rate of -0.0016 mm/min (same absolute value as for the compression tests). The *w* after failure was measured and the specimen was photographed to record the failure mode.

3.6.2.3. Consolidated drained tests under compression

One consolidated drained test (DSc1) was carried out in the stress path equipment in order to calculate the drained Poisson's ratio and help to define the critical state line in compression. The specimen was consolidated under K_0-conditions in Device A under a maximum vertical effective stress of 354 kPa and then isotropically consolidated in the stress path cell. During drained shearing, a strain rate of 0.0012 mm/min was used (slower than for the undrained case and within the range specified by BS 1377-8:1990 - refer to Table 2.3).

3.6.2.4. Isotropic consolidation tests

Two tests (NCL1 and NCL2) were performed in order to determine the parameters that define the ICL (and swelling lines) in the v - lnp' plane. The results were then compared to the findings from other researchers. Both samples were initially one-dimensionally consolidated in the consolidation Device A to vertical effective stresses of 594 kPa and 163 kPa respectively. After checking for saturation and measuring the initial p', both samples were subjected to the following stages:

Specimen NCL1: 5 consolidation stages, 3 unloading stages

Specimen NCL2: 5 consolidation stages, 3 unloading stages, 4 reloading stages

The isotropic preconsolidation pressure was determined from the results using the Casagrande method (Craig, 1992). Parameters λ_{ic}, κ_{ic} and N_{ic} were taken as the average results from both tests. Specimen NCL2 allowed the observation of any hysteretic behaviour of the soil during the unloading-reloading cycle.

3.6.2.5. K_0-consolidation and related tests

Three K_0-consolidation tests using on-sample LVDT's for a direct measurement of the radial deformation were initially proposed to be performed using the Stress Path cell in order to estimate K_0 and, at the same time, observe the performance of the software/equipment when using the K_0-Module. Two tests were carried out using the 'standard' top caps and the third using the extension top caps in order to observe any possible differences in the results. The calculated K_0 values were then compared to previous researchers' results.

The K_0-Module within GDSLAB has a particular way of conducting one-dimensional consolidation. Conventionally, when considering the K_0-consolidation of any given soil, it is the total vertical stress that is controlled and the total horizontal stress relates to this according to the relationship $\sigma_h = K_0 \cdot \sigma_v$, where $u = 0$, ensuring that lateral deformation does not occur. When using the K_0-Module in GDSLAB with direct measurement of the radial deformation, instead of varying the vertical stress it is the all-round CP that is increased at a certain rate, the on-sample instrumentation measures the radial strain and the system tries to keep the latter equal to zero by increasing the lower chamber volume (i.e. increasing the axial load). The lower chamber controller reacts to increments in the radial deformation equal or above 0.001 mm by pushing the piston in the base pedestal upwards by a distance equal to the amount that the radial transducer has changed every 2 - 3 seconds (the maximum rate being 0.005 mm/sec) until the radial transducer goes back to its initial position. The software is set up in this way because of computational advantages.

Due to some initial setbacks with the conditioning of the room (i.e. temperature changes and vibrations) observed during test Ko1, which strongly affected the results and will be commented on in Chapter 6, and also due to the initial poor performance of the K_0-GDSLAB module in performing such stress conditions when using the on-sample radial LVDT, six tests were finally carried out instead of three. The peculiarities of each of these tests are summarised in Table 3.11.

For tests Ko4 and Ko5, the latter using the extension caps, the indirect measurement option using the back-pressure volume (see Section 3.6.1.2) instead of the direct on-sample measurement was used. When using this option, an initial volume is calculated by the system based on the initial height and diameter of the specimen. Since the cross-sectional area is required to be constant, for every step in CP producing a variation in the back volume, a target height is calculated as the current volume divided by the area of the specimen. In this way the deviator stress increases as a result of the displacement of the lower chamber ram.

For test Ko6, the radial ±3 mm range Hall Effect device was used because it was necessary to have a full set of on-sample instrumentation working in order to reproduce some tunnelling induced stress paths at a later stage and the LVDT's did not seem to be good enough. According to GDS, the Hall Effect device tends to give fewer problems when testing soils although it is less durable and slightly less accurate.

The selected rate of increase in CP was slow enough in all these tests as to ensure full pore water pressure dissipation. A rate of 100 kPa/2 days was found appropriate and conventionally used. A rate of 50 kPa/2 days was also investigated during test Ko3 to see whether the results could be improved. None of the tests included unloading stages. The final *w* was measured for all the tests.

At the end of the one-dimensional consolidation in tests Ko4 and Ko5, the specimens were sheared undrained to failure under compression at a rate of strain of 0.0016 mm/min in order to compare the results with those obtained for isotropically consolidated specimens (Section 3.6.2.1). Specimen Ko6 was sheared under extension after one-dimensional consolidation at a constant rate of strain of - 0.0016 mm/min in order to compare the critical state to those obtained for isotropically consolidated specimens (Section 3.6.2.2).

At the end of test Ko3, two arbitrary undrained stress paths were carried out in order to test the performance of the Stress Path Module. The first stress path consisted on Δp = -20 kPa and Δq = +40 kPa. The second stress path consisted on Δp = +20 kPa and Δq = +20 kPa.

Table 3.11. Initial specifications for the K_0-consolidation tests

	In the consolidation Device A		In the stress path equipment		
Specimen code	**$\sigma_v'_{max}$ (kPa)**	***e* after consolidation**	**NC/OC (*)**	**Top caps used**	**Type of control to ensure K_0 conditions and improvements made (if any)**
Ko1	757	1.169	NC	Standard	Direct measurement using the LVDT1 (±2.5 mm range)
Ko2	1065	1.103	NC	Standard	Direct measurement using the LVDT1 (±2.5 mm range) [Vibrations and temperature control corrected]
Ko3	1065	1.121	NC	Standard	Direct measurement using the LVDT2 (±2.5 mm range) [Use of a different LVDT and calliper re-arrangement]
Ko4	643	1.187	NC	Standard	Indirect measurement using the back-volume change
Ko5	643	1.187	NC	Extension	Indirect measurement using the back-volume change
Ko6	643	1.199	NC	Standard	Direct measurement using the Hall Effect device (±3 mm range)

NOTES: NC, LOC: Normally consolidated or overconsolidated respectively

In addition to obtaining the coefficient of earth pressure at rest for the Speswhite Kaolin clay, another objective of using the K_0-Module in GDSLAB was to take the specimens for the simulation of tunnelling induced stress paths to the required stress state prior to tunnel excavation (see Section 3.6.3). In this sense, and after observing the poor performance of the K_0-Module together with the radial LVDT, an additional option was investigated during the study that consisted of the simulation of the K_0-consolidation using the Stress Path Module. In this option the condition of zero lateral strain was not necessarily maintained. One test with these characteristics was run coded KoAL1. The complete LVDT set (1 radial and 2 axial) was used in this case as well as the extension caps in order to run some tunnelling induced stress paths at the end of the consolidation, measure small-strain parameters and evaluate the overall system performance. The specimen was initially one-dimensionally consolidated in the consolidation Device A up to a vertical effective stress of 756 kPa giving a final void ratio of 1.169. The rate of stress application during the K_0-stress path, divided in 5 stages up to a maximum $\sigma_v' = 600$ kPa and $\sigma_h' = 384$ kPa, was around 50 kPa/2 days. The first stage went from the $q = 0$ state to the K_0-line following a stress path with an inclination of 65 ^{o}, this value being based on the observations made during previous K_0-consolidation tests.

3.6.3. Definition of Simplified Tunnel Induced Stress Paths and their Simulation in the Laboratory

Based on the results from PLAXIS (Section 3.3), stress changes at different points around SCL type tunnel/s under various initial soil stress conditions were identified and compared to the results presented by previous authors. The observed trends were simplified taking into account the limitations of the triaxial equipment and four types of stress paths were defined to be reproduced in the Stress Path cell as follows:

TYPE (i) Crown of single tunnel in normally consolidated soil $K_0<1$.

TYPE (ii) Springline of twin tunnels in normally consolidated soil $K_0<1$ (part of this being representative of the situation for single tunnels under the same initial stress conditions).

TYPE (iii) Crown of single tunnel in overconsolidated soil $K_0>1$.

TYPE (iv) Springline of twin tunnels in overconsolidated soil $K_0>1$ (part of this being representative of the situation for single tunnels under the same initial stress conditions).

All the reconstituted specimens prepared for stress path testing were K_0-consolidated in order to simulate the likely geological history of the natural soil (i.e. London Clay). This consisted of an initial consolidation in the Consolidation Device A up to a theoretical maximum vertical effective stress equal to 643 kPa. Afterwards, in the Stress Path cell, and after measuring the initial p', the specimens

were further K_0-consolidated to a state were $\sigma_h \cong 830$ kPa by using a rate of increase in CP of 50kPa/day. This, given the selected back-pressure of approximately 400 kPa, would correspond to a measured σ_v' close to 600 kPa. The reasons for selecting these two values (i.e. 643 kPa in Device A and 600 kPa in the Stress Path cell) will be discussed in Section 7.2. When unloaded under K_0 conditions for the overconsolidated specimens, the stress state was taken so as to have a K_0 value as close to 1.5 as possible (depending on individual test conditions) in order to simulate the $K_0 = 1.5$ case considered during FEA (Section 3.3.1.1). Ideally, the stress state during K_0-loading for the overconsolidated specimens should have been taken further so that at the end of the unloading stage the vertical stress was equal to that at the end of the K_0-consolidation for the normally consolidated specimens. This was impossible however due to the maximum working pressures of the Stress Path cell, therefore the same maximum stress levels during K_0-loading were used for both normally and overconsolidated states. For one-dimensional loading and unloading, the K_0-Module in GDSLAB was used together with the on-sample Hall Effect device and the extension caps.

After these K_0-stages, each of the stress paths would consist of the two following parts:

PART 1: Representing the excavation of the tunnel and consisting of an allowance for some relaxation of the stresses, at either the crown or the springline.

PART 2: Representing the placement of the tunnel support, at either the crown or the springline.

Both PARTS were performed under total stress control (defined in terms of p and q) in undrained conditions.

Tests TYPES (ii) and (iv) included also PARTS 3 and 4, which were equivalent to PARTS 1 and 2, but represented the excavation and placement of lining for the second of the twin tunnels respectively.

Readings during PARTS 1, 2, 3 and 4 were taken every 10 seconds. In order to define the stresses to be used, more emphasis was given to the relative orientation of the different PARTS and overall trend rather than to the magnitudes obtained during FEA. It should be noted that:

- The strains induced by tunnelling on (or close to) the ground surface fall within the small-strain range, but it would not necessarily be the case at points situated close to the tunnel opening.
- The overall strains induced in the laboratory during stress path testing would be mainly controlled by:
    - The initial conditions of the specimens.
    - The magnitude and orientation of the tunnelling induced stress paths followed for the present investigation.
    - The stress-strain behaviour of the soil.

The combination of these aspects could give rise to the generation of large strains at some point during some (or all) of the stress paths. In other words, not the whole stress path (i.e. the different PARTS) would fall within the small-strain range.

The simplifications taken from the PLAXIS results and from the conceptual idea of a cavity unloading when describing the stress paths were also carefully reviewed and will be presented in Chapter 7 together with the results from stress path testing. PARTS 1 (and 3) and 2 (and 4) were run over 8 and 3 hours respectively. The 8 hours timescale for PART 1 corresponded to the time necessary to excavate 1 m and was chosen based on data given by various authors (Table 3.12) from real excavations and FEA in London Clay. The timescale for PART 2 was selected only with the intention to simulate a lining that is placed in-situ faster than the advance of the excavation itself. For those tests simulating the excavation of side-by-side twin tunnels (i.e. SP2 and SP4), a time gap of about 12 hours was left between PARTS 2 and 3. This was done in an attempt to simulate the effect that the brief time gap, still under undrained conditions, between the excavation of the two tunnels could cause on the soil behaviour during the excavation of the second tunnel, and also for the convenience of the testing schedule.

Table 3.12. Some published values of rate of tunnel advance in London Clay

Reference	Soil	Excavation method	Rate of tunnel advance
Lee and Ng (2005)	London Clay	Shield	3 m/day
Burland et al. (2001)	London Clay – St. James's Park. 5 m diameter tunnels	Open face shield with mechanical back-hoe	8 hours (FEA)
	London Clay – Green Park and Waterloo. 5 m diameter tunnels	Open face shield with mechanical back-hoe	70 m/week
Clayton (2007)	London Clay – Heathrow Express – T4 Platform. 10 m diameter tunnels	Sprayed concrete lining	0.5 – 1.5 m/day
	London Clay – Heathrow Express – T4 Concourse. 9 m diameter tunnel	Sprayed concrete lining	1.5 – 3.5 m/day

Based on all these specifications, 7 tests were performed as specified in Table 3.13.

Table 3.13. List of stress path tests

Stress path type	Test code
TYPE (i)	SP1, SP1-c
TYPE (ii)	SP2, SP2B, SP2C
TYPE (iii)	SP3
TYPE (iv)	SP4

Some of the tests in Table 3.13 (SP2B and SB2C) were not initially planned, but were later added after encountering various shortcomings during testing. For the stress specifications in test SP2 the specimen reached failure during PART 1 because the increase in deviator stress induced an effective stress path close to the failure envelope in compression. The results from test SP2 were still relevant in the sense that the complete strain-stress curve up to failure could be recorded for a compression stress path. As a result of the soil failing during test SP2, another test coded SP2B was proposed with shorter stress path excursions, but still maintaining the overall trend observed during FEA. The stress paths increments for test SP2B were the very minimum possible given the precision of the volume/pressure controllers. Although on this occasion the soil stress state was still far from the yielding surface, the soil still failed and the analysis of the data saved during the test was not conclusive in order to establish the cause for the unexpected termination of the test.

A third test coded SP2C was performed that still aimed to represent the stress changes at the springline between twin tunnels for K_0<1. The total stress magnitudes used in SP2C were selected as to be sure that failure in compression would be avoided during the test. Some of the stress path features obtained in Chapter 4 were represented in this case, but the overall stress changes did not represent adequately the behaviour at a tunnel springline (e.g. the overall total horizontal stress increases when it should decrease). The results would however still serve the purpose of studying the performance of the various constitutive models.

An important point to note for all these tests (i.e. SP1, SP2, SP2B, SP2C, SP3 and SP4), is the fact that they were all carried out without allowing for creep deformations to occur between the end of the K_0-consolidation stage and the beginning of PART 1. According to Clayton and Heymann (2001) in their discussion on the paper by Powrie et al. (1998), the effects of creep on small-strain stiffness measurements during triaxial testing have to be considered. If creep rate is not allowed to dissipate sufficiently after a drained stress path then the strains from creep will be included as part of the subsequent stress excursions and it can give rise to underestimation of the soil stiffness. The authors refer to Jardine (1995) who recommended a ratio of creep rate to shear strain rate less than 1 % and also to Hight and Higgins (1995) who stated that creep rate prior to shearing should be less than 0.05 %/day (for a value of rate of undrained axial strain of 5 %/day).

The results presented by Atkinson et al. (1990) on reconstituted London Clay demonstrated that the soil stiffness during shearing is strongly affected by the previous recent stress history. According to this, the measured soil stiffness would therefore potentially depend on both the direction of the previous path (consolidation to the initial stress state in this case) and the direction of the subsequent undrained path. In this particular case Atkinson et al. (1990) used short rest periods (3 hours) before the undrained shearing. This would mean, for example, that if the stress state achieved at the end of the K_0-stages during the present experiments was approached along different incoming paths, the measured stiffness during equal subsequent tunnelling induced stress paths could be different in each

case. A decade later, Clayton and Heymann (2001) demonstrated that if enough creep is allowed at the end of the consolidation (the authors used in this case rest periods of between 1 and 3 days), then the effect of the recent stress history is erased and therefore the soil stiffness only depends on the direction of the subsequent shearing stress path. Since the approaching consolidation paths to the initial stress states used in the present investigation were kept constant, it was expected that the differences in stiffness would only be dependent on the orientation of each individual tunnelling induced stress path and therefore, in theory, time allowance for creep would not be required in order to remove the effects of the recent stress history. After considering these theories, one question arose however regarding how different the stiffness response of two soil samples would be if they had been consolidated along the same stress path, but just at the end of the consolidation process and before starting the shearing stage, one of them was allowed to creep and the other one was not. In this respect, Hight et al. (2007) have recently presented results from triaxial experiments on London Clay samples which were allowed to creep for longer periods than usual (≅ 7 days corresponding to a minimum strain rate of 0.002 %/hour) and these showed significantly lower normalized stiffness values ($E/1000p_0'$, p_0' being the mean effective stress prior to undrained shearing) than those previously established for London Clay. This would mean that the long resting periods do not only remove any effects of the recent stress history, but also have an impact on the initial measured soil stiffness, this tending to be smaller when long pause periods are allowed. This would hold true, based on Hight et al. (2007) results, for both stress paths involving, and not involving, a reversal in stress path direction after sample consolidation (although it is more obvious for the latter). Apart from the longer resting periods, Hight et al. (2007) believe that one of the factors inducing such difference is the rate of stress increment used during the approaching path. In compression, these differences in the measured stiffness are evident for axial strains below 0.05 %, but not so significant above this value. The differences are larger in extension. From the observations reported by Clayton and Heymann (2001), it is understood that the effects of recent stress history are erased when creep is allowed and therefore it virtually implies that only the orientation of the subsequent stress paths will dictate the variation in stiffness. From the results presented by Hight et al. (2007) however, it seems that, as well as removing the effects of the soil's most recent stress history, the occurrence of creep also gives rise to similar stiffness for compression and extension paths (undrained path involving or not a reversal in stresses) given the same value of p_0'.

If a model such as the 2-bubble model of Al-Tabbaa (1987) is considered (Figure 3.24) for a K_0-normally consolidated soil and also for a K_0-overconsolidated soil, then the condition of "not allowing for creep" at the end of the K_0-process would correspond to bubbles situated at positions A and A' respectively.

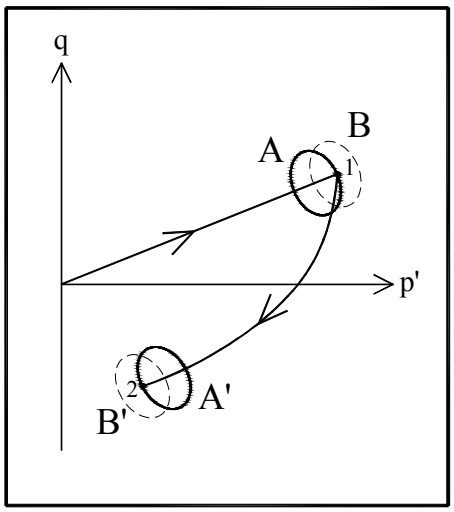

Figure 3.24. Location of the inner bubble in a kinematic hardening model with (B,B′) and without creep (A,A′) during K_0-consolidation

The observations made by Hight et al. (2007) seem to imply (e.g. similar response for compression than for extension) the bubbles being more centred to the final stress state at the end of the K_0-process (positions B and B′ for normally consolidated and overconsolidated soil respectively). This would explain the similar response observed by the authors when shearing either in compression or in extension from a common p_0' value and the difference observed by the authors with respect to previous work where less creep had been permitted. The amount of creep allowed could somehow control the amount of distance travelled by the stress state from position A (or A') in Figure 3.24 to position B (or B'). If Point 1 in Figure 3.24 is approached through different consolidation paths, the position of the kinematic bubble would be different for each case (Figure 3.25) and therefore the stiffness observed during subsequent undrained excursions would be potentially different as suggested by Atkinson et al. (1990).

If at the end of each of the incoming paths in Figure 3.25, time was allowed for creep to reduce to a minimum, then the three bubbles would start moving, getting closer (Figure 3.26a) until eventually all three would become the same bubble centred around Point 1 (Figure 3.26b).

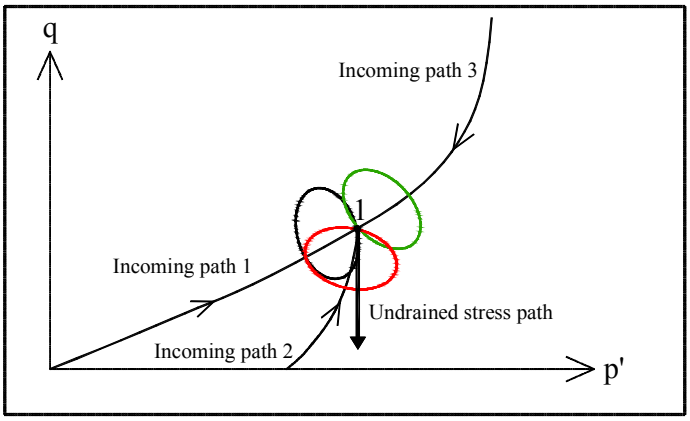

Figure 3.25. Location of the inner bubble in a kinematic hardening model when approaching the same point through different consolidation paths

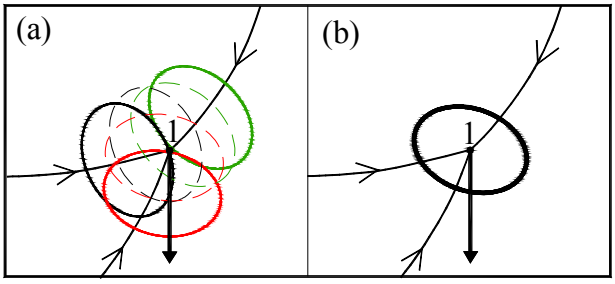

Figure 3.26. Location of the inner bubble in a kinematic hardening model when allowing for some creep (a) at the end of different consolidation paths. (b) represents the ideal final state after long creep

An undrained path such as that illustrated in Figure 3.26a starting at Point 1, would show smaller differences in stiffness for the three samples subjected to creep before being sheared (i.e. the recent stress history is partially erased) than the samples being under the same situation but without a rest period at the end of the incoming consolidation path (Figure 3.25). Figure 3.26a could hence show an idealized explanation of the observations made by Clayton and Heymann (2001). In Figure 3.26b, all the effects of the recent stress history would have been erased and this is what quite clearly can be extrapolated from Hight et al. (2007). Many more tests would be required in order to establish the amount of creep necessary to have the bubble centred at point 1 (Figure 3.26b) and this of course could well depend on many variables such as the soil type itself and the direction of the approaching path.

Various authors have used the concept of 'centreing' the kinematic surfaces in their analyses (e.g. Masin and Herle, 2005 with the Stallebrass and Taylor, 1997 model).

From the point of view of the present investigation the author found it of interest to observe the effect of reducing creep deformations to a certain threshold at the end of the K_0-stage. The reasons for the interest in this approach were two:

1) Partially corroborate the above theory.
2) Evaluating the possibility that the response of real soils affected by tunnel excavations in terms of stiffness could be affected by creep taking place over geological timescales.

For these reasons, one additional test coded SP1-c was performed. The stress path followed during this test would be equal to that during test SP1, so the only difference would be the allowance for drained creep between the end of the K_0-consolidation stage and the start of PART 1 under constant stresses. The condition of constant vertical and horizontal stresses was maintained using the Advanced Loading module in GDSLAB. Creep was allowed for 9.5 days. It should be noted that the condition of zero lateral strain may well not be maintained during creep since σ_v = constant, σ_h = constant and $\varepsilon_r = 0$ cannot be kept at the same time (i.e. it is possible with any two of them, but not with all three). u was maintained approximately constant (±5 kPa).

The author appreciates that laboratory creep times can never be compared to those occurring during the formation of natural soils, but at least, considering creep during some of the present experiments would potentially help in closer simulation and improve our understanding of real ground conditions.

Table 3.14 summarises some initial specifications for all the stress path tests finally performed during the present investigation.

With the equipment available, the anisotropy of the soil could not be investigated.

For every test, graphs showing the stress paths followed in terms of the vertical and horizontal total and effective stresses were given as well as any other recorded data such as the variation in u and the induced axial and radial strains. When readings from the two axial Hall Effect devices were available during the stress paths, a comparison of these was presented and the axial strain values were calculated by averaging both measurements. Due to the fact that the output given by GDSLAB is based on the external instrumentation, the q values were recalculated based on the on-sample measurements. The sign convention used for presenting the results is as follows: compressive stresses and strains related to this are considered positive and extension stresses and related strains are considered negative. Sometimes the strains were shown on a logarithmic scale to show in greater detail the small-strain range.

The author is aware that ideally at least two or three identical stress paths of each TYPE should have been performed for repeatability and in order to improve the interpretation of the results obtained. However the time constraints towards the end of the project made this impossible and the tests had to be planned accordingly.

Table 3.14. Initial specifications for the specimens used for the tunnelling induced stress path tests

Specimen code	$\sigma_v'_{max}$ in the consolidation Device A (kPa)	e after consolidation in Device A
SP1	643	1.235
SP1-c	643	1.181
SP2	643	1.241
SP2B	643	1.181
SP2C	643	1.253
SP3	643	1.187
SP4	643	1.211

The main aim at this point was to carefully define the right number of tests and their individual characteristics in order to obtain the maximum possible data within the time available. The solution that the author came up with is the one presented in this thesis, which although supplied only a limited amount of data it was enough to study and discuss each of the cases initially proposed and extract important conclusions with regard to how appropriate some well-known constitutive models are for their application in tunnel engineering. Additionally, some relevant issues in terms of the limitations involved in stress path testing could be flagged up which will certainly be useful for other people conducting similar tests.

3.7. SOIL MODEL TESTING AND EVALUATION USING SM2D

SM2D (Soil Model Testing Program in 2D) is part of the finite element suite DIANA-SWANDYNE II (Zienkiewicz et al., 1999; Chan, 2006). It can be described as a $2_{1/2}$ dimensional soil model testing program (i.e. the stress and strain z-direction is added in order to account for axisymmetric and plane strain analyses). The program was written in FORTRAN 95 and comprises:

1) Executables: -SM2D: Main program for calculation
   -SM2DGRH: Post-processing program for plotting graphs
2) Data input files: -sm2dfil: Model parameters, numerical control parameters and some test details
   -sm2dexp: Experimental data for comparison with the program results
   -sm2dplt: Selection of required graphics
3) Data output files: -sm2dsto: Comma separated files for export to Excel

Specific stress paths may require additional files.

Any consistent stress path can be simulated in SM2D under drained and undrained conditions. In SM2D, compression and extension are considered negative and positive respectively. In contrast, *u* is taken as positive in compression and vice versa. However, for the results presented in this thesis, stresses, strains and *u* have been considered compression positive and tensile negative to avoid confusion. From the various constitutive models available in the program, which are classified under the following categories: elastic, classical elasto-plastic, Cam-Clay, kinematic hardening and general plasticity models, only some were selected for the present investigation. The reasons behind the selection of the models are presented in the following section. The evaluation of the performance of the selected constitutive models in simulating the observed soil behaviour in the laboratory was done in two stages: (1) a preliminary evaluation using the experimental results obtained during conventional triaxial testing following the methodology in Section 3.6.2 (the results for this can be found in Chapter 8) and (2) a more tunnel-specific evaluation based on the results from the stress paths performed in accordance with the methodology in Section 3.6.3 (results in Chapter 9).

3.7.1. Selection of Models

The selection of the constitutive models used for the present investigation was based on the following criteria:

1. Commonly used in the United Kingdom.
2. The theoretical initial individual application.
3. Availability within the SM2D soil model library.
4. Availability in terms of having the models' source code for this to be modified and implemented in SM2D.
5. The continuing search during the present investigation to find a model that would fit well the data presented.

Based on the above criteria, the following models were selected. Those fully functional in SM2D before the start of this project have been indicated with the symbol ■. Some particularities related to the selection and application of each of the models are briefly described.

1. Isotropic linear elastic model (■)

   This model, although considered too simple to closely reproduce the observed soil behaviour in the laboratory, was used initially in order to become familiar with the operation of SM2D and ensure proper performance. Ward and Pender (1981), for example, pointed out that this model could never reproduce the behaviour of the soil during tunnelling.
2. Isotropic linear elastic perfectly plastic model (Mohr-Coulomb) (■)

The improvement with respect to the previous model is the fact that this includes a yield surface. This model was also considered too simple to reproduce the soil behaviour observed in the current investigation, but was selected because this model is still commonly used in practice.

3. Original Cam-Clay model (Roscoe and Schofield, 1963) (■)

   Although some shortcomings have been identified when using this model (Section 2.2.2.1), its performance was also tested during the initial stages of this investigation. The constant Poisson's ratio option (Section 2.2.2.1) was used for the present research.

4. Modified Cam-Clay model (Roscoe and Burland, 1968) (■)

   This model was selected because it is a very well established model, particularly for normally consolidated clays. The constant Poisson's ratio option (Section 2.2.2.1) was used for the present research.

5. Small-strain non-linear elastic model (Jardine et al., 1991)

   This model was selected because (1) the non-linear stiffness of the soils at small strains is a state-of-the-art topic nowadays, which explicitly implies that using a unique constant stiffness value for a given soil is wrong, (2) this is one of the few models for small-strain stiffness that has certainly come forward (at least in the United Kingdom) and (3) the present author wanted to evaluate how easy it is to use the model in general and for tunnelling in particular. The Jardine et al. (1991) model had the potential to be used in SM2D, but the program had to be updated (Chan, 2007) before this model could be used. This required a series of verifications before correct performance could be ensured. The mathematical relationships used for the definition of the shear and bulk modulus were the tangential expressions corresponding to Equations 2.25 and 2.26. The Jardine et al. (1991) model could be used in SM2D either on its own, basically for studying engineering problems where the induced strains fall within the small-strain range (0.001 to 0.000001), or in combination with a classical elastic-plastic model for problems where larger strains are expected. For the latter, and generally speaking, the capabilities of the overall model would be approximately the same as those offered by the yielding model. In SM2D, and for the present project, the Jardine et al. (1991) model was only used to reproduce the behaviour observed in the laboratory during the tunnelling induced stress paths, since it was only for these tests that appropriate equipment for measuring small strains was used and hence the small-strain parameters required by the model could be determined.

   With regard to establishing the small-strain parameters, the methodology initially proposed had to be modified as various limitations of the Jardine et al. (1986) and Jardine et al. (1991) models were identified when analysing and processing the results from the stress path testing presented in Chapter 7. These limitations were as follows:

a. The Jardine et al. (1986) and the Jardine et al. (1991) models were originally defined for single monotonic stress paths during triaxial tests being brought to failure in the laboratory. The application of the former was limited to the undrained behaviour of lightly overconsolidated clays under compression. The ultimate application of these models however, as for every other constitutive model, is their use in numerical analysis for the study of various engineering problems in which very variable stress paths occur during construction. In this respect, the authors of these small-strain models give no or only very little indication of how to incorporate the fact that:
   - The stiffness has been found to depend on the recent stress history (i.e. approaching consolidation stress path) (Atkinson et al., 1990).
   - Different stiffness responses are likely to be encountered along a stress path when sharp changes in load direction occur (i.e. multiple non-monotonic stress paths).

   For the former, Jardine et al. (1991) proposed using appropriate consolidation and stress paths in the laboratory to establish the right parameters. In their paper they explain for example how they used the model for the study of a deep basement. Parameters obtained from extension tests were specified for the soil being excavated whereas parameters obtained from compression tests were specified for the active zone. This is not straightforward in a tunnelling problem. For the second point above, the authors proposed re-setting the strain origins of the stiffness equations at the appropriate stage (i.e. kinematic nature of the model) and, if required, simultaneously changing the stiffness parameters. For real engineering problems however, this would assume knowledge of the exact soil previous history in the field and expected stress paths during construction, which is not likely to happen. Even if this information was available, performing the necessary laboratory testing would not be time/cost effective. Applying the model numerically under such conditions would not be easy either. It appears that the idea does not constitute a very sensible approach for the prediction of complicated studies. Even for the present case where the consolidation paths, as well as the non-monotonic undrained stress paths to be reproduced in SM2D, are known from the tests in the laboratory, the use of the model has been found to introduce many issues.

b. The Jardine models were established from data recorded during triaxial tests in which the soil was brought to failure, as previously stated. According to this, and although the model theoretically applies only over the small-strain range including an initial linear elastic part and a subsequent non-linear elastic part, a reasonably long stress path is needed in order to obtain all the model parameters. The curve fitting process goes to very large strains, therefore the model may also be said to include the elasto-plastic response. The elasto-plastic portion of the curve cannot be identified unless unloading is applied during testing.

Most of the stress paths proposed for the present investigation were not intended to reach failure, hence the whole stress-strain curve would not be available for the determination of the small-strain parameters. However, luckily as it happened, some stress paths tests unintentionally reached failure (e.g. SP2). The Jardine models therefore assume that in order to obtain the necessary soil parameters for a given stress path the soil needs to be taken to failure during laboratory testing, which may not always be feasible.

c. Jardine formulated the first relationship between $E_{u\ sec}$ and ε_a (Equation 2.15) based on conventional undrained triaxial tests. The present author assumes, since it is not explicitly explained in Jardine et al. (1991), that the relationships formulated for G_{sec} and K_{sec} were based on data from drained or undrained triaxial shear paths (for G_{sec}) and on drained triaxial shear paths (for K_{sec}). Not a single paper has been found that explains what the authors did with the soil behaviour experienced during the K_0-consolidation stage in their tests. In this respect it would be interesting, for example, to evaluate whether the same small-strain parameters can be used to represent the shear response during a pure shearing stress path and the shear behaviour during K_0-consolidation. Other similar approaches could also be investigated as, for example, whether the volumetric parameters determined from either a drained triaxial test or from a 'combined' shear-consolidation stage (e.g. K_0-consolidation) can be used indistinctly in a numerical analysis as a general description for the volumetric response of the soil.

d. The soil behaviour along a given consolidation path will potentially have two different parts, one elastic and one elasto-plastic. The elastic and elasto-plastic parts would be represented by the unloading-reloading lines and the ICL respectively in, for example, a v - lnp' plane. Various shortcomings were identified when the volumetric parameters had to be obtained from the K_0-consolidation results:

   - If considering the Jardine parameters determined from unloading-reloading lines only, then the volumetric behaviour of a soil with an initial state on the ICL would not be adequately modelled. It should be noted in this sense that the use of a classical elasto-plastic model such as Mohr-Coulomb for large strains would not have enough features to represent such volumetric behaviour during consolidation either.
   - The experimental q - ε_a and p' - ε_v curves for the shear and volumetric responses during K_0-loading could be represented by (1) a smooth curve enclosing the initial elastic response and the subsequent elasto-plastic behaviour, (2) two nearly linear paths. In the first case the shear and volumetric Jardine et al. (1991) parameters could be fitted to represent the complete behaviour, although the focus of interest

should be placed on the elastic portion. In the second case, G_{sec} and K_{sec} would be constant for both the elastic and the elasto-plastic phases.

- The fact that for some experiments the initial slope on the q - ε_a and p' - ε_v planes during for instance K_0-consolidation tended to be different from that during later unloading-reloading cycles (both theoretically in the elastic range), therefore different small-strain parameters should also be required in this respect.

From all these issues it was quite clear that obtaining the small-strain soil parameters from the stress paths proposed for the present investigation, as well as its later use in SM2D, would be very complicated. The methodology was therefore adapted in order to get the maximum information from the tests, but without spending time in actions that would not contribute to additional knowledge. With this aim, the test results were classified in three groups. *Group 1* would include those stress paths that were sufficiently long to obtain a complete set of small-strain parameters. This would basically include those stress paths reaching failure (or close to this) and the K_0-loading paths. *Group 2* would include those stress paths that were not long enough to get the complete variation in soil stiffness, but some parameters could still be obtained. *Group 3* would include those stress paths that were certainly too short for sensible fitting of the Jardine curves. The classification would be mainly made based on the q - ε_a results.

In addition to all the observations above, the present author wants to highlight the further difficulties that would come hand-to-hand if using in-situ samples instead. In such a case, the objective would be obtaining small-strain stiffness appropriate for the in-situ state of the soil but, given the magnitude of the strains being measured and disturbance issues, the measured stiffness may not be truly representative.

6. Multi-surface kinematic hardening model (Al-Tabbaa, 1987) (■)

This model was selected because:

- It was formulated based on results from tests on Kaolin clay.
- It has theoretically better capabilities in reproducing the soil response during unloading with elasto-plastic behaviour.
- It was proposed as a modification of the Modified Cam-Clay model to enable more accurate predictions for overconsolidated states (the model formulation implies that the soil in the dry side fails before reaching the boundary surface).

7. S-CLAY1 (Wheeler et al., 2003)

After having tested the above models, a search for other potential models to be used was carried out. Unfortunately, the difficulties in obtaining certain constitutive models were evident during the project. The most suitable model at the time, and one of the most recent,

because of its features and also because of the existing working relationship between the Birmingham and Strathclyde Universities was the S-CLAY1 model (Wheeler et al., 2003). Although the model was presented for normally consolidated and lightly overconsolidated soft clays and stated to be mostly suitable for problems not involving unloading where large plastic strains dominate (Section 2.2.2.3), its applicability to other soil conditions has been evaluated during the present research. Permission had to be obtained before the source code of the model could be used and again this required additional time in order to implement the appropriate subroutines in SM2D and to ensure correct implementation. The consideration of inherent soil anisotropy has been reported to improve the tunnelling predictions during numerical analyses by some authors (Rowe et al., 1983; Addenbrooke, 1996; Masin and Herle, 2005). However, not every finding corroborates this statement (Franzius et al., 2005). The 'inherent' soil anisotropy has not been considered in this project because of the limited facilities in the laboratory for measuring the required parameters. The only anisotropy being considered in the present project is the 'induced' anisotropy represented in the S-CLAY1 model by introducing rotational hardening. This additional feature in the S-CLAY1 model was expected to improve the predictions for the K_0-consolidated specimens.

3.7.2. Evaluation of the Small-strain Parameters

Due to the difficulty in establishing the Jardine et al. (1991) parameters, a specific methodology was developed for this.

Considering the type of stress paths performed for the present investigation, given the limited indications provided by the authors, and considering the shortcomings noted in the previous section, the following procedure was adopted:

(1) Selection of appropriate individual stress paths for the determination of the small-strain parameters:

This was done according to the following criteria after classifying the stress paths to Groups 1, 2 and 3 as defined in Section 3.7.1.

SHEAR BEHAVIOUR

For the undrained stress paths, the following three options were initially considered:

(a) Establishing the small-strain parameters from the data obtained experimentally during PART 1, assuming that this is the only path exhibiting truly initial linear elastic behaviour followed by a non-linear, but also fully recoverable response.

(b) Fitting the small-strain Jardine et al. (1991) parameters over the complete stress path sequence, giving more importance to the small-strain range.

(c) Fitting the Jardine et al. (1991) parameters for every individual stress path (each with a change in orientation) considering the soil conditions at the end of each path as being the initial conditions of the soil for the subsequent path, also for the calculation of the soil stiffness.

From the present author's point of view, using the parameters obtained in case (a) above would certainly ignore the different types of behaviour that could well be experienced during the subsequent stress paths, therefore this option was ruled out. Option (b) would be adopted for successive stress paths that did not involve major changes in direction from one to the next (i.e. monotonic or those close to monotonic). In this case, however, the model parameters would also be established for each individual PART (except PART 1). Option (c) was applied to those successive stress paths that experienced significant change in direction from one to the next, therefore potentially inducing new elastic behaviour.

In addition to the shear parameters determined for the undrained stress paths, these were also established based on the data obtained during the K_0-consolidation stages since q also changes during one-dimensional consolidation. For the K_0-consolidation stress paths, the following three options were considered:

(a) If the q - ε_a curve was smooth along the complete strain range, including the initial elastic portion and the subsequent elasto-plastic behaviour along the K_0-normally consolidation line, then the Jardine et al. (1991) parameters would be established in such a way that a unique curve would fit the whole set of data.

(b) If the q - ε_a curve was composed of various nearly linear parts, then constant G values would be established for each part.

(c) Independent parameters would be established for the swelling K_0-paths.

VOLUMETRIC BEHAVIOUR

Since the short-term tunnelling induced stress path testing did not involve any drained shear stress path, the volumetric small-strain parameters were determined only from the experimental data recorded during K_0-consolidation. The considerations were the same as those detailed above for the shear behaviour using the data from K_0-consolidation, but using the p' - ε_v data instead.

(2) Defining the variation in soil stiffness:

SHEAR BEHAVIOUR

For the undrained paths:

It was not possible to calculate the shear modulus (G_{sec}, G_t) directly from the raw data as these induced large fluctuations in the calculated values. Due to this, curve fitting using Excel was carried out as follows:

The q - ε_a relationship was plotted in order to identify which sort of curve/s would be able to closely fit the data. Based on these, various curves were plotted first by estimating the relevant curve parameters, and secondly by using the solver option within Excel to establish the optimum curve parameters that kept the error between the experimental and smoothed data (Equation 3.10) to a minimum.

$$Error = \frac{\Sigma\left(q_{\exp} - q_{smooth}\right)^2}{n} \quad \text{[Eq.3.10]}$$

(n = Number of points)

The Chin (1978) method was found to be suitable for certain shapes of the experimental curves. Chin's method, commonly used for the diagnosis of pile condition, states that the load-deflection relationship is of the form of a hyperbolic equation:

$$P = \frac{Q_{ult} w}{b + w} \quad \text{[Eq.3.11]}$$

where b is a positive constant, P is the load being applied, Q_{ult} is the ultimate load and w is the pile deflection. It can be observed that re-arranging the terms in Equation 3.11, w and w / P are related linearly (Equation 3.12).

$$\frac{w}{P} = \frac{w}{Q_{ult}} + \frac{b}{Q_{ult}} \quad \text{[Eq.3.12]}$$

In order to apply the Chin's method to the present case, the axial strain (ε_a) was plotted against the ratio of axial strain versus the deviator stress (ε_a / q). A linear trendline was fitted, if considered sensible, (sometimes the initial data had to be truncated due to initial oscillation of the system) and from this, which would be of the type $q = \varepsilon_a / (f_1 \cdot \varepsilon_a + f_2)$, the parameters f_1 and f_2 were obtained which allowed the calculation of a smoothed q for each given experimental ε_a value. This was later optimized using the solver function in Excel as previously explained.

In other cases it was found necessary to combine Chin's method with an equation of the following type in order to obtain a very close fit to the experimental data:

$$q = f_1 \cdot \varepsilon_a^{\left(\frac{1}{f_2}\right)} \quad \text{[Eq.3.13]}$$

Finally, G_{sec} and G_t could be calculated from the smoothed curve according to Equations 3.14 and 3.15 respectively.

$$G_{\text{sec}} = \frac{\left(\frac{q_i}{\varepsilon_{ai}}\right)}{3} \qquad \text{[Eq.3.14]}$$

$$G_t = \frac{\left[\frac{(q_{i+1} - q_i)}{(\varepsilon_{a\,i+1} - \varepsilon_{a\,i})}\right]}{3} \qquad \text{[Eq.3.15]}$$

For the K_0-paths:

Very similar procedures to the above were used but considering ε_s data instead of ε_a.

VOLUMETRIC BEHAVIOUR

It was intended to establish the secant and tangent bulk modulus (K_{sec}, K_t) from the K_0-consolidation stages. As with the shear response, it was not possible to calculate the bulk modulus directly from the raw data hence similar techniques to those used for the shear case were approached to smooth the experimental data. The data used in this case was p' - ε_v.

(3) Finding the Jardine et al. (1991) parameters:

The only indications found in the literature with regard to how to proceed in order to find the small-strain parameters for the shear and volumetric response are those given in Jardine et al. (1986) for the E_u - ε_a relationship. Due to this restricted information, the parameters were established during the present research from the smoothed data as follows:

SHEAR BEHAVIOUR

For the undrained stress paths:

From the smoothed secant shear data, the variation in $3G_{sec}/p'$ with respect to ε_a was plotted. Considering this relationship and Equation 2.24, an initial estimation of the shear parameters (*C1*, *C*2, *C3*, α and γ) was made based on the geometrical relationships illustrated in Figure 3.27.

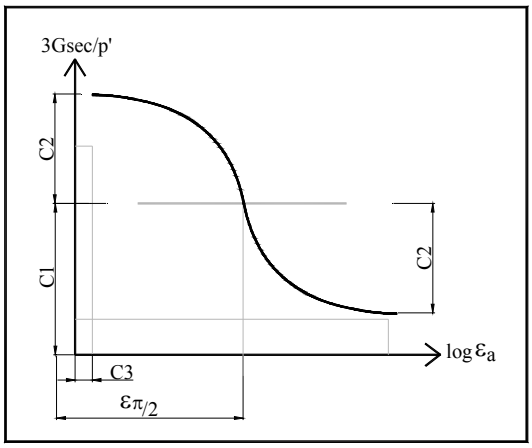

Figure 3.27. Geometrical relationship for the determination of the shear parameters *C1*, *C2* and *C3* (after Jardine et al., 1986)

$\varepsilon_{\pi/2}$ corresponded to the inflexion point of the curve. *C3* was chosen so that $3G_{sec}/p'$ was approximately constant. The first estimation of α was calculated according to Equation 3.16 (based on Equation 2.16) after finding γ by visual inspection or using the Excel solver function.

$$\alpha = \frac{\frac{\pi}{2}}{\log\left(\frac{\varepsilon_{\frac{\pi}{2}}}{C3}\right)^{\gamma}} \qquad \text{[Eq.3.16]}$$

This initial estimation was subsequently improved by using the solver function within Excel in order to ensure an optimum fitting over the whole strain range for both $3Gsec/p'$ - ε_a and q - ε_a, the latter being calculated according to Equation 3.18 based on the relationship between q and G_{sec} in Equation 3.17.

$$q = 3 \cdot G_{\sec} \cdot \varepsilon_a \qquad \text{[Eq.3.17]}$$

$$q = \varepsilon_a \cdot p' \cdot \left\{ C1 + C2 \cdot \cos\left[\alpha \cdot \left(\log\left(\frac{\varepsilon_a}{C3} \right) \right)^{\gamma} \right] \right\} \qquad \text{[Eq.3.18]}$$

For the K_0-paths:

In order to establish the small-strain Jardine parameters from the shear response during K_0-paths, the same procedure as above was used but using the q - ε_s data, hence using Equation 2.19 instead of Equation 2.24. The reason for this is the fact that Equation 2.23 is only valid for triaxial undrained tests.

VOLUMETRIC BEHAVIOUR

The procedure was similar to that used for the shear component, but using the relationship between $Ksec / p'$ and ε_v instead (Equation 2.20) for both K_0-loading and K_0-swelling. The parameters *C4*, *C5*, *C6*, δ and η were established. The Jardine prediction of p' values for the varying ε_v could then be calculated using the transformation in Equation 3.19 as indicated in Equation 3.20. In this equation p_0' makes reference to the initial p' value measured in the stress path cell.

$$K_{\sec} = \frac{p' - p_0'}{\varepsilon_v} \qquad \text{[Eq.3.19]}$$

$$p' = \frac{p_0'}{1 - \left\{ C4 + C5 \cdot \cos\left[\delta \cdot \left(\log\left(\frac{\varepsilon_v}{C6} \right) \right)^{\eta} \right] \right\} \cdot \varepsilon_V} \qquad \text{[Eq.3.20]}$$

The Jardine parameters established from the tests in Table 3.13 will be presented in Chapter 7.

3.7.3. Simulation of Conventional Triaxial Tests

Tests USc7, USc9, USe3, USe5, Ko5 and Ko6 (refer to Sections 3.6.2.1, 3.6.2.2 and 3.6.2.5) were simulated using SM2D. This allowed an evaluation of the suitability of the selected constitutive models in predicting the behaviour of Speswhite Kaolin clay under a wide range of conditions. Table 3.15 summarizes the constitutive models used for each simulation. The Jardine et al. (1991) model was not used at this stage because small strains had not been measured during the conventional triaxial testing presented in Chapter 6 and hence the small-strain parameters had not yet been obtained.

Table 3.15. Constitutive models used for SM2D simulation of conventional triaxial tests

	Test						
Constitutive model	**USc7**	**USc9**	**USe3**	**USe5**	**USe6**	**Ko5**	**Ko6**
Linear Elastic	√						
Mohr-Coulomb	√						
Original Cam-Clay	√						
Modified Cam-Clay	√	√	√	√	√	√	√
Al-Tabbaa (1987)	√	√	√	√	√	√	√
S-CLAY1						√	√

The modelling philosophy was as follows:

(1) A first set of SM2D runs was performed using the constitutive models specified in Table 3.15 for each individual test. The initial state details for each particular specimen were known.

Regarding the parameters to be used, there were two possible approaches. The first would be establishing a unique set of parameters from the data obtained in Chapter 6 and then evaluating the performance of each of the models based on these averaged parameters (common practice). Alternatively, there was the possibility of using specific parameters for each of the tests (e.g. M, ϕ) since these were available. This implies giving the constitutive model the very best parameters available hence, theoretically, the best chances to succeed for each test type. A very strict evaluation of the model's performance could then be made. The latter approach was selected for the present study.

A few parameters could not be established from the tests performed in Chapter 6. These were estimated as follows:

κ_0: This parameter was not established from the tests in Chapter 6 therefore it was taken from the results on isotropically swelled specimens for either lnv - lnp' or v - lnp'.

RVALU: A value of 0.2 was taken from Al-Tabbaa (1987).

XIVAL: A value of 1.5 was taken from Al-Tabbaa (1987). It should be noted that this is the least well defined parameter and cannot be easily found experimentally, but only defined by means of a parametric study.

α: It was estimated using Equation 2.11 with η being calculated using Equation 2.12 and M being that established for every particular test.

μ: It was estimated using the range specified in Equation 2.14.

β: It was estimated using Equation 2.13 with η and M being calculated as per α.

p_c': For the samples consolidated isotropically in the stress path cell before shearing, the isotropic consolidation stage was not simulated in SM2D. The preconsolidation pressure used for the analysis was therefore that known from the triaxial experiments. For the samples consolidated one-dimensionally before shearing, the K_0-consolidation stage was also included in SM2D. The reason for simulating the K_0-consolidation stage and not the isotropic stage was the fact that the critical state soil models do not have major problems in simulating the latter, provided that the correct preconsolidation pressure, λ, κ and N are given, but they have problems for one-dimensional conditions as previously commented in Section 2.3.1. For the K_0-consolidation stage two approaches were taken, stress-controlled (to observe the strain response predicted by the model) and strain-controlled (to observe the stress response predicted by the model). The stress-controlled option was in terms of total stresses. The preconsolidation pressure supplied for the K_0-consolidation stage would be that achieved in the consolidation Device A, but since this was

uncertain (according to findings presented in Chapter 5), such value was established as follows for each constitutive model:

Stress controlled simulations:

p_c' was established so that the overall axial strain during K_0-consolidation was coincident with the one obtained experimentally in the stress path cell. The value obtained was checked to ensure it was sensible knowing the approximate stress history in the consolidation Device A.

Strain controlled simulations:

The same p_c' established for the stress controlled case was used.

For tests USc7, USc9, USe3, USe5 and USe6, and as previously stated, only the shearing stage was simulated (using strain control up to a maximum axial strain equal to ±0.15 (compression / extension)) considering the initial soil conditions as those obtained at the end of the isotropic consolidation. For tests Ko5 and Ko6 the simulations included both the K_0-consolidation and the shearing stages, with the K_0-stage carried out both stress-controlled (total stresses) and strain-controlled as discussed before. It should be noted that for the former the radial strain is not necessarily zero. For the latter, two different options were used: (1) Fixing the maximum p' obtained experimentally at the end of the K_0 process (p'_{max}) and (2) Fixing the maximum ε_a reached experimentally at the end of the K_0 process (ε_{amax}). The strain-control option was already available within SM2D. The stress-control option was implemented especially for this project (Chan, 2007). The total stress path was given in an additional input file (Section 3.7). The shearing stage in tests Ko5 and Ko6 was always strain controlled. This is the program default, allows the observation of any likely hardening/softening of the soil and agrees with the testing procedure in the laboratory which was also strain controlled. The capabilities of the different constitutive models were evaluated by comparing the predicted values against the experimental data in the q - p', q - ε_a, u - ε_a and E_{sec} - ε_a planes.

(2) After this initial set of runs, a parametric study was carried out in order to evaluate the sensitivity of the best fitted model to the various parameters. The criteria used to establish the best model for each particular test was the performance of the models in simulating the experimental soil response in terms of stress, strain, stiffness and u at the same time. These sensitivity analyses also took into account the fact that the parameters used during the first runs, which were determined from previous laboratory testing, could be also subjected to some degree of error. A first group of analyses were carried out for tests USc7, USe5 and Ko6. For tests Usc9, USe3, USe6 and Ko5 only those parameters that were found to have a larger

influence were considered. From the sensitivity analyses the optimal values for the different parameters were established where possible. The weaknesses and strengths of each individual soil model were then discussed.

3.7.4. Simulation of Tunnelling Induced Stress Path Tests

The performance of the Modified Cam-Clay, Al-Tabbaa and S-CLAY1 models was further investigated, but in this case with particular application to tunnelling. The Jardine et al. (1991) small-strain model was added at this point in SM2D to observe whether any improvements could be obtained in the predictions. Three laboratory tests were used for this purpose: SP1 (Crown, K_0<1), SP2 (Springline, K_0<1) and SP3 (representative of K_0>1). The selection of these stress paths and no others from those listed in Table 3.13 was based on the observations made when fitting the Jardine et al. (1991) parameters to the data recorded during laboratory testing according to the methodology in Section 3.7.2.

In SM2D, both the K_0-consolidation stages and the subsequent tunnelling induced undrained paths were stress controlled. For this part of the evaluation of the constitutive models, a unique set of parameters was used, established from all the experiments carried out during this research as it would be done in normal engineering practice. The only exceptions to this were: e (initial conditions which are different for each test), M (different values were given to specimens sheared in compression and specimens sheared in extension as observed in tests Ko5 and Ko6) and parameters α and β in the S-CLAY1 model that depend on M.

The preconsolidation pressure (p_c') was in this case kept constant for all the models and equal to the average of the p_c' values found according to the previous section for the Modified Cam-Clay, Al-Tabbaa and S-CLAY1 models during the stress-controlled runs (i.e. 390 kPa).

NOTE: A complete list of all the laboratory experiments can be found in Appendix F.

Chapter 4: FINITE ELEMENT ANALYSIS

4.1. INTRODUCTION

This chapter presents the results obtained from PLAXIS v.8.2 and PLAXIS 3D Tunnel according to the methodology described in Section 3.3. Most of the results are expressed in terms of the variation of the total stresses at specific points in the ground given the final objective of these analyses. However, additional results are illustrated that allow assessing whether the stress paths obtained are sensible. The results are discussed in Section 4.3. The reader is referred back to Section 3.3.1.2 for a description on the nomenclature used for the PLAXIS analyses, which is used for some of the figures in this chapter.

4.2. RESULTS

4.2.1. 1-layer 2D Single Tunnel

Figure 4.1 illustrates the effect of using different ΣMstage values during the excavation stage on the stress paths at points A (above the crown) and B (to the side of the springline). Only the linear Elastic model was used in this case. 'Dry' conditions were assumed and the results are given for K_0 values below (0.593), equal and above "1" (1.5). Arrows have been added to indicate the direction of the stress path. Figure 4.2 illustrates the stress paths induced at A and B under variable K_0 conditions, but on this occasion considering both the excavation stage and the placement of the tunnel support. The linear Elastic, Mohr-Coulomb, Hardening and small-strain pre-yield Jardine et al. (1991) + Mohr-Coulomb models were used in this case under 'dry' conditions. Figure 4.3 illustrates the final deformed mesh and lining, the transverse surface settlement trough and total deformations for the elastic case for K_0 below and above "1". Only the elastic results are illustrated since the Mohr-Coulomb and Hardening models produced similar patterns of behaviour. Figure 4.4 compares the stress paths obtained at points A and B for 'dry' conditions and 'wet' conditions assuming linear elastic behaviour for the soil with K_0 both below and above "1".

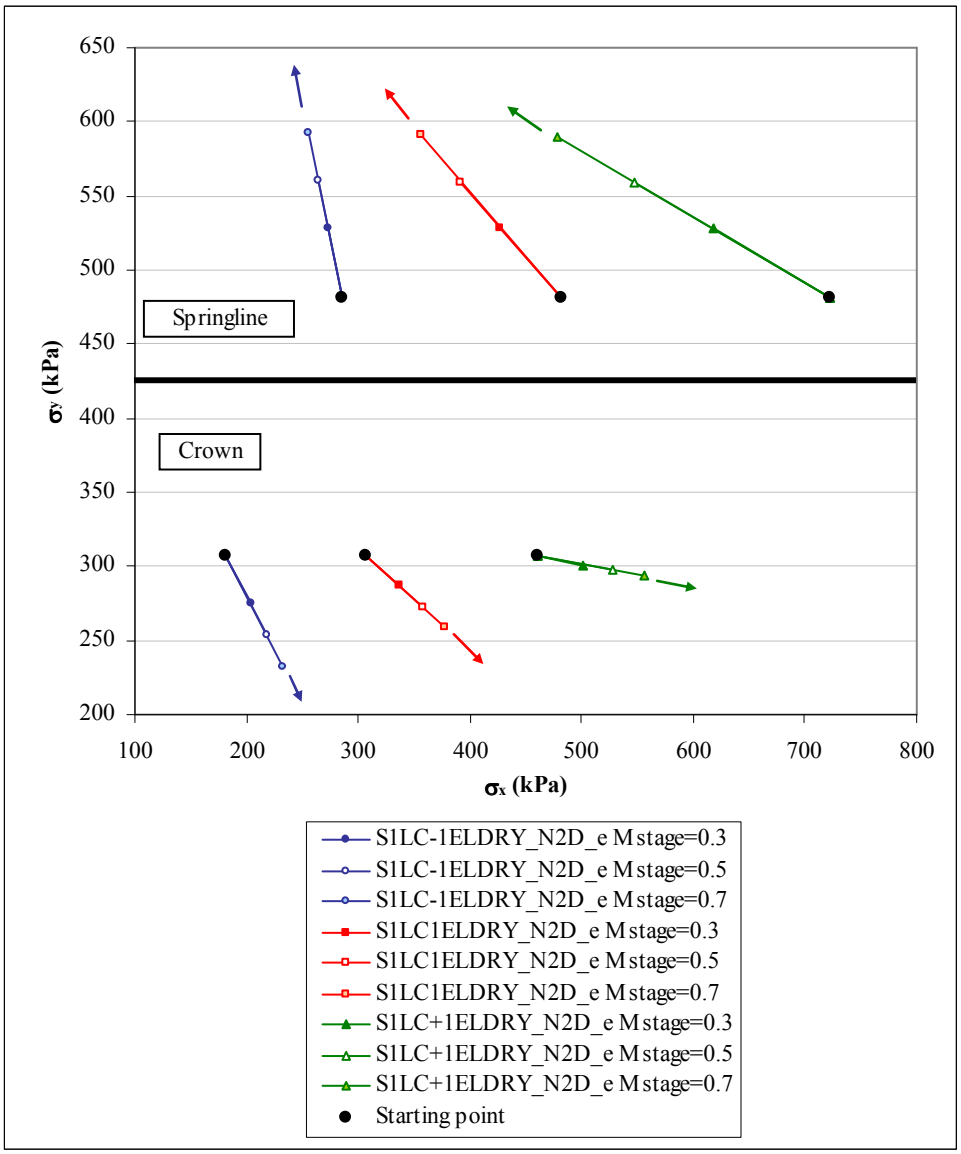

Figure 4.1. Stress paths at the crown and springlines of a single tunnel under K_0 conditions below (blue), equal to (red) and above "1" (green) using the Linear Elastic model. Only the excavation of the cavity has been considered as well as the progressive relaxation of the stresses controlled by the *ΣMstage* parameter

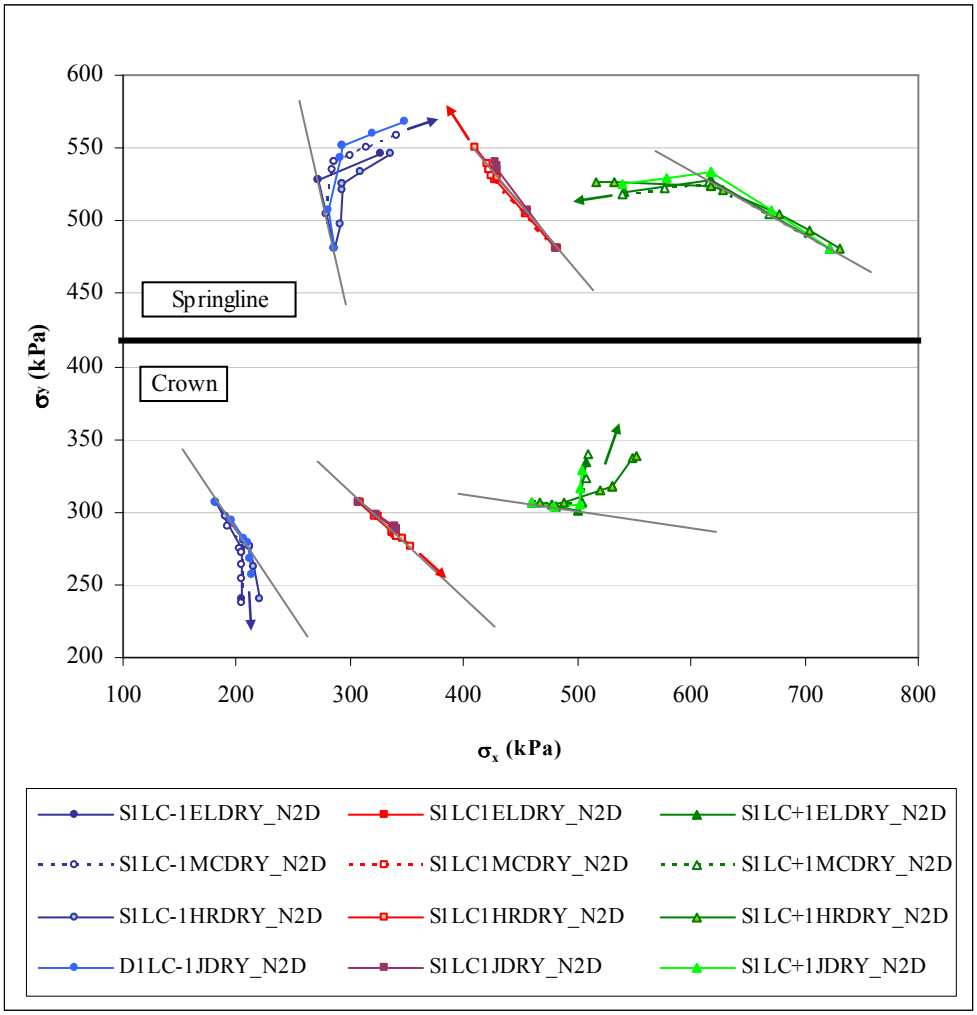

Figure 4.2. Stress paths at the crown and springlines of a single tunnel in terms of σ_y -σ_x under K_0 conditions below (blue), equal to (red) and above "1" (green) using the Elastic, Mohr-Coulomb, Hardening and Jardine et al. (1991)+Mohr-Coulomb models. Both the excavation of the cavity and the placement of the lining have been considered

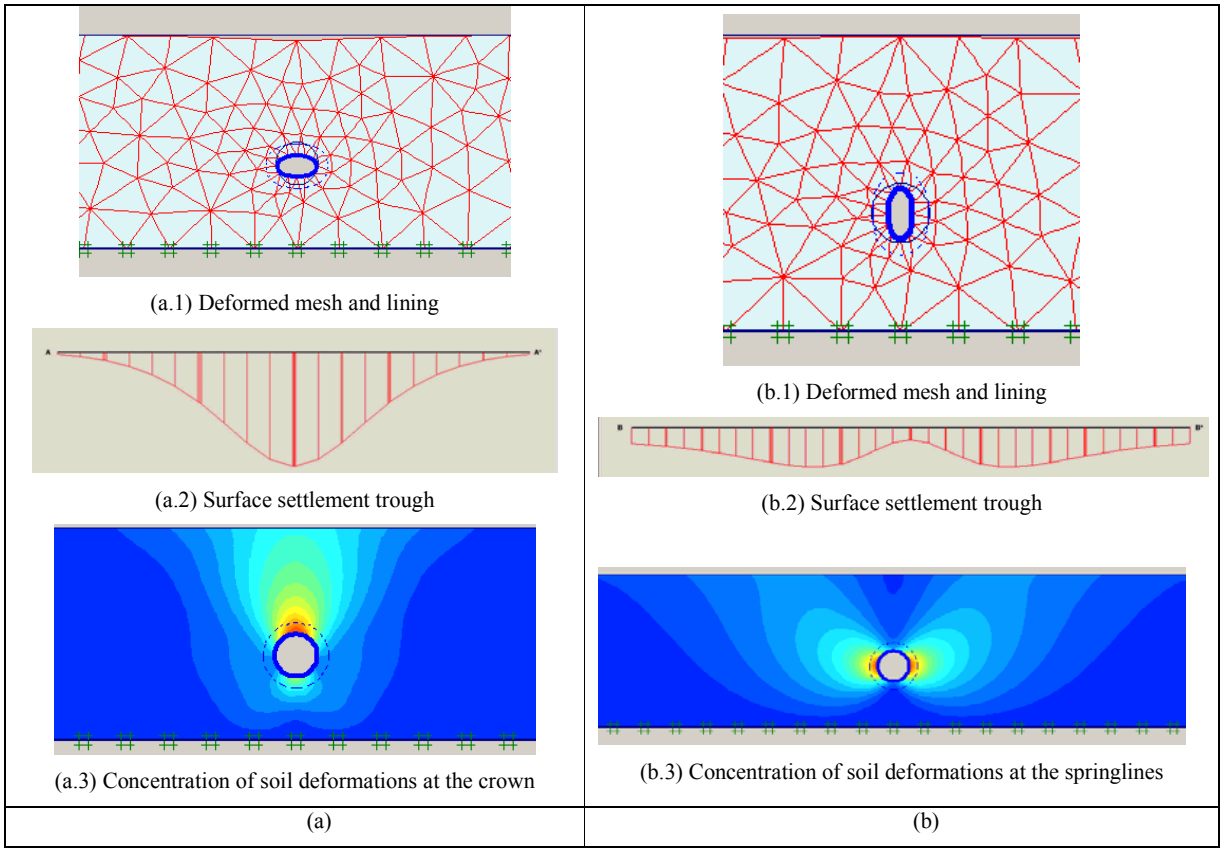

Figure 4.3. Typical settlement troughs and total displacements obtained during 2D PLAXIS elastic analyses: (a) K_0<1, (b) K_0>1

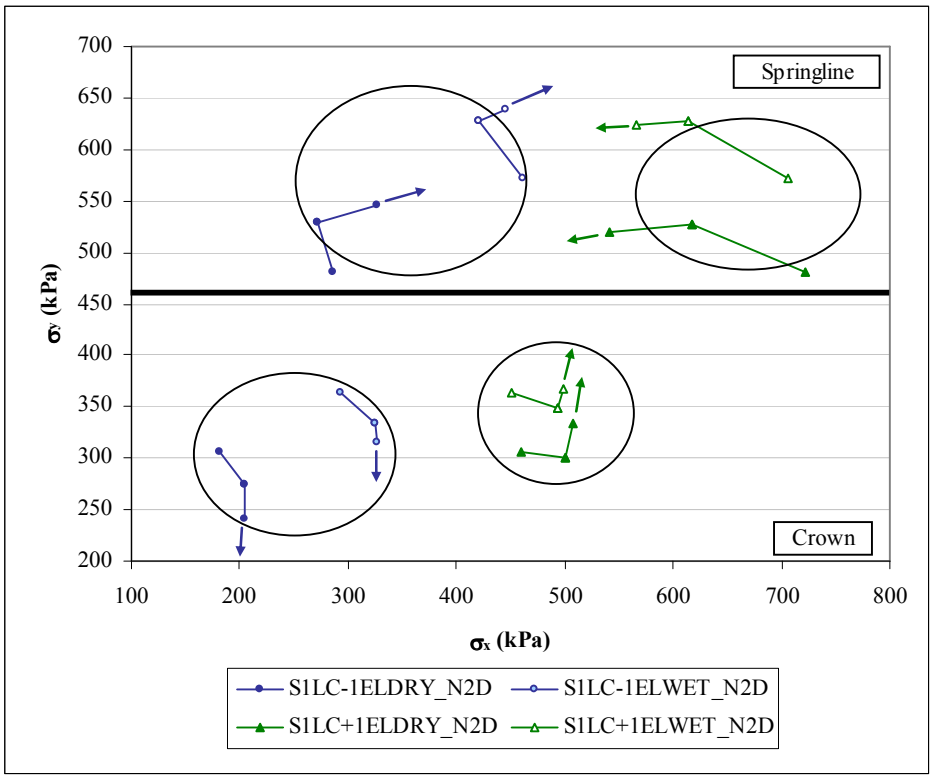

Figure 4.4. Comparison of stress paths at the crown and springlines of a single tunnel under K_0 conditions below (blue) and above "1" (green) using the Elastic model for both 'dry' and 'wet' conditions

4.2.2. 3-layer 2D Single Tunnel

The stress paths obtained at points A and B when three different soil layers were used in the analyses are illustrated in Figure 4.5 for K_0 below and above "1". The linear Elastic and Mohr-Coulomb models were used in this case. The stress paths include an initial excavation-relaxation stage and the subsequent application of the lining, as those in Figure 4.2.

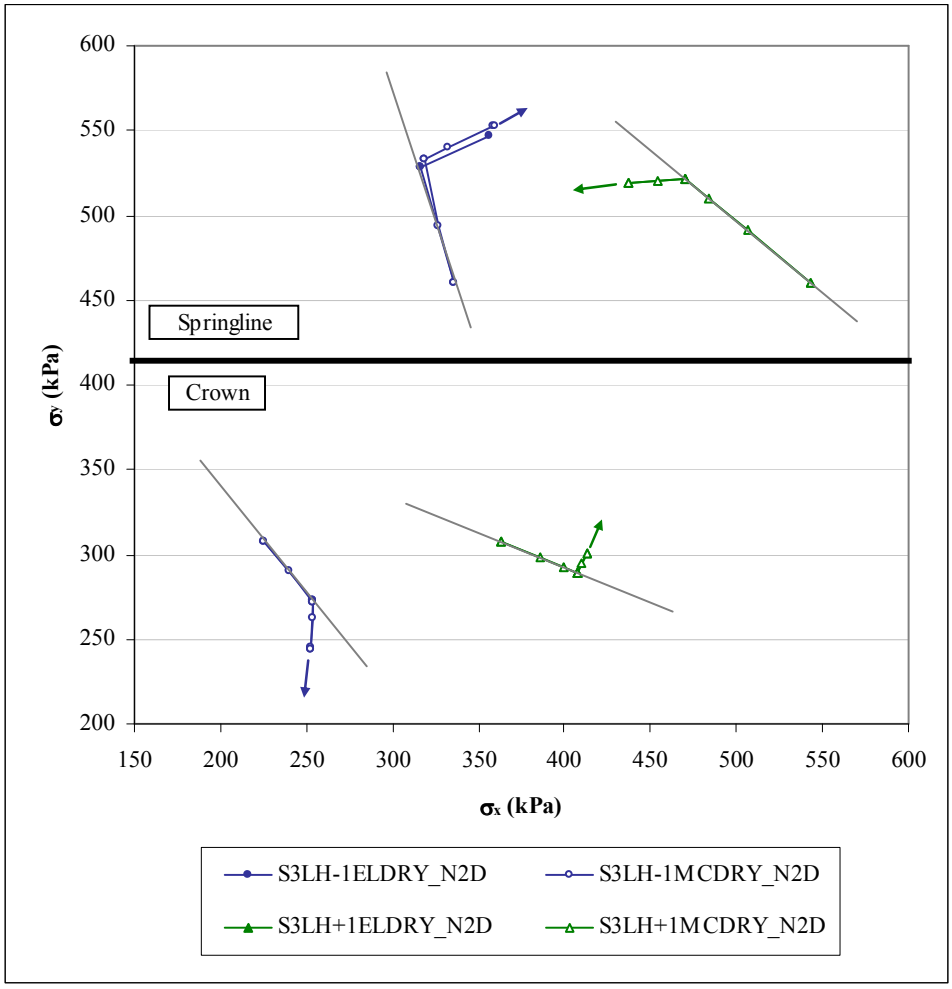

Figure 4.5. Stress paths at the crown and springlines of a single tunnel under K_0 conditions below (blue) and above "1" (green) using the Elastic and Mohr-Coulomb models and a 3-layer soil geometry

4.2.3. 1-layer 2D Twin Tunnels

Figures 4.6, 4.7 and 4.8 illustrate the stress paths at point C (springline) induced by the excavation of twin tunnels with distances between centrelines of 2.0 *d*, 2.5 *d* and 3.0 *d* respectively. The linear Elastic, Mohr-Coulomb and Hardening models were used in each case for K_0 conditions below, equal to and above "1". Figures 4.9, 4.10 and 4.11 show the transversal surface settlement troughs for the K_0<1 case using each of the constitutive soil models specified previously when the distances between the tunnel centrelines are 2.0 *d*, 2.5 *d* and 3.0 *d* respectively.

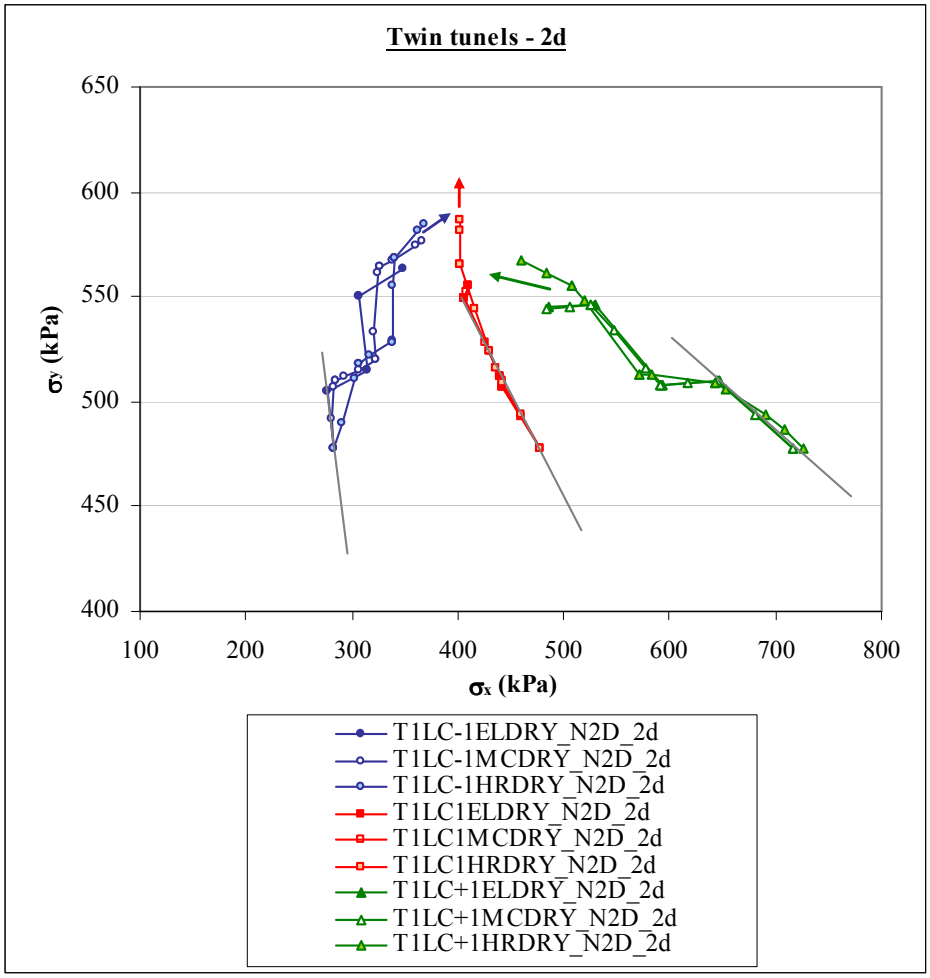

Figure 4.6. Stress paths at the springline between twin tunnels separated by a distance of 2.0 *d* between centrelines for K_0 conditions below (blue), equal to (red) and above "1" (green)

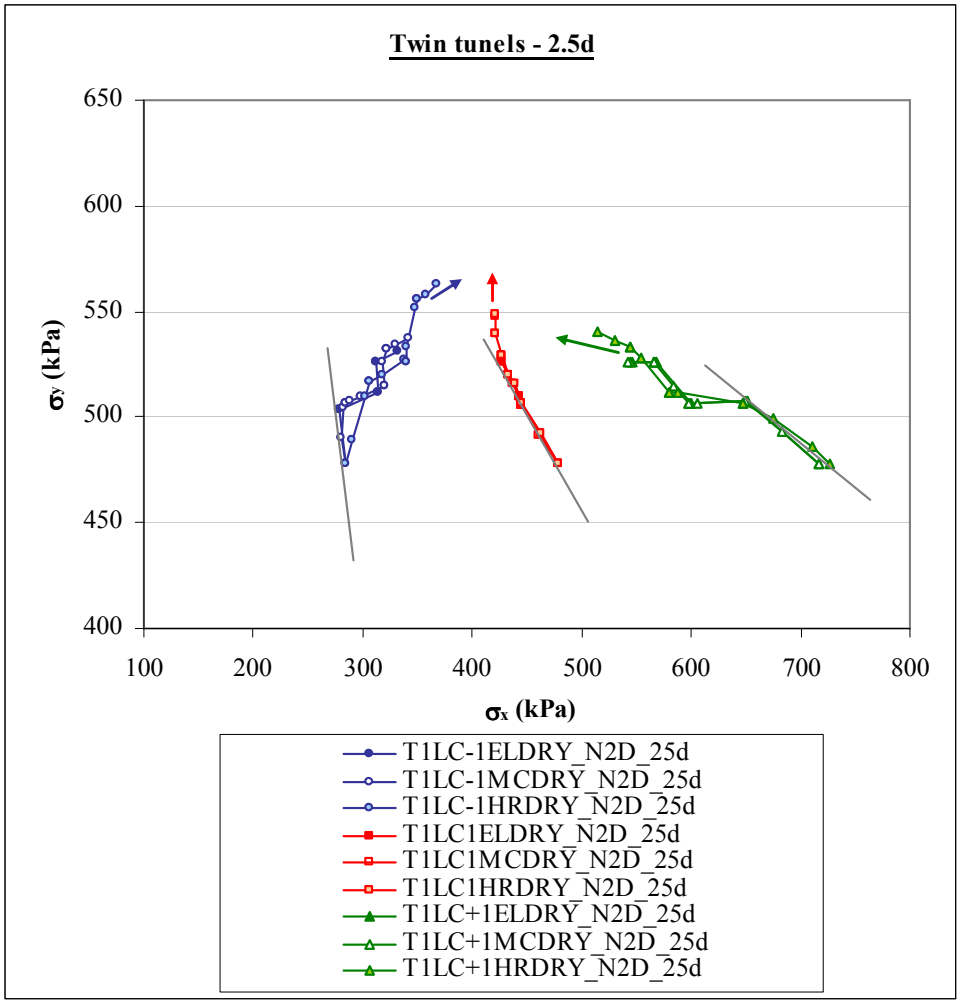

Figure 4.7. Stress paths at the springline between twin tunnels separated by a distance of 2.5 *d* between centrelines for K_0 conditions below (blue), equal to (red) and above "1" (green)

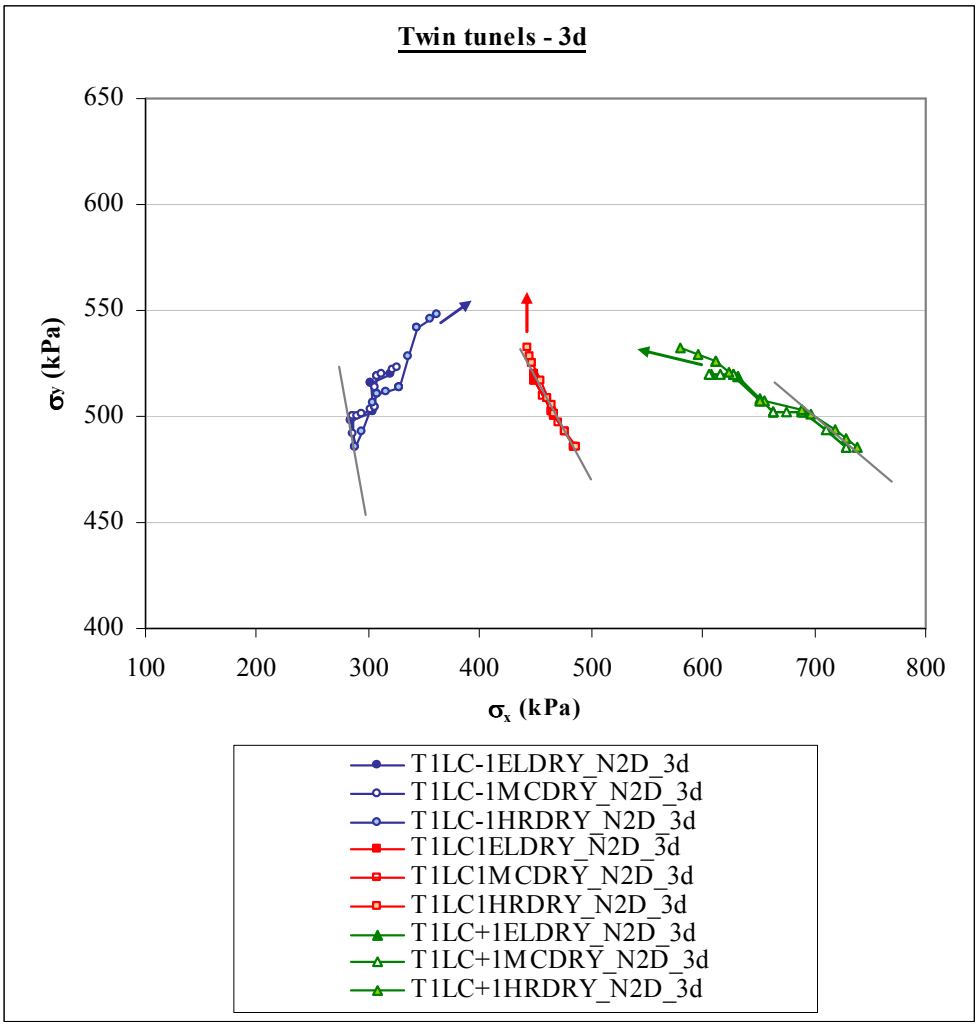

Figure 4.8. Stress paths at the springline between twin tunnels separated by a distance of 3.0 *d* between centrelines for K_0 conditions below (blue), equal to (red) and above "1" (green)

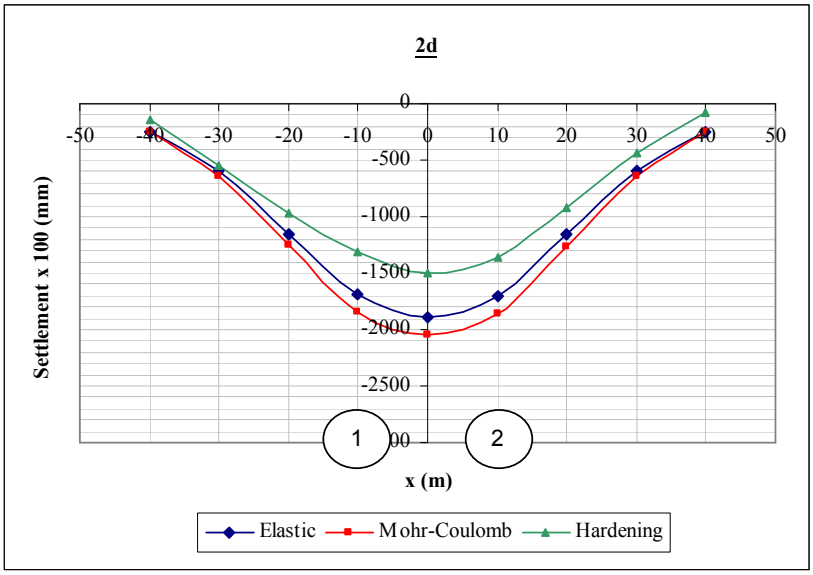

Figure 4.9. Calculated vertical transverse surface settlement troughs above twin tunnels separated 2.0 *d* between centrelines considering K_0<1 conditions and using the Elastic, Mohr-Coulomb and Hardening constitutive models

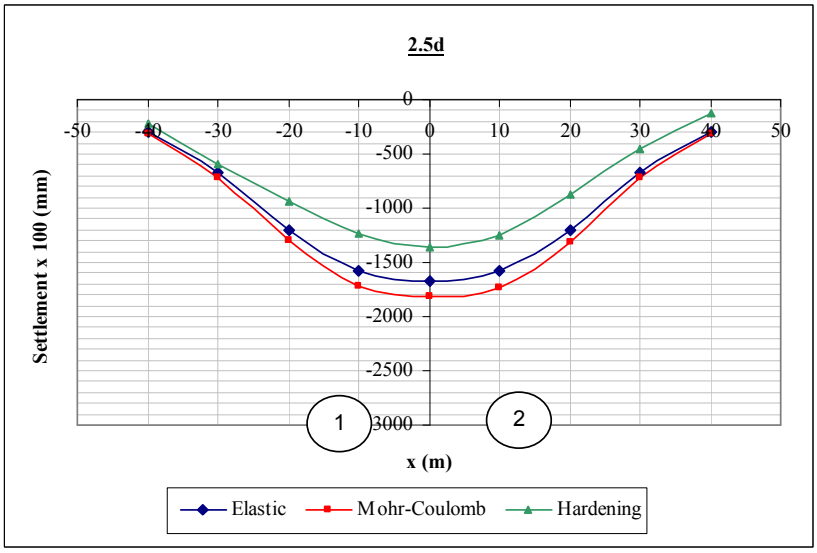

Figure 4.10. Calculated vertical transverse surface settlement trough above twin tunnels separated 2.5 *d* between centrelines considering K_0<1 conditions and using the Elastic, Mohr-Coulomb and Hardening constitutive models

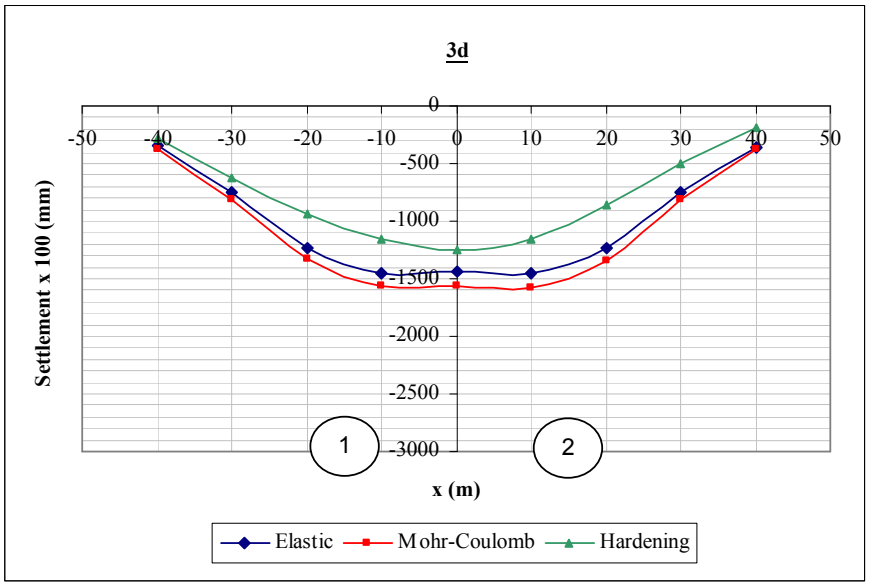

Figure 4.11. Calculated vertical transversal surface settlement trough above twin tunnels separated 3.0 *d* between centrelines considering K_0<1 conditions and using the Elastic, Mohr-Coulomb and Hardening constitutive models

4.2.4. Sensitivity Analyses

Figures 4.12, 4.13 and 4.14 illustrate the results from the sensitivity analyses performed in order to observe the dependency of the stress paths at points A and B to various soil, lining and analysis parameters, based on the S1LC1MCDRY_N2D, S1LC-1MCDRY_N2D and S1LC+1MCDRY_N2D analyses respectively. Figure 4.15 shows the results from the sensitivity analysis carried out based on S1LC+1HRDRY_N2D. The effect of having different initial stress conditions (i.e. a different K_0) in the ground on the surface settlement trough when using the Hardening model can be observed in Figure 4.16. The occurrence of plastic points in the ground for the different K_0 values is illustrated in Figure 4.17. The effect of using different *m* values for the Hardening model when $K_0 = 1.52$ on the transversal surface settlement profile is shown in Figure 4.18.

	$K_0 = 1$ (S1LC1MCDRY_N2D)	
	POINT A (CROWN)	**POINT B (SPRINGLINE)**
E	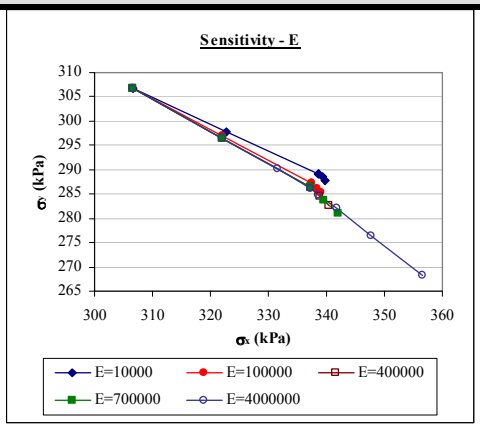	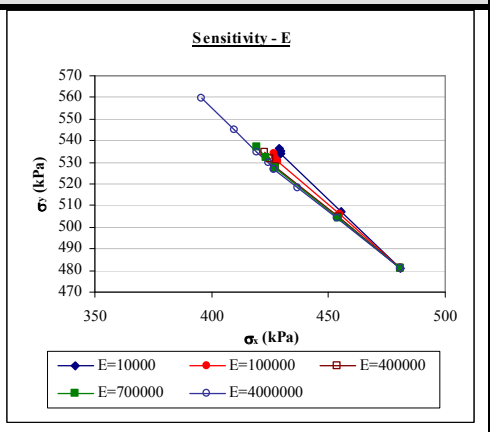
c'	No variation	No variation
ϕ'	No variation	No variation
ν_s	No variation	No variation
E_Δ	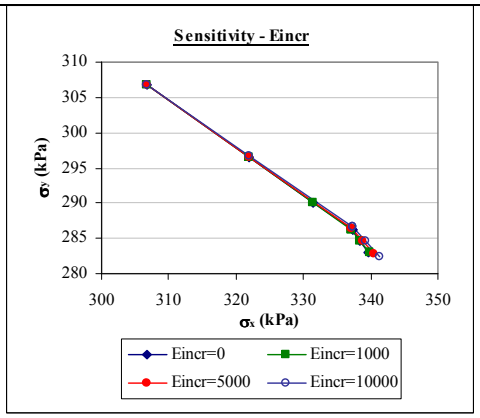	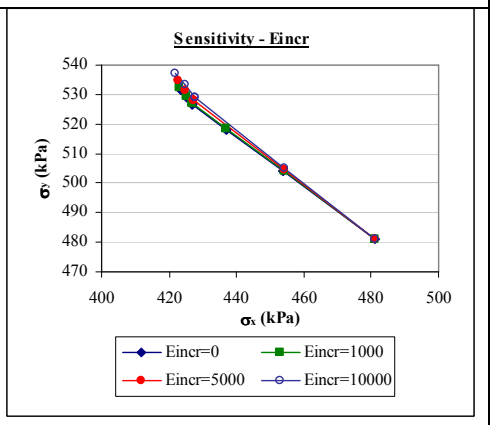
c_Δ	No variation	No variation
ψ	No variation	No variation

Figure 4.12. Sensitivity analysis with respect to the Mohr-Coulomb parameters, the lining properties and the mesh coarseness when $K_0 = 1$

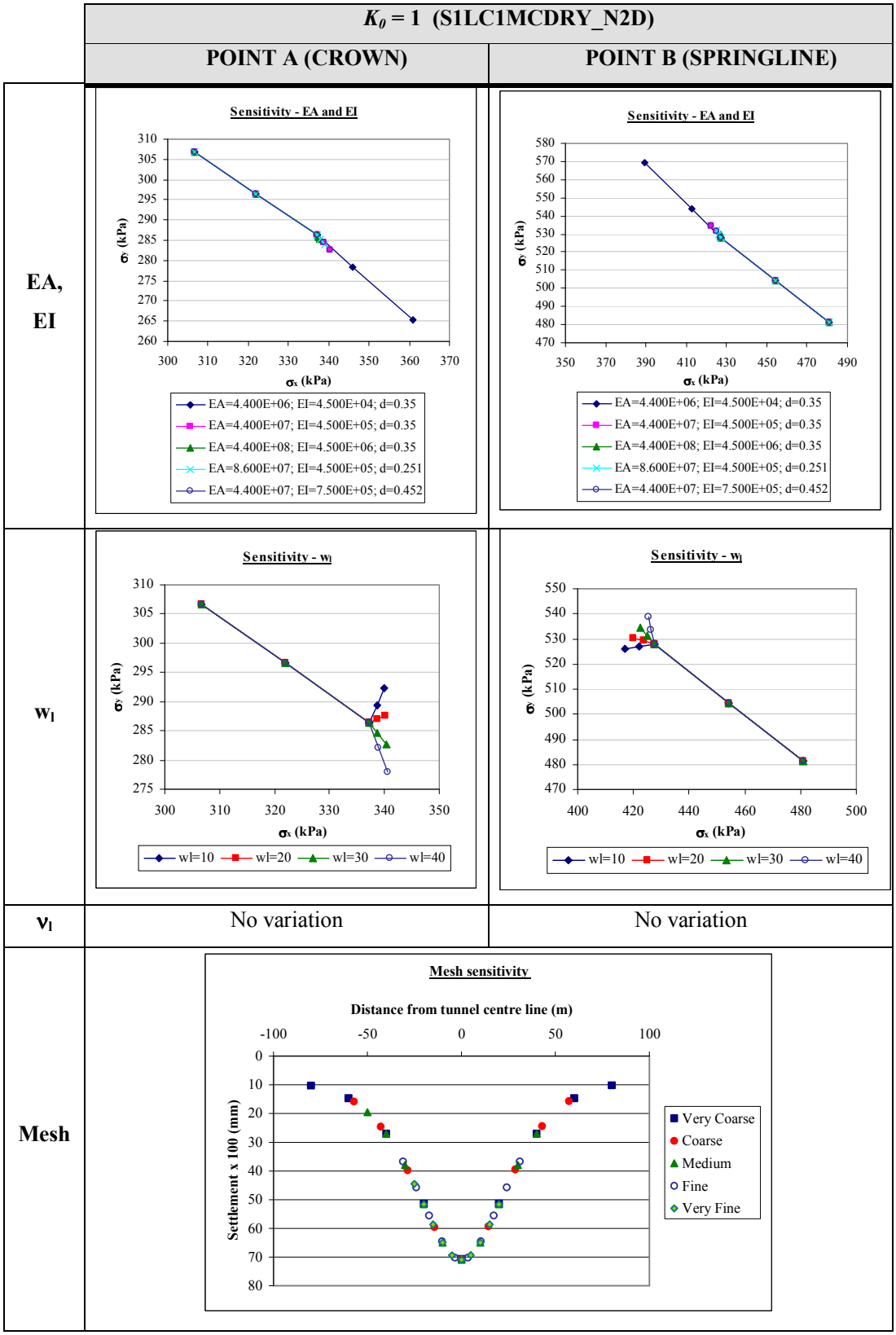

Figure 4.12 continuation. Sensitivity analysis with respect to the Mohr-Coulomb parameters, the lining properties and the mesh coarseness when $K_0 = 1$

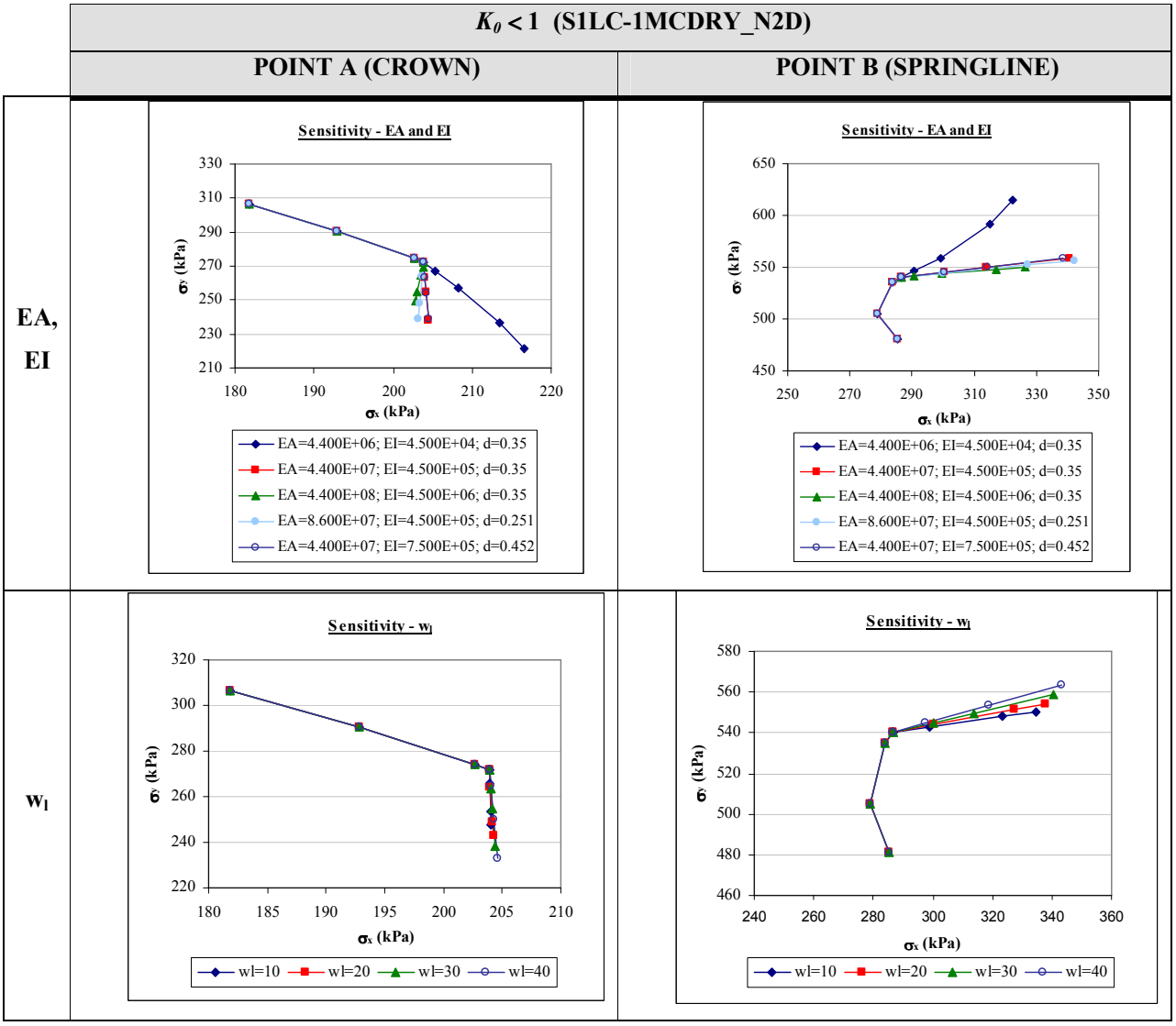

Figure 4.13. Sensitivity analysis with respect to the lining properties when K_0<1

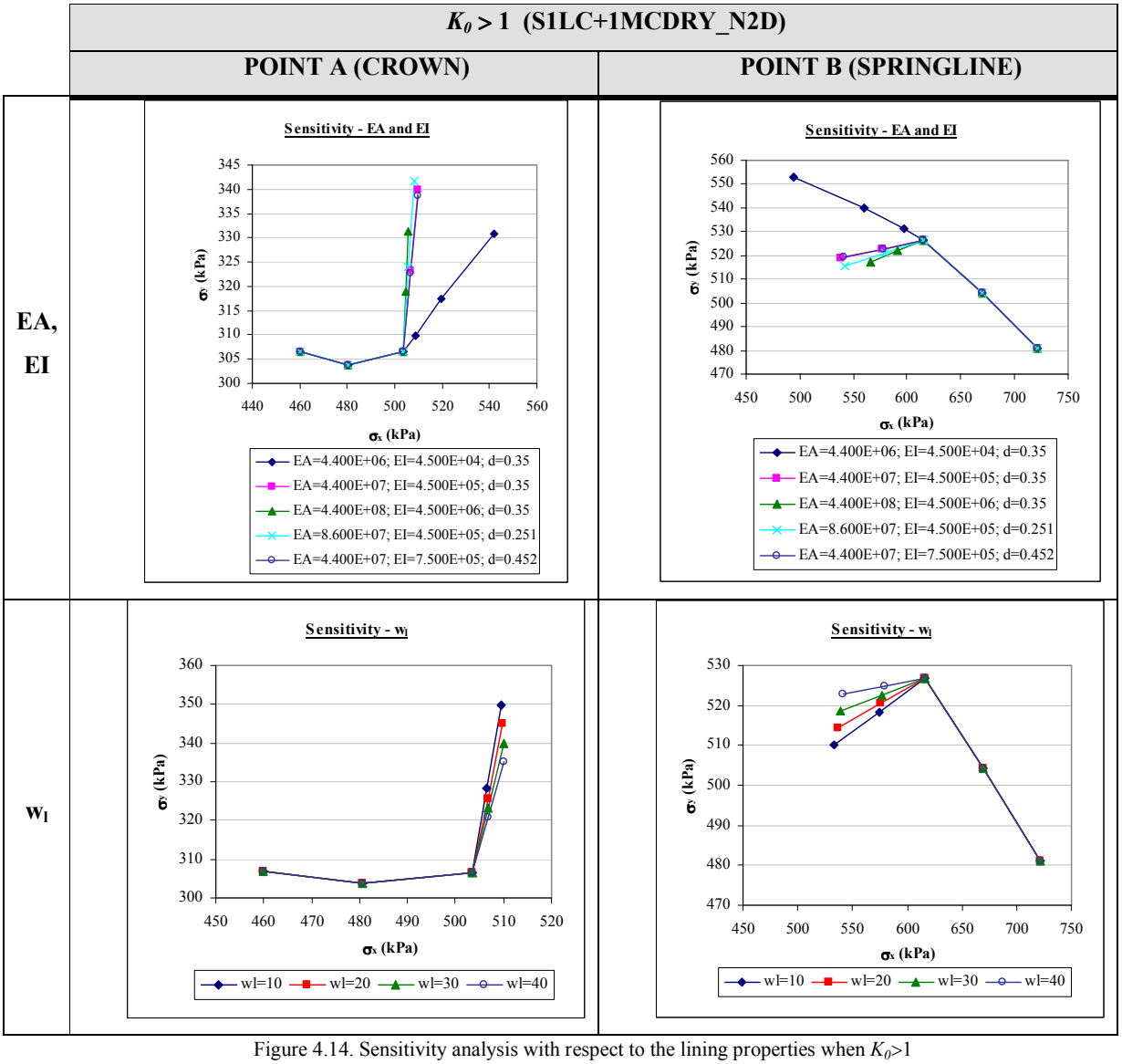

Figure 4.14. Sensitivity analysis with respect to the lining properties when K_0>1

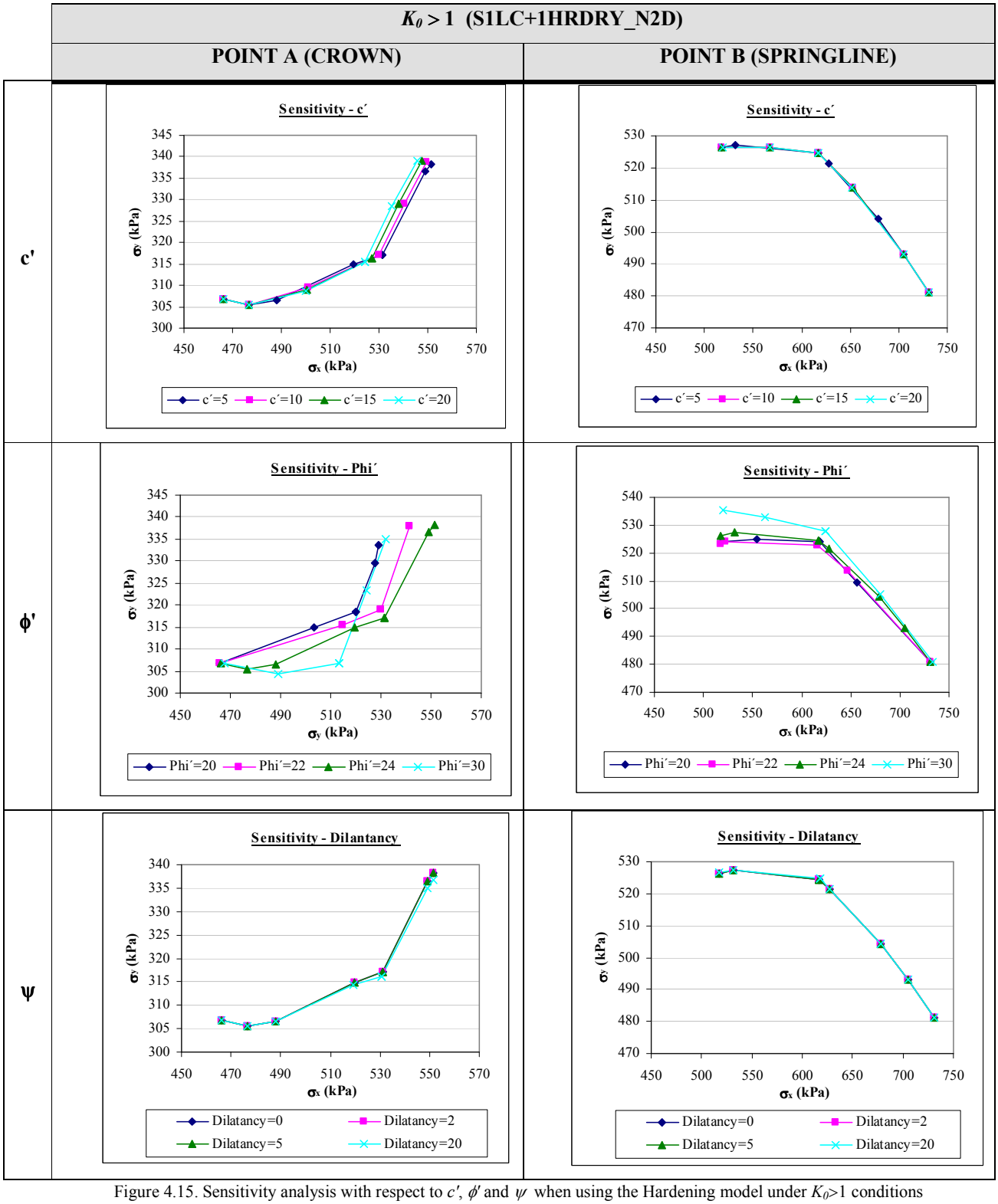

Figure 4.15. Sensitivity analysis with respect to c', ϕ' and ψ when using the Hardening model under K_0>1 conditions

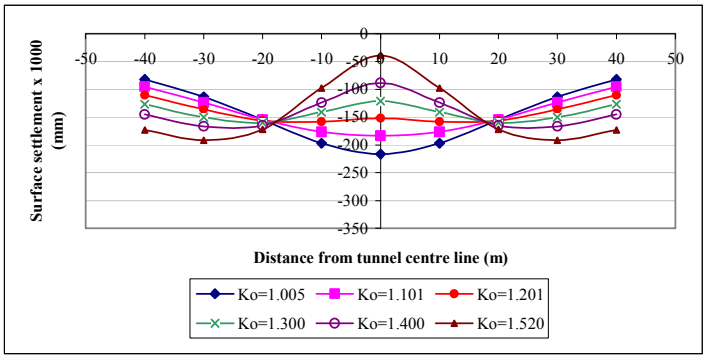

Figure 4.16. Surface settlement trough above a single tunnel when using the Hardening model for various K_0 values

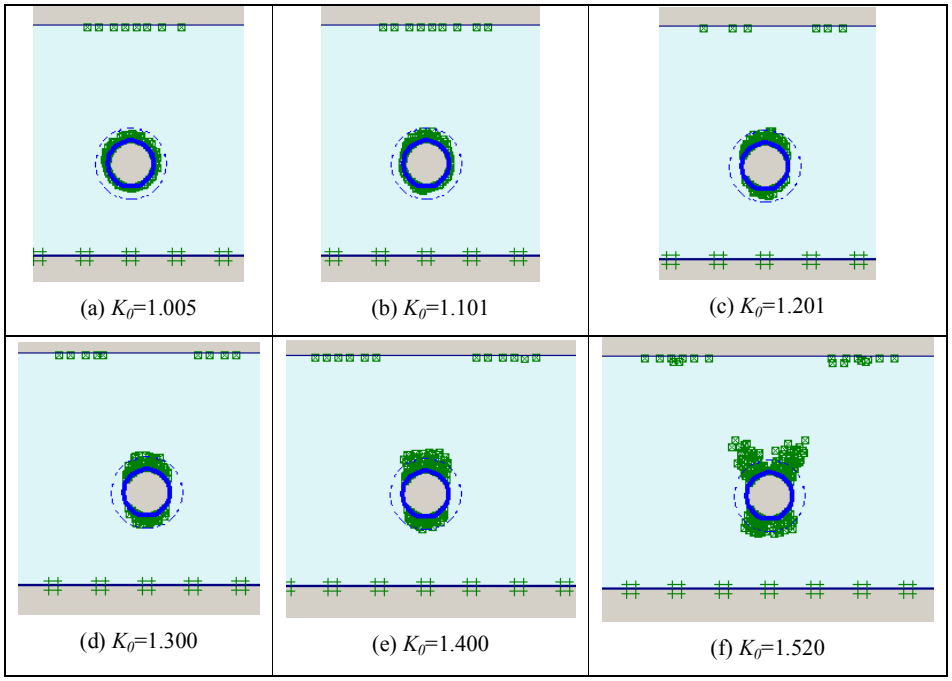

Figure 4.17. Occurrence of plastic points for increasing values of K_0 when using the Hardening model

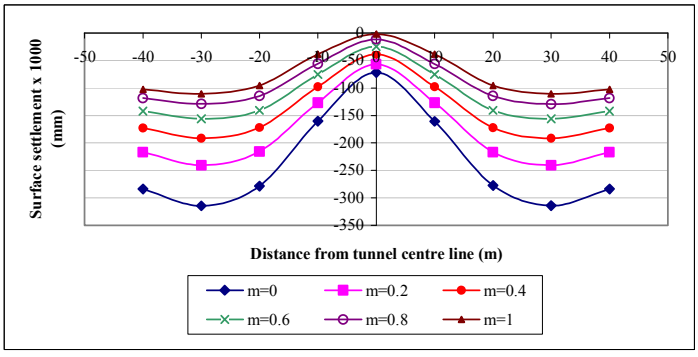

Figure 4.18. Surface settlement trough above a single tunnel when using the Hardening model and K_0 = 1.52 for various m values

4.2.5. 1-layer 3D Single Tunnel

Considering the initial stresses in the ground given by K_0 below, equal to and above unity and 'dry' conditions, the stresses at points A* (crown) and B* (springline) on the measurement section were calculated during the advance of the tunnel. Figure 4.19 illustrates the results for K_0<1 in terms of σ_x, σ_y and σ_z (according to PLAXIS coordinates) at points A* and B* varying with respect to the position of the front of the excavated tunnel for the Elastic, Mohr-Coulomb and Hardening models. Figures 4.20 and 4.21 illustrate the same but for K_0 equal to and above unity and only for the Mohr-Coulomb model. Figure 4.22 shows the stress paths at points A* and B* on the x - y plane for the Linear Elastic, Mohr-Coulomb and Hardening models for K_0 below, equal to and above "1".

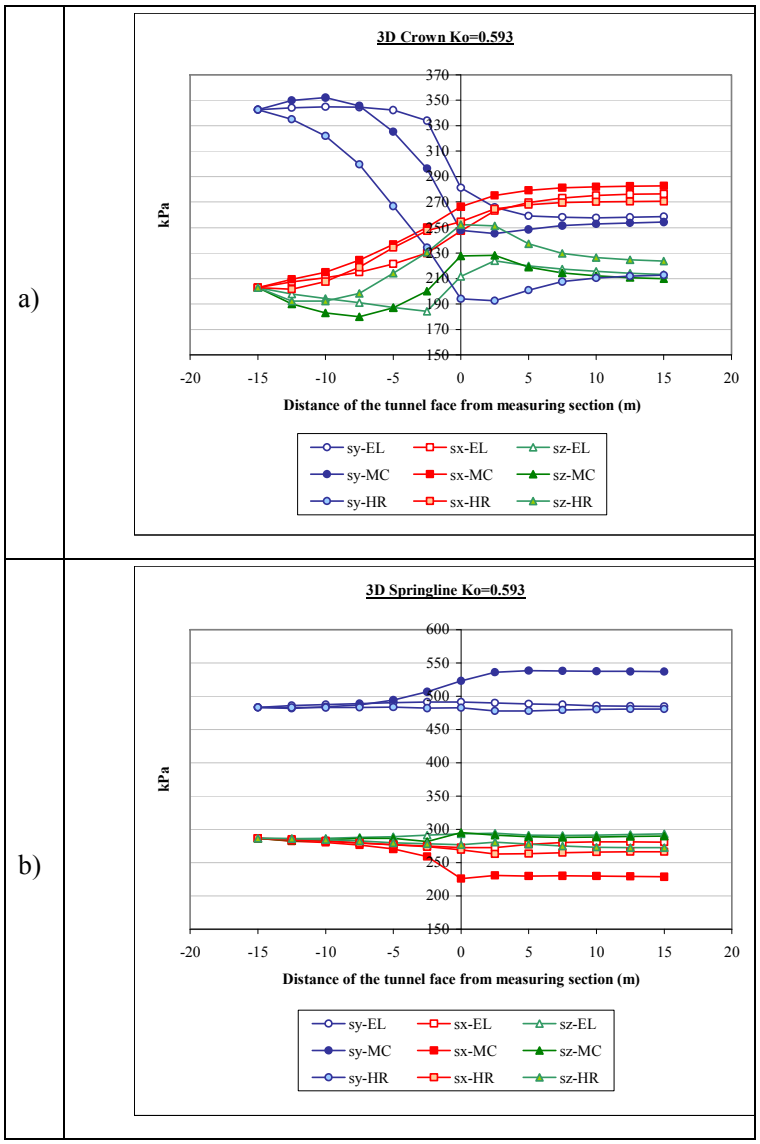

Figure 4.19. 3D-changes in σ_v, σ_x and σ_z at the measurement section points (a) A* and (b) B* with respect to the position of the tunnel face using the Elastic, Mohr-Coulomb and Hardening models when K_0<1

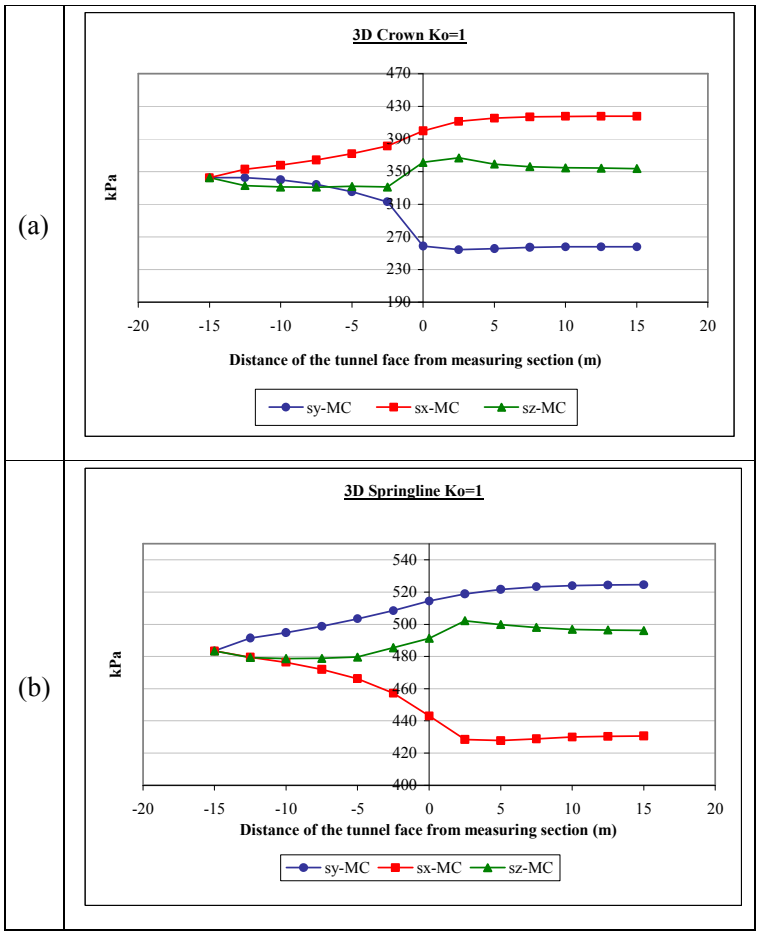

Figure 4.20. 3D-changes in σ_v, σ_x and σ_z at the measurement section points (a) A* and (b) B* with respect to the position of the tunnel face using the Mohr-Coulomb model when $K_0 = 1$

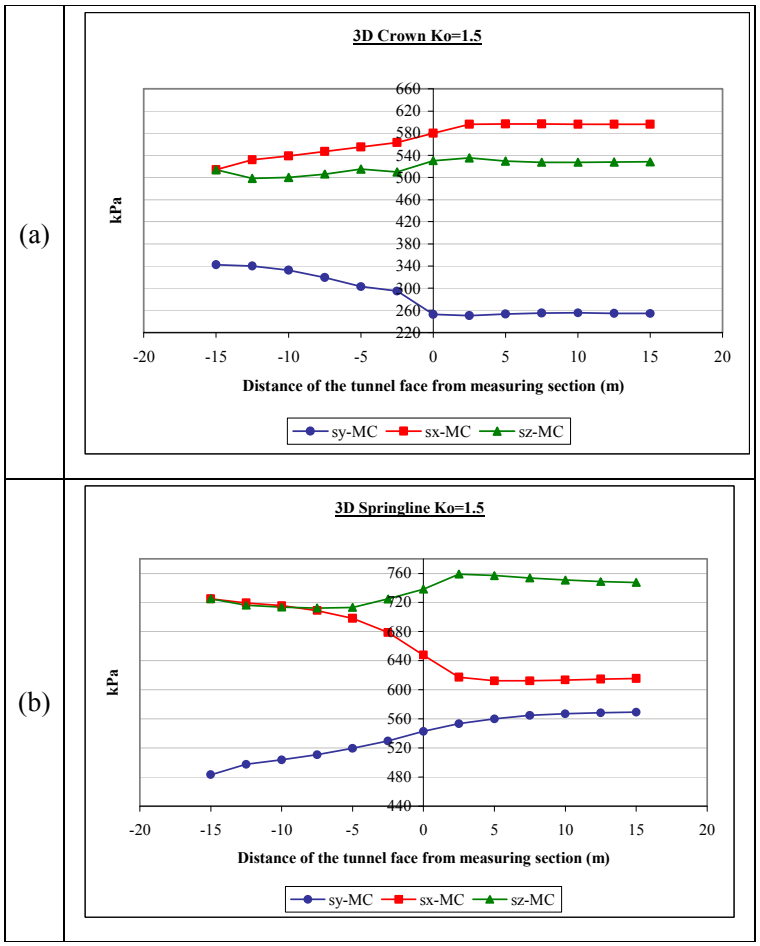

Figure 4.21. 3D-changes in σ_v, σ_x and σ_z at the measurement section points (a) A* and (b) B* with respect to the position of the tunnel face using the Mohr-Coulomb model when K_0>1

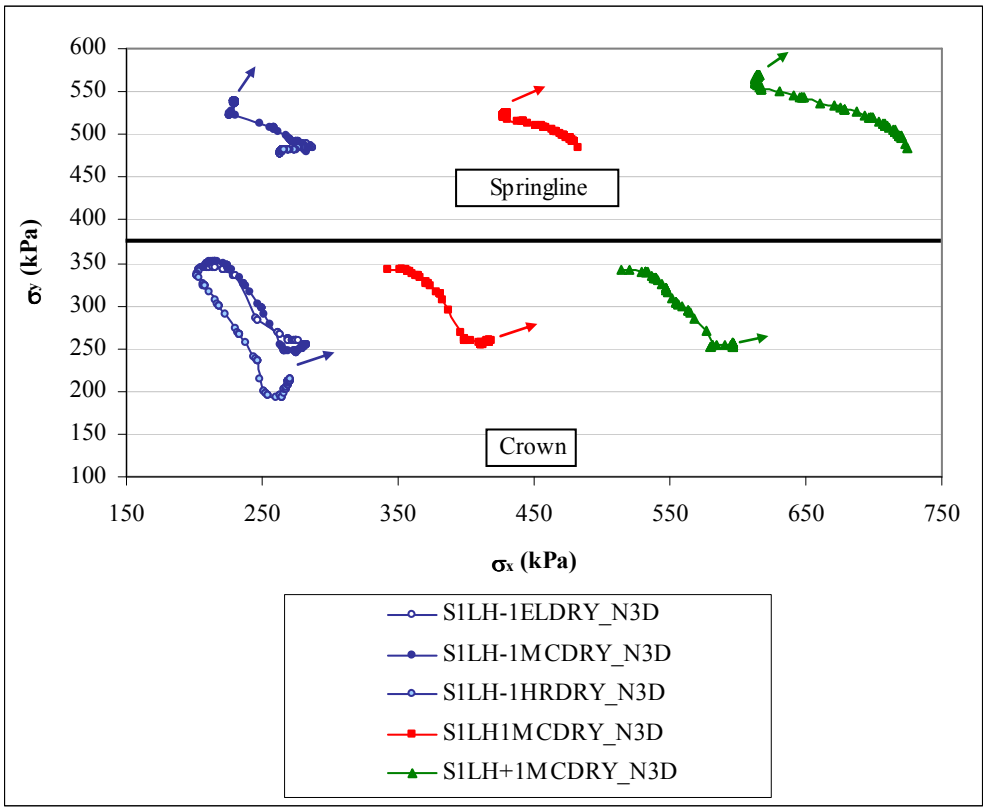

Figure 4.22. Stress paths at point A* and B* in terms of σ_x and σ_y using the Elastic, Mohr-Coulomb and Hardening models for K_0 below, equal to and above "1"

Figure 4.23 illustrates the longitudinal total displacements, the vertical and horizontal (in the *x*-direction) displacements on the x = -2.5 m plane, the transverse surface settlement trough and deformed tunnel contours as well as the three-dimensional surface settlement trough predicted by the Mohr-Coulomb model for K_0 below, equal to and above "1".

	K_0 = 0.593	K_0 = 1	K_0 = 1.5
(a)	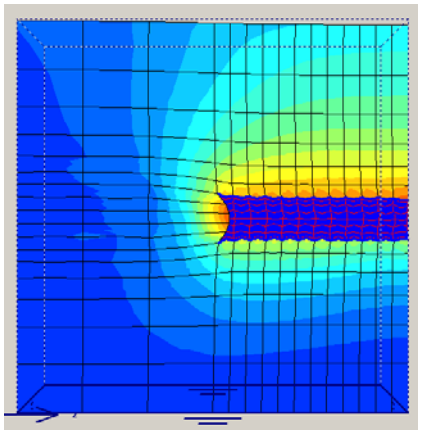 Displacements scaled 500times	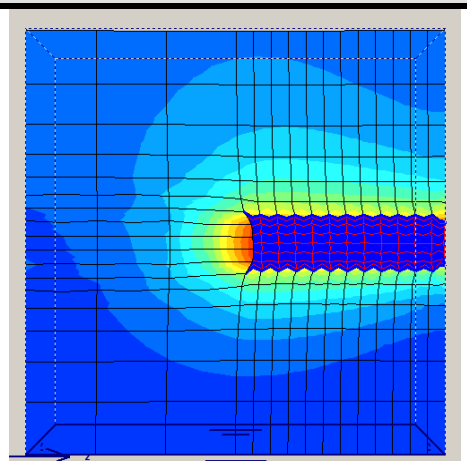 Displacements scaled 500times	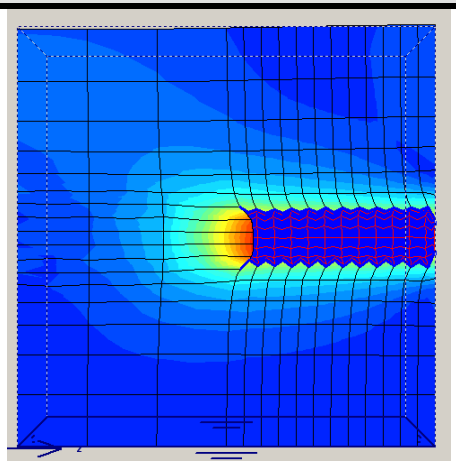 Displacements scaled 500times
(b)	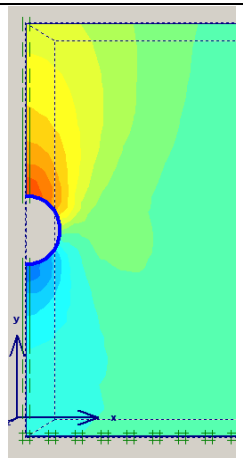 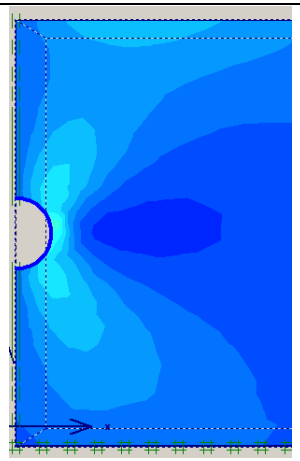	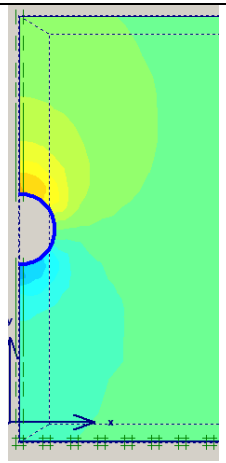 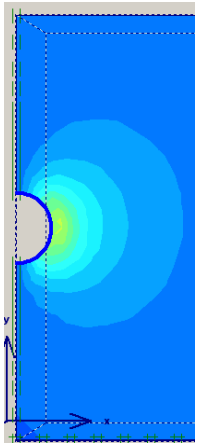	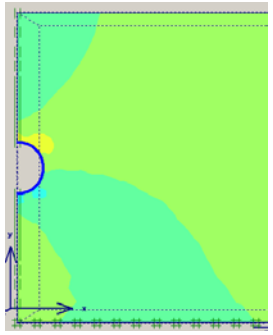 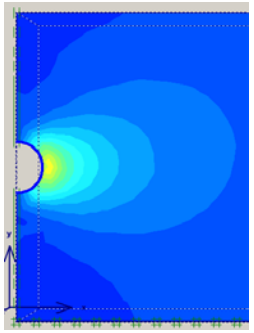

Figure 4.23. (a) Longitudinal total displacements, (b) Vertical and horizontal-x displacements on the x = -2.5 m plane, (c) Transverse surface settlement trough and deformed tunnel contour and (d) 3D surface settlement trough for K_0 below, equal to and above "1" using the Mohr-Coulomb criterion

	$K_0 = 0.593$	$K_0 = 1$	$K_0 = 1.5$
(c)	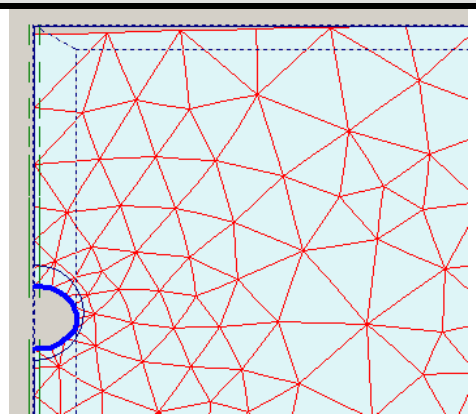 Displacements scaled 500times	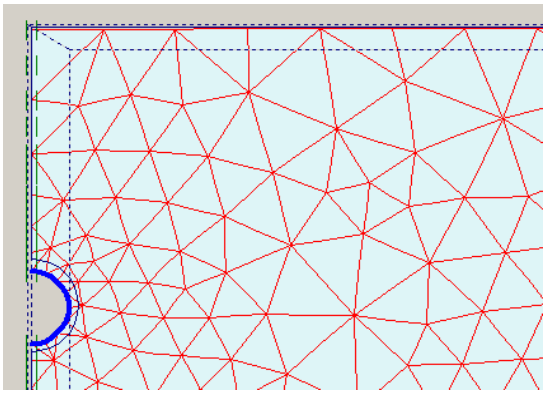 Displacements scaled 500times	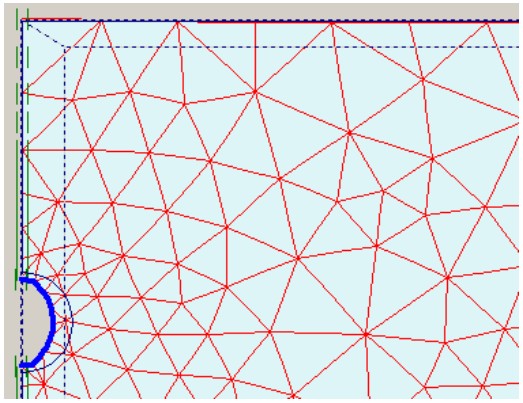 Displacements scaled 500times
(d)	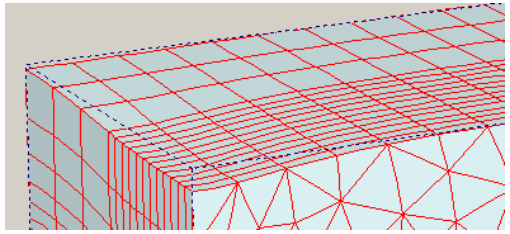 Displacements scaled 2000times	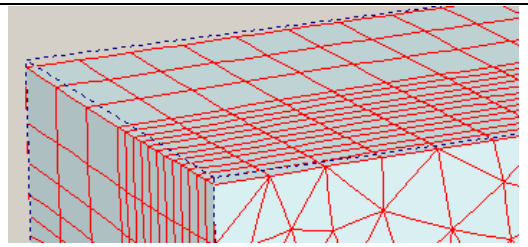 Displacements scaled 2000times	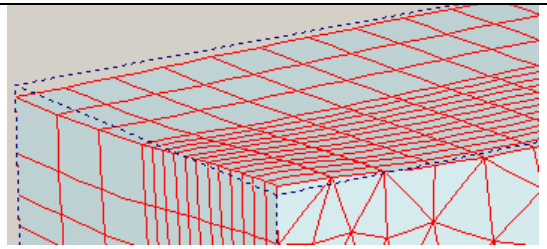 Displacements scaled 2000times

Figure 4.23 continuation. (a) Longitudinal total displacements, (b) Vertical and horizontal-*x* displacements on the x = -2.5 m plane, (c) Transverse surface settlement trough and deformed tunnel contour and (d) 3D surface settlement trough for K_0 below, equal to and above "1" using the Mohr-Coulomb criterion

4.3. DISCUSSION

This section discusses the 2D and 3D results presented in Section 4.2, investigates the soil-tunnel interaction mechanisms taking place during the analyses and evaluates the observed total stress trends.

4.3.1. 2D

4.3.1.1. Single tunnel

The stress paths derived from the 2D PLAXIS analyses at points A (above the crown) and B (springlines), and represented in terms of total vertical and horizontal stresses on a plane perpendicular to the tunnel axis, can be divided into two parts: the first corresponding to the excavation-relaxation of the soil (first construction stage in PLAXIS v.8.2), which will be named PART 1 according to the description in Section 3.6.3, and the second part corresponding to the application of the tunnel support (second construction stage) and named PART 2 in this thesis. In Figure 4.2, for example, these can be easily identified as the first and second segments of each of the stress paths, both of them generally with a clearly marked different orientation in the σ_y - σ_x plane, this being more obvious for the K_0>1 and K_0<1 cases. PARTS 1 and 2 vary when using the different constitutive models, but the trends are very similar. It should be noted that the stress changes given by PLAXIS during PART 2 may be somewhat exaggerated due to PART 1 being calculated as an incomplete staged construction in which only part of the out of balance stresses caused by the excavation are actually solved. Figure 4.1 considers only the excavation stage and it can be correlated to the same stage in Figure 4.2 for comparison. The stress paths during the excavation stage follow certain trends as indicated by the light grey lines in Figure 4.2, which can be again correlated with Figure 4.1 and are described in Table 4.1 for various K_0 conditions. These trends indicate that the slope σ_y / σ_x is higher for K_0<1, reducing for K_0 = 1 and further reducing for K_0>1 at both the crown and the springlines.

The present results have been compared to those from previous authors (Section 2.2.3) in order to observe whether similar trends during tunnel excavation (the first construction stage in PLAXIS) could be deduced from their data. In this sense, the decrease in σ_y and the increase in σ_x at points above the tunnel crown, as well as the decrease and increase in σ_x and σ_y respectively at the springline, and the ovalisation of the tunnel circumference have been previously stated by various authors (Mair, 1979; Ng and Lo, 1985; Lee and Rowe, 1989; Addenbrooke, 1996; Barla, 1999 and Bernat et al., 1999). These trends can be also related to the arching effect, which implies that the load at the tunnel crown is transferred to the sides during excavation creating positive (e.g. springline) and negative (above tunnel crown) arching zones as presented by Lee et al. (2006). The arching ratio is defined as the quotient between the change in vertical stress during tunnelling and the total overburden pressure times 100. As commented by the author, those elements that receive higher load transfers from adjoining yielding or flexible elements generate larger positive arching ratios, whereas those elements that shift load to the non-yielding parts will present negative arching ratios. Negative arching ratios were therefore higher at elements close to the tunnel

perimeter than at points above the tunnel centreline but closer to the ground surface. Similarly, larger positive arching ratios would be encountered at springline elements close to the tunnel opening than at those situated at the same depth but further distant from the tunnel. Negative arching ratios are therefore related to extension states and positive arching ratios to compressive states.

In terms of the relative variation between σ_y and σ_x, very similar trends to the ones observed from the present analyses can be deduced from the results presented by Barla (1999) (Section 2.2.3) for $K_0 = 1$ and $K_0 = 2$.

The decrease in σ_y (vertical extension conditions) and σ_x (vertical compression conditions) at the tunnel crown and springline respectively during excavation was also identified during this project when performing preliminary calculations using the Empirical method according to the methodology in Section 3.2 (see Appendix A – Section A.1). Since the *ΣMstage* parameter controls how much the soil is allowed to relax after excavation and just before placing the lining, increasing the *ΣMstage* values gives rise to a further decrease in σ_y at the crown and in σ_x at the springline as shown in Figure 4.1.

Table 4.1. Total 2D stress path trends predicted at points above the tunnel crown and at the springlines for K_0 conditions below, equal to and above "1"

Measurement point and K_0 conditions	σ_y (vertical)	σ_x (horizontal)	$p=(\sigma_y+(2\sigma_x))/3$	$s=(\sigma_y+\sigma_x)/2$	$q=\sigma_y-\sigma_x$	$q^*=\sigma_1-\sigma_3$	$t=(\sigma_y-\sigma_x)/2$	$t^*=(\sigma_1-\sigma_3)/2$
CROWN $K_0<1$	Decreases	Increases	Increases	Decreases	From + decreases (can go to -)	From - decreases	From + decreases (can go to -)	From - decreases
CROWN $K_0=1$	Decreases	Increases	Increases	Increases	From 0 decreases	From 0 increases	From 0 decreases	From 0 increases
CROWN $K_0>1$	Decreases	Increases	Increases	Increases	From - decreases	From + increases	From - decreases	From + increases
SPRINGLINE $K_0<1$	Increases	Decreases	Increases	Increases	From + increases	From - decreases	From + increases	From - decreases
SPRINGLINE $K_0=1$	Increases	Decreases	Decreases	Decreases	From 0 increases	From 0 decreases	From 0 increases	From 0 decreases
SPRINGLINE $K_0>1$	Increases	Decreases	Decreases	Decreases	From - increases (can go to +)	From + decreases (can go to -)	From - increases (can go to +)	From + decreases (can go to -)

Figure 4.4 shows that the stress path trends are unchanged when using either the groundwater level at the ground surface ('wet' conditions) or at the base of the geometry well below the tunnel invert ('dry' conditions).

When the geometry in the analysis is divided into three different layers in an attempt to reproduce more realistic conditions (i.e. soil properties varying with depth), the stress path trends are still the same as illustrated in Figure 4.5 at both the crown and the springlines.

Most of the PLAXIS analyses performed in this project involved the application of a tunnel support, hence the author has found it interesting to explain, in a simplified manner, the mechanisms that are occurring during the analyses that give rise to the observed stress paths (e.g. those shown in Figure 4.2) and why some of the parameters involved in the analyses and used for the sensitivity analysis have such a large effect on the second part of the stress paths (i.e. PART 2 corresponding to the application of the lining) as shown in Figures 4.12, 4.13 and 4.14. When a cavity is excavated in PLAXIS v.8.2 by removing part of the soil mesh elements and the soil is subsequently allowed to partially relax (β_{PL}-method), the equilibrium in the ground is altered and the soil suffers from two simultaneous effects: (1) movement of the ground towards the opening (convergence) and (2) uplift. Figure 4.24 illustrates these mechanisms in a simplified way for K_0 below and above "1".

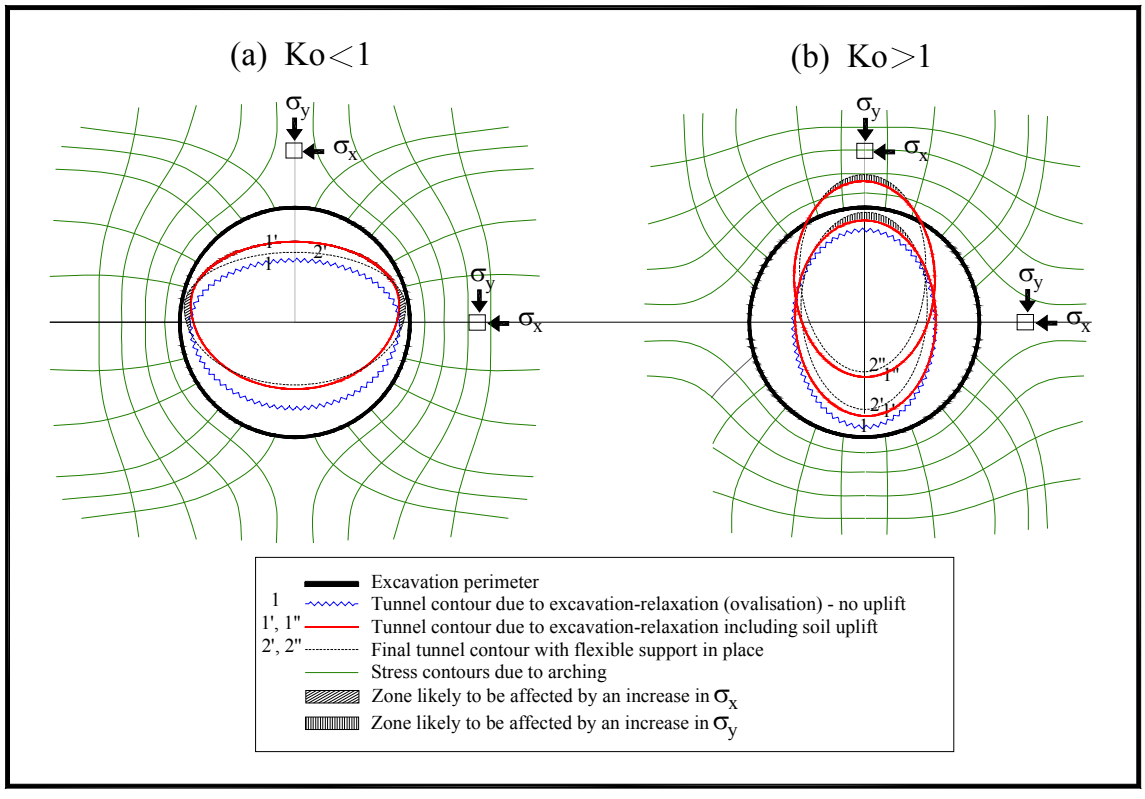

Figure 4.24. Idealised mechanisms occurring during a cavity unloading in PLAXIS for (a) Normally consolidated soil (K_0<1) and (b) Overconsolidated soil (K_0>1)

For K_0<1, the soil moves towards the opening with larger deformations at the tunnel crown than at the invert (even when having the weight of the soil above the tunnel being transferred to the sides due to arching) and larger at the invert than at the springlines (line "1" in Figure 4.24a) creating an oval-shaped tunnel contour with the largest axis being horizontal. Due to the uplift, the new tunnel contour is also pushed upwards (line "1' " in Figure 4.24a). The tunnel support is placed at some point according to the ground reaction curve in order to find the right balance between the soil deformations and final stresses applied on the lining. From this moment, the movements and changes in stress in the soil are largely controlled by the lining until equilibrium is reached (line "2' " in Figure 4.24a). This is why the flexural rigidity (EI), the axial stiffness (EA) and the weight (w_l) of the lining are the parameters to which the analyses are more sensitive, as illustrated in Figures 4.12, 4.13 and 4.14. The stiffer the lining the larger the final stresses applied on it and the smaller the soil deformations. At the crown, for a lining with some flexibility, σ_y will continue reducing (but less) and therefore some vertical deformation will still occur. At the springline, as the tunnel is squeezed further, the lining is pushed away towards the ground that is probably still converging and therefore an increase in horizontal stress at the springline can be observed. Theoretically, the stiffer the lining, the lower the increment in σ_x at the springline and the lower the decrease in σ_y occurring at the crown and so a smaller overall settlement would be obtained at the ground surface. This effect is not very clear at the springline in Figure 4.14 since the variation in σ_y at this position in the ground may be having a large effect. The effect of w_l when K_0<1 at the springline is an increase in both σ_y and σ_x, being larger for heavier linings. At the crown, the effect in σ_x is almost negligible, but σ_y is shown to further decrease for heavier linings.

Under K_0>1 conditions, the mechanism is virtually the same, but reversed between the crown and springline and slightly more complicated. In this case, due to the excavation, the soil moves towards the cavity with larger deformations at the springline followed by the crown and invert respectively creating an oval-shaped tunnel contour with the largest dimension being vertical (line "1" in Figure 4.24b). If the uplift effect is added, then, depending on its magnitude, the new tunnel contour would be moved either to "1' " or to "1" ". At the springline, when the tunnel support is placed, the decrease in σ_x (and so the deformations) will be restricted until equilibrium is reached. Since the tunnel will be further squeezed during this construction stage, the lining pushes the soil upwards at the crown that is still moving towards the opening and hence the vertical stress at points above the tunnel crown could well increase further until attaining the final tunnel shape represented by lines "2" or "2" " in Figure 4.24b. It should be noted that situation "2' " would give rise to a surface settlement trough similar to those illustrated in Figures 4.3b2, whereas "2" " would give rise to a net heave on the ground surface. Theoretically, for a stiffer lining the increase in σ_y at points above the tunnel crown should be smaller and the other way round, but this is not clearly observed in Figure 4.12 since the variation in σ_x may be having a large effect. The effect of w_l

when K_0>1 at the springline is such that the lighter the lining the larger is the decrease in both σ_y and σ_x. At the crown, the effect in σ_x is almost not noticeable and the increase in σ_y is shown to be larger for the less heavy linings.

The effect of *EI* and *EA* is more obvious for K_0<1 and K_0>1 and the effect of w_l is more obvious for K_0 = 1.

The orientation of PART 2 on the stress paths has been shown to be dependent on the parameters of the lining (also for the K_0 = 1 case in Figure 4.12) compared to PART 1, which is virtually unaffected by the varying conditions in the analyses.

It can be observed in Figure 4.12 that varying c', ϕ' and ψ have no influence in the results. This is only true, however, because plasticity was not occurring (or only very localised just on the tunnel crown and invert for K_0>1 and at the springline for K_0<1) in the Mohr-Coulomb analyses and these parameters only intervene when the soil reaches plastic conditions. Since the number of plastic points was found to increase when using the Hardening model for K_0 values increasing above "1" as shown in Figure 4.17, a sensitivity analysis with respect to c', ϕ' and ψ was carried out using this constitutive model concentrating on the K_0 = 1.5 condition. The results illustrated in Figure 4.15 indicate that these parameters do not have much effect on the stress path trends. From the three parameters, ϕ' has the largest effect, especially at the crown. Part of this variation is, however, related to the fact that the OCR of the clay was modified in the analyses for each ϕ' in order to keep K_0 constant and equal to about 1.5, as previously stated in Section 3.3.1.6.

The coarseness of the mesh used for the analyses has been shown not to affect the results in terms of the surface settlement trough as illustrated in Figure 4.12.

Regarding the final shape of the surface settlement trough, the present results show that for K_0<1 the convergence effect is larger than the uplift at all points in the ground hence a net settlement is observed at the ground surface. For K_0>1 however, the mechanisms have generally been found to give a net transverse surface settlement trough of the wrong shape (i.e. different from a Gaussian-shaped curve, with the maximum settlement not occurring at the tunnel centreline) due to localised heave in the vicinity of the tunnel corresponding to a situation such as "2' " in Figure 4.24b. This effect has been observed in Figures 4.3b2 and 4.16, in the latter case for values of K_0 above 1.1 and when using the more advanced non-linear Hardening model (using m = 0.4). Using different values for the parameter m in the Hardening model, which controls the stiffness dependency to the stress level, gives rise to different magnitudes for the surface settlements, but the shape remains the same as illustrated in Figure 4.18. If larger values of *ΣMstage* are used, the predicted settlements are also larger as expected, but the transverse shape illustrated in Figure 4.3 remains for certain values of K_0. It should be noted that the use of the user defined small-strain pre-yield Jardine et al. (1991) + Mohr-Coulomb model did not significantly improve the prediction of the surface settlement profiles for K_0>1 during the present investigation. The settlement

trough width calculated by PLAXIS in the K_0>1 case is also much wider than for K_0<1 due to the concentration of soil deformations at the springlines as illustrated in Figure 4.3b3.

Since it was not the intention of the present study to simulate and back-analyse a real case study, but the identification of general trends in stress changes induced by hypothetical tunnel excavations, the concept of accuracy of the predictions in reproducing real field data was not really applicable and has therefore not been investigated in detail. However some obvious shortcomings have been identified, including the tendency to predict relatively shallow and wide profiles and the shape of the surface transverse settlement trough identified earlier on the surface settlement trough for values of K_0 above "1". Both observations had been previously reported (Section 2.2.2).

These predicted surface settlements for K_0>1 are believed to be incorrect mainly because reported in-situ measurements are normally of similar shape to those for K_0 below unity conditions. On the other hand however, other references can be found in the literature that report on uplift movements being registered in-situ during the excavation of a tunnel in K_0 above unity conditions (e.g. Myrianthis, 1981). The author referred to the definition of the stress created after erection of the lining and setting of the grout as a matter of speculation, but noted a tendency for uplift above the tunnel crown. This uplift had been recorded for example by Attewell and Farmer (1974), who reported an increasing vertical diameter and decreasing horizontal diameter of the clay surrounding the recently erected lining. The K_0 effect on the excavation of shallow tunnels has also been studied by Guedes de Melo and Santos Pereira (2000) by means of two and three-dimensional FEA using ABAQUS. One of their findings was that the larger the value of K_0, the smaller the settlements at the ground surface.

It should also be pointed out that in the current investigation the tunnels have been excavated as full-sections rather than in steps and the lining has been assumed to be uniform all around the tunnel contour and equal for all K_0 cases. It is believed that the heave effects may be reduced by dividing the excavation of the cavity into different stages and perhaps using variable lining properties along the tunnel periphery.

The performance of the constitutive models used for the present analyses is believed to be limited by the fact that none of them has features to account, at the same time, for some well established patterns in soil behaviour that have been reported to control the mechanisms occurring when tunnelling and therefore improve the predictions (e.g. anisotropy, elasto-plasticity during unloading, non-linear elastic stiffness). For the purposes of the present analyses, however, the simple geometries and construction sequences used as well as the constitutive models available in PLAXIS v.8.2 were considered appropriate as a preliminary insight into the problem. From these analyses, very consistent stress paths patterns have been obtained at points above the tunnel crown and at the tunnel springline, given the small deformations induced during the proposed tunnel constructions, and these could be easily reproduced in the stress path cell. Until this point nothing has been said with regard to the occurrence of shear stresses at points A and B during the tunnelling process. As briefly introduced in Section 3.3.1.4, very small shear stresses were expected at points above the tunnel crown (such as point A). From the two-dimensional analyses of single

tunnels the maximum shear stress ($\sigma_{xy} = \sigma_{yx}$) value at point A was found to be -1.73 kPa corresponding to the Mohr-Coulomb model in K_0 below unity conditions. At the springline (point B), the maximum shear stress was -17.8 kPa, this being obtained using the Jardine model also in K_0 below unity conditions. The assumption of no rotation in the triaxial cell during stress path testing may therefore be more unrealistic when representing the conditions at the tunnel springlines. It was additionally observed that at the springlines the shear stresses were negative for K_0<1, negative but very small for K_0 = 1 and positive for K_0>1. For both the K_0<1 and K_0>1 cases, the magnitude of the negative or positive shear stress respectively was found to increase for the different constitutive models according to the following order: Elastic, Mohr-Coulomb, Hardening and Jardine.

4.3.1.2. Twin tunnels

The stress paths obtained at a point situated at the springline between twin tunnels show virtually the same trends as those observed for single tunnels, but repeated twice (see Figures 4.6, 4.7 and 4.8). The first PART 1 and PART 2 corresponds to the excavation and placement of the lining respectively for the first tunnel. The second PART 1 and PART 2, named here PARTS 3 and 4 respectively, corresponds to the excavation and placement of the support for the second tunnel. The change in stresses is observed to be larger for the distance of 2.0 *d* between tunnel centrelines, and further decrease for 2.5 *d* and 3.0 *d* as expected. With respect to the surface settlement troughs, and given the findings of other authors with respect to the asymmetry towards the second tunnel, it can be noticed in Figures 4.9, 4.10 and 4.11 that the Hardening model is the only one predicting a small asymmetry and this is most noticeable for tunnels separated by 2.0 *d*. The maximum transverse surface settlement trough has been found to decrease for increasing distance between the tunnels. Comparing the settlements predicted by the Elastic, Mohr-Coulomb and Hardening models it can be said that:

i) The predicted values are very similar when using the Elastic and Mohr-Coulomb criteria, but larger for the latter due to the plastic deformations induced in some areas around the tunnels.
ii) For the cases considered in the present investigation, the Hardening model has been found to give the smallest and also narrowest settlements. Although the Hardening model could eventually predict larger settlements than the Elastic or Mohr-Coulomb models because of its distinction between virgin unloading and unloading-reloading stiffness, which reduces the effect of heave, it has been found not to be true in the present analyses because this feature of the model also reduces the amount of settlement due to convergence.
iii) These differences between the settlement profiles predicted by the three constitutive models are also partially created by the fact that the parameters selected for the Hardening model do not exactly match those used for Mohr-Coulomb (Section 3.3.1.5), and also because the Hardening model takes into account other factors such as the OCR of the soil.

In terms of the induced shear stresses at point C, these were found again to be larger for the Mohr-Coulomb model than for the Elastic and larger for the Hardening model that for the Mohr-Coulomb. The shear stresses were observed to increase (tending to be negative for the K_0<1 case and positive for the K_0>1 case) during the excavation and the application of support to the first tunnel and later decrease (i.e. stress tensor rotating again in the opposite direction) during the excavation and application of support to the second tunnel. As for the single tunnel case, the shear stresses become negative during the construction of the first tunnel in K_0<1 conditions and positive in K_0>1 conditions. The maximum shear stresses were found to be -20 kPa for the K_0<1 case and 11.5 kPa for the K_0>1 case.

4.3.2. 3D

Figure 4.23 illustrates the differences in terms of deformations predicted by PLAXIS 3D for increasing K_0 values. For the K_0 = 0.593 case, the vertical deformations well exceed the horizontal values, with the former being larger at the tunnel crown than at the invert. This can be seen to progressively change towards the K_0 = 1.5 case in which the vertical deformations are very small and it is the horizontal deformation towards the opening that are dominant.

The surface settlement trough is of the type expected by using empirical methods for K_0=0.593, both in the transverse and longitudinal case, with pre-convergence occurring in front of the tunnel face and the maximum settlement developing far behind this. However the trough is shallower and wider in the numerical prediction. For the K_0 = 1 case, the surface settlement trough is similar in shape to the one predicted for K_0 = 0.593, but shallower and extends further in front of the tunnel face. In this way, Figure 4.23a illustrates how the volume of soil affected in front of the excavated tunnel increases for increasing K_0 values, and could be partially controlled by applying support to the face. When K_0 = 1.5, PLAXIS predicts the ground surface to heave especially above the first constructed slices in the model. This shows that the resulting heave effect is larger in the 3D models than in the 2D models. Lee and Ng (2002) also found the longitudinal ground settlement to be different than a cumulative probability function curve for K_0 = 1.5 due to the heave observed behind an open face excavation (with no face support) during 3D analyses with ABAQUS using isotropic and anisotropic elastic perfectly-plastic (Drucker-Prager) models.

The larger concentration of vertical deformations above the first slice of the tunnel in Figure 4.23a for K_0 = 0.593 and K_0 = 1 is due to the soil in this area not having the support from a previously supported section when excavated as explained in Section 3.3.1.1. Varying the conditions in this first construction stage during the analyses was found to have a large impact on the surface settlement trough close to the starting point, however these results have not been presented here because they are not relevant to the main aim of this project.

All these predictions are sensible and agree well with the observations made based on the 2D results.

The stress conditions in a triaxial cell impose two main limitations when it comes to the selection of stress paths to be simulated:

i) The rotation of the stresses due to the advancing tunnel cannot be reproduced;

ii) σ_x cannot be different from σ_z.

Other considerations will be also required and will be commented on in Section 7.3. As a result of i), the 3D PLAXIS results have not been studied in terms of principal stresses but in terms of σ_x, σ_y and σ_z. Due to the limitation in point ii), the radial pressure for stress path testing in the triaxial cell has to be carefully selected in order to be representative of the main trends of behaviour in the soil.

The changes in total stresses σ_y, σ_x and σ_z at points A* (crown) and B* (springline) due to the advancing tunnel face show two types of behaviour: (1) before reaching the measurement section, and (2) after passing the measurement section (see Figures 4.19, 4.20 and 4.21). The effect of excavating and supporting the slices of tunnel before reaching the measurement section at points A* and B*, although inducing rotation of the stress tensor, is similar to the one produced by the excavation stage in the 2D analyses with regards the type of changes in σ_x and σ_y induced over time. At the crown, σ_y decreases (more for $K_0 = 0.593$ than for $K_0 = 1.5$) and σ_x increases by a smaller amount compared to the decrease in σ_y. σ_z varies less than the other two components and its value is generally constantly being somewhere in between the other two values with the exception of the $K_0 = 0.593$ case in which σ_z stays below σ_x. At the springlines, σ_x decreases (more for the $K_0 = 1.5$ case) and σ_y increases (although the increase is smaller than the decrease in σ_x). σ_z varies only marginally in general with its magnitude being in between σ_y and σ_x, but becoming higher than σ_x when $K_0 = 1.5$.

Once the tunnel face is at the measurement section and beyond, the effect at points A* and B* of constructing the tunnel is different because the soil at those points starts noticing the effects of having the lining in place. This involves mechanisms similar to the one explained before referring to Figure 4.24.

The differences observed by using the different constitutive models for the $K_0 = 0.593$ case (Figure 4.19) are significant in terms of the magnitude of the total stresses induced by tunnelling. This is especially true with respect to σ_y at the crown and both σ_y and σ_x at the springline, however the trends are very similar.

The predicted variations in σ_y could easily be reproduced in the triaxial cell, but as stated earlier, a further assessment of σ_x and σ_z was required in order to appropriately define the changes in radial stress for the subsequent representative triaxial stress path testing. In this way, since the magnitude of σ_z was observed to generally lie between those of σ_y and σ_x, with the exception of points above the crown for K_0=0.593 and the points at the springline for $K_0 = 1.5$, the final assumption taken would be that of considering σ_x acting on all horizontal radial directions for any soil element. The 3D stress paths at points A* and B* were therefore represented in terms of σ_y and σ_x during the excavation of the 30 m long tunnel as illustrated in Figure 4.22 and similar trends in behaviour to those shown from the 2D analyses in Figure 4.2 can be observed.

From the literature review, the research by Jacobsz (2002) was found to be of particular interest as these results were based on physical modelling rather than FEA, and they were not conditioned by the constitutive relationship being used. These results showed similar trends in behaviour to those found in the present numerical study in terms of the σ_y - σ_x changes for the K_0<1 case with respect to points above the crown during tunnel excavation.

The main observations regarding shear stresses (σ_{xy}, σ_{yz} and σ_{zx}) at points A and B during 3D simulations are as follows, both due to the shape of the developing settlement trough ahead of the advancing tunnel face until reaching plane strain conditions:

- Large σ_{yz} (maximum of 67 kPa) being induced at the tunnel crown for K_0 below, equal and above unity.
- Large σ_{zx} at the springline for K_0 = 1 and K_0>1 (maximums of 37 and 74 kPa respectively).

The study of such shear stresses permitted the author to corroborate the inevitable limitations of the stress path cell in order to closely reproduce stress changes around tunnel openings.

4.4. SUMMARY

This chapter has presented the total stress paths occurring at the crown and springline of a single circular tunnel and at the springline in between twin circular tunnels from undrained 2D and 3D FEA using PLAXIS. The depth of the tunnels has been approximately 30 m. The soil parameters used have resembled those of a stiff clay. The various model variables have been clearly stated. Various K_0 initial conditions have been used and sensitivity analyses have been carried out in order to evaluate the dependency of the stress paths to the different parameters involved in the analyses. The observed trends have been discussed and related to the mechanisms occurring in PLAXIS and also to observations by previous authors.

The results from this chapter have been used to assist with the choice of stress paths to be subsequently reproduced in the laboratory (Chapter 7).

Chapter 5: STUDY OF THE CHARACTERISTICS OF THE RECONSTITUTED SAMPLES

5.1. INTRODUCTION

As stated in Section 3.5 an initial group of samples was prepared to evaluate the performance of consolidation Device A, investigate the characteristics / quality of the samples and assess their repeatability. During the preparation of this first group of samples, a number of shortcomings were identified that may have some impact in the subsequent triaxial tests, as well as affect the interpretation of the soil behaviour, therefore a detailed study into the significance of these observations was carried out as part of the present investigation. This chapter presents the results from the four investigation stages in which the study was divided. The discussion for this chapter is provided alongside the results since the sequence of events dictated the course of the investigation.

Initially, the results from the LL and PL tests performed on both Kaolin clays commonly used in the Soils Laboratory at the University of Birmingham (Section 3.4) are provided, as well as the determination of *Gs* for the Speswhite Kaolin clay finally selected.

Most of the results presented in this chapter have been previously published (Valls-Marquez et al., 2008).

5.2. INDEX TESTS AND DETERMINATION OF G_S

The results from the Index tests performed on both Kaolin clays specified in Section 3.4 are compiled in Table 5.1, as well as the average specific gravity for the Speswhite Kaolin clay.

The *LL* and *PL* values obtained for English China clay PURAFLO 50 agree well with the values reported by Doroudian and Vucetic (1995) (Table 2.4). The *LL* and *PL* values obtained for Speswhite Kaolin clay agree very well with the average values reported by Kim (1996) and with other values also presented in Table 2.4. It should be noted that although most of the clays reported in Table 2.4 fall within the zone of high plasticity clay or silt in the Casagrande Plasticity chart (British Standard BS 5930:1999), some Kaolin clays would correspond to other categories. For instance, the Speswhite Kaolin clay used by Hird and Hajj (1995) would be classified as a very high plasticity clay. The *Gs* value experimentally obtained during this study also agrees with previously reported values (Section 2.3.7). For comparison with the idealised context previously presented in Section 3.2, the *PL* and *LL* of London Clay have been reported to be: [*PL*: 25 %; *LL*: 70 %] (Atkinson et al., 1990), [*PL*: 20 % to 33 %; *LL*: 44 % to 85 %] (Mott MacDonald, 1991), [*PL*: 30 %; *LL*: 75 %] (Atkinson, 1993) and [*PL*: 20 % to 30 %; *LL*: 54 % to 85 %] (Burland et al., 2001).

Table 5.1. Index tests and G_s results

	***LL* (%)**	***PL* (%)**	**G_s**
English China clay PURAFLO 50	Average 56 Variability: 54.9 – 57.8	Average 31 Variability: 30.2 – 31.8	-
Speswhite Kaolin clay	Average 65 Variability: 65.1 – 65.3	Average 33 Variability: 33 – 33.01	Average 2.6 Variability: 2.597 -2.597

5.3. STAGE 1 - PRELIMINARY INVESTIGATION

This section summarises the results gained from the study of the samples listed in Tables 3.6 and 3.7 and exposes the first shortcomings encountered.

5.3.1. *e* - σ_v' Relationship

The change in void ratio with vertical effective stress (σ_v') measured for the samples listed in Table 3.6 during K_0-consolidation in Device A, is shown in Figure 5.1. A similar graph, but compiling the results for all the samples prepared for the present project, can be also found in Appendix C-Figure C.1. The results show that after a stress of about 150 kPa the variability in void ratio between the different tests was small with differences of about 0.1 for the same stress level. For effective stresses below 150 kPa, differences in void ratio as large as 0.4 were observed (Figure 5.2). These larger differences for σ_v' below 150 kPa have been considered to be due to friction between the piston/tube and the rod/frame, and also due to the compliance of the drainage layer. These results additionally indicate that the type of water used for the preparation of the samples does not appear to have any significant effect on the consolidation of this particular Speswhite Kaolin clay. It has to be noticed however that the effect could be potentially noticeable if using a different type of clay because of soil-water chemical interactions.

Figure 5.3 illustrates some of the verifications that primary consolidation had been attained at the end of each of the loading stages using the square root of the time method. The results correspond to those recorded during the preparation of sample IN 1.8 (Table 3.6).

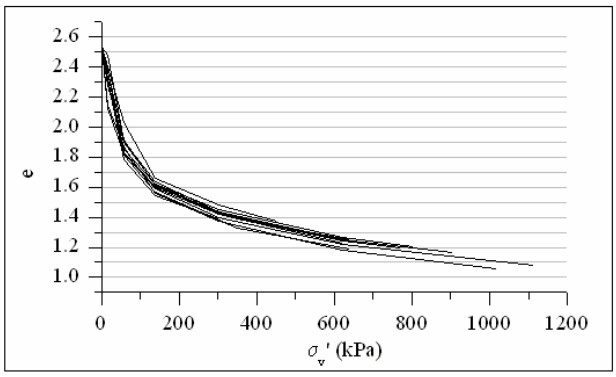

Figure 5.1. Void ratio change with σ_v' during the K_0-consolidation of Speswhite Kaolin slurry under different conditions

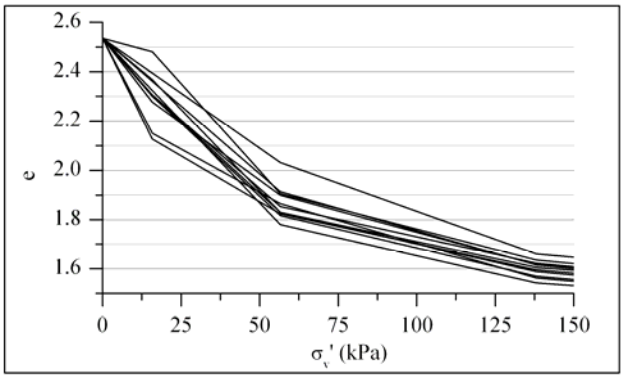

Figure 5.2. Detail of the void ratio change during the K_0-consolidation for σ_v' below 150 kPa

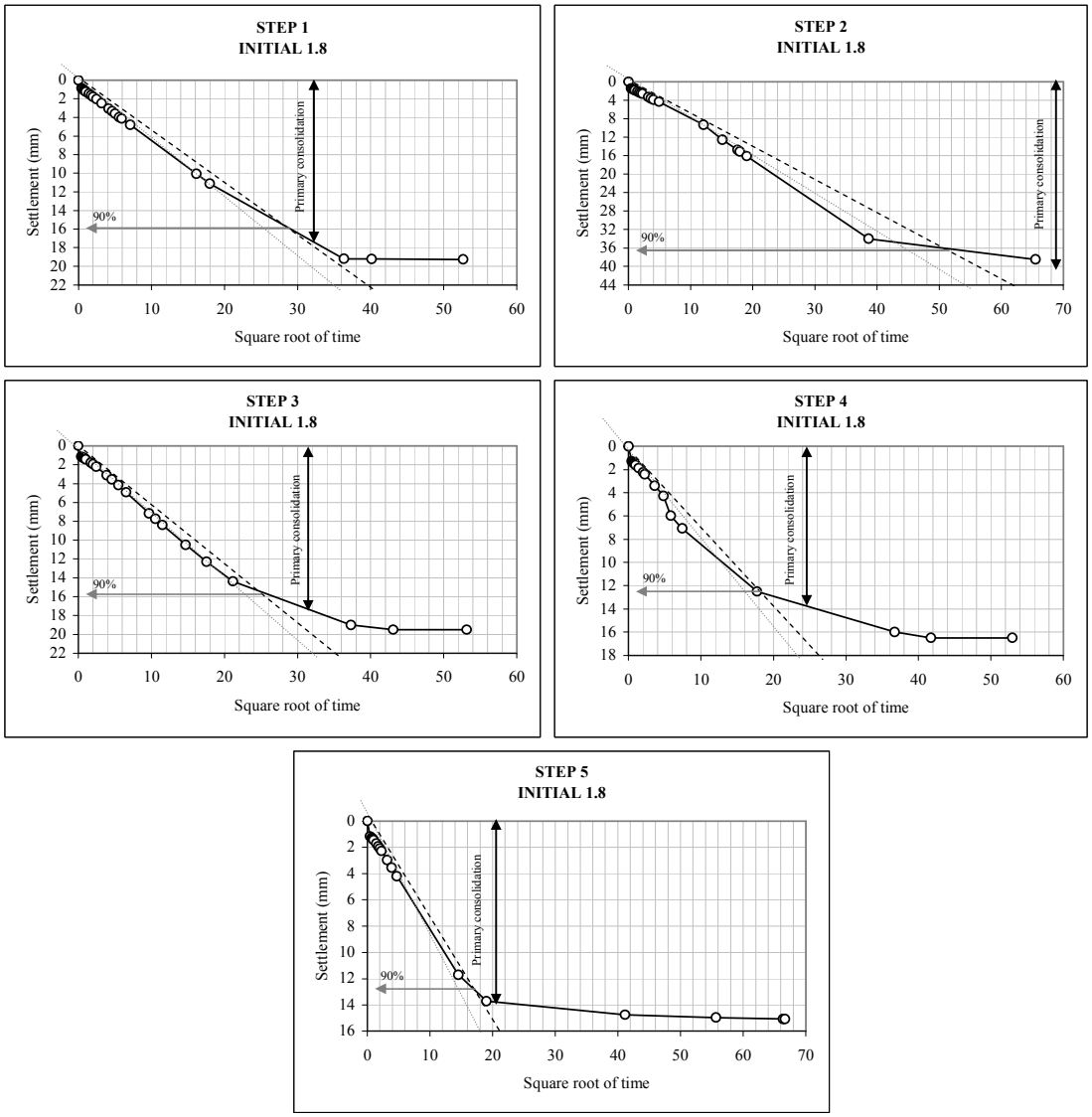

Figure 5.3. Laboratory consolidation curves during the different loading steps in the preparation of sample IN 1.8 using the square root of the time fitting method (British Standard 1377-5:1990)

5.3.2. c_u - *IL* Relationship

Figure 5.4 illustrates the c_u - *IL* relationship found at the maximum value of the vertical effective stress ($\sigma_v'_{max}$). The trendline presented only considers the samples prepared using tap water. The rest of the samples are shown to agree well with such relationship. In the same figure, the relationship between c_u and *IL* proposed by Muir Wood (1990) for remoulded soils, and described by Equation 5.1, is also shown.

$$c_u = 2 \cdot 100^{(1-IL)} = 200 \cdot e^{-4.6052 \cdot IL} \qquad \text{[Eq.5.1]}$$

.

Comparing Muir Wood's predictions to the results obtained during the present investigation, the latter were found to be displaced towards the right meaning that for the same value of *IL* larger c_u values were obtained.

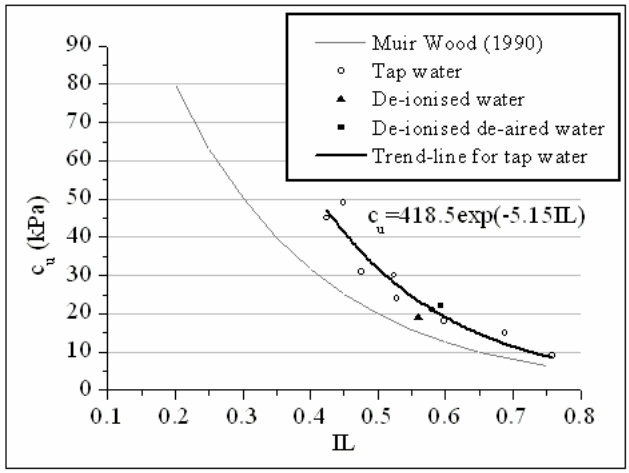

Figure 5.4. c_u - *IL* relationship for reconstituted Speswhite Kaolin samples with an initial *w* equal to 1.5 *LL*, c_u being measured by a hand vane

5.3.3. c_u - $\sigma_v'_{max}$ Relationship

Figure 5.5 illustrates the relationship between c_u and the maximum applied vertical effective stress, the former having been measured by a hand vane. Based on these results, a $\sigma_v'_{max}$ of 1340 kPa would be the minimum required in order to obtain a soil with high undrained shear strength (75 kPa to 150 kPa according to British Standard BS EN ISO 14688-2:2004) and therefore it could not be attainable using the consolidation Device A, but the Device B (Section 3.5.1.2).

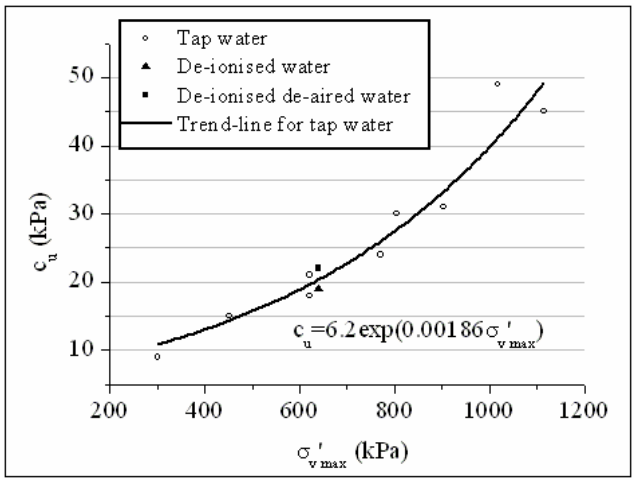

Figure 5.5. c_u - $\sigma_v'_{max}$ relationship for reconstituted Speswhite Kaolin samples with an initial *w* equal to 1.5 *LL*, c_u being measured by a hand vane

5.3.4. w - $\sigma_v'_{max}$ Relationship

Figure 5.6 shows the relationship between the average measured final w and the maximum effective vertical stress. The trendline considers in this case the results from all the samples listed in Table 3.6.

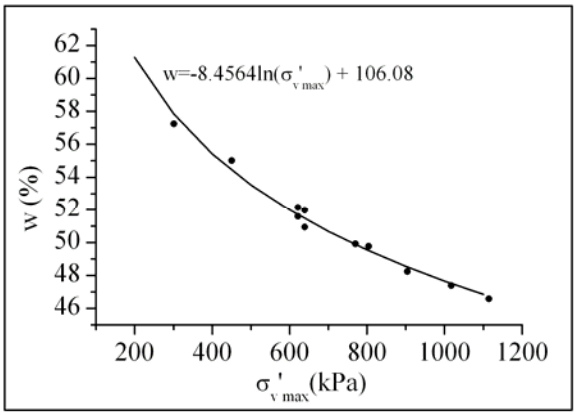

Figure 5.6. w - $\sigma_v'_{max}$ relationship for one-dimensionally consolidated Speswhite Kaolin reconstituted samples with an initial w equal to 1.5 LL

5.3.5. UU Tests

The results from the triaxial unconsolidated undrained tests listed in Table 3.7 are summarised in Table 5.2. The specimens tended to fail forming a 'barrel' shape close to the base of the specimen as illustrated in Figure 5.7.

Table 5.2. Results from the unconsolidated undrained tests

Specimen code	p_0' (kPa)	B	c_u measured (kPa)	c_u calculated using equation in Figure 5.4 (kPa)	w_i (%)	w_f (%)
UU2	178	0.93	43.0	25	47.7	49.48
UU3	Not measured	Not measured	78.7	45	45.7	46.09
UU4	Not measured	Not measured	36.7	13	52.5	54.40
UU6	Not measured	Not measured	70.0	45	44.7	44.67

Figure 5.7. Mode of failure for specimen UU2

5.3.6. *p′* Measurements in the Triaxial Cells

The measurement of the initial p' in the triaxial cell for specimen UU2 was found to be 178 kPa, which is far below the calculated value using Skempton (1954) Equation 2.28. Similar observations were made when performing preliminary tests using specimens retrieved from the samples listed in Table 3.6. After noticing this, a graph was prepared that illustrates measured against calculated p' values for all the specimens used for the present project. This graph can be found in Appendix C - Figure C.2.

5.3.7. Shortcomings from STAGE 1

Based on the results from STAGE 1, a number of shortcomings were identified that are listed below. As a result of these, the reliability of the results illustrated in Figures 5.4, 5.5 and 5.6 was questioned. A more in-depth follow-up investigation was therefore carried out to account for the significance of these observations and the results will be presented and discussed in the following sections.

Shortcoming 1: w (IL) - c_u - $\sigma_v'_{max}$ relationships

Large disagreements were found in the literature with respect to w (IL) - c_u - $\sigma_v'_{max}$ relationships. For example, Atkinson et al. (1987) gave a value of $c_u = 20$ kPa for $\sigma_v'_{max} = 60$ kPa and $w = 58$ % (± 1 %) ($IL = 0.77$). This is very different from the findings illustrated in Figures 5.3 and 5.4, which for the same IL value suggest a value of c_u close to 8 kPa related to a $\sigma_v'_{max}$ value just above 130 kPa. For the same IL, Muir Wood (1990) curve predicts a c_u value close to 6 kPa.

Shortcoming 2: c_u measurements

c_u values measured during the unconsolidated undrained tests were found to be larger than the ones measured by the hand vane for similar values of $\sigma_{v'max}$ (Table 3.7, Table 5.2 and Figure 5.5).

According to the triaxial values, only a $\sigma_{v'max}$ of approximately 1070 kPa would be required in order to have a c_u = 75 kPa, compared to the 1340 kPa previously stated in Section 5.3.3 based on the hand vane results. This being the case, the consolidation Device A would be just suitable for the purpose also accounting for the problems envisaged with the Device B (Section 3.5.1.2).

Shortcoming 3: p' measurements

Although part of the large differences observed in Appendix C - Figure C.2 between the measured and the predicted values of the initial p' may be attributed to disturbances occurring during extrusion, trimming and specimen preparation (Section 2.3.2), it was thought that the processes taking place inside the consolidation Device A may be also having a substantial effect.

Shortcoming 4: Internal soil fabric

Based on a careful visual inspection of the samples after consolidation, some fabric could be intuited. It should be noted that the word 'fabric' (i.e. arrangement of the particles) and not 'bonding' (interparticle forces of various natures) (Cotecchia and Chandler, 1997) is used in this case because the latter was not specifically studied. However, although bonding is more normal for natural clays, some of it may have well occurred during preparation due for instance to some sort of interaction between the water and the clay chemistry. The platy kaolin particles seemed to be forming a concave macro-fabric resulting in soil samples that would be clearly anisotropic but not necessarily cross-anisotropic as would be expected. This supposed (at this stage) fabric was first observed by taking some dry samples to failure by tension (Figure 5.8).

Figure 5.8. Concave fabric created in the soil during one-dimensional consolidation

Sheeran and Krizek (1971) also noted the occurrence of curved surfaces and linked them to the various techniques used to place the slurry into the cylinder. The selected technique for the present study was kept unchanged for repeatability and it is believed not to be responsible for the concave surfaces encountered. The results from the observation of subsamples C1A, C1B and C1C (Section 3.5.5.2) in the Scanning Electron Microscope (SEM) are illustrated in Tables 5.3, 5.4 and 5.5. From these, the following main observations were made:

- The concave arrangement of the clay particles was more pronounced towards the base of the samples than close to the top. This can be seen for example comparing the figures in Tables 5.3 and 5.5. The concave fabric can be particularly well observed on a horizontal cross-section in Table 5.3 - Figures 1 and 8. Linear arrangements are visible in most of the figures in Table 5.3. Figures 2, 6, 9 and 10 are particularly of interest in this respect. Some white lines have been superimposed on these figures indicating the orientation of the particles. On a vertical cross-section, the concave fabric was also well identified. Figures 1 and 2 in Table 5.4 are a good example of this. In Table 5.5, illustrating the top of the sample, some alignment of particles was observed in Figures 1 and 5, but no specific orientation could be established in the other parts of subsample C1C.
- The fabric created in the soil was visible in the SEM at scales from 5 μm above.

Table 5.3. Scanning Electron Microscope images of a horizontal cross-section C1A close to the base of sample C1

SUBSAMPLE C1A

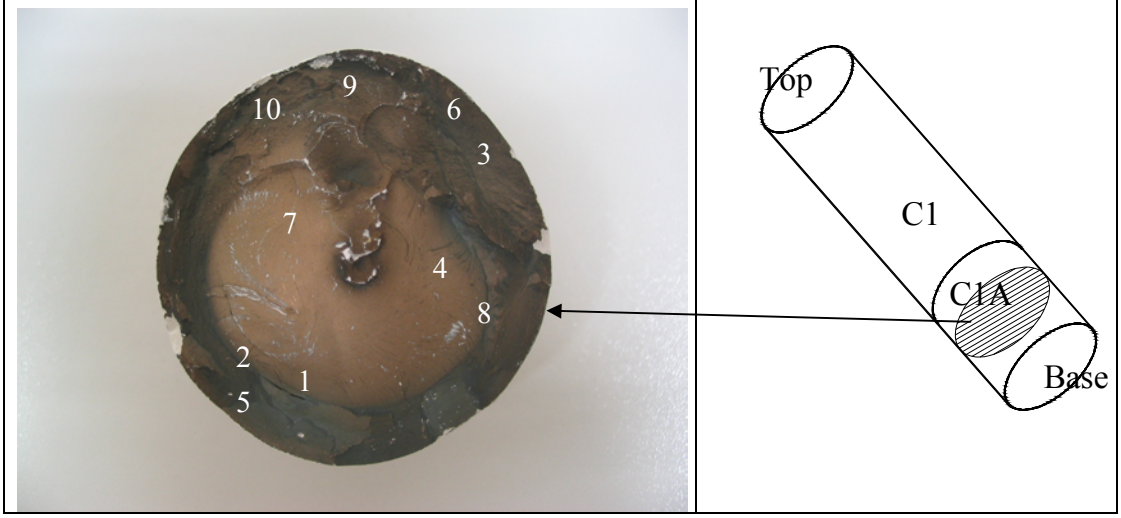

SUBSAMPLE C1A

1 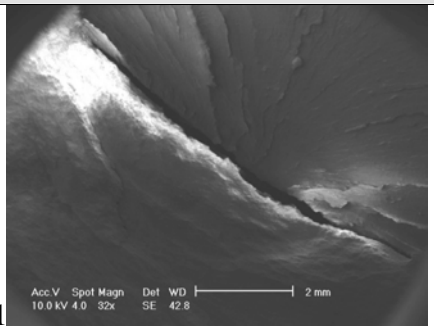

2 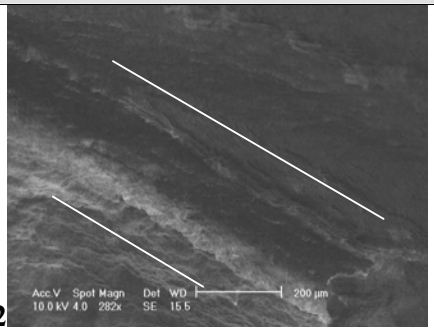

3 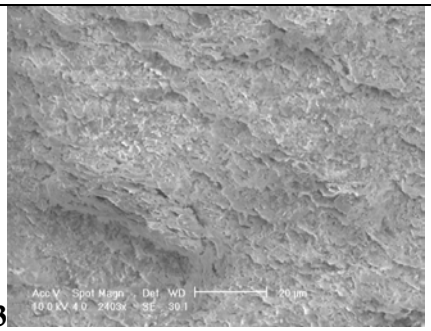

4 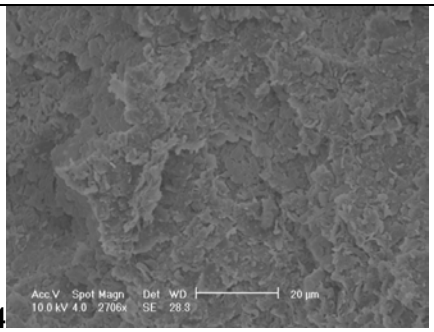

5 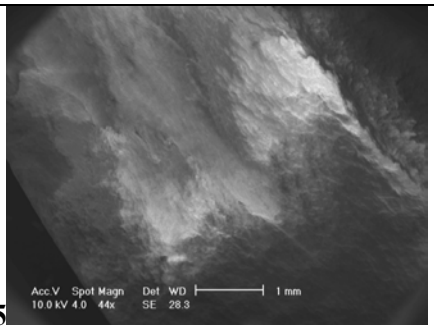

6 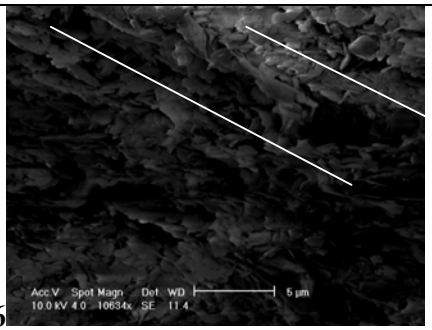

7 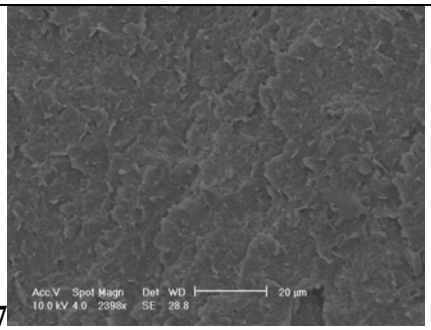

8 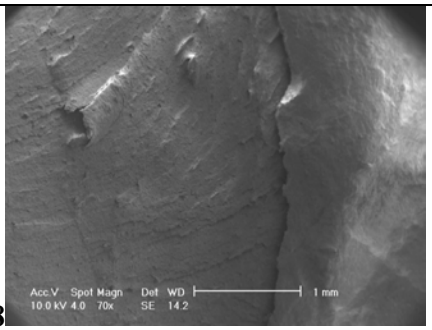

9 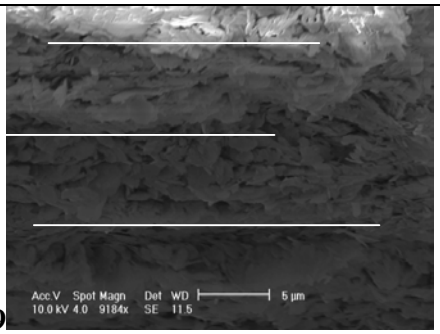

10 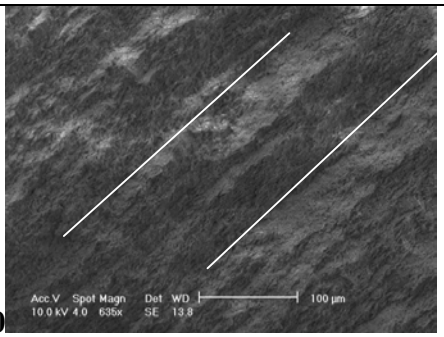

Table 5.4. Scanning Electron Microscope images of the vertical cross-section C1B close to the base of sample C1

SUBSAMPLE C1B

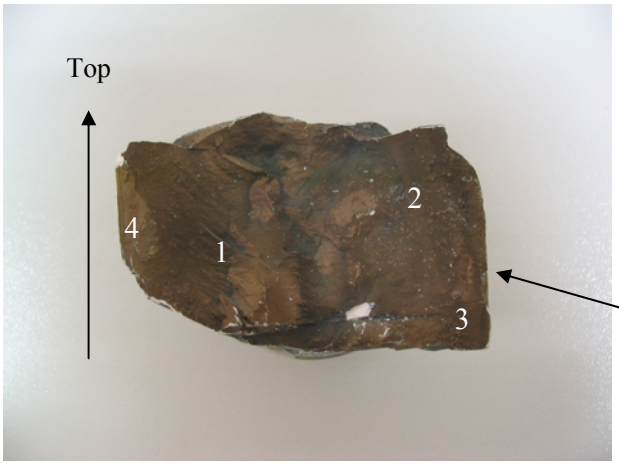

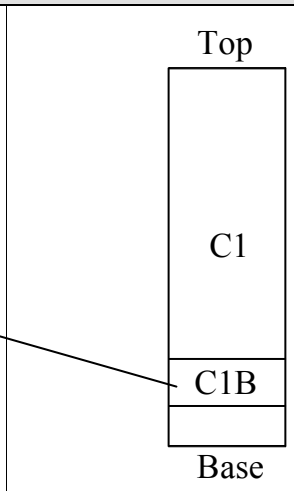

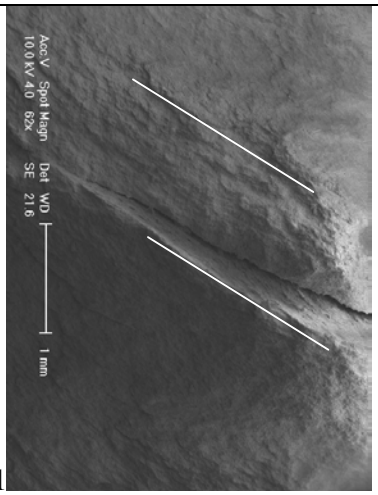

1

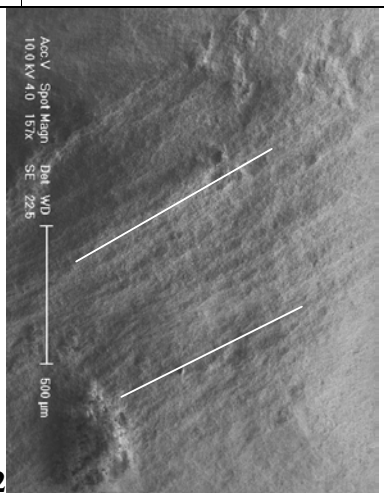

2

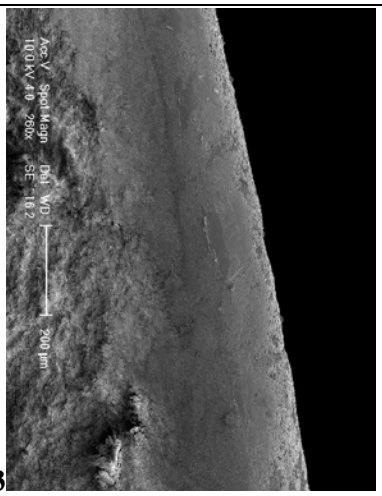

3

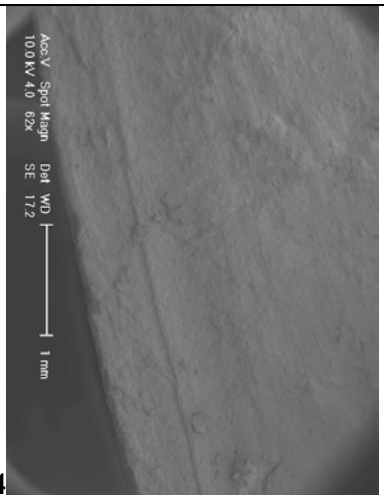

4

Table 5.5. Scanning Electron Microscope images of a horizontal cross-section C1C close to the top of sample C1

SUBSAMPLE C1C

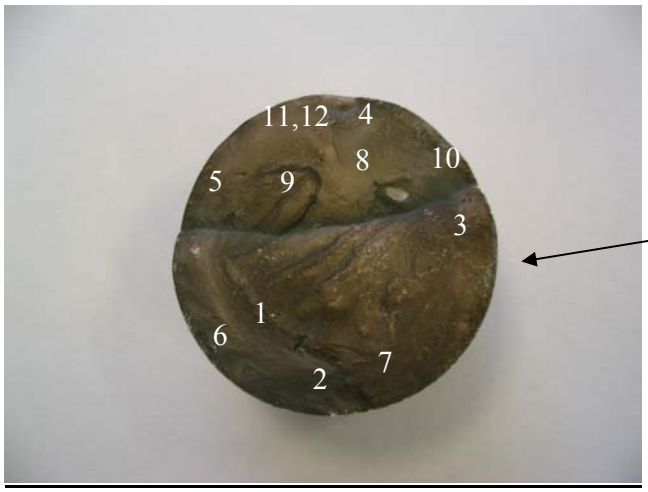

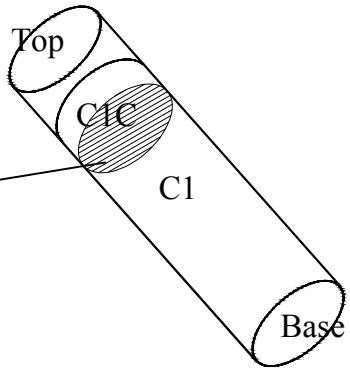

1

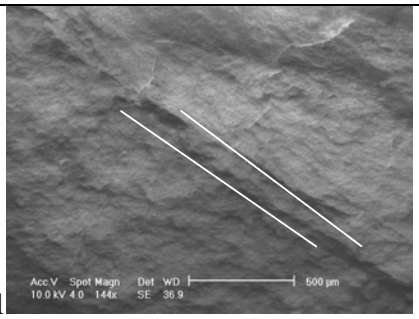

2

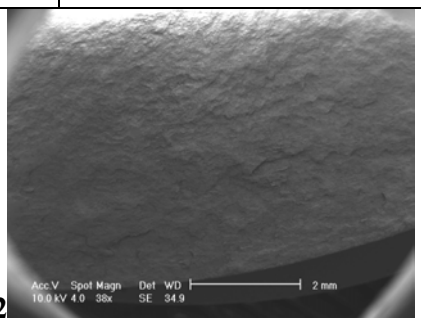

3

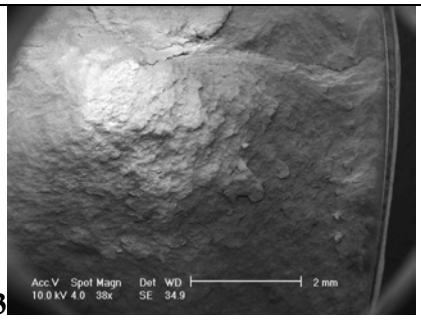

4

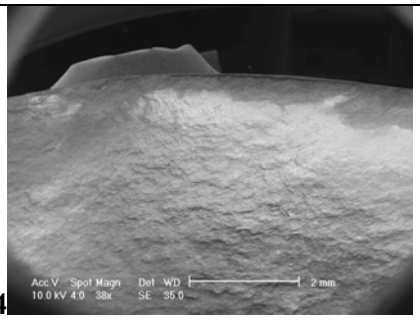

5

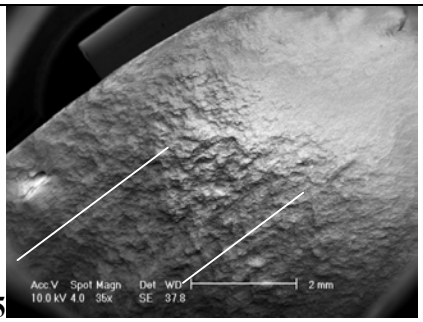

6

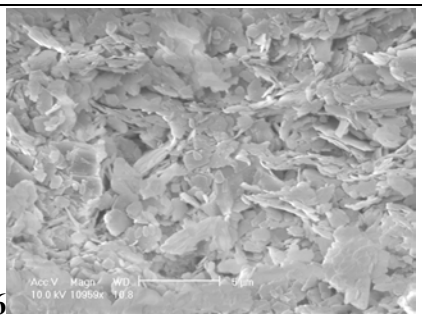

SUBSAMPLE C1C

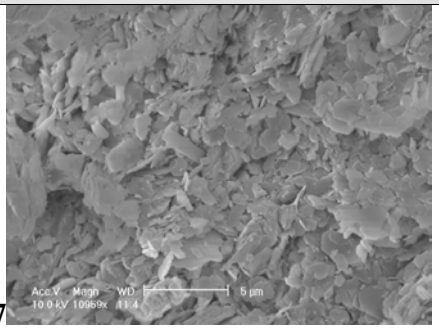

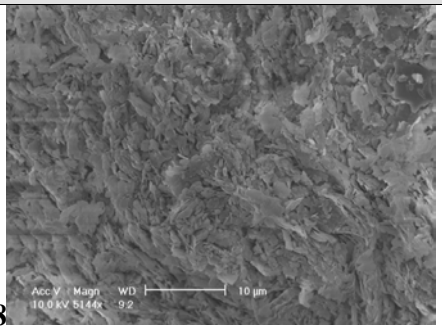

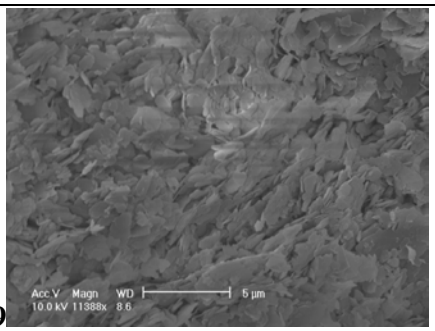

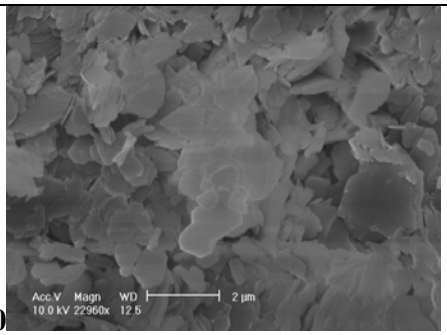

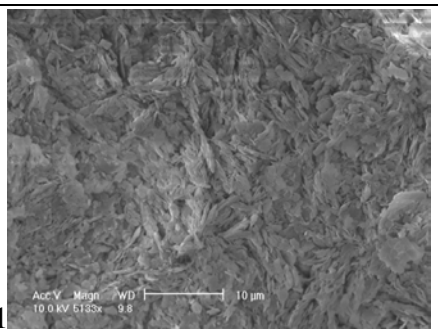

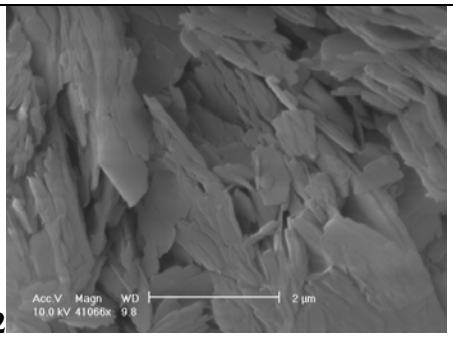

Shortcoming 5: Moisture content distribution

A more detailed observation of the moisture content data for the different samples showed that taking an average value from various sub-samples and correlating this with the c_u value measured at the top of the sample (as performed for Figures 5.4, 5.5 and 5.6) was probably not appropriate because w varied throughout the samples. A certain pattern could be seen intuitively but needed of further investigation.

5.4. STAGE 2 - SECONDARY INVESTIGATION

5.4.1. Variation of *w* along the Samples' Length

The observed distribution of w along the length of samples "w1" and "w2" is shown in Figure 5.9. This figure typically shows w to be minimum at the top, increasing closer to the base of the sample

and again reducing at the very bottom. This was also obvious by visual inspection of the samples as shown in Figure 5.10.

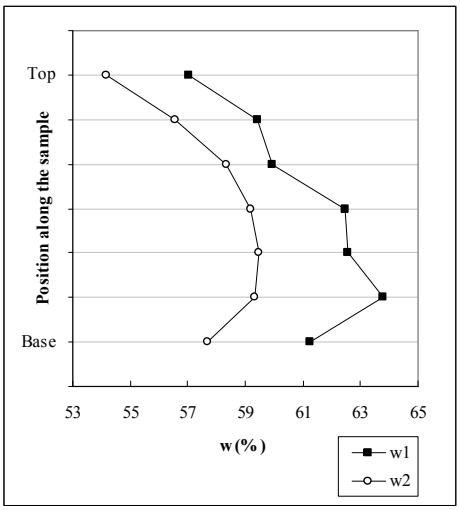

Figure 5.9. Moisture content distribution along Speswhite Kaolin samples after one-dimensional consolidation

Figure 5.10. Visual inspection of one of the samples showing differences in *w* along its length

In addition to this, all *w* measurements taken for the samples prepared for the present project have been compiled and illustrated in Appendix C - Figure C.3. It can be seen that all the data, only with the exception of test IN 1.7, agrees well with the pattern shown in Figure 5.9.

This pattern illustrated in Figures 5.9 and C.3 has been related to the mode of failure during unconsolidated undrained tests in Section 5.3.5.

The maximum w variation throughout the samples created in the consolidation Device A (of length normally between 170 and 220 mm depending on $\sigma_v'_{max}$) was found to be between 5.2 and 8.7 %, with this magnitude being independent of the $\sigma_v'_{max}$ applied onto the slurry.

With reference to the results shown in Figure 5.4, where c_u values were measured at the top of the samples and w was determined from various sub-samples at the base of the samples, it was now clearer why the experimental curve was transposed towards the right. Considering that the actual w could have been as much as 8.7 % lower at the position where c_u was measured than the value taken at the base, the current experimental trendline in Figure 5.4 would get closer to that predicted by Muir Wood (1990).

5.4.2. Alternative Method for the Measurement of c_u

The results from the fall-cone test on the specimen "c_uw" are summarised in Figure 5.11 and indicate a clear relationship between the measured w values and the estimated c_u.

An average value for a 100 mm specimen trimmed from the centre of the sample would suggest a value of c_u = 32.9 kPa. The test carried out on the specimen "UU4" subjected to the same $\sigma_v'_{max}$ gave a value of 36.7 kPa, so it is in close agreement with the fall-cone method. The hand vane tests gave values of approximately 14 kPa for the same $\sigma_v'_{max}$, which is under half the value obtained from the triaxial and cone penetrometer tests. Although the results from the hand vane were assumed to be more unreliable due to the fact that perfect verticality and constant rate of stress were difficult to achieve during the test, differences are expected just by the nature of each test and the different shearing mechanisms induced. Therefore, all the relationships presented before that include c_u only make sense when this is measured by a hand vane. When considering the c_u values measured during the fall-cone or the triaxial tests, the results get closer to those given by Atkinson et al. (1987) (Section 5.3.7).

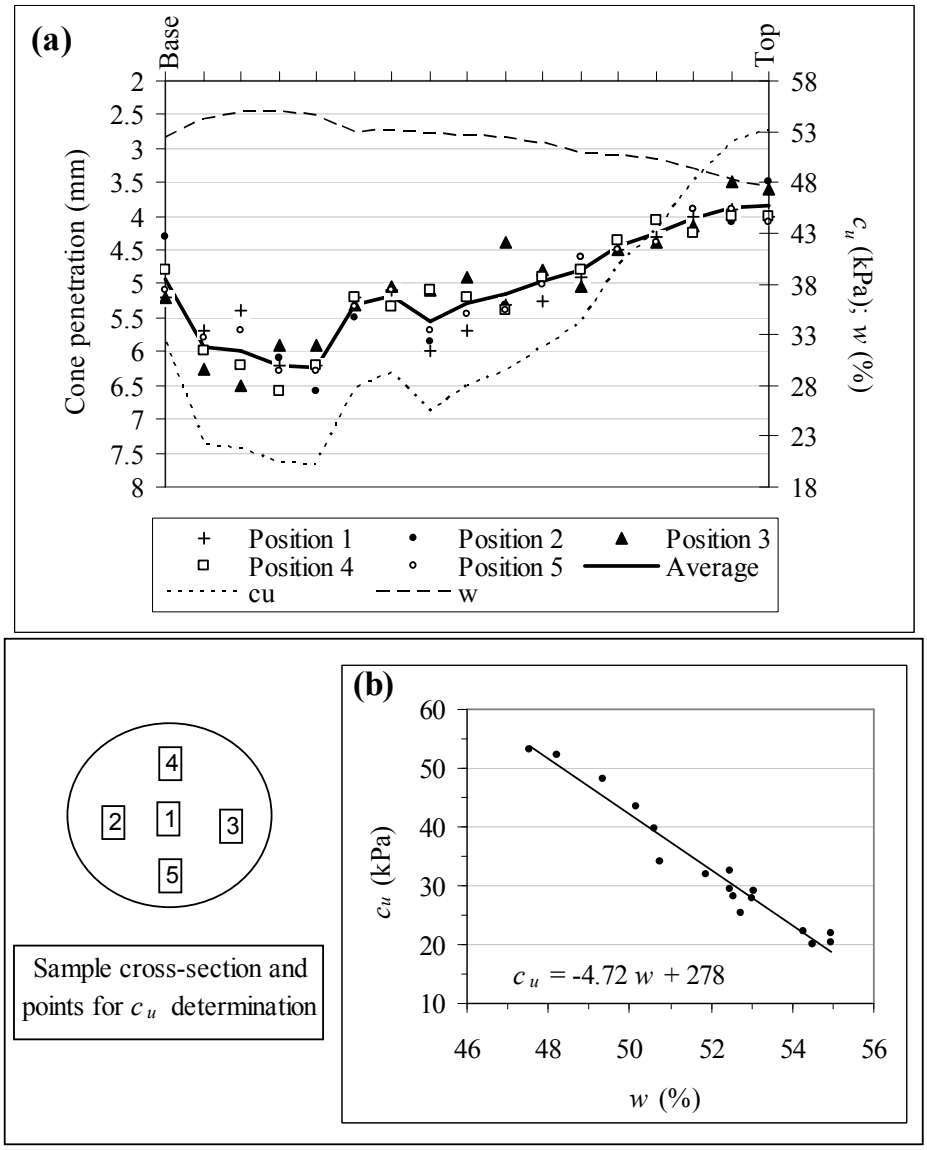

Figure 5.11. Fall-cone test results for sample 'c_uw': (a) Moisture content, cone penetration and c_u distributions along the sample length, (b) Discrete c_u - w relationship

5.4.3. Evaluating the Reasons for the Low p' Measured Values

Considering the observations described above that occur during the K_0-consolidation process, it was apparent that part of the differences between measured and predicted p' values (Appendix C - Figure C.2) could be due to mechanical and physical disturbances during sample extrusion and specimen preparation for testing, but part of it could be related to the fact that not all the vertical pressure applied to the sample in the consolidation device was being transmitted to the soil. Further evidence for this came during this project from the isotropic and K_0-consolidation tests performed in the Stress Path cell (Sections 3.6.2.4 and 3.6.2.5) which, by evaluating the preconsolidation pressure,

suggested that specimens retrieved from the central part of some K_0-consolidated samples had only been subjected to about 50 - 60 % of the theoretical $\sigma_v'_{max}$ applied at the top. Other researchers (personal communications) have also encountered similar results, but details are generally not published. The patterns illustrated in Figures C.2, 5.9 and 5.11 suggest that the vertical stress actually being applied decreases almost linearly with depth with the reduced *w* at the very base possibly due to the proximity of the soil to the bottom drainage. Potential reasons for this reduction in vertical stress along the samples could be a combination of (1) the relative dimensions of the consolidation chamber (i.e. length to diameter ratio) and (2) friction issues. Atkinson et al. (1987) also found some differences in p' and attributed these to side friction in the oedometer and disturbances during transfer to the triaxial cell.

5.5. STAGE 3 - PORE WATER PRESSURE MEASUREMENTS DURING K_0-CONSOLIDATION

The results from tests F01, F02, F03 and F04 are illustrated in Figure 5.12. Note that in Figures 5.12c and 5.12d the pore water pressure at point U does not increase during the third and fourth stress increments because by this time the point was already situated above the top of the soil due to settlement. The observations made are as follows:

i) Points U and I were found to receive similar stress levels, with a common tendency however for the U measurement to be under the I value. This apparent response was related to the proximity of U to the top piston where undrained conditions did not really exist. This definitely limited the maximum pressures measurable at U. As expected, the difference in *u* between U and I was more obvious for increasing stresses and also larger for test F03 due to the top boundary conditions (ballotini balls instead of a rigid plastic disc). As I is the point less affected by the drainage when the vertical stress is applied (i.e. can be considered to have undrained behavior in the short term), it could be said quantitatively that:

   i.i) When the stress was applied in stages without letting the excess pore water pressure dissipate between each stage (tests F01 and F02), around 60 to 80 % (increasing with increasing stress) of the load applied at each stage actually reached point I with small variations between tests.

   i.ii) When the four stress stages were applied allowing for drainage between each stage (which has been the method used for preparing samples during the present research and also for tests F03 and F04), the load being transmitted to the soil at point I during each stage was found to be between 40 and 70 %, but in this case tending to decrease for increasing stress. This was considered to be due to the friction between the piston and the acrylic tube increasing during the drained periods. Again small variations were observed between tests.

ii) Point B always received smaller stresses, even when the drainage at the base was impeded (i.e. full excess *u* was measured), the amount of which varied for every test and is believed to greatly depend on small variations of the device alignment. This variability, together with the low *w* measured at the very base of the soil makes this part of the specimen less suitable for sample trimming. Quantitatively it could be said that:

ii.i) For tests F01 and F02, the percentage of stress reaching point B at each stage was between 30 and 75 %. As for point I, the percentage increased with increasing stress.

ii.ii) For test F03, at point B the percentage of applied stress at each stage was within the range 30 - 60 %, again decreasing with increasing stress as for point I under the same test conditions.

iii) The maximum undrained response, in terms of *u* at point B, took longer to occur than at points U and I.

iv) Excluding the first load stage in tests F03 and F04 (seating pressure), the excess pore water pressure at U drained very quickly, reaching equilibrium after a maximum of 11 hours. A maximum of two days were required for complete pore water pressure dissipation at point I if two-way drainage was used, and longer if the soil was allowed to drain only one-way. As expected, the excess *u* at point B decreased faster than at point I with two-way drainage and more slowly when the drainage was only upwards.

All these observations explain the water content pattern observed throughout the samples in Figures C.2, 5.9 and 5.11.

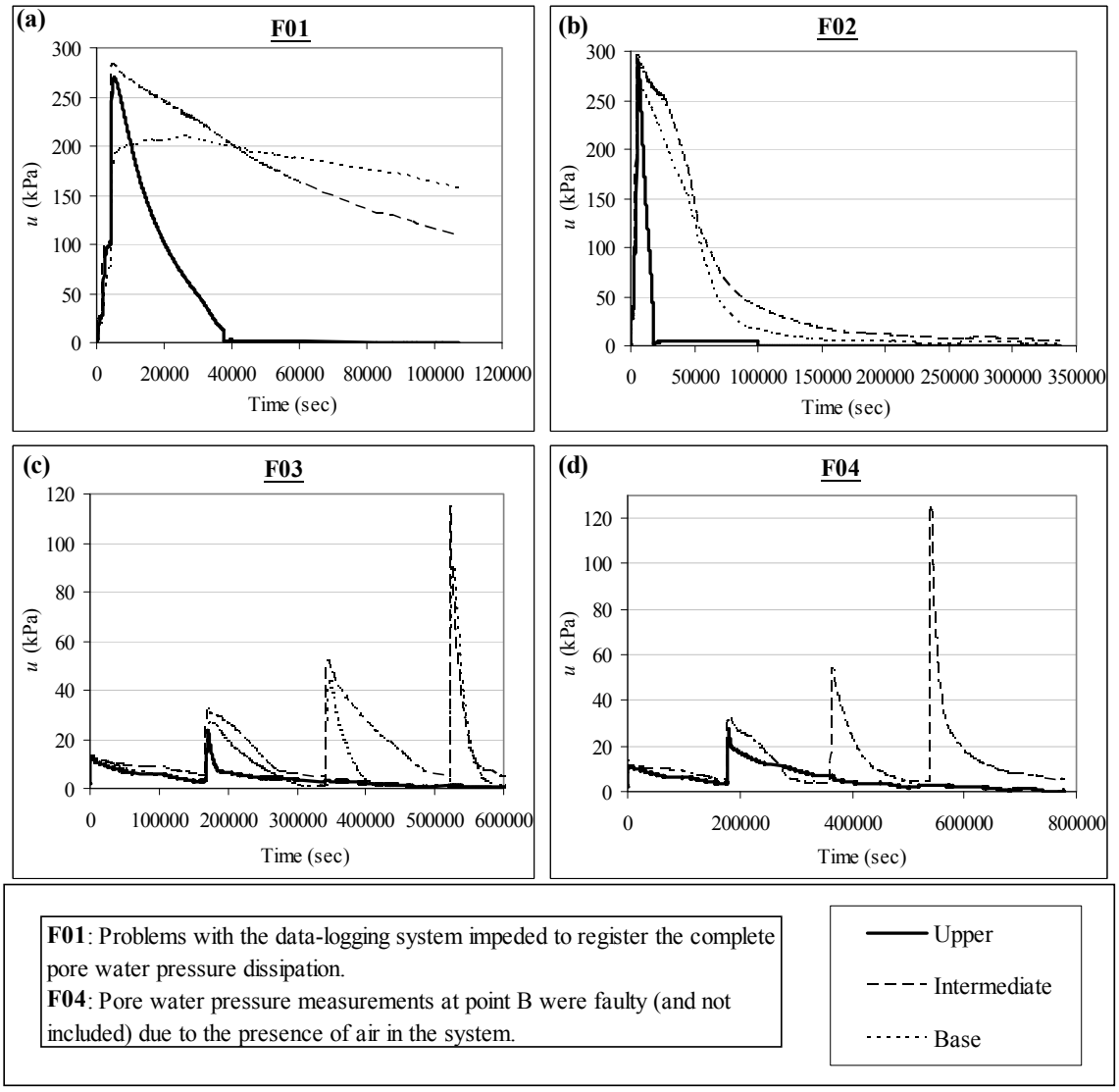

Figure 5.12. Pore water pressure measurements at three points equally spaced along the consolidation device (Upper, Intermediate and Bottom) during K_0-consolidation in tests (a) F01, (b) F02, (c) F03 and (d) F04

5.6. STAGE 4 – MODIFICATIONS TO DEVICE A

Based on the pore water pressure measurements and the distribution of stresses within the samples observed during STAGE 3 (Section 5.5), the internal soil fabric observed in Section 5.3.7 was attributed to the following processes occurring during consolidation:

- The concave orientation of the clay particles, this being more pronounced towards the base of the samples, would be produced by (1) friction between the soil and the acrylic tube and (2) the vertical movement of the soil particles due to gravity and the influence of the bottom drainage, taking into account that this part of the sample is subjected to a quite low percentage of the vertical stress theoretically being applied at the top.

- The flatter disposition of the clay particles close to the top of the samples would correspond to the expected settlement under a rigid piston, but this being slightly affected by the tube friction.

In order to reduce friction within the consolidation chamber, the use of liquid oil WD-40 and dry PTFE spray were investigated at the beginning of the project. Silicon grease had also previously been used at Birmingham with no success (Burns, personal communication, 2005). WD-40 was used for the present work (specimen INWD) and this did not introduce major variations in the soil behaviour (measured in terms of *e* changes) and so agreed well with the relationships indicated in Figures 5.4, 5.5 and 5.6. It was noted however that when WD-40 was used, the soil and oil mixed together when the slurry was poured into the consolidation tube and the final samples appeared to be more heterogeneous. PTFE spray was also found to be unsuitable since some components in the spray reacted with the acrylic tube, although this may be suitable if other materials are used for the consolidation chamber.

The idea of using Teflon as an inner lining (Sheeran and Krizek, 1971; Indraratna and Redana, 1998; Prashant and Penumadu, 2005) was also approached, but some difficulties were experienced in finding suppliers and certain types of Teflon (i.e. sheets) would have reduced the internal tube diameter. Some search into other available coatings was also carried out. For instance, some enquiries were made with regard to the ultra low friction (0.01 - 0.06) solid lubricant MoST. The manufacturers concluded that due to the way this was deposited, using a vacuum method, it would not be appropriate to be placed on the internal walls of the tubes used for the consolidation Device A. Their advice with regard to other coatings was that these would quite likely transfer to the soil.

At a later stage in the project, the observations made from samples A100-1 and A110-2 demonstrated that some fabric inside the samples is still formed when 100 mm inner diameter tubes are used, although perhaps in this case the concavity is not so much pronounced close to the base of the samples. Figure 5.13 shows the fabric encountered from top to base in intact surfaces within sample A100-1 after being dried in the oven at 105 degrees, these being representative of the observations made in both specimens A100-1 and A100-2. Based on the void ratio evolution with effective vertical stress however, which is illustrated in Figure 5.14, it was deduced that the percentages of the vertical stress being actually applied to the soil were larger in this case than when a 50 mm inner diameter tube was used. More tests on 100 mm diameter samples including higher stress levels than the ones used for samples A100-1 and A100-2 would be however necessary to be certain in this respect. The results previously presented in Figure 5.1 are added in Figure 5.14 as a matter of comparison.

(a)

(b)

(c)

(d)

Detail:

(e)

Figure 5.13. Internal fabric from top (a) to base (e) in the sample A100-1 K_0-consolidated in the 100 mm inner diameter modified Device A

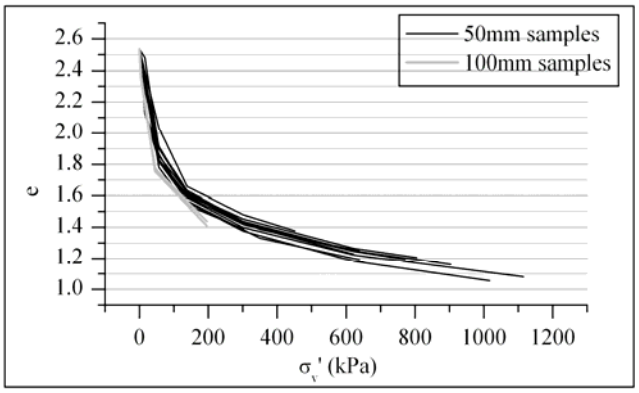

Figure 5.14. Void ratio change with σ_v' during the K_0-consolidation of sample A100-1 compared to data in Figure 5.1

5.7. IMPLICATIONS OF THE FINDINGS

Although the results presented in this chapter are specific for the consolidation Device A, they illustrate the type of issues that can be encountered when preparing reconstituted samples from a slurry and demonstrate that the effect of these on the specimens should be carefully evaluated and certainly not ignored.

By comparing this to other previous experiences, it can be concluded that the characteristics of the specimens created during the present investigation may well be similar but never quite the same as those prepared by other consolidation techniques, therefore these need to be individually assessed. Likely problems experienced during consolidation, as well as details of the characteristics of the prepared samples, are not generally published. Only a few studies were encountered after the present observations were made. Lin and Penumadu (2005) reported a non-homogeneous *w* distribution along their hollow cylindrical 50 mm diameter x approximately 230 mm long Kaolin clay samples with a maximum towards the centre. The authors reported that even using Teflon on the walls of the consolidometer, a 5 % difference in *w* was still found in the soil, with a maximum at the centre of the sample (slightly displaced towards the base). Schmidt (2006) prepared London clay samples in a 106 mm inner diameter plastic pipe and found a 10 % moisture content variation over a 200 mm long sample with the maximum value situated approximately at its centre. Gasparre (2005), who also used acrylic tubes with long length to diameter ratio for preparing 38 mm reconstituted specimens, reported inhomogeneities due to frictional resistance and non-uniform *w* along the samples, but these were not quantified. Some investigations in the 1970's were also found that studied the performance of various one-dimensional consolidation devices. Sheeran and Krizek (1971) for example noted the occurrence of curved surfaces with no apparent relation to the consolidation stress and linked them to the various techniques used to place the slurry into the cylinder. It was also noted after re-reading Al-Tabbaa's thesis that the author referred to one previous experience at the University of Cambridge

(Amerasinghe, 1973) reporting on load losses of about 40 % between the top and the bottom of the sample during consolidation due to side friction.

For a given sample, Figure 5.15 illustrates the sequence of thoughts along this study until realising that the dimensions of the consolidation chamber (i.e. length and diameter) together with the friction created between the different parts of the consolidation Device A were limiting the amount of vertical effective stress actually being transmitted to the sample. Point "A" represents the state of the sample at the end of the K_0-consolidation assuming that all the $\sigma_{v\,max}'$ applied at the top had been transmitted to the whole soil body. "B" represents the estimated state after extrusion using Skempton's Equation 2.28 assuming 'perfect' unloading (see Section 2.3.2). "B' " represents the expected state of a trimmed specimen assuming various sources of disturbance. Point "B" " corresponds to the initial value of p' measured in the triaxial cell well below that expected at "B' ". Based on the later observations made, which indicated that the samples were being consolidated along their lengths to variable percentages of the applied $\sigma_{v\,max}'$ on top (represented by point "A' "), the measured "B' " values appeared to be more sensible.

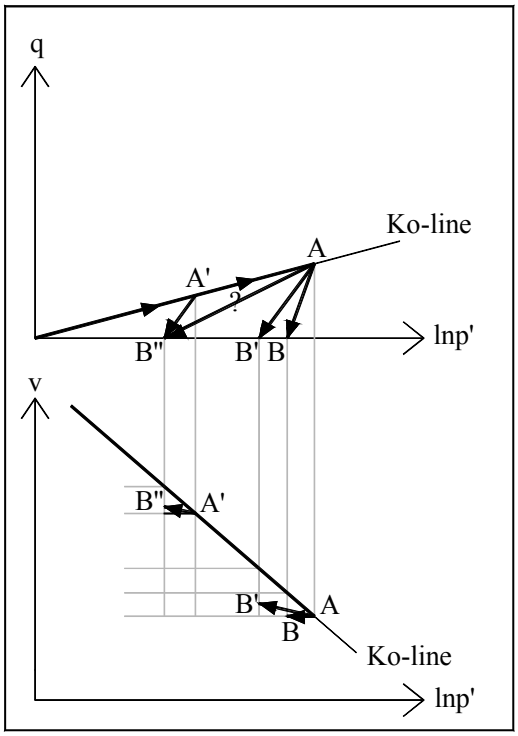

Figure 5.15. Theoretical and real stress history of the K_0-consolidated specimens

Due to the heterogeneous stress, w and c_u distributions observed within the samples, unique relationships between these (e.g. equation in Figure 5.4) cannot be given for each of the samples, as it

does only represent an average of all the possible values within the soil. The void ratios in Figure 5.1 are actually also an average of the real partial values within the soil. This was one of the mistakes made at the beginning of this investigation.

The implications of these non-homogeneities within the soil will largely depend on the final use of the trimmed specimens. If the type of subsequent tests allow for further consolidation stages to be conducted in the triaxial cell, which would be preferable, this would eventually help to create a more homogeneous specimen and the effect in soil behaviour could be small, although again difficult to evaluate. Knowing the approximate degree of consolidation gained in the consolidation device is also seen as an advantage, especially in cases like this in which a large amount of stress is getting lost during the process of consolidation. Unfortunately, some problems can be experienced with triaxial tests that do not allow for further consolidation, such as the conventional unconsolidated undrained tests. Some examples of potential issues that can arise in this case are barrelling towards the base of the specimen during shearing (e.g. Section 5.3.5) and problems with the interpretation of the results if the specimen is assumed to have been consolidated to a certain $\sigma_v'_{max}$ and this has not been the case. In addition to these examples concerning triaxial testing, the fact that the properties of the samples vary along their length can also be inconvenient if the objective of using the consolidation device is to create homogeneous samples of a specific stiffness or *w* for other purposes. Based on the results from these investigations it was decided to trim all the subsequent specimens from the middle-upper part of the samples to avoid as much as possible the region in which the concave surfaces were observed to be more pronounced and also to have a more even distribution of water contents.

Some people tend to believe that the preparation of samples by one-dimensional consolidation is a very trivial matter, something not to worry too much about and the issues reported in this chapter seem to be (a posteriori) obvious to some people. However, we all make the same mistakes again and again. Researchers consolidate their samples using various types of consolidation techniques generally copied from other previous researchers without questioning anything about the performance of the system and the peculiarities of the prepared specimens. If someone has ever systematically studied or observed any limitations, the results have certainly been 'glossed over' either by the authors or by the publishing journals who do not appear interested in this sort of information. More attention should be given to these more 'basic' concepts since they can have major implications during subsequent testing therefore potentially affecting the experimental results. The point that the author wants to make here is the fact that although perhaps some of the induced fabric and variable *w* observed in the present investigation may not be completely removed even using other improved consolidation techniques, these shall not be hidden, but on the contrary, they should be identified as clearly as possible in order to enable a better control over subsequent tests.

5.8. SUMMARY

This chapter has presented the thorough observations made during the preparation and preliminary testing of K_0-reconstituted samples from slurry in terms of their repeatability, homogeneity, disturbances during preparation hence ultimately their quality. The interpretation of such aspects has benefit from techniques such as the Scanning Electron Microscope that allowed observing the clay particles within the samples. Despite all the observations reported being directly related to the specific consolidation device used for the present investigation, similar effects can potentially occur using other apparatus. Carrying out this evaluation of the characteristics of the samples was found to be imperative in order to avoid misinterpretation of subsequent results. This also allowed taking an informed view on how to obtain the most appropriate specimens for later triaxial and stress path testing. It is hoped that this chapter raises some of the issues likely to occur when preparing reconstituted specimens and provide some guidance for future researchers.

Chapter 6: LABORATORY TESTS PART I:

CRITICAL STATE FRAMEWORK FOR SPESWHITE KAOLIN CLAY

6.1. INTRODUCTION

This chapter presents the results from the tests performed on specimens of Speswhite Kaolin clay according to the methodology in Section 3.6.2. A discussion of the results presented is given in Section 6.3. This includes problems encountered during the experiments together with the sequence of actions taken in order to finally obtain the desired results. The deduced parameters for the soil can be also found in the discussion section.

6.2. RESULTS

6.2.1. Isotropically Consolidated Undrained and Drained Tests Under Compression

The results from the isotropically consolidated undrained and drained tests sheared under compression are summarised in Table 6.1. The behaviour of the specimens in terms of q - p', q - $\varepsilon_a(\%)$ and u - *time* are illustrated in Figures 6.1, 6.2 and 6.3 respectively. Figure 6.4 illustrates the mode of failure for the specimens shared undrained. The response of these, and all the other specimens tested during this project, during saturation was very consistent with a small drop in pore water pressure during the first increment in cell pressure that will be discussed at a later stage in this chapter. A typical pore water response has been illustrated in Figure 6.5.

Table 6.1. Results from the isotropically consolidated undrained and drained tests under compression

Specimen code	Initial p' measured in the triaxial cell (kPa)	B value	Maximum p' during isotropic consolidation (kPa)	BP (kPa)	p' before shearing (kPa)	σ_1 at peak strength (kPa)	σ_3 at peak strength (kPa)	u at failure (kPa)	ε_a at failure (%)	w_f (%)
USc2	13 (*)	Failed								
USc3	105	0.99	105	-	105	558	468	410	3.21	-
Usc4	85	0.97	155	310	155	629	470	381	7.64	-
Usc5	113	0.99	226	334	226	770	560	453	8.31	-
Usc6	5 (*)	1.00	575	320	580	Failed				
USc7	121	0.93	1011	379	1011	1854	1400	990	10.65	39.22
USc8	Failed									
USc9	139	0.99	974	320	796	1544	1121	743	9.38	39.07
USc10	46	0.98	477	311	477	1014	800	600	8.11	43.20
USc11	146	0.97	146	-	146	607	500	412	5.15	47.19
DSc1	40	0.99	340	320	340	1021	656	BP=320	15.52	41.27

NOTES: (*) Unexpected low values of p'

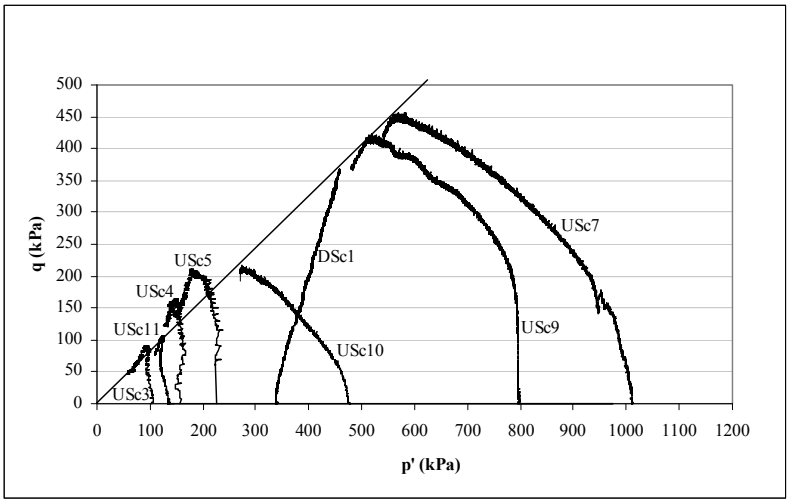

Figure 6.1. Failure envelope for the isotropically consolidated specimens sheared in compression

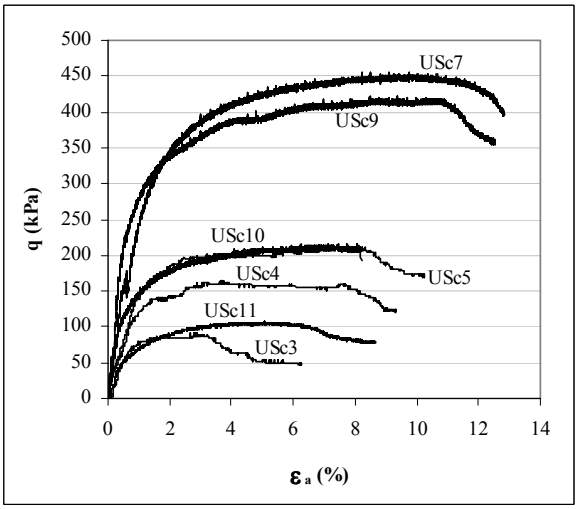

Figure 6.2. q -ε_a relationship for specimens sheared in compression in undrained conditions

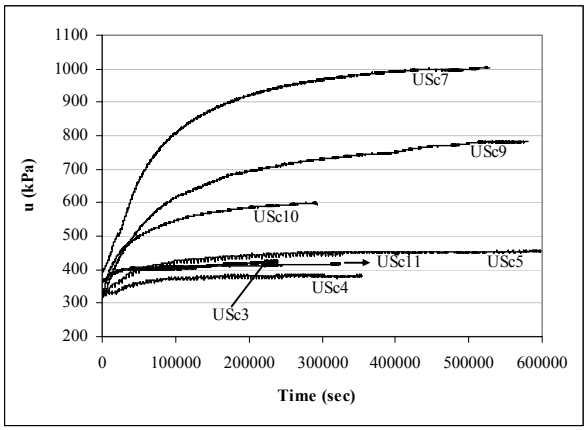

Figure 6.3. *u -Time* measurements during undrained shearing in compression

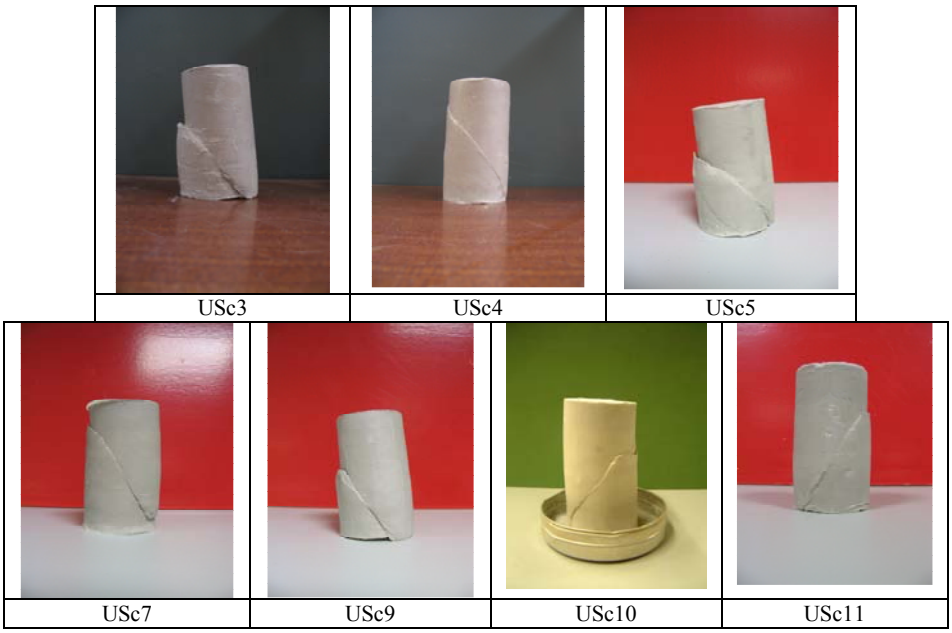

Figure 6.4. Modes of failure for the specimens sheared undrained in compression

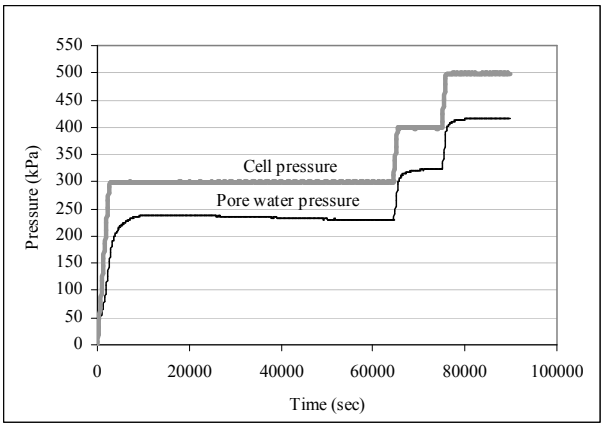

Figure 6.5. Typical pore water pressure response during B-check

6.2.2. Isotropically Consolidated Undrained Tests Under Extension

The results from the isotropically consolidated undrained tests sheared in extension are summarised in Table 6.2. The behaviour of the specimens in terms of q - p', q - $\varepsilon_a(\%)$ and u - *time* are illustrated in Figures 6.6, 6.7 and 6.8 respectively. Figure 6.9 illustrates the mode of failure for these specimens.

Table 6.2. Results from the isotropically consolidated undrained tests under extension

Specimen code	Initial p' measured in the triaxial cell (kPa)	B value	Maximum p' during isotropic consolidation (kPa)	BP (kPa)	p' before shearing (kPa)	σ_h at peak strength (kPa)	σ_v at peak strength (kPa)	u at failure (kPa)	ε_a at failure (%)	w_f (%)
USe1	98	0.98	300	602	398	Failed				
USe2	60	0.99	290	600	350	Failed				
USe3	51	1.0	234	459	234	700	611	531	-6.33	46.70
USe4	44	0.99	392	500	392	900	737	634	-8.59	43.96
USe5	72	0.99	592	300	497	800	565	451	-10.96	42.11
USe6	120	0.92	1117	382	218	600	367	174	-9.65	39.73

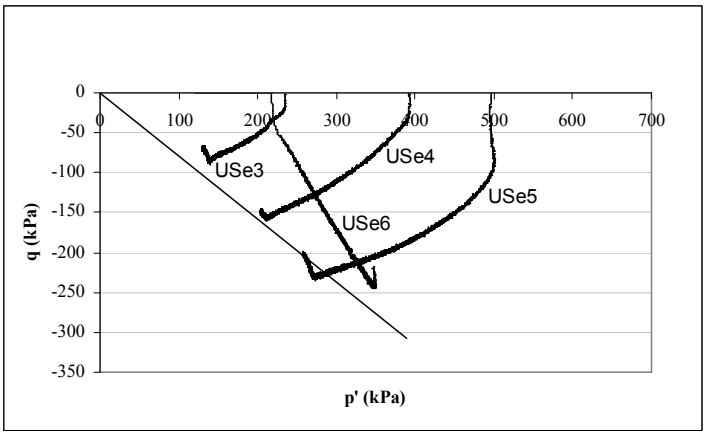

Figure 6.6. Failure envelope for the isotropically consolidated specimens sheared in extension

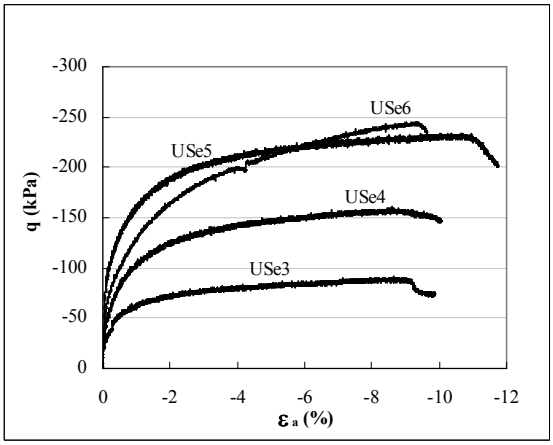

Figure 6.7. q -ε_a relationship for specimens sheared in extension in undrained conditions

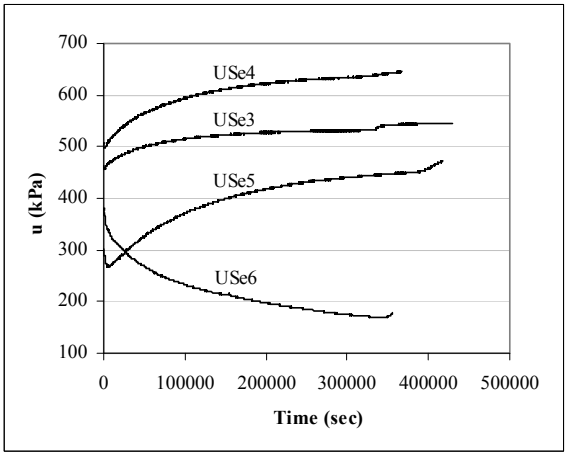

Figure 6.8. u - *Time* measurements during undrained shearing in extension

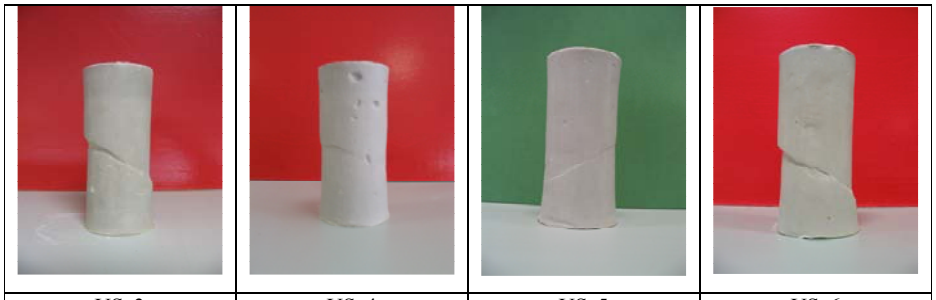

USc3	USc4	USe5	USc6

Figure 6.9. Modes of failure for the specimens sheared undrained in extension

6.2.3. Isotropic Consolidation Tests

The results from staged isotropic consolidation tests are summarised in Table 6.3 and presented in Figure 6.10.

Table 6.3. Results from the isotropic consolidation tests

Specimen code	Initial p' measured in the triaxial cell (kPa)	B value	BP (kPa)	Maximum initial Consolidation pressure p' (kPa)	Minimum Unloading (Swelling) pressure p' (kPa)	Maximum Reloading pressure p' (kPa)	w_f (%)
NCL1	94	0.96	355	1010	568	-	39.94
NCL2	17	0.98	323	472	174	570	42.73

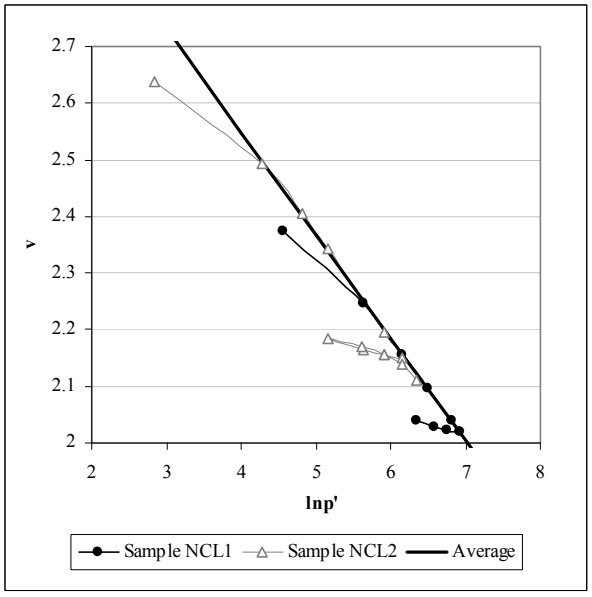

Figure 6.10. Definition of the normally consolidated and unloading-reloading lines based on tests NCL1 and NCL2

6.2.4. K_0-consolidation and Related Tests

The results from the K_0-consolidation tests, the KoAL1 simulation and the shearing tests after K_0-consolidation are summarized in Table 6.4. Figures 6.11, 6.12 and 6.13 show the results from the one-dimensionally consolidation tests Ko1, Ko2 and Ko3 in the q - p' plane. Figure 6.14 illustrates the stress paths performed after K_0-consolidation in test Ko3, as well as the evolution of u with time. Figures 6.15 and 6.16 illustrate respectively the proposed stress path for test KoAL1 and the measurements in terms of q - p and p - *time*. Figure 6.17 shows the results from the one-dimensional consolidation and undrained shearing during tests Ko4 and Ko5. Figure 6.18 illustrates the results during K_0-consolidation and undrained shearing under extension in terms of q - p' changes during test Ko6. The radial Hall Effect device readings during the different stages of the Ko6 test (B-Check, K_0-consolidation and undrained shearing) are shown in Figure 6.19. It should be noted that because of the arrangement of the radial calliper, the deformation measured by the device is twice the actual deformation experienced by the specimen. Figure 6.20 illustrates the one-dimensional normal consolidation lines in the v - lnp' resulting from tests Ko4, Ko5 and Ko6. Figure 6.21 illustrates the change in u with time during undrained shearing in tests Ko4, Ko5 and Ko6. Figure 6.22 shows the mode of failure for specimens Ko4, Ko5 and Ko6.

Table 6.4. Results from the K_0-consolidation and related tests

Specimen code	Initial p' measured in the triaxial cell (kPa)	B value	BP (kPa)	Increment in cell pressure during K_0-consolidation (kPa)	w_f (%)	K_0 value deduced	σ_1 at peak strength (kPa)	σ_3 at peak strength (kPa)	q at peak strength (kPa)	u at failure (kPa)
Ko1	72	0.98	530	400	42.80	0.64	-	-	-	-
Ko2	172	0.94	433	300	43.24	0.64	-	-	-	-
Ko3	165	0.94	433	350	42.62	0.64	-	-	-	-
Ko4	65	1.0	438	210	45.83	0.64	878	710	168	574
Ko5	83	0.95	317	250	43.96	0.65	859	653	206	472
Ko6	98	0.94	404	190	46.15	0.665	566	690	-124	500
KoAL1	185	0.96	315	Failed			-	-	-	-

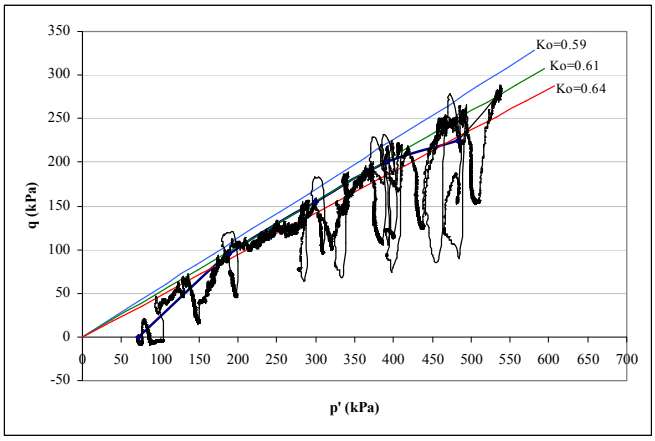

Figure 6.11. One-dimensional consolidation during test Ko1 using on-sample LVDT's

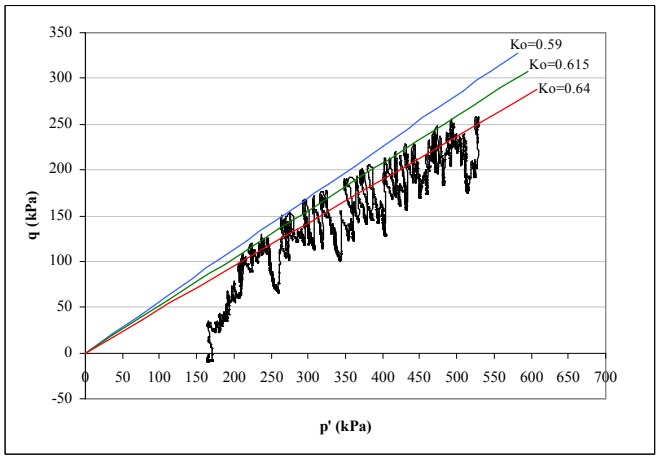

Figure 6.12. One-dimensional consolidation during test Ko2 using on-sample LVDT's

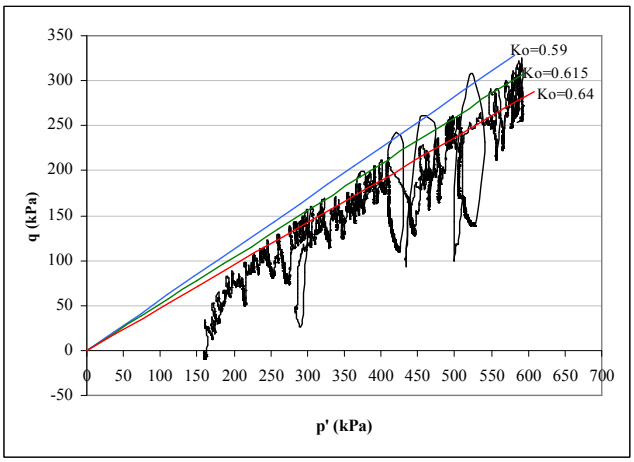

Figure 6.13. One-dimensional consolidation during test Ko3 using on-sample LVDT's

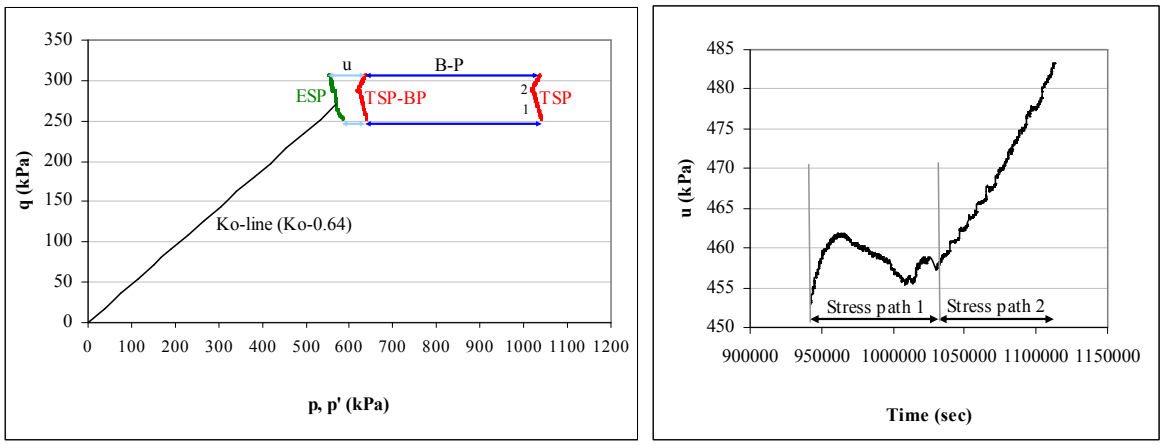

Figure 6.14. Results from the stress paths performed after the one-dimensional consolidation in test Ko3
BP: Back-pressure; *u*: Pore water pressure; ESP: Effective stress path; TSP: Total stress path

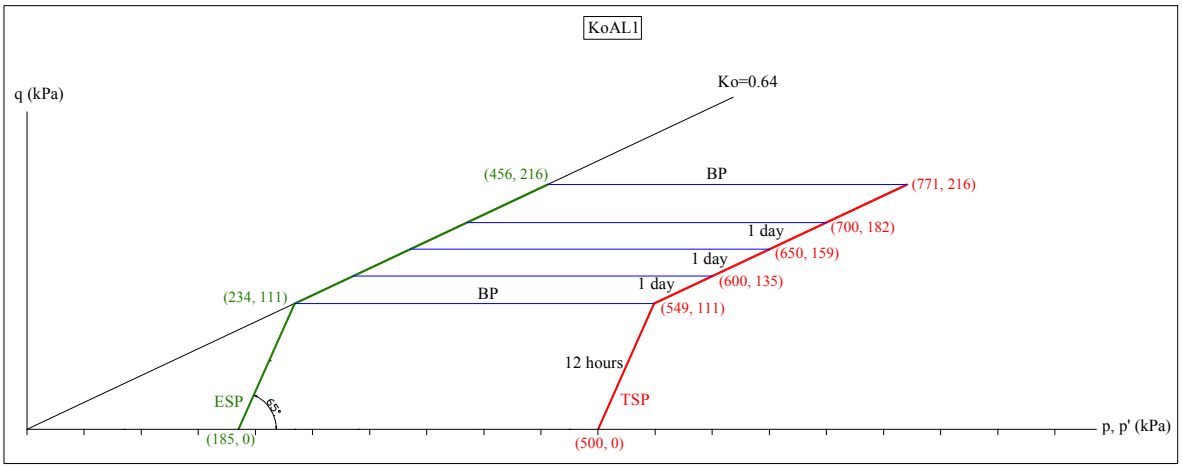

Figure 6.15. Proposed stress path for the simulation of K_0-consolidation during test KoAL1
BP: Back-pressure; ESP: Effective stress path; TSP: Total stress path

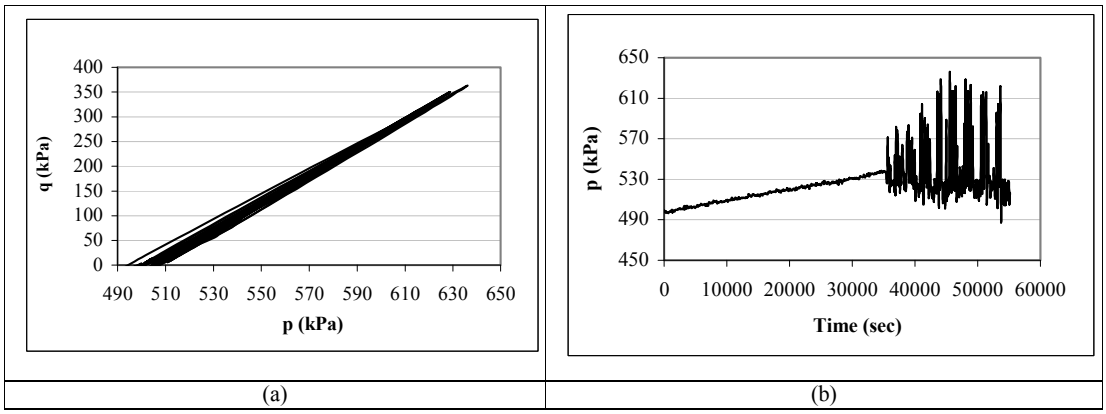

Figure 6.16. Results from test KoAL1

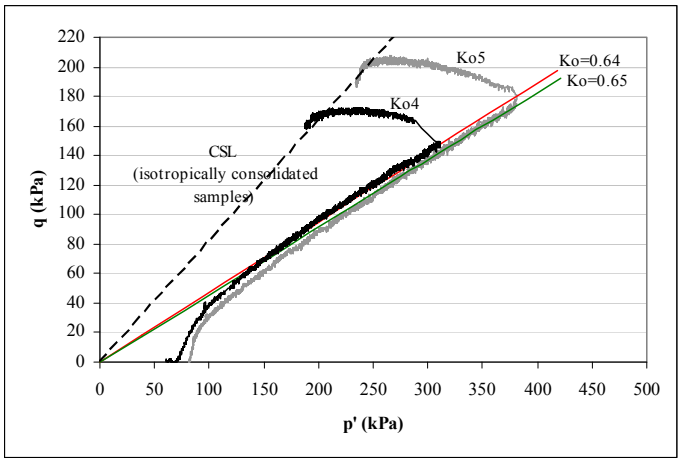

Figure 6.17. One-dimensional consolidation (using the specimen volume change option) and undrained shearing in compression during tests Ko4 and Ko5

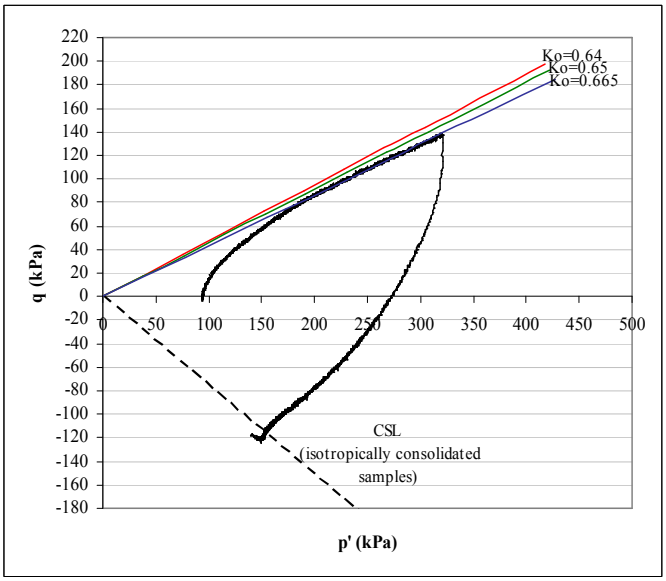

Figure 6.18. One-dimensional consolidation (using the Hall Effect device) and undrained shearing in extension during test Ko6

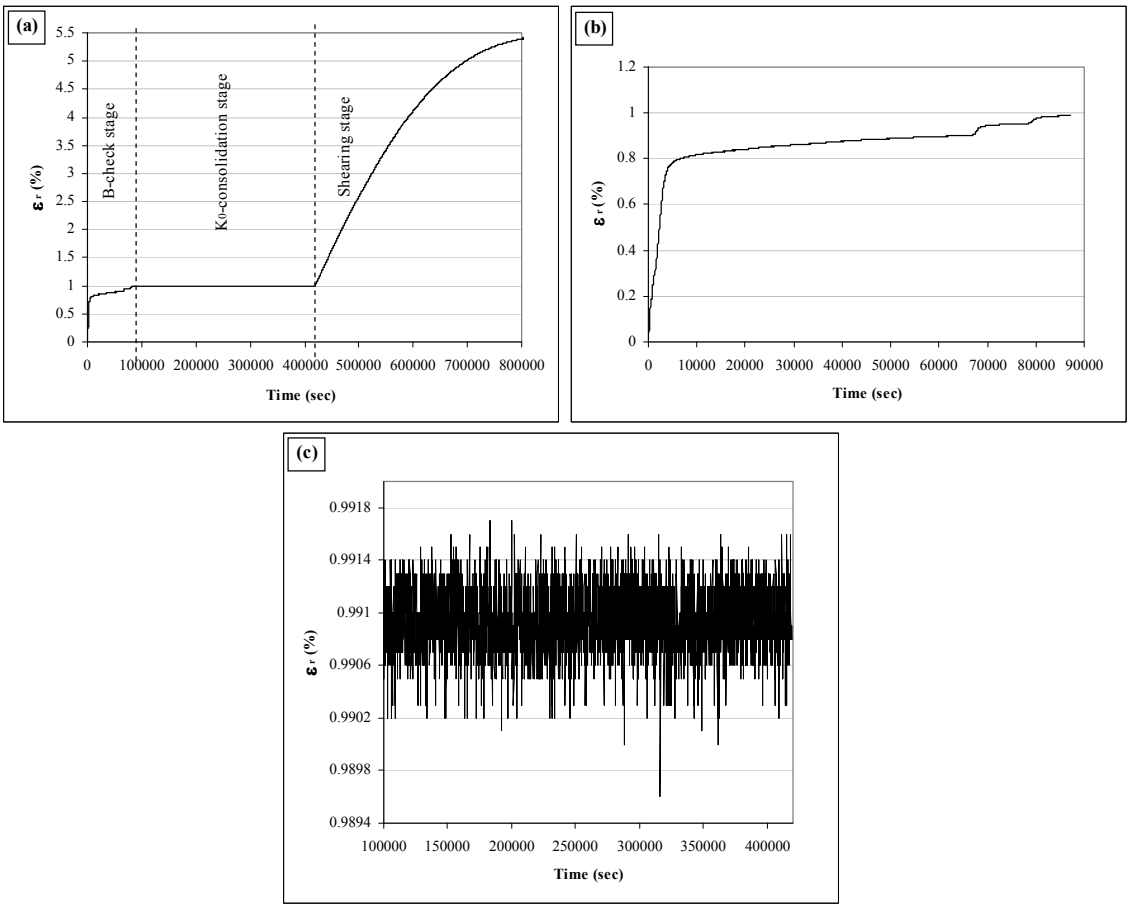

Figure 6.19. (a) Radial Hall Effect device measurements during test Ko6, (b) Detail of the radial strain during the B-check stage and (c) Detail of the radial strain during the K_0-consolidation stage

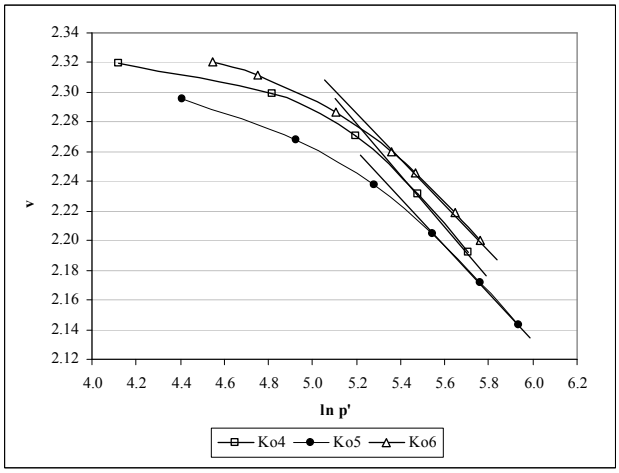

Figure 6.20. One-dimensional normal consolidation lines in the *v* - *lnp'* plane obtained during tests Ko4, Ko5 and Ko6

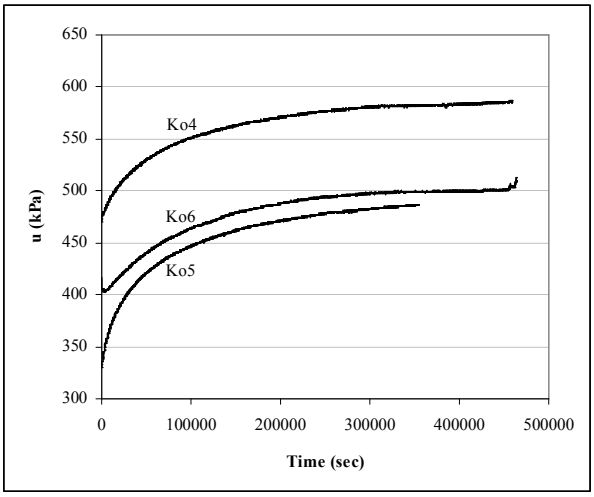

Figure 6.21. Pore water pressure changes with time during undrained shearing in tests Ko4, Ko5 and Ko6

Ko4	Ko5	Ko6

Figure 6.22. Modes of failure for various K_0-consolidated specimens

6.3. DISCUSSION

The findings illustrated in this section are the result of a very thorough process of learning and putting into practice the different techniques involved in conventional and advanced triaxial testing. During the process, some problems and shortcomings were encountered and have been explained in detail in order to facilitate the work of other researchers conducting similar tests. One of the reasons for presenting these issues is the lack of detail encountered by the author in published papers and theses with respect to the precise way of conducting this type of work, including limitations of the equipment and problems encountered, which may save some time on future projects undertaken at universities that start from a similar level of experience.

When the conventional triaxial test equipment was used, many problems were encountered as previously stated in Section 3.6.1.3, these being aggravated by the general poor initial condition of the laboratory equipment as briefly stated in Chapter 1. For example, test USc2 failed because of various

problems with the testing system, especially with the back-pressure. Test USc6 failed because of problems with the dial gauge that resulted in a large axial load initially being applied to the specimen during docking. During test USc5, the cell pressure was fixed to 570 kPa, which in theory was well below the maximum stress allowed by the compressed air system. However, it was observed that the compressed air supply worked in such a way that the pressure would rise to a maximum (690 kPa) and then drop, for safety reasons, to 550 kPa and back again following a constant frequency. Therefore this introduced a constant fluctuation in the cell pressure of 20 kPa that invalidated the test. The volume change unit did not work properly for tests USc4 and USc5 and therefore the changes in specimen height (and therefore in specimen cross-sectional area) during consolidation were estimated rather than measured based on the final *w*. Test USc8 was invalidated because of an unexpected power cut in the laboratory.

The shape of the stress paths in the q - p' plane during undrained shearing in tests USc3, USc4 and USc5 (Figure 6.1) were initially questioned and thought to be wrong probably due to the problems previously stated experienced with the equipment. Such soil behaviour was, however, later confirmed by test USc11 performed in the Stress Path cell. This shape for the stress path is related to the fact that these specimens were either not further consolidated (tests USc3 and USc11) or isotropically consolidated, but below the isotropic preconsolidation pressure (tests USc4 and USc5). This meant that the behaviour during shearing is different than that expected for normally consolidated specimens such as USc7 or USc10. The non-homogeneity observed along the length of the samples (Chapter 5) could also be affecting the results in these tests. The maximum shear strength obtained for specimens USc4 and USc5 were well above the critical state line described by the other specimens. This is likely to be related to the way in which the specimen dimensions were determined (i.e. based on the final *w* instead of using the volume change unit). The behaviour observed during tests USc9 (lightly overconsolidated) and DSc1 (drained) agreed well with the rest of the tests. From the tests performed in the Stress Path cell, the cohesion and Mohr-Coulomb friction angle in compression for isotropically consolidated specimens were estimated and are summarized in Table 6.5. In order to establish the friction angle, Equation 6.1 was used.

$$M_c = \frac{p'}{q'} = \frac{6 \cdot \sin \phi_c^{'}}{3 - \sin \phi_c^{'}} \qquad \text{[Eq.6.1]}$$

Table 6.5. Critical state parameters in compression for isotropically consolidated specimens

	Strength parameters	
Mc_{ic}	$c_c'_{ic}$ (kPa)	$\phi_c'_{ic}$ (°)
0.818	0	21.10 (~ 21)

From test DSc1, in which the specimen was sheared drained under compression, a Poisson's ratio (ν) equal to 0.347 was calculated. The apparent undrained Poisson's value was confirmed to be equal to 0.5 during the undrained tests.

With respect to the extension tests performed during the present study, tests USe1 and USe2 failed because the specimens became slightly out of line during the B-check and/or during isotropic consolidation, and also, and more importantly, because there was a leak at the top of the cell that made it impossible to create a good seal between the two parts of the extension caps. Tests USe3, USe4 and USe5 were used in order to define the critical state line under extension for isotropically consolidated samples. The parameters are summarised in Table 6.6 and indicate a larger friction angle in extension (calculated using Equation 6.2) than in compression. It should be noted that in this case the results from test USe3 reduce the average friction angle, which without considering this test would be around 28 degrees. This was not surprising at all since it was during test USe3 that a leak was finally identified at the top of the cell. This unfortunately required various successive rearrangements (e.g. filling and emptying the cell and performing the corresponding B-checks) and therefore the specimen was quite likely to have been affected in some way. As a comparison, the friction angle for London Clay has been reported to be 14.5 º to 30 º (Mott MacDonald, 1991), 22 º (Simpson, 1992), 23 º (Atkinson, 1993), 26.5 º for the unweathered London clay (Chandler et al., 1998) and 24 º to 28 º (Burland et al., 2001).

$$M_e = \frac{p'}{-q'} = \frac{6 \cdot \sin\phi_e'}{3 + \sin\phi_e'} \qquad \text{(with } q' = \sigma_v - \sigma_h\text{)} \qquad \text{[Eq.6.2]}$$

Table 6.6. Critical state parameters in extension for isotropically consolidated specimens

	Strength parameters	
Me_{ic}	$c_e'_{ic}$ (kPa)	$\phi_e'_{ic}$ (º)
0.759 0.817	0	25.88 (~ 26) 28.28 (~ 28): Without including data from test USe3

The way in which the extension tests are performed can introduce additional sources of error and therefore the accuracy is believed to be lower than during the more conventional compression tests. This is mainly because of the use of the Advanced Loading Module (see Section 3.6.2.2), which might introduce additional specimen deformations during the B-check and consolidation stages. The deformation of the specimens was measured using the external LVDT.

The condition of constant u at failure for the specimens sheared either in compression or in extension was reached as illustrated in Figures 6.3 and 6.8 respectively. An initial reduction in u during shearing is observed in tests USe5.

The critical state parameters reported in Table 6.7 were obtained by averaging the results from the isotropic consolidation tests NCL1 and NCL2 as illustrated in Figure 6.10.

Table 6.7. Normal consolidation line and swelling line parameters

λ_{ic}	κ_{ic}	N_{ic}
0.1817	0.03	3.275

The K_0-consolidation tests, together with the on-sample instrumentation, formed the basis for the subsequent stress path testing (Chapter 7) therefore it was important to get these aspects right. Unfortunately however there were many setbacks until high quality results were achieved. These caused a lot of time to be invested in finding the causes for the poor performance of the system when reproducing the required stress conditions, testing the different methods available, repairing equipment and using new devices not initially envisaged. This occurred until nearly the end of the project and represented a major issue in terms of achieving the aim and objectives of the study.

When the K_0-Module in GDSLAB was used for the first time using the direct measurement option with the ±2.5 mm radial on-sample LVDT's the results were very poor. The outcome is illustrated in Figure 6.11. On this occasion the results were sent to GDS. The fluctuations were linked to a poor temperature control of the room (small fluctuations in Figure 6.11) and to interferences from mobile phones (large fluctuations in Figure 6.11). From this graph, although being very likely affected by the large stress cycles, an initial K_0 value of approximately 0.64 was estimated from the results corresponding to p' values between 200 and 275 kPa. Before attempting to do another test, temperature control was installed in the room as part of the laboratory refurbishment and the LVDT was checked for effects from vibrations, mobile phones (as suggested by GDS) and other electrical apparatus. None of these proved to affect the LVDT, but it was found that closing the door to the room, which was, unfortunately, too close to the cell did affect the LVDT response. This was resolved before starting test Ko2. Despite this, and although some of the large fluctuations were removed, the results were still far from being acceptable as shown in Figure 6.12. A K_0 value around 0.64 was also estimated in this case. After this test, all the potential sources of error in the system during one-dimensional consolidation were identified and carefully checked. This meant that the LVDT, the mounting calliper characteristics, the lower chamber friction, the load cell, the pore water pressure transducer, the three volume/pressure controllers and the software all had to be checked. As an example of these investigations, Figure 6.23 illustrates the different correlations made between the load cell, radial deformation (on-sample LVDT), axial displacement (external LVDT) and u readings during test Ko1. These correlations, which were also performed for test Ko2, indicated that the readings recorded were correct and that something was occurring physically in the cell since all the transducers showed the same type of response simultaneously. It can be seen in Figure 6.23 that excluding the peak

fluctuations due to the closing of the door, the rest of the fluctuations occur when the radial displacement (measured by the internal LVDT) does not respond to the successive slow increments in cell pressure during the K_0 process. As a result of this, the following loop occurs: as the system does not detect any variation in diameter (i.e. theoretically the K_0 conditions are maintained), the lower chamber diaphragm does not move (i.e. the axial displacement does not vary) and therefore the deviator stress reduces (see the load cell readings in Figure 6.23) because the specimen deforms under drained conditions. Whenever the radial LVDT moves again the system tries to bring this to its initial position and the process is not slow enough to keep u constant and equal to the back-pressure. After these observations, test Ko3 was carried out using another same-range LVDT and loosing the hinge in the mounting calliper. The result is illustrated in Figure 6.13, which is no better than the previous results. At this stage the problem was considered to be definitely caused by the radial LVDT pin getting randomly stuck (and then suddenly moving) inside the LVDT during the deformation of the specimen (due to the curvature being induced into the device and the rigidity of this). Additional causes for the observed problem could be due to the design of the radial calliper itself.

Yueyang (2008) found similar problems and introduced some modifications to the 'conventional' arrangement. These modifications consisted of: (1) The introduction of a glued rounded metallic pin between the specimen and one of the pads to allow the armature to move more freely; (2) gluing the metallic support that holds the LVDT pin to the radial armature rather than using the 'standard' bolts to ensure a less rigid contact between the pin and the LVDT body. These modifications helped improve his results, but strains below $1x10^{-4}$ could not be registered. Such modifications were not introduced during the present investigation because of time constraints. From the Ko3 test at p' between 300 kPa and just above 400 kPa a K_0 value again equal to 0.64 was estimated. At the end of the K_0-consolidation in test Ko3, an arbitrary stress path was carried out to evaluate the performance of the Stress Path GDSLAB Module (Figure 6.14). It should be noted that the stress state at the beginning of the first part had already varied from that calculated using K_0=0.64. The stress path module worked well and the pore water pressures were also measured successfully. Only the radial LVDT was used in this test and so the axial strains could not be measured.

Due to the poor performance of the K_0-module when using the LVDT's, an alternative method was investigated as shown in Figure 6.15 (test KoAL1). Even using this method, the measurement of radial strains during subsequent stress paths would still be an issue if the observed problems during K_0-consolidation were caused by the radial on-sample instrumentation, as the device would be required to measure small strains during subsequent stages.

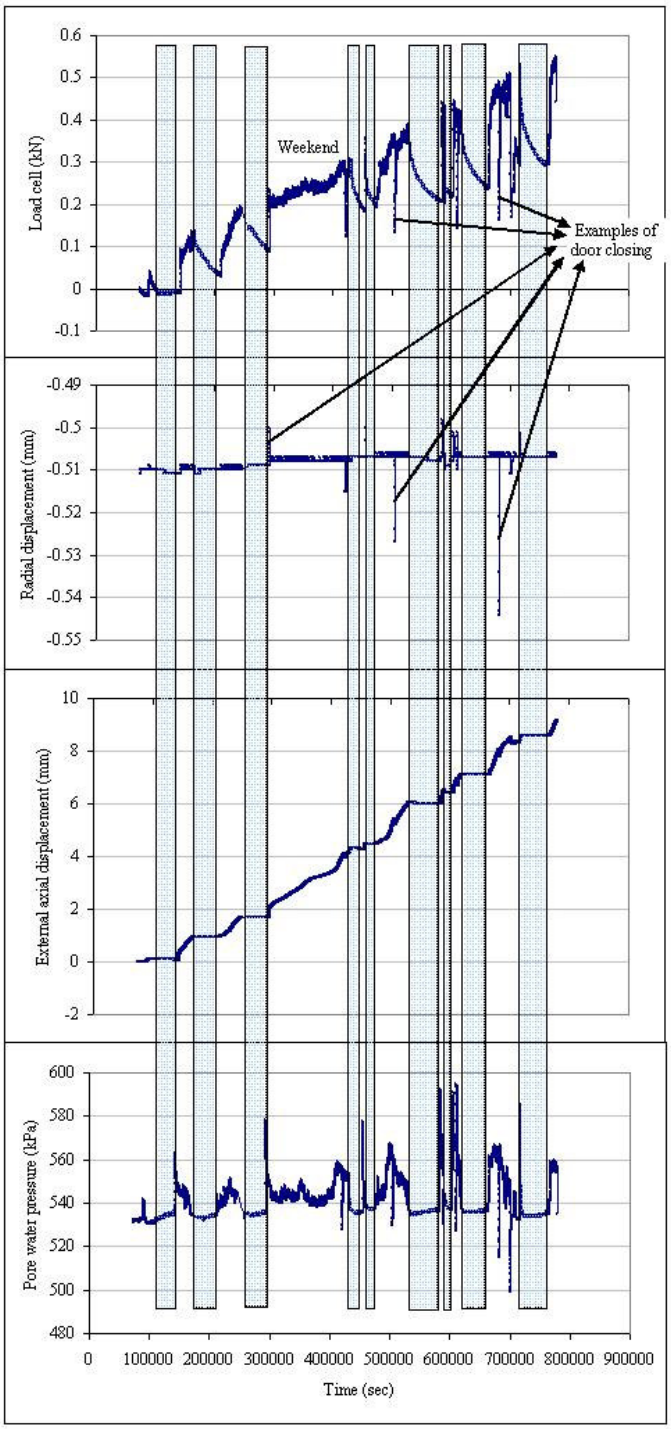

Figure 6.23. Correlations between the load cell, radial and axial deformations and the pore water pressure readings during test Ko1. The vertical columns relate the same observed behaviour between the different plots

Unfortunately, test KoAL1 could not be completed because the whole system became unstable showing many unexpected and extremely large fluctuations in test data (Figure 6.16). The engineers from GDS were contacted after this, and they updated the software and identified a large electrical interference between the LVDT's signal amplifier and the RS232 (Figure 3.18c). This was probably generated by water getting into one of the LVDT's after GDS had changed the cables to a new more flexible version (Section 3.6.1.2.3).

The K_0-Module option for performing one-dimensional consolidation by controlling the back volume was also investigated during tests Ko4 and Ko5 and these results are shown in Figure 6.17. The improvement was evident with respect to the performance of GDSLAB when the LVDT was used as a direct measurement of the radial strain. Based on test Ko4, a K_0 value of 0.64 was estimated, which confirms that the average trend obtained during tests Ko1, Ko2 and Ko3 was correct. From test Ko5, however, a value of K_0 equal to 0.65 was deduced. Part of the difference could be due to the use of the extension caps in test Ko5 instead of the standard ones. With respect to the behaviour of the samples in the v-lnp' plane, a larger variability can be observed in Figure 6.20 for tests Ko4, Ko5 and Ko6 when compared to the isotropic consolidated tests illustrated in Figure 6.10. The critical state parameters obtained for tests Ko4, Ko5 and Ko6, as well as the average values, are reported in Table 6.8.

Table 6.8. K_0-consolidation line parameters

	λ_0	N_0	K_0
Ko4	0.167	3.143	0.64
Ko5	0.160	3.093	0.65
Ko6	0.153	3.082	0.665
Average	0.160	3.106	0.65

At the end of the one-dimensional consolidation in test Ko4, the specimen was sheared undrained under compression. At the beginning of the shearing phase some problems occurred due to the last upgrade of the GDSLAB software that gave rise to an uncontrollable increase in the rate of strain. This demonstrated that sometimes the software updates correct some problems but may create new ones. After correcting this problem, the shearing continued successfully. Sample Ko5 was also sheared undrained under compression. Both samples failed at stress states that suggest a Mc_0 value and $\phi_c'_0$ in compression coincident with those previously obtained for isotropically consolidated specimens.

The results from test Ko6, in which a ±3 mm range radial Hall Effect device was used (see Figure 6.18), show an excellent performance for the device. This proves that the design of the GDS radial calliper-radial LVDT set has some deficiencies and requires further improvement before it can be used for accurate measurement of radial deformations at least in soils of similar characteristics to the one

used for the present investigation. From the results obtained in this test, a K_0 value equal to 0.665 was deduced. The shearing stage in extension at the end of the K_0-consolidation in test Ko6 showed the specimen failing at a stress state that agrees well with the failure envelope previously obtained for the three isotropically consolidated samples, with the friction angle ($\phi_e'_0$) being in good agreement with the average 28 degrees in Table 6.6. Figure 6.19 was useful in quantifying: (1) the radial deformation induced during B-check due to re-equilibrium of water; (2) the level of accuracy in keeping the radial strain equal to zero during K_0-consolidation; (3) the radial strain occurring during undrained shearing. With respect to the radial deformation during the B-check stage, three marked steps can be observed corresponding to the three increments in cell pressure applied during saturation (i.e. 0 - 300, 300 - 400 and 400 - 500 kPa respectively). It can be noticed that most of the deformation occurs during the first step. This reduction in cross-sectional area occurs because the specimen sucks water from the porous stones during specimen preparation in the cell (i.e. the volume increases) and once the cell pressure is increased, the water slowly returns to the porous stones (i.e. the volume decreases and hence the diameter). In fact, both changes in volume compensate each other and these are not required to be taken into account during the test to evaluate the specimen dimensions. It should be also noted that if the reduction in specimen height during the B-check stage when using the extension caps and the Advanced Loading Module is taken from the external transducer, which significantly overestimates this, the error when calculating subsequent stresses will be large. Additionally, since in theory this part of the test is undrained (i.e. $\Delta V = 0$), this reduction in specimen height is correlated by GDSLAB to an increase in cross-sectional area, which is in fact wrong. It should be additionally noted that the same phenomenon (i.e. apparent change in specimen volume during B-check) also occurs when checking the B value under "pure" isotropic conditions (i.e. when using the standard caps), but this is not registered by the system (i.e. the system considers the specimen dimensions being unchanged during the process). This issue, together with the fact that most of the excess u within the specimen tends towards equilibrium (i.e. the existing gradients dissipate), can give rise to a detectable reduction in u after having reached the initial maximum during this first cell pressure increment. An example of this was illustrated in Figure 6.5.

The condition of zero radial strain during K_0-consolidation was perfectly maintained during test Ko6 with maximum oscillations of 0.0017 mm being registered by the Hall Effect device. The radial deformation during undrained shearing was smooth until the magnetic pin came out of range (at about 3.5 mm). From all the tests performed in this chapter, test Ko6 is the only one in which a comparison could be made between internal and external measurements (i.e. between the radial deformation measured by the Hall Effect device during undrained shearing and the one calculated by the software based on the axial deformation measured by the external LVDT). This comparison is illustrated in Figure 6.24. In this particular case the difference between these two measurements was found to be large only when the soil was close to failure. Before reaching failure, the radial strain measured by the

Hall Effect device was bigger than that calculated by GDSLAB. It should be noted that the specimen cross-sectional area calculated by GDSLAB at the beginning of the shearing stage will always depend on the back-volume and the external LVDT values registered during K_0-consolidation according to Equation 3.8 despite using the K_0-Module. Potential inaccuracies in the back-volume can come from temperature changes mainly. With respect to the specimen area calculated during K_0-consolidation by GDSLAB using Equation 3.8, if the diameter is supposed to stay unchanged then the term ΔBV (back-volume), which corresponds to the increment in sample volume, should be equal to $Do \cdot \Delta H$, being Do the initial specimen diameter and $\cdot \Delta H$ the change in specimen height according to the external LVDT. However, reviewing the data during test Ko6, it has been observed that, since most of the time this volume is different than $Do \cdot \Delta H$, the system calculations give rise to an area that changes over time although theoretically this should be constant (and the radial on-sample Hall Effect device shows this). Differences in specimen area between that calculated by GDSLAB and that measured based on the on-sample instrumentation have been found not to have a large impact when it comes to calculating stresses (e.g. q at failure).

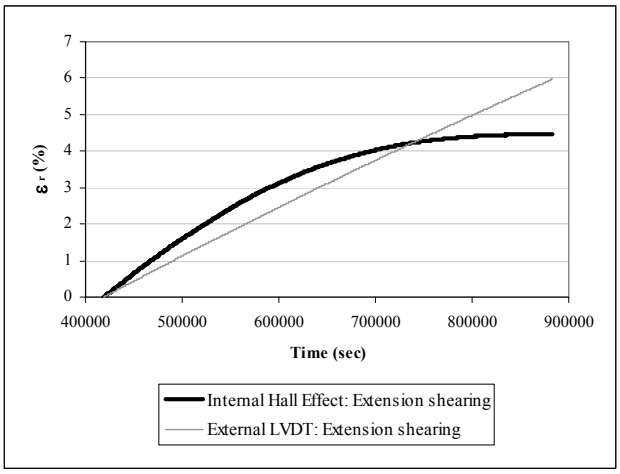

Figure 6.24. Difference between the radial strains measured by the on-sample Hall Effect device and those calculated based on the external LVDT during undrained shearing in test Ko6

A unique critical state line in the v - lnp' plane was deduced based on all the available failure states (i.e. isotropically and K_0-consolidated specimens; sheared specimens in compression and in extension) and this is illustrated in Figure 6.25.

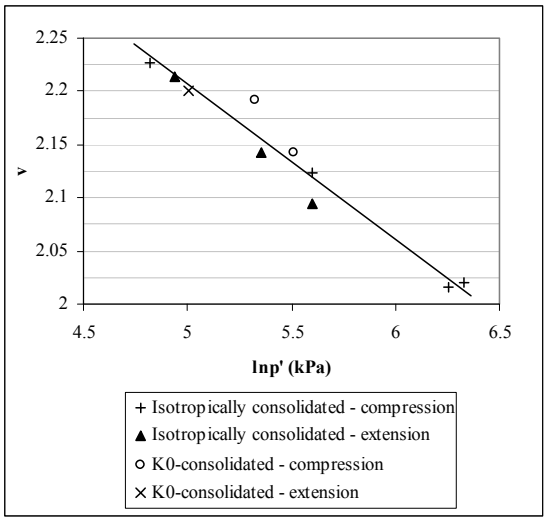

Figure 6.25. Critical state line in the *v* - *lnp'* plane

Table 6.9 summarises the parameters for the critical state line in the *v* - *lnp'* plane based on the results illustrated in Figure 6.25.

Table 6.9. Critical state line parameters

λ_{cs}	Γ
0.145	2.931

By examining the findings available in the published literature in terms of K_0 values and the critical state and consolidation parameters previously presented in Section 2.3.7, it can be observed than some disagreement exists with respect to whether the isotropically consolidated and the K_0-consolidated specimens share the same critical state parameters or not, and also with respect to the compression and extension states. This also applies for soils other than Speswhite Kaolin clay.

The laboratory data obtained from undrained triaxial tests under compression and extension for both isotropically and K_0-consolidated specimens was represented on a π-plane together with the failure envelopes for the Mohr-Coulomb, Lade-Duncan, Pande-Zienkiewicz, Matsuoka-Nakai and Drucker-Prager as illustrated in Figure 6.26. The Mohr-Coulomb envelope was fitted for the average compression friction angle in Table 6.5 (i.e. 21 ^{o}) and therefore the laboratory data in compression fits well on the π-plane representation with some points lying just on the envelope and others being slightly inside or outside this. The extension data, however, shows a larger spread, with one point lying on the Mohr-Coulomb envelope (corresponding to test USe3, which is likely to have been subjected to disturbance as described earlier in this section), but the other three points are well outside this envelope. The Mohr-Coulomb criterion is therefore not truly appropriate because if the compression results are fixed then the envelope underestimates the soil strength in extension.

Although the results are not conclusive, and further tests would be desirable, the Drucker-Prager model seems to be the most appropriate in reproducing the behaviour of the Speswhite Kaolin clay used for the present study.

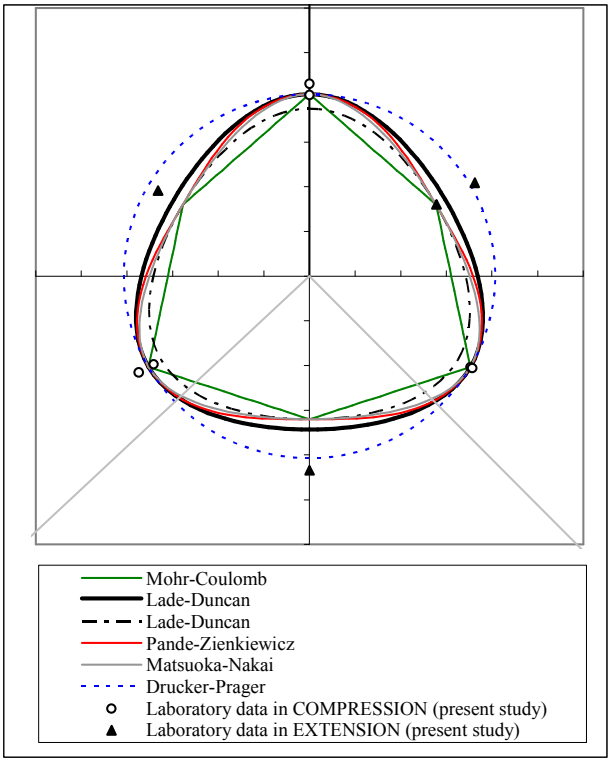

Figure 6.26. π-plane representation of the laboratory data for compression and extension triaxial states

6.4. SUMMARY

This chapter has presented the results from a wide range of triaxial testing on reconstituted Speswhite Kaolin clay specimens. From these, critical state parameters have been established that will be used later on in this research (Chapters 8 and 9). The limitations and issues encountered whilst performing the tests, in particular those requiring on-sample instrumentation, have been described in detail. Apart from determining the intrinsic parameters for this particular soil, these tests also served the purpose of learning on the use of conventional triaxial equipment and more state-of-the-art stress path testing before attempting to carry out more difficult stress path tests in Chapter 7.

Chapter 7: LABORATORY TESTS PART II:

STRESS PATH TESTING

7.1. INTRODUCTION

This chapter presents the results obtained from the laboratory stress path tests listed in Table 3.13 according to the methodology in Section 3.6.3. From these, the Jardine et al. (1991) small-strain parameters were obtained according to the methodology in Section 3.7.2 and these are also presented.

Before presenting the laboratory results:

- Section 7.2 describes the one-dimensional stress history to which the specimens were subjected in Device A and in the stress path cell in order to achieve the required initial stress conditions and explains the reasons for using the selected stress levels.
- Based on the results obtained from PLAXIS (Chapter 4), and the Speswhite Kaolin parameters defined in Chapter 6, the stress paths to be reproduced are defined in Section 7.3 in terms of total stresses.

A discussion of the results presented is given in Section 7.6.

7.2. INITIAL SOIL CONDITIONS

As previously stated briefly in Section 3.6.3, all the normally consolidated specimens tested using the stress path method were initially consolidated in Device A up to a theoretical (see Chapter 5) maximum vertical effective stress of 643 kPa. After sample trimming and preparation, the specimens were further consolidated one-dimensionally in the stress path cell to a horizontal total stress equal to 830 kPa, which experimentally corresponded to a vertical effective stress of approximately 600 kPa. There were various reasons for the selection of these values and these are described as follows:

1 The observations made in Chapter 5 (Section 5.3.7) indicated that a σ_v' of 1070 kPa was required in order to obtain firm to stiff specimens (i.e. a minimum c_u of 75 kPa), but it was later observed that in fact the specimens that were thought to have been consolidated to 1070 kPa could have been consolidated to a much lower σ_v' (perhaps even 50 % of this value). Assuming therefore that a σ_v' of about 1070 kPa / 2 = 535 kPa would be sufficient to prepare a firm specimen, a final σ_v' in the stress path cell above this value was considered to be adequate.

2 Specimen Ko5 (see Chapter 6) had been consolidated in Consolidation Device A to a σ_v' of 643 kPa (theoretical vertical effective stress), further consolidated in the triaxial cell to a σ_v' of 495 kPa and the undrained shear strength when sheared from a K_0 state was found to be close to 103 kPa (i.e. in the firm to stiff range).

3 In order to remove some of the soil disturbance occurring during specimen preparation, the specimen should ideally be further consolidated (exceeding the preconsolidation pressure) in the stress path cell (related to the SHANSEP method, see Section 2.3.2).

4 The stress state of the soil at the end of the K_0-consolidation had to be such that it would allow a reasonable margin for the stress state to be changed during tunnelling induced stress paths without reaching failure. The failure envelopes in compression and in extension were based on the results presented in Chapter 6 and these are illustrated in Figure 7.1 in a more convenient form. The limitations of the equipment in terms of maximum allowable working pressures were also taken into account.

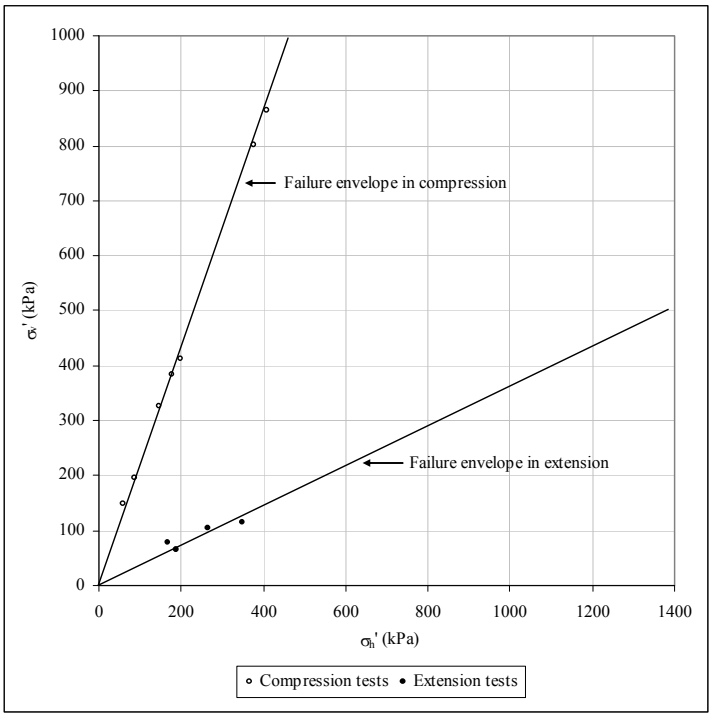

Figure 7.1. Failure envelopes in compression and extension for the Speswhite Kaolin clay based on the experimental data presented in Chapter 6

For the overconsolidated specimens ($K_0 \cong 1.5$) the vertical effective stress was taken to a final value of approximately 100 kPa.

Although strictly speaking a soil element at the tunnel springline would have been consolidated to a higher vertical pressure than a soil element situated above the tunnel crown and would have a lower overconsolidation ratio, all the specimens (i.e. those used for the reproduction of stress conditions at the crown and those for the reproduction of stress conditions at the springline) were prepared in the same way for simplicity.

It must be noted that the main aim when preparing the specimens for stress path testing was more a case of reaching the desired soil stiffness and overconsolidation ratio than that of exactly reproducing the condition of a soil element at a given depth. This makes sense particularly for the normally consolidated specimens since the likely stress states to which a soil element at 30 m depth is subjected in normally consolidated conditions (e.g. σ_v = 600 kPa, σ_v' = 300 kPa, σ_h' = 195 kPa and σ_h = 495 kPa (assuming K_0 = 0.65)) would not have given rise to stiff samples, at least not during K_0-consolidation at laboratory scale.

7.3. DEFINITION OF TUNNEL INDUCED STRESS PATHS FOR LABORATORY SIMULATION

From the results in Chapter 4, corresponding to the FEA of single and twin tunnels using PLAXIS, special attention was given to the relative variation of the vertical and horizontal total stresses at the different ground positions for the stages corresponding to the excavation of the tunnel and the placement of the lining. These relative variations were found to be quite constant during the tunnel excavation stage, but not during the placement of the lining (see Section 4.2.4). For the excavation stage (PART 1, and also PART 3 for the twin tunnels), the slopes of the stress variation on a σ_v - σ_h plane for K_0 values below 1 (i.e. 0.65) and above 1 (i.e. 1.5) at both the crown and the springlines were noted. Although for each K_0 value a slight difference in slope was observed for points above the tunnel crown and at the tunnel springlines, an average was taken to simplify the process during laboratory testing. The K_0 = 1 case was not reproduced in the laboratory since the differences in behaviour were expected to be more significant for K_0 above and below unity. For the stage corresponding to the placement of the tunnel support (PART 2, and also PART 4 for the twin tunnels), since the variation in σ_h and σ_v was found to be very sensitive to the type of soil and lining parameters involved in the analyses, a fixed 45 ^{o} was selected for simplicity. This was only changed to 15 ^{o} for the stress path at the springline between twin tunnels under K_0>1 conditions in order for the general stress trend to agree better with previous observations in Chapter 4. It should be noted that the stress path PARTS corresponding to the placement of the tunnel lining always acted as 'stabilising' stages in the sense that these either moved the stress path away from the failure envelope or restrained it from reaching failure. For the case of a point situated at the springline between the twin tunnels, the stress changes for K_0 values below and above "1" were found to be virtually the same as those occurring at the springline of a single tunnel, but duplicated (Sections 4.2.1 and 4.2.3). Due to this, and for the springlines, only the stress paths occurring around twin tunnels were simulated in the laboratory, with PARTS 1 and 2 being representative of the first tunnels and PARTS 3 and 4 being representative of the second tunnel. The targeted stress paths defined for each test are presented in Table 7.1. These were described according to the finite element results in Chapter 4, the methodology in Section 3.6.3, the precision of the equipment and the possible stress states region in Figure 7.1 given the individual

stress levels attained during K_0-consolidation. As previously stated in Section 3.6.3, tests SP2B and SB2C were not initially planned, but were later added due to the various shortcomings encountering during testing. It should be noted that for most of the tests the stress paths were very close to failure and therefore the stress path definition was greatly restricted. In some cases even conducting stress excursions smaller than initially desired, the soil reached failure. Total stress increments below 10 kPa were undesirable due to the precision of the volume/pressure controllers, but these were sometimes unavoidable.

Table 7.1. Change in vertical and horizontal total stress magnitudes aimed during tests SP1, SP1-c, SP2, SP2B, SP2C, SP3 and SP4

$K_0 < 1$		
Test	**Stage**	**Scheme**
SP1 and SP1-c Crown Single tunnel	PART 1: Tunnel excavation	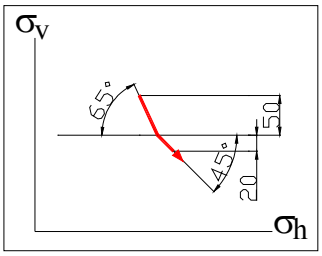
	PART 2: Lining placement	
SP2 Springline Single & Twin tunnels	PART 1: 1st Tunnel excavation	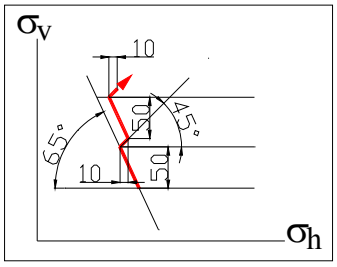
	PART 2: 1st Tunnel lining	
	PART 3: 2nd Tunnel excavation	
	PART 4: 2nd Tunnel lining	
SP2B Springline Single & Twin tunnels	PART 1: 1st Tunnel excavation	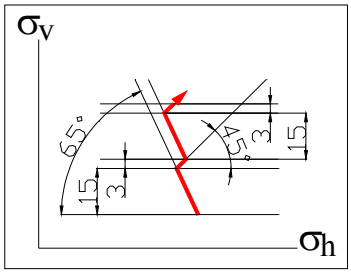
	PART 2: 1st Tunnel lining	
	PART 3: 2nd Tunnel excavation	
	PART 4: 2nd Tunnel lining	
SP2C Springline Single & Twin tunnels	PART 1: 1st Tunnel excavation	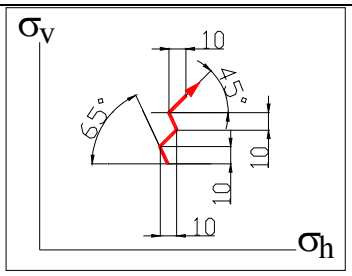
	PART 2: 1st Tunnel lining	
	PART 3: 2nd Tunnel excavation	
	PART 4: 2nd Tunnel lining	

Table 7.1 continuation. Change in vertical and horizontal total stress magnitudes aimed during tests SP1, SP1-c, SP2, SP2B, SP2C, SP3 and SP4

$K_0 > 1$		
Test	**Stage**	**Scheme**
SP3 Crown Single tunnel	PART 1: Tunnel excavation	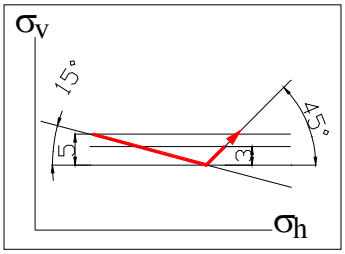
	PART 2: Lining placement	
SP4 Springline Single & Twin tunnels	PART 1: 1st Tunnel excavation	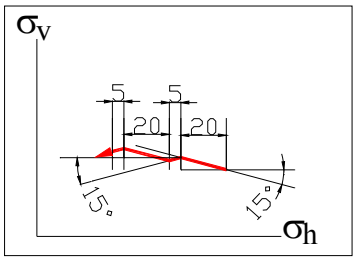
	PART 2: 1st Tunnel lining	
	PART 3: 2nd Tunnel excavation	
	PART 4: 2nd Tunnel lining	

When defining the stress paths in Table 7.1, and after making sure that the stress excursions could be reproduced in the stress path equipment, many simplifications were made with respect to the in-situ real conditions based on the following considerations:

- Likely rotations of the stress tensor due to the three-dimensional advance of the tunnel cannot be reproduced because of the limited stress conditions that can be performed within the cell.
- The triaxial cell constraints make it also impossible to vary the intermediate principal stress independently from σ_1 and σ_2.
- The way in which compression and extension states are reproduced in the cell are not exactly the same as those occurring in-situ around a tunnel. When a tunnel is excavated, those points situated on a vertical line above the tunnel centre line suffer unloading due to the removal of soil from underneath. This results in stress rotation. If the soil is capable of withstanding the deviated stresses, then arching occurs close to the tunnel perimeter and most of the overburden is supported by the resulting stresses. When the strength of the soil is not sufficient, this would require some sort of support and in the worst case the soil would collapse. The soil would then deform according to the new distribution of stresses over time until equilibrium (naturally or artificially) is reached. The amount of deformation would be determined by the particular stress-strain relationship of the soil, but the effect of gravity would also play a role. The soil close to the ground surface could be considered to follow the movement of the soil underneath, but even when arching occurs, the deformations would be more noticeable close

to the tunnel opening and these would be absorbed towards the ground surface. This is what creates extension states at points above the tunnel crown.

However, these conditions cannot be reproduced in the laboratory, where the sample (in which one end could be assumed to be representative of a soil element closer to the tunnel opening and the other end representative of a soil element closer to the ground surface) is axially unloaded equally along its length and the gravity effect is not present.

7.4. RESULTS

Due to the large amount of data compiled during laboratory testing, only one complete set of graphs is shown in this chapter. This corresponds to tests SP1 and SP1-c. All the other graphs can be found in Appendix D. Some plots from Appendix D have been also included in Section 7.6 for clarity and practical purposes if reference has been made to them as part of the discussion.

7.4.1. Crown of Single Tunnel. *Ko*<1 (Tests SP1 and SP1-c)

The data obtained during tests SP1 and SP1-c are shown together in Figures 7.2 to 7.14 in order to compare the differences in soil behaviour introduced due to creep after K_0-consolidation. Some relevant laboratory data have been also summarized in Table 7.2 that illustrates the similarities between both test conditions.

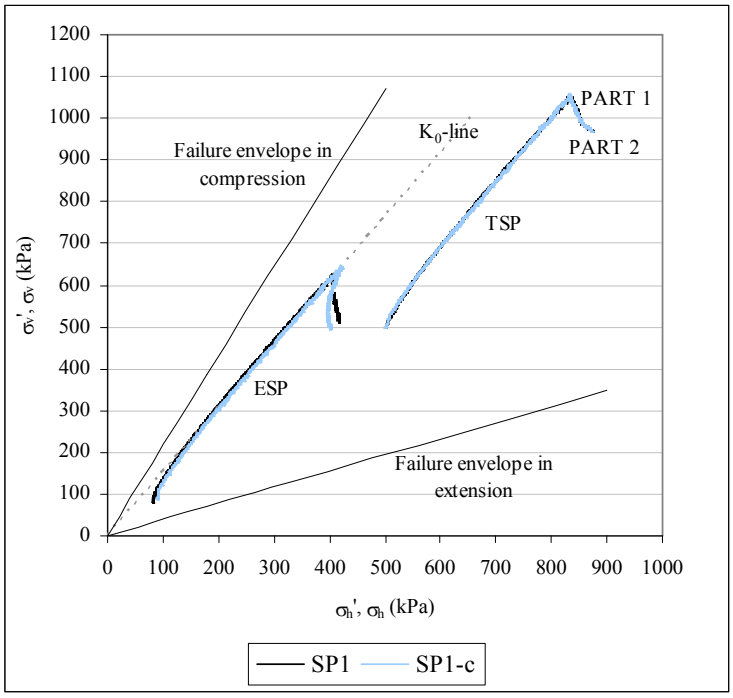

Figure 7.2. Total and effective experimental stress paths during tests SP1 and SP1-c.

BP: Back-pressure, TSP: Total stress path, ESP: Effective stress path

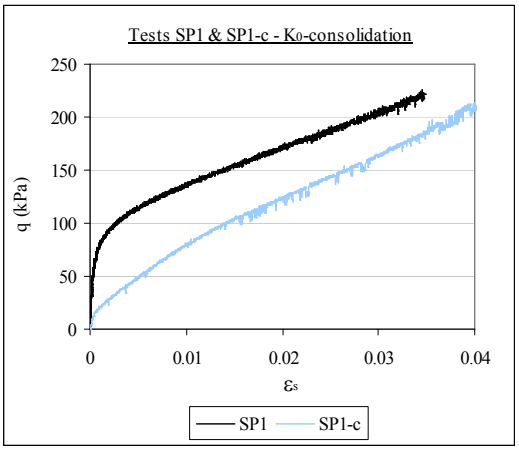

Figure 7.3. Tests SP1 and SP1-c. q - ε_s relationship during the K_0-consolidation stage

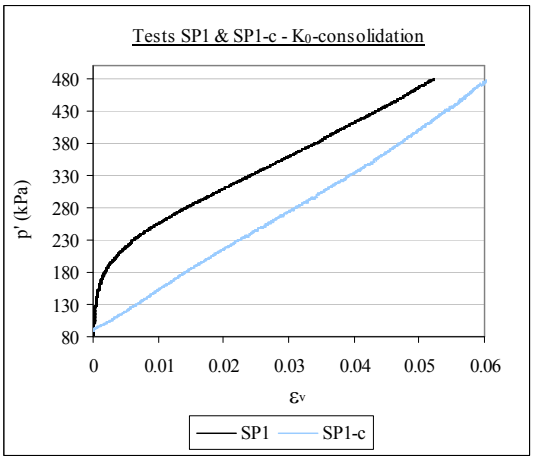

Figure 7.4. Tests SP1 and SP1-c. p' - ε_v relationship during the K_0-consolidation stage

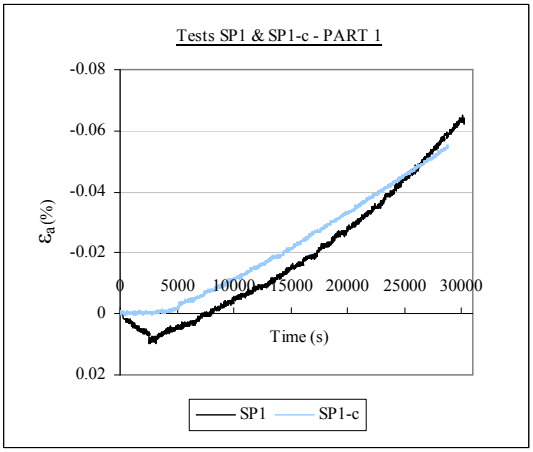

Figure 7.5. Tests SP1 and SP1-c. Variation in ε_a with time measured by the two axial on-sample Hall Effect devices

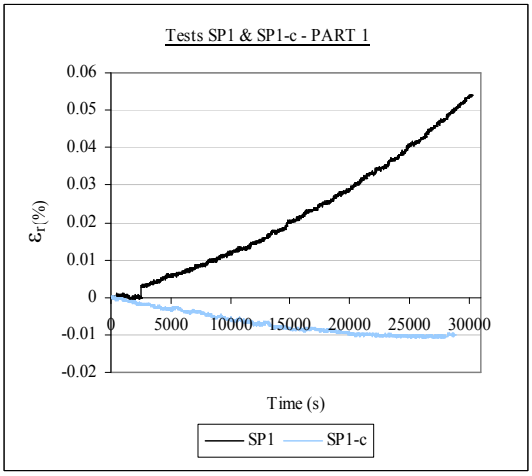

Figure 7.6. Tests SP1 and SP1-c. Variation in ε_r with time measured by the radial on-sample Hall Effect device

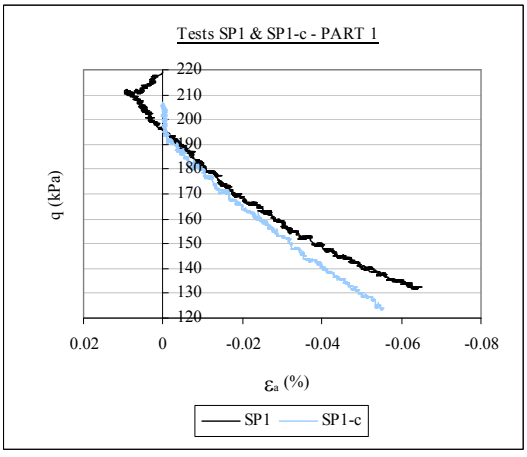

Figure 7.7. Tests SP1 and SP1-c. q - ε_a relationship during PART 1

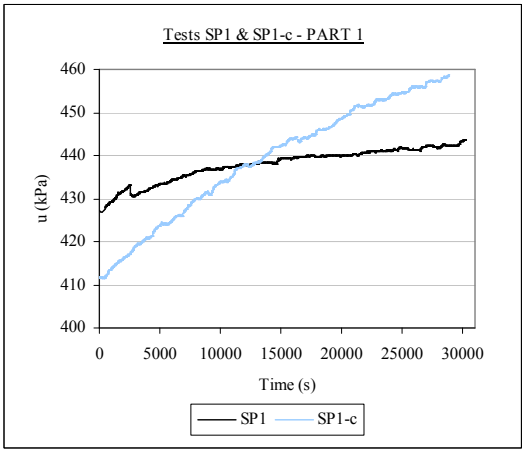

Figure 7.8. Tests SP1 and SP1-c. Variation in u with time during PART 1

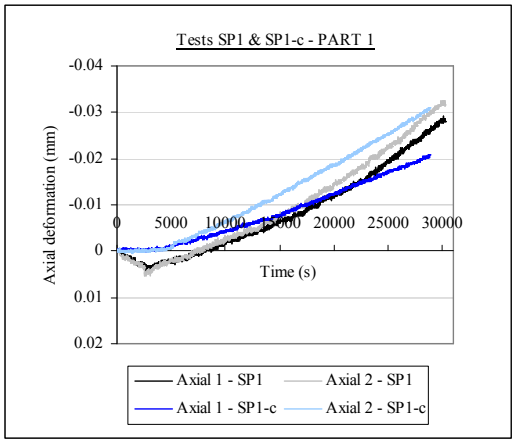

Figure 7.9. Tests SP1 and SP1-c. Comparison between the axial deformation registered by both axial Hall Effect devices during PART 1

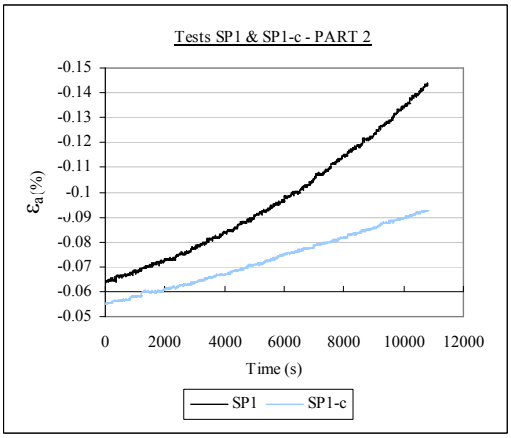

Figure 7.10. Tests SP1 and SP1-c. Variation in ε_a with time during PART 2 measured by the two axial on-sample Hall Effect devices

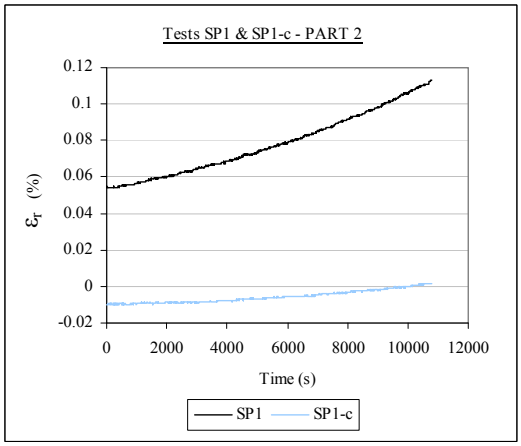

Figure 7.11. Tests SP1 and SP1-c. Variation in ε_r with time during PART 2 measured by the radial on-sample Hall Effect device

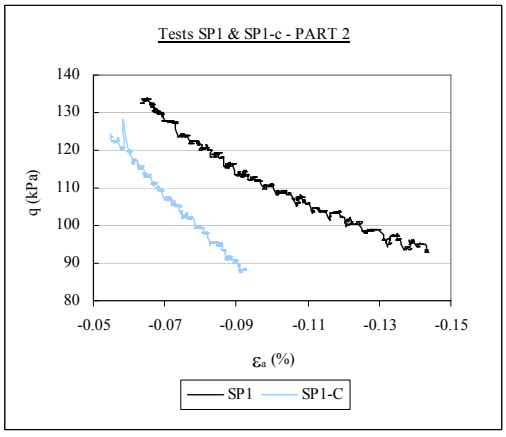

Figure 7.12. Tests SP1 and SP1-c. q - ε_a relationship during PART 2

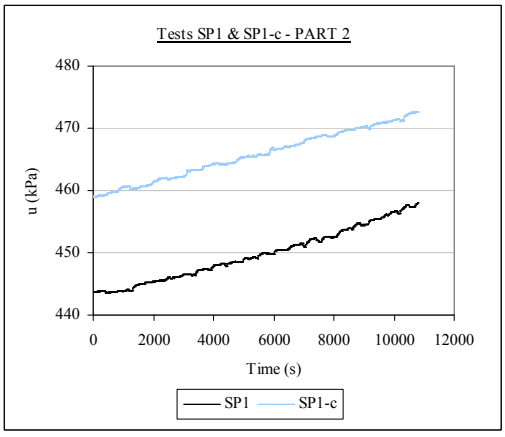

Figure 7.13. Tests SP1 and SP1-c. Variation in u with time during PART 2

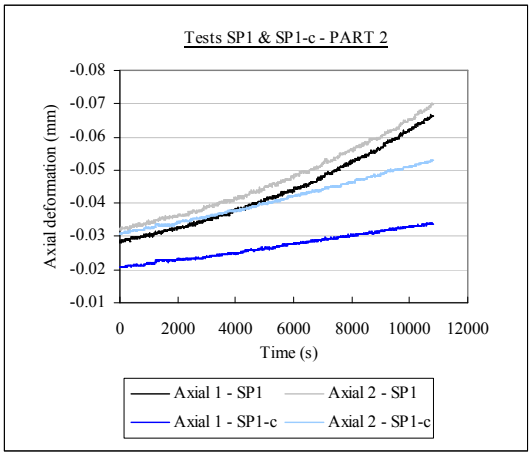

Figure 7.14. Tests SP1 and SP1-c. Comparison between the axial deformation registered by both axial Hall Effect devices during PART 2

Table 7.2. Summary of laboratory data during tests SP1 and SP1-c

	Before K_0-consolidation			After K_0-consolidation			End of test
	p'_0 (kPa)	B	u_0 (kPa)	σ_v (kPa)	σ_h (kPa)	u (kPa)	w (%)
SP1	87	0.94	417	1051.475	833	427	43.81
SP1-c	91	0.96	416	1051.038	832	412	43.05

7.4.2. Springline of Twin Tunnels. *Ko*<1 (Tests SP2, SP2B and SP2C)

The data obtained during test SP2 is illustrated in Appendix D - Figures D.1 to D.7. The initial B and p' values were 0.92 and 65 kPa respectively. One of the Hall Effect devices failed during this test. The specimen failed during this test because the increase in deviator stress induced an effective stress path that reached the failure envelope in compression. The failure mode of the specimen is shown in Figure D.8. The final w was 44.2 %.

The data obtained during test SP2B are illustrated in Appendix D - Figures D.9 to D.16. The initial B and p' values were 0.93 and 99 kPa respectively. As with test SP2, the soil also reached failure during PART 1. However the cause on this occasion could not be established from the recorded data. Only the data before the system went out of control have been presented in the Figures D.9 to D.16. The failure mode of the specimen is illustrated in Figure D.17. The final w was 45.80 %.

The data obtained during test SP2C is illustrated in Appendix D - Figures D.18 to D.41. The initial B and p' values were 0.93 and 106 kPa respectively. In this test the four PARTS were successfully completed without reaching failure. The final w was 43.8 %.

7.4.3. Crown of Single Tunnel. *Ko*>1 (Test SP3)

When the sample for test SP3 was set up, the system failed towards the end of the K_0-loading stage as huge fluctuations in all sensors were detected after 7 days of perfect performance. The test had to be terminated at this point and only the K_0 value could be reported (Table 7.10). The cause of the failure was identified as two of the Hall Effect devices having been damaged by water getting inside them, specially the radial one which controls the K_0-consolidation module. This just confirmed, considering the level of care during the testing, how delicate the Hall Effect devices are. Three new sensors were purchased at this point, but these were of the type conventionally commercialized by GDS made of aluminium. Unlike the ones made from titanium, these were reported by GDS not to have problems with leaks but to be more sensitive to corrosion. Another specimen was prepared at this point for test SP3. The data obtained during the test are presented in Appendix D - Figures D.42 to D.54. The initial B and p' values were 0.95 and 84 kPa respectively. It should be noted that from the middle to the ultimate part of the Ko-loading stage, the q - p' path was quite unstable. This was related to friction in the lower chamber increasing when the piston was getting closer to the upper part of the chamber. Friction can occur due to soil particles clogging the chamber during successive use of the cell. As a result it was decided to start the unloading stage earlier than initially intended in order to move the lower chamber piston in the opposite direction in the hope of improving the situation. The K_0 value achieved at the end of the one-dimensional swelling was 1.487. The final w was 46.39 %.

7.4.4. Springline of Twin Tunnels. *Ko*>1 (Test SP4)

The data obtained during test SP4 are illustrated in Appendix D - Figures D.55 to D.74. The initial B and p' values were 0.95 and 99 kPa respectively. The K_0 value achieved at the end of the one-dimensional swelling was 1.418. The final w was 46.0 %.

7.5. DETERMINATION OF THE SMALL-STRAIN PARAMETERS

According to the methodology in Section 3.7.1, the individual stress paths were classified in Groups 1, 2 and 3 as indicated in Table 7.3. The change in soil stiffness and the Jardine et al. (1991) parameters for the shear and volumetric behaviour of the soil were obtained from some representative tests in Groups 1 and 2. The results are presented in the following sections.

Table 7.3. Classification of tests into Groups 1, 2 and 3 according to the methodology in **Section 3.7.2**

	Stress path
Group 1	• K_0-loading for all tests • K_0-unloading for Tests SP3 and SP4 • PART 1 Test SP2 • PART 1 Test SP3
Group 2	• PARTS 1 & 2 Test SP1 • PART 2 Test SP1 • PARTS 1 & 2 Test SP1-c • PART 2 Test SP1-c • PART 3 Test SP4
Group 3	• PART 1 Test SP2B • PARTS 1 to 4 Test SP2C • PART 2 Test SP3 • PARTS 1, 2 & 4 Test SP4

7.5.1. Shear Response

The curve fitting methods used for each particular test are summarized in Table 7.4. The same table gives indications on corresponding figures in Appendix D – Section D.2 for curve fitting, variation in shear stiffness and degree of precision of the Jardine et al. (1991) curves in fitting the experimental data. Table 7.5 summarises the Jardine et al. (1991) parameters determined for each test.

The method established for the determination of the small-strain parameters during K_0-consolidation (Section 3.7.2) could have been applied to any of the K_0-loading paths available. However, since it was already obvious from the data presented in Section 7.4 that fitting the Jardine et al. (1991) curve to the different test data would potentially give different parameters, only one set of data was considered. The main aim was to derive a full set of parameters and demonstrate that the procedure defined in the methodology works. Test SP1 was selected for this purpose because the initial elastic and the subsequent elasto-plastic parts were more clearly differentiated. For this particular case, various curve fitting methods that gave good matching to the laboratory data were employed. The first method consisted of an equation of the type $q = f_1 \cdot \varepsilon_s^{\left(\frac{1}{f_2}\right)}$ because the relationship ε_s / q - ε_s was not linear and hence Chin's method was not applicable. The second method consisted of Chin's method being applied on $\varepsilon_s / (q / p')$ - ε_s. Other methods were tried with either similar or worse success. The fitting achieved by Chin's method on $\varepsilon_s / (q / p')$ - ε_s was particularly good. All these methods were, however, found to have a common limitation in the sense that they predict quite different q values at small strains than those measured experimentally and hence predict an inaccurate initial shear modulus. The q - ε_s fitting achieved using the different methods is illustrated in Figure D.90. The Jardine et al. (1991) parameters were not established for this particular case since it was

clear from the other data presented in this chapter that there is no unique set of parameters that can fit all the experimental data.

Table 7.4. Shear response during stress path testing: Curve fitting method, variation in shear modulus and Jardine et al. (1991) fitting accuracy

Test	Curve fitting method	Variation in shear modulus	Jardine et al. (1991) fitting
PART 1 Test SP2	Optimized average of (1) Chin's method ($q = \frac{\varepsilon_a}{f_1 \cdot \varepsilon_a + f_2}$) and (2) equation $q = f_3 \cdot \varepsilon_a^{\left(\frac{1}{f_4}\right)}$ (Figure D.75)	Figure D.76	Figure D.77 (Error: 0.886)
PART 1 Test SP3	Optimized average of (1) Chin's method ($q = \frac{\varepsilon_a}{f_1 \cdot \varepsilon_a + f_2}$) and (2) equation $q = f_3 \cdot \varepsilon_a^{\left(\frac{1}{f_4}\right)}$ (Figure D.78)	Figure D.79	Figure D.80 (Error: 0.074)
PARTS 1 & 2 Test SP1	Chin's method with $q = \frac{\varepsilon_a}{f_1 \cdot \varepsilon_a + f_2}$ (Figure D.81)	Figure D.82	Figure D.83 (Error: 0.189)
PART 2 Test SP1	Chin's method with $q = \frac{\varepsilon_a}{f_1 \cdot \varepsilon_a + f_2}$ (Figure D.84)	Figure D.85	Figure D.86 (Error: 0.005)
K_0-unloading Test SP3	Chin's method with $q = \frac{\varepsilon_s}{f_1 \cdot \varepsilon_s + f_2}$ (Figure D.87)	Figure D.88	Figure D.89 (Error: 1.972)
K_0-loading Test SP1	Chin's method on ε_s - ε_s/(q/p') (Figure D.90)	-	-

The error is calculated using Equation 3.10

Table 7.5. Jardine et al. (1991) shear parameters obtained from experimental data

	C1	*C2*	*C3*	*α*	*γ*	$\varepsilon_{s\,min}$	$\varepsilon_{s\,max}$	G_{min}
PART 1 – Test SP2	71.00	63.00	4.10E-05	1.336	0.828	3.637E-06	3.200E-02	974
PART 1 – Test SP3	217.77	182.92	2.128E-05	1.270	0.895	1.784E-06	1.000E-02	1129
PARTS 1 & 2 – Test SP1	2.36E-13	366.00	9.95E-06	0.319	1.569	5.482E-06	2.633E-03	25449
PART 2 – Test SP1	2.36E-13	204.00	9.95E-06	0.423	1.322	5.478E-06	1.365E-03	16779
K_0-unloading – Test SP3	367.00	176.00	2.087E-05	1.039	1.286	8.660E-06	1.500E-02	4483

Note 1: For the undrained stress paths, the relationship $\varepsilon_s = \sqrt{3} \cdot \varepsilon_a$ was used in order to obtain ε_s from ε_a

Note 2: Note that *C3*, $\varepsilon_{s\,min}$ and $\varepsilon_{s\,max}$ are presented as decimals and not as a percentage. Multiply by 100 in order to get %

7.5.2. Volumetric Response

The curve fitting methods used for each particular test are summarized in Table 7.6. The same table gives indications on corresponding figures in Appendix D - Section D.2 for curve fitting, variation in bulk modulus and degree of precision of the Jardine et al. (1991) curves in fitting the experimental data. Table 7.7 summarises the Jardine et al. (1991) parameters determined from the data obtained during K_0-loading in Test SP1. The Jardine et al. (1991) parameters were not established for the K_0-unloading stage in Test SP3 for the same reason as previously stated for the shear response during the K_0-consolidation stage in Test SP1.

Table 7.6. Volumetric response during stress path testing: Curve fitting method, variation in bulk modulus and Jardine et al. (1991) fitting accuracy

Test	Curve fitting method	Variation in bulk modulus	Jardine et al. (1991) fitting
K_0-loading Test SP1	Optimized average of (1) Chin's method on the transformed space $\frac{(p' - p_0')}{p'}$ ($p' = \frac{p_0' \cdot (f_1 \cdot \varepsilon_v + f_2)}{\varepsilon_v \cdot (f_1 - 1) + f_2}$) and (2) equation $p' = f_3 \cdot \varepsilon_v^{\left(\frac{1}{f_4}\right)}$ (Figure D.91)	Figure D.92	Figure D.93 (Error: 27.35)
K_0-unloading Test SP3	Chin's method with $p' = \frac{\varepsilon_v}{f_1 \cdot \varepsilon_v + f_2}$ (Figure D.94).	Figure D.95	-

The error is calculated using Equation 3.10 but using p' instead of q

Table 7.7. Jardine et al. (1991) volumetric parameters obtained from experimental data

	C4	*C5*	*C6*	δ	η	$\varepsilon_{v\,min}$	$\varepsilon_{v\,max}$	K_{min}
K_0-consolidation – Test SP1	936.9	880.861	4.75E-05	1.8346	0.5713	5E-05	9.9E-03	12074

Note 1: Note that *C6*, $\varepsilon_{v\,min}$ and $\varepsilon_{v\,max}$ are presented as decimals and not as a percentage. Multiply by 100 in order to get %

7.6. DISCUSSION

This section has been divided in two parts. The first presents and discusses the issues identified while performing the stress paths in the laboratory in addition to those shortcomings already commented in Section 7.4. The second serves the same purpose, but with respect to the evaluation of the change in soil stiffness during the stress path excursions and the definition of the Jardine et al. (1991) parameters.

7.6.1. Stress Path Testing

(1) As previously stated in Section 3.6.3, the output readings and calculated data given by GDSLAB are based on the external measurements rather than on the internal on-sample instrumentation, therefore all the data was re-calculated accordingly in order to discover any likely differences. Similarly and as previously mentioned in Section 6.3, specimen cross-sectional variations were calculated by GDSLAB during K_0-consolidation. These have been however found not to give significant differences in σ_v and related stress magnitudes (e.g. q), hence not having much impact when calculating parameters such as K_0. In order to confirm these observations, the area calculated by GDSLAB during one-dimensional consolidation in test SP2 and that calculated based on the on-sample Hall Effect device measurements are illustrated in Figure 7.15. The corresponding calculated $\sigma_{v'}$ - $\sigma_{h'}$ relationship, based on both measurements, is shown in Figure 7.16 together with the same procedure conducted for test Ko6 (see Chapter 6).

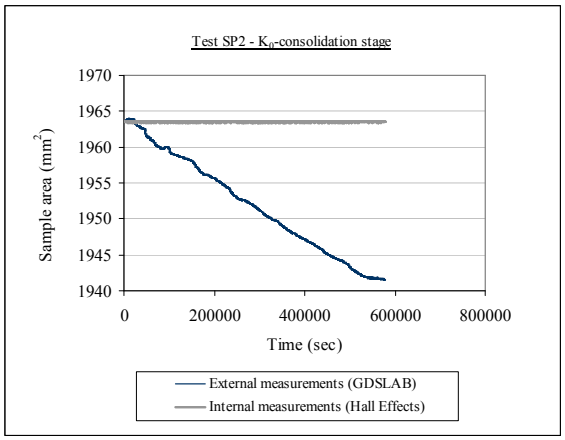

Figure 7.15. Test SP2. Variation in specimen area during K_0-consolidation as measured by both internal and external instrumentation

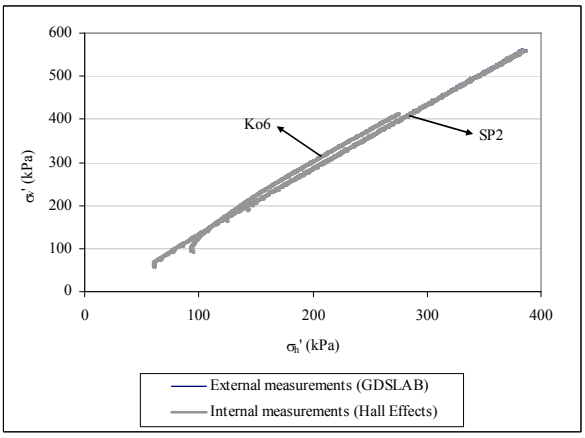

Figure 7.16. Tests SP2 and Ko6. Calculated $\sigma_{v'}$ - $\sigma_{h'}$ variation during K_0-consolidation based on both internal and external specimen area measurements

(2) The issue commented in the previous point regarding the change in sample area during K_0-consolidation, could eventually introduce significant differences between the values calculated by GDSLAB during the subsequent stress paths and those re-calculated using the on-sample measurements. It was found that such differences were very small, but still important to take into account when concerned with small-strain behaviour. As an example, Table 7.8 shows the values reached at the end of PART 1 in tests SP2 and SP2C.

Table 7.8. Differences between GDSLAB-calculated data (external transducers) and user-calculated data (internal transducers) at the end of PART 1 in tests SP2 and SP2C

		BASED ON EXTERNAL MEASUREMENTS			BASED ON INTERNAL MEASUREMENTS				
Test (PART 1)	**Load cell pressure (kN)**	**ε_a (%)**	**Area (mm^2)**	**c_u (kPa)**	**ε_a (%)**	**Area based on axial Hall Effect devices (mm^2)**	**c_u based on axial Hall Effect devices (kPa)**	**Area based on radial Hall Effect device (mm^2)**	**c_u based on radial Hall Effect device (kPa)**
SP2	0.120	2.628	1993.917	30.091	2.556	2015.005	29.776	2047.465	29.304
SP2C	0.023	0.074	1950.103	5.897	0.093	1965.333	5.851	1965.652	5.850

(3) Judging from the results, the author believes that for an appropriate study of the soil behaviour at small strains, even more accurate equipment should be used, perhaps for instance, the GDS Advanced Pressure/Volume Controllers, which has a pressure resolution of 0.1 kPa instead of the 1 kPa of the current equipment. The problem observed with the equipment used for the present investigation was primarily identified when changing from one test-type to another (i.e. GDSLAB modules) or test conditions (e.g. from drained to undrained conditions). During test SP2 PART 1 for example, the total vertical stress was set up to increase and the all-round pressure to decrease (i.e. q increases). However, for the first 6-7 minutes q decreased (only around 1 kPa) instead of increasing due to the system relaxing slightly and the specimen length still showed a continuous decrease. Similar behaviour could be observed at the beginning of PART 1 in test SP2C since q was being adjusted by the software (i.e. fluctuating slightly) before starting to increase, and very small positive axial strains were already being registered. This type of phenomenon made it difficult to calculate the soil stiffness at small strains, as this gave rise to the calculation of very large initial negative stiffness. At the beginning of PART 1 in test SP1 something slightly different occurred that is easily identifiable in Figures 7.5 and 7.7. Although q decreased over time as expected, the axial strain was observed to increase (i.e. being positive) during the first 50 minutes. A rational explanation for this could not be found as 50 minutes was considered too long for initial system adjustment.

(4) During some of the tests (e.g. PART 2 Test SP2C - Figure D.29, PART 2 Test SP4 - Figure D.65), because the variations in stresses were small, and because of the precision of the pressure/volume controllers, the system struggled to follow the targets set.

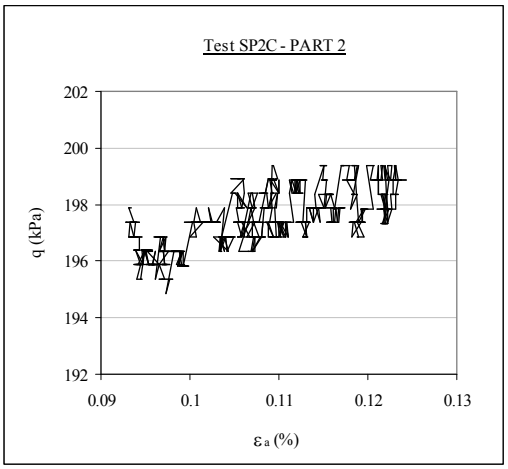

Figure D.29. Test SP2C. q - ε_a relationship during PART 2

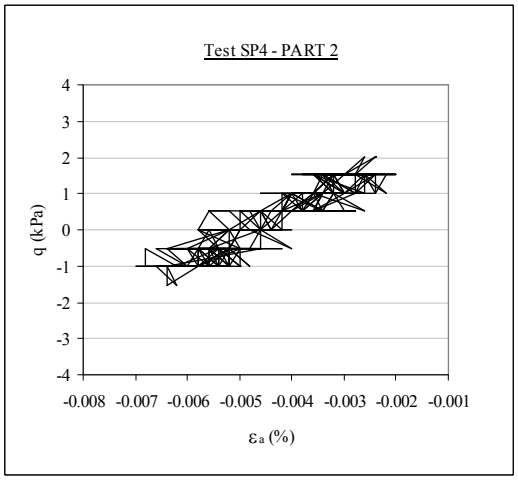

Figure D.65. Test SP4. q - ε_a relationship during PART 2

(5) The accuracy of the Hall Effect devices is better than 0.8 % FRO as previously stated in Section 3.6.1.2.3. Considering the range over which the various devices were linear (from ±2.3 to about ±2.9 mm), the expected accuracy was approximately between 0.036 and 0.046. This means between 0.0007 and 0.0009 in terms of strain when measured over 50 mm. Although the device resolution can be more than 10 times higher than the accuracy quoted (see Appendix A – Section A.1), the on-sample deformation measurements registered during the present laboratory tests, which were sometimes as small as 0.0001 mm (i.e. strain: $2 \cdot 10^{-6}$), could be in fact under or over-estimated by the accuracy value just stated. The devices seemed to be very stable down to 0.1 micron, but ideally specific calibrations should have been undertaken to assess the accuracy and the repeatability, for example, over a 0.1 mm range. This could not be done during this study due to the lack of facilities for this calibration.

(6) The relatively large differences between the readings from the two axial Hall Effect devices in test SP3 for example (Figures D.49 and D.54), were attributed, in addition to the different precision of the two devices, to a likely small tilting of the specimen and imperfections in the specimen - top/base caps contact. Although the latter would normally have a larger impact on the external measurements, the internal instrumentation would not be totally free from these undesirable effects.

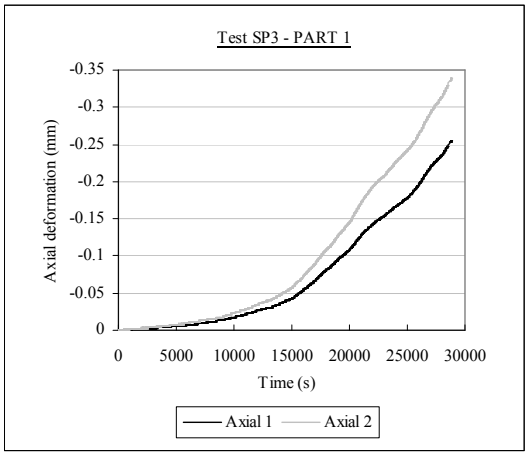

Figure D.49. Test SP3. Comparison between the axial deformation registered by both axial Hall Effect devices during PART 1

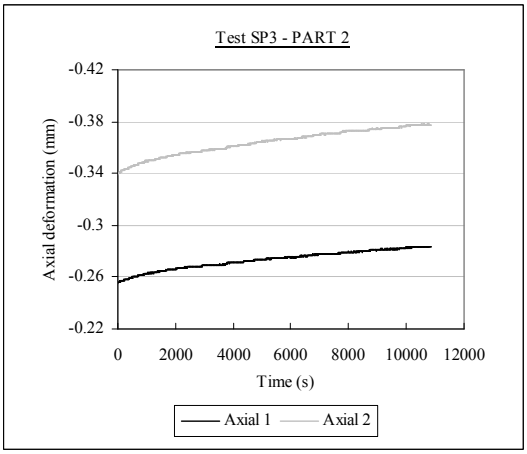

Figure D.54. Test SP3. Comparison between the axial deformation registered by both axial Hall Effect devices during PART 2

(7) Comparing PARTS 1 in tests SP2 (Figures D.4 to D.7) and SP2C (Figures D.22 to D.25), the effects of using different rates of stress for testing were easily identified. The initial 10 kPa increment in total vertical stress in test SP2 took 2 hours to complete. The same stress increment, but in test SP2C, took 8 hours. The differences have been summarized in Table 7.9. According to these results, the faster the rate of stress increment, the smaller the pore water pressures that develop and the less the soil deforms, therefore higher soil stiffness is computed. Similar results, with regard to the soil stiffness, have been reported by Jardine et al. (1991).

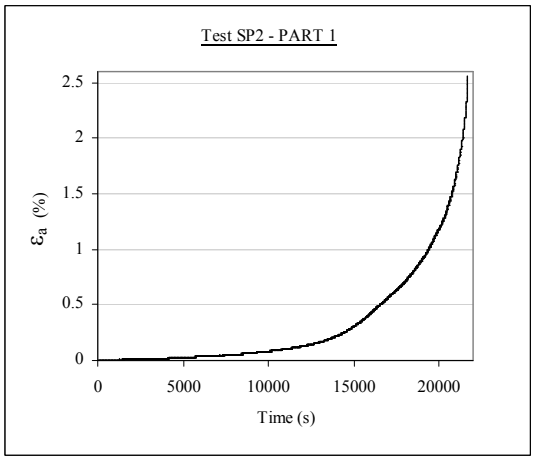

Figure D.4. Test SP2. Variation in ε_a with time during PART 1 measured by the axial on-sample Hall Effect device

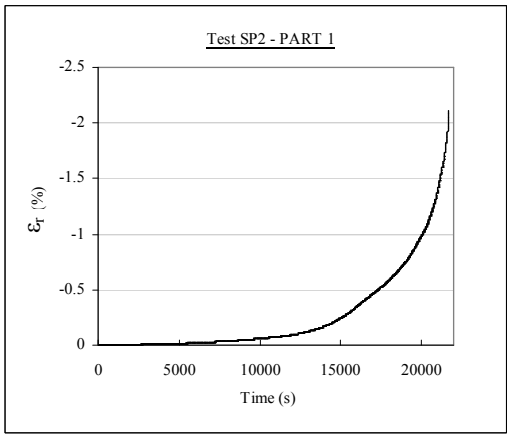

Figure D.5. Test SP2. Variation in ε_r with time during PART 1 measured by the radial on-sample Hall Effect device

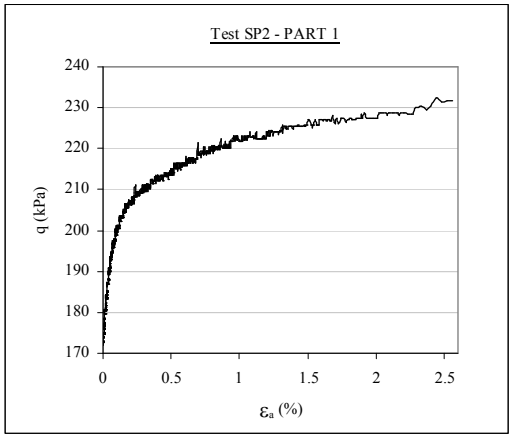

Figure D.6. Test SP2. q - ε_a relationship during PART 1 based on the Hall Effect device internal measurements

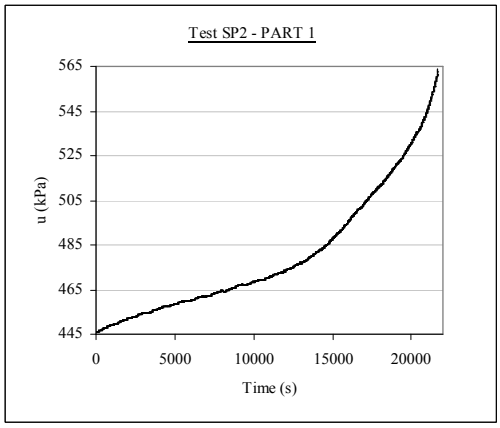

Figure D.7. Test SP2. Variation in u with time during PART 1

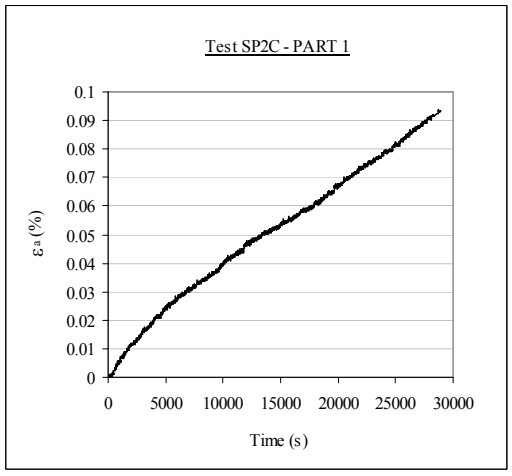

Figure D.22. Test SP2C. Variation in ε_a with time during PART 1 measured by the axial on-sample Hall Effect device

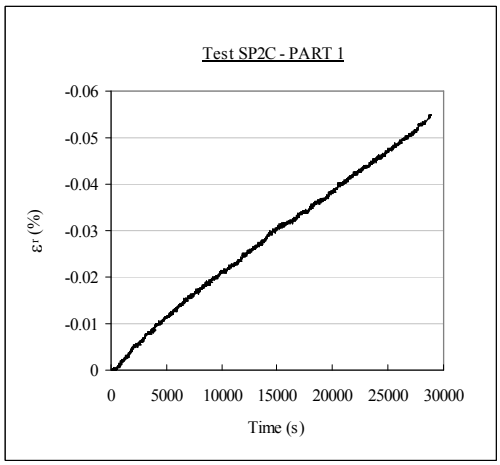

Figure D.23. Test SP2C. Variation in ε_r with time during PART 1 measured by the radial on-sample Hall Effect device

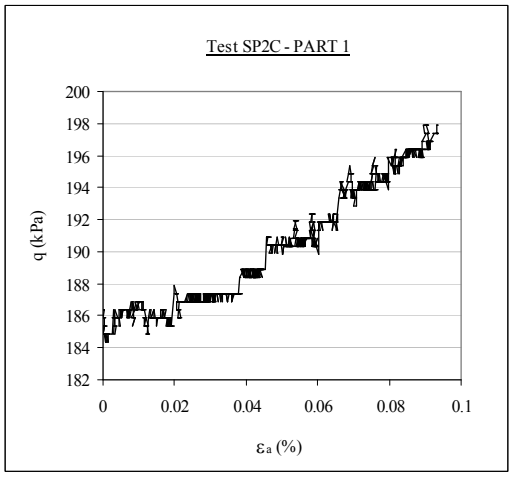

Figure D.24. Test SP2C. q - ε_a relationship during PART 1

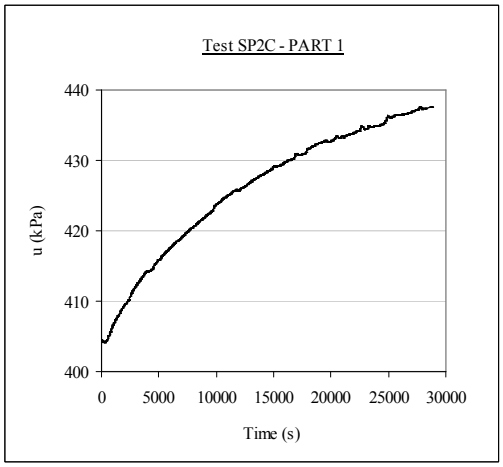

Figure D.25. Test SP2C. Variation in u with time during PART 1

Table 7.9. Differences observed between tests SP2 and SP2C due to strain rates used during testing

	SP2	SP2C
Test duration (hours)	2	8
$\Delta\sigma_v$ (kPa)	10	10
$\Delta\varepsilon_a$ (%)	0.0448	0.0935
$\Delta\varepsilon_r$ (%)	-0.0303	-0.0549
Δu (kPa)	16.23	33.03

(8) Some variability in the K_0-value was observed during the present tests as summarised in Table 7.10.

Table 7.10. Variability in computed K_0 values during K_0-consolidation in the triaxial cell

Test	K_0
SP1	0.665
SP1-c	0.665
SP2	0.685
SP2B	0.665
SP2C	0.69
SP3-failed	0.68
SP3	0.63
SP4	0.63

(9) When stress paths corresponding to the excavation of consecutive twin tunnels were reproduced (see test SP2C for example), there were about 12 hours between PARTS 2 and 3 in which the stress state was not changed but maintained constant under undrained conditions. The soil response during this interval of time was recorded as follows:

- ε_a (%) went from 0.123 to 0.194 (Figure 7.17)
- ε_r (%) went from -0.065 to -0.089 (Figure 7.18)
- u went from 448.53 to 456.75 kPa (Figure 7.19)

This observed soil response has been mainly attributed to undrained creep occurring within the specimen at constant stress and also partially to the system precision. This sort of deformation was also reported by Barla (1999) towards the end of the tunnelling induced stress paths excursions that the author performed in the laboratory. Although the numbers indicate very small changes taking place in the soil during the 12 hours, the observations were considered relevant since the order of magnitude is similar to the response observed during PARTS 1 and 2.

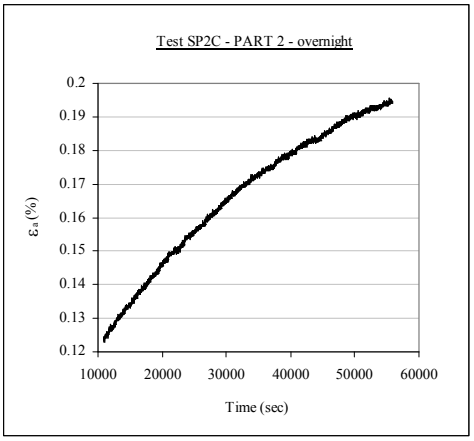

Figure 7.17. Test SP2C. Variation in ε_a during PART 2-overnight under constant stress undrained conditions

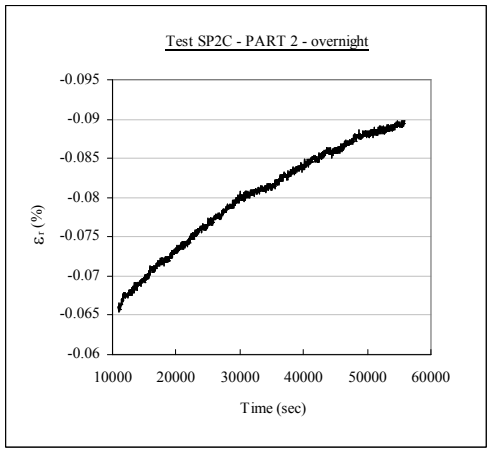

Figure 7.18. Test SP2C. Variation in ε_r during PART 2-overnight under constant stress undrained conditions

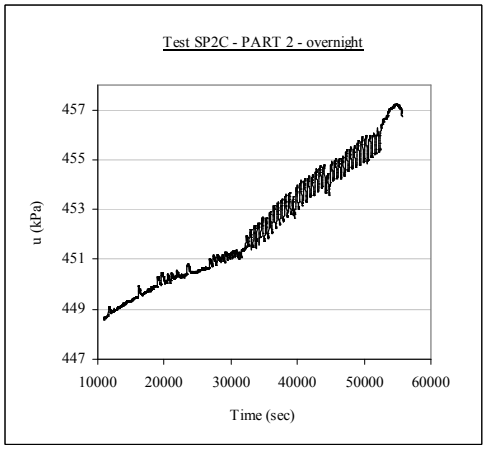

Figure 7.19. Test SP2C. Variation in *u* during PART 2-overnight under constant stress undrained conditions

(10) The main difference between the response observed in tests SP1 and SP1-c (including creep at the end of the K_0-consolidation stage) was the variation in radial strain during PART1 (Figure 7.6). Significant differences can also be observed in terms of *u* during PART 1 (Figure 7.8). The readings of the various variables during creep at the end of K_0-consolidation indicated very small variations: σ_v from 1049.9 kPa to 1051.3 kPa; σ_h constant; Axial Hall Effect device 1: 1.572 to 1.695; Axial Hall Effect device 2: 1.864 to 2.055; Radial Hall Effect device from -0.895 mm to -0.917 mm; u from 420.5 kPa to 411.8 kPa. Based on these, the response was not expected to be so different for both tests. The intended direct comparison of initial stiffness during PART 1 in tests SP1 and SP1-c (Section 3.6.3) was not possible. This was unfortunate

but it was no longer pursued given the limited time available and the fact that this was not one of the main objectives of the present investigation but rather an additional interesting topic. Further tests of the same type should be performed before being able to extract any relevant conclusion.

(11) A distinctively different soil response was observed during PART 1 in test SP4. It was also only during this test and test SP3, both with K_0 values above unity, that a drop in *u* was registered (Figures D.48 and D.62). This is consistent with the overconsolidated conditions.

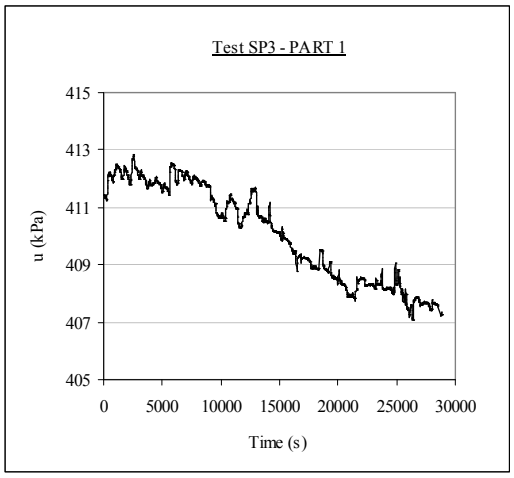

Figure D.48. Test SP3. Variation in *u* with time during PART 1

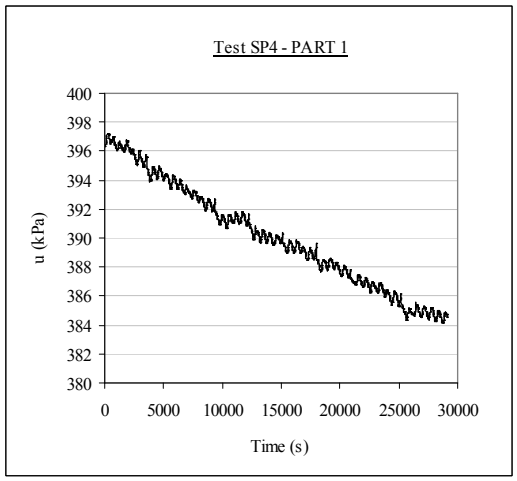

Figure D.62. Test SP4. Variation in *u* with time during PART 1

(12) The slopes of the swelling line in both planes *v* - *lnp'* (κ) and *lnv* - *lnp'* (κ*) were calculated from test SP3 since the volume change measurement at the moment of changing from loading to unloading in test SP4 was somewhat irregular. These were found to be 0.039 and 0.018 respectively. The parameter θ in Schmidt (1966)´s Equation 2.30 was also established using the same data, as 0.483 and 0.489 (average 0.486) for tests SP3 and SP4 respectively. Both values fall within the range 0.40 to 0.50 as suggested by many previous authors (Schmertmann, 1975; Meyerhof, 1976; Simpson et al., 1981). It was noted, however, that according to these experiments, and only for the Speswhite Kaolin clay used in this study, a much better fitting could be achieved by using Equation 7.1 with $A1 = 0.41$ and $A2 = 0.66$ as illustrated in Figure 7.20.

$$K_0^{oc} = A1 \cdot \ln(OCR) + A2 \qquad \text{[Eq.7.1]}$$

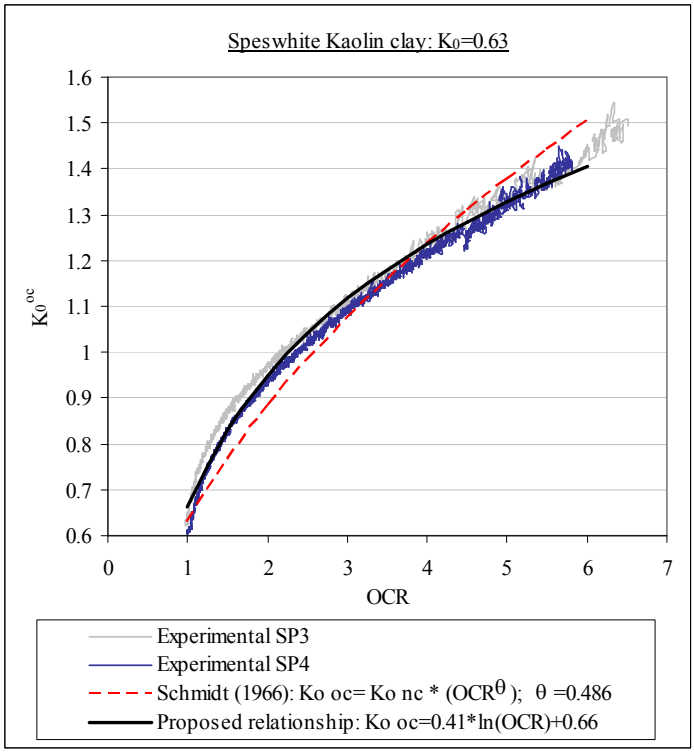

Figure 7.20. Fitting of experimental K_0-OCR data during tests SP3 and SP4

(13) It can be extrapolated from Figures 7.2, D.1, D.42 and D.55 that in general during excavation and before placing the lining:

For K_0<1: The elements at the springline are closer to failing in compression than the elements at the crown are from failing under extension.

For K_0>1: The elements at the crown are potentially closer to failing in extension than the elements at the springline are from failing under compression.

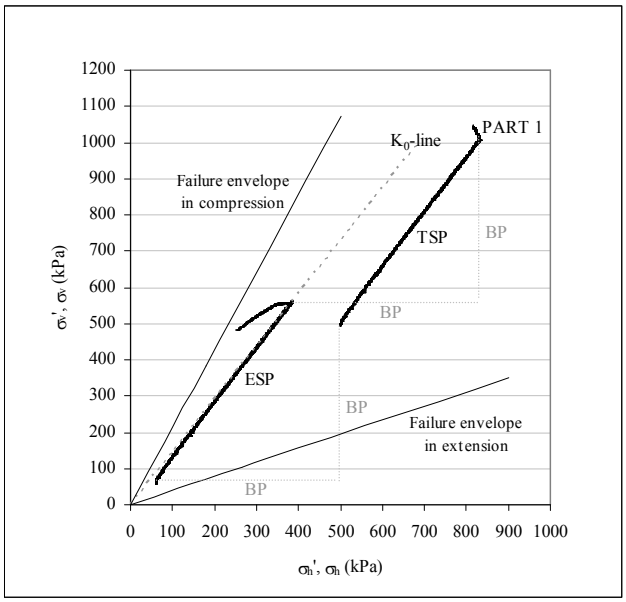

Figure D.1. Total and effective experimental stress paths during test SP2.

BP: Back-pressure, TSP: Total stress path, ESP: Effective stress path

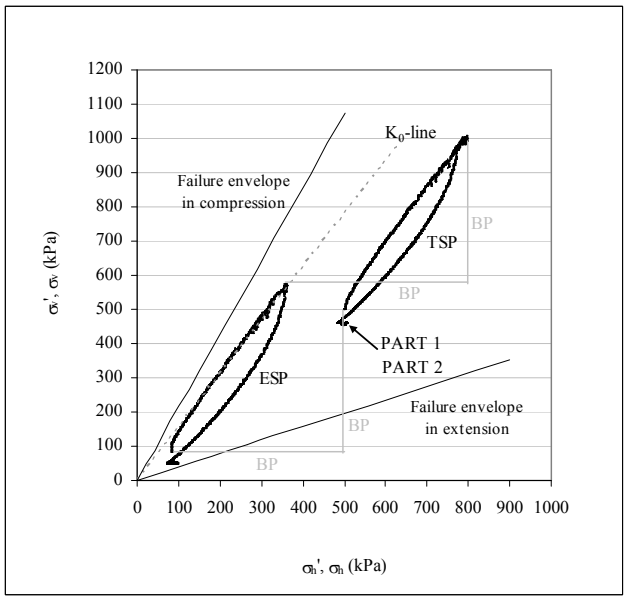

Figure D.42. Total and effective experimental stress paths during test SP3.

BP: Back-pressure, TSP: Total stress path, ESP: Effective stress path

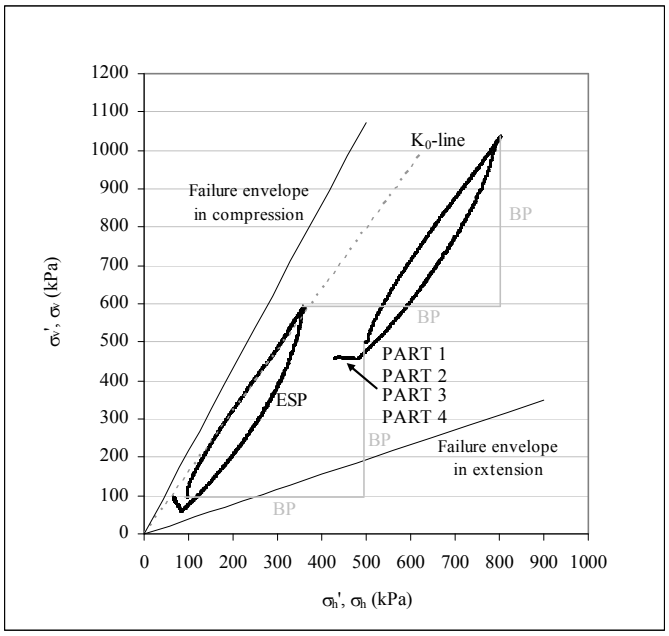

Figure D.55. Total and effective experimental stress paths during test SP4.
BP: Back-pressure, TSP: Total stress path, ESP: Effective stress path

7.6.2. Variation in Soil Stiffness and Evaluation of the Jardine et al. (1991) Parameters

(1) All the stress-strain curves were found to be suitably fitted using Chin´s method, an equation of the type $\sigma = f_3 \cdot \varepsilon^{\left(\frac{1}{f_4}\right)}$ or a combination of both. Additional tests would be necessary in order to establish whether this is generally applicable or mainly a function of the type of tests performed during the present investigation in combination with other factors such as, for example, the rates of strain and the particular triaxial equipment used.

(2) Finding the Jardine et al. (1991) parameters that would fit both the $3G_{sec} / p' - \varepsilon$ (or $K / p' - \varepsilon_v$) and the corresponding $q - \varepsilon$ (or $p' - \varepsilon_v$) at the same time was complicated to achieve (e.g. Figures D.77 and D.93), particularly for the volumetric case.

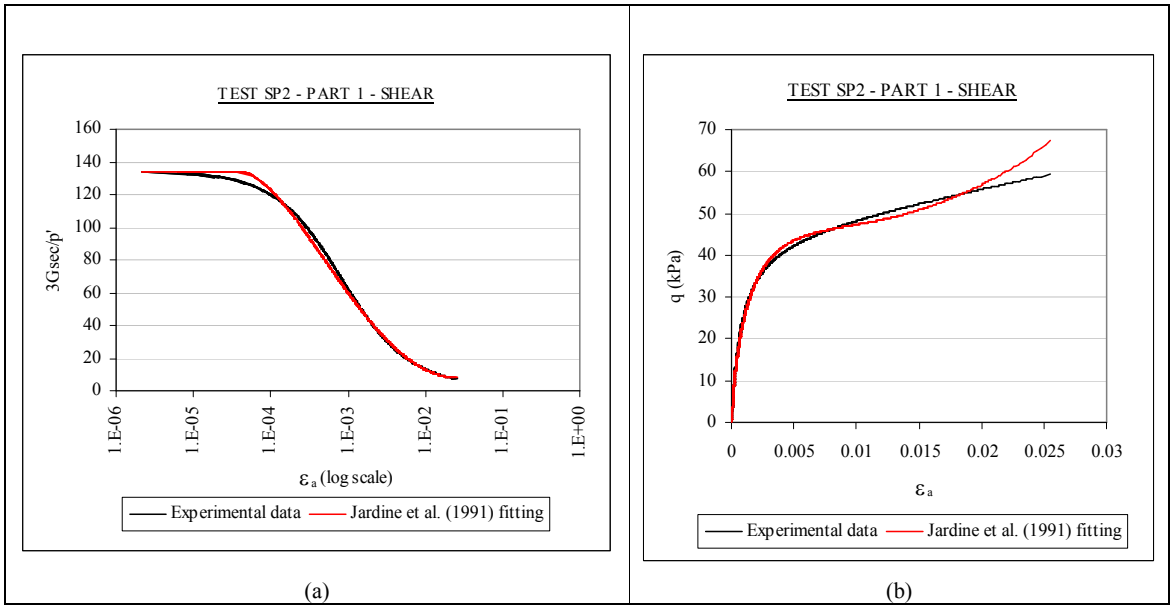

Figure D.77. Test SP2. Jardine et al. (1991) fitting to experimental data during PART 1: (a) fitting $3Gsec / p'$, (b) fitting q

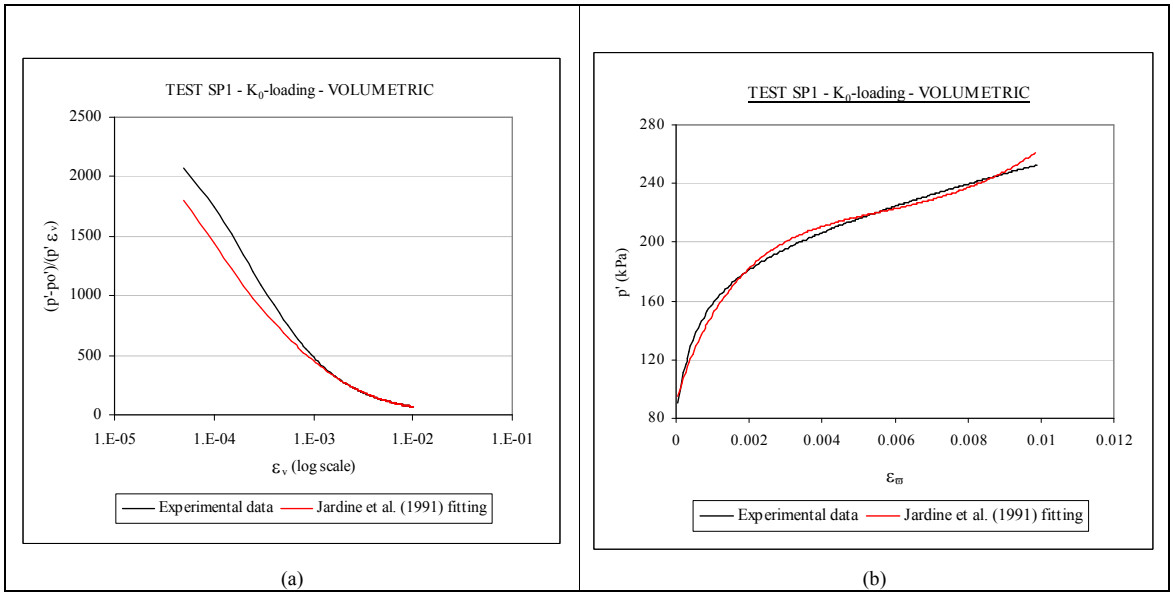

Figure D.93. Test SP1. Jardine et al. (1991) fitting to volumetric experimental data during K_0-loading: (a) fitting K / p', (b) fitting p'

(3) As stated in Section 3.7.1, regarding the Jardine models, most of the stress paths reproduced in the laboratory for the present investigation did not reach failure, hence the stress-strain curve was not complete (e.g. Figure D.85). Despite this, and as demonstrated in this chapter, parameters C1, C2, C3 and C4 could still be found that nicely fit the observed soil behaviour. Due to the relatively short length of the stress paths however, the parameters C1 and C3 can

be very small and certainly very different from C2 and C4 respectively. This has proved to be a large obstacle for the numerical application of the model since this, although generally referring to the elastic behaviour of the soil, requires the definition of the complete stress-strain relationship to failure. This was corroborated, for example, using some of the parameters obtained in this chapter for various PLAXIS 2D analyses not related to this project using the DLL developed by Rouainia at the University of Newcastle. For the shear response, for example, the following message would appear at the beginning of the calculation stage: "The variable (G) has an undefined value".

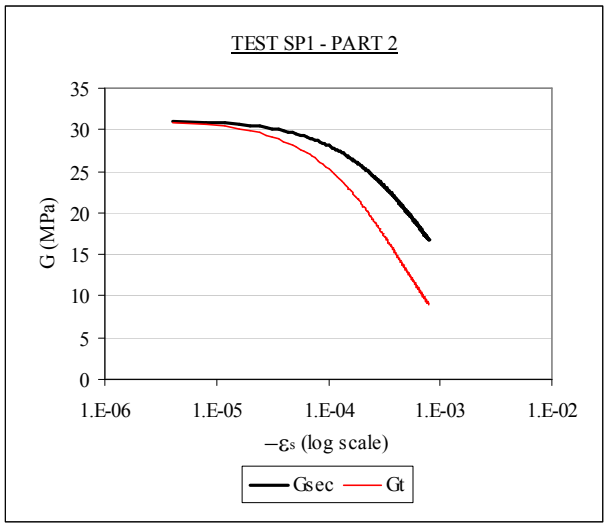

Figure D.85. Test SP1. G_{sec} (and G_t) - ε_s relationship using only data during PART 2

(4) It seems to be widely corroborated, based on recent laboratory testing, that the elastic stiffness of soils is highly non-linear. This theory would imply that those models that use a constant stiffness value for the soil would not be appropriate even at small-strain levels. However, based on the results presented in this chapter, which show that different parameters would be necessary in order to represent the soil behaviour along different stress paths (in agreement with Jardine et al., 1991), it seems that using either the Jardine et al. (1986) model or the Jardine et al. (1991) model for a general analysis, together with a classical elasto-plastic yielding envelope for large strains, may not be necessarily better. Based on the present results, and also taking into account the preliminary observations made in Section 3.7.1, the present author believes that these two small-strain models are at a very initial stage of development and that in order for these to be more realistically correlated to the real soil behaviour under variable conditions, these should be formulated within a more general framework (e.g. critical state) that takes into account the likely different states of the soil. It has been noted in the

literature that there have been some attempts to do so (e.g. Puzrin and Burland, 2000). At the current stage of development however, this new model is very complicated, includes various surfaces, a considerable number of parameters and appears to be very difficult to integrate numerically, at least for users other than the authors. Jardine et al. (1991) used the best knowledge they had to that date and it is certainly a good starting point for including the non-linear response of soils at small strains in constitutive modeling, but the model should be reviewed on the light of more recent findings. In the Jardine et al. (1991) paper the authors reported that "it is possible to simulate many of the characteristics seen in well instrumented stress path tests using relatively simple models, which can be applied to analyse complex civil engineering problems". The present author agrees with the former. Some parameters can be always found that make the relationships presented in the Jardine et al. (1991) paper for G and K fit the experimental data. However, extrapolating that to the analysis of engineering problems may be a too large step. Lake et al. (1996) thought that this non-linear response may assist in understanding the observed soil response around tunnels and may help in obtaining better results from finite element modelling. The present results show that further work is necessary before this can be achieved.

(5) From the previous statement, a question arises that refers to the current, and at least apparent, success of the Jardine models in closely reproducing available in-situ data: How can these models give good results, even better than others (e.g. as reported by Jardine et al. (1991) based on experience to date), having all the issues previously identified and being essentially so simple? The answer to this question is not straightforward. The present author has identified three possible reasons for this, the arguments being largely based on the present observations. The first reason would be the fact that when used, for example, in a numerical analysis, many other factors play a part and conventional engineering practice tends to modify some parameters, always within a reasonable range and using judgment, until a reasonable fit between prediction and observed values is achieved (Potts, 2003). The second is the fact that for engineering problems where the strains fall within the small to the very-small range, even if the proposed stress-strain curve is not very realistic, at such strain levels it may be still more accurate than those given by other constitutive models that do not look in detail into what is happening at that level of strain. The third reason is perhaps the way in which we perceive the success of the different models available. Perhaps one should think that it is not that these simple models give better predictions than some other more sophisticated models, but the fact that quite often these sophisticated models do not give better solutions than those achieved using fairly simple classical models (e.g. Mohr-Coulomb).

(6) Despite the different sets of Jardine et al. (1991) parameters determined from the present experiments, for practical reasons and adopting the way in which this model is normally used (based on available literature), a unique set was selected for use into the soil model tester SM2D (Chapter 9) as follows:

- Shear behaviour: Those corresponding to PART 1 Test SP2 (Table 7.5). These results were chosen because the stress path reached failure hence the stress-strain curve was complete for the purpose of establishing the small-strain parameters.
- Volumetric behaviour: Those corresponding to K_0-loading Test SP1 (Table 7.7).

  The K_0-process was the same for all the specimens therefore the parameters obtained from any of the tests should be applicable for the others with some allowance for the experimental differences observed (e.g. Figure 7.3 and D.2). The reason for using the K_0-loading in Test SP1 is the fact that the Jardine et al. (1991) parameters were only established for this stage. Additionally, K_0-loading was considered more relevant than K_0-unloading since only 2 out of the 7 tests involved swelling of the specimen.

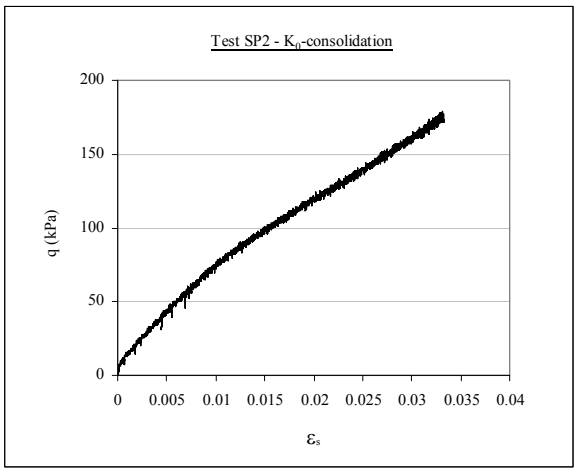

Figure D.2. Test SP2. q - ε_s relationship during the K_0-consolidation stage

7.7. SUMMARY

This chapter has presented the results from tunnel specific stress path testing on reconstituted Speswhite Kaolin specimens. The stress paths followed intended to reproduce the geological history of a soil plus the stress paths induced by tunnelling. The latter were based on the results obtained in Chapter 4 for various K_0 values and for a choice of locations around the tunnel(s), and were run under undrained conditions to simulate the quick behaviour of a stiff clay. Also in this chapter, the small-strain Jardine et al. (1991) parameters to be used in Chapter 9 have been established from the various experimental results. The findings and issues encountered during either stress path testing or whilst identifying the small-strain parameters have been also presented and discussed. The results from this chapter will be compared against the various constitutive soil models' predictions in Chapter 9.

Chapter 8: EVALUATION OF SOIL CONSTITUTIVE MODEL PERFORMANCE FOR CONVENTIONAL TRIAXIAL TESTING

8.1. INTRODUCTION

This chapter evaluates the capacity of the Modified Cam-Clay, Al-Tabbaa and S-CLAY1 models in simulating the response of Speswhite Kaolin clay during conventional triaxial testing presented in Chapter 5 according to the methodology in Section 3.7.3. A discussion of the results is given at the end of this chapter. The comparison between the different models has been more visual, looking at the overall general trends, than actually quantifying the error (e.g. using an expression similar to Equation 3.10) between experimental and predicted values.

8.2. RESULTS USING PARAMETERS DEDUCED FROM EXPERIMENTAL WORK

8.2.1. Normally Isotropic Consolidated Kaolin Sheared in Compression

The evaluation in this case was performed using the experimental observations during test USc7. The soil parameters and the initial soil conditions used for the different constitutive models listed in Table 3.15 are summarised in Table 8.1. Figures 8.1 to 8.4 illustrate the q - p', q - ε_a, u - ε_a and E_{sec} - ε_a predictions in comparison to the laboratory data. The most suitable model in this case was the Modified Cam-Clay model.

Table 8.1. Soil parameters and initial state data for test USc7

p_o' ([A])	u_o	e_o	p_c'	E_{50}	c_c' ([B])	ϕ_c'	ν
1021	379	1.016	1021	25000	0.1	21	0.34
M	λ_{ic}	κ_{ic}	λ_{ic}^*	κ_{ic}^*	*RVALU*	*XIVAL*	
0.809	0.18	0.03	0.086	0.017	0.2	1.5	

([A]) This is the initial mean effective stress just before shearing;

([B]) The implementation of the Mohr-Coulomb model in SM2D does not accept $c'_c = 0$, so a very small value was used.

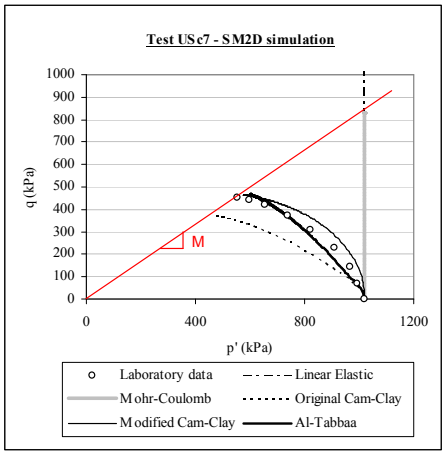

Figure 8.1. Measured versus predicted q - p' relationship during test USc7

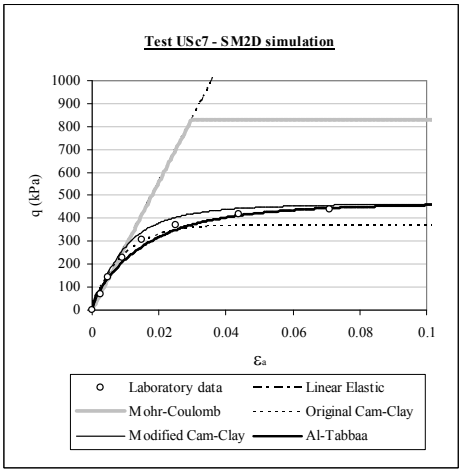

Figure 8.2. Measured versus predicted q - ε_a relationship during test USc7

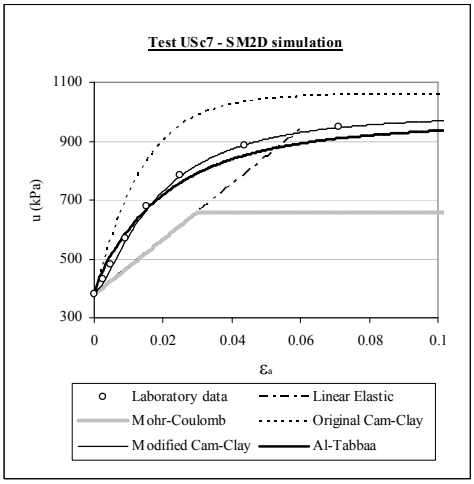

Figure 8.3. Measured versus predicted u - ε_a relationship during test USc7

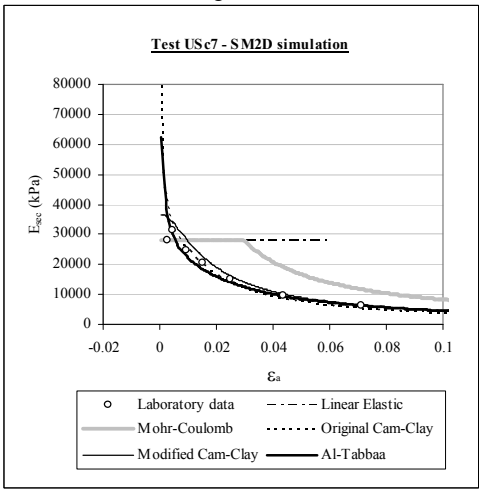

Figure 8.4. Measured versus predicted E_{sec} - ε_a relationship during test USc7

8.2.2. Lightly Isotropic Overconsolidated Kaolin Sheared in Compression

The evaluation in this case was performed using the laboratory data from test USc9. The soil parameters and the initial soil conditions used for the different constitutive models listed in Table 3.15 are summarised in Table 8.2. Figures 8.5 to 8.8 illustrate the q - p', q - ε_a, u - ε_a and E_{sec} - ε_a predictions compared to the laboratory data. The most suitable model in this case was the Al-Tabbaa model.

Table 8.2. Soil parameters and initial state data for test USc9

p_o' (A)	u_o	e_o	p_c'	ν	M
797	324	1.030	980	0.34	0.814
λ_{ic}	κ_{ic}	λ_{ic}^*	κ_{ic}^*	*RVALU*	*XIVAL*
0.18	0.03	0.086	0.017	0.2	1.5

(A) This is the initial mean effective stress just before shearing

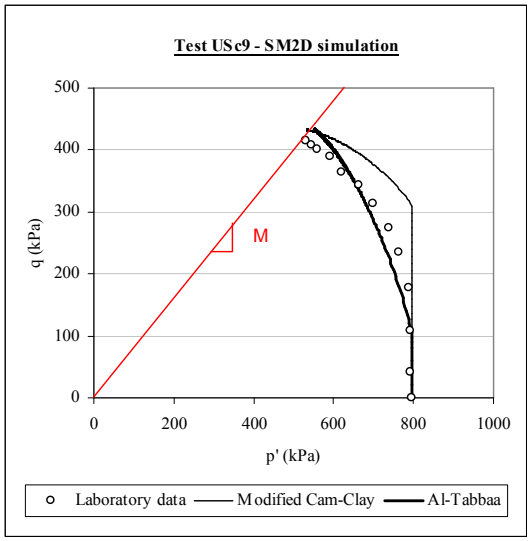

Figure 8.5. Measured versus predicted q - p' relationship during test USc9

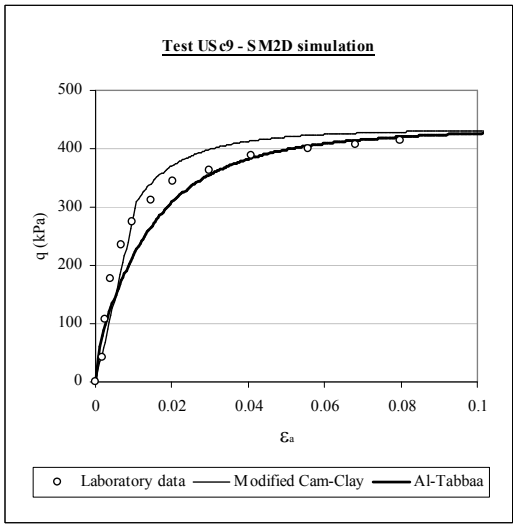

Figure 8.6. Measured versus predicted q - ε_a relationship during test USc9

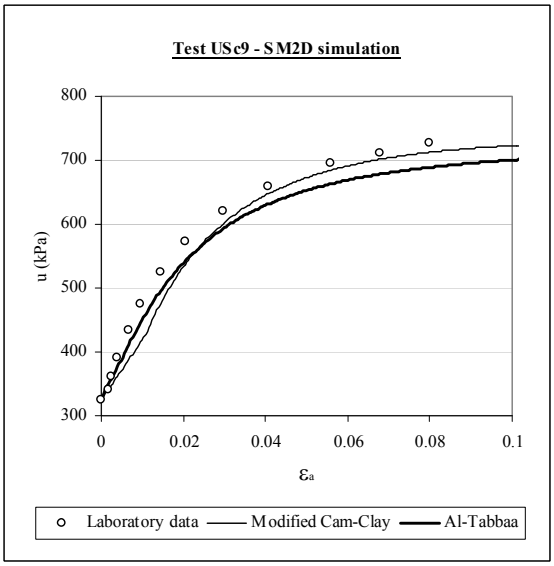

Figure 8.7. Measured versus predicted u - ε_a relationship during test USc9

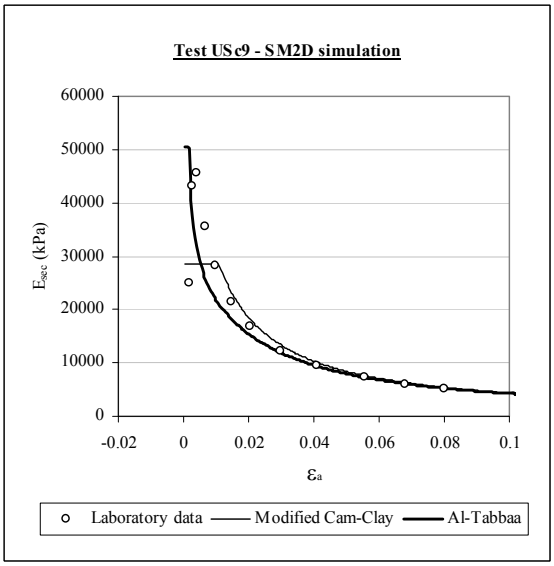

Figure 8.8. Measured versus predicted E_{sec} -ε_a relationship during test USc9

8.2.3. Normally Isotropic Consolidated Kaolin Sheared in Extension

The evaluation in this case was performed based on the experimental data from test USe3. The soil parameters and the initial soil conditions used for the different constitutive models listed in Table 3.15 are summarised in Table 8.3. Figures 8.9 to 8.12 illustrate the q - p', q - ε_a, u - ε_a and E_{sec} - ε_a predictions compared to the laboratory data. The most suitable model in this case was the Al-Tabbaa model.

Table 8.3. Soil parameters and initial state data for test USe3

p_o' ([A])	u_o	e_o	p_c'	ν	M
235	464	1.283	235	0.34	0.642
λ_{ic}	κ_{ic}	λ_{ic}*	κ_{ic}*	*RVALU*	*XIVAL*
0.18	0.03	0.086	0.017	0.2	1.5

([A]) This is the initial mean effective stress just before shearing

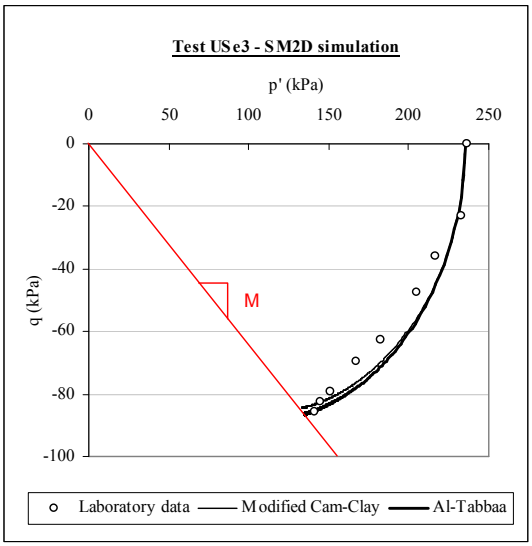

Figure 8.9. Measured versus predicted q - p' relationship during test USe3

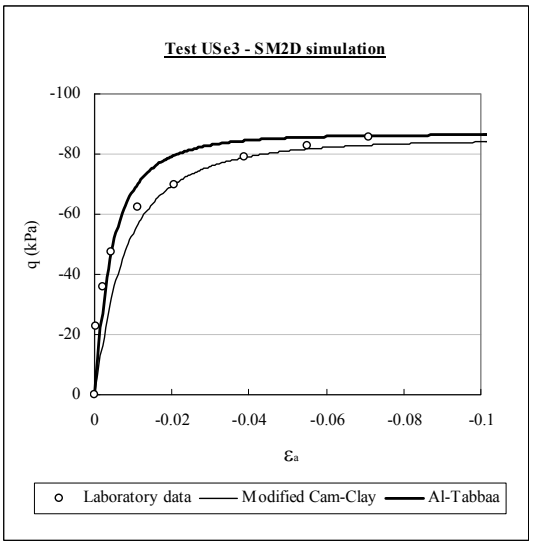

Figure 8.10. Measured versus predicted q - ε_a relationship during test USe3

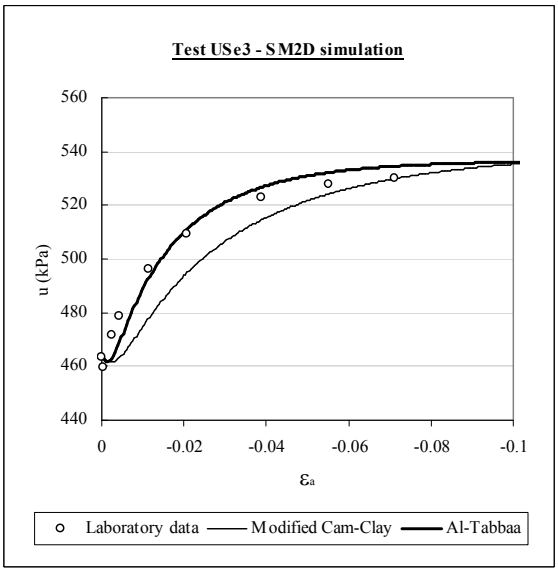

Figure 8.11. Measured versus predicted u - ε_a relationship during test USe3

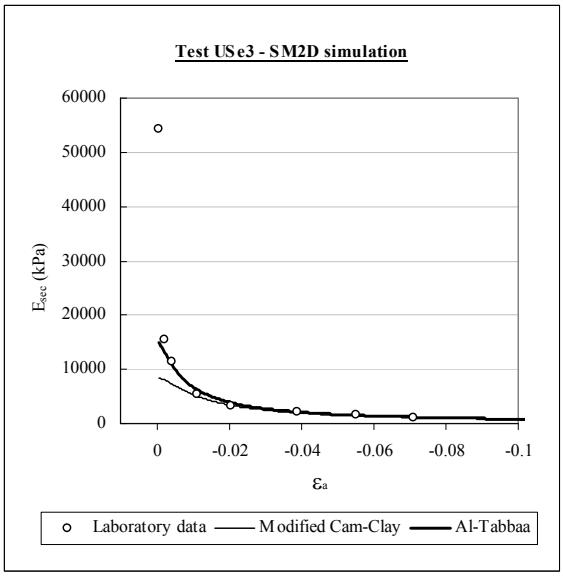

Figure 8.12. Measured versus predicted E_{sec} - ε_a relationship during test USe3

8.2.4. Lightly Isotropic Overconsolidated Kaolin Sheared in Extension

The evaluation in this case was performed using the experimental observations during test USe5. The soil parameters and the initial soil conditions used for the different constitutive models listed in Table 3.15 are summarised in Table 8.4. Figures 8.13 to 8.16 illustrate the q - p', q - ε_a, u - ε_a and E_{sec} - ε_a predictions compared to the laboratory data. The most suitable model in this case was the Al-Tabbaa model.

Table 8.4. Soil parameters and initial state data for test USe5

p_o' (^{A})	u_o	e_o	p_c'	ν	M
498	301	1.120	595	0.34	0.868
λ_{ic}	κ_{ic}	λ_{ic}^*	κ_{ic}^*	*RVALU*	*XIVAL*
0.18	0.03	0.086	0.017	0.2	1.5

(^{A}) This is the initial mean effective stress just before shearing

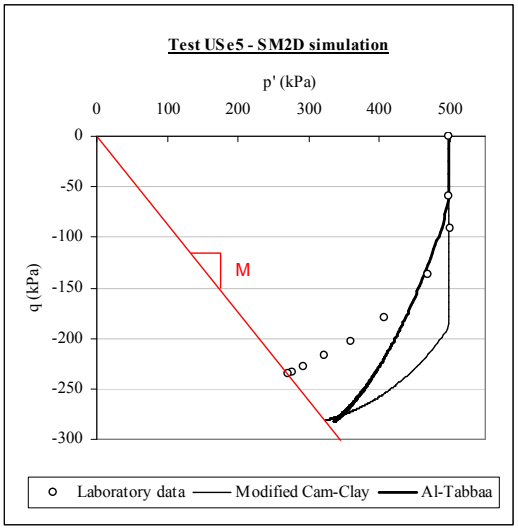

Figure 8.13. Measured versus predicted q - p' relationship during test USe5

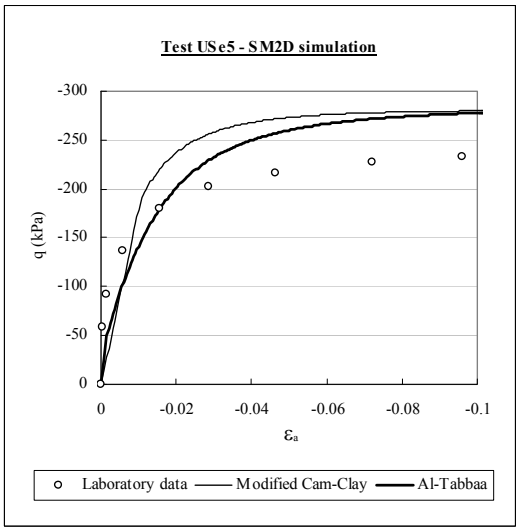

Figure 8.14. Measured versus predicted q - ε_a relationship during test USe5

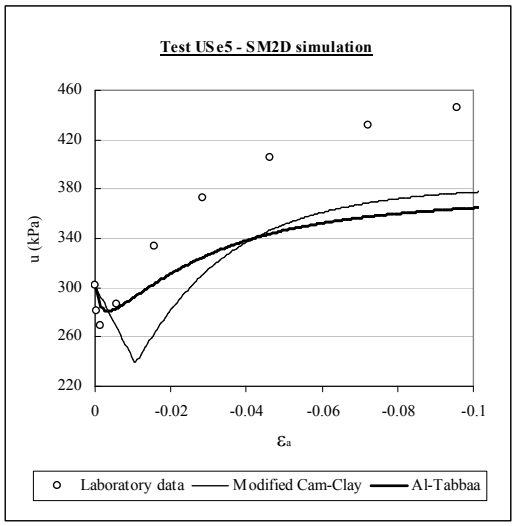

Figure 8.15. Measured versus predicted u - ε_a relationship during test USe5

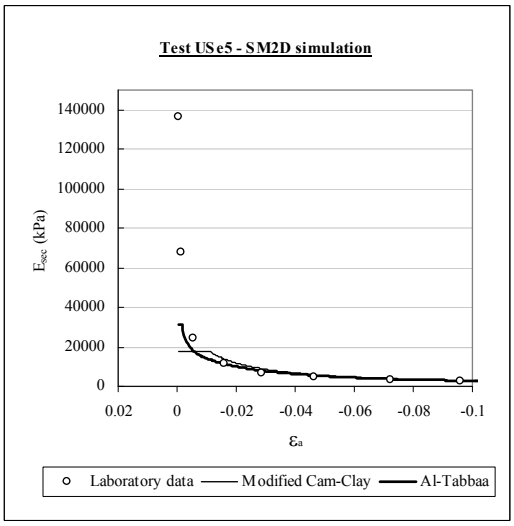

Figure 8.16. Measured versus predicted E_{sec} -ε_a relationship during test USe5

8.2.5. Heavily Isotropic Overconsolidated Kaolin Sheared in Extension

The evaluation in this case was performed based on the experimental data recorded during test USe6. The soil parameters and the initial soil conditions used for the different constitutive models listed in Table 3.15 are summarised in Table 8.5. Figures 8.17 to 8.20 illustrate the q - p', q - ε_a, u - ε_a and E_{sec} - ε_a predictions compared to the laboratory data. The most suitable model in this case was the Al-Tabbaa model.

Table 8.5. Soil parameters and initial state data for test USe6

p_o' ([A])	u_o	e_o	p_c'	ν	M
218	382	1.145	1118	0.34	0.704
λ_{ic}	κ_{ic}	λ_{ic}^*	κ_{ic}^*	*RVALU*	*XIVAL*
0.18	0.03	0.086	0.017	0.2	1.5

([A]) This is the initial mean effective stress just before shearing

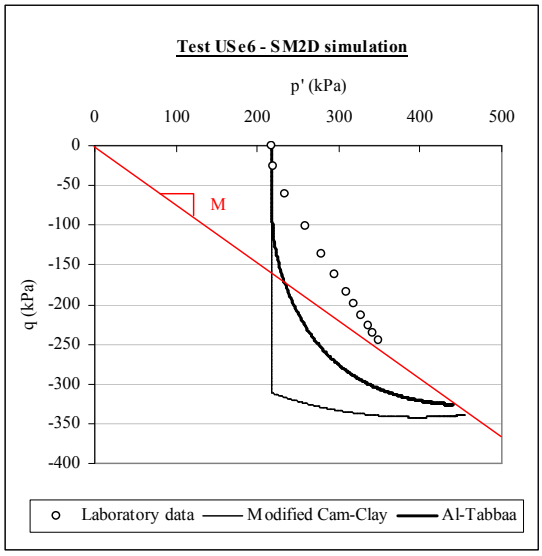

Figure 8.17. Measured versus predicted q - p' relationship during test USe6

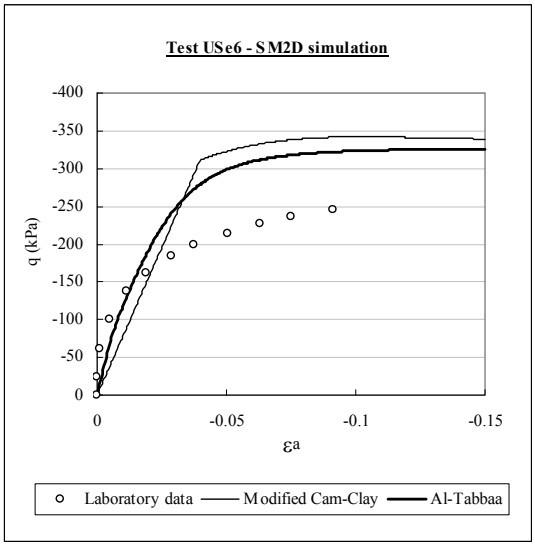

Figure 8.18. Measured versus predicted q - ε_a relationship during test USe6

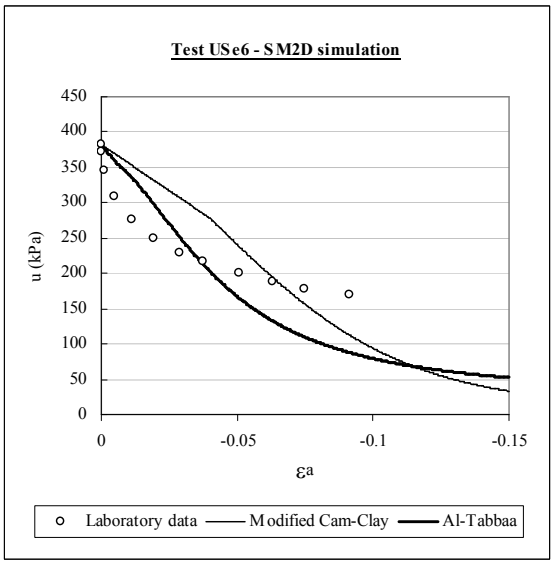

Figure 8.19. Measured versus predicted u - ε_a relationship during test USe6

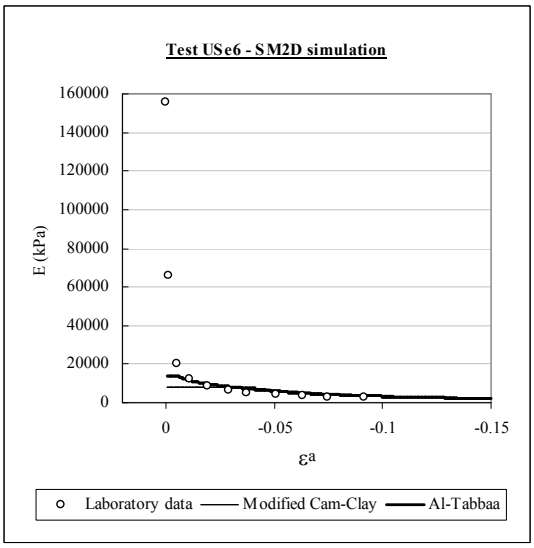

Figure 8.20. Measured versus predicted E_{sec} -ε_a relationship during test USe6

8.2.6. Normally K_0-consolidated Kaolin Sheared in Compression

The evaluation in this case was performed using the experimental observations during test Ko5. The soil parameters and the initial soil conditions used for the different constitutive models listed in Table 3.15 are summarised in Table 8.6. It should be noted that in this case the values of κ_0 and κ_0* correspond to those obtained from isotropically consolidated specimens as there was not yet data

available during swelling under K_0 conditions. Figures 8.21 to 8.24 illustrate the q - p', q - ε_a, u - ε_a and E_{sec} - ε_a predictions compared to the laboratory data when using both stress control and strain control during the K_0-stage from point p_0' in SM2D. Although the radial strain data is not presented in here, such results were also examined and confirmed that the condition of zero radial strain was only maintained for the strain controlled runs, not during the stress controlled case. For test Ko5 none of the three constitutive models proved to be much better than the others.

Table 8.6. Soil parameters and initial state data for test Ko5

p_o' (^{A})	u_o	e_o	p_c'	ν	M	λ_0	κ_0	λ_0^*
83	0	1.187	472 (MCC) 388 (Al-Tabbaa) 440 (S-CLAY1)	0.34	0.823	0.16	0.03	0.073
κ_0^*	*RVALU*	*XIVAL*	p'_{max}	ε_{amax}	α	μ	β	*POP*
0.017	0.2	1.5	380	0.067	0.25	65	0.42	220

(^{A}) This is the mean effective stress measured initially in the stress path cell

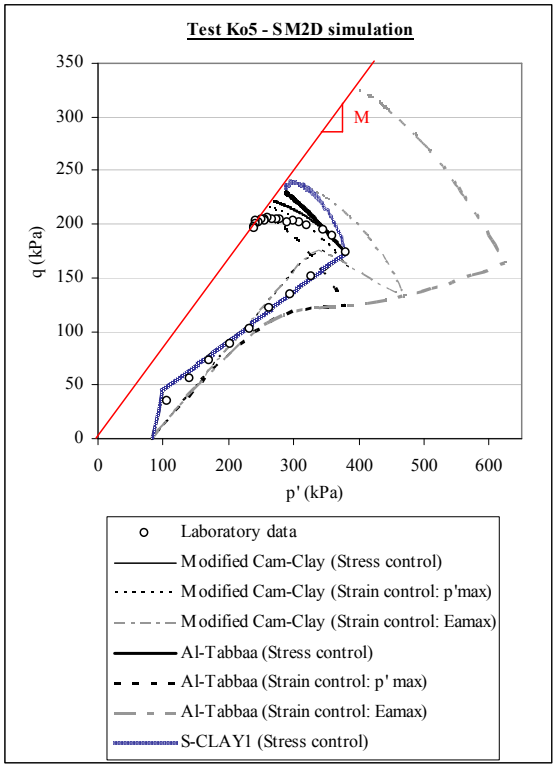

Figure 8.21. Measured versus predicted q - p' relationship during test Ko5

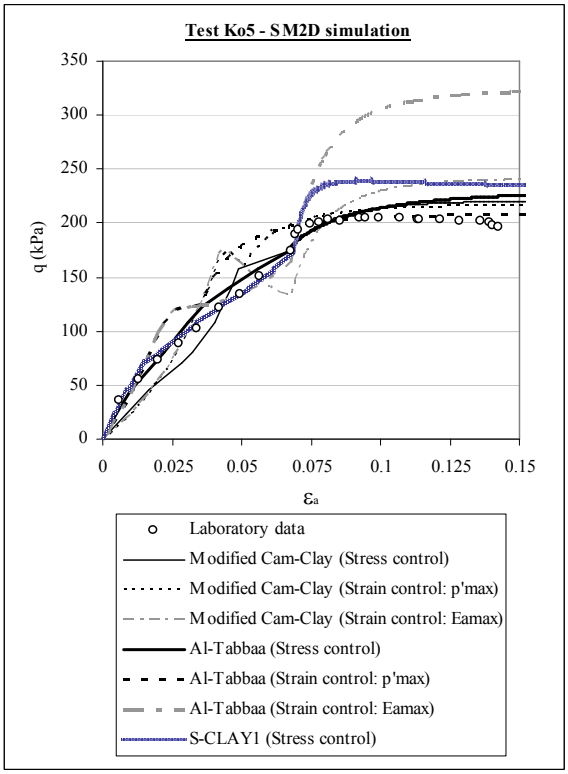

Figure 8.22. Measured versus predicted q - ε_a relationship during test Ko5

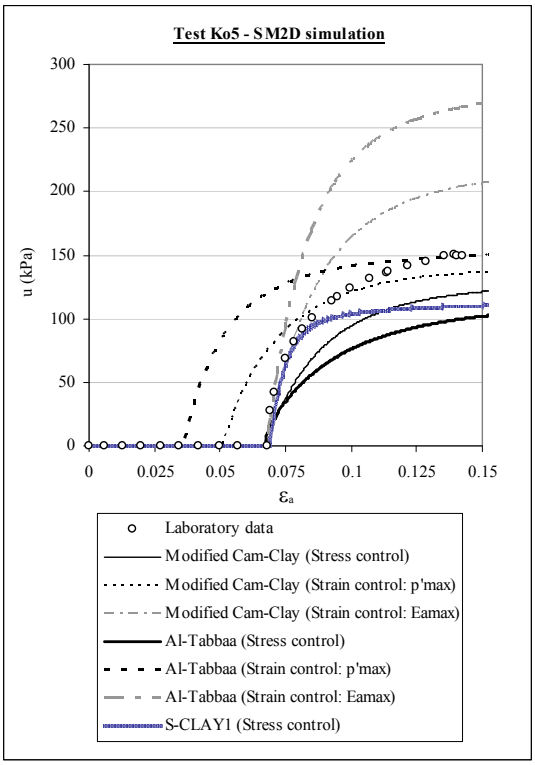

Figure 8.23. Measured versus predicted u - ε_a relationship during test Ko5

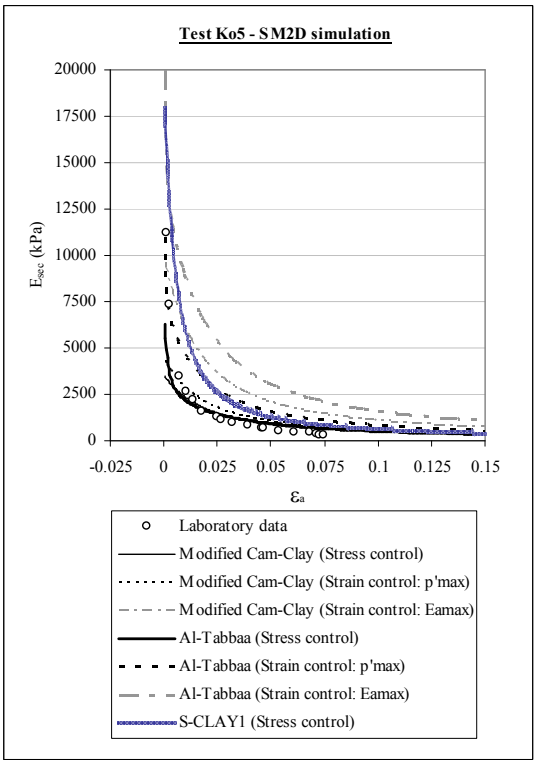

Figure 8.24. Measured versus predicted E_{sec} -ε_a relationship during test Ko5

8.2.7. Normally K_0-consolidated Kaolin Sheared in Extension

The evaluation in this case was performed using the laboratory data from test Ko6. The soil parameters and the initial soil conditions used for the different constitutive models listed in Table 3.15 are summarised in Table 8.7. As for test Ko5, the values of κ_0 and κ_0* correspond to those obtained from isotropically consolidated specimens. Figures 8.25 to 8.28 illustrate the q - p', q - ε_a, u - ε_a and E_{sec} - ε_a predictions compared to the laboratory data. As for Ko5, the condition of zero radial strain was only maintained for the strain controlled runs, not during the stress controlled case. The most suitable model in this case was the S-CLAY1 model.

Table 8.7. Soil parameters and initial state data for test Ko6

p_o' ([A])	u_o	e_o	p_c'	ν	M	λ_0	κ_0	λ_0*
98	0	1.199	386 (MCC) 322 (Al-Tabbaa) 340 (S-CLAY1)	0.34	0.836	0.153	0.03	0.069
κ_0*	RVALU	XIVAL	p'_{max}	ε_{amax}	α	μ	β	POP
0.017	0.2	1.5	320	0.054	0.26	65	0.81	170

([A]) This is the mean effective stress measured initially in the stress path cell

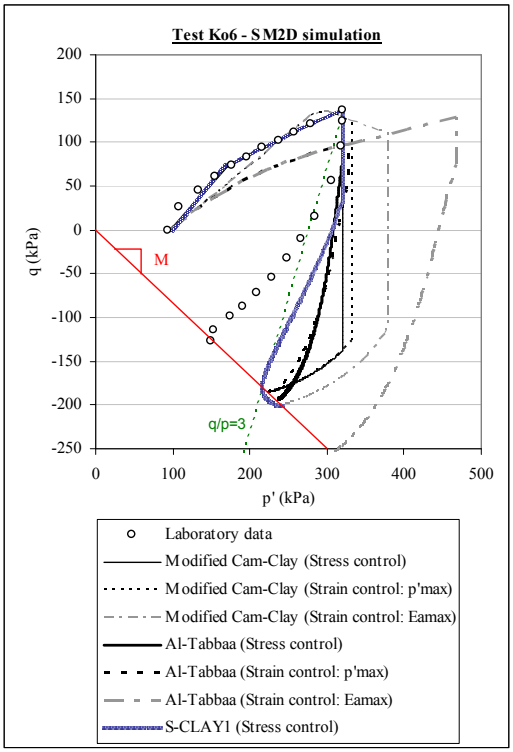

Figure 8.25. Measured versus predicted q - p' relationship during test Ko6

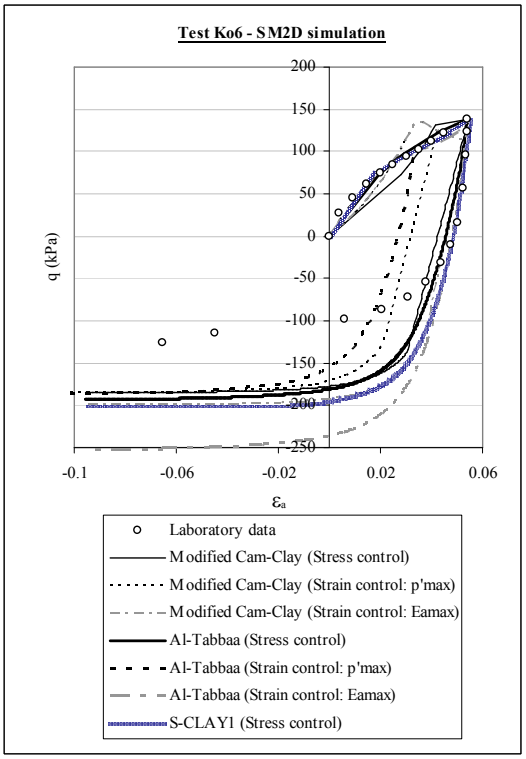

Figure 8.26. Measured versus predicted q - ε_a relationship during test Ko6

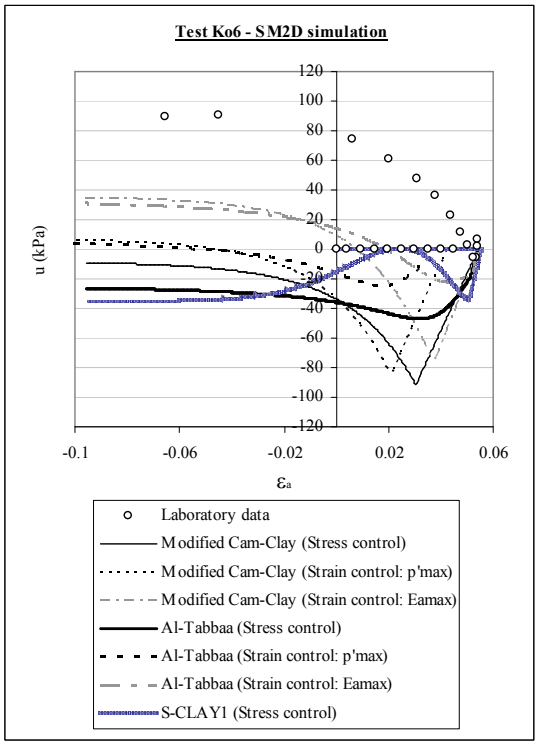

Figure 8.27. Measured versus predicted u - ε_a relationship during test Ko6

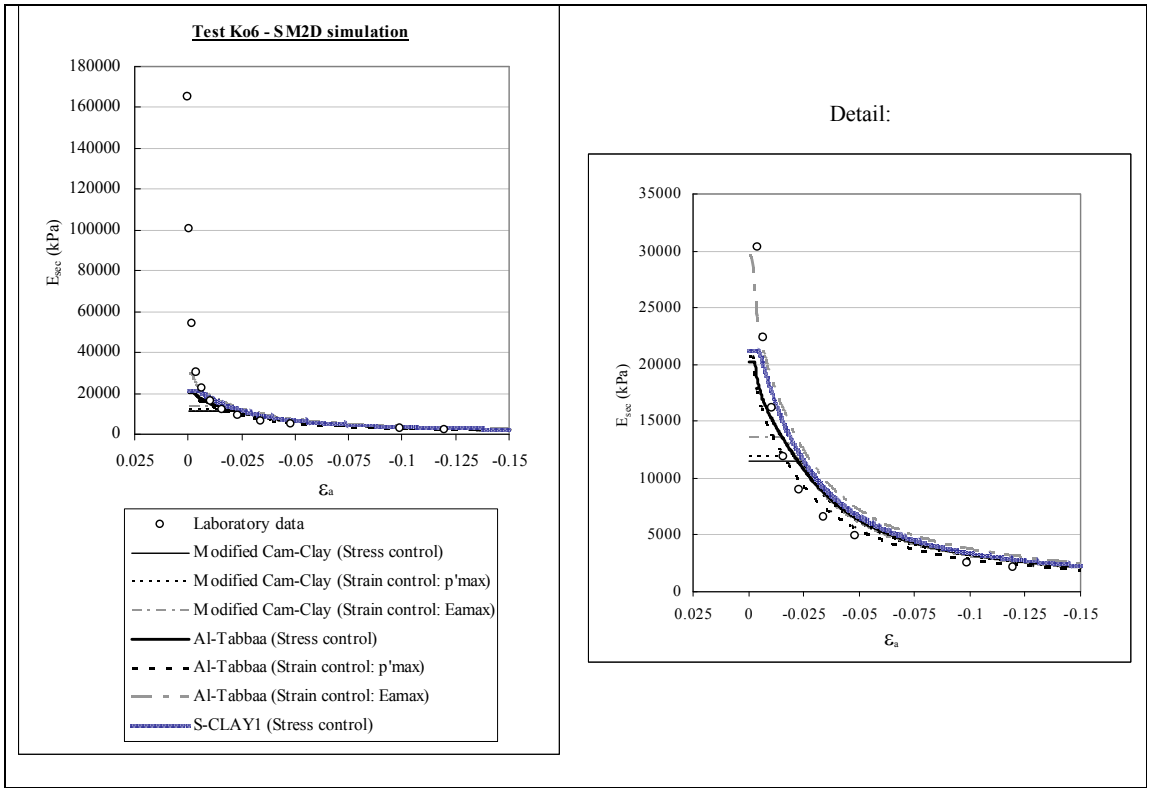

Figure 8.28. Measured versus predicted E_{sec} -ε_a relationship during test Ko6

8.3. PARAMETRIC STUDY: OPTIMAL CHOICE OF PARAMETERS

8.3.1. Sensitivity Analysis I

TEST USe5

For test USe5, the sensitivity of the Al-Tabbaa model to λ_{ic}^*, κ_{ic}^*, υ, *M, RVALU* and *XIVAL* were studied according to the methodology given in Section 3.7.3. The parameters that were found to mainly control the results were κ_{ic}^*, *RVALU* and *XIVAL*. The results corresponding to these parameters are illustrated in Figures 8.29 to 8.40. The graphs showing the effect of the other parameters can be found in Appendix E - Figures E.1 to E.12. Grammatikopoulou (2004) also found the two-surface model to be sensitive to *RVALU* and *XIVAL* because they introduced a non-smooth transition from elastic to elasto-plastic behaviour once yield was initiated. This was not explicitly observed in the present results.

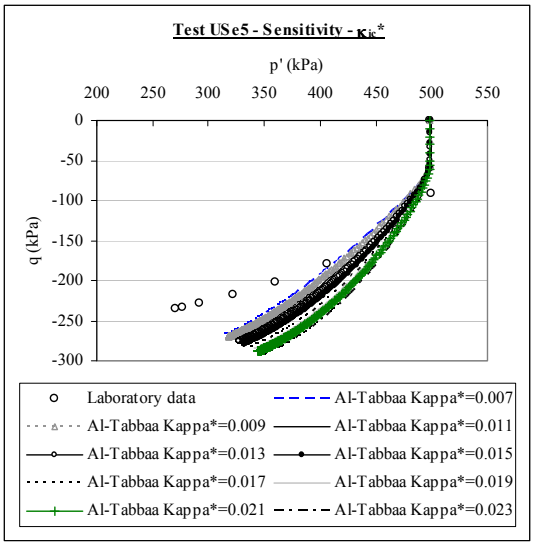

Figure 8.29. Sensitivity of the Al-Tabbaa model to κ_{ic}* in terms of the q - p' behaviour during test USe5

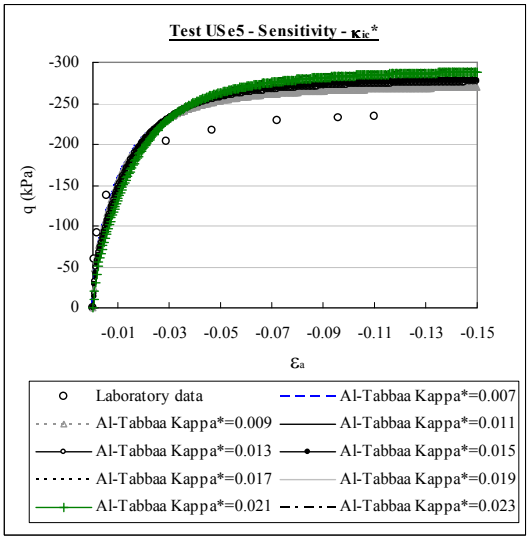

Figure 8.30. Sensitivity of the Al-Tabbaa model to κ_{ic}* in terms of the q - ε_a behaviour during test USe5

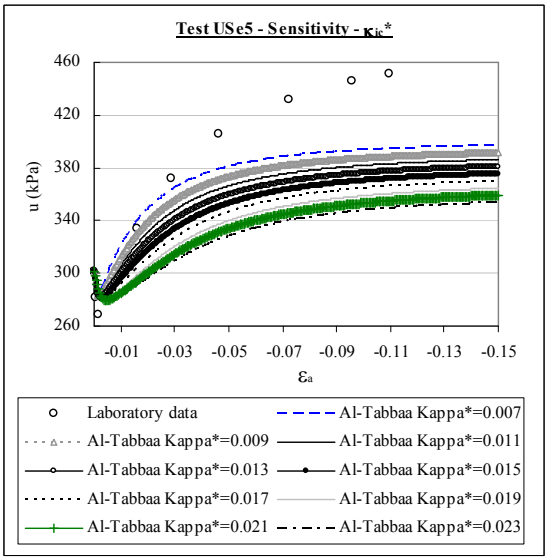

Figure 8.31. Sensitivity of the Al-Tabbaa model to κ_{ic}* in terms of the u - ε_a behaviour during test USe5

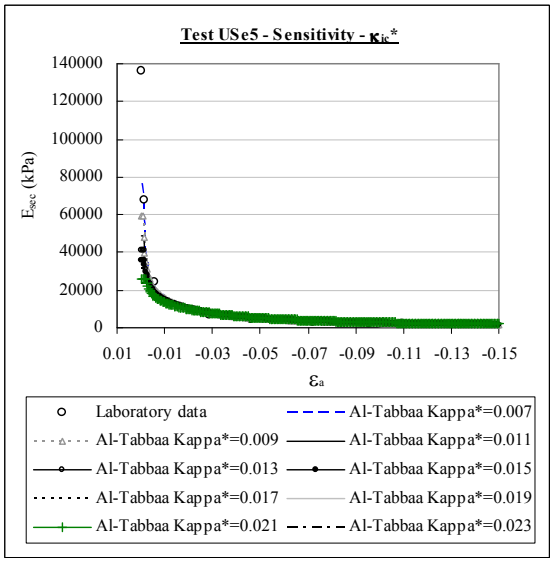

Figure 8.32. Sensitivity of the Al-Tabbaa model to κ_{ic}* in terms of the E_{sec} -ε_a behaviour during test USe5

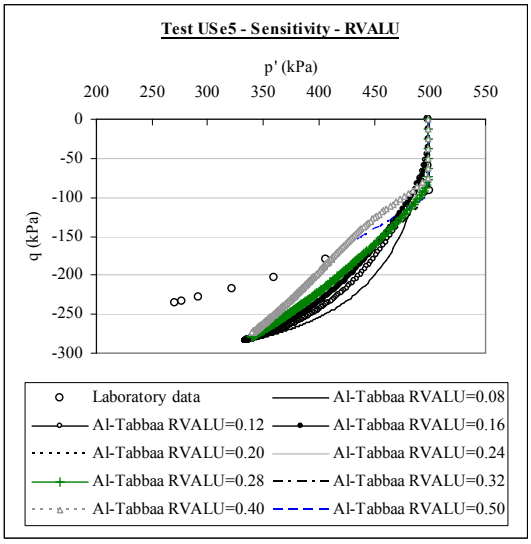

Figure 8.33. Sensitivity of the Al-Tabbaa model to *RVALU* in terms of the q - p' behaviour during test USe5

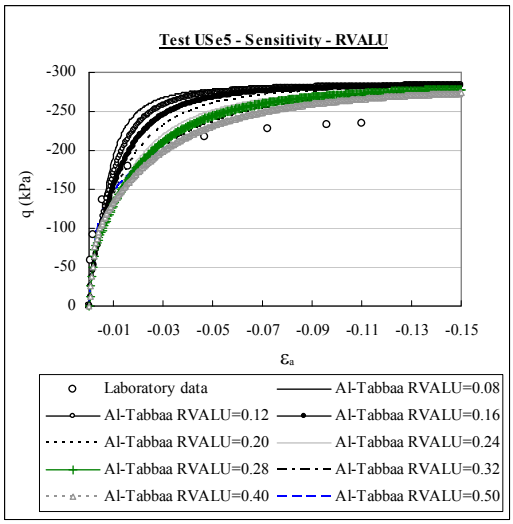

Figure 8.34. Sensitivity of the Al-Tabbaa model to *RVALU* in terms of the q - ε_a behaviour during test USe5

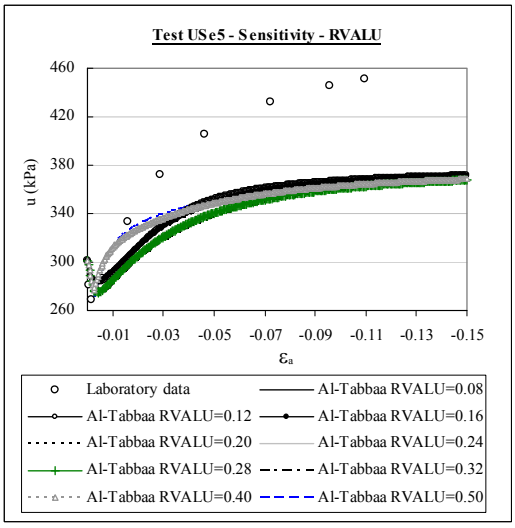

Figure 8.35. Sensitivity of the Al-Tabbaa model to *RVALU* in terms of the u - ε_a behaviour during test USe5

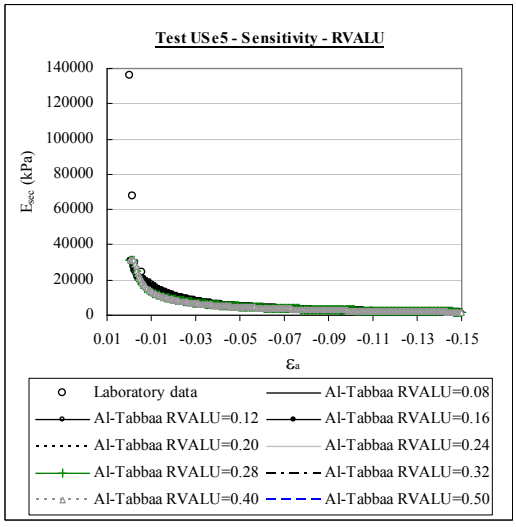

Figure 8.36. Sensitivity of the Al-Tabbaa model to *RVALU* in terms of the E_{sec} -ε_a behaviour during test USe5

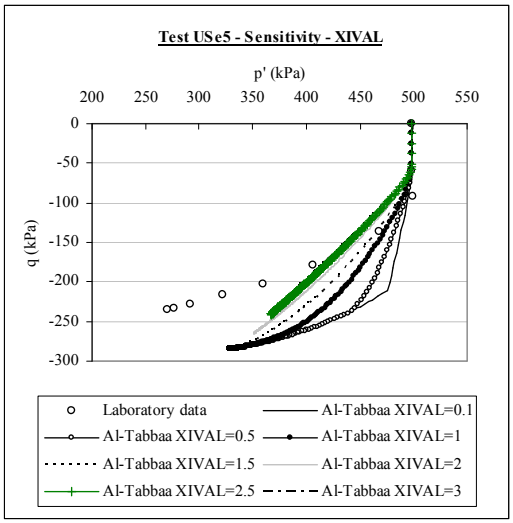

Figure 8.37. Sensitivity of the Al-Tabbaa model to *XIVAL* in terms of the q - p' behaviour during test USe5

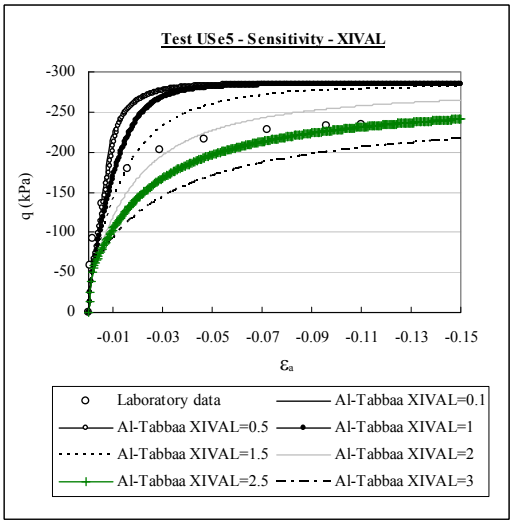

Figure 8.38. Sensitivity of the Al-Tabbaa model to *XIVAL* in terms of the q - ε_a behaviour during test USe5

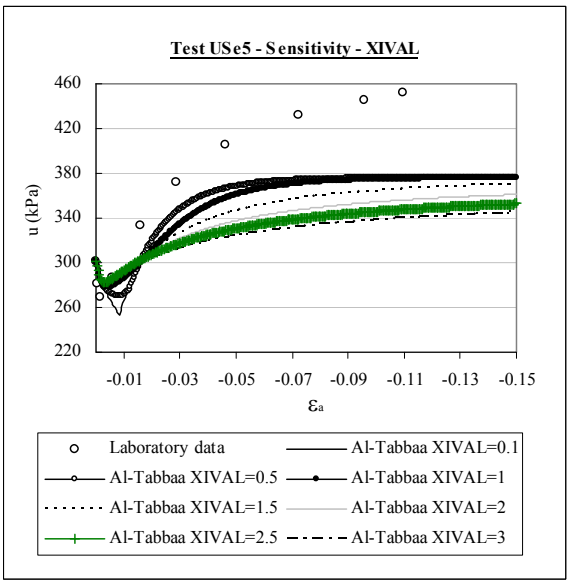

Figure 8.39. Sensitivity of the Al-Tabbaa model to *XIVAL* in terms of the u - ε_a behaviour during test USe5

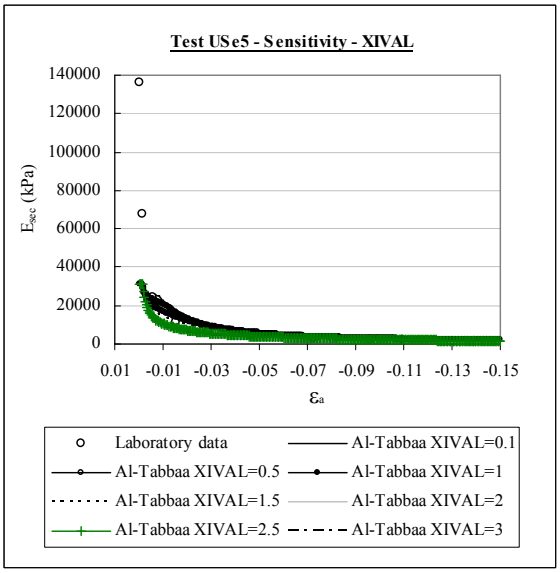

Figure 8.40. Sensitivity of the Al-Tabbaa model to *XIVAL* in terms of the E_{sec} -ε_a behaviour during test USe5

TEST USc7

For test USc7, the sensitivity of the Modified Cam-Clay model to λ_{ic}, κ_{ic}, υ and M and that of the Al-Tabbaa model with regard to κ_{ic}*, *RVALU* and *XIVAL* (these being chosen after the sensitivity analysis carried out on test USe5) were studied according to the methodology given in Section 3.7.3. The parameters that were found to mainly control the results were κ_{ic}, υ, *RVALU* and *XIVAL*. The results corresponding to these parameters are illustrated in Figures 8.41 to 8.60. The graphs showing the effect of the other parameters can be found in Appendix E - Figures E.13 to E.20.

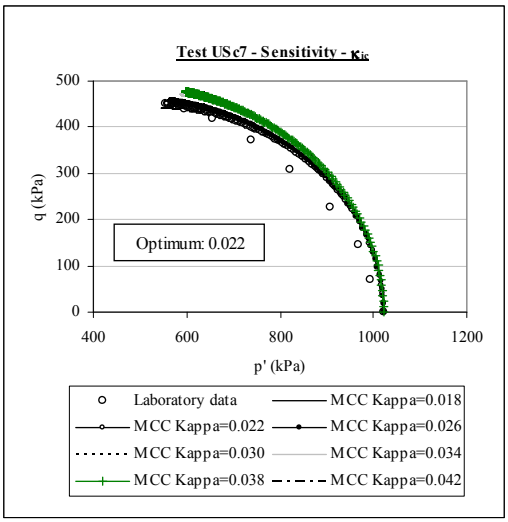

Figure 8.41. Sensitivity of the Modified Cam-Clay model to κ_{ic} in terms of the q - p' behaviour during test USc7

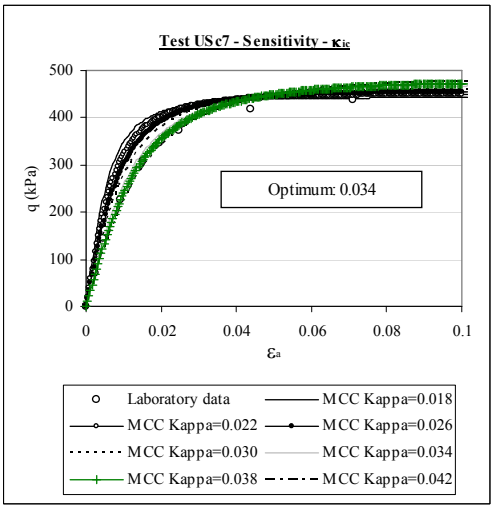

Figure 8.42. Sensitivity of the Modified Cam-Clay model to κ_{ic} in terms of the q - ε_a behaviour during test USc7

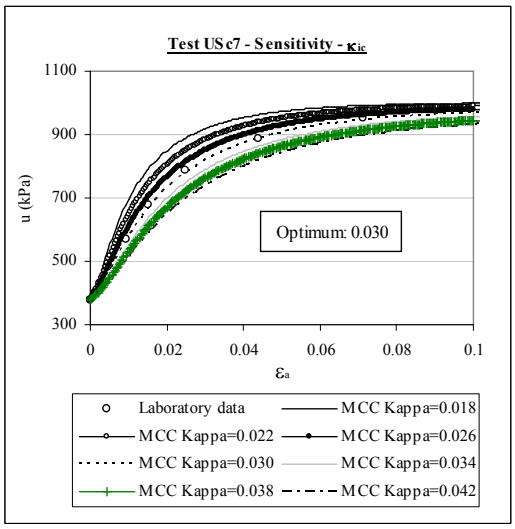

Figure 8.43. Sensitivity of the Modified Cam-Clay model to κ_{ic} in terms of the u - ε_a behaviour during test USc7

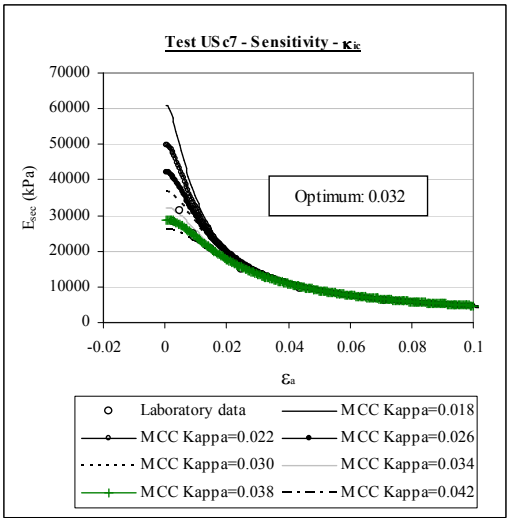

Figure 8.44. Sensitivity of the Modified Cam-Clay model to κ_{ic} in terms of the E_{sec} -ε_a behaviour during test USc7

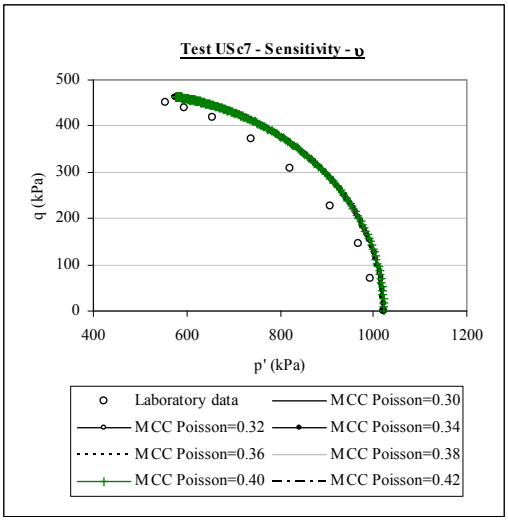

Figure 8.45. Sensitivity of the Modified Cam-Clay model to υ in terms of the q - p' behaviour during test USc7

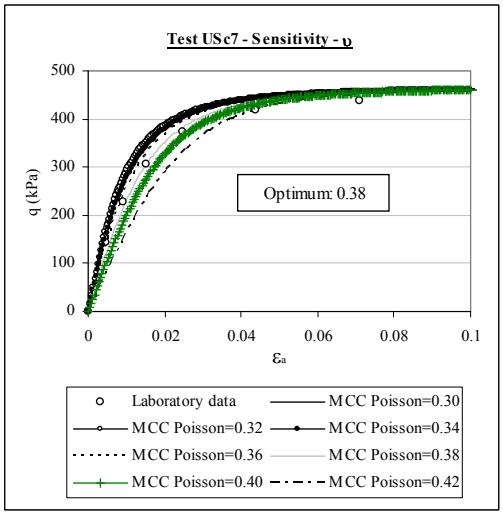

Figure 8.46. Sensitivity of the Modified Cam-Clay model to υ in terms of the q - ε_a behaviour during test USc7

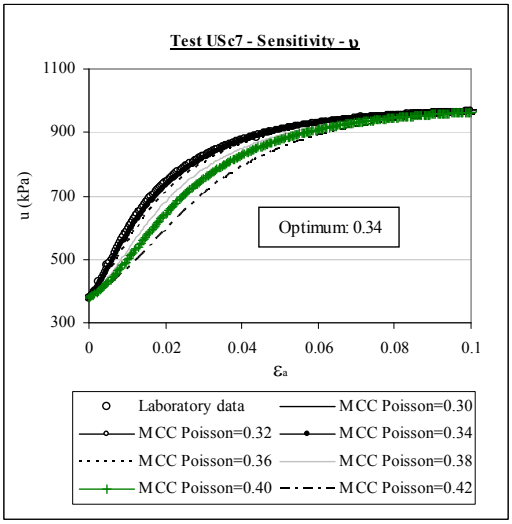

Figure 8.47. Sensitivity of the Modified Cam-Clay model to υ in terms of the u - ε_a behaviour during test USc7

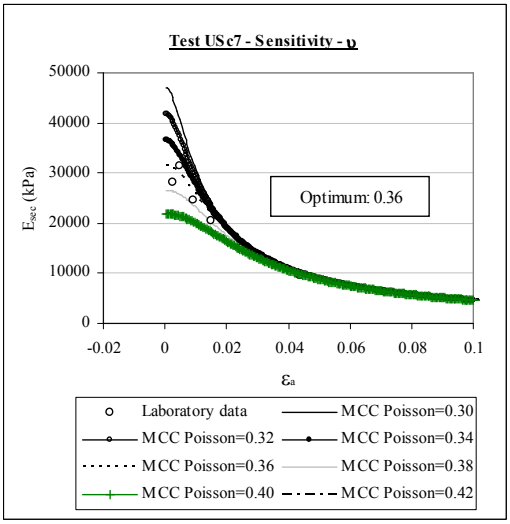

Figure 8.48. Sensitivity of the Modified Cam-Clay model to υ in terms of the E_{sec} -ε_a behaviour during test USc7

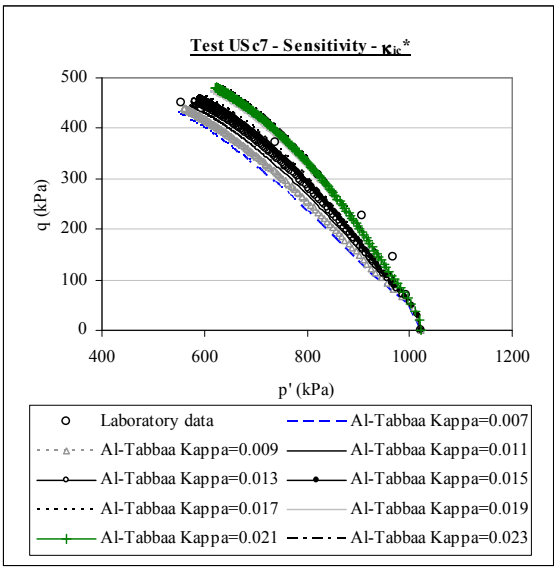

Figure 8.49. Sensitivity of the Al-Tabbaa model to κ_{ic}^* in terms of the q - p' behaviour during test USc7

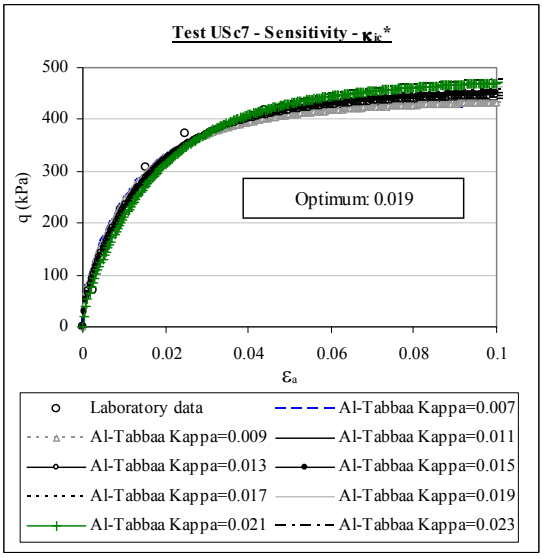

Figure 8.50. Sensitivity of the Al-Tabbaa model to κ_{ic}^* in terms of the q - ε_a behaviour during test USc7

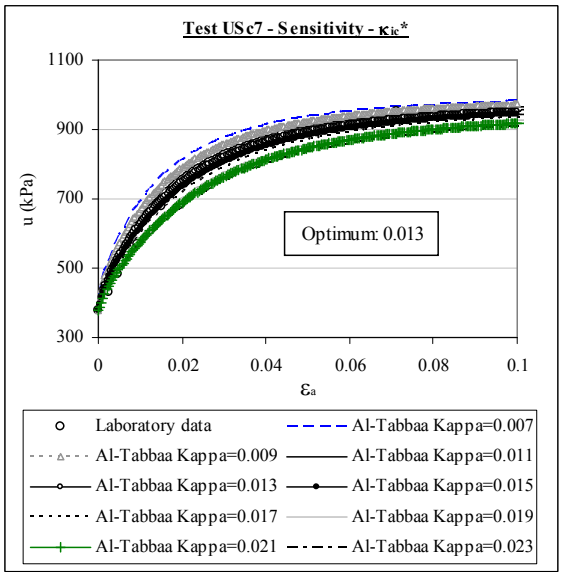

Figure 8.51. Sensitivity of the Al-Tabbaa model to κ_{ic}^* in terms of the u - ε_a behaviour during test USc7

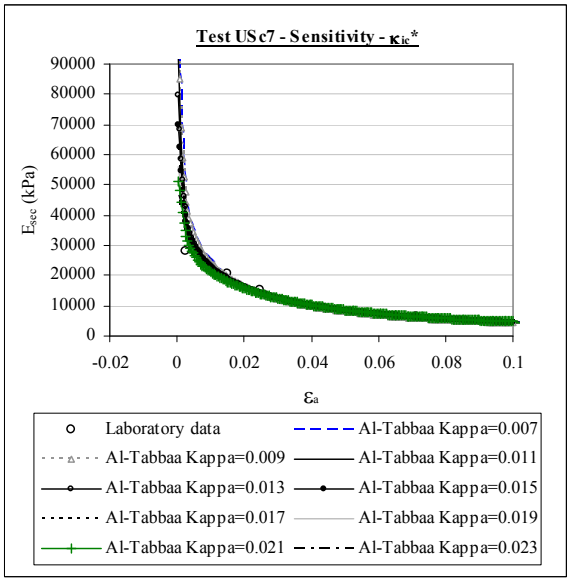

Figure 8.52. Sensitivity of the Al-Tabbaa model to κ_{ic}^* in terms of the E_{sec} -ε_a behaviour during test USc7

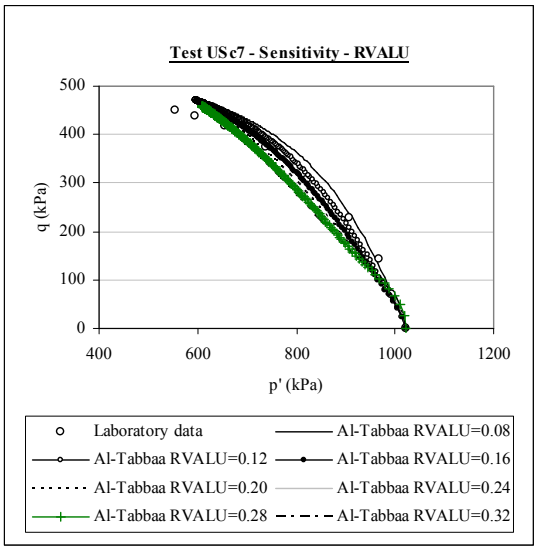

Figure 8.53. Sensitivity of the Al-Tabbaa model to *RVALU* in terms of the q - p' behaviour during test USc7

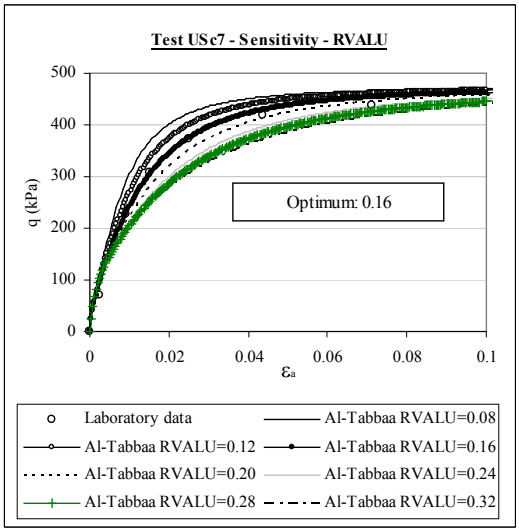

Figure 8.54. Sensitivity of the Al-Tabbaa model to *RVALU* in terms of the q - ε_a behaviour during test USc7

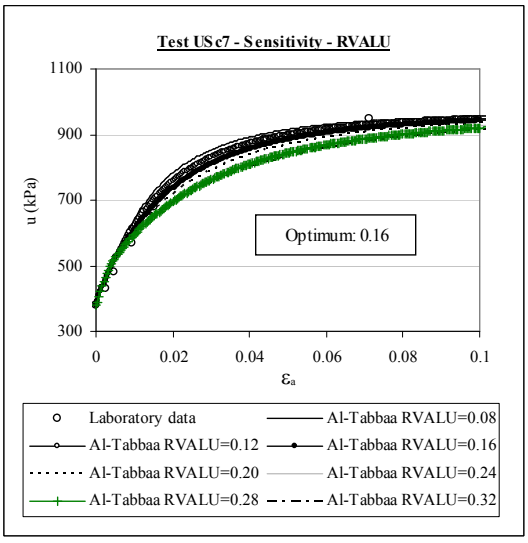

Figure 8.55. Sensitivity of the Al-Tabbaa model to *RVALU* in terms of the u - ε_a behaviour during test USc7

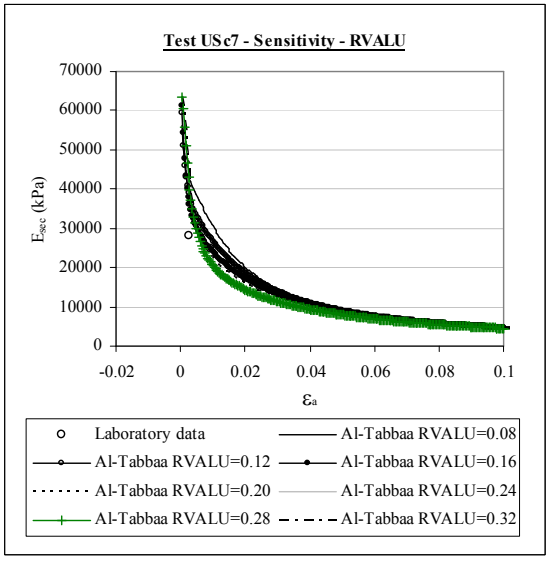

Figure 8.56. Sensitivity of the Al-Tabbaa model to *RVALU* in terms of the E_{sec} - ε_a behaviour during test USc7

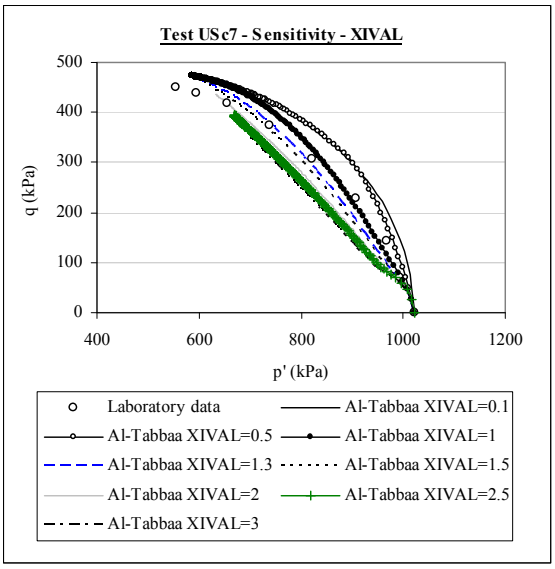

Figure 8.57. Sensitivity of the Al-Tabbaa model to *XIVAL* in terms of the q - p' behaviour during test USc7

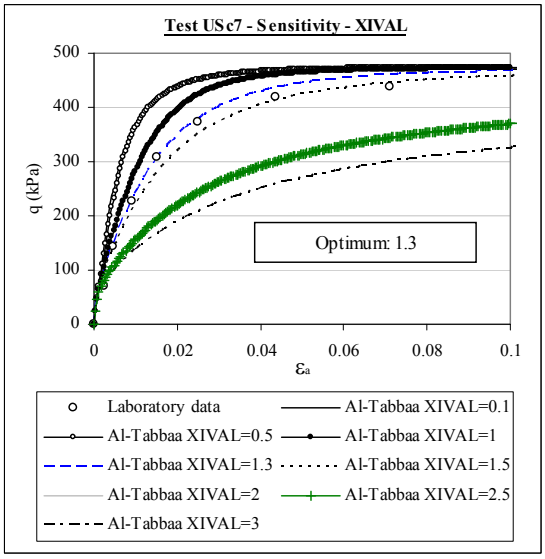

Figure 8.58. Sensitivity of the Al-Tabbaa model to *XIVAL* in terms of the q - ε_a behaviour during test USc7

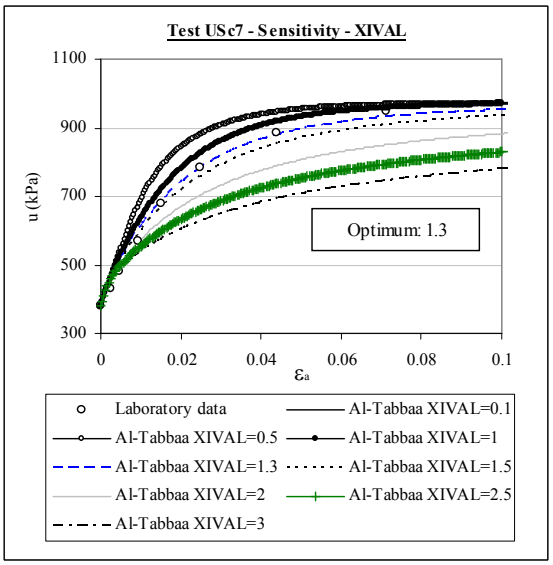

Figure 8.59. Sensitivity of the Al-Tabbaa model to *XIVAL* in terms of the u - ε_a behaviour during test USc7

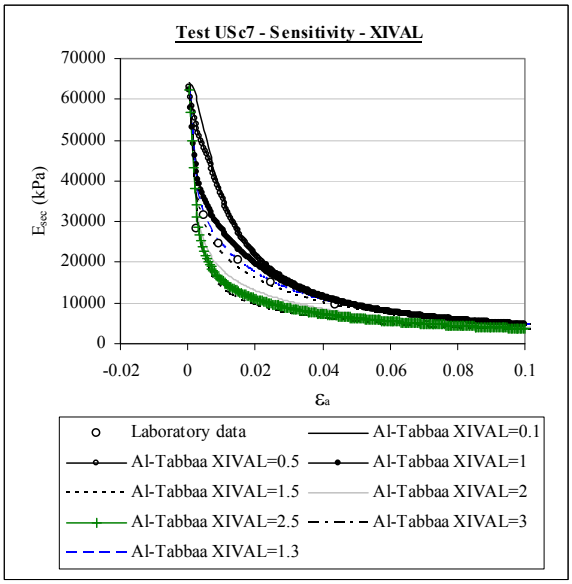

Figure 8.60. Sensitivity of the Al-Tabbaa model to *XIVAL* in terms of the E_{sec} -ε_a behaviour during test USc7

TEST Ko6

For test Ko6, the sensitivity of the S-CLAY1 model to κ_0, λ_0, υ, M, μ, β and α were studied according to the methodology given in Section 3.7.3. The parameters that were found to mainly control the results were κ_0 and β. The results corresponding to these parameters are illustrated in Figures 8.61 to 8.68. The graphs showing the effect of the other parameters can be found in Appendix E - Figures E.21 to E.40.

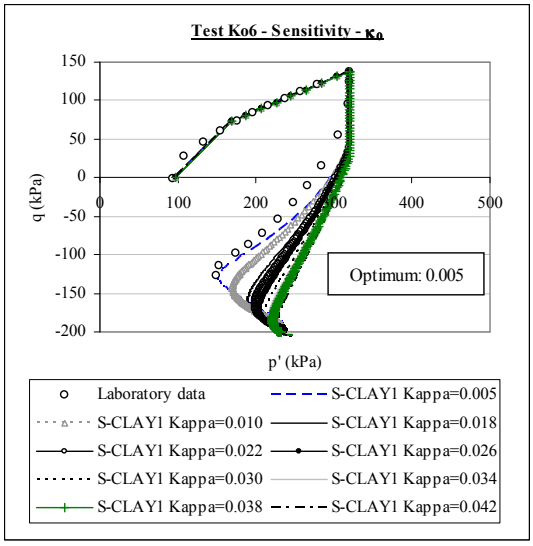

Figure 8.61. Sensitivity of the S-CLAY1 model to κ_0 in terms of the q - p' behaviour during test Ko6

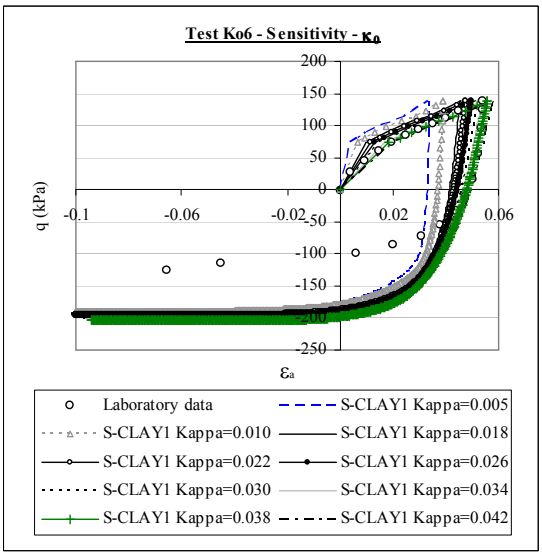

Figure 8.62. Sensitivity of the S-CLAY1 model to κ_0 in terms of the q - ε_a behaviour during test Ko6

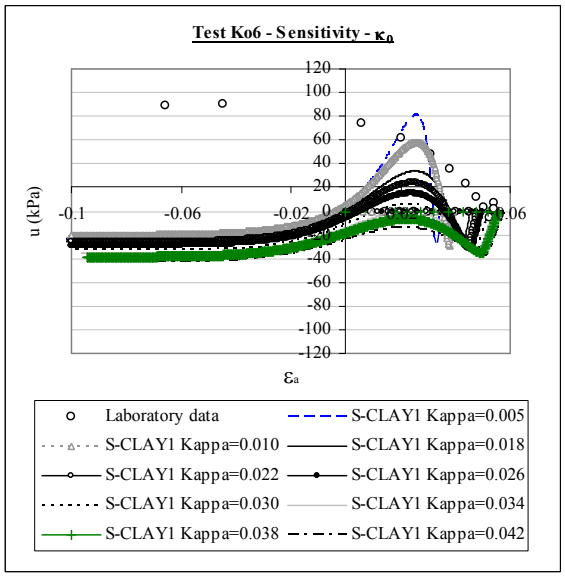

Figure 8.63. Sensitivity of the S-CLAY1 model to κ_0 in terms of the u - ε_a behaviour during test Ko6

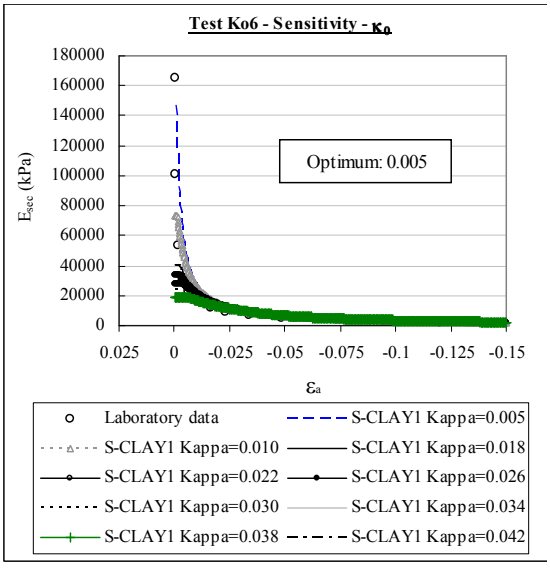

Figure 8.64. Sensitivity of the S-CLAY1 model to κ_0 in terms of the E_{sec} - ε_a behaviour during test Ko6

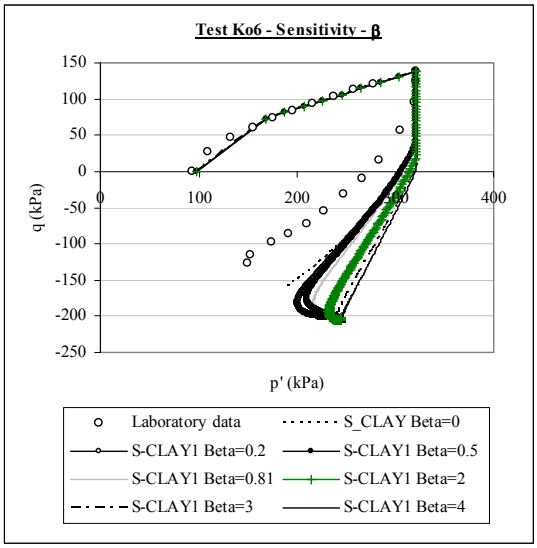

Figure 8.65. Sensitivity of the S-CLAY1 model to β in terms of the q - p' behaviour during test Ko6

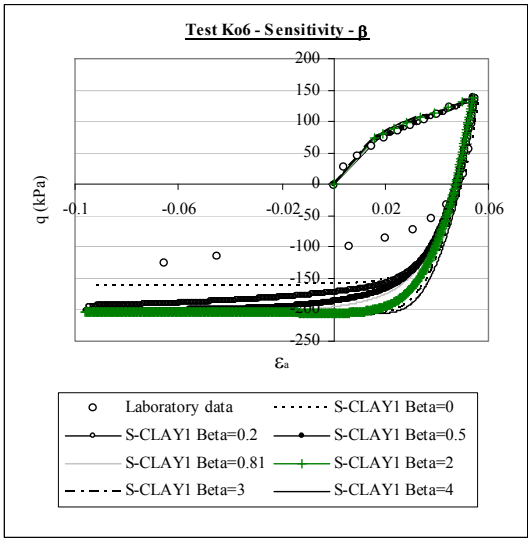

Figure 8.66. Sensitivity of the S-CLAY1 model to β in terms of the q - ε_a behaviour during test Ko6

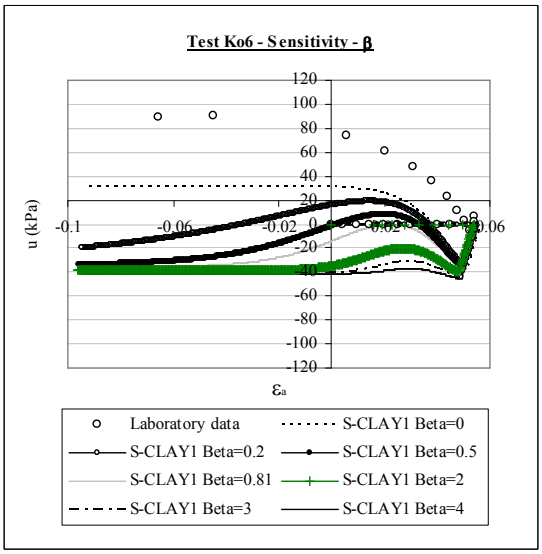

Figure 8.67. Sensitivity of the S-CLAY1 model to β in terms of the u - ε_a behaviour during test Ko5

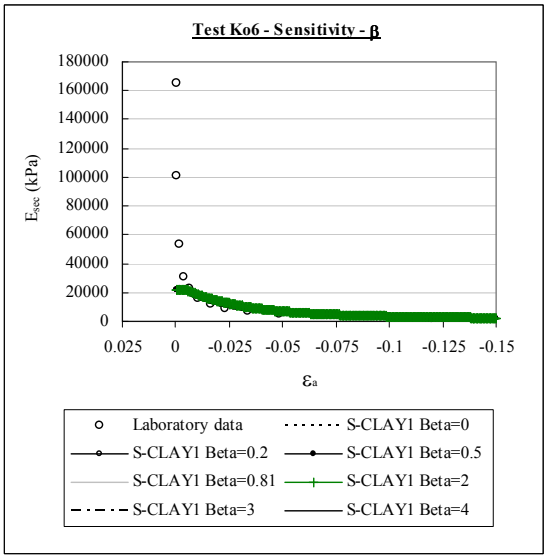

Figure 8.68. Sensitivity of the S-CLAY1 model to β in terms of the E_{sec} -ε_a behaviour during test Ko5

8.3.2. Sensitivity Analysis II

TEST USc9

The results corresponding to test USc9 are illustrated in Figures 8.69 to 8.80.

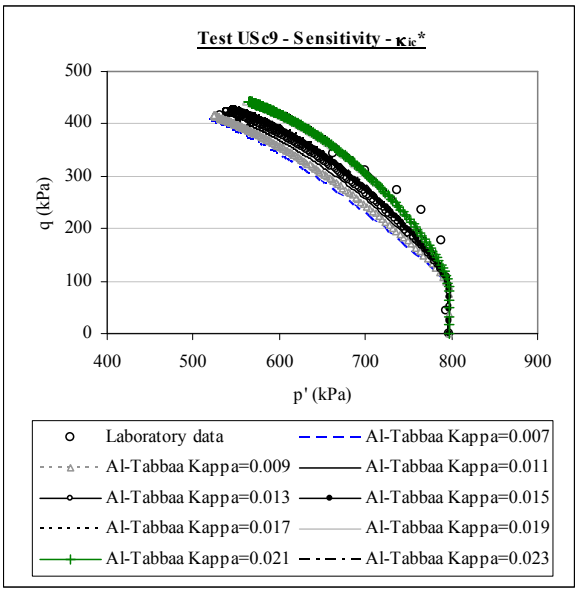

Figure 8.69. Sensitivity of the Al-Tabbaa model to κ_{ic}^* in terms of the q - p' behaviour during test USc9

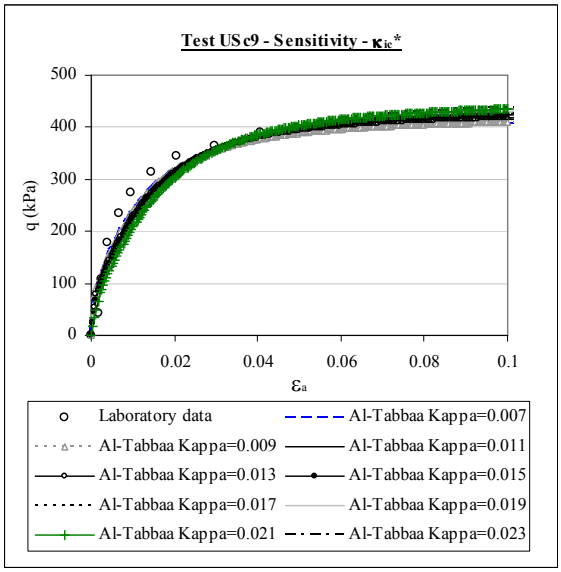

Figure 8.70. Sensitivity of the Al-Tabbaa model to κ_{ic}^* in terms of the q - ε_a behaviour during test USc9

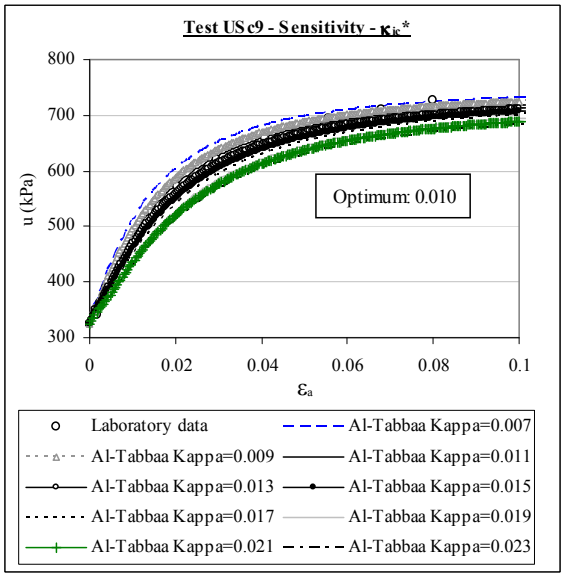

Figure 8.71. Sensitivity of the Al-Tabbaa model to κ_{ic}^* in terms of the u - ε_a behaviour during test USc9

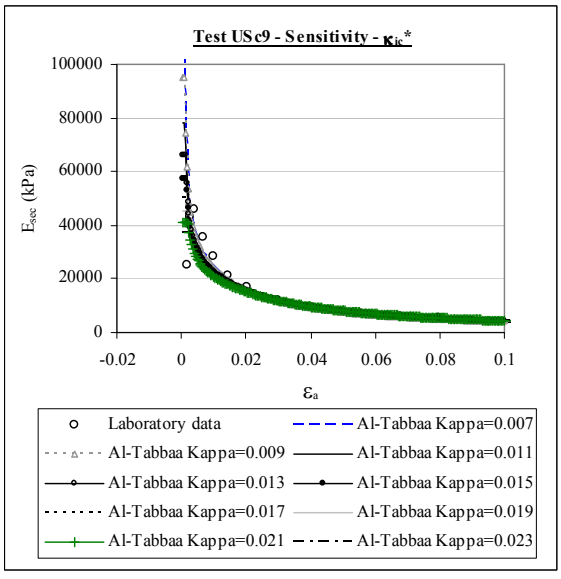

Figure 8.72. Sensitivity of the Al-Tabbaa model to κ_{ic}^* in terms of the E_{sec} -ε_a behaviour during test USc9

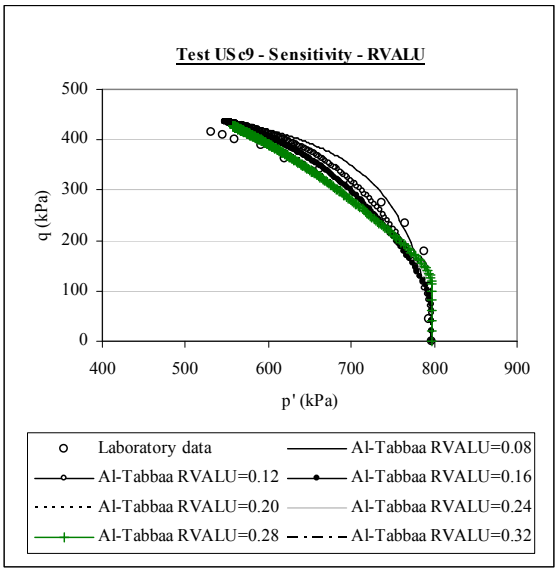

Figure 8.73. Sensitivity of the Al-Tabbaa model to $RVALU$ in terms of the q - p' behaviour during test USc9

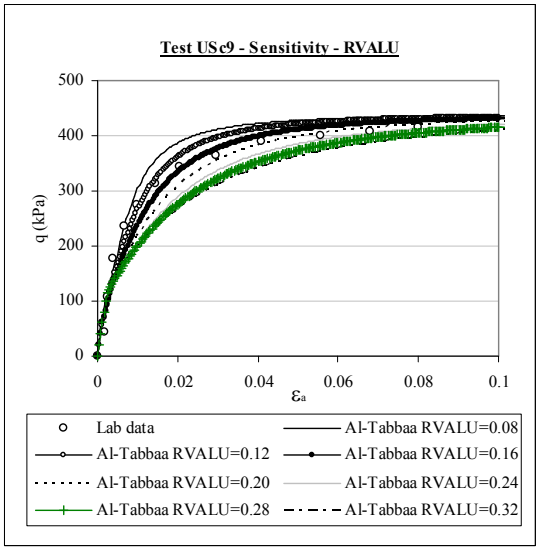

Figure 8.74. Sensitivity of the Al-Tabbaa model to $RVALU$ in terms of the q - ε_a behaviour during test USc9

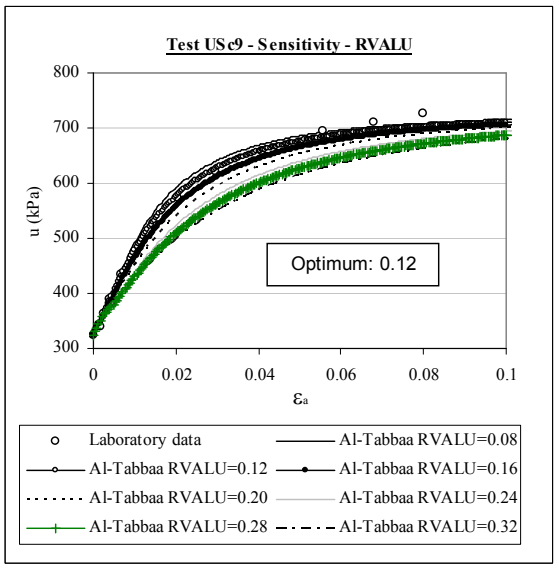

Figure 8.75. Sensitivity of the Al-Tabbaa model to $RVALU$ in terms of the u - ε_a behaviour during test USc9

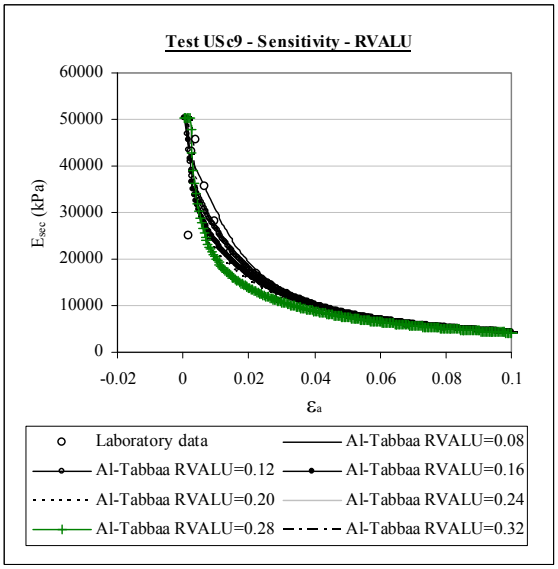

Figure 8.76. Sensitivity of the Al-Tabbaa model to $RVALU$ in terms of the E_{sec} -ε_a behaviour during test USc9

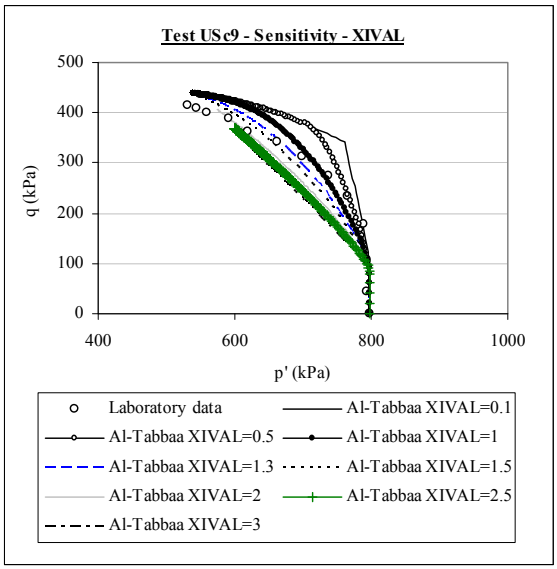

Figure 8.77. Sensitivity of the Al-Tabbaa model to XIVAL in terms of the q - p' behaviour during test USc9

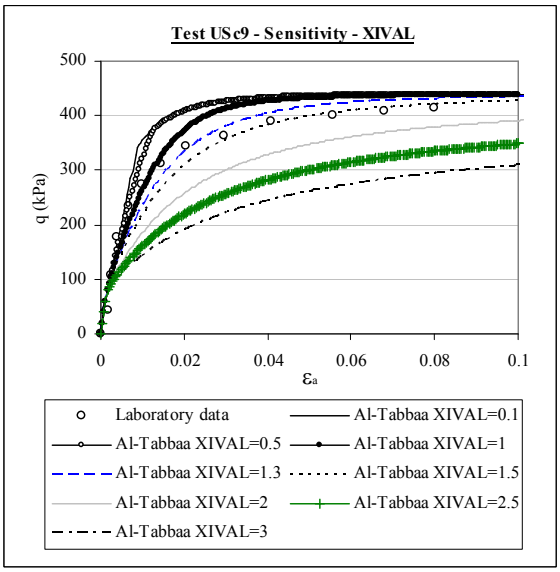

Figure 8.78. Sensitivity of the Al-Tabbaa model to *XIVAL* in terms of the q - ε_a behaviour during test USc9

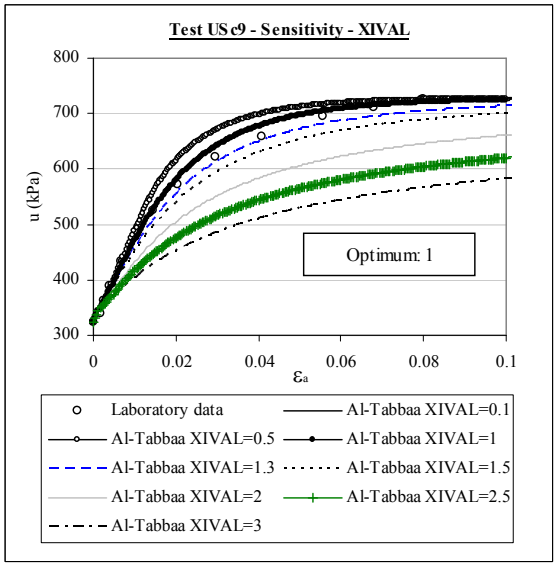

Figure 8.79. Sensitivity of the Al-Tabbaa model to *XIVAL* in terms of the u - ε_a behaviour during test USc9

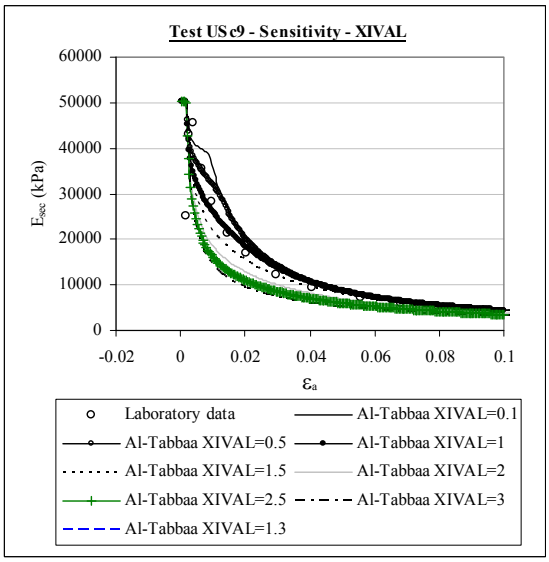

Figure 8.80. Sensitivity of the Al-Tabbaa model to *XIVAL* in terms of the E_{sec} -ε_a behaviour during test USc9

TEST USe3

The results corresponding to test USe3 are illustrated in Figures 8.81 to 8.92.

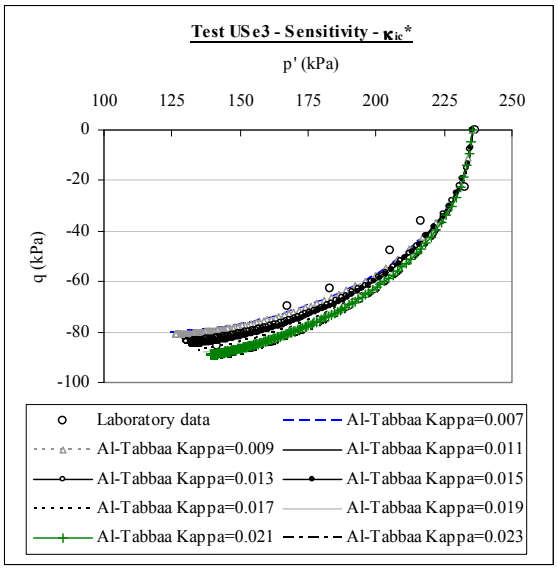

Figure 8.81. Sensitivity of the Al-Tabbaa model to κ_{ic}^* in terms of the q - p' behaviour during test USe3

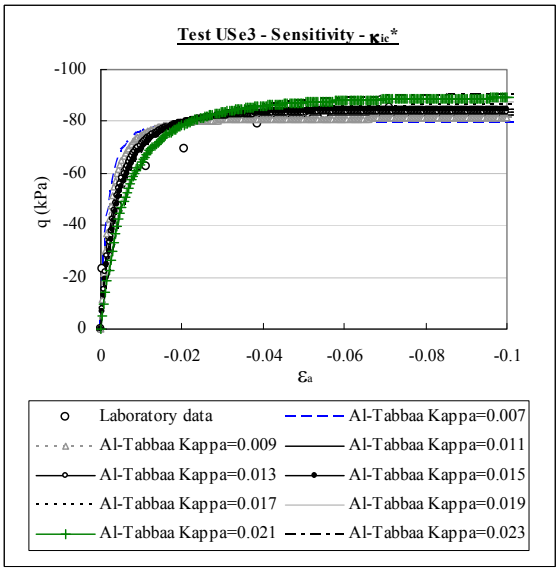

Figure 8.82. Sensitivity of the Al-Tabbaa model to κ_{ic}^* in terms of the q - ε_a behaviour during test USe3

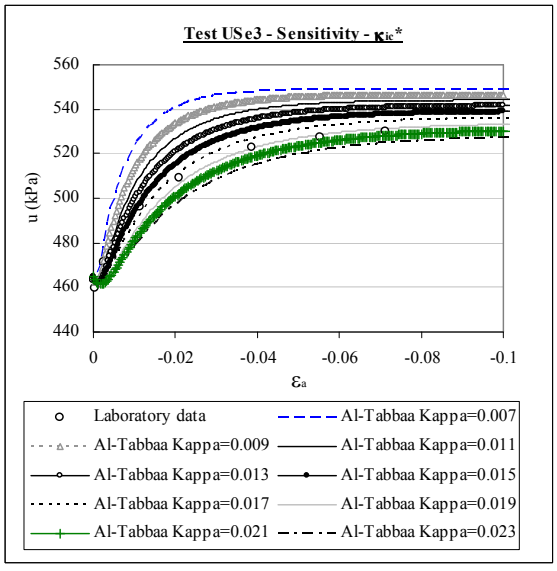

Figure 8.83. Sensitivity of the Al-Tabbaa model to κ_{ic}^* in terms of the u - ε_a behaviour during test USe3

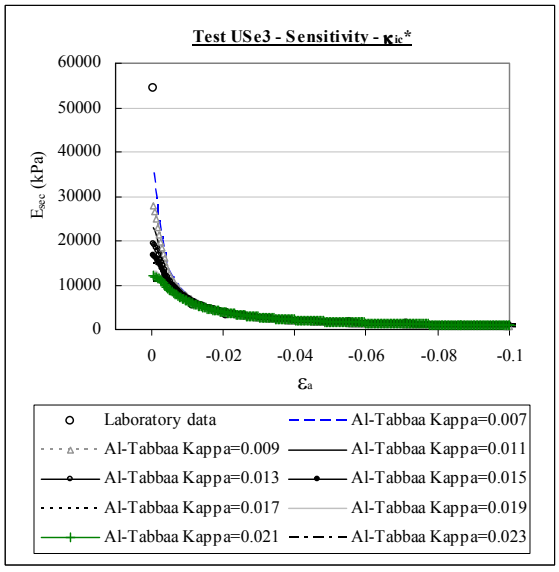

Figure 8.84. Sensitivity of the Al-Tabbaa model to κ_{ic}^* in terms of the E_{sec} -ε_a behaviour during test USe3

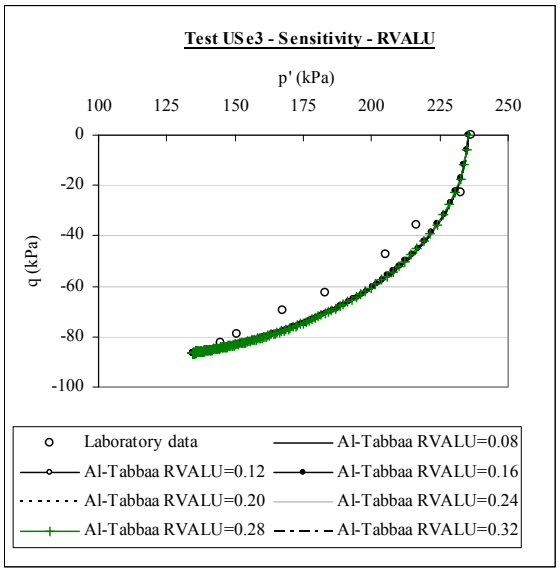

Figure 8.85. Sensitivity of the Al-Tabbaa model to $RVALU$ in terms of the q - p' behaviour during test USe3

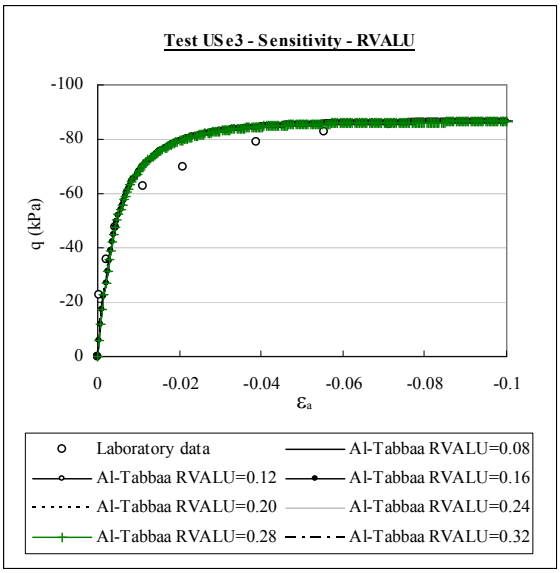

Figure 8.86. Sensitivity of the Al-Tabbaa model to $RVALU$ in terms of the q - ε_a behaviour during test USe3

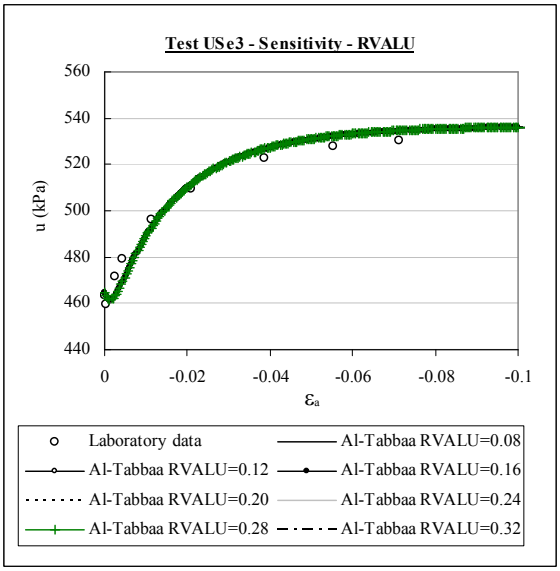

Figure 8.87. Sensitivity of the Al-Tabbaa model to $RVALU$ in terms of the u - ε_a behaviour during test USe3

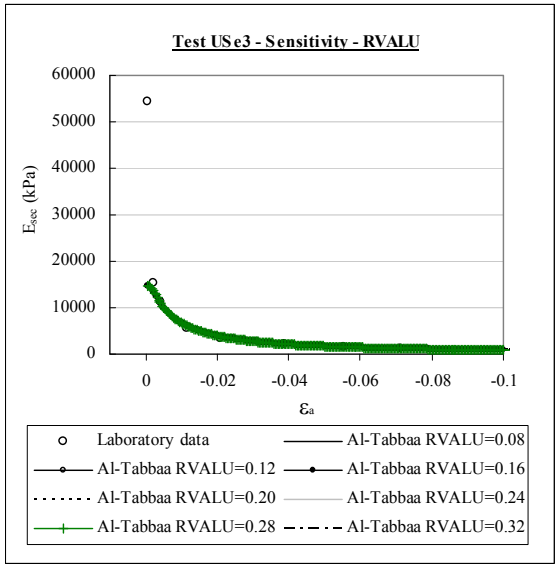

Figure 8.88. Sensitivity of the Al-Tabbaa model to $RVALU$ in terms of the E_{sec} -ε_a behaviour during test USe3

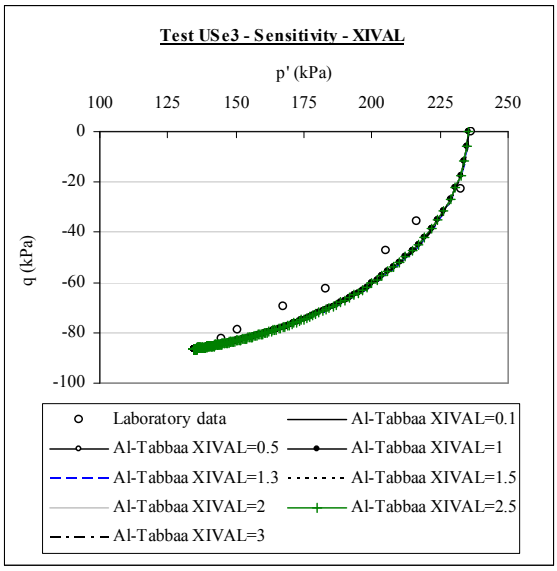

Figure 8.89. Sensitivity of the Al-Tabbaa model to XIVAL in terms of the q - p' behaviour during test USe3

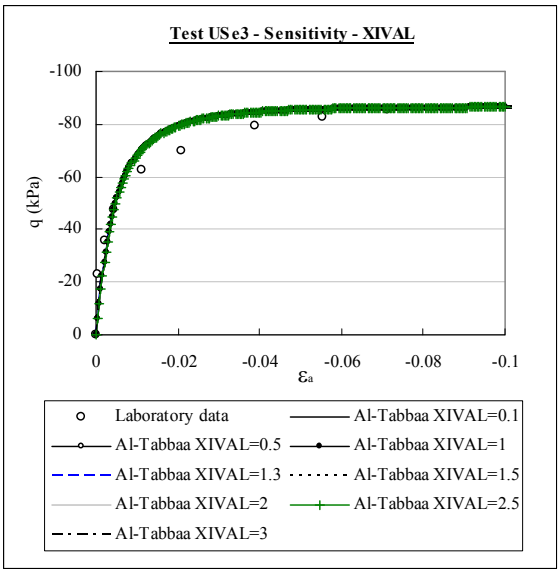

Figure 8.90. Sensitivity of the Al-Tabbaa model to *XIVAL* in terms of the q - ε_a behaviour during test USe3

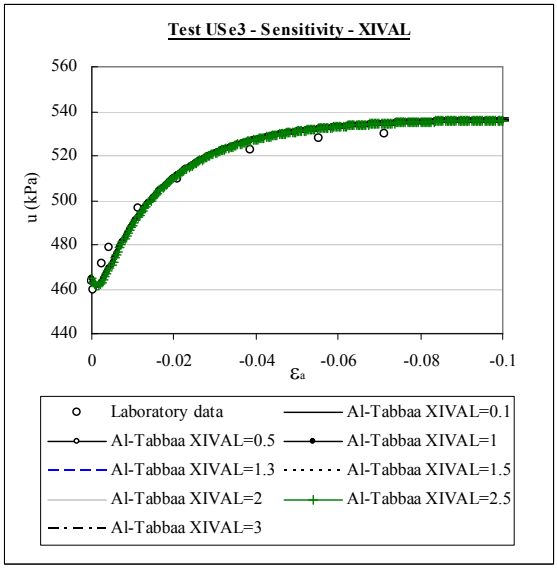

Figure 8.91. Sensitivity of the Al-Tabbaa model to *XIVAL* in terms of the u - ε_a behaviour during test USe3

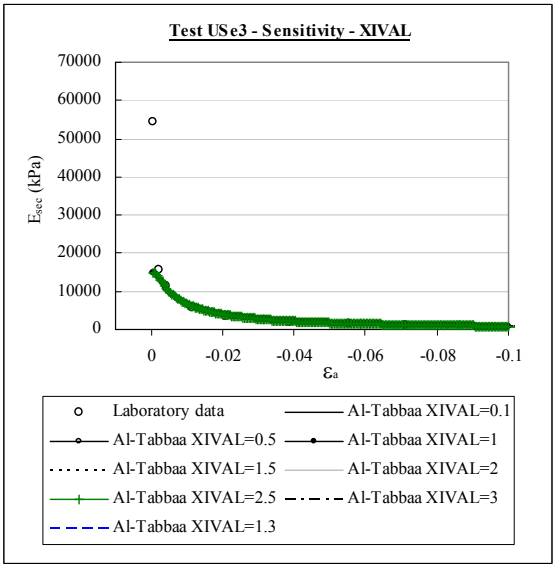

Figure 8.92. Sensitivity of the Al-Tabbaa model to *XIVAL* in terms of the E_{sec} - ε_a behaviour during test USe3

TEST USe6

The results corresponding to test USc9 are illustrated in Figures 8.93 to 8.104.

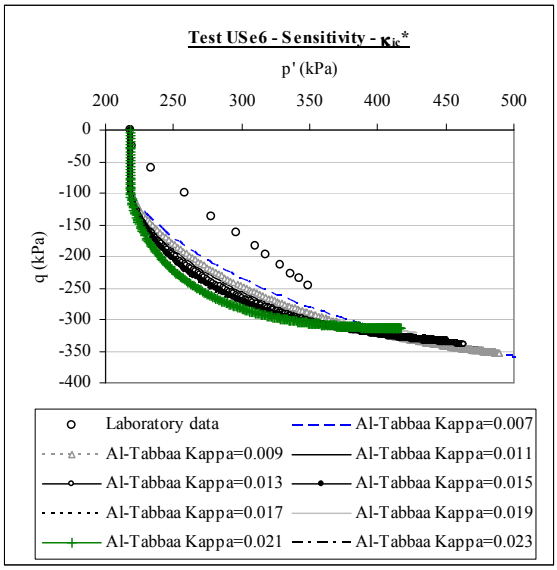

Figure 8.93. Sensitivity of the Al-Tabbaa model to κ_{ic}^* in terms of the q - p' behaviour during test USe6

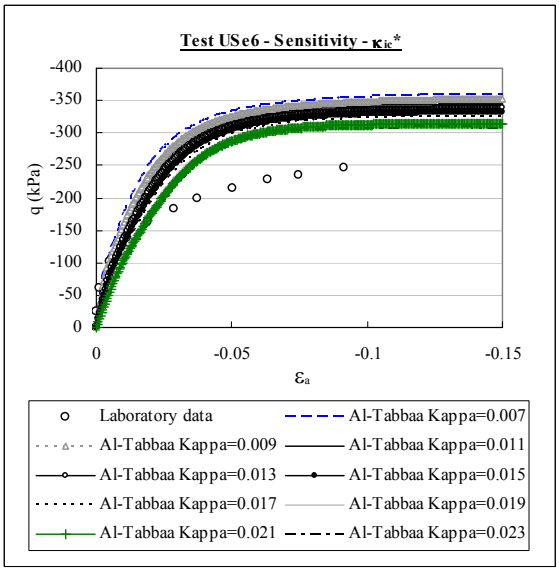

Figure 8.94. Sensitivity of the Al-Tabbaa model to κ_{ic}^* in terms of the q - ε_a behaviour during test USe6

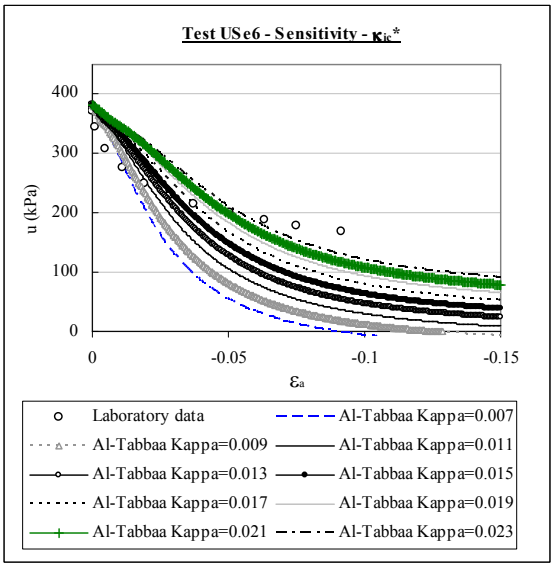

Figure 8.95. Sensitivity of the Al-Tabbaa model to κ_{ic}^* in terms of the u - ε_a behaviour during test USe6

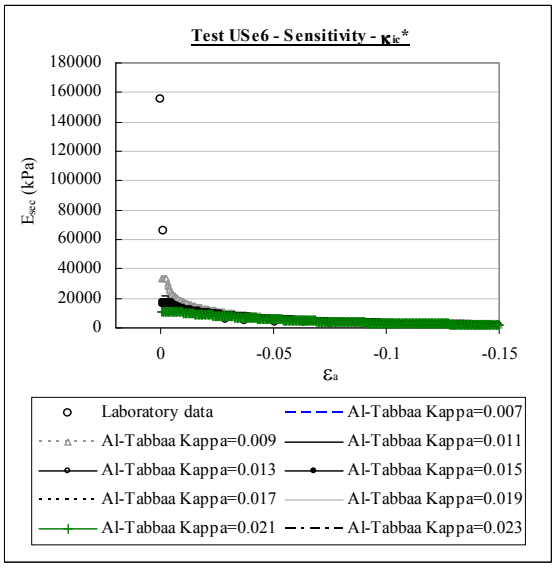

Figure 8.96. Sensitivity of the Al-Tabbaa model to κ_{ic}^* in terms of the E_{sec} - ε_a behaviour during test USe6

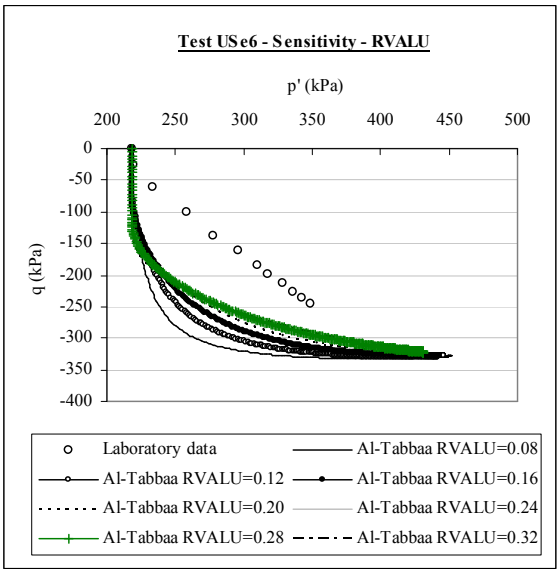

Figure 8.97. Sensitivity of the Al-Tabbaa model to $RVALU$ in terms of the q - p' behaviour during test USe6

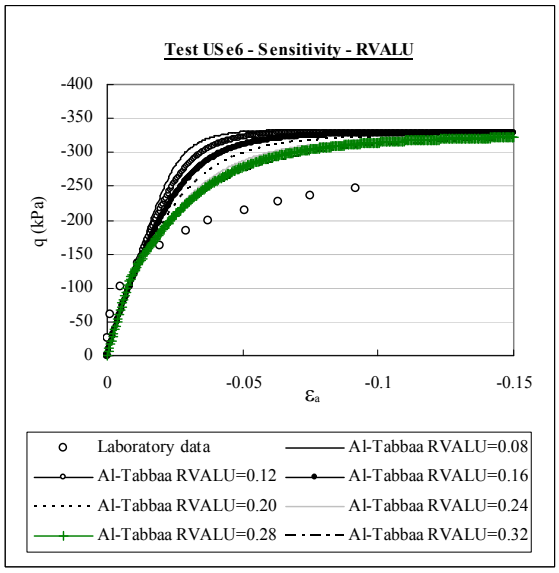

Figure 8.98. Sensitivity of the Al-Tabbaa model to $RVALU$ in terms of the q - ε_a behaviour during test USe6

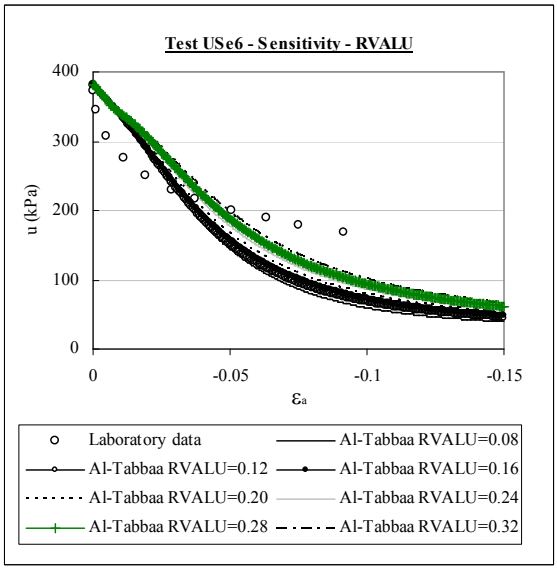

Figure 8.99. Sensitivity of the Al-Tabbaa model to $RVALU$ in terms of the u - ε_a behaviour during test USe6

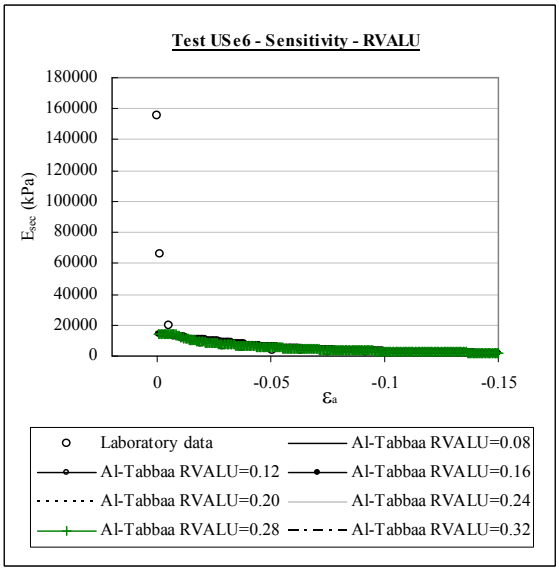

Figure 8.100. Sensitivity of the Al-Tabbaa model to $RVALU$ in terms of the E_{sec} -ε_a behaviour during test USe6

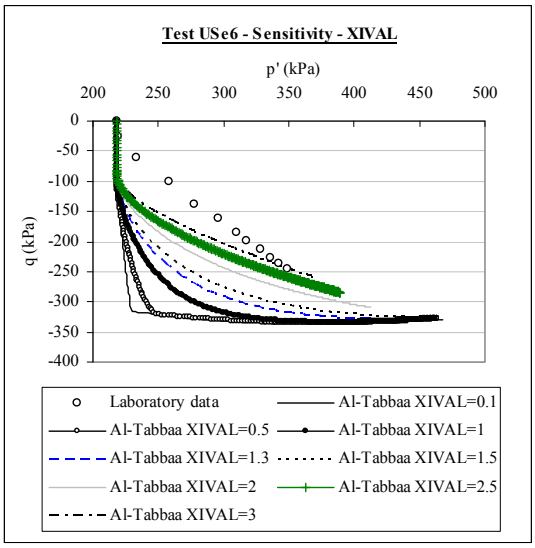

Figure 8.101. Sensitivity of the Al-Tabbaa model to XIVAL in terms of the q - p' behaviour during test USe6

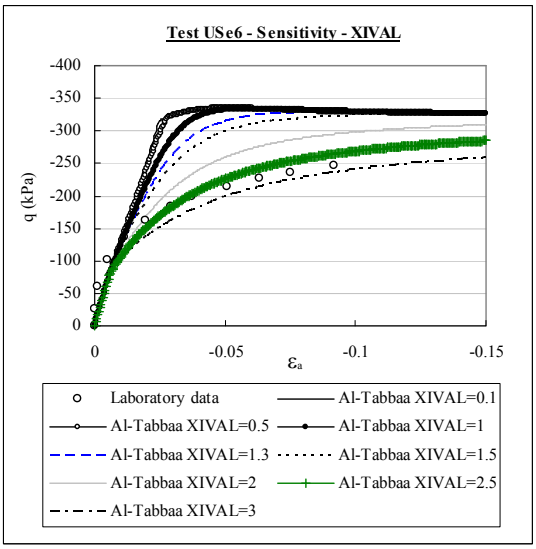

Figure 8.102. Sensitivity of the Al-Tabbaa model to *XIVAL* in terms of the q - ε_a behaviour during test USe6

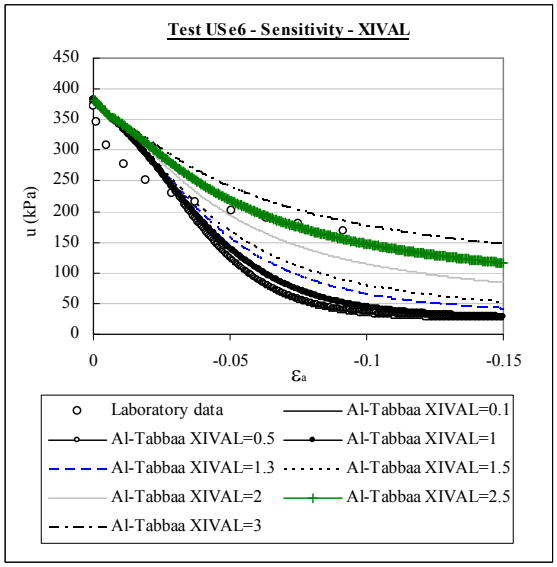

Figure 8.103. Sensitivity of the Al-Tabbaa model to *XIVAL* in terms of the u - ε_a behaviour during test USe6

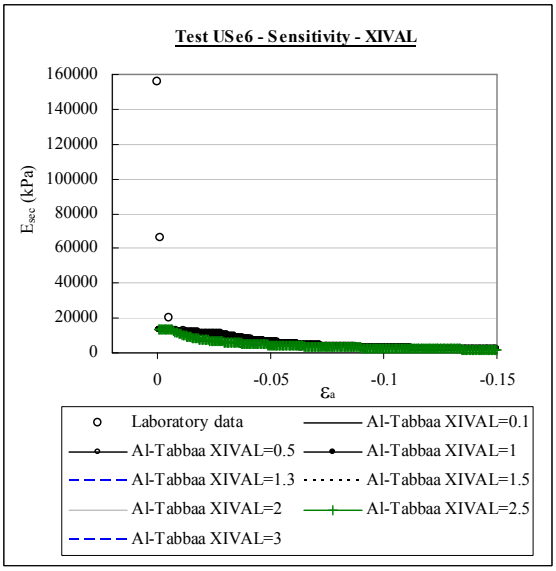

Figure 8.104. Sensitivity of the Al-Tabbaa model to *XIVAL* in terms of the E_{sec} - ε_a behaviour during test USe6

TEST Ko5

The results corresponding to test Ko5 are illustrated in Figures 8.105 to 8.132.

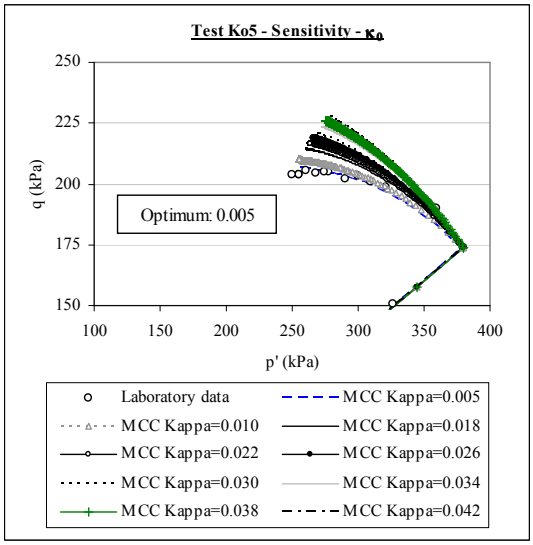

Figure 8.105. Sensitivity of the Modified Cam-Clay model to κ_0 in terms of the q - p' behaviour during test Ko5

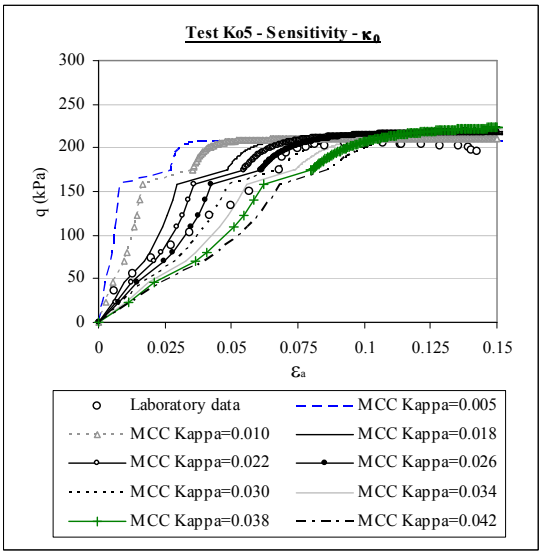

Figure 8.106. Sensitivity of the Modified Cam-Clay model to κ_0 in terms of the q - ε_a behaviour during test Ko5

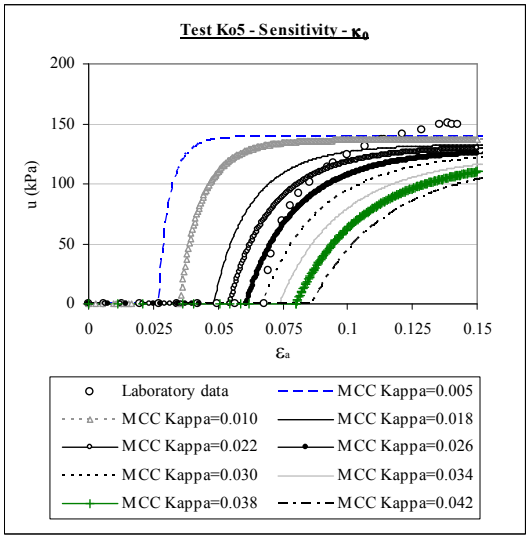

Figure 8.107. Sensitivity of the Modified Cam-Clay model to κ_0 in terms of the u - ε_a behaviour during test Ko5

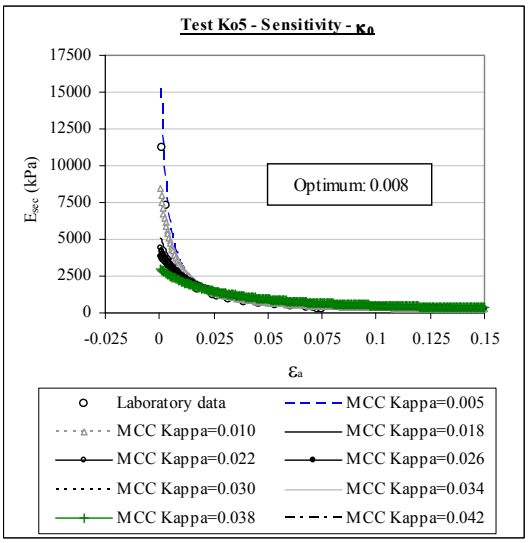

Figure 8.108. Sensitivity of the Modified Cam-Clay model to κ_0 in terms of the E_{sec} -ε_a behaviour during test Ko5

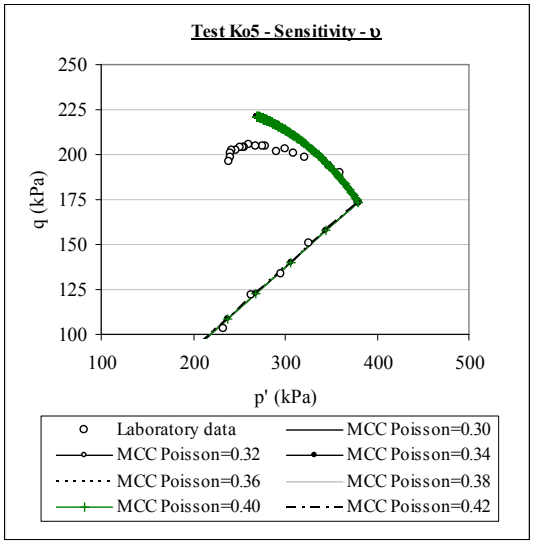

Figure 8.109. Sensitivity of the Modified Cam-Clay model to υ in terms of the q - p' behaviour during test Ko5

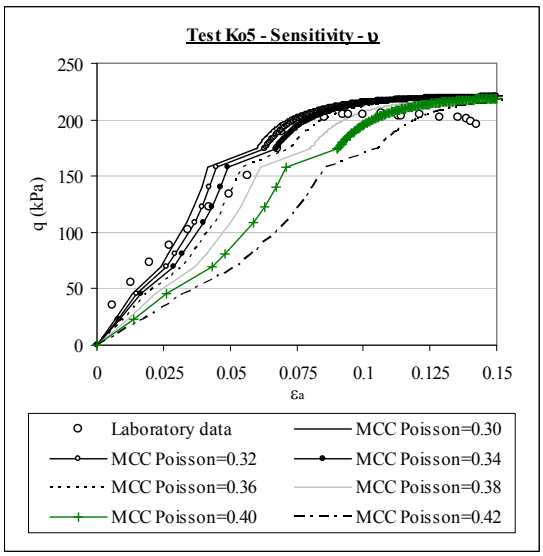

Figure 8.110. Sensitivity of the Modified Cam-Clay model to υ in terms of the q - ε_a behaviour during test Ko5

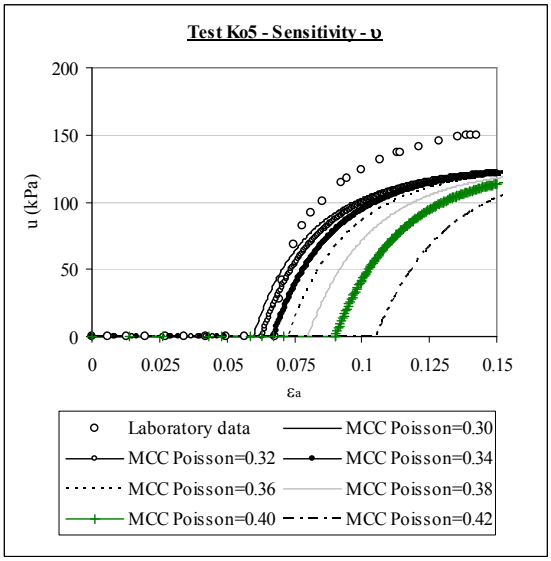

Figure 8.111. Sensitivity of the Modified Cam-Clay model to υ in terms of the u - ε_a behaviour during test Ko5

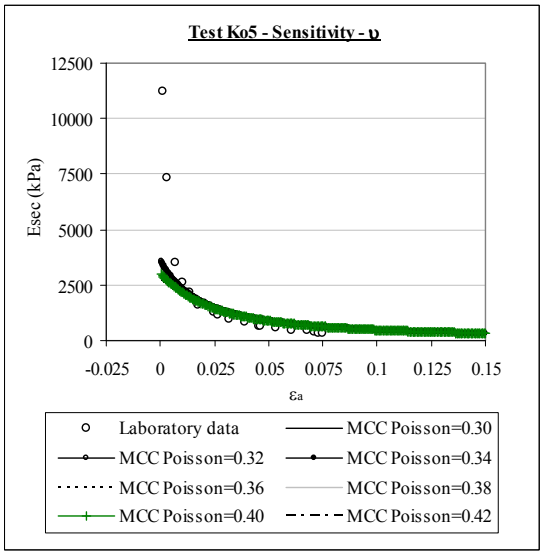

Figure 8.112. Sensitivity of the Modified Cam-Clay model to υ in terms of the E_{sec} -ε_a behaviour during test Ko5

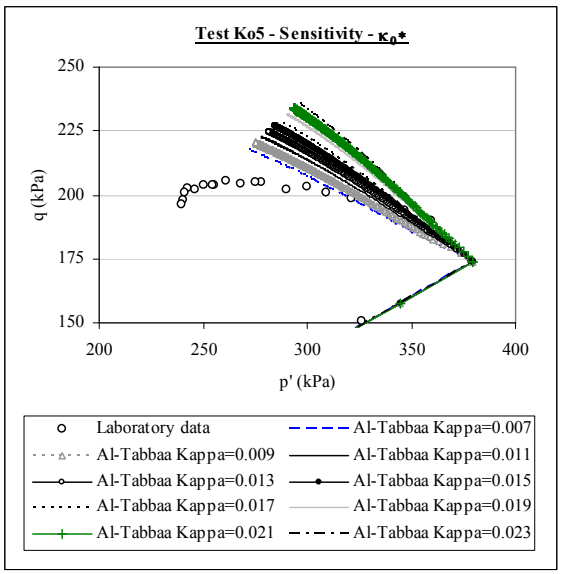

Figure 8.113. Sensitivity of the Al-Tabbaa model to κ_0* in terms of the q - p' behaviour during test Ko5

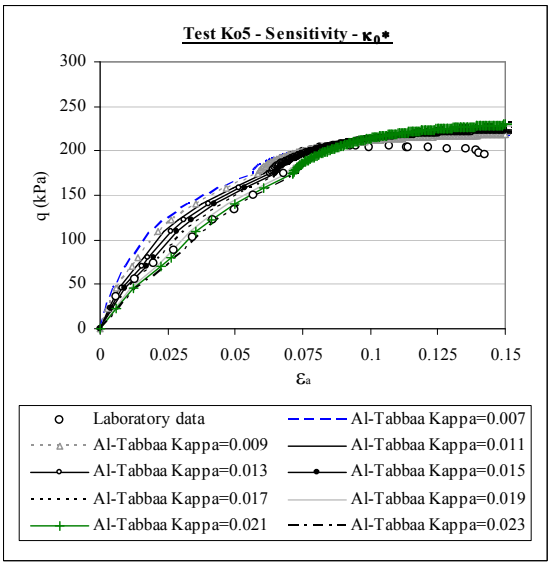

Figure 8.114. Sensitivity of the Al-Tabbaa model to κ_0* in terms of the q - ε_a behaviour during test Ko5

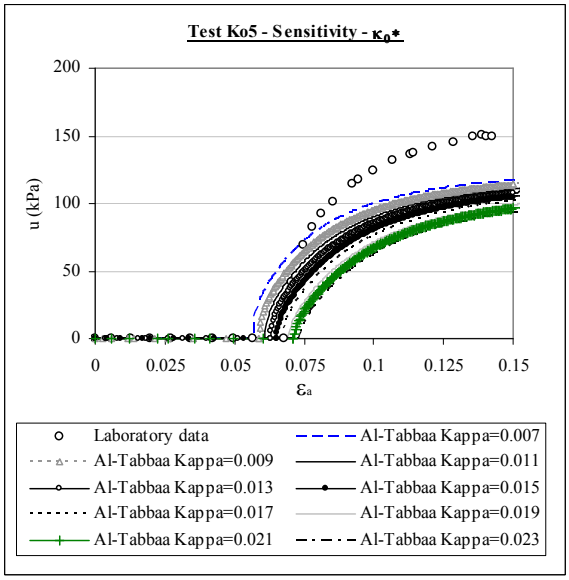

Figure 8.115. Sensitivity of the Al-Tabbaa model to κ_0* in terms of the u - ε_a behaviour during test Ko5

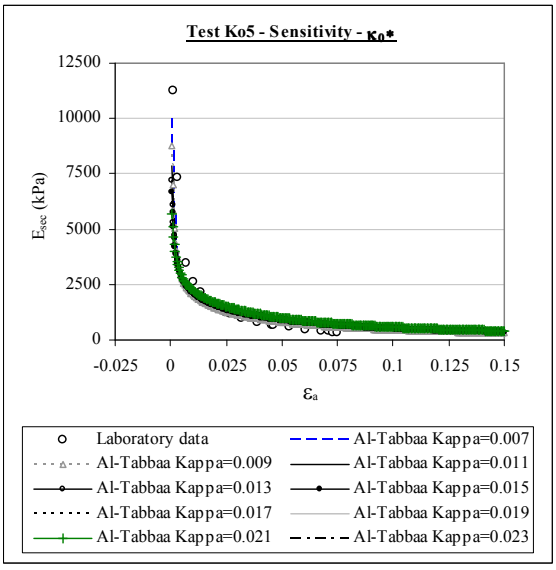

Figure 8.116. Sensitivity of the Al-Tabbaa model to κ_0* in terms of the E_{sec} -ε_a behaviour during test Ko5

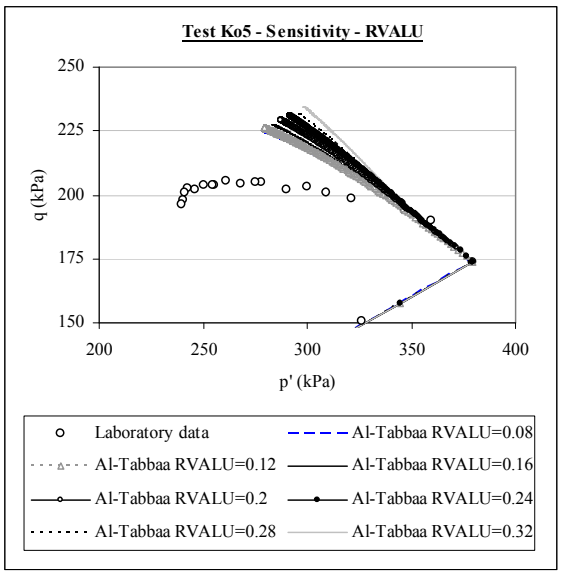

Figure 8.117. Sensitivity of the Al-Tabbaa model to *RVALU* in terms of the q - p' behaviour during test Ko5

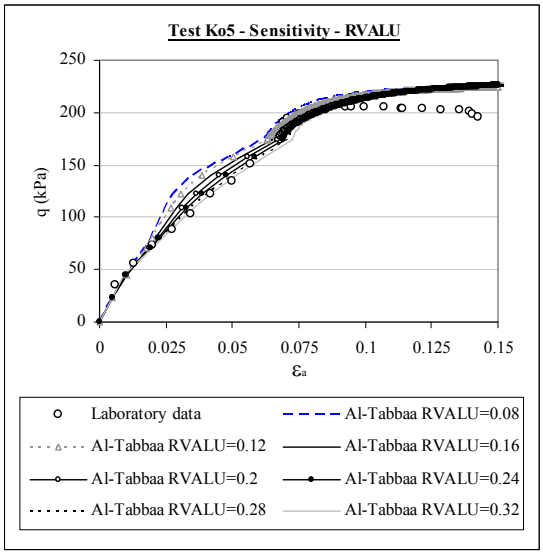

Figure 8.118. Sensitivity of the Al-Tabbaa model to *RVALU* in terms of the q - ε_a behaviour during test Ko5

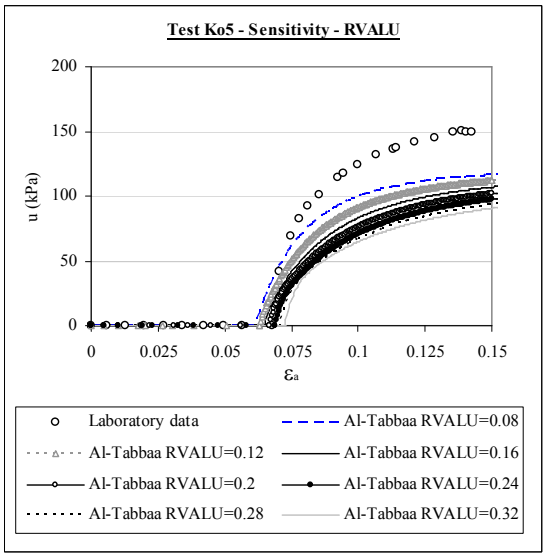

Figure 8.119. Sensitivity of the Al-Tabbaa model to *RVALU* in terms of the u - ε_a behaviour during test Ko5

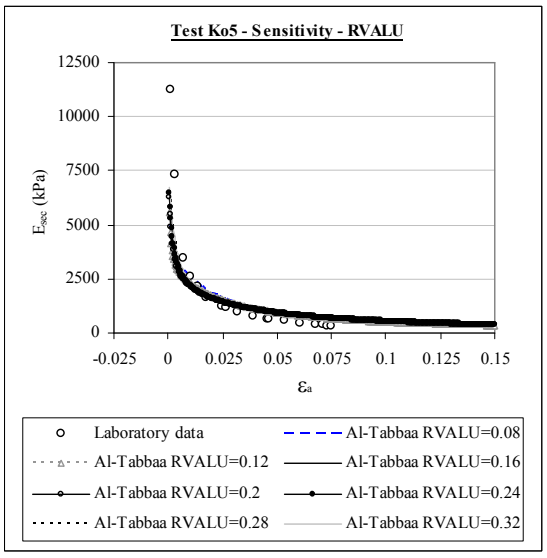

Figure 8.120. Sensitivity of the Al-Tabbaa model to *RVALU* in terms of the E_{sec} -ε_a behaviour during test Ko5

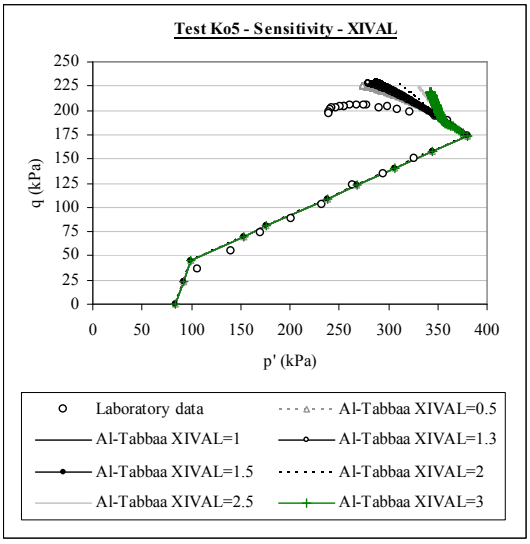

Figure 8.121. Sensitivity of the Al-Tabbaa model to *XIVAL* in terms of the q - p' behaviour during test Ko5

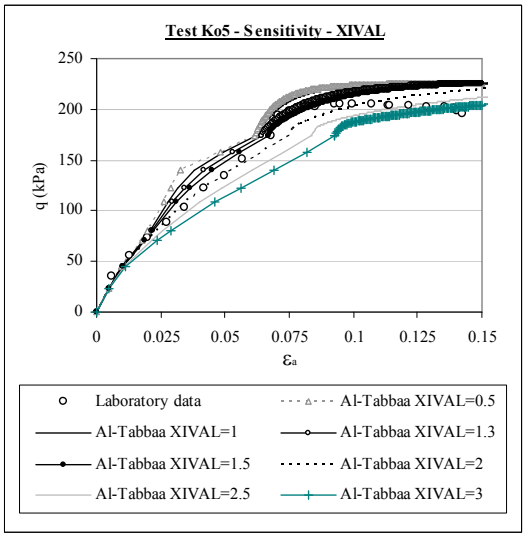

Figure 8.122. Sensitivity of the Al-Tabbaa model to *XIVAL* in terms of the q - ε_a behaviour during test Ko5

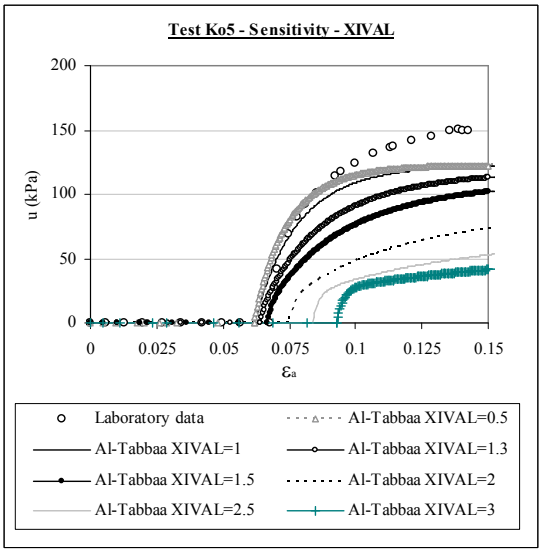

Figure 8.123. Sensitivity of the Al-Tabbaa model to *XIVAL* in terms of the u - ε_a behaviour during test Ko5

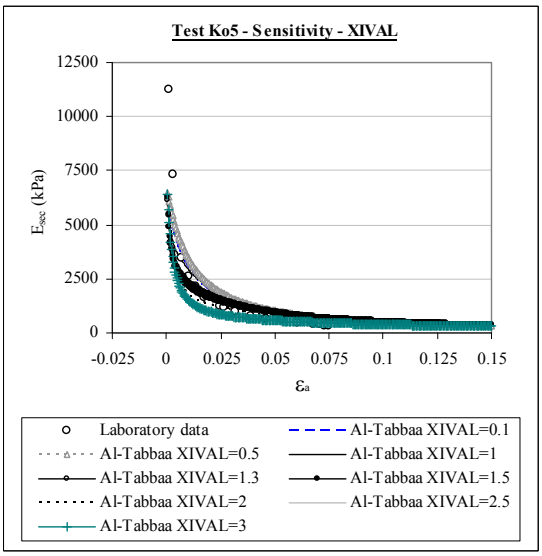

Figure 8.124. Sensitivity of the Al-Tabbaa model to *XIVAL* in terms of the E_{sec} -ε_a behaviour during test Ko5

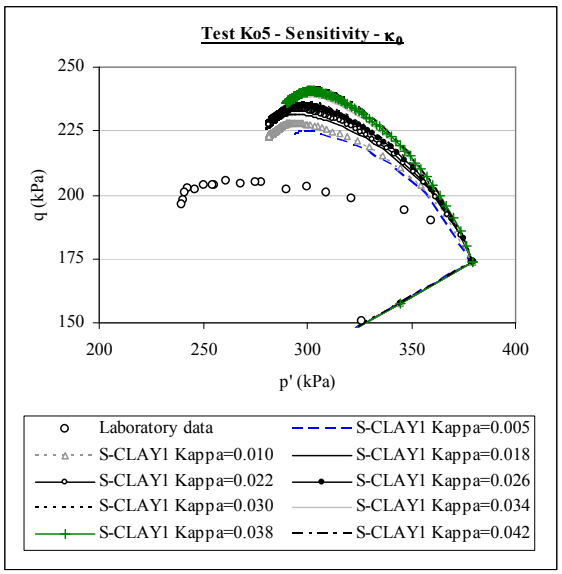

Figure 8.125. Sensitivity of the S-CLAY1 model to κ_0 in terms of the q - p' behaviour during test Ko5

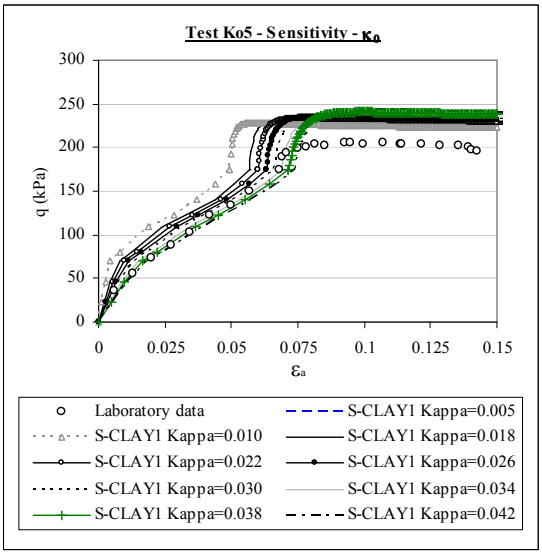

Figure 8.126. Sensitivity of the S-CLAY1 model to κ_0 in terms of the q - ε_a behaviour during test Ko5

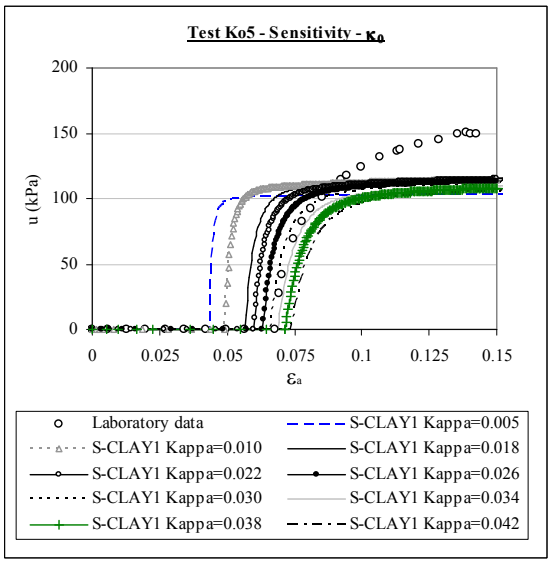

Figure 8.127. Sensitivity of the S-CLAY1 model to κ_0 in terms of the u - ε_a behaviour during test Ko5

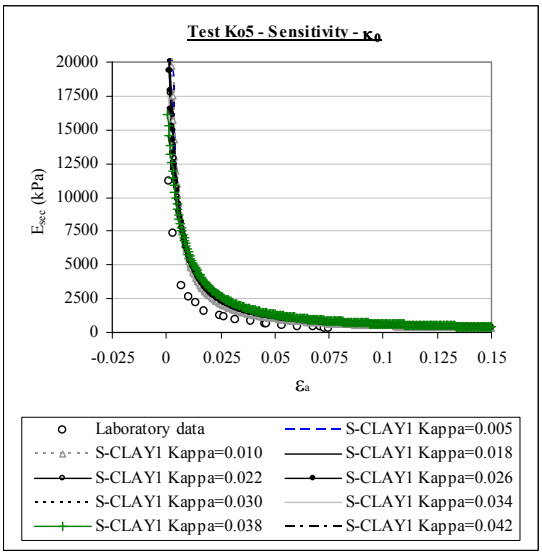

Figure 8.128. Sensitivity of the S-CLAY1 model to κ_0 in terms of the E_{sec} -ε_a behaviour during test Ko5

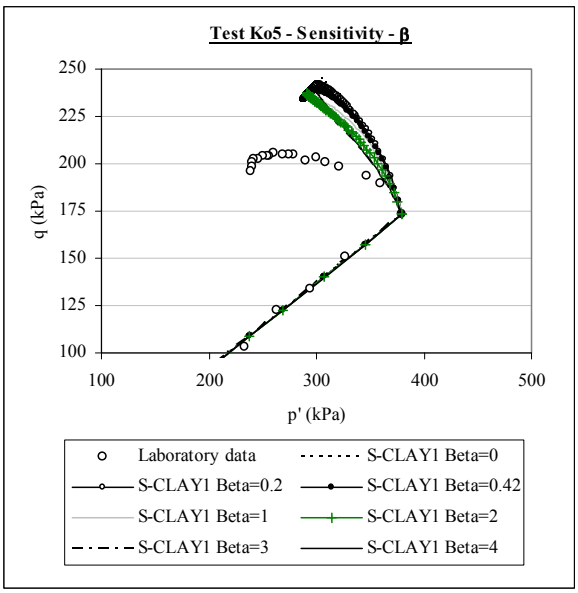

Figure 8.129. Sensitivity of the S-CLAY1 model to β in terms of the q - p' behaviour during test Ko5

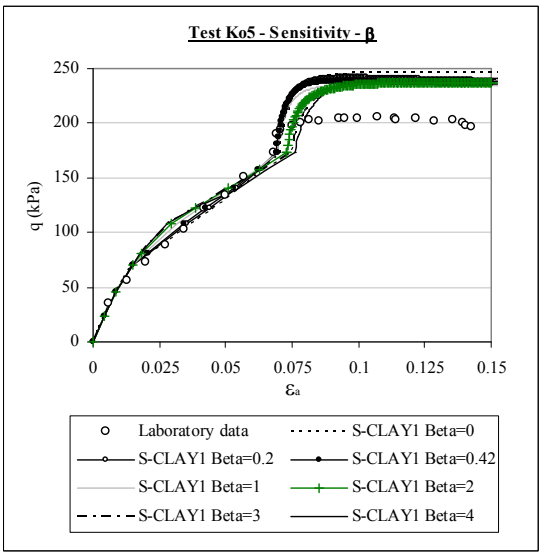

Figure 8.130. Sensitivity of the S-CLAY1 model to β in terms of the q - ε_a behaviour during test Ko5

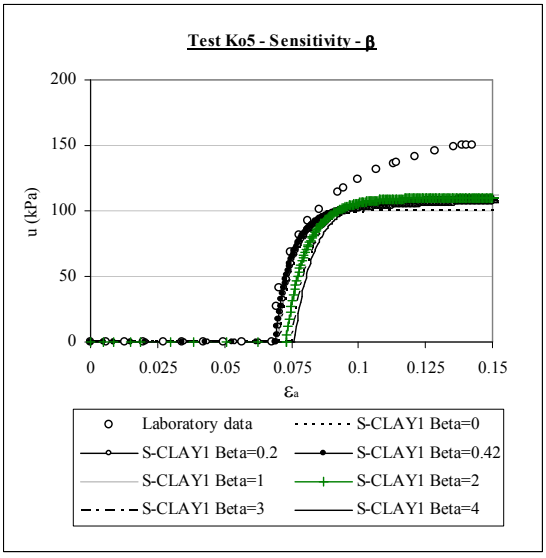

Figure 8.131. Sensitivity of the S-CLAY1 model to β in terms of the u - ε_a behaviour during test Ko5

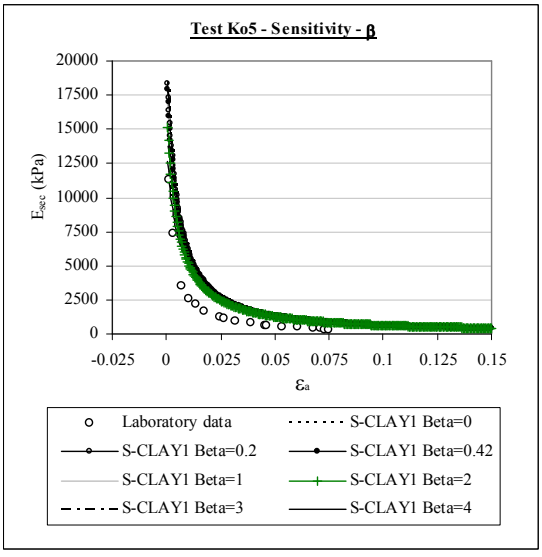

Figure 8.132. Sensitivity of the S-CLAY1 model to β in terms of the E_{sec} -ε_a behaviour during test Ko5

8.4. DISCUSSION

The data presented in this chapter has allowed an initial evaluation of the selected constitutive models with regard to their accuracy in predicting a wide range of reconstituted soil conditions (soil consolidated isotropically or one-dimensionally to different stress levels) and shearing modes (compression or extension). As previously highlighted in Section 3.7.1, the Linear Elastic and the Mohr-Coulomb models did not have enough features to simulate the behaviour of the soil as a whole in terms of stresses, strains and generation of u. For example, the Mohr-Coulomb model predicts a vertical elastic stress path in the q - p' space until reaching the failure surface therefore greatly overestimating the strength of the material. In order to achieve a more accurate prediction, a constant c_u (i.e. zero effective friction angle and hence Mohr-Coulomb reducing to the Tresca criterion) should be used instead, but the model would still be too crude. These classical models have been only used for test USc7.

For normally isotropic consolidated Kaolin sheared in compression (test USc7; Figures 8.1. to 8.4), the Modified Cam-Clay model was found to perform in general better than the Al-Tabbaa model, but both were capable of dealing well with the experimentally observed patterns.

The opposite occurs when considering the behaviour of lightly overconsolidated Kaolin (test USc9; Figures 8.5 to 8.8). In this case, the Al-Tabbaa model was found to be slightly better than the Modified Cam-Clay model, particularly for the prediction of the q - p' path and the initial stiffness response which was underestimated by the Modified Cam-Clay model. In terms of the u - ε_a relationships, it could be observed for both USc7 and USc9 (Figures 8.3 and 8.7), that Al-Tabbaa tends to predict higher and lower u than the Modified Cam-Clay model for strains below and above $\cong$0.02 respectively. This gives rise to a better prediction of u at small strains by the Al-Tabbaa model and vice versa for the Modified Cam-Clay.

When it comes to the reproduction of the behaviour of isotropically consolidated Kaolin sheared in extension (tests USe3, USe5 and USe6; Figures 8.9 to 8.20), it was observed that only the normally consolidated case (USe3) could be reasonably simulated by either model (Al-Tabbaa and Modified Cam-Clay), with the Al-Tabbaa model being again more accurate. The q - p' paths did not agree well with the experimental observations for both lightly and heavily overconsolidated Kaolin (Figures 8.13 and 8.17), mostly for the Modified Cam-Clay model due to the prediction of pure elastic behaviour (i.e. constant p') inside the yielding surface. This was more obvious for the heavily overconsolidated soil. The curvature introduced by the elasto-plastic unloading behaviour considered in the Al-Tabbaa model improved the prediction, but this was still far from the experimental observations. Both models largely overestimate q at failure for both lightly and heavily overconsolidated soils. In the lightly overconsolidated case u was underpredicted, although the general trend was correctly demonstrated (Figure 8.15). On the contrary, the decrease in u during shearing in the heavily overconsolidated case

was overestimated (Figure 8.19). None of the models was good at predicting the high initial soil stiffness (higher than for the compressive cases) observed in the three cases (i.e. normally consolidated, lightly and heavily overconsolidated). However, the Al-Tabbaa model was quite accurate in predicting the soil stiffness for strains above approximately -0.01.

It was noticed when analysing the results that a better approximation to the experimental observations was achieved for test USe6 if a preconsolidation pressure of 800 kPa was used instead of 1118 kPa. However and since the preconsolidation pressures for each test were known, these were maintained constant and equal to the experimental values during the simulations with SM2D.

The results obtained for tests Ko5 and Ko6 are more complicated and require further explanation. In test Ko5 (Figure 8.21) for example, the first runs to be performed (using Mohr-Coulomb, Al-Tabbaa and S-CLAY1) were stress controlled and p_c' was determined so that the axial strains during K_0-consolidation coincided with those measured in the laboratory as previously stated in Section 3.7.3. Under these conditions, the predicted behaviour during shearing was similar to that obtained experimentally, but the peak deviator stress was always overestimated. Something important to notice is the fact that due to the rotated yielding surface in the S-CLAY1 model, this predicts a q - p' path during undrained shearing in test Ko5 that deviates more from the experimental data than that of the Al-Tabbaa or Modified Cam-Clay models. Due to this, the pore water pressures during the undrained shearing stage were underestimated, with the overall trend being better reproduced by the Modified Cam-Clay and Al-Tabbaa models than by the S-CLAY1 model (Figure 8.23). The overall q - ε_a trend during both K_0-consolidation and shearing was better predicted by the S-CLAY1 model (Figure 8.22). The initial stiffness, however, was greatly overestimated by the S-CLAY1 model and tending to be underestimated by the Modified Cam-Clay and Al-Tabbaa models run under stress control.

The subsequent runs were performed under strain controlled conditions until achieving either the maximum axial strain ($\varepsilon_{a\ max}$) or the maximum mean effective stress (p'_{max}) values obtained during K_0-consolidation in the laboratory. The p_c' values were the same as those used for the stress controlled runs. It was observed that in order to achieve the p'_{max} obtained experimentally, the axial strains predicted by the model during one-dimensional consolidation were too small. Similarly but opposite, in order to fit the maximum axial strain, a greatly overpredicted final p' was required (Figure 8.21).

In all the runs involving strain control, the stress paths followed in order to maintain zero lateral strain did not coincide with the experimental K_0-path (e.g. Figures 8.21 and 8.22). Within the elastic zone, the stress path that maintains K_0 conditions presents a constant slope that is different from the experimental one and that depends on the soil Poisson's ratio according to equation.

$$\frac{\Delta q}{\Delta p'} = \frac{3 \cdot (1 - 2\upsilon)}{(1 + \upsilon)} \qquad \text{[Eq.8.1]}$$

If the straining continues beyond the elastic region then the plastic formulation controls the orientation of the stress path. Something similar occurs for the Al-Tabbaa model, but the unrealistic curvature in the stress path is smoothed due to elasto-plastic behaviour inside the bounding surface. If the p_c' value were to be modified for the different strain controlled runs, slightly better fits could be achieved, but never better than those obtained using the stress controlled option.

Based on the observations above, one may argue that using a smaller preconsolidation input pressure, individually established as it was done for the stress controlled analyses, should be used. Doing this, the elastic zone would be reduced and therefore the strains would increase during p'_{max} - controlled analyses. Similarly, the required p' during K_0-consolidation to reach the experimentally measured strains would decrease during $\varepsilon_{a\ max}$ - controlled analyses. This option was investigated, but although the reasoning above is correct, the prediction still diverged from the experimental results and still showed the drop in q due to the differences in stress ratio for the elastic and elasto-plastic regions of the K_0-path. Some of the preconsolidation pressure values may not even be sensible considered the stress history of the soil in the consolidation Device A. Just as an indication, some of the investigations made in this respect are illustrated in Figure 8.133. Values of p_c' equal to 240, 280, 300, 388 and 400 kPa were used.

Another option likely to reduce this unrealistic shape of the stress path for the strain-controlled runs was modifying the value of κ. Considering, for example the Modified Cam Clay model, it was observed in Section 8.2.6 that using $\kappa = 0.030$: (1) Induced too small $\varepsilon_{a\ max}$ in the analyses that were run specifying p'_{max} (see for example Figure 8.23) and (2) Gave rise to too large p' in those analyses where $\varepsilon_{a\ max}$ was specified (see for example Figure 8.21). In an attempt to improve these predictions and taking into account the relationship between p', κ and ε_a (Equation 2.5), higher values of κ were investigated for both cases ($\kappa = 0.032$, 0.034, 0.036, 0.038 and 0.040). The results are illustrated in Figure 8.134. Increasing κ allowed improving some of the fitting to the experimental data (see for example Figure 8.134(e) for $\kappa = 0.036$), but most of the model's predictions (e.g. q - p' behaviour during shearing and ε_a during K_0-consolidation) still diverged from the laboratory data.

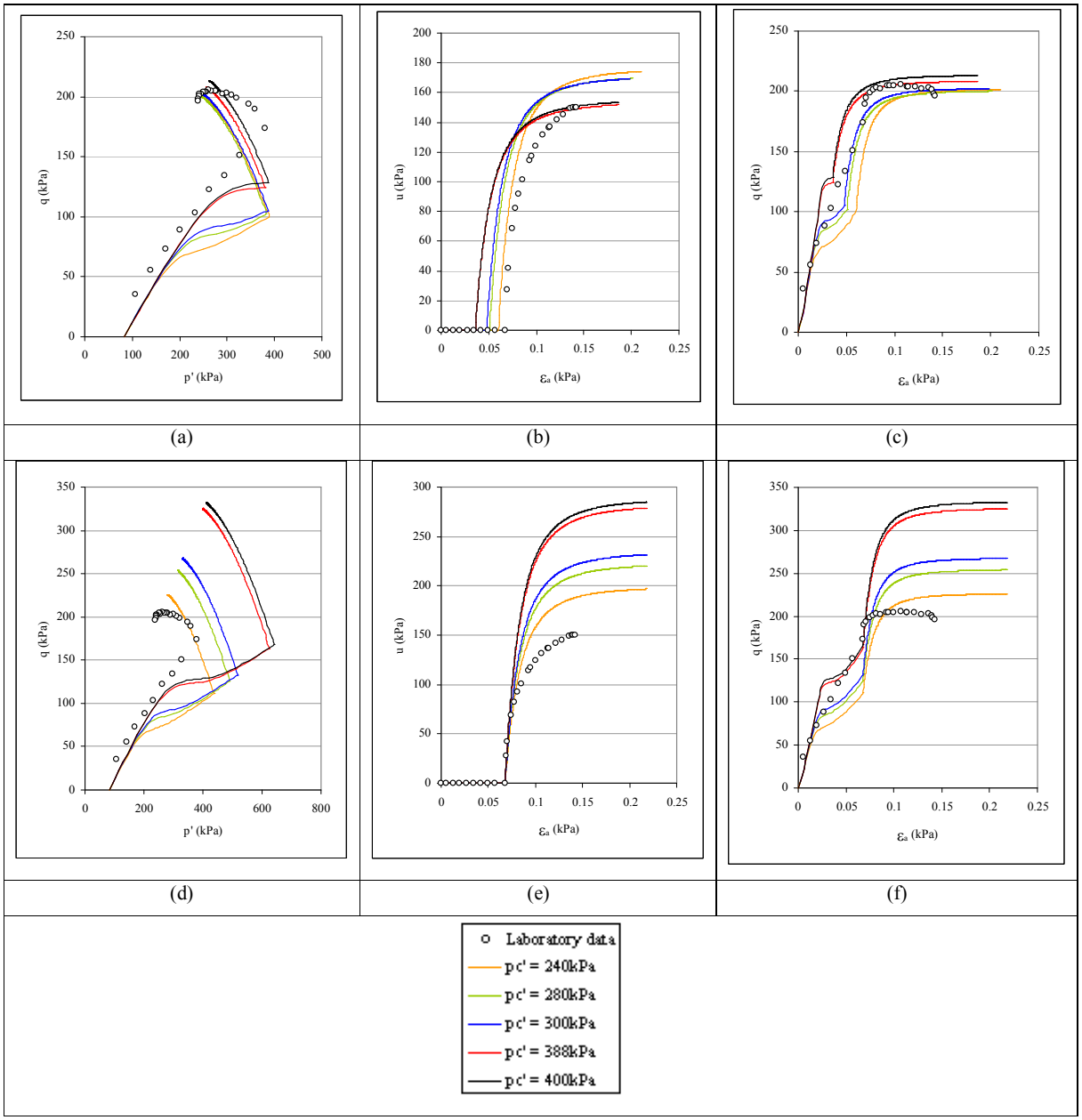

Figure 8.133. Al-Tabbaa predictions using SM2D for the behaviour of Speswhite Kaolin clay in test Ko5: (a,b,c) Using preconsolidation pressures of 1240, 280, 300, 388 and 400 kPa for analyses controlling p'_{max}; (d,e,f) Using the same preconsolidation pressures but for analyses controlling $\varepsilon_{a\ max}$

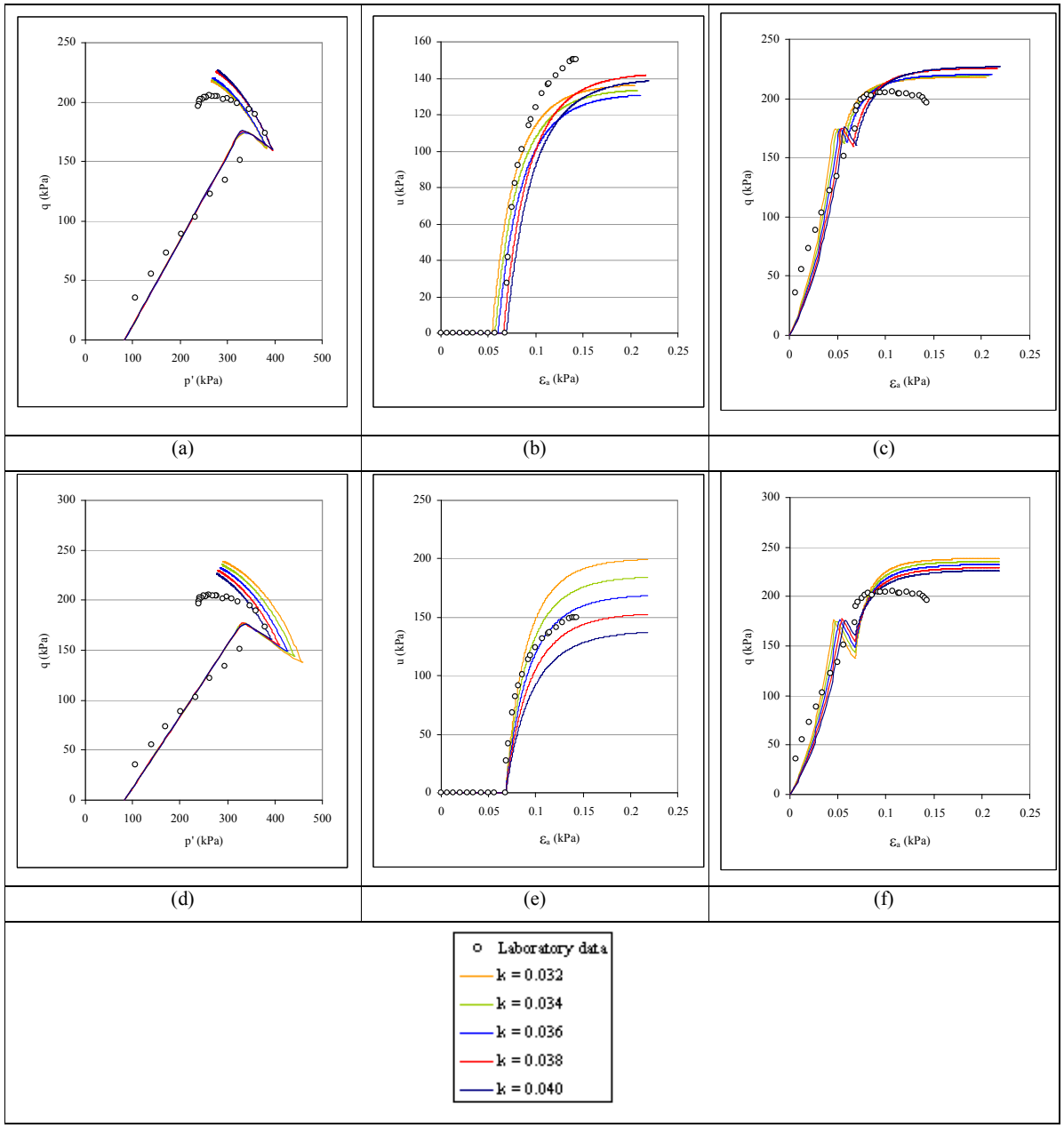

Figure 8.134. Modified Cam Clay predictions using SM2D for the behaviour of Speswhite Kaolin clay in test Ko5: (a,b,c) Increasing κ (0.032, 0.034, 0.036, 0.038, 0.040) for the analysis based on p'_{max}; (d,e,f) Increasing κ (0.032, 0.034, 0.036, 0.038, 0.040) for the analysis based on $\varepsilon_{a\,max}$

None of the runs, neither stress nor strain-controlled, using the experimentally obtained parameters, were found to be accurate in predicting peak q, u and stiffness changes during straining. The three stress-controlled predictions had, however, potential for improvement by using optimized parameters.

In test Ko6, similar trends were observed. Shearing in extension instead of in compression, however, became an additional issue in this particular case. The Modified Cam-Clay could not fit the experimental observations because of the long constant p' path predicted in the elastic region during unloading (Figure 8.25). The Al-Tabbaa model improved this situation, again due to the consideration of elasto-plastic unloading, but it was still far from closely reproducing the experimental curvature observed in the q - p' plane. As a result of this, q (being negative in this case) was greatly overpredicted in all the simulations. Since all the predicted effective stress paths during shearing were to the right of the total stress path, the models induced negative u when in fact these were found to be positive during the experiments (Figure 8.27). The S-CLAY1 model was found to slightly improve the predictions in terms of the q - p' path thanks to the rotated yield surface, but still overpredicted q in extension and could not simulate the correct u. In terms of stiffness, all the simulations were quite good in predicting the soil response for strains above -0.025 (some of them also from approximately -0.0125 to -0.0250), but could not cope with the high initial stiffness observed during the experiments. The fact that out of the soil models used none was found to be particularly suitable for this test, which more closely represents some of the likely conditions to be encountered in-situ during tunnelling (i.e. K_0-consolidated soils sheared in extension), was of particular relevance for the present investigation.

The sensitivity analyses carried out on tests USc7, USe5 and Ko6 allowed for more informed discussions with regard to the accuracy of the different models. These additional findings can be summarized as follows:

- As commonly stated by most researchers, the vast majority of constitutive models work better for normally isotropic consolidated specimens sheared in compression than in any other case. This was also observed during the present investigation with test USc7. The sensitivity analyses for the Modified Cam-Clay model, demonstrated that the initial predictions using experimentally obtained parameters could be further improved by modifying some of these. The observations were, however, not always sensible. For example, although the results were found not to depend too much on λ_{ic}, using a larger λ_{ic} value (0.195 instead of 0.180; Figures E.13 to E.16) was found to marginally improve the predictions. Considering such an increase would not be reasonable however given the small variation obtained in λ_{ic} during tests NCL1 and NCL2 (Section 6.2.3). The analyses were found to be quite sensitive to κ_{ic} (Figures 8.41 to 8.44). The problem with this parameter was that different optimum values were found for fitting the various relationships (e.g. 0.034 and 0.030 for the q - ε_a and u - ε_a relationships respectively). This means that modifying this value would help improving the prediction of

some of the patterns of soil behaviour, but would make others worse. The same happened with υ (Figures 8.45 to 8.48) and M (Figures D.17 to D.20), although for the latter a reduced M value (from 0.809 to 0.780) seems to improve the predictions. As for λ_{ic}, it would not make much sense modifying M so much from its experimentally obtained value. For the Al-Tabbaa model it was of interest to observe that both RVALU and XIVAL could be optimized (Figures 8.53 to 8.60). The following values were found to improve the predictions for the normally isotropic consolidated case sheared in compression in comparison to those proposed by Al-Tabbaa (1997) for Speswhite Kaolin clay:

RVALU: 0.16
XIVAL: 1.30

A setback, however, appears since even with these optimized values the initial stiffness of the soil during shearing was overestimated.

- For test USe5, the sensitivity analysis was performed on the Al-Tabbaa model parameters as this model was found to be most suitable for this particular test conditions. Similarly as for USc7, the parameters that mainly control the predicted behaviour were found to be κ_{ic}, *RVALU* and *XIVAL*. However, in this case, it was very difficult, if not impossible, to establish optimum values. The observed soil response could not be properly predicted in this case simply by optimizing some parameters, but changes in the formulation of the models would be required. For the axial E_{sec} - ε_a relationship, 'optimum' values were established for strains above -0.005 as follows: $\upsilon = 0.32$, $RVALU = 0.24$, $XIVAL = 1.5$. It should be noted that these values of *RVALU* and *XIVAL* are inconsistent with those previously established for tests USc7.
- The sensitivity to the various parameters used in the S-CLAY1 model was investigated using the experimental data from test Ko6 run under stress control. In this particular test the parameters that mainly control the outcome were found to be κ_0, υ, β, α, *and* μ. Again, as for test USe5, improving the prediction was very difficult. The curvature observed during undrained shearing in extension in the q - p' plane was only closely predicted by using a κ_0 value equal to 0.005 (Figure 8.61). The value of $\kappa_0 = 0.030$ used for the first runs was taken from the isotropically consolidated samples (κ_{ic}) and therefore the slope of the swelling lines of K_0-consolidated specimens could have been different from this. The value 0.005 seemed initially a bit low, however when compared to the results presented by Al-Tabbaa (1997) for example, who found κ_0 to be larger than κ_{ic}, this being also true for κ_0* and κ_{ic}*. The author found a value of κ* = 0.013 (similar to the value obtained in the present study were κ_{ic}* is equal to 0.017) to be appropriate if a single value was required to characterize the behaviour during both isotropic and one-dimensional unloading. Test SP3, performed at a later stage than

the conventional triaxial testing (Chapter 7), corroborated these observations since the values of κ_0 and κ_0* were established as 0.039 and 0.018 respectively. The value of $\kappa_0 = 0.005$ gave rise to a much better prediction of the initial soil stiffness magnitude (Figure 8.64), but did not help in simulating better overall q and u - ε_a responses (Figures 8.62 and 8.63).

Based on the sensitivity analysis II (tests USc9, USe3, USe6 and Ko5) the following additional observations were made:

- Little improvement could be achieved to the prediction of the experimentally observed soil behaviour during test USc9 by modifying some of the parameters to which the model had been found to be more sensitive to during the sensitivity analysis in test USe5. The parameter XIVAL was found to have a large effect on the model predictions (Figures 8.77 to 8.80).
- As for USc9, there was little room for improvement in tests USe3 and USe6. The initial stiffness of the soil was always underestimated (e.g. Figures 8.88 and 8.96).
- The fact that *RVALU* and *XIVAL* had a negligible effect on the results for test USe3 (Figures 8.85 to 8.92), in comparison to test USc7 which was also normally consolidated but sheared under compression, gave rise to an important observation. The preconsolidation pressure was specified in SM2D as $p_c' / 2$ for the Al-Tabbaa model. Since p_c' for tests USc7 and USe3 were 1021 kPa and 235 kPa respectively, $p_c' / 2$ was established as 511 kPa and 117 kPa respectively. Although the difference was small in both cases (511 kPa x 2 = 1022 kPa compared to 1021 kPa and 117 kPa x 2 = 234 kPa compared to 235 kPa), the initial stress state was situated inside and on the edge of the kinematic bubble for USc7 and USe3 respectively, and this was why the size of the bubble (i.e. the length of the initial elastic path) and also *XIVAL* was relevant in test USc7 but not in test USe3. If a $p_c' / 2 = 510$ kPa was used for USc7, *RVALU* and *XIVAL* did not have any effect either on the soil response.
- The sensitivity analyses carried out on test Ko5 for the Modified Cam-Clay, Al-Tabbaa and S-CLAY1 models indicated that kappa (either κ_0 or κ_0*) has a large effect on adjusting the soil initial stiffness response (e.g. Figures 8.108 and 8.116). For the three models, modifying some of the parameters would require varying p_c' in order to achieve correct axial strains during K_0-consolidation (e.g. Figures 8.106 and 8.107). Again, as in test Ko6, but for the Modified Cam-Clay model in this case, the prediction in terms of q - p' paths during shearing using the Al-Tabbaa model could be improved by using $\kappa_0 = 0.005$ (Figure 8.105). Improving the predictions obtained using Al-Tabbaa was more difficult than with the Modified Cam-Clay, mainly in terms of q - p' paths, although for the latter and as commented earlier the value of $\kappa_0 = 0.005$ was not considered sensible. The sensitivity analysis carried out on the S-CLAY1 model proved that, even by varying the soil parameters, the initial soil stiffness during the shearing stage continued being overestimated (e.g. Figure 8.128), the q - p' paths were far

from the experimental ones (e.g. Figure 8.129) (as for Al-Tabbaa) and the u response was poorly predicted (e.g. Figure 8.131).

Al-Tabbaa (1997) also compared her model´s predictions with her experimental results on Speswhite Kaolin clay. Direct comparison between Al-Tabbaa's findings and the present study is not straightforward due to the difference between the tests carried out in both studies. The best association can be made based on Al-Tabbaa's two undrained tests up to failure, one initiated from isotropic conditions and the other from one-dimensional conditions. Based on these, the author reported a good agreement between the predicted and the experimental response. This statement was rather vague, particularly based on the graphs presented. For example, for the one-dimensionally consolidated sample, a simulation reproducing exactly the same test conditions was not presented. Additionally, the results were also presented in terms of stress paths on the q - p' plane and shear strain contours only. The experimental and predicted data in terms of u and stiffness for instance were not presented. Since very limited data on undrained stress paths to failure had been obtained during Al-Tabbaa (1997)´s research, q - p' and strain contours data by Parry and Nadarajah (1973) were alternatively presented for both isotropic and one-dimensional cases. Such data showed many similarities with the predictions using the Al-Tabbaa model. A graph showing together both the experimental and the predicted results for the same (or very close) test conditions would have allowed a much better evaluation of the model though. The model predicts symmetrical stress paths for compression and extension for isotropically consolidated samples. This could not be investigated in detail by Al-Tabbaa either, because none of the samples during the study was brought to failure in extension. The accuracy of the model was therefore mainly evaluated by Al-Tabbaa based on results obtained during cyclic tests starting from different stress conditions and during isotropic and one-dimensional consolidation tests including various stages of unloading-reloading.

Wheeler et al. (2003) studied the accuracy of S-CLAY1 in predicting the yielding points and volumetric strains during drained stress paths at various values of stress ratio q/p' and found this to be better than the Modified Cam-Clay model, therefore demonstrating the success of incorporating the rotational component of hardening for the particular cases being analysed. This success was particularly true for reconstituted specimens where bonding and destructuration are absent according to Wheeler et al. (2003), since for natural soils the volumetric strains tended to be considerably underpredicted, this being most clearly shown for high values of stress ratio. Undrained shearing was not included in their experiments.

The S-CLAY1 model assumes isotropic elasticity inside the yield surface. Combining the rotational hardening in the S-CLAY1 model with the elasto-plastic unloading in the Al-Tabbaa model would probably help in improving the predictions in test Ko6, for example.

In order to achieve better predictions of soil stiffness at small strains, particularly for extension states, small-strain non-linearity should be also incorporated into the formulation. The accuracy of the Jardine et al. (1991) model in predicting the variation in soil stiffness at small strains will be evaluated in Chapter 9.

8.5. SUMMARY

In this chapter some of the conventional triaxial texts performed on reconstituted Speswhite Kaolin specimens and presented in Chapter 6 have been reproduced in SM2D using mainly the Modified Cam-Clay, Al-Tabbaa and S-CLAY1 models. Other more simple models have been also added for comparison. The performance of the three models has been evaluated based on the level of agreement between the experimental measurements and the numerical predictions. The assessment in this case has not taken into account on-sample strain measurements because these were not undertaken during 'conventional' triaxial testing. Sensitivity analyses have been also carried out in order to establish which parameters have a larger effect onto the models' predictions.

Chapter 9: EVALUATION OF SOIL CONSTITUTIVE MODEL PERFORMANCE FOR TUNNELLING INDUCED STRESS PATH TESTING

9.1. INTRODUCTION

This chapter evaluates the capacity of the Modified Cam-Clay, Al-Tabbaa, S-CLAY1 and Jardine models in simulating the response of Speswhite Kaolin clay (presented in Chapter 7) to tunnelling induced stress paths according to the methodology in Section 3.7.4. The results are discussed in Section 9.3. The comparison between the different models has been more visual, looking at the overall general trends, than actually quantifying the error between experimental and predicted values.

9.2. RESULTS

9.2.1. Crown of Single Tunnel. K_o<1 (Test SP1)

The Jardine et al. (1991) parameters used in SM2D for test SP1 were those specified in Section 7.6.2 - bullet point (6). The parameters used for the other constitutive models have been summarised in Table 9.1. Figures 9.1 to 9.4 show the predictions of the four models in comparison to the recorded laboratory data.

Table 9.1. Soil parameters for test SP1

ν	M	λ	λ^*
0.34	0.836	0.1565	0.0710
κ	κ^*	p'_c	
0.030	0.017	390	
RVALU	*XIVAL*	β	
0.2	1.5	0.8119	
μ	α	e_o	
75	0.260	1.3996	

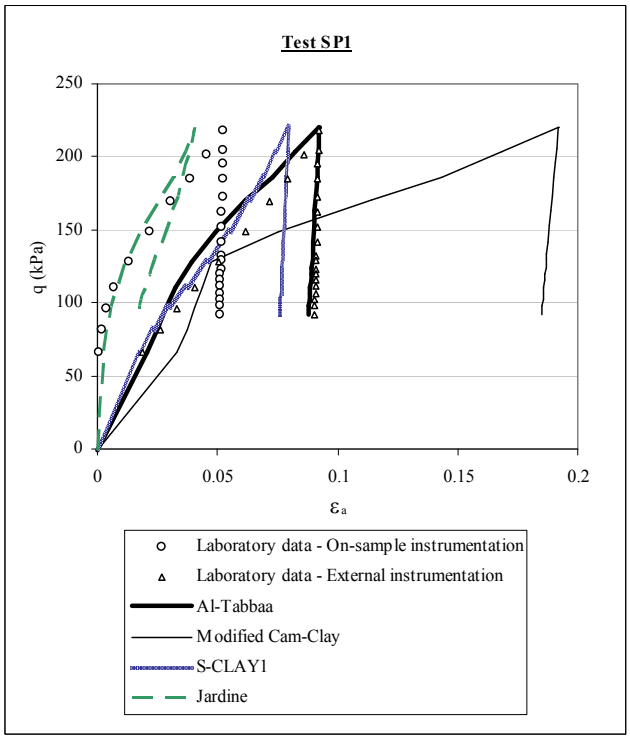

Figure 9.1. Measured versus predicted q - ε_a relationship during test SP1

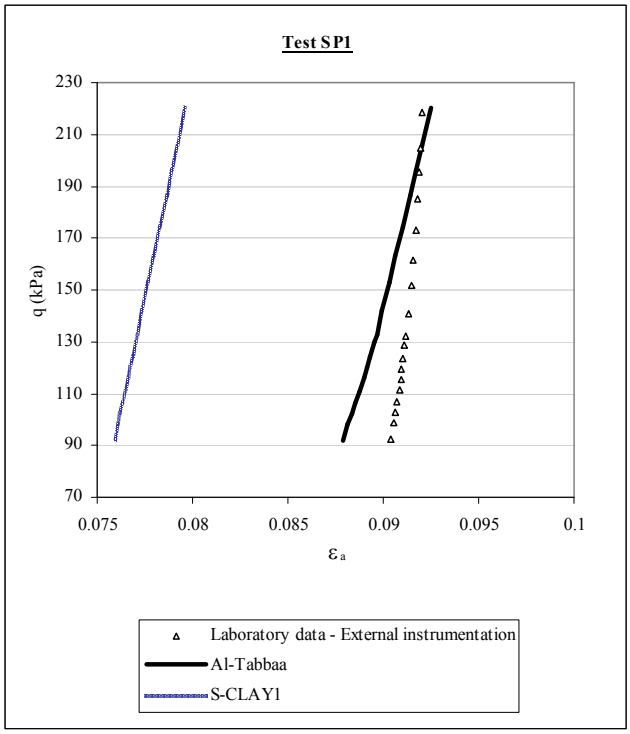

Figure 9.2. Measured versus predicted q - ε_a relationship during undrained shearing in test SP1

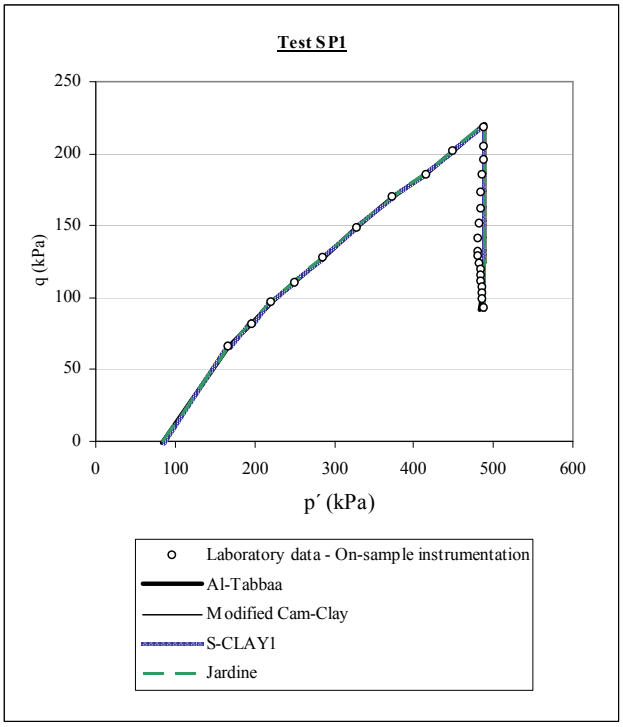

Figure 9.3. Measured versus predicted q - p' relationship during test SP1

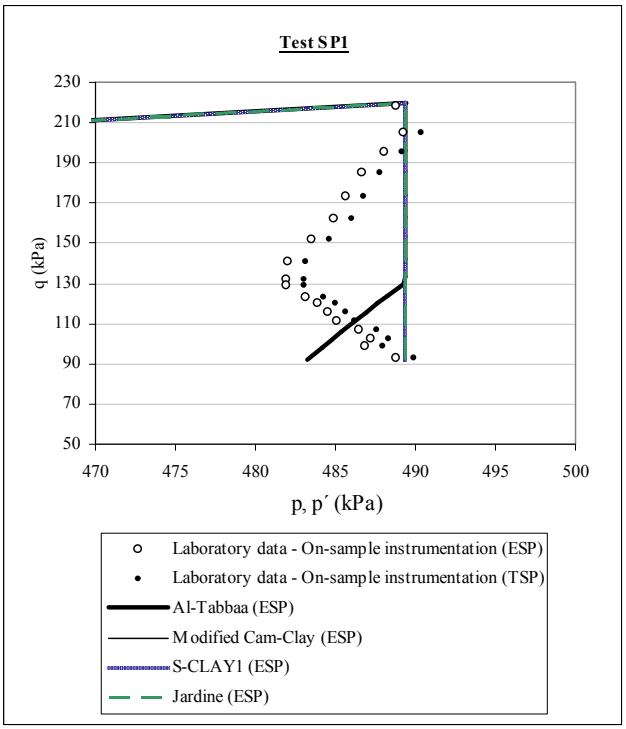

Figure 9.4. Measured versus predicted q - p, p' relationship during undrained shearing in test SP1

9.2.2. Springline of Twin Tunnels. K_o<1 (Test SP2)

The Jardine et al. (1991) parameters used in SM2D for test SP1 were those specified in Section 7.6.2 - bullet point (6). The parameters used for the other constitutive models have been summarised in Table 9.2, but only those that differ from the parameters in Table 9.1 have been given.

Table 9.2. Soil parameters for test SP2

M	β	α	e_o
0.823	1.1930	0.225	1.4518

Figures 9.5 to 9.8 show the predictions of the four models in comparison to the recorded laboratory data.

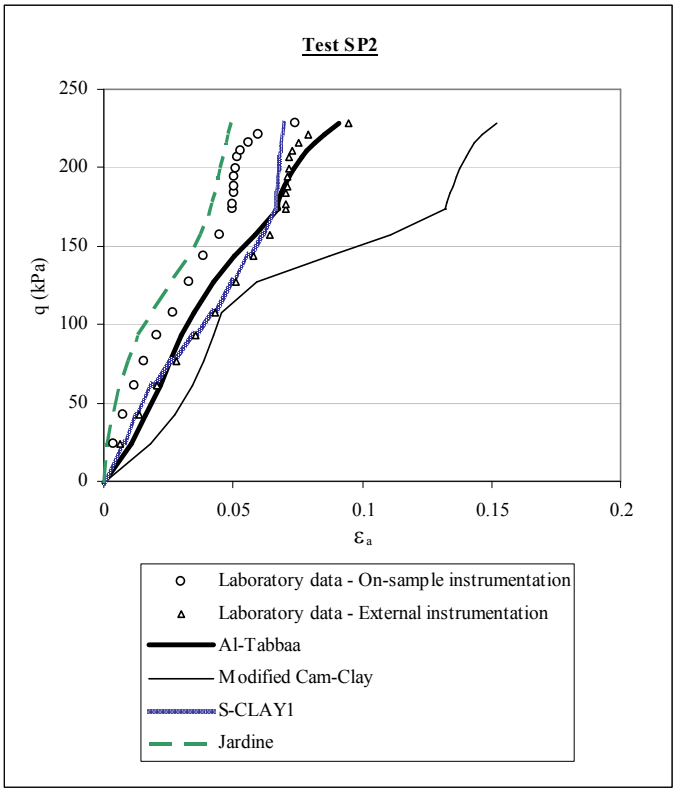

Figure 9.5. Measured versus predicted q - ε_a relationship during test SP2

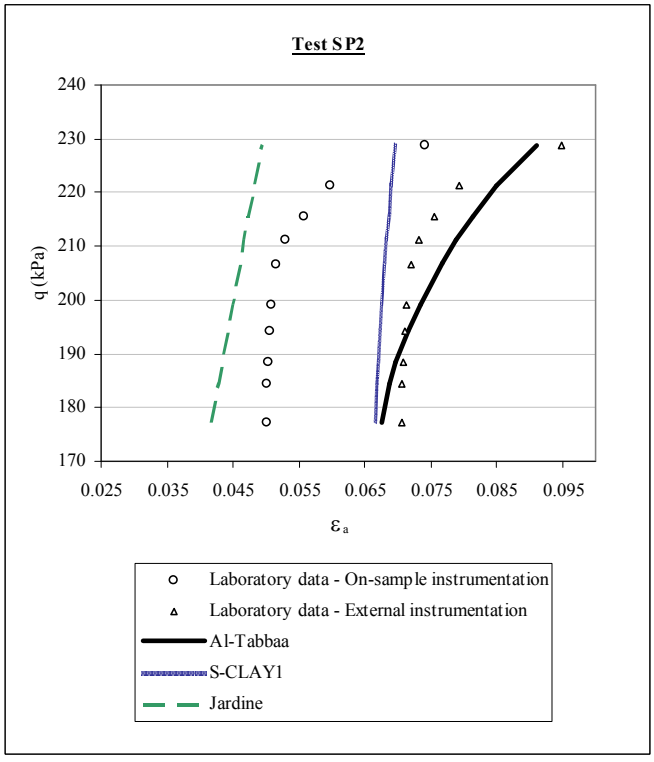

Figure 9.6. Measured versus predicted q - ε_a relationship during undrained shearing in test SP2

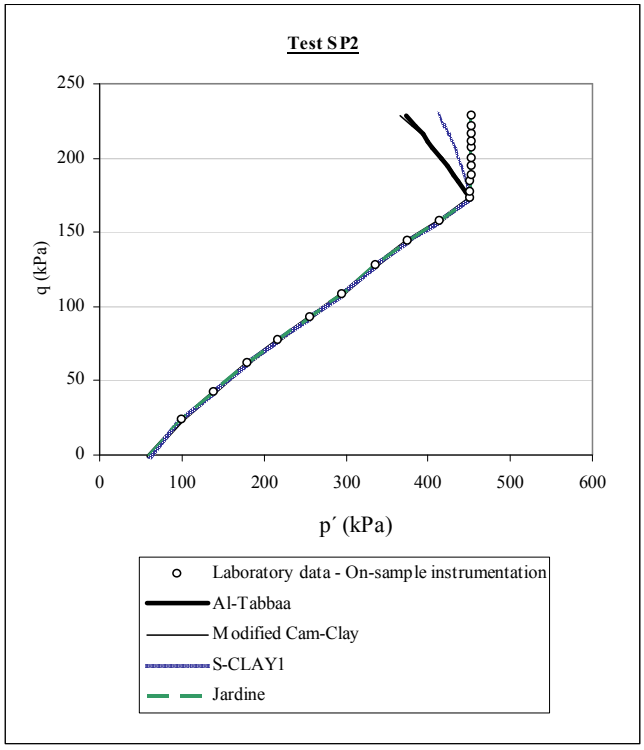

Figure 9.7. Measured versus predicted q - p' relationship during test SP2

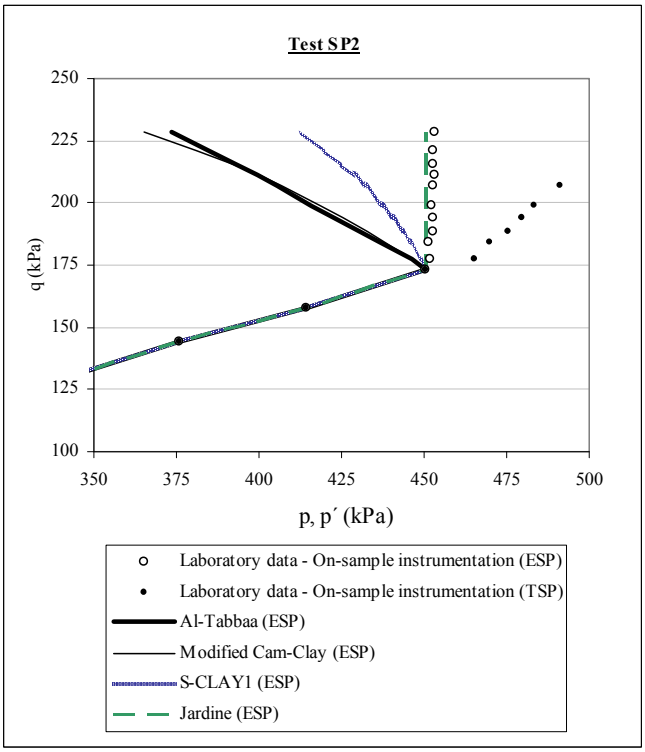

Figure 9.8. Measured versus predicted q - p, p' relationship during undrained shearing in test SP2

9.2.3. Crown of Single Tunnel. K_o>1 (Test SP3)

The Jardine et al. (1991) parameters used in SM2D for test SP1 were those specified in Section 7.6.2 - bullet point (6). The parameters used for the other constitutive models have been summarised in Table 9.3, but only those that differ from the parameters in Table 9.1 have been given.

Table 9.3. Soil parameters for test SP3

β	α	e_o
1.0720	0.338	1.3990

Figures 9.9 to 9.12 show the predictions of the four models in comparison to the recorded laboratory data.

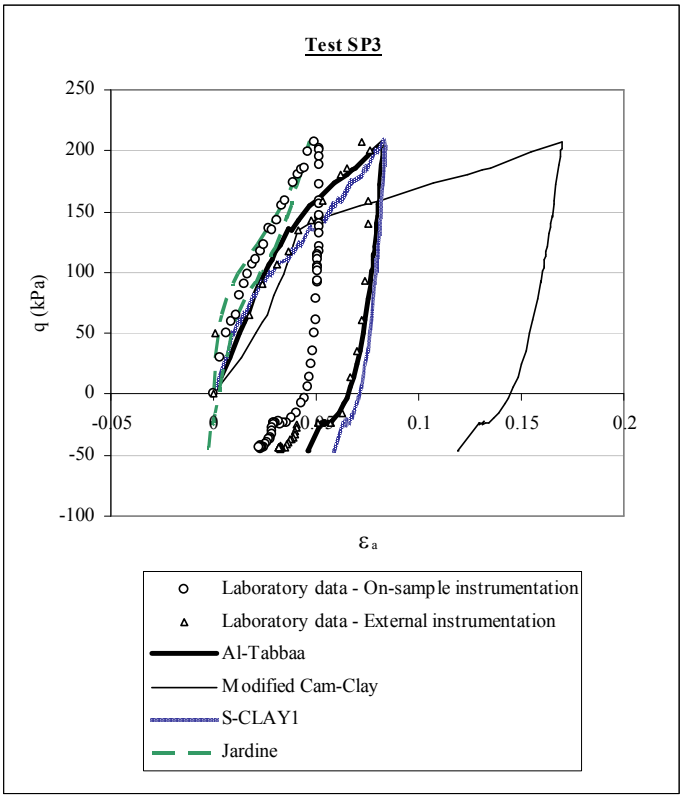

Figure 9.9. Measured versus predicted q - ε_a relationship during test SP3

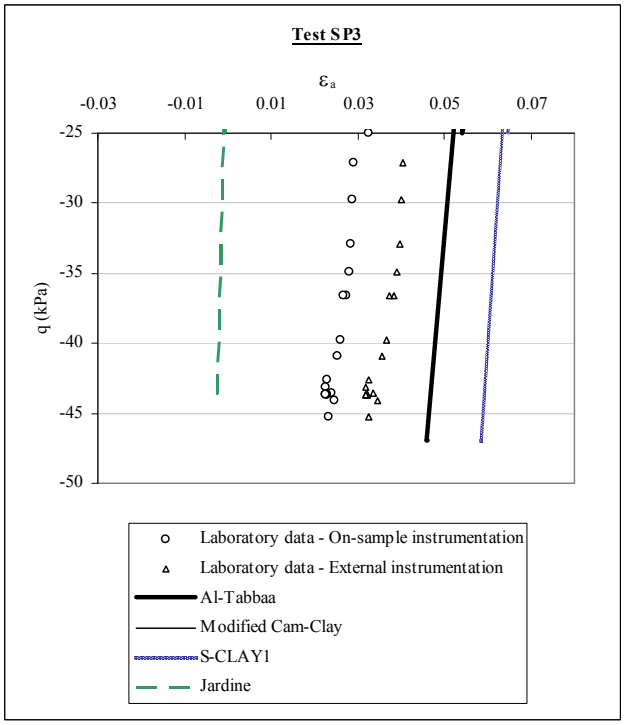

Figure 9.10. Measured versus predicted q - ε_a relationship during undrained shearing in test SP3

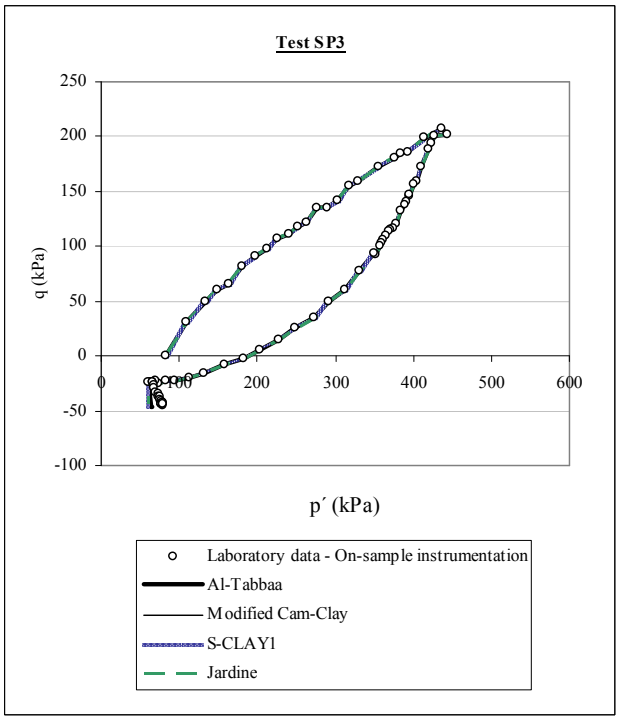

Figure 9.11. Measured versus predicted q - p' relationship during test SP3

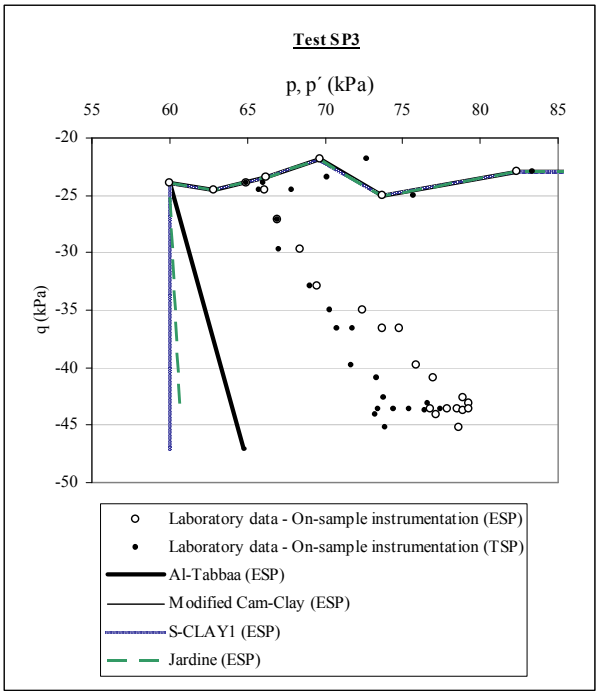

Figure 9.12. Measured versus predicted q - p, p' relationship during undrained shearing in test SP3

9.3. DISCUSSION

Some significant observations can be made based on the presented results. These have been summarised as follows:

- The Al-Tabbaa model is considerably successful in simulating the complete observed q - ε_a response in the laboratory (i.e. during K_0-consolidation and subsequent undrained shearing) when such strains are those measured using external instrumentation (Figures 9.1, 9.2, 9.5, 9.6, 9.9 and 9.10). The agreement achieved during K_0-consolidation (loading and unloading) is remarkable. The agreement is good with the external measurements and not with the on-sample readings because the model parameters were established in Chapter 6 from external LVDT's readings. In order to evaluate how close the predictions could be to the on-sample measurements, another set of critical state parameters would be therefore required. Only having these new parameters could this feature be completely assessed. It should be noted that the new set of parameters would differ from those currently found in the literature (e.g. Section 2.3.7) which are typically based on external measurements. Based on the currently available data, it has been found that the predictions can be made to agree better with the on-

sample strains if different p'_c values are used (e.g. 250 kPa instead of the 195 kPa specified in Table 9.1 for Test SP3). However, the necessary p'_c values would not be sensible given the initial consolidation history in the consolidation Device A.

- The S-CLAY1 model was also calibrated against external measurements. The S-CLAY1 model´s predictions have many similarities to those produced by the Al-Tabbaa model, but are generally worse (e.g. Figures 9.5 and 9.12), one of the reasons being the consideration of elastic behaviour within the yield surface.
- The Modified Cam-Clay model was also calibrated against external measurements. This model can predict the shape of the q - ε_a response during K_0-unloading and the given undrained shearing paths, but it greatly overpredicts the strains occurring during one-dimensional loading (Figures 9.1, 9.5 and 9.9) due to the fact that an average initial p_c' = 195 kPa is used and this model would need a higher value of p_c' for the same strain (refer to Tables 8.6 and 8.7 for example).
- The Jardine model is only moderately successful in simulating the complete observed q - ε_a response in the laboratory, with such strains being those measured using on-sample instrumentation. Unlike the Al-Tabbaa, Modified Cam-Clay and the S-CLAY1 models, the parameters for the Jardine et al. (1991) model were established for specific strain records based on on-sample measurements (Chapter 7). Due to this, this is the only constitutive model, out of the four investigated during this project, that fits well the on-sample strain response. However, and due to the reasons already discussed in Section 3.7.1 and Chapter 7, the overall performance can be (and is in this particular case) worse than that of the Al-Tabbaa and S-CLAY1 models. This relates to the fact that even though different sets of Jardine et al. (1991) parameters are required for different stress paths / test conditions, only one is selected during conventional modelling. At the end of Chapter 7, a unique set of parameters was specified to be used in SM2D despite the wide scatter observed from the various tests carried out in the laboratory (Section 7.6.2 - bullet point (6)). The shear parameters were obtained from PART 1 Test SP2. The volumetric parameters were obtained from K_0-loading Test SP1. Keeping this in mind it is obvious why the prediction of the soil response during K_0-consolidation in SM2D for test SP1 is better than the prediction of the soil behaviour during the undrained shearing part (Figure 9.1). Similarly, this helps to understand why the prediction of the soil response during one-dimensional consolidation in SM2D is worse for test SP2 (Figure 9.4) and even worse for test SP3, which includes a K_0-unloading part (Figure 9.7).

  Other difficulties observed when establishing the Jardine parameters in Chapter 7 are now clearly observed as well. Two examples of this are (1) the differences between measured and predicted behaviour at the end of the K_0-consolidation in test SP1 (Figure 9.1) and the fitting, also towards the end of the consolidation, of the Jardine et al. (1991) curve to the volumetric

experimental data (Figure D.93(b)), (2) the differences between measured and predicted soil behaviour at the end of the undrained shearing in test SP2 (Figure 9.5) and the fitting, also towards the end of PART 1, of the Jardine et al. (1991) curve to the shear experimental data (Figure D.77(b)). It should be noted however that some of these differences between measured and predicted behaviour during K_0-consolidation are not only due to the reasons given above but also due to the fact that the soil response in this case is also partially controlled by the shear parameters. In an attempt to prove the above points further, test SP1 was re-run in SM2D but using the specific Jardine shear parameters established for this test (Table 7.5) instead of using those from test SP2. This should theoretically improve the predictions but it was noted that the Poisson´s ratio became out of range during the iterative process and hence the program stopped running. This was sorted by introducing three new options in SM2D: (1) Resetting υ while keeping the E the same, (2) Resetting υ while keeping the G the same and (3) Resetting υ while keeping the K the same. If υ was negative, it was reset to zero. If υ was larger than or equal to 0.5, it was reset to 0.49. For case (3) for example, using the original value of K and the newυ, new values of E and G were then calculated. After sorting out this initial problem, which is a known limitation in the Jardine et al. (1991) model, it was identified, as expected, that the magnitude of the shear parameter C2 (i.e. 366) had a very large effect on the soil behaviour during K_0-consolidation and hence worsened the predictions during one-dimensional consolidation. The prediction of the q - ε_a response during the undrained paths was improved as expected. Figure 9.13 shows these observations.

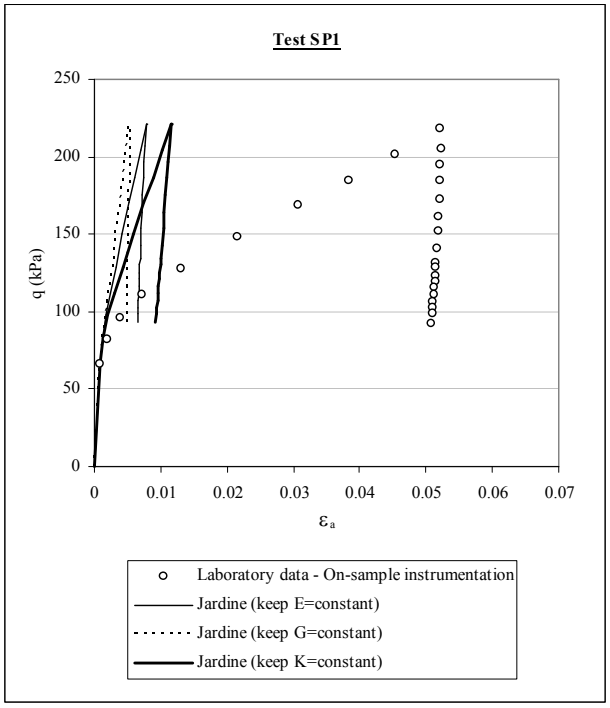

Figure 9.13. Measured versus predicted *q - p, p′* relationship during undrained shearing in test SP1 using shear and volumetric test-specific parameters from Table 7.5

- The accuracy of the predictions in the SM2D runs presented has been evaluated based on both the K_0-consolidation and the undrained shear stages. Despite the fact that some FEA include the stress history of the soil as one of the construction stages in order to obtain more accurate initial stress distributions, the large strains occurring during K_0-consolidation (i.e. formation of the soil) are not that relevant to tunnelling problems. It is the soil behaviour during excavation (typically in the small-strain range for points situated outside the vicinity of the excavation) that certainly matters. Based on this, one may argue that during the analysis of ´real´ engineering problems the Jardine model could produce more accurate results than some of the other models investigated, because of the way the parameters are calibrated in the small-strain range. This would be particularly true if the stress state is far from failure or yield as the effect of the small-strain stiffness is dominant in this case. The present findings show that this is not necessarily the case. The fitting to the experimental data corresponding to the undrained shear stages is not appreciably better than those achieved by the other models (e.g. Figure 9.6). In addition to this, it should be noted that even if the K_0-consolidation stage corresponding to the geological formation of the soil is ignored in the analysis, real life tunnel excavations are complex processes that can potentially include several drained and undrained stages and

abrupt changes in stress path direction. This would mean that the application of the Jardine model would be equally complex.

- The agreement between the models´ predictions and the experimental observations in terms of effective stresses during undrained shearing are generally poor. This is because for the same total stress path the experiment and the models do not agree in terms of whether the soil is already experiencing plastic strains or not. In test SP1 for example (Figure 9.3), all the models except Al-Tabbaa (for PART 2 because this is the only model that can predict elasto-plastic response inside the yielding surface) predict a pure elastic undrained path with constant p', when in fact the experimental path visibly deviates from the vertical solution despite being inside the yield surface. As an example, Figure 9.14 shows the movement of the inner bubble and the bounding surface in the Al-Tabbaa model during test SP1. The differences between prediction and measured can therefore be due to various reasons:
    - Perhaps the soil is behaving inelastically instead that purely elastically (i.e. elasto-plastic behaviour inside the yielding/bounding surface) as considered in the Al-Tabbaa model.
    - Perhaps the soil has an elastic response but although constant volume is assumed, and ensured in the model, some volume change occurred during the experiment that created the deviation from the numerical elastic effective path. Also the Skempton parameter B is considered to be equal to 1 in the models, but it is never this value during the laboratory tests.

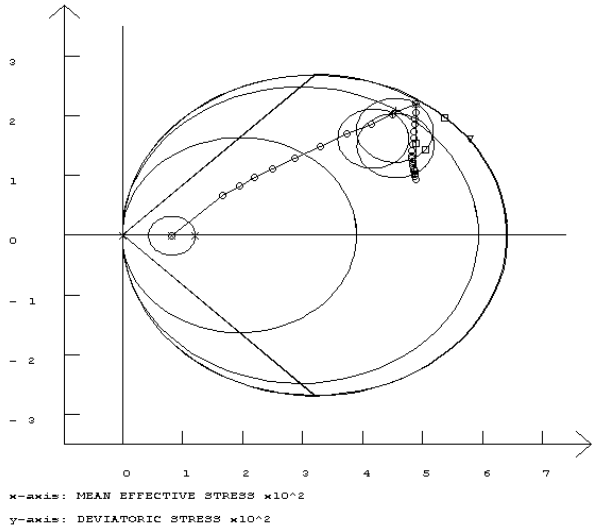

Figure 9.14. Movement of the inner bubble and the bounding surface in the Al-Tabbaa model during test SP1. The white dots correspond to the experimental data

In this sense it would be necessary to repeat the test before making any further judgements about the models.

In test SP2 (Figure 9.8), only the Jardine model simulates what seems to be an elastic response of the soil (i.e. p' = constant path) whereas all the other models definitely show some degree of plasticity, hence the curvature of the effective stress paths (see for example Figure 9.15 for the Al-Tabbaa model). In this case however, although the state of the soil just before undrained shearing was also on the yielding surface (as per SP1), plastic deformations were expected because the subsequent total stress path was directed to the outside of the yielding surface until reaching failure under compression. The experimental response doe not agree with conventional patterns of behaviour (e.g. Figure 8.21).

In test SP3 the initial soil state falls within the yielding surface. The experimental results in test SP3 deviate from pure elastic behaviour under undrained conditions, therefore presents some similarities to test SP1 (i.e. likely elasto-plastic response within the yielding surface). In this case the total stress path was indeed very close to the critical state line in extension therefore some sort of plastic response was less unexpected (see for example Figure 9.16 for the Al-Tabbaa model). In this case only the Al-Tabbaa model, and the Jardine model to some extent, manage to reproduce the tendency observed in the experimental effective stress path. It should be noted, however, that the models predict positive u whereas the experimental results indicate a reduction in u during extension at the tunnel crown. This does not occur for test SP1, also subjected to extension but starting from K_0<1 conditions (Figure 9.4).

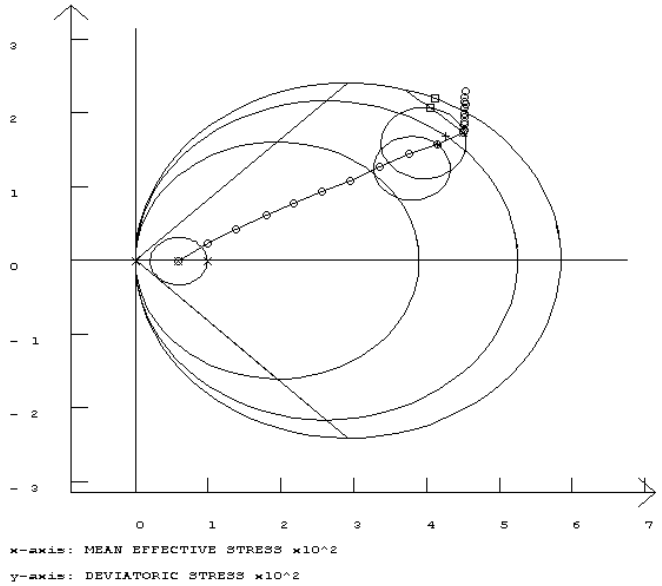

Figure 9.15. Movement of the inner bubble and the bounding surface in the Al-Tabbaa model during test SP2. The white dots correspond to the experimental data

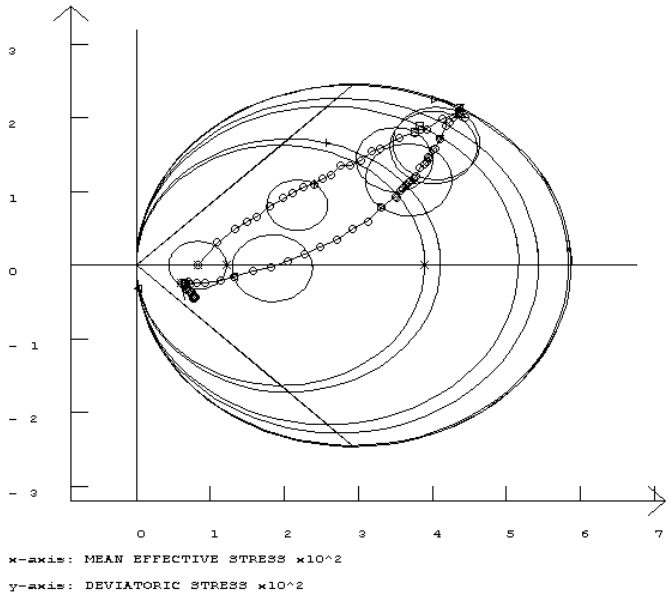

Figure 9.16. Movement of the inner bubble and the bounding surface in the Al-Tabbaa model during test SP3. The white dots correspond to the experimental data

- In relation to all these observations, the variation in stiffness during undrained shearing was also found not to agree well with the soil behaviour observed during laboratory testing. As an example, Figures 9.17 and 9.18 show the measured and predicted secant Young modulus during the undrained stress paths at the end of the K0-consolidation for tests SP1 and SP2. Only the results from the Al-Tabbaa, Modified Cam-Clay and S-CLAY1 models are shown. The predictions by the Jardine model are illustrated in Figures 9.19 and 9.20 against the on-sample strains rather than considering the external measurements. Both the S-CLAY1 and Modified Cam-Clay predict a constant Esec for test SP1, which is under extension. Due to the small magnitude of the increments in total stress during undrained shearing in test SP3, with considerable fluctuation (see Figures D.47 and D.52), the total stress paths defined in SM2D could not be based on these. The overall total stress increment (two steps from Table 7.1) had to be used to avoid the model not converging due to high sensitivity to data fluctuation. For this reason a figure showing the detailed variation of E with axial strain for test SP3 has not been shown in this chapter.

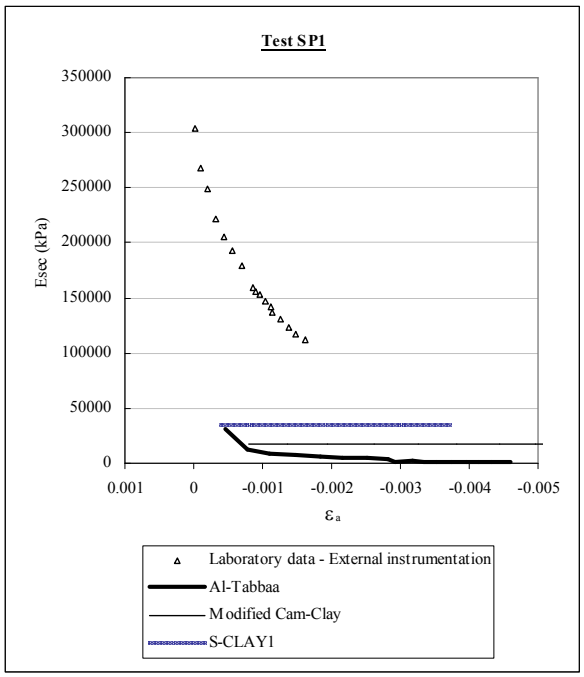

Figure 9.17. Measured versus predicted E_{sec} -ε_a relationship during undrained shearing in test SP1 for the Al-Tabbaa, MCC and S-CLAY1 models

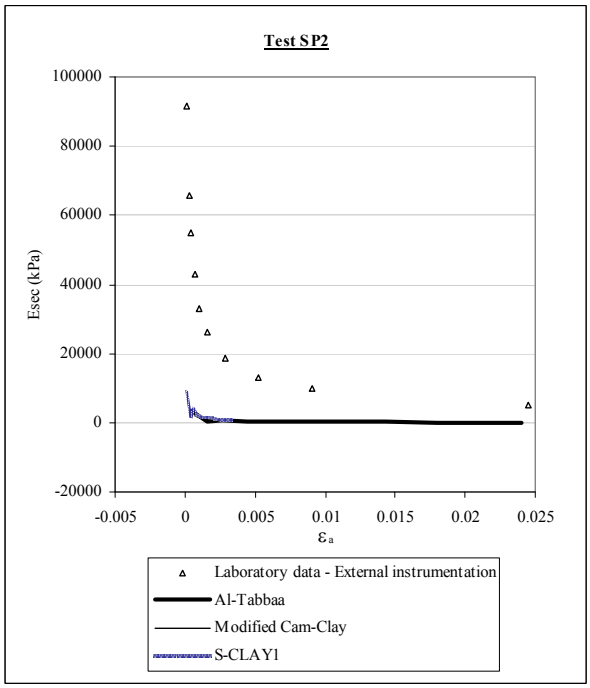

Figure 9.18. Measured versus predicted E_{sec} -ε_a relationship during undrained shearing in test SP2 for the Al-Tabbaa, MCC and S-CLAY1 models

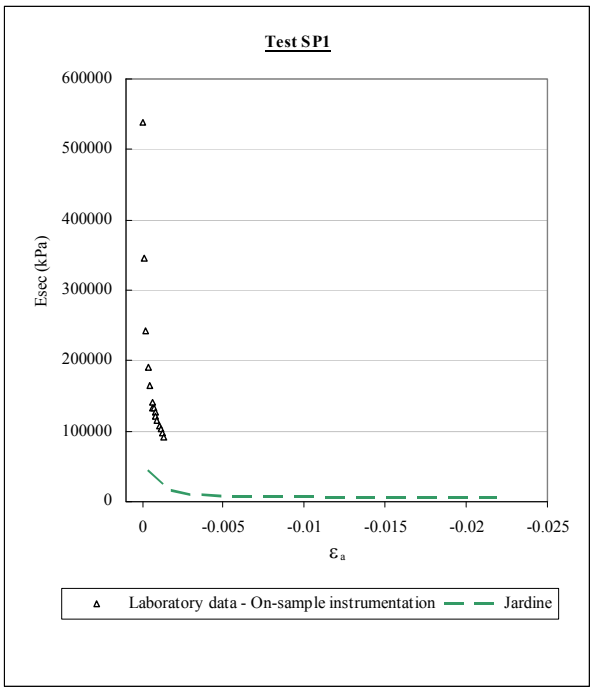

Figure 9.19. Measured versus predicted E_{sec} -ε_a relationship during undrained shearing in test SP1 for the Jardine model

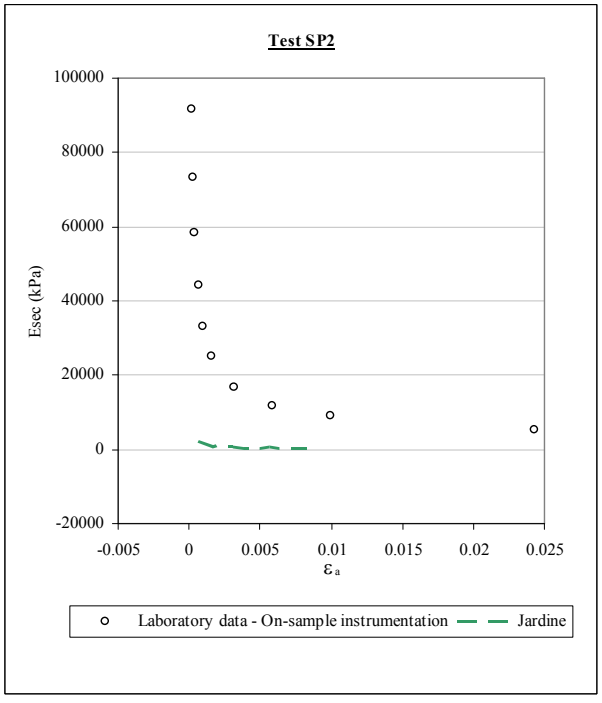

Figure 9.20. Measured versus predicted E_{sec} -ε_a relationship during undrained shearing in test SP2 for the Jardine model

- Based on the observations mentioned previously, there are various actions that could potentially improve the predictions achieved:
    - Including (if not available yet for the particular constitutive model) elasto-plasticity inside the yielding surface.
    - Introducing two additional terms in Equation 2.4 as indicated in Equation 9.1 so that the volumetric response (hence u) would also depend on the variation in q.

$$\begin{bmatrix} \delta\varepsilon_v^e \\ \delta\varepsilon_s^e \end{bmatrix} = \begin{bmatrix} \frac{1}{\mathrm{K}'} & J \\ J & \frac{1}{3G'} \end{bmatrix} \cdot \begin{bmatrix} \delta p' \\ \delta q \end{bmatrix} \qquad \text{[Eq.9.1]}$$

    - In particular, for the Al-Tabbaa model, modifying the size of the inner bubble in order to force the curvature of the stress path to match that observed experimentally.
    - Also, for the Al-Tabbaa model, introducing the small-strain concept inside the kinematic bubble in order to improve stiffness predictions.

9.4. SUMMARY

In this chapter some of the tunnelling-induced stress paths established in Chapter 4 and simulated in the laboratory (Chapter 7), have been reproduced in SM2D using the Modified Cam-Clay, Al-Tabbaa, S-CLAY1 and Jardine models. By comparing the intrinsic experimental observations with the numerical predictions, the capabilities of each of the models have been assessed. Stress paths representative of the various conditions (i.e. K_0 initial state and a soil element at either the tunnel crown or at the springline) have been selected for such purpose. Knowing the models' limitations already identified in Chapter 8, the present chapter has focused on tunnel-specific features, the relevance of accurately simulating the soil behaviour at small strains and on the implications of using either external or on-sample measurements for model calibration. Some suggestions have been given on how to improve the models' predictions.

Chapter 10: CONCLUSIONS AND SUGGESTIONS FOR FUTURE RESEARCH

10.1. INTRODUCTION

This thesis has combined four main topics: tunnelling, finite element analysis, advanced laboratory testing on stiff clay and constitutive modelling. The novelty in this project has consisted first of all in the way the four topics above have been combined in order to assess the suitability of four constitutive models for tunnelling problems, secondly on the inclusion of the S-CLAY1 model which has not been extensively validated to date, and finally, on the way that some aspects have been approached and presented (e.g. issues related to the preparation of reconstituted specimens, methodology for establishing the Jardine et al. (1991) small-strain parameters). All the aims and objectives listed in Section 1.2, motivated by an extensive review of related previous literature, have been successfully achieved. The main conclusions from this thesis are given in the following sections.

10.2. TOTAL STRESS PATHS DUE TO TUNNELLING

The 2D and 3D analyses presented in Chapter 4 were run using some of the constitutive models available in PLAXIS at the time and also the small-strain Jardine et al. (1991) model. Fifty-three analyses, not including the sensitivity analyses, were carried out. Despite the various variables involved in the different analyses, some clear trends in terms of total stress paths at the tunnel crown and springlines of a single tunnel (and also at the springline in between twin tunnels) were observed. The stress changes during the excavation of the tunnel itself were shown to be almost independent of the soil parameters used. However, the stress changes taking place during the placement of the lining were found to vary significantly mainly as a function of the lining parameters.

Although other observations (e.g. width of the surface settlement trough and magnitude of the settlements) were not validated, the overall soil response was reviewed in order to ensure that the main patterns were sensible.

Previously reported observations mainly in terms of heave observed for ground conditions with initial K_0>1 when ´too simplistic´ models are used were corroborated during the present analyses.

The predicted total stress paths at the crown and springline of a single tunnel were found to show a very repeatable trend. This consists of the slope of the σ_y / σ_x path during tunnel excavation decreasing for increasing K_0 initial values. In general, during excavation, the vertical stress reduces at the tunnel crown and increases at the tunnel springline while the horizontal stress tends to increase at the crown and decrease at the springline. The effects on the stress field created after the placement of the lining are more complex than this and mainly depend on the lining properties and the initial stress

state of the soil (i.e. K_0 value). The mechanisms occurring in PLAXIS (i.e. interactions between the soil and lining under specific K_0-conditions) that gave rise to the obtained stress paths have been illustrated and discussed.

The stress paths on a soil element in between twin tunnels seem to indicate that at that specific location the ground experiences something which is close to the effect at the springline of a single tunnel, but repeated twice.

10.3. RECONSTITUTED SAMPLES

A large number of the reconstituted samples prepared for the present investigation in consolidation Device A (purpose-built for this project) were thoroughly studied in order understand more about their properties, hence about their quality and that of the trimmed specimens. The results were presented in Chapter 5. This quality, despite being unique to the consolidation device and extrusion methods used for this project, could be potentially no different in substance from that of samples prepared by other researchers using similar methods worldwide. Some papers were found after the present observations that confirm this statement.

The initial belief that all the vertical stress applied onto the sample in the consolidation Device A was being transmitted to the soil gave rise to some misunderstandings in terms of the c_u, initial p' values measured in the triaxial cell and moisture contents. The results obtained did not seem to agree with what would be expected and with what had been reported by some previous researchers. This motivated a more in-depth investigation that proved that only a certain percentage of the stress being applied during one-dimensional consolidation was in fact reaching the soil. This was found to be due to (1) friction in the device and (2) the consolidation chamber length to diameter ratio. The percentage could be as low as 30% close to the base of the cell. This effect was found to improve slightly, but definitely not to completely disappear, if a cell of twice the diameter was used (i.e. 100 mm) instead of 50 mm.

The effect of this on the samples was found to be a non-homogeneous distribution of moisture content, and hence c_u and p', along their length. The moisture content was found to be minimum at the top, increasing towards the base and reducing at the very bottom. Measured c_u values using the Fall-cone Swedish test were found to agree very closely with such patterns. The c_u values obtained during UU triaxial testing were found to agree well with the fall-cone test measurements whereas the c_u values measured using a 12.7 mm hand vane were much lower.

Another effect of such a distribution of stresses within the samples was the appearance of a concave fabric, which again did not disappear when using a 100 mm diameter cell. These surfaces were observed in a Scanning Electron Microscope and the images taken have also been presented.

All these observations helped enormously in planning the subsequent triaxial and stress path tests and also in specifying the correct parameters and initial soil state during the numerical simulations in SM2D.

10.4. CRITICAL STATE PARAMETERS FOR SPESWHITE KAOLIN CLAY

All the specimens used for triaxial testing were trimmed from the middle-upper part of the reconstituted samples to avoid, as much as possible, some of the issues presented in the previous section. Even so, some effects were observed such as barrelling of the specimens during UU tests.

The critical state parameters obtained during the present investigation, and presented in Chapter 6, were found to agree well with previously reported data for other kaolin clays (i.e. within a similar range).

These preliminary triaxial tests were carried out, however, not only in order to find specific parameters for the soil used but also in order to learn how to carry out the tests in the most broad sense of the expression since training was not provided and there were no other researchers doing similar work at the time in the Department. There was also no previous experience in the Department with regard to the use of on-sample instrumentation and the execution of extension tests. In addition to this, the tests had to be planned not only in order to pursue the various objectives of the project but also so that the timing would fit with the purchase of new equipment. Acquiring new equipment was particularly important in order to produce results that were of comparable quality to those presented by other universities with broader experience in the field.

Chapter 6 therefore focused on the parameters obtained for the Speswhite Kaolin clay and also on the problems encountered and on the performance of the various equipment used.

The shortcomings came basically from two different sources. Firstly the poor state of the laboratory for a significant proportion of the research period. On-sample measurements require a highly controlled environment (i.e. controlled temperature, no vibrations) and this was not accessible until refurbishment took place in the laboratory. Secondly, the limitations of the equipment itself (new and old). The biggest lesson learned from the latter was the very poor performance of the GDS LVDT transducers for the measurement of radial strains. This was overcome by using the GDS Hall Effect devices. The performance of these was excellent, but they are very delicate and tend not to last very long based on the current experience. The numerous setbacks during this stage of the research restricted the number of tests that could be done. However the tests that were eventually conducted were of high quality.

Chapter 3 provided detailed guidance on how to perform tests that are not covered in the available standards (e.g. extension).

10.5. REPRODUCING TUNNELLING-INDUCED TOTAL STRESS PATHS IN THE LABORATORY

Six total stress paths were defined in order to be reproduced in the laboratory based on the stress trends observed in the PLAXIS analyses. These intended to reproduce not only the stress changes induced by tunnelling during excavation and lining placement, but also the geological formation of the soil. The latter consisted of either K_0-loading only (NC soil) or K_0-loading and unloading (OC soil). None of these tests considered creep at the end of the one-dimensional consolidation. For this reason, one additional test was proposed that considered creep in order to evaluate the effects of this on the soil behaviour during subsequent stress paths. All the tests took into account additional considerations such as the failure envelopes in compression and in extension for the particular Speswhite Kaolin clay and the capabilities and limitations of the equipment used. Axial and radial Hall Effect devices were used for the seven tests.

All the measurements in terms of q, p', ε_a, ε_r, u, ε_s, ε_v changes have been presented in Chapter 7. The differences between the axial deformations measured by the two Hall Effect devices have been also reported, which is unfortunately quite uncommon.

The dedication given in this thesis to the definition of a comprehensible methodology for the determination of the Jardine et al. (1991) parameters is of particular relevance. Despite some of the stress paths being too short given the precision of the equipment, the Jardine et al. (1991) small-strain parameters for both shear and volumetric behaviour could be successfully determined. These results were also presented in Chapter 7. The best laboratory results were used for such purpose. Whilst doing this, and also initially by examination of the model´s origin and formulation, many significant observations were made. The two main ones were as follows:

- The formulation of the model allows fitting a curve to all (or most) of the laboratory results for both the shear and the volumetric response, which makes this model theoretically more accurate than others (e.g. linear elasticity) in describing the variation of stiffness at small strains as observed in recent years for a variety of soils.
- However, the model, in its current state of development at least, is too crude to be able to be used in numerical analyses of geotechnical problems unless very refined techniques (both numerical and in the laboratory) are used.

The reasons for the latter conclusion are as follows:

Each stress path has been found to require a different set of parameters, particularly those involving sharp changes in stress direction. The shear behaviour of the soil is also very likely going to be different during certain undrained stress paths than during a combined shear-consolidation stage (e.g. K_0-consolidation). The same occurs in terms of the volumetric behaviour. As a result of these, unless accurate and representative stress paths are reproduced in the laboratory and unless the small-

strain parameters are changed during the analysis, which is quite unlikely in conventional practice, any similarity between real measurements and numerical predictions is more of a 'coincidence' than something with a theoretical basis.

10.6. EVALUATION OF THE CAPABILITIES OF THE MODIFIED CAM-CLAY, AL-TABBAA, S-CLAY1 AND SMALL-STRAIN JARDINE MODELS

A first stage looked at the capabilities of the Modified Cam-Clay, Al-Tabbaa and SCLAY1 models in reproducing the intrinsic behaviour of Speswhite Kaolin clay during conventional triaxial testing. The S-CLAY1 model was relatively new and its validity had not been extensively proved to date. The results for this stage were presented in Chapter 8. A second stage looked at the same, but with regard to the soil behaviour monitored during some representative tunnelling stress paths presented in Chapter 7. The Jardine et al. (1991) model was added and evaluated at this stage because on-sample small-strain measurements were available from the tunnelling induced stress path tests. The results for this second stage were presented in Chapter 9. All the comparisons between the models' predictions and the experimental data were made using the soil model testing program SM2D.

The main conclusions from the first stage were as follows:

- The Modified Cam-Clay model is suitable for modelling normally consolidated Speswhite Kaolin clay sheared in compression and in extension from an isotropically consolidated state. The model´s predictions are still acceptable for lightly overconsolidated clay sheared in compression, but these worsen when the lightly overconsolidated Speswhite Kaolin clay is sheared in extension.
- The behaviour of lightly isotropically overconsolidated clay during both compression and extension is simulated slightly better by the Al-Tabbaa model, but the error is still significant, particularly for the extension case.
- The behaviour of heavily isotropically overconsolidated Speswhite Kaolin clay sheared in extension was not closely simulated by the Modified Cam-Clay and the Al-Tabbaa models, with again the Al-Tabbaa model being only slightly more accurate.
- The prediction of the secant Young modulus during shearing was acceptable in compression for both the Modified Cam-Clay and the Al-Tabbaa models, but far from the experimental results when the specimens were sheared in extension.
- Stress control has to be used for the specimens consolidated under K_0-conditions in order to achieve a realistic path during one-dimensional consolidation.
- None of the three models managed to match closely the experimental observations made when subjecting one of the normally K_0-consolidated specimens to undrained shearing under compression. The curvature of the effective stress path was not properly followed since the pore water pressures were underpredicted. This was worst for the S-CLAY1

model due to the curvature of the yielding surface. The Al-Tabbaa and S-CLAY1 models did not improve significantly the predictions given by the simpler Modified Cam-Clay.

- The three models were also not particularly good when shearing in extension after one-dimensional consolidation, although the S-CLAY1 model shown slightly improved capabilities in following the experimental curvature in the q - p' plane. The rotation of the yielding surface proved to be of help in this case.
- Again the simulation of the stiffness of the soil during shearing is better in compression than in extension in the case of K_0-consolidated soil.
- The models showed high sensitivity to the following parameters: the slope of the loading-unloading lines in either the lnv - lnp' space or the v - lnp' space (for the three models), υ (for the Modified Cam-Clay and mainly), $RVALU$ and $XIVAL$ (for the Al-Tabbaa model) and β (for S-CLAY1). It was impossible, however, to find a set of adjusted parameters that managed to improve the predictions as a whole. Attaining a good fit to some of the soil features observed means, at least at the moment, worsening the predictions when the soil is tested under different conditions.

The main conclusions from the second stage were as follows:

- Since the Al-Tabbaa model was calibrated against external deformation measurements, the model did not fit, as expected, the on-sample soil response. However, the Al-Tabbaa model predicts very well the stress - strain behaviour during K_0-loading and unloading if considering the strains measured by external instrumentation in the laboratory. The Al-Tabbaa's model predictions in this respect were better than those achieved by the S-CLAY1 model.
- The overall experimental axial strains during undrained tunnelling stress paths were reasonably well predicted by the Al-Tabbaa model, again with such strains corresponding to external measurements.
- In order to evaluate how close the Al-Tabbaa model's predictions could be to the on-sample measurements, another set of critical state parameters would be required. Only having these new parameters could this aspect be completely assessed.
- Following the observations made in the previous sections regarding the capabilities of the Jardine et al. (1991) model, this part of the project did no more than corroborate the fact that this model is not necessarily better than the other models assessed herein, beyond the fact that it takes the small-strain concept into consideration and therefore can individually fit any stress-strain response at this level.
- Accurately reproducing the small and very-small strain behaviour of soils can indeed be relevant for some engineering problems. However, this should be treated with caution.

Although being concerned with strains at such levels can be seen as potentially bringing accuracy to our work, it can be criticised in relation to the degree of reliability associated with laboratory testing at that level of strain. The impact that specimen disturbances and variable testing methods have in the behaviour of soils has been reported on numerous occasions. It seems sensible to assume that such issues will have a much larger impact when intending to measure strains in the small and very-small ranges. In addition to this, the new generation of transducers are very sensitive, hence they do not only measure strains accurately but can also pick up on any other undesirable external effects (e.g. small vibrations, temperature fluctuation). Due to these, the author believes that at the moment, and at least for tunnelling problems, there are limitations within the models' formulations, other than the inclusion or non-inclusion of small-strain non-linearity, that need resolving more urgently.

The above observations imply that none of the models investigated has currently enough capabilities as to be used successfully in tunnelling problems, hence the poor predictions often encountered during design and research as reported in the literature. There are still large limitations in terms of predicting the behaviour of overconsolidated clay, in particular during extension paths. These limitations are fundamental to tunnelling problems and should be given priority alongside other improvements being made to the models before accurate predictions can be made. In addition, most models available have the basis of their formulation in laboratory testing that used external instrumentation. These models should be reviewed in the light of more recent observations, such as the ones presented herein. Based on the present results, the Al-Tabbaa model appears to be a model with high potential if some modifications are made in its formulation. The consideration of elasto-plasticity during both loading and unloading inside the bounding surface is a clear improvement with respect to the other models used in this project. This model has also the advantage that it is not extremely complex in its current form (i.e. just one additional bubble inside the bounding surface and not too many parameters required). The most immediate modifications should include:

- Tackling the behaviour of clays on the dry side of critical.
- Differentiating between compression and extension. This could be done along the lines of Grammatikopoulou et al. (2002).

Other potential improvements could come from:

- Incorporating the small-strain concept inside the elastic kinematic bubble.
- Coupling volumetric and shear behaviour.

This conclusion is obviously drawn on the basis of the presented results, which the author understands to be broad in terms of the variables taken into account (i.e. normally consolidated and overconsolidated states, isotropically and K_0-consolidated specimens, compression and extension states, stress paths for single tunnels and an attempt to reproduce those at the springline in between twin tunnels), but limited in number with respect to guaranteeing repeatability. Some of the tunnelling undrained stress paths were also very short hence potentially fairly sensitive to the accuracy of the volume/pressure controllers. As a result of this, some suggestions for future work are given below.

10.7. SUGGESTIONS FOR FUTURE RESEARCH

Based on the main findings presented previously, and following the same line of thoughts, the author would like to propose some opportunities for future research as follows:

- The present investigation has reported on non-homogeneities in the samples created during one-dimensional consolidation in a purpose-built device. Although some modifications to this apparatus were approached (e.g. methods of reducing internal friction and the effect of length to diameter ratio of the consolidation chamber), the device was kept unchanged for this study due to time constraints and also for repeatability. Future research could focus on studying various arrangements, evaluating the quality of the samples for each particular device, quantifying the individual limitations and perhaps proposing the most optimum alternative.
- In terms of stress path testing, it would be of interest to:
    - Reproduce exactly the same tunnelling induced stress paths followed during the present investigation on the same Speswhite Kaolin clay in order to evaluate the degree of repeatability and therefore the potential influence of the various triaxial and on-sample equipment, user and methodology.
    - Perform similar stress paths on the same material but going to higher pressures (this requires different equipment) in order to avoid being so close to the critical state line as in the present investigation for some of the tests (e.g. SP3 and SP4).
    - Perform similar tests but including an additional K_0-loading stage as part of the geological history of the soil (i.e. loading - unloading - reloading).
    - Carry out supplementary research in terms of the effects of creep on the soil behaviour when subjected to stress paths similar to the ones followed in the present investigation. It should be noted that in this thesis only one of the tunnelling induced stress paths considered creep at the end of the K_0-stage (test SP1-c).
    - Test other clays in order to confirm the applicability of including some of the present observed features in the constitutive models´ formulations.

- Regarding the equipment used, further research should be carried out that would consider performing similar tests but using:
  - For example the Advanced Pressure/Volume GDS controllers that have a higher resolution (0.1 kPa instead of 1 kPa).
  - On-sample instrumentation of higher accuracy.
  - A mid-probe water pressure cell in order to double-check homogeneity within the specimen at all times during testing and to avoid end effects.
- Further development is required if the GDS LVDT´s (or a similar device) wants to be used on a normal basis for the measurements of radial deformations on-sample.
- On the subject of the Jardine et al. (1991) small-strain parameters, it could be investigated whether the equations that have been found to fit the experimental stress-strain data presented in this thesis (e.g. Chin´s method) also fit the new data.
- Four constitutive models were selected for the present research: Modified Cam-Clay, Al-Tabbaa, S-CLAY1 and Jardine et al. (1991). Future research could look at the capabilities of other models such as, for example, those formulated by Stallebrass and Taylor (1997) and Rouainia and Wood (2000). The effects of considering inherent anisotropy in the formulation could be also investigated.
- An obvious opportunity for future investigation would consist of taking the data presented in this thesis, and, if possible, some additional data as indicated above for further validation, and make the necessary modifications to some or all of the four selected models so that their predictions match better the experimental observations.

The author of this thesis hopes that this and future assessments on the performance of current constitutive models add to our understanding on soil behaviour hence offering a chance for further improvement of our predictive tools.

REFERENCES

Addenbrooke, T.I. (1996) Numerical analysis of tunnelling in stiff clay. **PhD Thesis**. Imperial College of Science Technology and Medicine. University of London.

Addenbrooke, T.I. and Potts, D.M. (1996) Twin tunnel construction - Ground movements and lining behaviour. **International Symposium on Geotechnical Aspects of Underground Construction in Soft Ground**. 441 - 446.

Addenbrooke, T.I. Potts, D.M. and Puzrin, A.M. (1997) The influence of pre-failure soil stiffness on he numerical analysis of tunnel construction. **Géotechnique**. Vol. 47. No. 3. 693 - 712.

Al-Tabbaa, A. (1987) Permeability and stress-strain response of Speswhite kaolin. **PhD Thesis**. University of Cambridge.

Amerasinghe, S.F. (1973) The stress-strain behaviour of clay at low stress levels and high overconsolidation ratio. **PhD Thesis**. University of Cambridge.

Anandarajah, A. and Zhao. D. (2000) Triaxial behaviour of kaolinite in different pore fluids. **Journal of Geotechnical and Geoenvironmental Engineering**. Vol. 126. No. 2. 148 - 156.

Atkinson, J.M. (1993) **An introduction to the mechanics of soils and foundations through critical state soil mechanics**. McGraw-Hill Book Co.

Atkinson, J.H. and Bransby, P.L. (1978) **The mechanics of soils. An introduction to critical state soil mechanics**. University Series in Civil Engineering. Mc.Graw Hill. NY. USA.

Atkinson, J.H. and Sallfors, G. (1991) Experimental determination of soil properties. **Proceedings of the 10th ECSMFE**. Florence. Vol. 3. 915 - 956.

Atkinson, J.M., Richardson, D. & Robinson, P.J. (1987) Compression and extension of K_0 normally consolidated kaolin clay. **Journal of Geotechnical Engineering**. Vol. 113. No. 12. 1468 - 1481.

Atkinson, J.H., Charles, J.A. and Mhach, H.K. (1990) Examination of erosion resistance of clays in embankment dams. **Quarterly Journal of Engineering Geology**. London. Vol. 23. 103 - 108.

Attewell, P.B. (1978) Ground movements caused by tunnelling in soil. **Proceedings of the Conference on Large Ground Movements and Structures**. Cardiff. Geddes (ed). Pentech Press. London. 812 - 948.

Attewell, P.B. and Farmer, I.W. (1974) Ground deformations resulting from shield tunnelling in London Clay. **Canadian Geotechnical Journal**. Vol. 11. No. 3. 380 - 395.

Attewell, P.B., Yeates, J. and Selby, A.R. (1986) **Soil Movements Induced by Tunnelling and their Effects on Pipelines and Structures**. Methuen, Inc., NY.

Augarde, C.E., Burd, H.J. and Houlsby, G.T. (1995) A three-dimensional finite element model of tunnelling. In: Pande, G.N., Pietruszczak, S. (eds.). **Numerical Models in Geomechanics. NUMOG V**. Balkema. 457 - 462.

Baldi, G., Hight, D.W. and Thomas, G.E. (1988). A reevaluation of conventional triaxial test methods. In: Robert T. Donaghe, Ronald C. Chaney and Marshall L. Silver (eds.). **Advanced Triaxial Testing of Soil and Rock**. ASTM STP 977. Philadenphia. 219 - 263.

Barla, M. (1999) Tunnels in swelling ground. Simulation of 3D stress paths by triaxial laboratory testing. **PhD Thesis**. Politecnico di Torino.

Bernat, S., Campou, B. and Dubois, P. (1999) Assessing a soft soil tunnelling numerical modelling using field data. **Géotechnique**. Vol. 49. No. 4. 427 - 452.

Berre, T. (1982) Triaxial testing at the Norwegian Geotechnical Institute. **Geotechnical Testing Journal**. GTJODJ. Vol. 5. No. 1/2. 3 - 17.

Bishop, A.W. and Henkel, D.J. (1962) **The measurement of soil properties in the triaxial test**. Edward Arnold. London. Second Edition.

Bishop, A.W. and Wesley, L.D. (1975) A hydraulic triaxial apparatus for controlled stress path testing. **Géotechnique**. Vol. 25. No. 4. 657 - 670.

Bracegirdle, A. and Mair, R.J. (1996) A methodology for evaluating potential damage to cast iron pipes induced by tunnelling. In: Mair and Taylor (eds). **Geotechnical aspects of Underground Construction in Soft Ground**. Balkema. Rotterdam. 659 - 664

Brinkgreve. R.B.J., Bakker, K.J. and Bonnier, P.G. (2006) The relevance of small-strain soil stiffness in numerical simulation of excavation and tunnelling projects. **Proceedings for the 6th Erupean Conference on Numerical Methods in Geotechnical Engineering**. Schweiger, H.F. (ed.). Taylor & Francis Group. London. 133 - 139.

British Standard BS 1377-2:1990. Soils for civil engineering purposes. Classification tests.

British Standard BS 1377-7:1990. Soils for civil engineering purposes. Shear strength tests (total stresses).

British Standard BS 1377-8:1990. Soils for civil engineering purposes. Shear strength tests (effective stresses).

British Standard BS EN ISO 14688-2:2004. **Geotechnical investigation and testing - Identification and classification of soil. Principles for a classification** (AMD Corrigendum 16928).

British Standard BS: 1377-5: 1990. **Methods of test for soils for engineering purposes. Compressibility, permeability and durability tests.**

British Standard BS 5930:1999. **Code of practice for site investigation.**

Burland, J.B. (1990) On the compressibility and shear strength of natural clays. **Géotechnique**. Vol. 40. No. 3. 329 - 378.

Burland, J.B. and Symes, M. (1982) A simple axial displacement gauge for use in the triaxial apparatus. **Géotechnique**. Vol. 32. No. 1. 62 - 65.

Burland, J.B., Standing, J.R. and Jardine R.J. (2001) Building response to tunnelling. Volume 1: Projects and methods. **Case studies from construction of the Jubilee Line Extension.** London.

Burland, J.B., Rampello, S., Georgiannou, V.N. et al. (1996) A laboratory study of the strength of four stiff clays. **Géotechnique**. Vol. 46. No. 3. 491 - 514.

Burns, B. (2006) Internal erosion of earth embankments. **PhD Thesis**. University of Birmingham.

Callisto, L. and Rampello, S. (2002) Shear strength and small-strain stiffness of a natural clay under general stress conditions. **Géotechnique**. Vol. 52. N0. 8. 547 - 560.

Chan, A.H.C. (2006) **User manual for SM2D - Soil Model Tester for 2-dimensional application**. School of Civil Engineering. University of Birmingham.

Chan, A.H.C. (2007) **User manual for SM2D - Soil Model Tester for 2-dimensional application**. School of Civil Engineering. University of Birmingham.

Chandler, R.J., Willis, M.R., Hamilton, P.S. et al. (1998) Tectonic shear zones in the London Clay Formation. **Géotechnique**. Vol. 48. No. 2. 257 - 270.

Chapman, D.N., Rogers, C.D.F. and Hunt, D.V.L. (2004) Predicting the settlements above twin tunnels constructed in soft ground. **Proceedings of the 30th ITA-AITES World Tunnel Congress**. Singapore. Vol. 19. No. 4 - 5.

Chin, F.K. (1978) Diagnosis of pile condition. **Geotechnical Engineering Journal**. Vol. 9. 85 - 104.

Clayton, C.R.I. and Heymann, G. (2001) Stiffness of geomaterials at very small strains. **Géotechnique**. Vol. 51. No. 3. 245 - 255.

Clayton, C.R.I. and Khatrush, S.A. (1986) A new device for measuring local axial strains on triaxial specimens. **Géotechnique**. Vol 36. No. 4. 593 - 597.

Clayton, C.R.I., Hight, D.W. and Hopper, R.J. (1992) Progressive destructuring of Bothkennar clay: implications for sampling and reconsolidation procedures. **Géotechnique**. Vol. 42. No. 2. 219 - 239.

Clayton, C.R.I., Theron, M. and Best, A.I. (2004) The measuremtn of vertical shear-wave velocity using side-mounted bender elements in the triaxial apparatus. **Géotechnique**. Vol. 54. No. 7. 495 - 498.

Clough, G.H. and Leca, E. (1989) Model and design method with focus on use of finite element methods for soft ground tunnelling. Review paper. In: **Tunnels et Micro-tunnels en Terrain Meuble du Chantier à la Théorie**. Presse de l' Ecole Nationale des Ponts et Chaussées. Paris. 531 - 573.

Coatsworth, A.M. and Hobbs, N.B. (1984) Computer-controlled triaxial soil testing equipment in a commercial laboratory. **Ground Engineering**. Vol. 17. No. 7. 19 - 23.

Cooke, R.W. and Price, G. Horizontal inclinometers for the measurement of vertical displacement in the soil around experimental foundations. In: Field Instrumentation in Geotechnical Engineering. Butterworths. London. 112 - 125.

Cooper, M.L. (2001) Tunnel-induced ground movements and their effects on existing tunnels and tunnel linings. **PhD Thesis**. University of Birmingham.

Cooper, M.L., Chapman, D.N. and Rogers, C.D.F. (2002) Prediction of settlement in existing tunnel caused by the second of twin tunnels. **Transportation Research Record. Design of Structures**. No. 1814. 103 - 112.

Cording, E.J. and Hansmire, W.H. (1975) Displacements around soft ground tunnels. **Proceedings of the 5th Pan-American Conference on Soil Mechanics and Foundation Engineering**. Buenos Aires. Vol. 4. 571 - 633.

Costa Filho, L de M. (1985) Measurement of axial strains in triaxial tests on London Clay. **Geotechnical Testing Journal**. American Society for Testing and Materials. Vol. 8. No. 1. 3 - 13.

Cotecchia, F. and Chandler, R.J. (1997) The influence of structure on the pre-failure behaviour of a natural clay. **Géotechnique**. Vol. 47. No. 3. 523 - 544.

Craig, R.F. (1992) **Soil Mechanics**. Chapman and Hall (eds). Fifth Edition.

Cuccovillo, T. and Coop, M.R. (1997) The measurement of local axial strains in triaxial tests using LVDT´s. **Géotechnique**. Vol. 47. No. 1. 167 - 171.

Dafalias, Y.F. (1975) On cyclic and anisotropic plasticity: (i) A general model including material behaviour under stress reversals, (ii) Anisotropic hardening for initially orthotropic materials. **PhD Thesis**. University of California. Berkeley.

Dasari, G.R. (1996) Modelling the variation of soil stiffness during sequential construction. **PhD Thesis**. University of Cambridge.

Dean, A.P. and Basset, R.H. (1995) The Heathrow Express Trial Tunnel. **Proceedings of the Institution of Civil Engineers**. Geotechnical Engineering. Issue 113. 144 - 156.

Dimmock, P.S. and Mair, R.J. (2007) Estimating volume loss for open-face tunnels in London Clay. **Proceedings of the Institution of Civil Engineers**. Geotechnical Engineering 160. Issue GE 1. 13 - 22.

Doran, I.G., Sivakumar, V., Graham, J. et al. (2000) Estimation of in situ stresses using anisotropic elasticity and suction measurements. **Géotechnique**. Vol. 50. No. 2. 189 - 196.

Doroudian, M. and Vucetic, M. (1995) A direct simple shear device for measuring small-strain behavior. **ASTM Geotechnical Testing Journal**. Vol. 18. No. 1. 69 – 85.

Hall, E. H. (1879) On a new action of the magnet on electric currents. **Americal Journal of Mathematics**. Vol. 2. 287 - 292.

Eberhardt, E. (2001) Numerical modelling of three-dimension stress rotation ahead of an advancing tunnel face. **International Journal of Rock Mechanics and Mining Sciences**. Vol. 38. 499 - 518.

Eisenstein, Z. (1986) "The contribution of numerical analysis to the design of shallow tunnels". In: Dungar and Studer (eds.). **Geomechanical Modelling in Engineering Practice**. Balkema. Rotterdam. 135 - 165.

Elmes, D. (1985) Creep and viscosity of two kaolin clays. **PhD Thesis**. Cambridge University.

Fannin, R.J. (1986) Geogrid reinforcement of granular layers of soft clay - a study at model scale and full scale. **D. Phil. Thesis**. Oxford University.

Fearon, R.E. and Coop, M.R. (2000) Reconstitution: what makes an appropriate reference material? **Géotechnique**. Vol. 50. No. 4. 471 - 477.

Franzius, J.N., Potts, D.M. and Burland, J.B. (2005) The influence of soil anisotropy and K_0 on ground surface movements resulting from tunnel excavation. **Géotechnique**. Vol. 55. No. 3. 189 - 199.

Garga, V.K. and Khan, M.A. (1991) Laboratory evaluation of K_0 for overconsolidated clays. **Canadian Geotechnical Journal**. Vol. 28. 650 - 659.

Ghaboussi, J. and Ranken, R.E. (1977) Interaction between two parallel tunnels. **International Journal for Numerical and Analytical Methods in Geomechanics**. Vol. 1. 75 - 103.

Ghaboussi, J., Ranken, R.E. and Karshenas, M. (1979) Analysis of subsidence over soft ground tunnels. **Proceedings of the International Conference on Evaluation and Prediction of Subsidence**. London. 182 - 196.

Grammatikopoulou, A. (2004) Development, implementation and application of kinematic hardening models for overconsolidated clays. **PhD Thesis**. Imperial College. University of London

Grammatikopoulou, A., Zdravkovic, L. and Potts, D.M. (2002) The effect of a kinematic yield surface on the predicted behaviour of an embankment. In: Pande, G.N., Pietruszczak, S. (eds.). **Numerical Models in Geomechanics. NUMOG VIII**. Balkema. 553 - 560.

Gue, S.S. (1984) Ground heave around driven piles in clay. **PhD Thesis**. Oxford University.

Guedes de Melo, P.F.M. and Santos Pereira, C. (2000) The role of the soil K_0 value in numerical analysis of shallow tunnels. **International Symposium on Geotechnical Aspects of Underground Construction in Soft Ground**. Fujita, Kusakabe and Miyazaki (eds.). Balkema. Tokyo. 379 - 384.

Hagiwara, T., Grant, R.J., Calvello, M. et al. (1999) The effect of overlying strata on the distribution of ground movements induced by tunnelling in clay. In: **Soils ans Fundations**. Japanese Geotechnical Society. Vol. 39. No. 3. June. 63 - 73.

Hansbo, S. (1957) A new approach to the determination of the shear strength of clay by the fall-cone test. **Swedish Geotechnical Institution Publications**. Vol. 14.

Hansbo, S. 1994. **Foundation Engineering**. Developments in Geotechnical Engineering. Elsevier. Vol. 75.

Hartkorn, P. (1997) High definition in-situ stress measurements in tunnelling. **International Journal of Rock Mechanics and Mining Sciences and Geomechanics**. Elsevier Science Ltd. Vol. 34. No. 3. Paper No. 123.

Hassal, S. and Rouainia, M. (2004) Finite element modelling of small strain soil behaviour. Application to tunnels. **12th Annual Conference. Association of Computational Mechanics in Engineering**. Cardiff. School of Engineering.

Hau, K. W. (2003) Application of a three-surface kinematic hardening model to the repeated loading of thinly surfaced pavements. **PhD thesis**. University of Nottingham.

Hight D.W. and Higgins, K.G. (1995) An approach to the prediction of ground movements in engineering practice: background and applications. In: S. Shibuya, T. Mitachi and S. Miura (eds.). **Pre-failure deformation of geomaterials**. Balkema. 909 - 945.

Hight, D.W., Gasparre, A., Nishimura, S. et al. (2007) Characteristics of the London Clay from the Terminal 5 site at Heathrow Airport. Géotechnique. Vol. 57. No. 1. 3 - 18.

Hight, D.W., Boese, R., Butcher, A.P. et al. (1992) Disturbance of the Bothkennar clay prior to laboratory testing. **Géotechnique**. Vol. 42. No. 2. 199 - 217.

Hird, C.C. and Hajj, A.R. (1995) A simulation of tube sampling effects on the stiffness of clays. **Geotechnical testing Journal**. Vol. 18. No.1. 3 - 14.

Hunt, D. (2004) Predicting the ground movements above twin tunnels constructed in London clay. **PhD Thesis**. University of Birmingham.

Indraratna, B. and Redana, I.W. (1998) Laboratory determination of smear zone due to vertical drain installation. **Journal of Geotechnical and Geoenvironmental Engineering**. Vol.124. No.2. 180 - 184.

Jacky, J. (1948) Pressure in silos. **Proceedings of the 2nd International Conference on Soil Mechanics and Foundation Engineering**. Vol. 1. 103 - 107.

Jacobsz. S.W. (2002) The effects of tunnelling on piled foundations. **PhD Thesis**. University of Cambridge.

Jardine, R.J. (1985) Investigation of pile-soil behaviour, with special reference to the foundations of offshore structure. **PhD Thesis**. Imperial College. University of London.

Jardine, R.J., John, H.D.St., Potts, D.M. et al. (1991) Some practical applications of a non-linear ground model. **Proceedings for the 10th European Conference in Soil Mechanics and Foundation Engineering**. Balkema. Florence. 223 - 228.

Jardine, R.J., Symes, M.J. and Burland, J.B. (1984) The measurement of soil stiffness in the triaxial apparatus. **Géotechnique**. Vol. 34. No. 3. 323 - 340.

Jardine, R.J., Potts, D.M., Fourie, A.B. and Burland, J.B. (1986) Studies of the influence of non-linear stress-strain characteristics in soil-structure interection. **Géotechnique**. Vol. 36. No. 3. 377 - 396.

Karakus, M. (2007) Appraising the methods accounting for 3D tunnelling effects in 2D plane strain FE analysis. **Tunnelling and Underground Space Technology**. Vol. 22. 47 - 56. Science Direct. Elsevier.

Karakus, M. and Fowell, R.J. (2005) Back analysis for tunnelling induced ground movements and stress redistribution. **Tunnelling and Underground Space Technology**. Vol. 20. No. 6. 514 - 524.

Karstunen, M., Wiltafsky, C., Krenn, H. et al. (2006) Modelling the behaviour of an embankment on soft clay with different constitutive models. **International Journal for Numerical and Analytical Methods in Geomechanics**. Vol. 30. 953 - 982.

Kim, S. (1996) Model testing and analysis of interactions between tunnels in clay. **PhD Thesis**. University of Oxford.

Kim, S. (2004) Interaction behaviours between parallel tunnels in soft ground. **Proceedings of the 30th ITA-AITES World Tunnel Congress**. Singapore. Vol. 19. No. 4 - 5.

La Rochelle, P., Sarrailh, J., Tavenas, F. et al. (1980) Causes of sampling disturbance and design of a new sampler for sensitive soils. **Canadian Geotechnical Journal**. Vol. 18. 51 - 66.

Ladd, C.C. and Foott, R. (1974) New design procedures for stability of soft clays. **Journal of the Geotechnical Engineering Division**. American Society of Civil Engineers. 763 - 786.

Lake, L.M., Rankin, W.J. and Hawley, J. (1992) Prediction and effects of ground movements caused by tunnelling in soft ground beneath urban areas. **CIRIA Project Report 30**. Construction Industry Research and Information Association. London.

Lake, L.M, Rankin, W.J. and Hawley, J. (1996) Prediction and effects of ground movements caused by tunnelling in soft ground beneath urban areas. **Project Report 30. CIRIA**. Mott MacDonald.

Lambe, T.W. (1967) Stress path method. **Journal of the Soil Mechanics and Foundations Division. Proceedings of the Americal Society id Civil Engineers**. Vol. 93. No. SM6. 309 - 331.

Lambe, T.W. (1973) Predictions in soil engineering. **Geotechnique**. Vol. 23. No. 2. 149-202.

Leca, E. (1989) Analysis of NATM and shield tunnelling in soft ground. **PhD Thesis**. Virginia Polytechnic Institute and State University. USA.

Lee, G.T.K. and Ng, C.W.W. (2002) Three-dimensional analysis of ground settlements due to tunnelling: Role of K_0 and stiffness anisotropy. **Geotechnical Aspects of Underground Construction in Soft Ground**. Kastner, Emeriault, Dias and Guilloux (eds.). Lyon. 617 - 622.

Lee, G.T.K. and Ng, C.W.W. (2005) Effects of advancing open face tunnelling on an existing loaded pile. **Journal of Geotechnical and Geoenvironmental Engineering**. Vol. 131. No. 2. 193 - 201.

Lee, K.M. and Rowe, R.K. (1989) Deformations caused by surface loading and tunnelling: the role of elastic anisotropy. **Géotechnique**. Vol. 39. No. 1. 125 - 140.

Lee, C.J, Wu, B.R., Chen, H.T. and Chiang, K.H. (2006). Tunnel stability and arching effects during tunneling in soft clayey soil. **Tunnelling and Underground Space Technology**. Vol. 21. No. 2. 119 - 132..

Liaki, C. (2006) Physicochemical study of electrokinetically treated clay using carbon and steel electrodes. **PhD Thesis**. University of Birmingham.

Lo, K.Y., Ng, M.C. and Rowe, R.L. (1984) Predicting settlement due to tunnelling in clays. **Proceedings Geotech. '84 - Tunnelling in Soil and Rock**. Atlanta. Georgia (ASCE). 47 - 76.

Lo Presti, D.C.F., Pallara, O., Cavallaro, A. et al. (1999) Influence of reconsolidation techniques and strain rate on the stiffness of undisturbed clays from triaxial tests. **Geotechnical Testing Journal**. Vol. 22. No. 3. 211 - 225.

Lunardi, P. (2000) The design and construction of tunnels using the approach based on the analysis of controlled deformation in rocks and soils. **Tunnels and Tunnelling International**. Special supplement. May. 3 - 30.

Mair, R.J. (1979) Centrifugal modelling of tunnelling construction in soft clay. **PhD Thesis**. University of Cambridge.

Mair, R.J. (1996) Settlement effects of bored tunnels. Session Report. **Proceedings International Symposium on Geotechnical Aspects of Underground Construction in Soft Ground**. R.J. Mair and R.N. Taylor (eds.). Balkema. London. 43 - 53.

Mair, R.J. and Taylor, R.N. (1997) Theme lecture: Bored tunnelling in the Urban Environment. **Proceedings 14th International Conference on Soil Mechanics and Foundation Engineering**. Hamburg.

Mair, R.J., Taylor, R.N. and Bracegirdle, A. (1993) Subsurface settlement profiles above tunnels in clay. Géotechnique. Vol. 43. No. 2. 315 - 320.

Mair, R.J., Hight, D.W. and Potts, D.M. (1992) Finite element analyses of settlements above a tunnel in soft ground. **TRRL CR265**. Crowthorne. Berks.

Martos, F. (1958) Concerning an approximate equation of subsidence trough and its time factors. **International Strata Control Congress**. Leipzig. 191 - 205.

Masin, D. & Herle, I. (2005) Numerical analyses of a tunnel in London clay usign different constitutive models. **Proceedings of the 5th International Symposium TC28 Geotechnical Aspects of Underground Construction in Soft Ground**. Amsterdam. The Netherlands. 595 - 600.

Mayne, P.W. and Kulhawy, F.H. (1982) K_0-OCR relationships in soil. **Journal of the Geotechnical Engineering Division. Proceedings of the American Society of Civil Engineers**. Vol. 108. No. GT6. 851 - 872.

Menzies, B.K. (1988) A computer controlled hydraulic triaxial testing system. In: **Advanced Triaxial Testing of Soil and Rocks**. American Society for Testing and Materials. 82 - 94.

Meyerhof, G.G. (1976) Bearing capacity and settlement of pile foundations. **Journal of the Geotechnical Engineering Division. Proceedings of the American Society of Civil Engineers**. Vol. 102. No. GT3. 197 - 228.

Mitchell, J.K. and Soga, K. (2005) **Fundamentals of soil behaviour**. 3rd Edition. John Wiley and Sons.

Mott MacDonald. (1991) **Jubilee Line Extension. Geotechnical Investigation Sectional Interpretative Report. No. 1: Green Park to Canada Water. Volumes 1, 2 and** 4. April.

Muir Wood, D. (1990) **Soil behaviour and critical state soil mechanics**. Cambridge University Press.

Myrianthis, M.L. (1981) Stress path approach for a tunnel driven in stiff clay. In: Resendiz and Romo (eds.). **Soft-Ground Tunnelling**. Balkema. 79 - 84.

Negro, A. and Queiroz, P.B. (2000) Prediction and preformance: A review of numerical analyses for tunnels. **International Symposium on Geotechnical Aspects of Underground Construction in Soft Ground**. Fujita, Kusakabe and Miyazaki (eds.). Balkema. 409 - 418.

New, B.M. and Bowers, K.H. (1994) Ground movement model validation at the Heathrow Express trial tunnel. **Tunnelling 94. Proceedings of the 7th International Symposium of the Institution of Mining and Metallurgy and British Tunnelling Society**. London. Chapman and Hall. 310 - 329.

New, B.M. and O'Reilly, M.P. (1991) Tunnelling Induced ground movements: predicting their magnitude and effects. In: Geddes. J.D. (ed). **Ground Movements and Structures**. Pentech Press. 671 - 697.

Ng, C.W.W. (1999) Stress paths in relation to deep excavations. **Journal of Geotechnical and Geoenvironmental Engineering**. Vol. 125. No.5. 357 - 363.

Ng, M.C. and Lo, Y. (1985) The measurements of soil parameters relevant to tunnelling in clays. **Canadian Geotechnical Journal**. Vol. 22. 375 - 391.

Ng, R.M.C. and Lo, K.Y. (1986) The measurements of soil parameters relevant to tunnelling in clays. **Canadian Geotechnical Journal**. Vol. 22. 375 - 391.

O'Reilly, M.P. and New, B.M. (1982) Settlements above tunnels in the United Kingdom - their magnitude and prediction. **Proceedings of Tunnelling' 82 Symposium. Institution of Mining and Metallurgy**. London. 173 - 181.

Panet, M and Guenot, A. (1982) Analysis of convergence behind the face of a tunnel. **Proceedings Tunnelling 82. Institution of Mining and Metallurgy**. London. 197 - 204.

Parry, R.H.G. and Nadarajah, V. (1973) A volumetric yield locus for lightly overconsolidated clays. Technical Note. **Géotechnique**. Vol. 23. No. 3. 450 - 453.

Peck, R.B. (1969) Deep excavations and tunnelling in soft ground. State of the art report. **7th International Conference on Soil Mechanics and Foundations Engineering**. Mexico City. 225 - 290.

Potts, D.M. and Zdravkovic, L. (2001) **Finite element analysis in geotechnical engineering: Application**. London. Thomas Telford Publishing.

Potts, D.M. and Zdravkovic, L. (1999) **Finite element analysis in geotechnical engineering: Theory**. London. Thomas Telford Publishing.

Potts, D.M. (2003) Numerical analysis: a virtual dream or practical reality? - Introduction. The 42th Rankine Lecture (2002). **Géotechnique**. Vol. 53. No. 6. 535 - 573.

Powell, D. and Clayton, C. (2007) SCL tunnelling in stiff clays: recent experience and future needs. **Collection of key note lectures for the ITA-AITES World Tunnel Congress 2007**. Prague. 33 - 50.

Powrie, W., Pantelidou, H. and Stallebrass, S.E. (1998). Soil stiffness in stress path relevant to diaphragm walls in clay. **Géotechnique**. Vol. 48. No. 4. 483 - 494.

Prashant, A. and Penumadu, D. (2005) A laboratory study of normally consolidated kaolin clay. **Canadian Geotechnical Journal**. Vol. 42. 27 - 37.

Puzrin, A.M. and Burland, J.B. (2000) Kinematic hardening plasticity formulation of small strain behaviour of soils. **International Journal for Numerical and Analytical Methods in Geomechanics**. Vol. 24. 753 - 781.

Rampello, S., Viggiani, G.M.B. and Amorosi, A. (1997) Small-strain stiffness of reconstituted clay compressed along constant triaxial effective stress ratio paths. **Géotechnique**. Vol. 47. No. 3. 475 - 489.

Rankin, W.J. (1988) Ground movements resulting from urban tunnelling: predictions and effects. **Conference on Engineering Geology of Underground Movements**. Nottingham. BGS. 79 - 92.

Roscoe, K. H. and Burland, J. B. (1968) On the generalized stress-strain behaviour of ´wet clay´. In: Heyman and Leckie (eds.). **Engineering plasticity**. Cambridge University Press. 535 - 609.

Roscoe, K.H. and Schofield, A.N. (1963) Mechanical behaviour of an idealised ´wet clay´. **Proceedings of the 2nd European Conference on Soil Mechanics and Foundation Engineering**. Wiesbaden. Vol. 1. 47 - 54.

Rossato, G., Ninis, N.L. and Jardine, R.J. (1992) Properties of some kaolin-based model clay soils. **Geotechnical Testing Journal**. GTJODJ. Vol. 15. No. 2. 166 - 179.

Rouainia, M. and Wood, D. (2000) A kinematic hardening constitutive model for natural clays with loss of structure. **Géotechnique**. Vol. 50. No. 2. 153 - 164.

Rouainia, M., Sheng, D. and Zhao, J. (2005) Influence of structure degradation on the behaviour of embankments on soft soil. **13th ACME Conference**. University of Sheffield. 39 - 42.

Rowe, R.K., Lo, K.Y. and Kack, G.J. (1983) A method of estimating surface settlement above tunnels constructed in soft ground. **Canadian Geotechical Journal**. Vol. 20. 11 - 22

Schanz, T., Vermeer, P.A. and Bonnier, P.G. (1999) The Hardening Soil Model: Formulation and verification. In: Brinkgreve, R.B.J. **Beyond 2000 in Computational Geotechnics**. Balkema. Rotterdam. 281 - 290.

Schmertmann, J.H. (1975) Measurement of in-situ strength. **Proceedings of the Conference on In-Situ Measurement of Soil Properties**. Americal Society of Civil Engineers. 55 - 138.

Schmidt, B. (1969) Settlements and ground movements associated with tunnelling in soil. **PhD Thesis**. University of Illinois.

Schmidt, B. (1966) Discussion of ´Earth pressures at rest related to stress history´ by Brooker and Ireland (1965). **Canadian Geotechnical Journal**. Vol. 3. No. 4. 239 - 242.

Selby, A.R. (1988) Surface movements caused by tunnelling in two-layer soil. In: Geological Society Engineering. **Engineering Geology of Underground Movements**. Geology Special Publication. No. 5. 71 - 77.

Sheeran, D.E. and Krizek, R.J. (1971) Preparation of homogeneous soil specimens by slurry consolidation. **Journal of Materials**. American Society for Testing and Materials. Vol.6. No. 2. 356 - 373.

Siddique, A., Clayton, C.R.I. and Hopper, R.J. (1999) The effects of varying centreline tube sampling disturbance on the behaviour of reconstituted clay. **Geotechnical Testing Journal**. GTJODJ. Vol. 22. No. 3. 245 - 256.

Simpson, B. (1992) Retaining structures: displacement and design. **Géotechnique**. Vol. 42. No. 4. 541 - 576.

Simpson, B., Calabresi, G., Graham, J. et al. (1981) The effect of anisotropic elasticity on the yielding characteristics of overconsolidated natural clay. **Canadian Geotechnical Journal**. Vol. 38. 251 - 137.

Sivakumar, V., Doran, I.G., Graham, J. et al. (2001) Relationship between K_0 and overconsolidation ratio: a theoretical approach. **Géotechnique**. Vol. 52. No. 3. 225 - 230.

Skempton , A.W. (1954) The pore pressure coefficients A and B. **Géotechnique**. Vol. 4. No. 4. 186 - 187.

Skempton, A.W. and Bjerrum, L. (1957) A contribution to the settlement analysis of foundations on clay. **Géotechnique**. Vol. 7. No. 4. 168 - 178.

Skinner, A.E. (1975) The effect of high pore water pressures on the mechanical behaviour of sediments. **PhD Thesis**. Imperial College. University of London.

Smith, M. G. (1993) A laboratory study of the Marchetti dilatometer. **D.Phil. Thesis**. University of Oxford.

Stallebrass, S.E. (1990) Modelling the effects of recent stress history on the deformation of overconsolidated clays. **PhD Thesis**. City University. London.

Stallebrass, S.E.and Taylor, R.N. (1997) The development and evaluation of a constitutive model for the prediction of ground movements in overconsolidated clay. **Géotechnique**. Vol. 47. No. 2. 235 - 253.

Standing, J.R. and Burland, J.B. (2005) Investigating variations in tunnelling volume loss - a case study. **Proceedings of the 5th International Symposium in Geotechnical Aspects of Underground Construction in Soft Ground**. Amsterdam. June. Session 2. 113 - 118.

Swoboda, G. (1979) Finite element analysis of the New Austrian Tunnelling Method (NATM). **Proceedings of the 3rd International Conference on Numerical Methods in Geomechanics**. Aachen. Vol. 2. 581 - 586.

Tang, D.K.W., Lee, K.M. and Ng, C.W.W. (2000) Stress paths around a 3-D numerically simulated NATM tunnel in stiff clay. In: Fujita and Miyazaki (eds). **Geotechnical Aspects of Underground Construction in Soft Ground. Kusakabe**. Balkema. Rotterdam. 443 - 449.

Taylor, R.N. (1998) Modelling of tunnel behaviour. **Proceedings of the Institution of Civil Engineers. Geotechnical Engineering**. July. 127 - 132.

Urciuoli, G., Russo, C., Desideri, A. et al. (1996) Pore pressure generation and equalization around a circular tunnel in soft clays. In: Mair and Taylor (eds). **Geotechnical Aspects of Underground Construction in Soft Ground**. Balkema. Rotterdam. 621 - 625.

Valls-Marquez, M., Chapman, D.N. and Ghataora, G.S. (2008) Preparation of K_0-consolidated reconstituted samples in the laboratory. **International Journal of Geotechnical Engineering**. J. Ross Publishing. Braja M. Das (ed.). Vol. 2. No. 4. 343 – 354.

Viggiani, G. and Atkinson, J.H. (1995) Interpretation of bender element tests. **Géotechnique**. Vol. 45. No. 1. 149 - 154.

Viggiani, G. and Atkinson, J.H. (1997) Interpretation of bender element tests - Discussion. **Géotechnique**. Vol. 47. No. 4. 873 - 877.

Viggiani, G.M.B, Soccodato, F.M. & Burghignoli, A. (2005) A study of the interaction between the new C Line of Roma Underground and the Aurelian Wall. **Proceedings of the 5th International Symposium TC28 Geotechnical Aspects of Underground Construction in Soft Ground**. Amsterdam. The Netherlands.

Ward, W.H. and Pender, M.J. (1981) Tunnelling in soft ground - General report. **Proceedings of the 10th International Conference on Soil Mechanics and Foundation Engineering**. Stockholm. Session II. Vol. 4. 261 - 275.

Wheeler, S.J., Naatanen, A., Karstunen, M. et al. (2003) An anisotropic elastoplastic model for soft clays. **Canadian Geotechnical Journal**. Vol. 40. pp. 403-418.

Whittaker, B.N. and Frith, R.C. (1990) **Tunnelling: Design, Stability and Construction**. The Institution of Mining and Metallurgy. London.

Yeates, J. (1985) The response of buried pipelines to ground movements caused by tunnelling in soil. In: Geddes. J.D. (ed). **Ground Movements and Structures**. Pentech Press. Plymouth. 145 - 160.

Yueyang, Z. (2008) In situ testing for foundation performance prediction. **PhD Thesis**. University of Cambridge.

Zienkiewicz, O.C., Chan, A.H.C., Pastor, M. et al. (1999) **Computational geomechanics with special reference to earthquake engineering**. John Wiley and Sons Ltd. Chichester.

Zytinski, M., Randolph, M.F. Nova, R. et al. (1978) On modelling the unloading-reloading behaviour of soils. **International Journal Numerical Analaysis Methods in Geomechanics**. Vol. 2. 87 - 93.

Appendix A: CHAPTER 3 – ADDITIONAL INFORMATION

A.1. EMPIRICAL METHOD: PRELIMINARY CALCULATIONS

A.1.1. INTRODUCTION

This section presents the results obtained during the preliminary calculations carried out using the Empirical Method in order to gain an initial appreciation of the soil deformations induced by tunnelling in an idealised field situation such as that introduced in Section 3.2. The geometry considered for the calculations is illustrated in Figure A.1.1. The coordinates *x*, *y* and *z* correspond to the criterion in Figure 3.2.

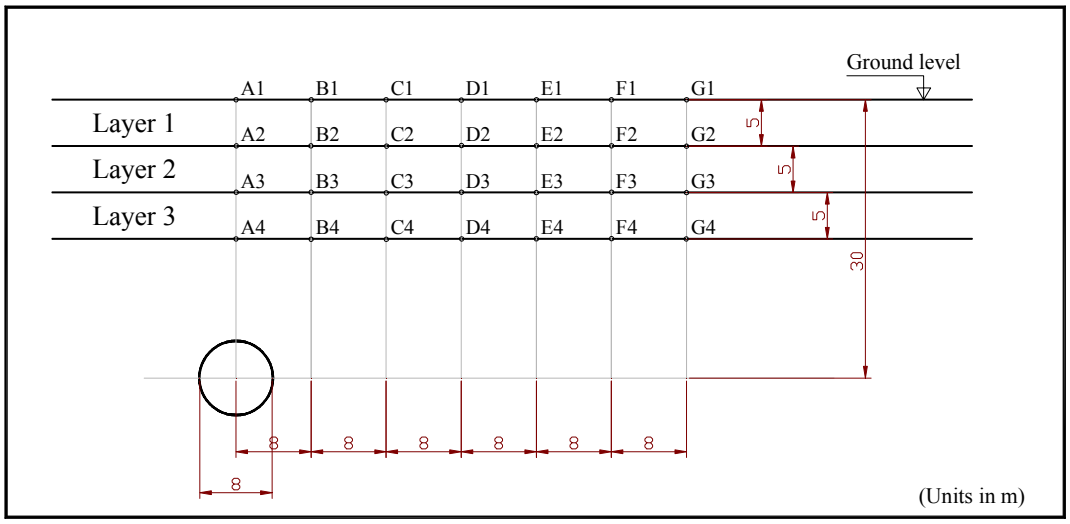

Figure A.1.1 Geometry and mesh used for the preliminary calculations using the Empirical Method

The geometry comprised of a 8 m diameter tunnel, with its axis level situated at a depth of 30 m below the ground surface. The grid was formed by 18 rectangles (28 nodes) being 8 m wide (y-coordinate) and 5 m deep (z-coordinate). Vertical deformations were calculated at each node and strains were calculated considering the deformations at consecutive nodes on the grid in the *z* direction. Three calculations were carried out in which the volume of the settlement trough (*Vs*), considered to be the same as the volume loss at the tunnel level (*Vl*) for clays in undrained conditions, was taken as 0.5 %, 1 % and 2 % of the tunnel cross sectional area (in m^2). These values were selected from values reported in the literature for tunnels excavated in stiff clay for variable depths, diameters, and excavation methods. Examples of this are:

- Attewell et al. (1986): 1 to 2 % for stiff fissured clays.

- O'Reilly and New (1982): 1 to 2 % for shield or non-supported ~4 m diameter tunnels excavated in stiff fissured London Clay.
- Mair (1996): 0.5 to 1.5 % for NATM tunnels in London Clay (based on a review on previous published papers).
- Standing and Burland (2005): 1.1 to 3.3 % for shield tunnelling into London Clay as part of the Jubilee Line Extension.
- Dimmock and Mair (2007): 1.1 % at the Jubilee Line extension beneath Elizabeth House when excavating 5 – 6 m diameter twin tunnels in London Clay using an open face NATM method.

The maximum surface settlement (W_{max}) in mm, occurring at point (0,0,0), was calculated using Equation A.1.1:

$$W_{\max} = \frac{V_S}{\sqrt{2\pi} \cdot i_y} \cdot 1000 \quad \text{[Eq.A.1.1]}$$

where the trough width parameter (i_y) (in m) was calculated using O´Reilly and New (1982) relationship for cohesive materials (Equation A.1.2).

$$i_y = 0.5 \cdot Z_0 \quad \text{[Eq.A.1.2]}$$

Z_0 being the depth (in m) from the ground surface to the tunnel axis. For other points on the ground surface with *y* coordinate different than "0", the vertical deformation was calculated using Equation A.1.3.

$$W_{(y)} = W_{\max} \cdot \exp\left(-\frac{y^2}{2i_y{}^2}\right) \quad \text{[Eq.A.1.3]}$$

For sub-surface points ($z > 0$), Equation A.1.3 was used but i_y was calculated using Equation A.1.4 by Mair et al. (1993).

$$i_y = K \cdot (z_0 - z) \quad \text{[Eq.A.1.4]}$$

where K was calculated using Equation A.1.5.

$$K = \frac{0.175 + 0.325 \cdot \left(1 - \frac{z}{z_0}\right)}{1 - \frac{z}{z_0}} \quad \text{[Eq.A.1.5]}$$

Mair et al. (1993) claimed to obtain better predictions of sub-surface movements in London Clay using this new formulation in comparison to that presented by O'Reilly and New (1982).

Zones in compression (positive strain) and in extension states (negative strain) were then identified as well as the extent of the soil deformations. Graphs were plotted comparing the strains at 0 - 5 m, 5 - 10 m and 10 - 15 m depth for the different values of *Vs*.

A.1.2. RESULTS

Figures A.1.2, A.1.3 and A.1.4 illustrate the strains at different *y* and *z* positions (0-5 m, 5-10 m and 10-15 m respectively) into the ground for different values of the volume loss. Figure A.1.5 illustrates the settlement trough at different depths for a volume loss of 2 %. The predictions given by various authors in terms of the position of the vector focus and the width of the surface settlement trough are also indicated.

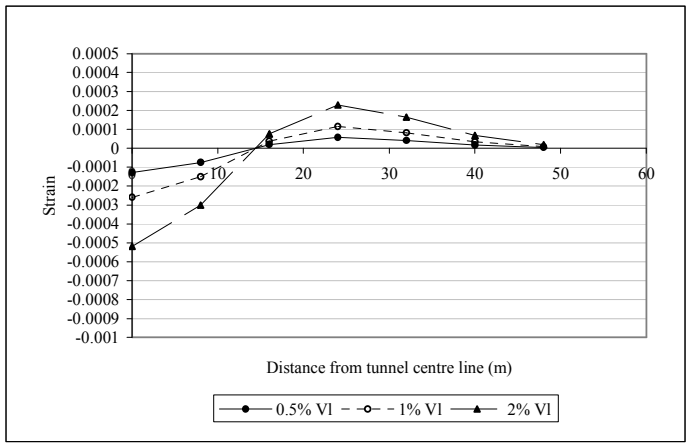

Figure A.1.2. Vertical strains at 0-5 m depth for various values of *Vl*

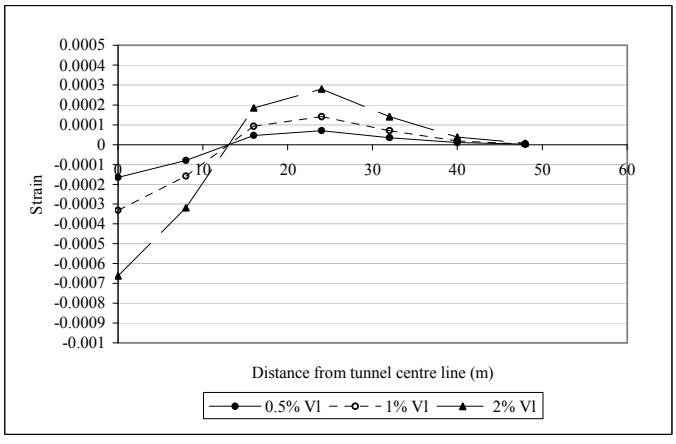

Figure A.1.3. Vertical strains at 5-10 m depth for various values of *Vl*

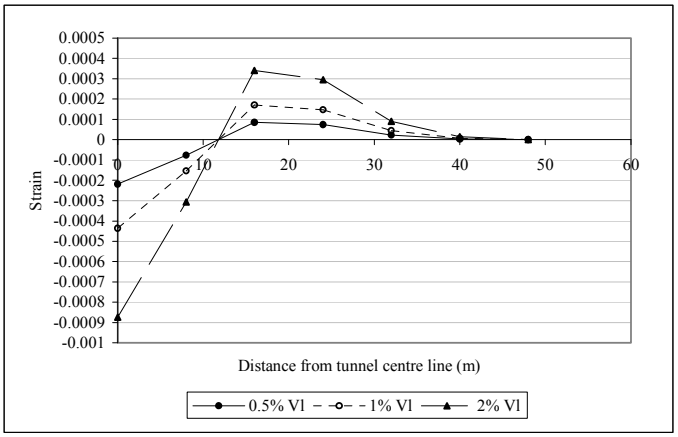

Figure A.1.4. Vertical strains at 10-15 m depth for various values of *Vl*

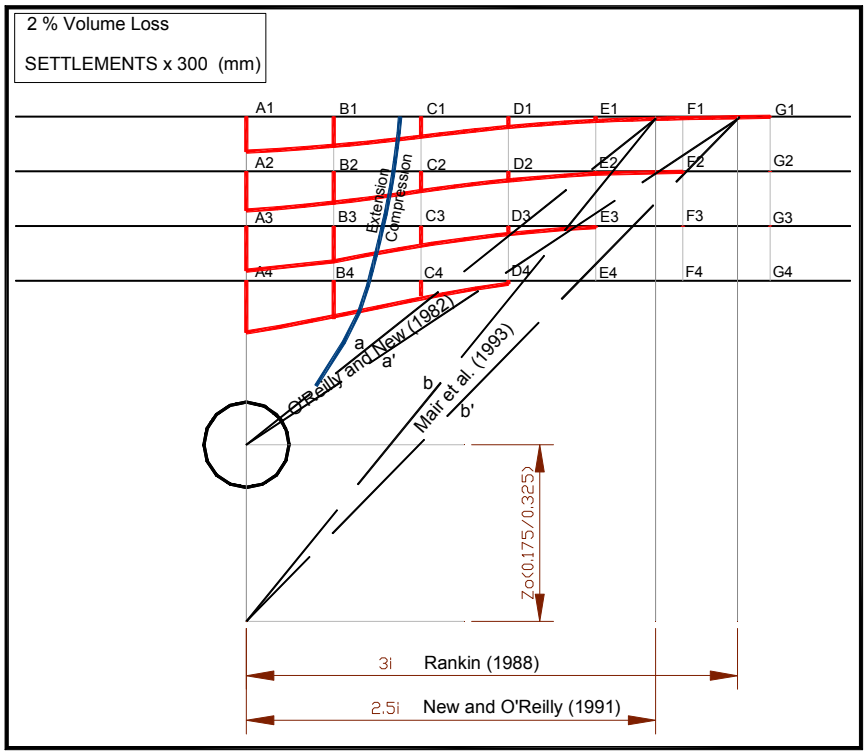

Figure A.1.5. Layout and extent of the settlement trough at various depths for a *Vl=2 %*..

The boundary between vertical compression and extension states in the ground is also indicated

A.1.3. DISCUSSION

The results predicted by the Empirical Method are well known. The calculations performed in this chapter helped to visualise the following:

1. Variations in the settlement trough with depth. The maximum settlement being above the tunnel centreline with its magnitude increasing with depth, and the settlement trough width reducing with depth. The maximum extent of the transverse surface settlement trough is well described either by 2.5i or 3i depending on the magnitude of the settlement that is considered negligible.
2. Zones affected by vertical extension (therefore horizontal compression) corresponding to a certain volume of soil directly above the tunnel (including the tunnel crown) and up to the ground surface level.
3. Zones affected by vertical compression (therefore horizontal extension) including the soil at the tunnel springlines and all the volume up to the ground surface level.
4. The range of magnitudes for the strains likely to be found around a tunnel excavated in clay were found to be in the range:
   a. $1 \cdot 10^{-4}$ - $1 \cdot 10^{-7}$ for a volume loss of 0.5 %
   b. $1 \cdot 10^{-4}$ - $1 \cdot 10^{-7}$ for a volume loss of 1 %
   c. $1 \cdot 10^{-4}$ ($\cong 1 \cdot 10^{-3}$) - $1 \cdot 10^{-6}$ for a volume loss of 2 %

   It should be noted however, that at the points of interest for this study (e.g. above the tunnel crown) the strains are in the order of $1 \cdot 10^{-4}$ for the three different volume losses investigated, and these increase with volume loss and depth (i.e. the stresses are larger near the tunnel opening) getting close to the range $1 \cdot 10^{-3}$ for a volume loss of 2 %.

According to the magnitudes of the strains above and a graph indicating the relationship between shear strain and the shear modulus (Figure 2.25), the expected strain levels in this hypothetical case would be within the small and very small-strain range. The study of the soil behaviour at this level of strain will therefore be of interest for the present investigation. It should be noted that if volume losses above 2 % were used for the calculations, which are not so uncommon, the range of strains induced in the ground would be larger at some points as it is the case for the range of strains suggested for tunnels in Figure 2.25.

The direct measurement devices being considered for purchase for the present investigation were the following:

- ±2.5 mm range LVDT: Accuracy ($\varepsilon \cong 1 \cdot 10^{-4}$); Resolution ($1.5 \cdot 10^{-6}$)
- ±5 mm range LVDT: Accuracy ($\varepsilon \cong 2 \cdot 10^{-4}$); Resolution ($3 \cdot 10^{-6}$)
- ±3 mm range Hall Effect: Accuracy ($\varepsilon \cong 4.5 \cdot 10^{-4}$); Resolution ($1.7 \cdot 10^{-6}$)

Based on the ranges of strain previously discussed, the ±2.5 mm range LVDT set was considered the most appropriate for the present study due mainly to its better accuracy and better durability (convenient for this and other projects to come) when compared to the Hall Effect device.

Since the strains occurring in the soil during tunnel induced stress paths will be measured during this investigation in the laboratory using cylindrical 50 mm diameter x 100 mm long specimens, the expected range of strains could vary considerably from those calculated above. The measured strains in the specimens will inevitably depend on the initial properties of the specimens (e.g. stiffness). It must be noted here that identical stress changes will never have the same effect (in terms of magnitude) in the field (vast extension of soil) compared to those in the laboratory (small portion of soil). The observed trends in the laboratory are, however, expected to be representative of the in-situ ground behaviour.

A.2. UNDRAINED TRIAXIAL TEST SIMULATION IN PLAXIS

One undrained triaxial test was simulated in 2D PLAXIS in order to better understand the differences between the soil parameters used for the Mohr-Coulomb, Hardening and Jardine et al. (1991) models and evaluate their effects in the predicted soil behaviour. A 1 m x 1 m geometry was modelled in axysymmetric conditions as illustrated in Figure A.2.1. Two distributed loads (A and B in Figure A.2.1) were applied in order to simulate the all-round pressure. A vertical prescribed displacement was also applied to simulate the strain controlled loading during shearing. The water level was set up at the base of the geometry and initial stresses were not generated prior to calculation. The calculation process was divided into two phases. The first phase consisted on a plastic staged construction in which both loads A and B were set up to increase to 300 kPa ignoring undrained conditions so that the soil could consolidate under such pressure. This gave rise to a complete dissipation of the pore water pressures within the soil and therefore to a homogeneous distribution of effective stresses of 300 kPa at all points. The second construction phase consisted on a displacement controlled shearing stage where, maintaining the previous all-round pressure, the vertical deformation was increased to 20 cm.

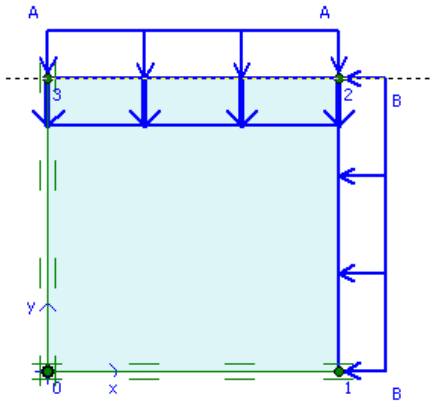

Figure A.2.1. Geometry used for the simulation of an undrained triaxial test in PLAXIS 2D

Figure A.2.2 illustrates the stress-strain relationships obtained for the three constitutive models. The initial deformations induced during isotropic consolidation were different for the Jardine et al. (1991) model. This is because the bulk modulus in Mohr-Coulomb and in the Hardening model is constant and in the Jardine et al. (1991) model it is very small initially (i.e. a large initial volumetric deformation occurs) and decreases for increasing p'. This in particular however did not have any implications during the simulation of tunnel excavations (Table 3.1) because none of them included consolidation stages.

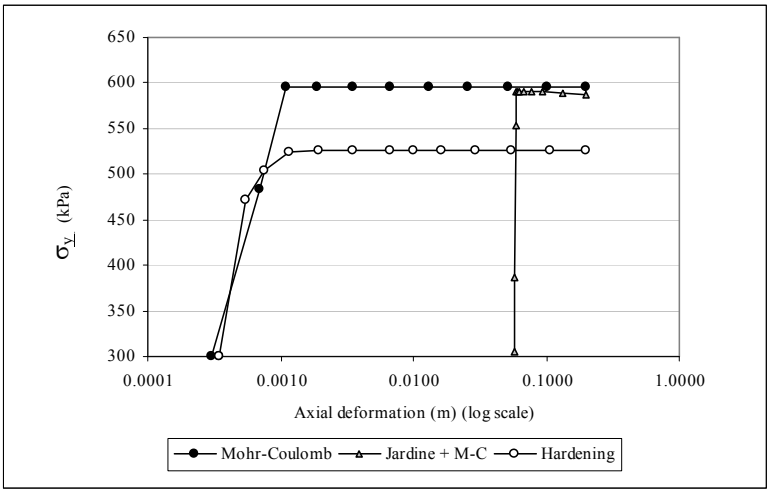

Figure A.2.2. Stress-strain responses during an undrained triaxial test in PLAXIS for various constitutive soil models

A.3. LARGE STRESS PATH EQUIPMENT

This equipment was developed by British Gas for testing 200 mm diameter x 400 mm long specimens of granular materials (Figure A.3.1).

The advantages of using such an apparatus were thought to be:

- The uniqueness of the equipment.
- The potentially more representative results due to the size of the specimens.
- The possibility of comparing the results with those obtained from the Bishop and Wesley GDS Standard Stress Path triaxial equipment if both apparatus could have been used at some point.

The equipment and related information (e.g. manuals) were in a very poor state. Once all the parts were put together and identified, arrangements were made to check for the operation of the whole system. However, even with the help of the last employee who used the equipment at Loughborough it was not possible to make it work. The system was in an extremely deteriorated state. In addition, the equipment sketches and some of the manuals were mainly from what seemed to be an older version of the equipment, there were no operational notes available, the hardware / software were too old, the multiple connections were not clear and there was no direct access to water and compressed air supplies. Finally, the health and safety requirements in the laboratory did not permit some of the tests required for re-setting the device. More than three months were spent working on this equipment with little success, including also doing some surveys for potential suppliers of the required parts for such non-standard sized equipment. It may be of interest in this section to quote Precision Dippings Marketing Ltd as one of the contacts that was established for the manufacturing of 200 mm (diameter) x 400 mm (length) x 0.5 mm (thickness) membranes. Also a 200 mm (inner diameter) x 5 m (length) pipe was kindly donated by Durapipe UK for the preparation of K_0-consolidated samples. There were some disadvantages as well in the use of this equipment. These were mainly in terms of time and number of tests that could be performed considering the difficulties involved in handling the large specimens and operating this huge apparatus. Considering all the pros and cons it was eventually decided to stop working on this equipment and think about other alternatives. Nevertheless, substantial progress was made setting up the equipment and new information was gained during this time. The notes and sketches produced, although not included in this thesis, will be extremely useful in the future if someone wishes to continue working with this device.

(a)

(b)

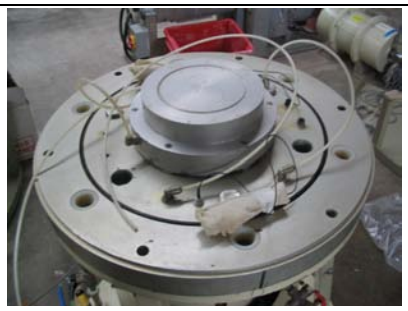

(c)

(d)

Figure A.3.1. Large stress path equipment: (a) Laboratory view and details of (b) the data-logger, (c) the base pedestal of the cell and (d) some connections to the cell

A.4. ZERO PRESSURE DATUM AND CALIBRATION OF THE STRESS PATH CELL STANDARD COMPONENTS

It is recommended that the zero pressure datum in the GDS computer-controlled Stress Path device is fixed at least once a month. The various equipment components involved are:

-The pore water pressure transducer;

-The back-pressure volume/pressure controller;

-The cell pressure volume/pressure controller.

This initial setting up is fundamental to ensure a clear understanding of what is occurring in the system and also for proper post-processing of the results. Different options are being used by different users and although GDS suggested that variations in fixing the pressure datum would only give differences of a few kPa, from the author's point of view these can affect the results, to a more or lesser extent, and so it would be desirable for the future to establish a standard method. The procedure used for this study was as follows:

1) The lower chamber piston was moved until it was situated at half its travel.
2) The pore water pressure port at the base pedestal was flushed to remove any trapped air.
3) A stainless steel hollow spacer was placed inside the cell instead of the specimen to support the top cap with the back-pressure line connected and full of water so as to simulate standard conditions during the tests, but without obstructing the pore water pressure port at the base pedestal.
4) The cell was then tightened in place and filled with de-aired water just up to half the height of the specimen (i.e. 50 mm from the top of the base pedestal for a 100 mm long specimen) leaving the upper bleed valve on the top of the cell open. The pipe from the cell pressure controller was then connected to the cell pressure port on the cell full of water.
5) At this point, with the back pressure and cell pressure valves open, the three controllers above were zeroed. The pore water pressure transducer was zeroed using the appropriate screen on the computer.

In this way, differences in readings between cell pressure, back pressure and pore water pressure would be mainly caused by the different accuracies and resolutions of each component.

Similarly, the lower chamber volume/pressure controller and the load cell have to be zeroed simultaneously. This was done at the beginning of each test when the cell was full of water, the cell pressure was set to zero and there was no vertical stress applied on the specimen. This would account for the weight of the specimen and piston in the case of the lower chamber, and for changes in temperature in the case of the load cell.

The components requiring calibration were calibrated at the start of the laboratory work and periodically thereafter. The volume/pressure controllers were calibrated by connecting them to each other and taking the back pressure as the reference, since this had previously been sent to GDS for a complete service (including calibration). The reason for sending this controller for servicing and not the other two is the fact that it is from this controller that readings of all the volume changes in the specimen are calculated and so it requires the best possible accuracy. The cell pressure and lower chamber controllers were never found to diverge more than ±1 kPa from the back pressure controller. The pore water pressure transducer was calibrated by filling the cell with water and once closed to the atmosphere, applying successive increments in cell pressure, after setting the zero pressure datum as explained above. The external displacement transducer was calibrated using a Wykeham Farrance calibration device with precision micrometer. A new 5 kN submersible load cell had to be purchased during the project due to a fault with the original one. Both cells were initially calibrated by the manufacturer and periodically tested afterwards in the laboratory using a dummy sample in an empty cell subjected to increments in the lower chamber pressure. The lower chamber pressure and load cell values are related to each other by using the area of the diaphragm in the movable base pedestal.

Appendix B: CHAPTER 5 - TAP WATER ANALYSIS

Table B.1 lists the results from a quality report on the tap water supplied to the area where the University of Birmingham is located. The data was provided by Severn Trent Water and corresponds to the period between 1-1-05 and 31-12-05.

Table D.1. Results from the analysis of the tap water supplied to the area where the University of Birmingham is located. Data supplied by Severn Trent Water

			Concentration or value (all samples)			
Parameter	**Units**	**No. Samples taken**	**Minimum**	**Average**	**Maximum**	**PCV***
MANDATORY:						
1,2 Dichloroethane	µg/l	8	0.080	0.090	0.120	3
Aldrin	µg/l	8	0.02	0.002	0.002	0.03
Alpha-HCH	µg/l	8	0.01	0.001	0.001	0.1
Aluminium	µg/l	76	5.000	10.803	21.000	200
Antimony	µg/l	8	0.240	0.240	0.240	5
Arsenic	µg/l	8	0.500	0.500	0.500	10
Benzene	µg/l	8	0.060	0.083	0.150	1
Benzo 3,4 Pyrene	µg/l	8	0.001	0.001	0.001	0.01
Beta-HCH	µg/l	8	0.002	0.002	0.002	0.1
Boron	mg/l	8	0.010	0.012	0.013	1
Bromate	µg/l	8	0.600	0.675	0.800	10
Cadmium	µg/l	8	0.230	0.230	0.230	5
Chlordane A	µg/l	8	0.002	0.002	0.002	0.1
Chlorothalonil	µg/l	8	0.001	0.001	0.001	0.1
Chromium	µg/l	8	0.340	0.340	0.340	50
Cis-Permethrin	µg/l	8	0.001	0.001	0.001	0.1
Colour	mg/l	38	0.400	1.042	2.700	20
Copper	mg/l	8	0.001	0.012	0.050	2
Cyanide	µg/l	8	0.220	0.308	0.590	50
Cyfluthrin	µg/l	8	0.040	0.040	0.040	0.1
Cypermethrin	µg/l	8	0.040	0.040	0.040	0.1
D.D.E.-Para Para	µg/l	8	0.002	0.002	0.002	0.1
D.D.E.-Ortho Para	µg/l	8	0.002	0.002	0.002	0.1
D.D.T.-Ortho Para	µg/l	8	0.002	0.002	0.002	0.1
D.D.T.-Para Para	µg/l	8	0.002	0.002	0.002	0.1
Delta – HCH	µg/l	8	0.002	0.002	0.002	0.1
Deltamethrin	µg/l	8	0.002	0.002	0.020	0.1
Dichlobenil	µg/l	8	0.001	0.001	0.001	0.1
Dieldrin	µg/l	8	0.002	0.002	0.002	0.03
E.coli	No. / 100ml	204	0.000	0.000	0.000	0
Endosulfan A	µg/l	8	0.001	0.001	0.001	0.1
Endosulfan B	µg/l	8	0.004	0.004	0.004	0.1
Endrin	µg/l	8	0.002	0.002	0.002	0.1
Enterococci	No. / 100ml	8	0.000	0.000	0.000	0
Fenvalerate	µg/l	8	0.020	0.020	0.020	0.1
Fluoride	mg/l	8	0.750	0.894	0.980	1.5
Gamma – HCH	µg/l	8	0.002	0.002	0.002	0.1
Heptachlor	µg/l	8	0.002	0.002	0.002	0.03
Heptachlor epoxide	µg/l	8	0.002	0.002	0.002	0.03
Hexachlorobenzene	µg/l	8	0.001	0.001	0.001	0.1
Hexachlorobutadiene	µg/l	8	0.002	0.002	0.002	0.1

			Concentration or value (all samples)			
Parameter	**Units**	**No. Samples taken**	**Minimum**	**Average**	**Maximum**	**PCV***
Iron	µg/l	76	7.000	30.118	110.000	200
Isodrin	µg/l	8	0.002	0.002	0.002	0.1
Lead	µg/l	8	1.000	1.875	5.400	25
Manganese	µg/l	38	1.500	1.753	3.400	50
Mercury	µg/l	8	0.015	0.031	0.140	1
Methoxychlor	µg/l	8	0.002	0.002	0.002	0.1
Nickel	µg/l	8	1.400	2.600	11.000	20
Nitrate	mg/l	8	1.110	1.814	3.410	50
Nitrite	mg/l	8	0.002	0.003	0.005	0.5
Nitrite / Nitrate Calculated	mg/l	8	0.260	0.260	0.260	<1
Odour	Dilution Number	76	0.000	0.000	0.000	3 at 25^0C
PAH	µg/l	8	0.000	0.000	0.000	0.1
PCB – Arochlor 1254	µg/l	8	0.003	0.003	0.003	0.1
pH	pH value	76	8.000	8.639	9.100	Max.9.5, Min.6.5
Selenium	µg/l	8	0.440	0.440	0.440	10
Sodium	Mg/l	8	4.100	5.000	8.100	200
T.D.E.-Ortho Para	µg/l	8	0.002	0.002	0.002	0.1
T.D.E.-Para Para	µg/l	8	0.002	0.002	0.002	0.1
Taste	Dilution Number	76	0.000	0.000	0.000	3 at 25^0C
Tetrachloroethene and Trichloroethene	µg/l	8	0.000	0.000	0.000	10
Tetrachloromethane	µg/l	8	0.020	0.033	0.040	3
Total Pesticides	µg/l	8	0.000	0.000	0.001	0.5
Total Trihalomethanes	µg/l	8	22.500	35.988	67.400	100
Trans-Permethrin	µg/l	8	0.002	0.02	0.002	0.1
Trichlorobenzene	µg/l	8	0.001	0.001	0.001	0.1
Turbidity	NTU	38	0.050	0.117	1.230	4
NON-MANDATORY:						
Free Chlorine	mg/l	204	0.000	0.126	0.340	No numerical limit applies
Total Chlorine	mg/l	204	0.030	0.184	0.410	No numerical limit applies
Ammonium	mg/l	76	0.021	0.023	0.038	0.5
Chloride	mg/l	8	7.300	9.538	15.200	250
Clostridium perfringens	No. / 100ml	38	0.000	0.000	0.000	0
Coliform Bacteria	No. / 100ml	204	0.000	0.020	3.000	0
Colony Count After 72 hours at 22^0C	No. / 100ml	76	0.000	4.592	89.000	No numerical limit applies
Colony Count After 47 hours at 37^0C	No. / 100ml	76	0.000	4.750	78.000	No numerical limit applies
Conductivity	µS/cm at 20^0C	38	98.000	113.053	178.000	2500
Gross Alpha Activity	Bq/l	8	0.020	0.035	0.078	0.1 (Guidance only)
Gross Beta Activity	Bq/l	8	0.010	0.025	0.035	1 (Guidance only)
Sulphate	Mg/l	8	10.400	14.400	25.000	250
Total Organic Carbon	Mg/l	8	0.910	1.159	1.770	No numerical limit applies

* PCV: Prescribed concentration or value for mandatory parameters and specified limit or value for non-mandatory parameters

Appendix C: CHAPTER 5 - ADDITIONAL FIGURES

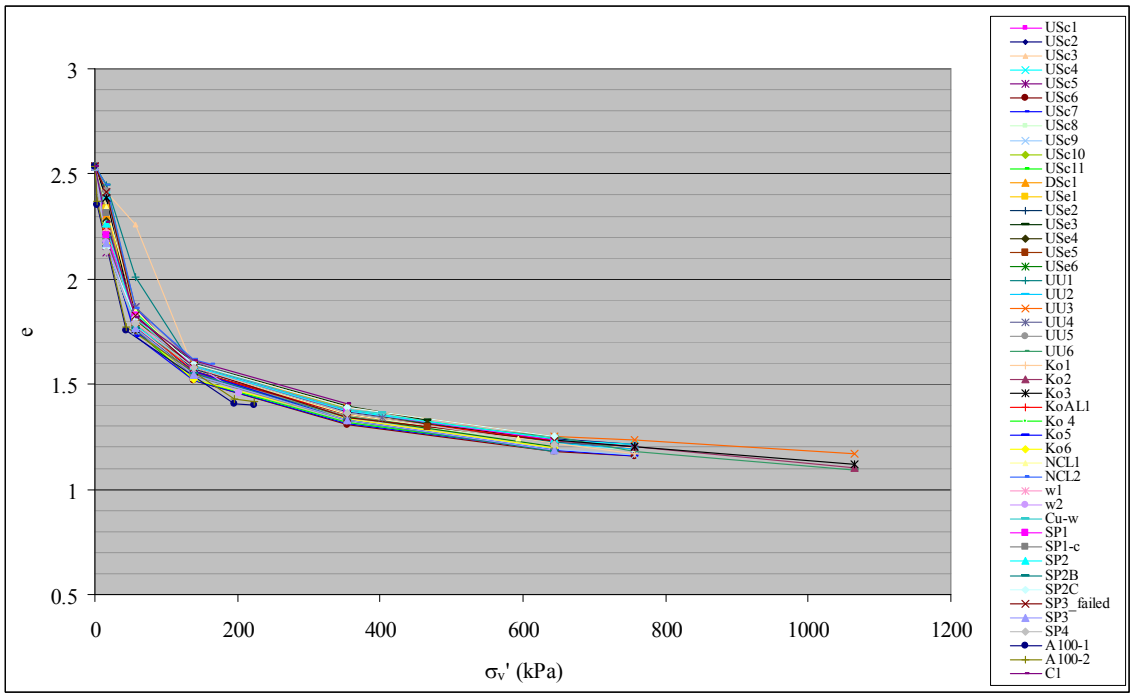

Figure C.1. Void ratio evolution with vertical effective stress during K_0-consolidation of Speswhite Kaolin samples in Device A

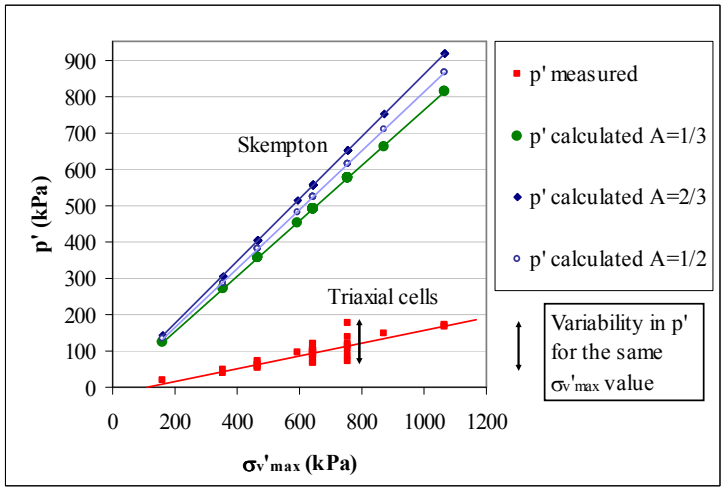

Figure C.2. Difference between calculated and measured initial p' values in the triaxial cell for Speswhite Kaolin specimens reconstituted from slurry in Device A

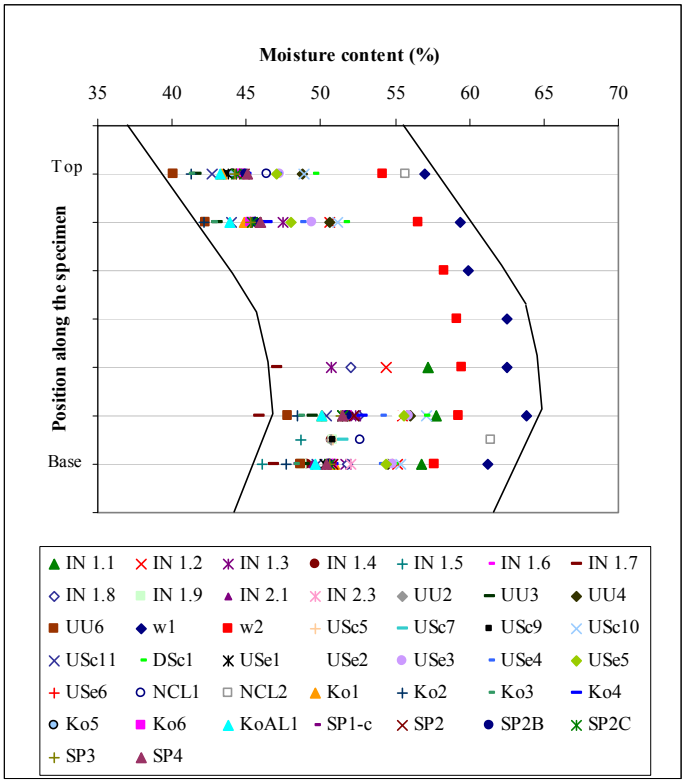

Figure C.3. Final moisture content measurements along Speswhite Kaolin samples reconstituted from slurry in Device A

Appendix D: CHAPTER 7 – ADDITIONAL FIGURES

(Some of these figures in this appendix have been also presented in Chapter 7 for practical purposes).

D.1. STRESS PATH TESTING

SPRINGLINE. TWIN TUNNELS. K_0<1

Test SP2

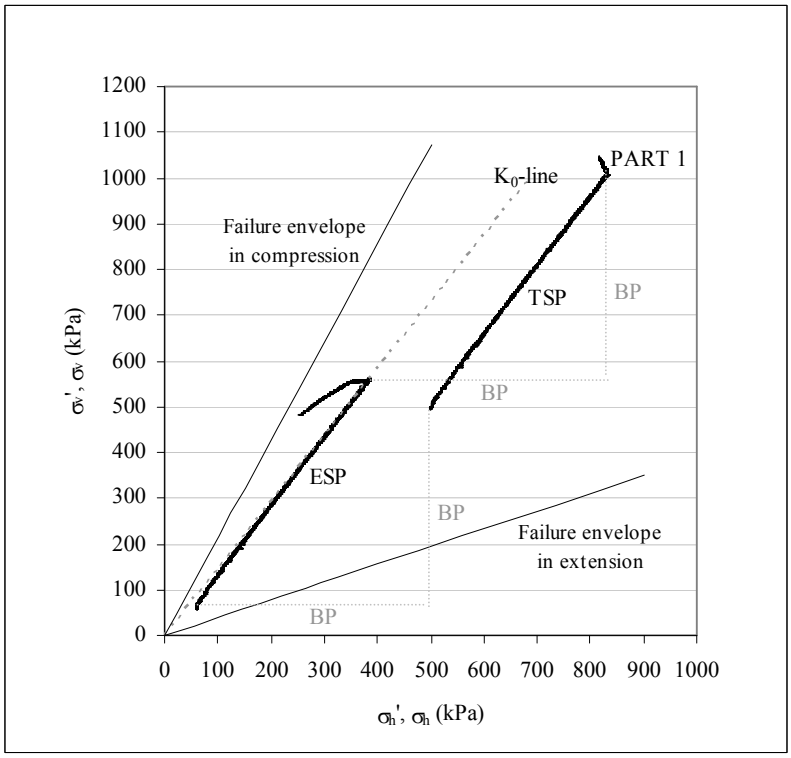

Figure D.1. Total and effective experimental stress paths during test SP2.

BP: Back-pressure, TSP: Total stress path, ESP: Effective stress path

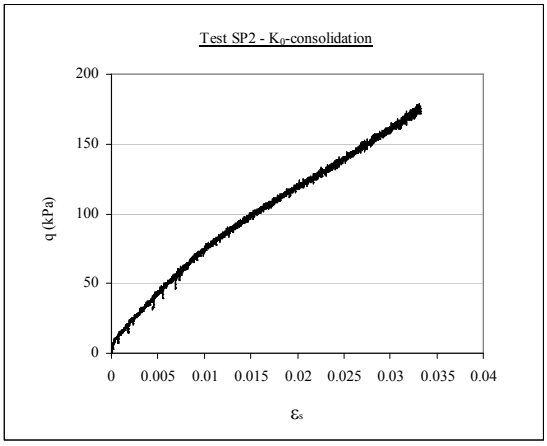

Figure D.2. Test SP2. q - ε_s relationship during the K_0-consolidation stage

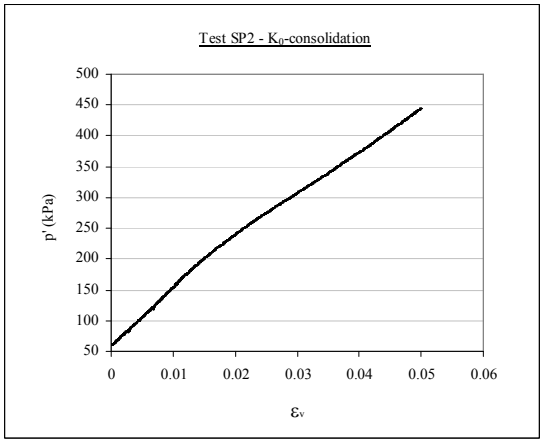

Figure D.3. Test SP2. p' - ε_v relationship during the K_0-consolidation stage

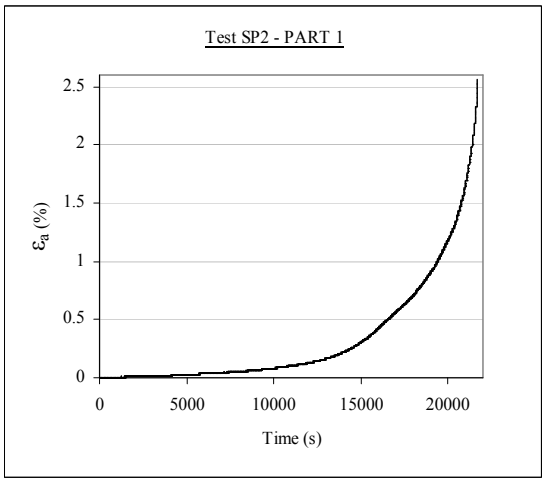

Figure D.4. Test SP2. Variation in ε_a with time during PART 1 measured by the axial on-sample Hall Effect device

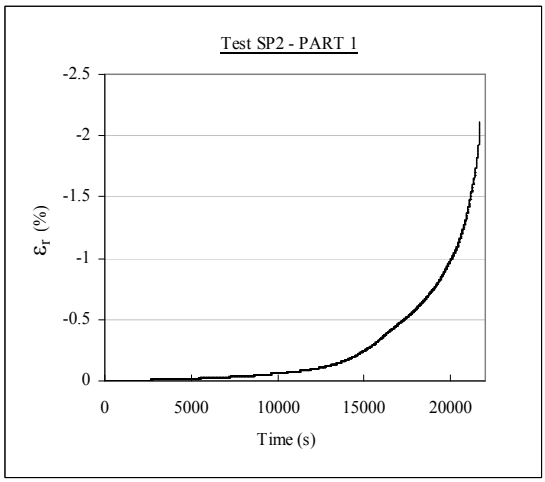

Figure D.5. Test SP2. Variation in ε_r with time during PART 1 measured by the radial on-sample Hall Effect device

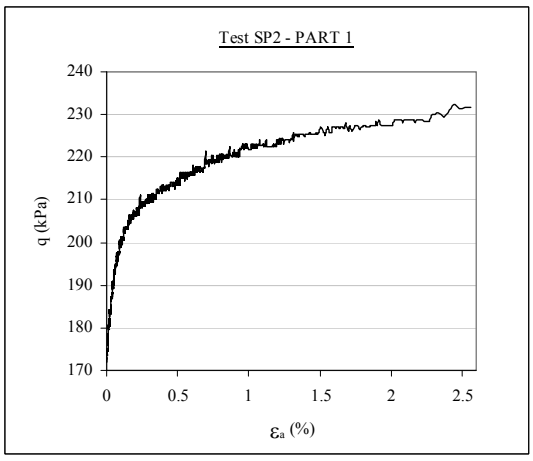

Figure D.6. Test SP2. q - ε_a relationship during PART 1 based on the Hall Effect device internal measurements

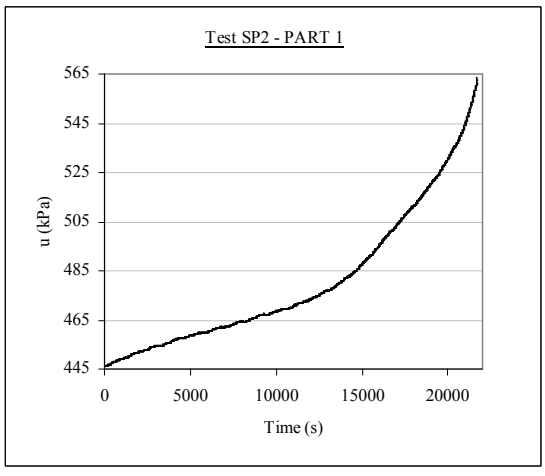

Figure D.7. Test SP2. Variation in u with time during PART 1

Figure D.8. Mode of failure during test SP2

Test SP2B

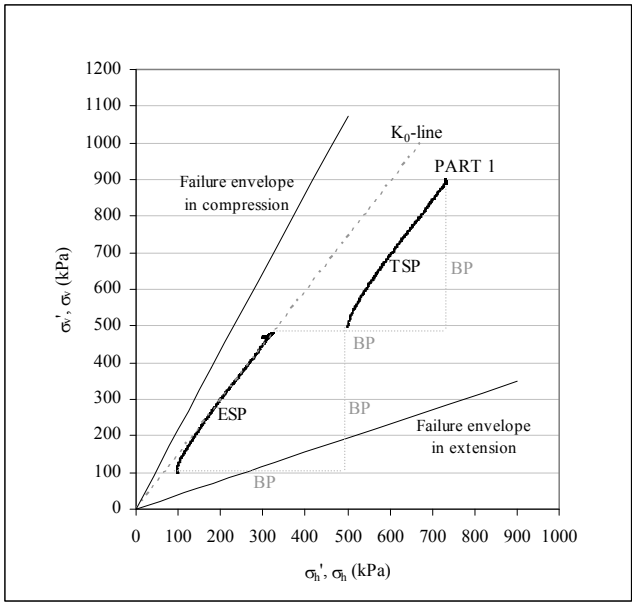

Figure D.9. Total and effective experimental stress paths during test SP2B. BP: Back-pressure, TSP: Total stress path, ESP: Effective stress path

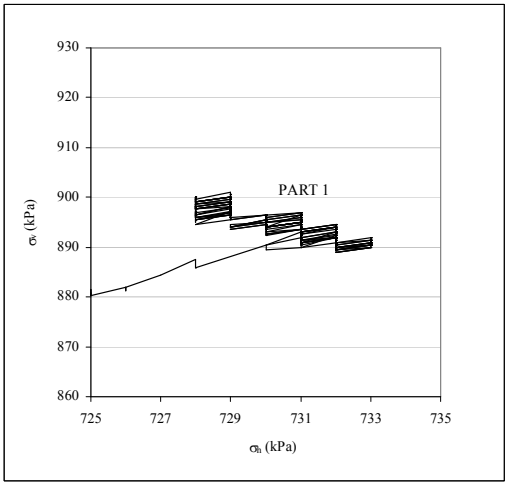

Figure D.10. Detail of the total stress paths during test SP2B from Figure 7.23

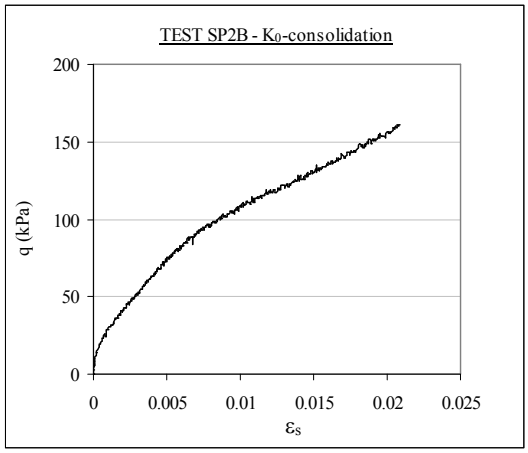

Figure D.11. Test SP2B. q - ε_s relationship during the K_0-consolidation stage

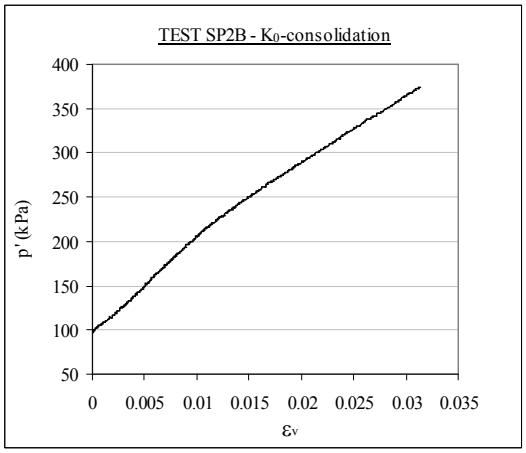

Figure D.12. Test SP2B. p' - ε_v relationship during the K_0-consolidation stage

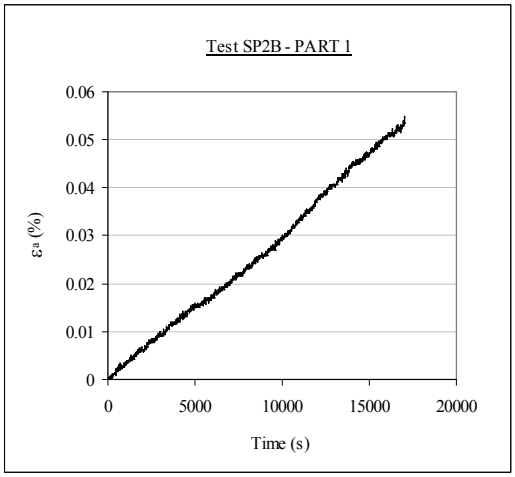

Figure D.13. Test SP2B. Variation in ε_a with time during PART 1 measured by the axial on-sample Hall Effect device

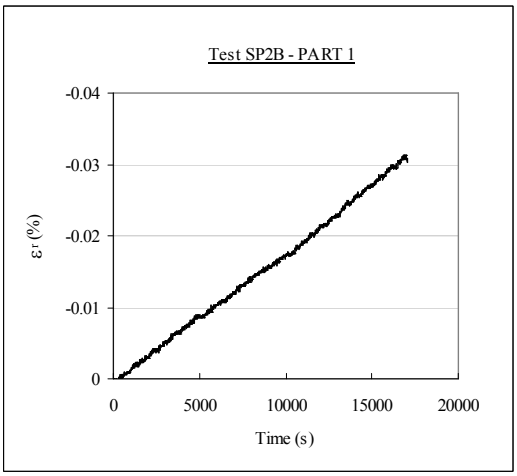

Figure D.14. Test SP2B. Variation in ε_r with time during PART 1 measured by the radial on-sample Hall Effect device

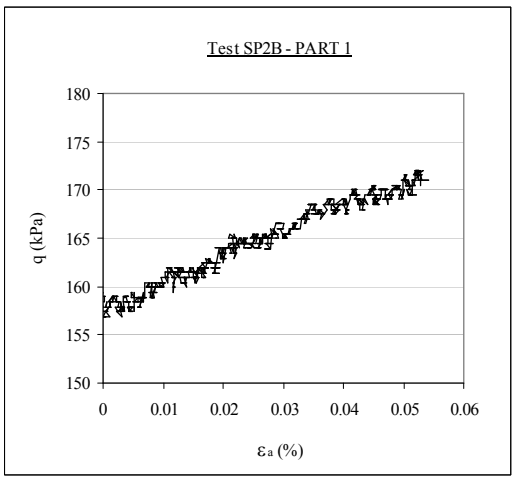

Figure D.15. Test SP2B. q - ε_a relationship during PART 1 based on the Hall Effect device internal measurements

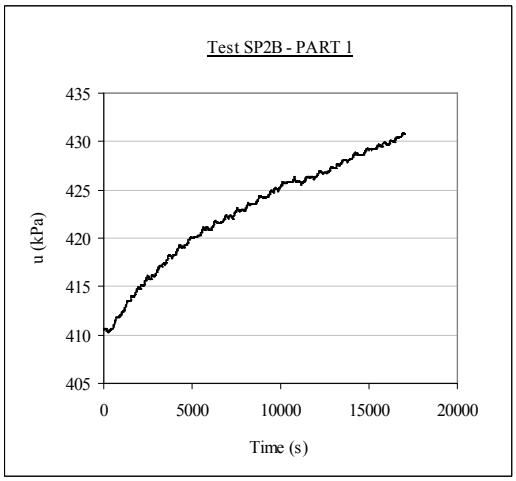

Figure D.16. Test SP2B. Variation in u with time during PART 1

Figure D.17. Mode of failure during test SP2B

Test SP2C

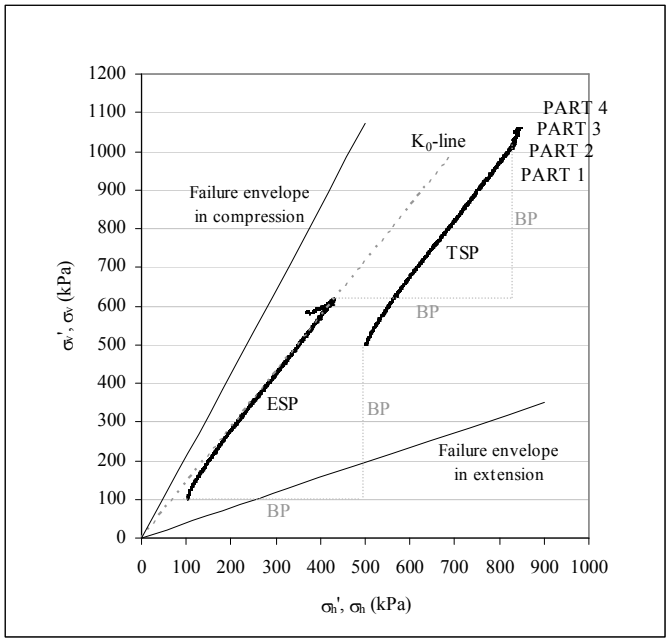

Figure D.18. Total and effective experimental stress paths during test SP2C. BP: Back-pressure, TSP: Total stress path, ESP: Effective stress path

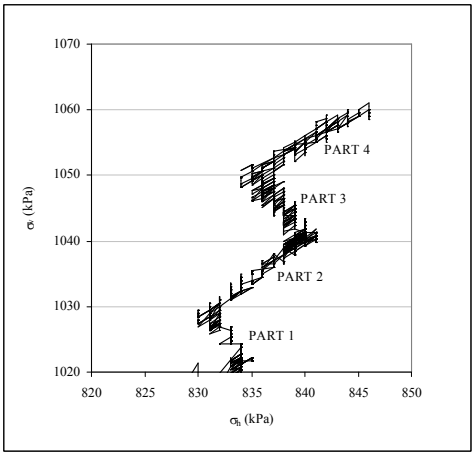

Figure D.19. Detail of the total stress paths during test SP2C from Figure 7.32

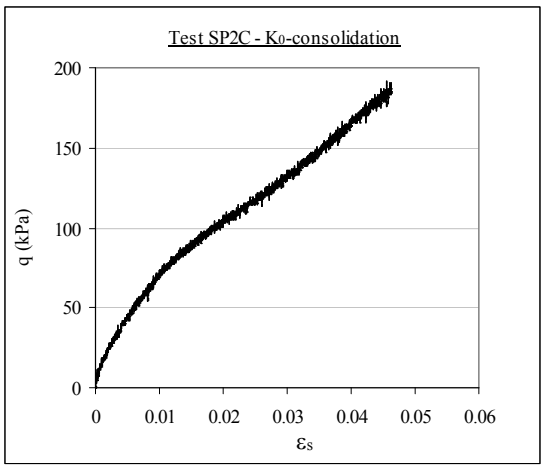

Figure D.20. Test SP2C. q - ε_s relationship during the K_0-consolidation stage

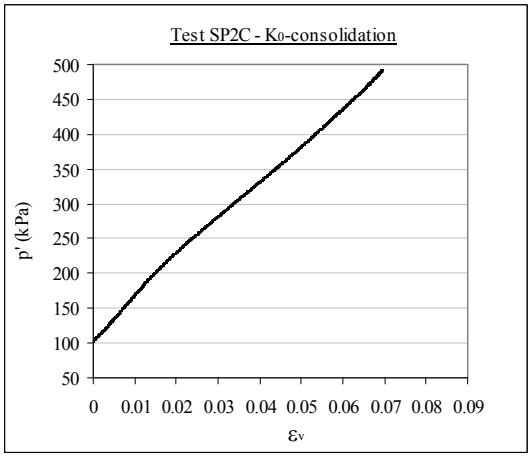

Figure D.21. Test SP2C. p' - ε_v relationship during the K_0-consolidation stage

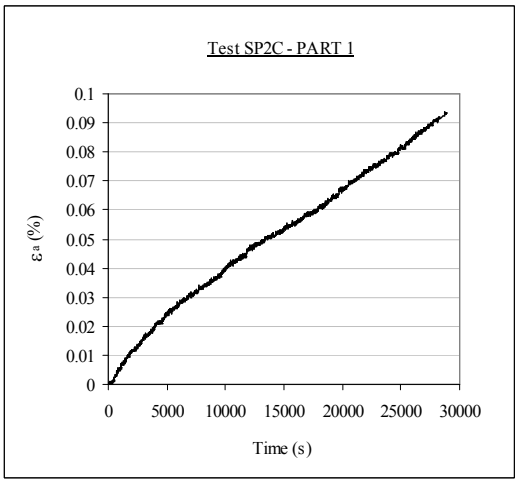

Figure D.22. Test SP2C. Variation in ε_a with time during PART 1 measured by the axial on-sample Hall Effect device

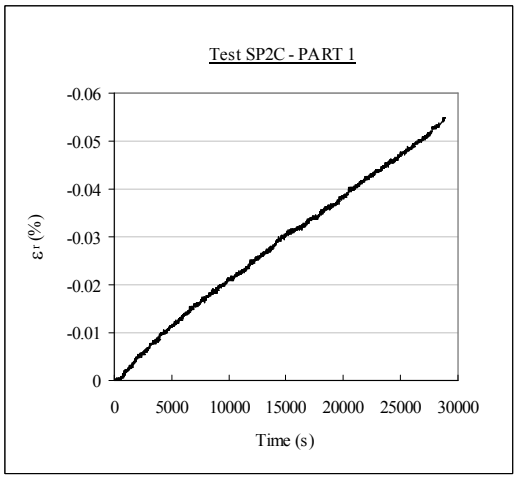

Figure D.23. Test SP2C. Variation in ε_r with time during PART 1 measured by the radial on-sample Hall Effect device

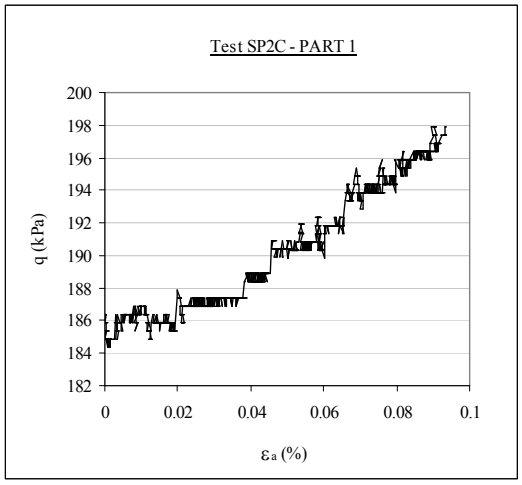

Figure D.24. Test SP2C. q - ε_a relationship during PART 1

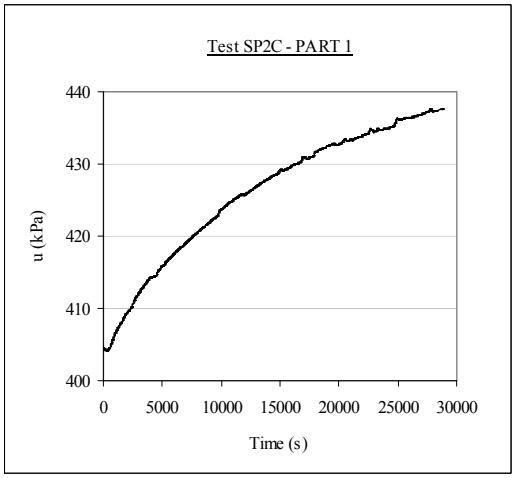

Figure D.25. Test SP2C. Variation in u with time during PART 1

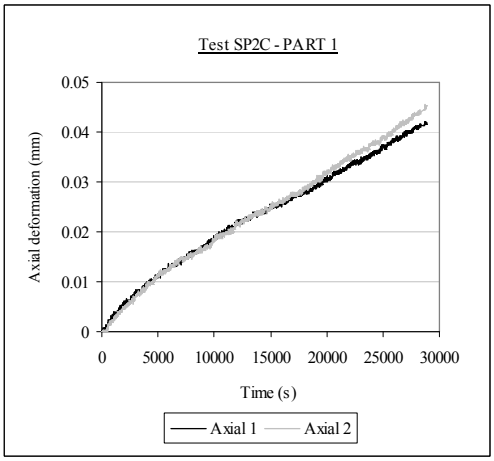

Figure D.26. Test SP2C. Comparison between the readings of both axial Hall Effect devices during PART 1

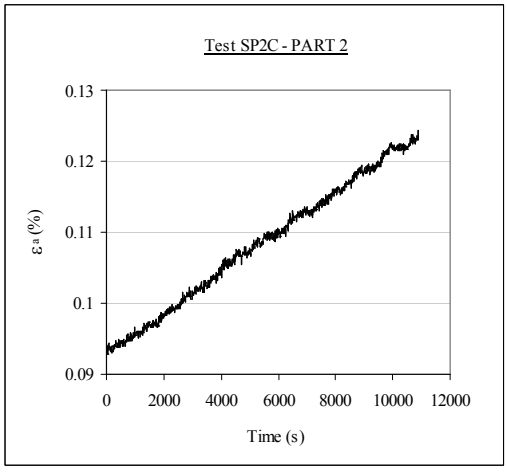

Figure D.27. Test SP2C. Variation in ε_a with time during PART 2 measured by the axial on-sample Hall Effect device

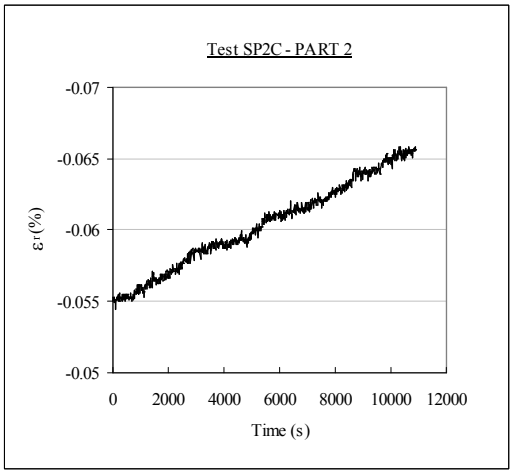

Figure D.28. Test SP2C. Variation in ε_r with time during PART 2 measured by the radial on-sample Hall Effect device

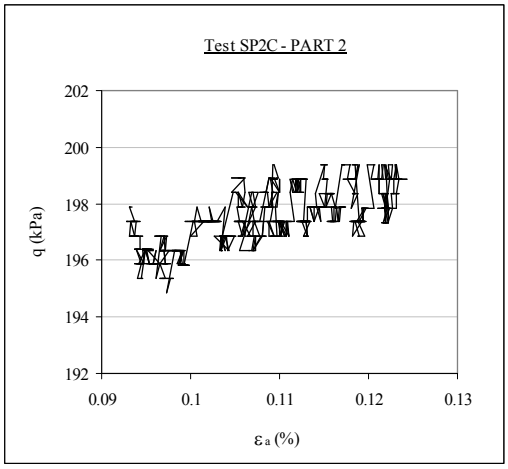

Figure D.29. Test SP2C. q - ε_a relationship during PART 2

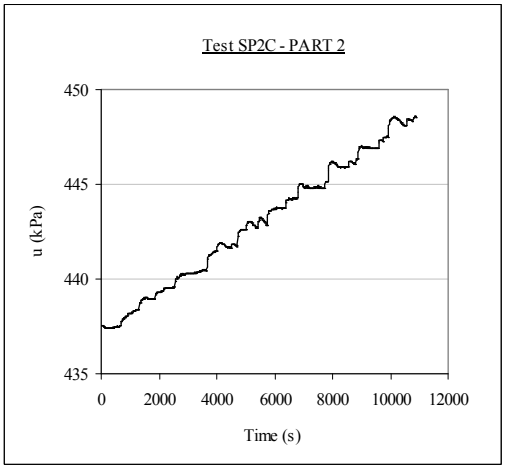

Figure D.30. Test SP2C. Variation in u with time during PART 2

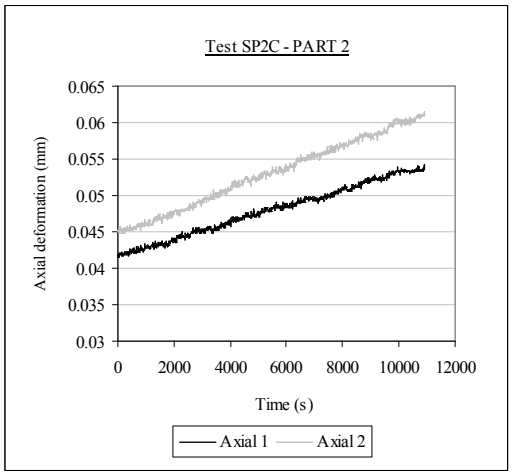

Figure D.31. Test SP2C. Comparison between the readings of both axial Hall Effect devices during PART 2

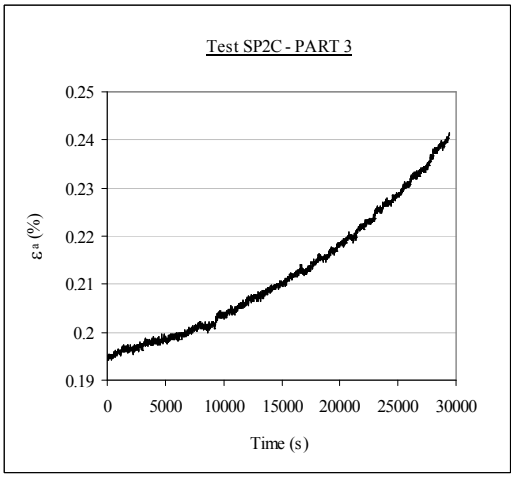

Figure D.32. Test SP2C. Variation in ε_a with time during PART 3 measured by the axial on-sample Hall Effect device

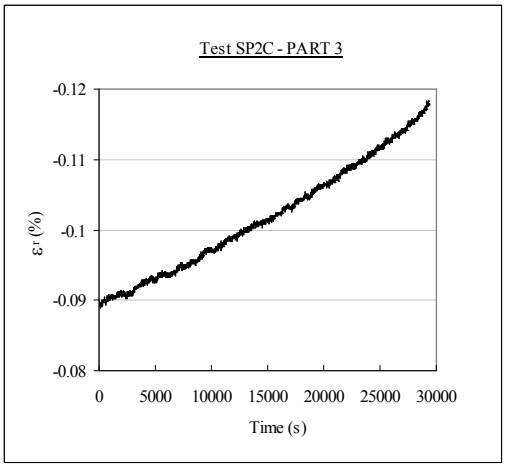

Figure D.33. Test SP2C. Variation in ε_r with time during PART 3 measured by the radial on-sample Hall Effect device

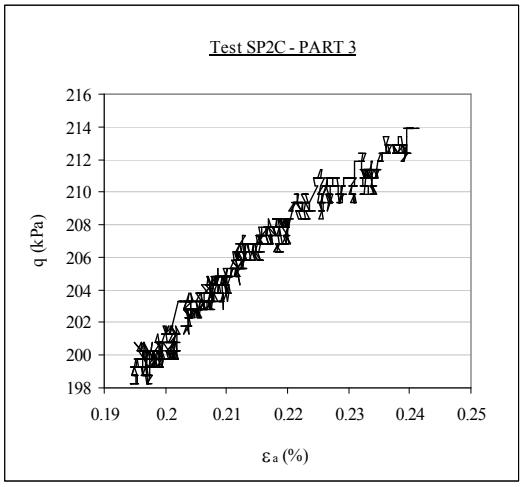

Figure D.34. Test SP2C. q - ε_a relationship during PART 3

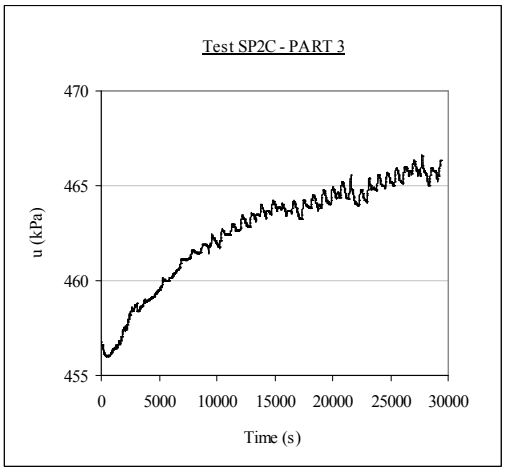

Figure D.35. Test SP2C. Variation in u with time during PART 3

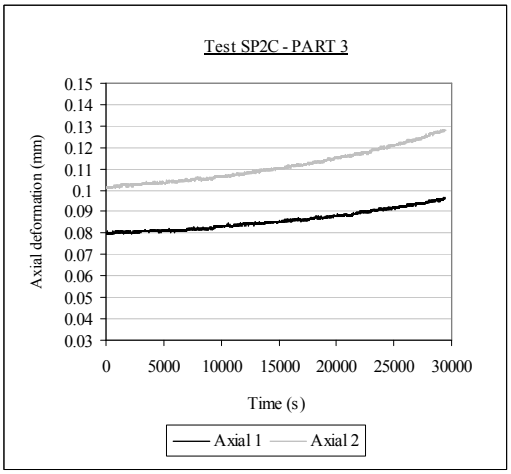

Figure D.36. Test SP2C. Comparison between the readings of both axial Hall Effect devices during PART 3

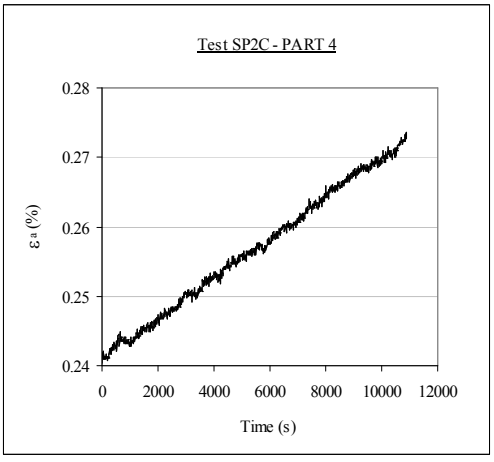

Figure D.37. Test SP2C. Variation in ε_a with time during PART 4 measured by the axial on-sample Hall Effect device

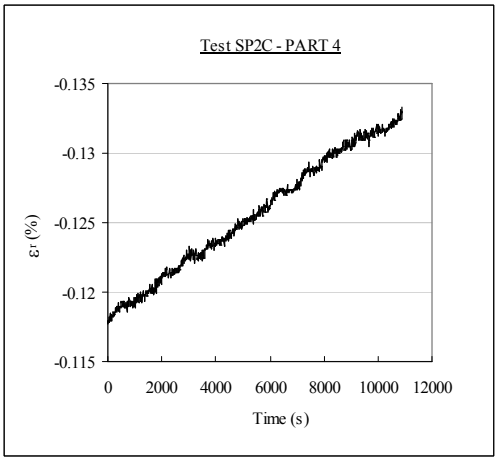

Figure D.38. Test SP2C. Variation in ε_r with time during PART 4 measured by the radial on-sample Hall Effect device

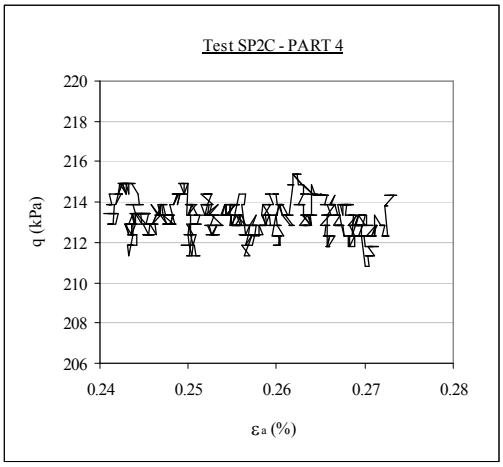

Figure D.39. Test SP2C. q - ε_a relationship during PART 4

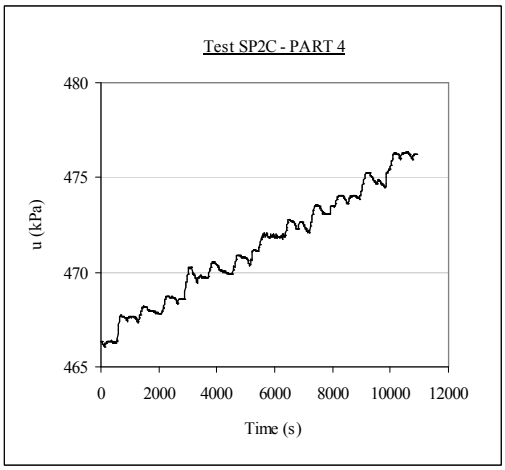

Figure D.40. Test SP2C. Variation in u with time during PART 4

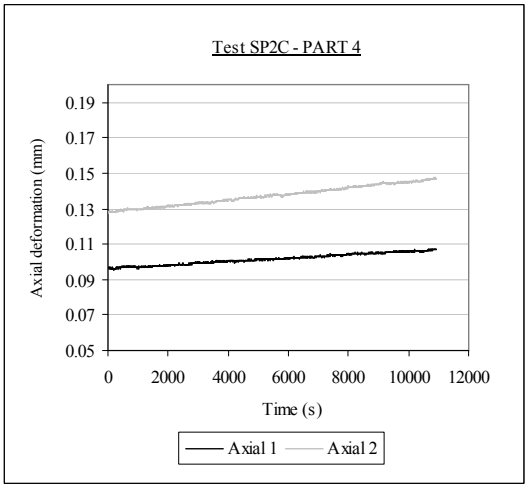

Figure D.41. Test SP2C. Comparison between the readings of both axial Hall Effect devices during PART 4

CROWN. SINGLE TUNNEL. K_0>1

Test SP3

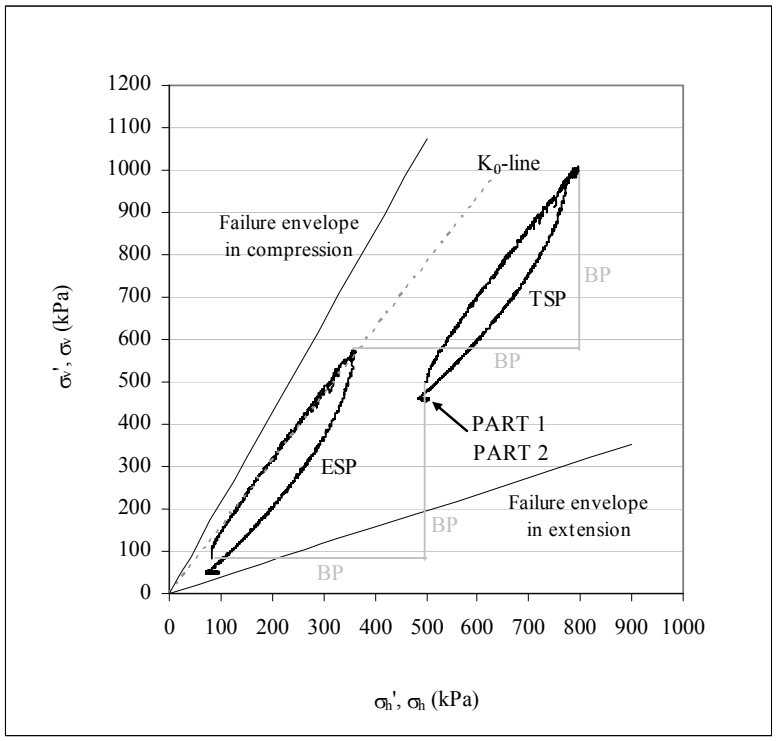

Figure D.42. Total and effective experimental stress paths during test SP3.
BP: Back-pressure, TSP: Total stress path, ESP: Effective stress path

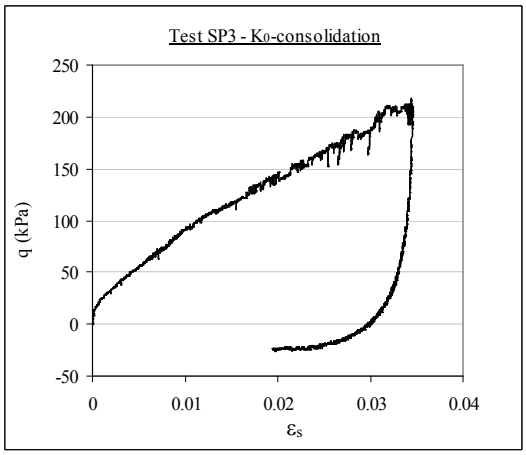

Figure D.43. Test SP3. q - ε_s relationship during the K_0-consolidation stage

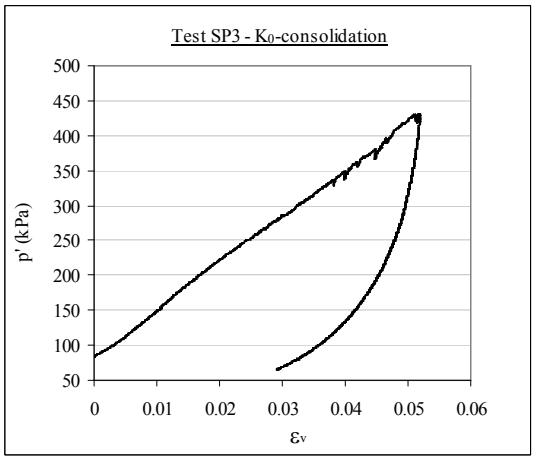

Figure D.44. Test SP3. p' - ε_v relationship during the K_0-consolidation stage in test SP3

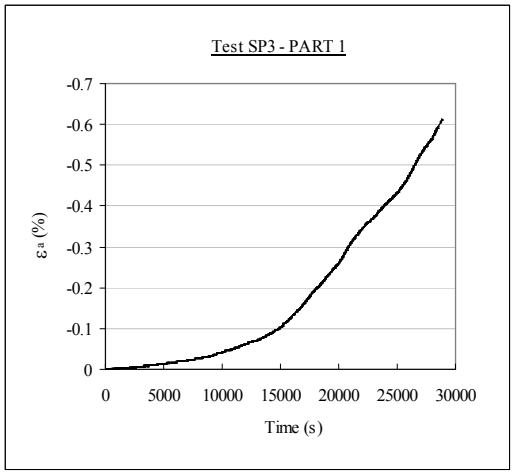

Figure D.45. Test SP3. Variation in ε_a with time during PART 1 measured by the two axial on-sample Hall Effect device

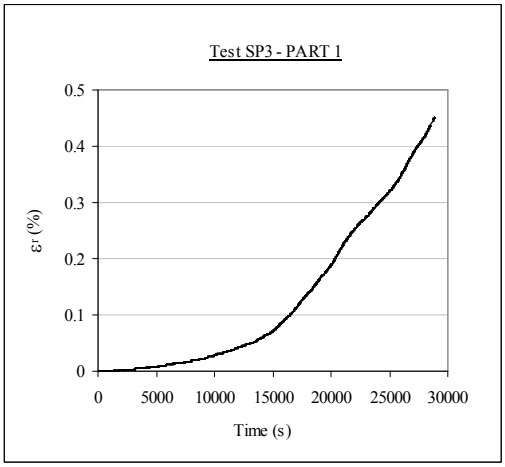

Figure D.46. Test SP3. Variation in ε_r with time during PART 1 measured by the radial on-sample Hall Effect device

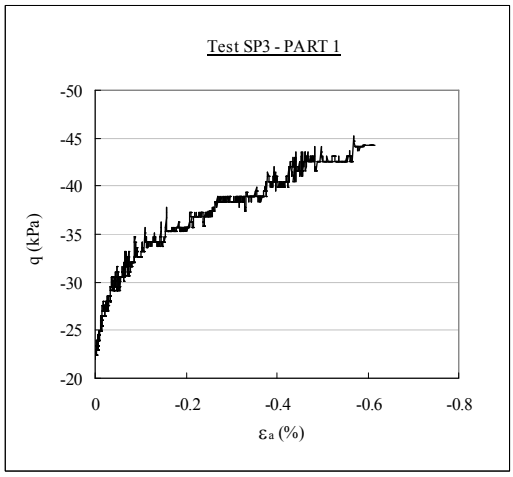

Figure D.47. Test SP3. q - ε_a relationship during PART 1

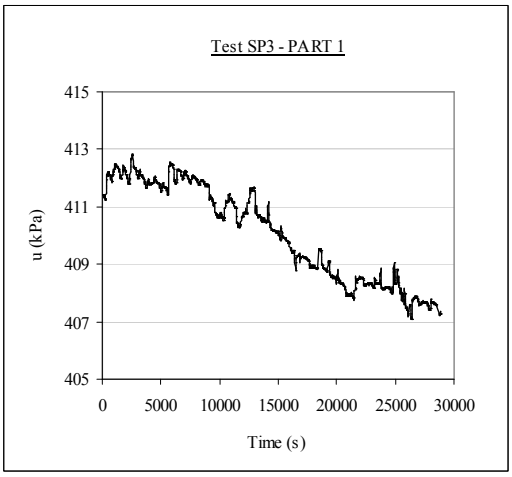

Figure D.48. Test SP3. Variation in u with time during PART 1

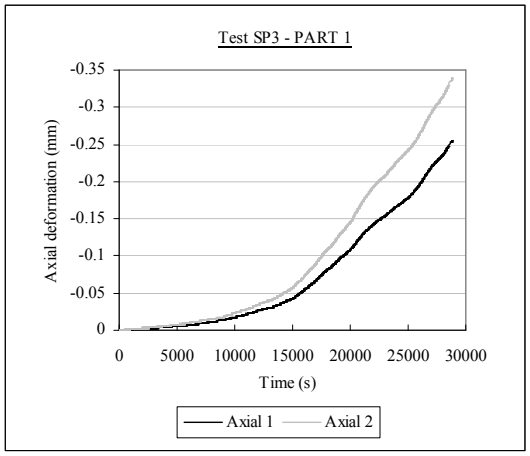

Figure D.49. Test SP3. Comparison between the axial deformation registered by both axial Hall Effect devices during PART 1

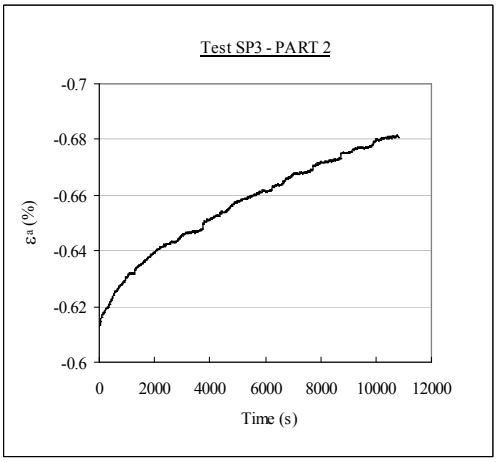

Figure D.50. Test SP3. Variation in ε_a with time during PART 2 measured by the two axial on-sample Hall Effect device. The sample length decreases over time

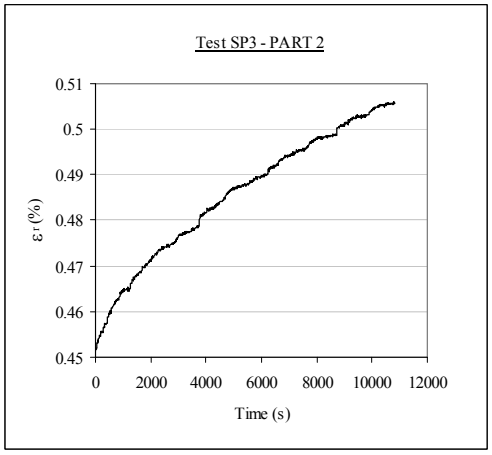

Figure D.51. Test SP3. Variation in ε_r with time during PART 2 measured by the radial on-sample Hall Effect device. The sample diameter increases over time

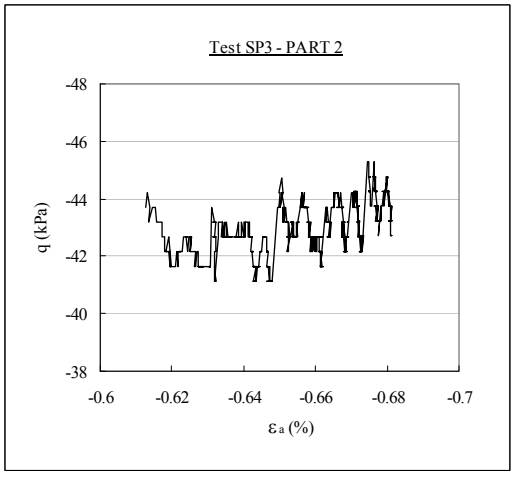

Figure D.52. Test SP3. q - ε_a relationship during PART 2

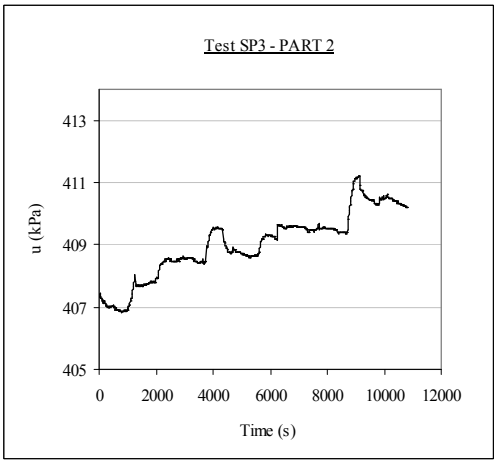

Figure D.53. Test SP3. Variation in u with time during PART 2

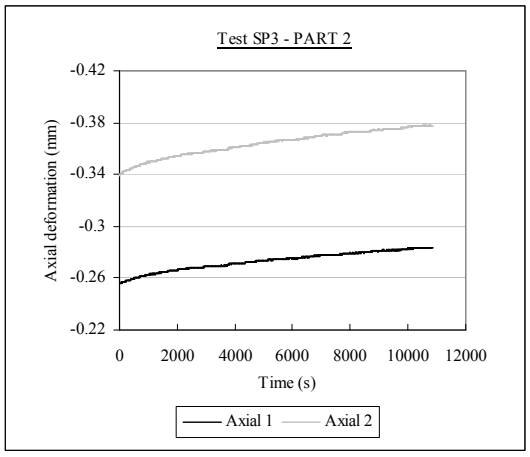

Figure D.54. Test SP3. Comparison between the axial deformation registered by both axial Hall Effect devices during PART 2

SPRINGLINE. TWIN TUNNELS. K_0>1

Test SP4

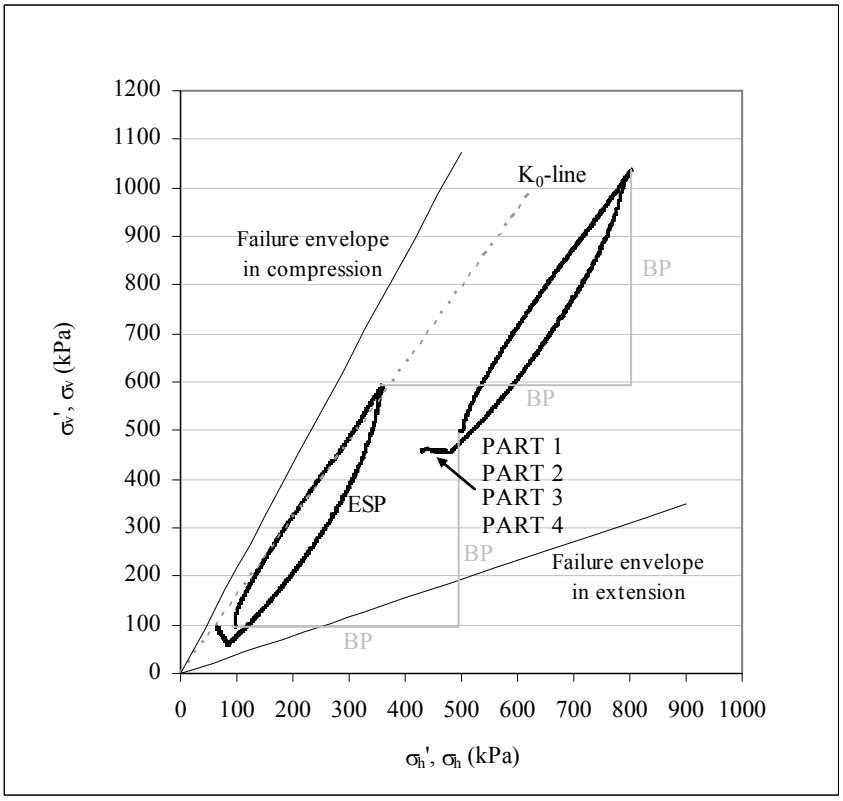

Figure D.55. Total and effective experimental stress paths during test SP4.
BP: Back-pressure, TSP: Total stress path, ESP: Effective stress path

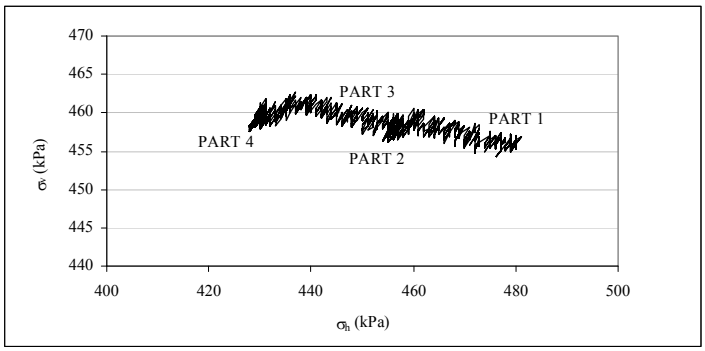

Figure D.56. Detail of the total stress path during test SP4 from Figure 7.69

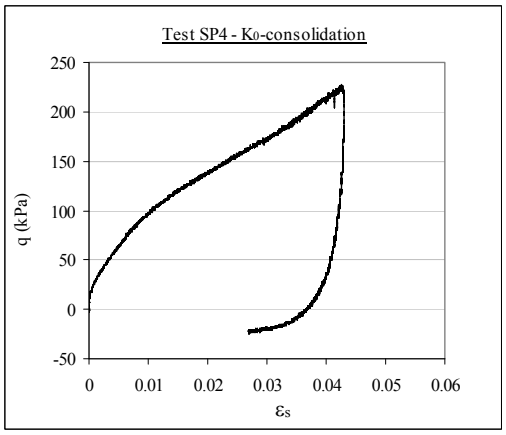

Figure D.57. Test SP4. q - ε_s relationship during the K_0-consolidation stage

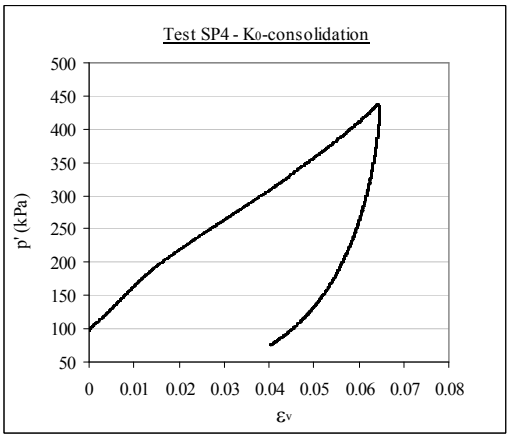

Figure D.58. Test SP4. p' - ε_v relationship during the K_0-consolidation stage

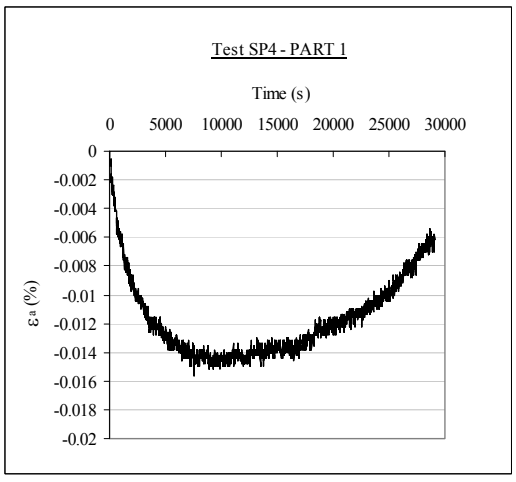

Figure D.59. Test SP4. Variation in ε_a with time during PART 1 measured by the axial on-sample Hall Effect device

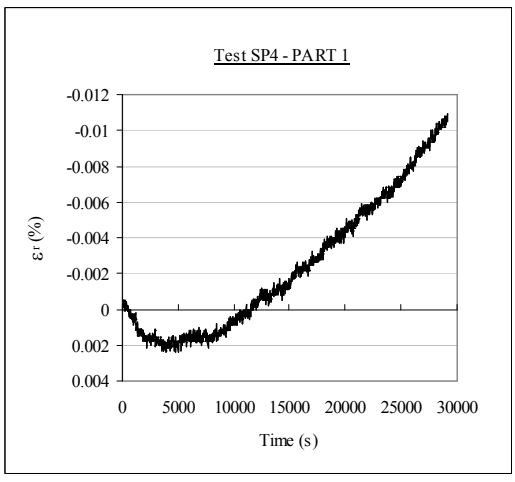

Figure D.60. Test SP4. Variation in ε_r with time during PART 1 measured by the radial on-sample Hall Effect device

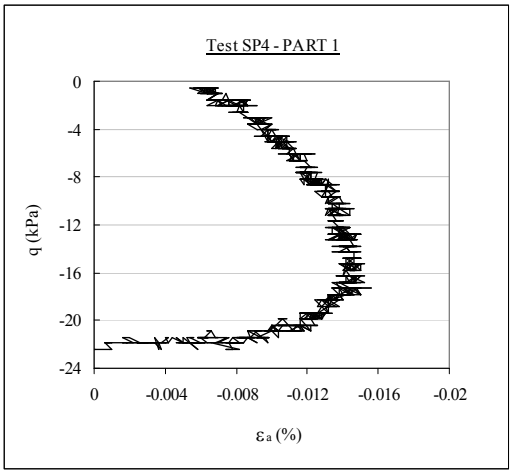

Figure D.61. Test SP4. q - ε_a relationship during PART 1

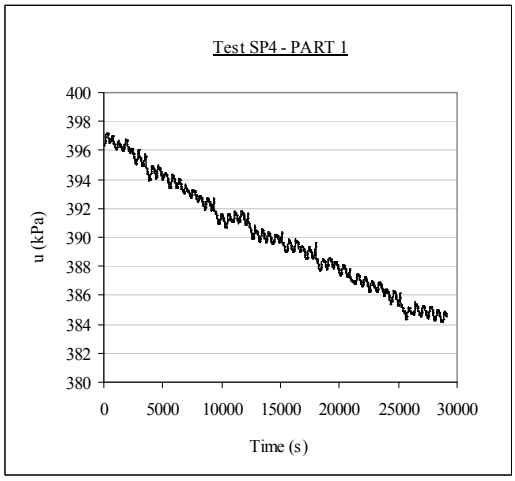

Figure D.62. Test SP4. Variation in u with time during PART 1

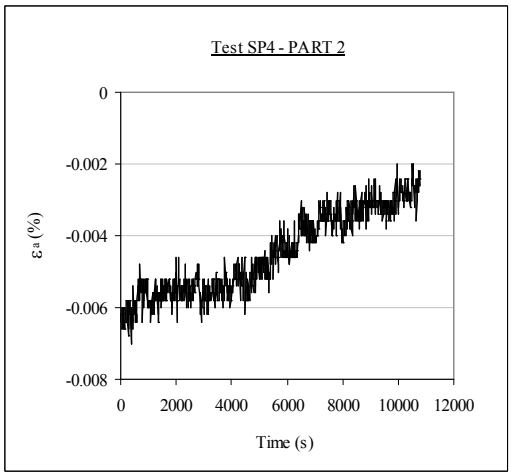

Figure D.63. Test SP4. Variation in ε_a with time during PART 2 measured by the axial on-sample Hall Effect device

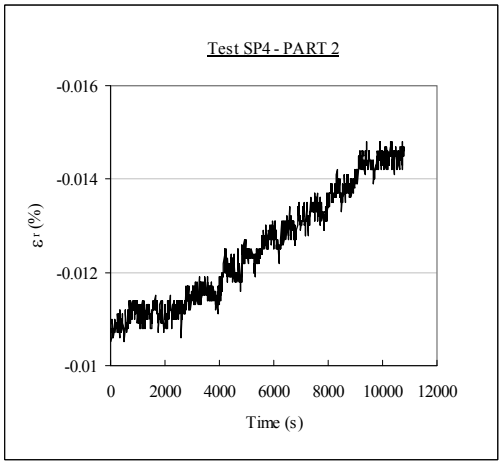

Figure D.64. Test SP4. Variation in ε_r with time during PART 2 measured by the radial on-sample Hall Effect device

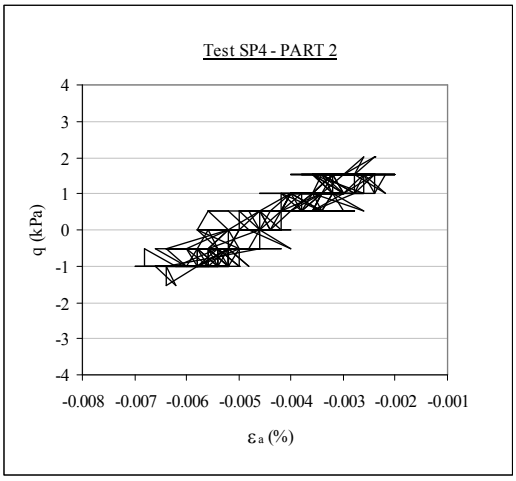

Figure D.65. Test SP4. q - ε_a relationship during PART 2

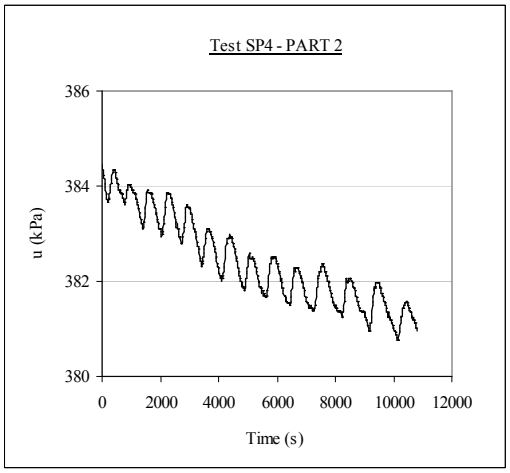

Figure D.66. Test SP4. Variation in u with time during PART 2

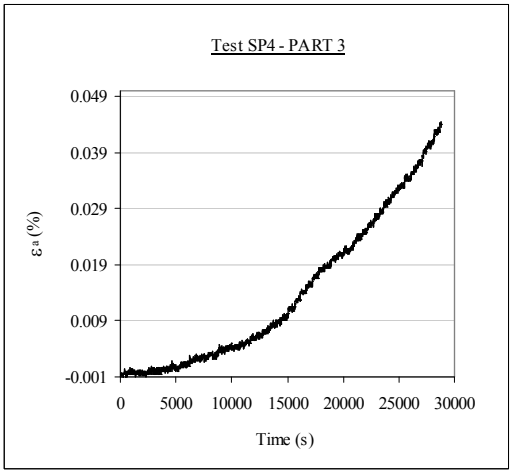

Figure D.67. Test SP4. Variation in ε_a with time during PART measured by the axial on-sample Hall Effect device

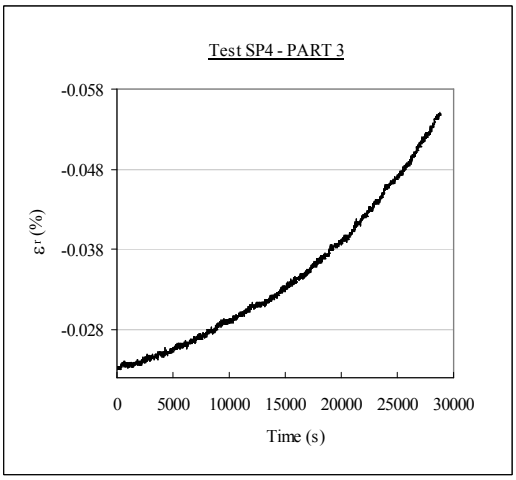

Figure D.68. Test SP4. Variation in ε_r with time during PART 3 measured by the radial on-sample Hall Effect device

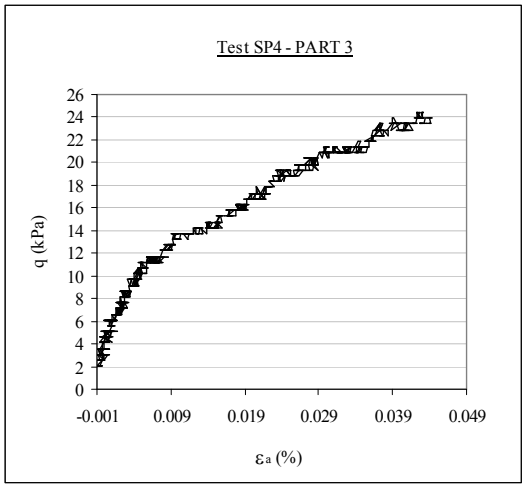

Figure D.69. Test SP4. q - ε_a relationship during PART 3

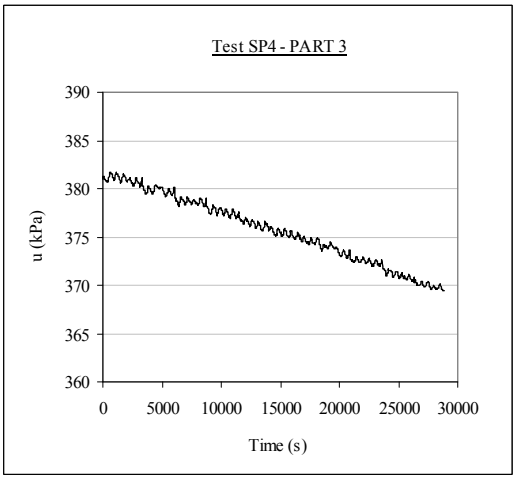

Figure D.70. Test SP4. Variation in u with time during PART 3

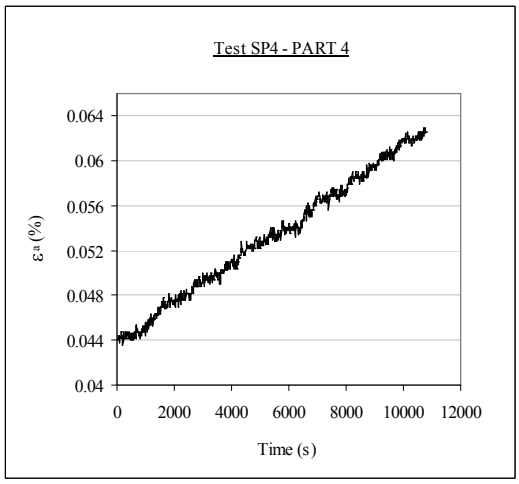

Figure D.71. Test SP4. Variation in ε_a with time during PART 4 measured by the axial on-sample Hall Effect device

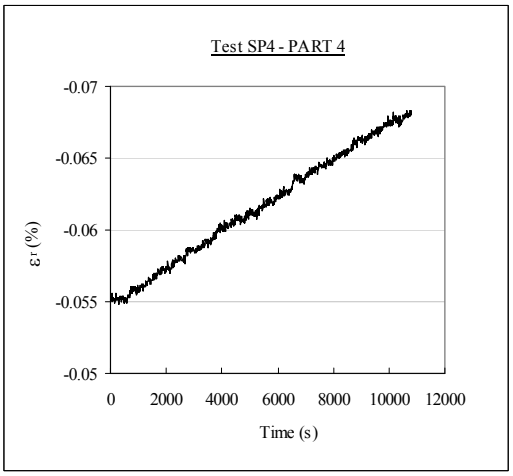

Figure D.72. Test SP4. Variation in ε_r with time during PART 4 measured by the radial on-sample Hall Effect device

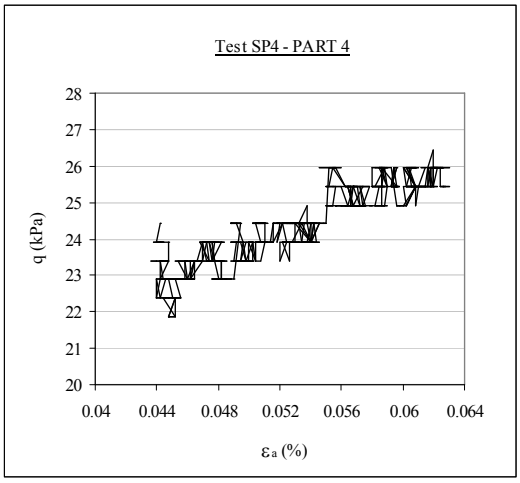

Figure D.73. Test SP4. q - ε_a relationship during PART 4

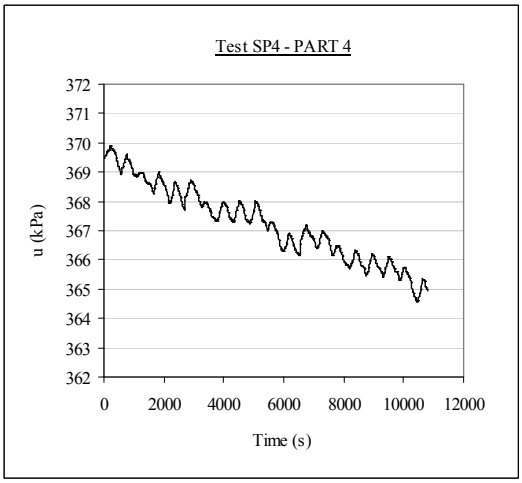

Figure D.74. Test SP4. Variation in u with time during PART 4

D.2. VARIATION IN SOIL STIFFNESS AND EVALUATION OF THE JARDINE ET AL. (1991) SMALL-STRAIN PARAMETERS

D.2.1. SHEAR RESPONSE

PART 1 Test SP2

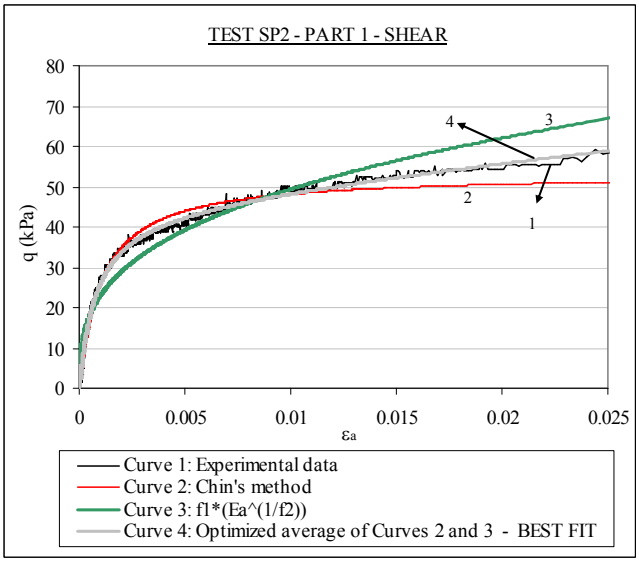

Figure D.75. Test SP2. Curve fitting for the shear response during PART 1. f_1 and f_2 are curve parameters

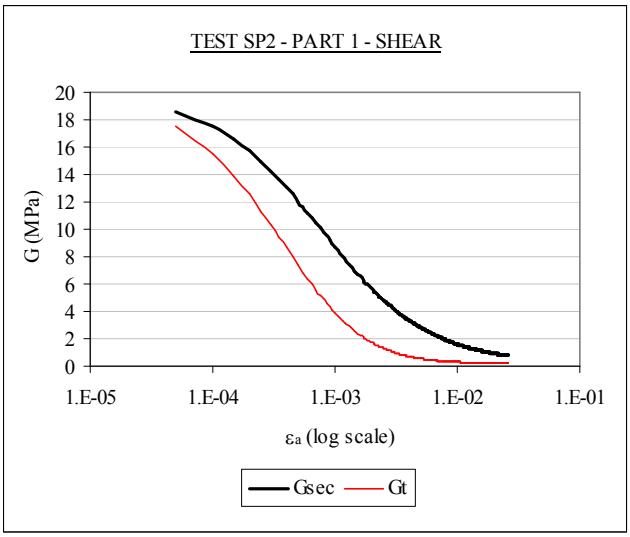

Figure D.76. Test SP2. G_{sec} (and G_t) - ε_s relationship during PART 1

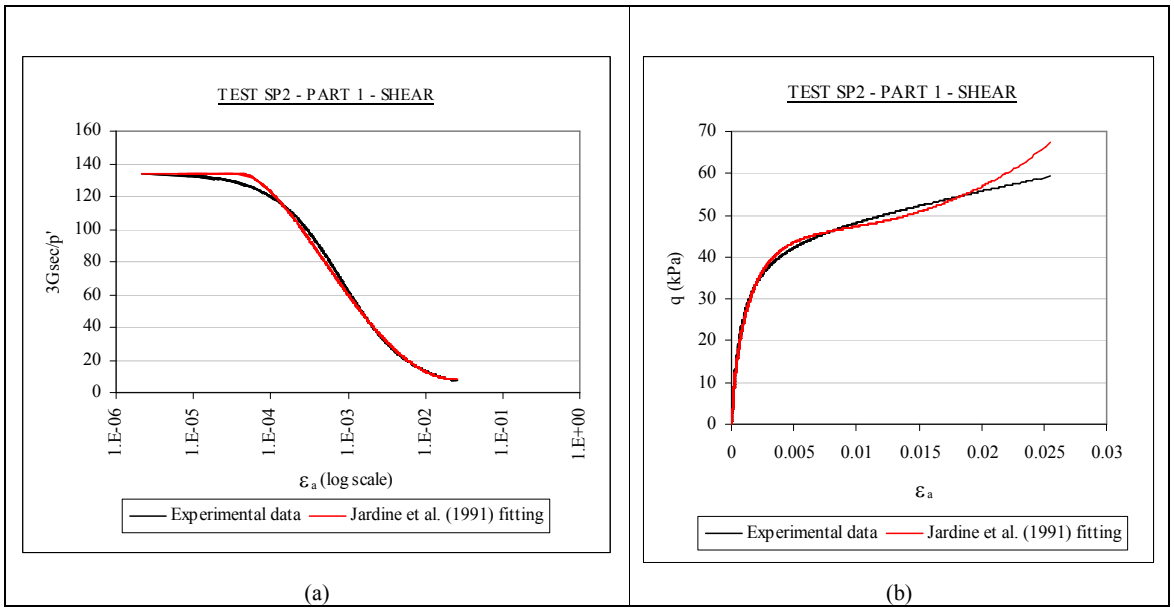

Figure D.77. Test SP2. Jardine et al. (1991) fitting to experimental data during PART 1: (a) fitting $3G_{sec} / p'$, (b) fitting q

PART 1 Test SP3

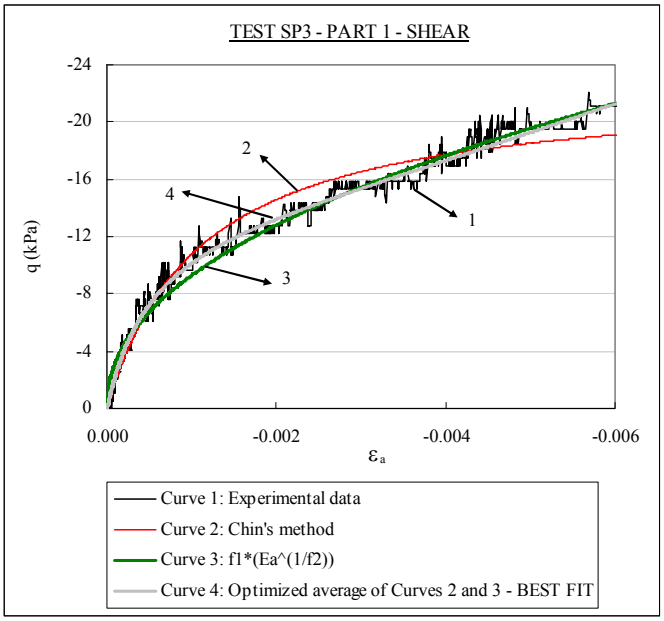

Figure D.78. Test SP3. Curve fitting for the shear response during PART 1. f_1 and f_2 are curve parameters

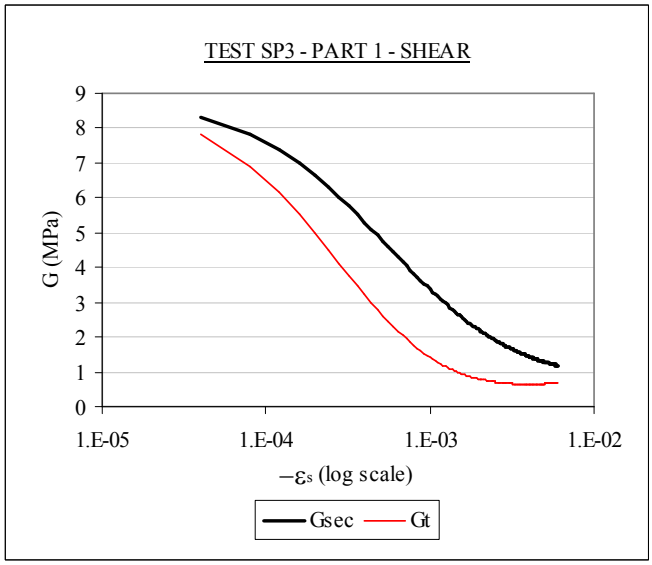

Figure D.79. Test SP3. G_{sec} (and G_t) - ε_s relationship during PART 1

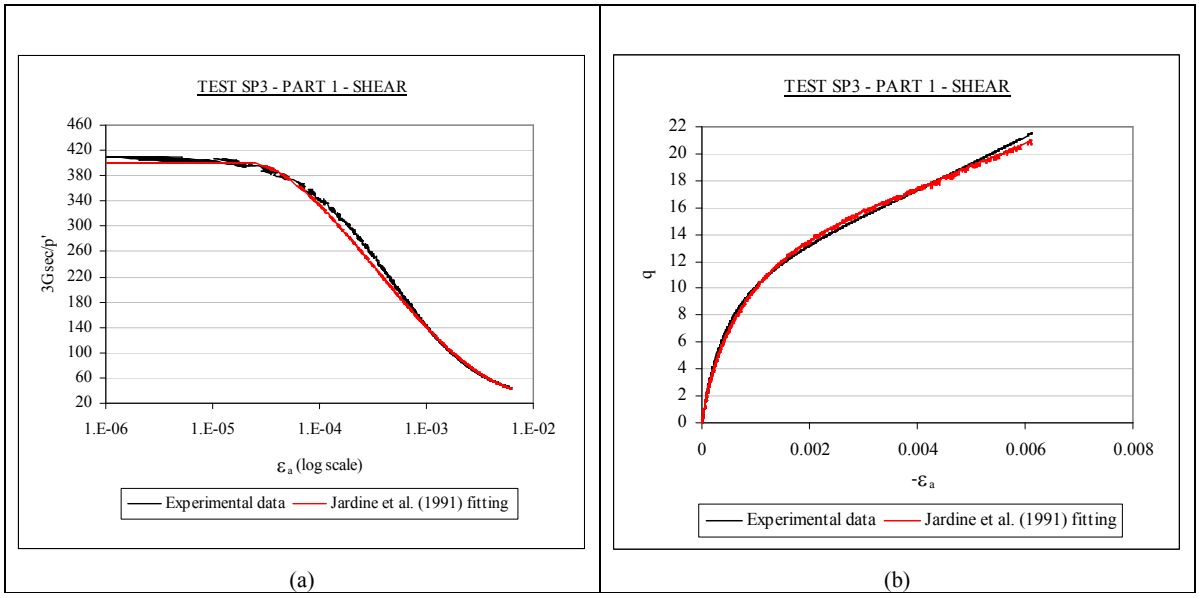

Figure D.80. Test SP3. Jardine et al. (1991) fitting to experimental data during PART 1: (a) fitting $3G_{sec} / p'$, (b) fitting q

PART 1 & 2 Test SP1

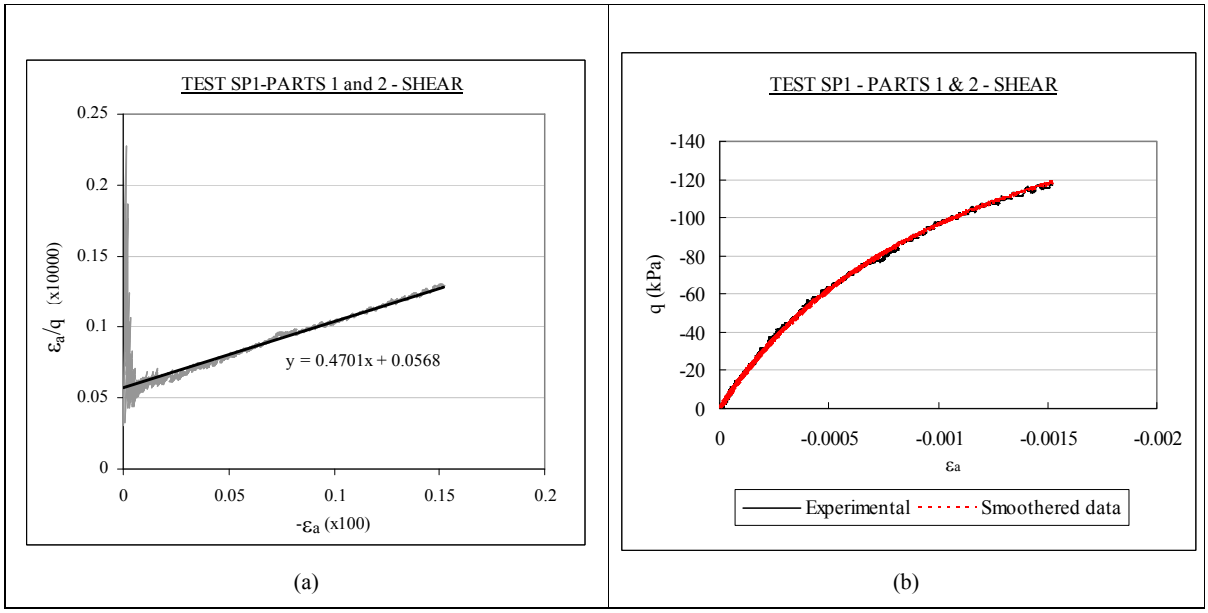

Figure D.81. Test SP1. (a) Chin (1978) method on (ε_a / q) -ε_a data during PARTS 1 and 2; (b) Chin's fitting on (ε_a / q) -ε_a data

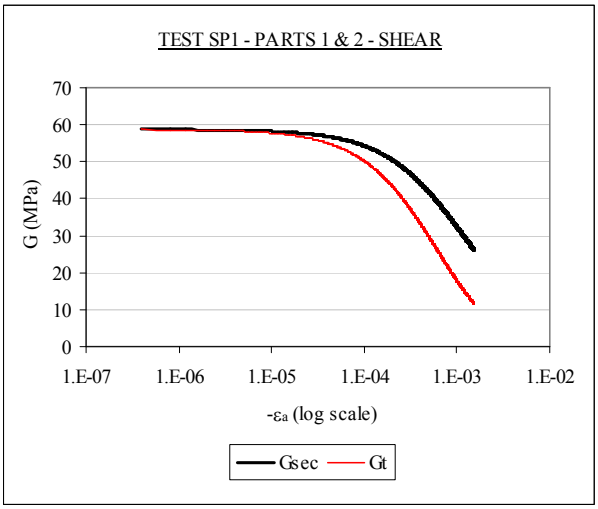

Figure D.82. Test SP1 G_{sec} (and G_t) - ε_s relationship during PARTS 1 and 2. Only the portion of the soil response where the axial strains are negative has been considered

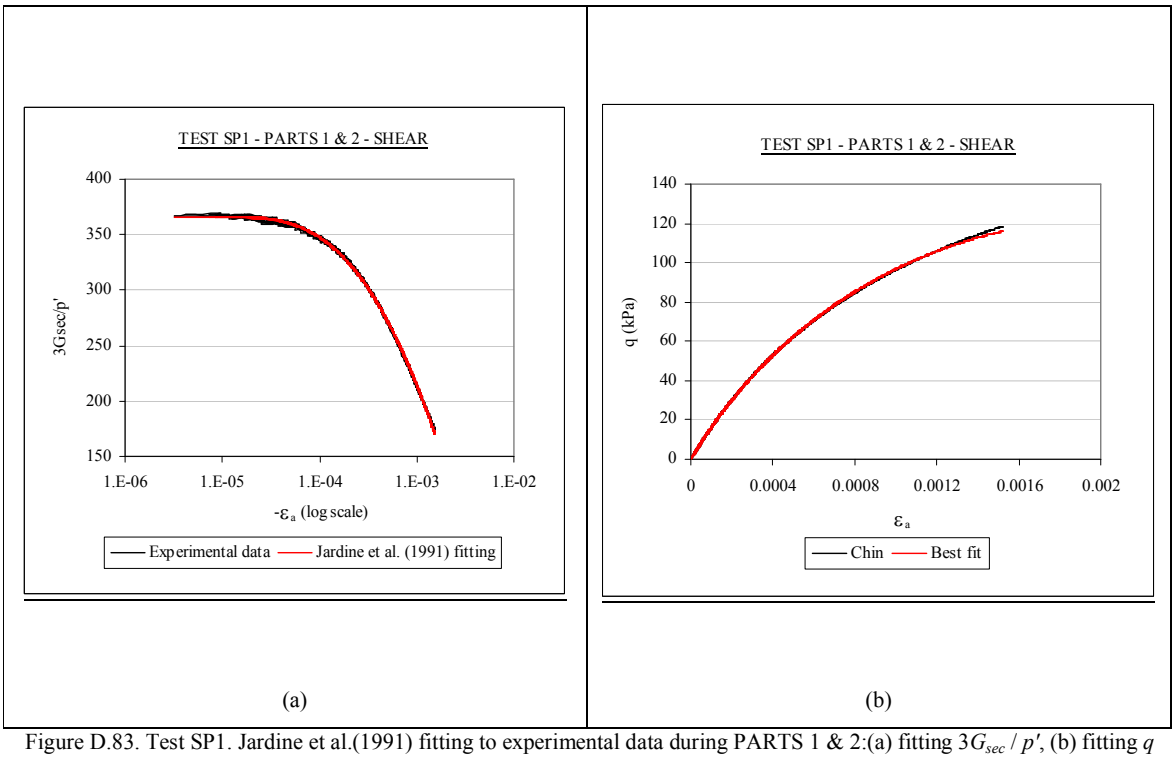

Figure D.83. Test SP1. Jardine et al.(1991) fitting to experimental data during PARTS 1 & 2:(a) fitting $3G_{sec}$ / p', (b) fitting q

PART 2 Test SP1

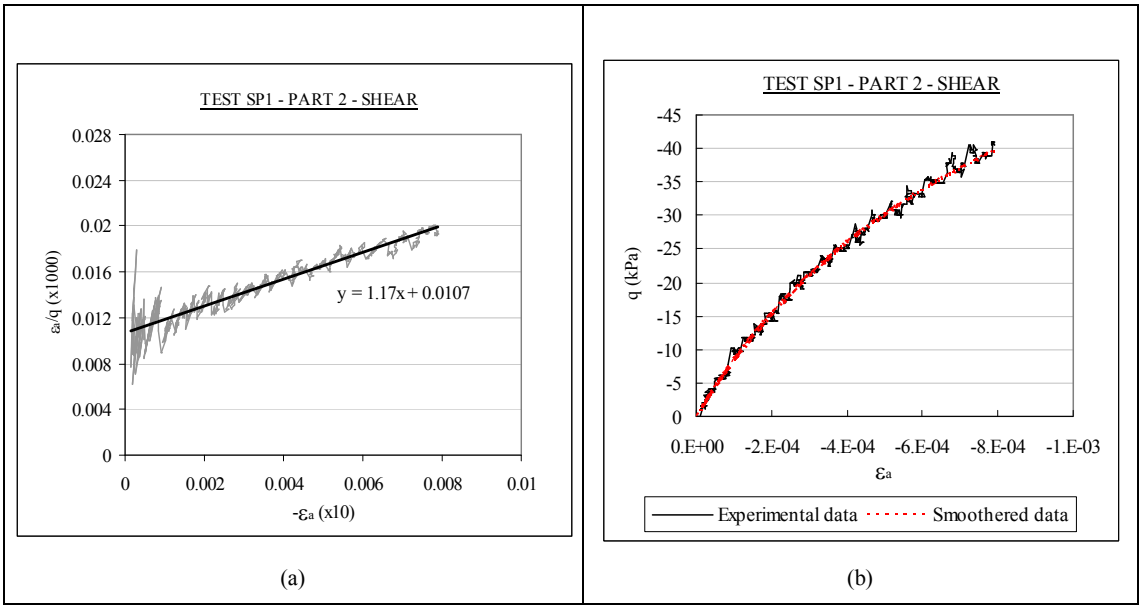

Figure D.84. Test SP1. (a) Chin (1978) method on q - ε_a data during PART 2 only; (b) Chin's fitting on q - ε_a data

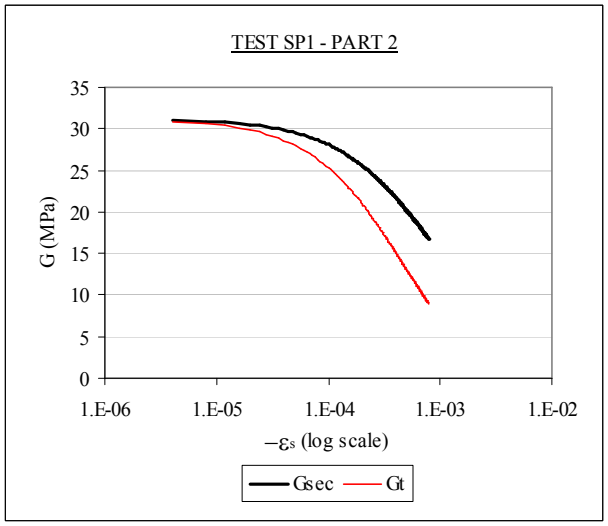

Figure D.85. Test SP1. G_{sec} (and G_t) - ε_s relationship using only data during PART 2

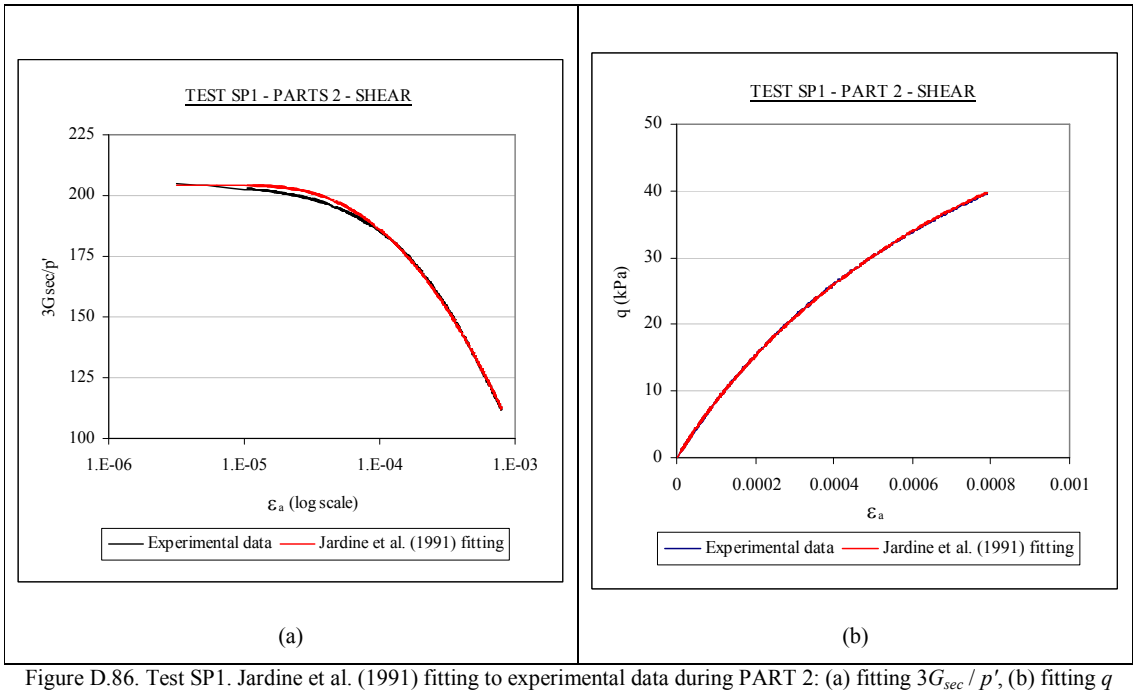

Figure D.86. Test SP1. Jardine et al. (1991) fitting to experimental data during PART 2: (a) fitting $3G_{sec} / p'$, (b) fitting q

K_0-unloading Test SP3

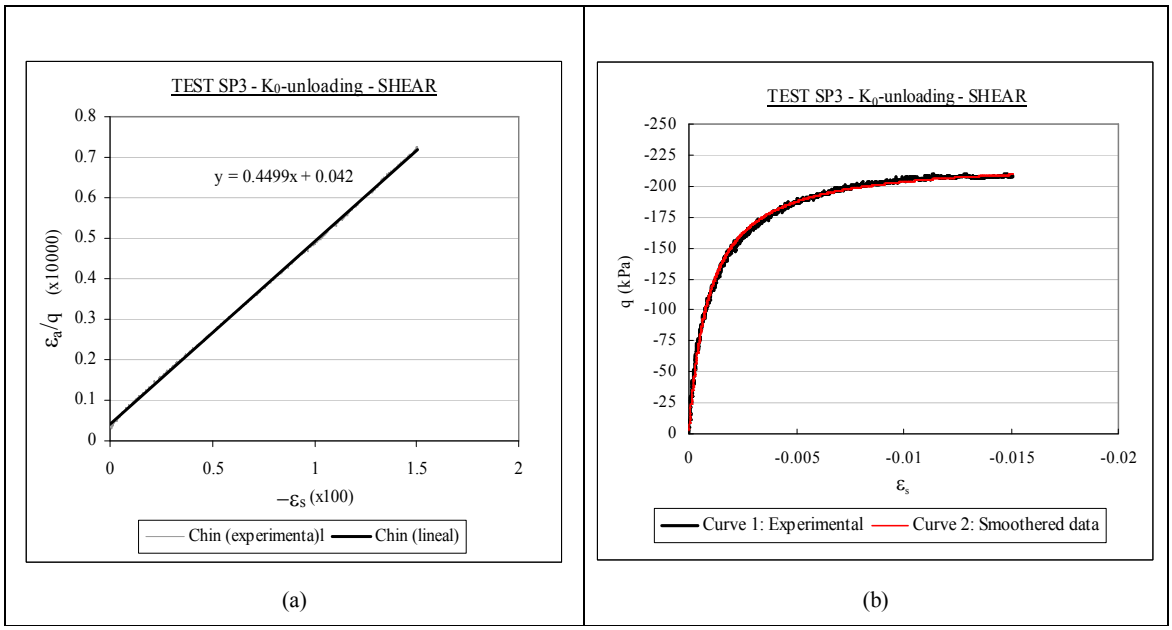

Figure D.87. Test SP3. (a) Chin (1978) method on q - ε_s data during K_0-unloading; (b) Chin's fitting on q - ε_s data

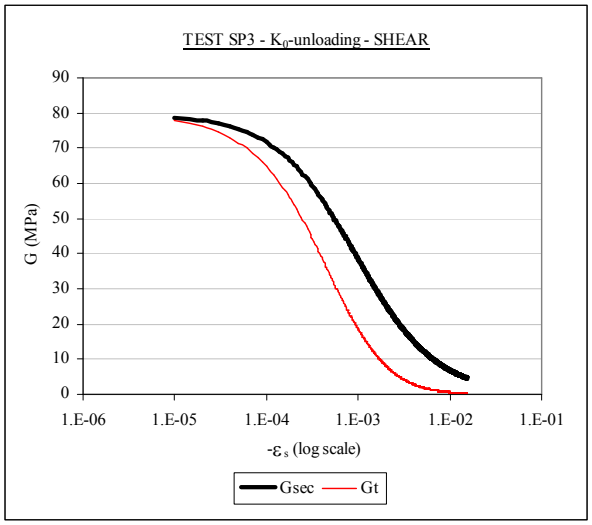

Figure D.88. Test SP3. G_{sec} (and G_t) - ε_s relationship using only data during K_0-unloading

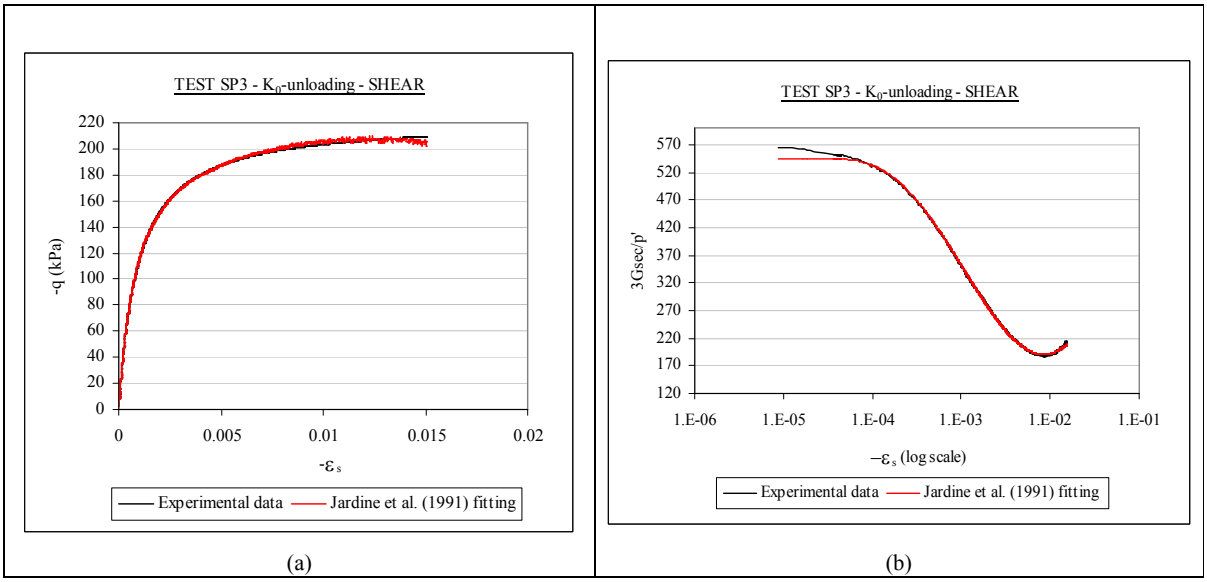

Figure D.89. Test SP3. Jardine et al. (1991) fitting to experimental data during K_0-unloading:(a) fitting $3G_{sec} / p'$, (b) fitting q

K_0-loading Test SP1

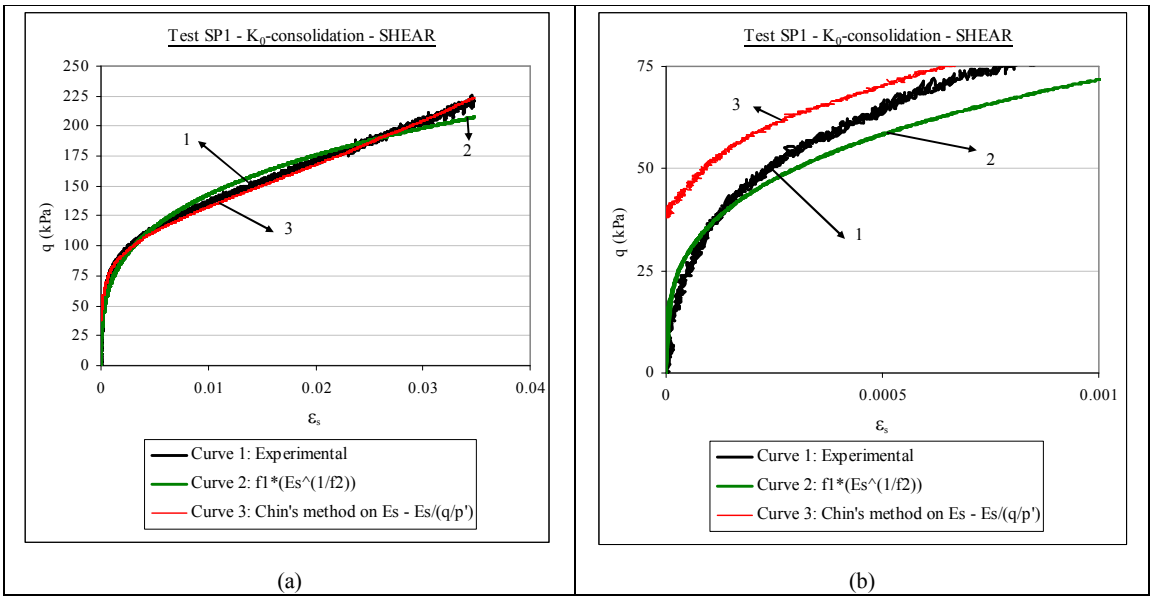

Figure D.90. Test SP1. (a) Curve fitting for the shear response during K_0-consolidation. f_1 and f_2 are curve parameters. (b) Detail for strains below 0.001

D.2.2. VOLUMETRIC RESPONSE

K_0-loading Test SP1

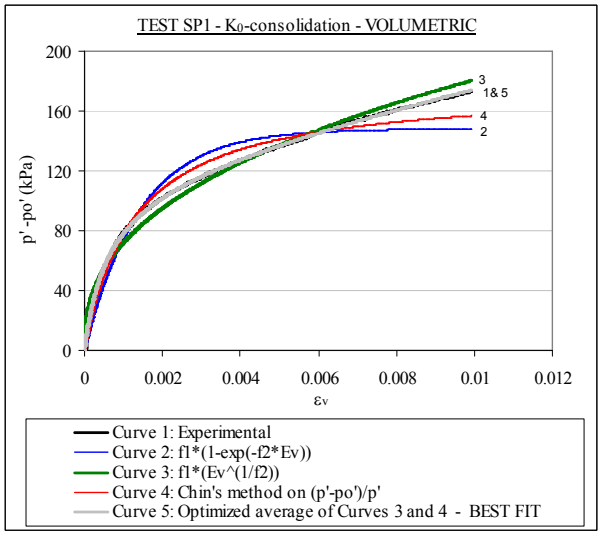

Figure D.91. Test SP1. Curve fitting for the volumetric response during the K_0-consolidation stage. f_1 and f_2 are curve parameters

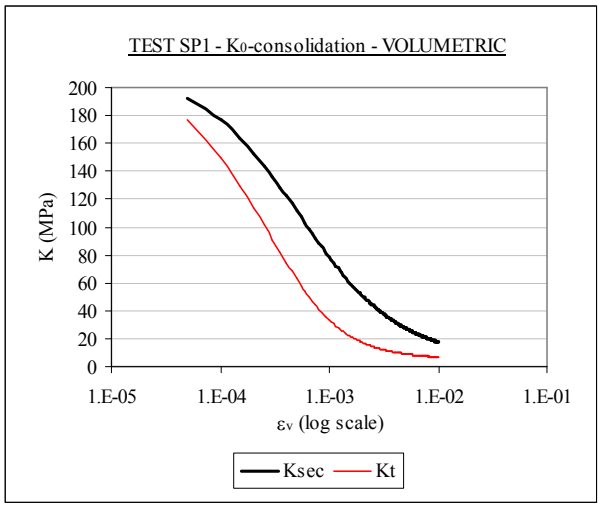

Figure D.92. Test SP1. K_{sec} (and K_t) - ε_v relationship during the K_0-consolidation stage

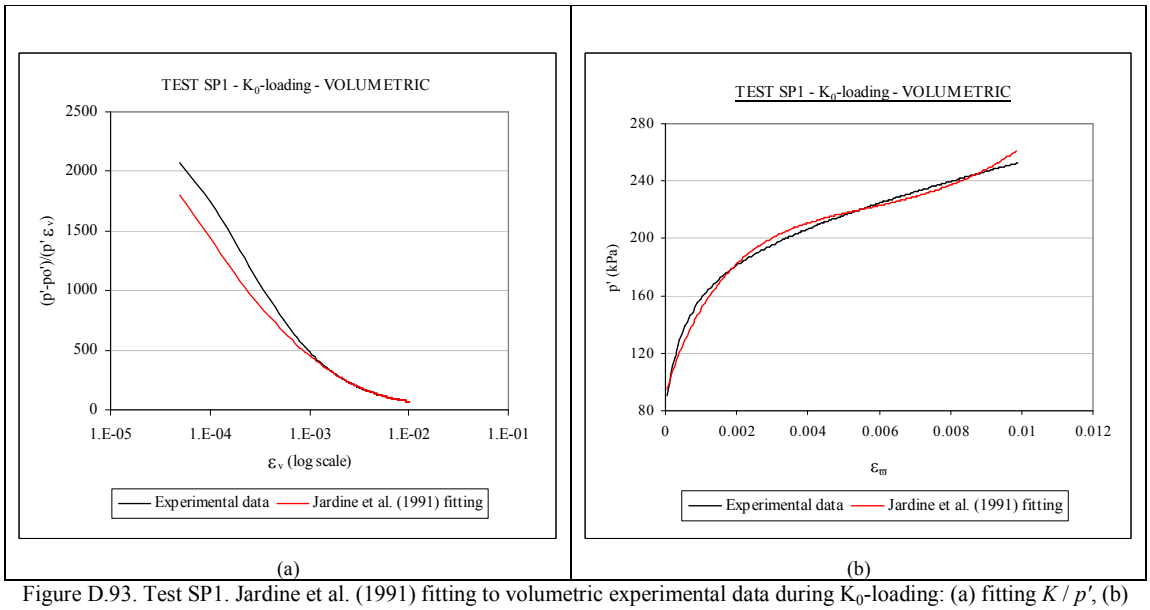

Figure D.93. Test SP1. Jardine et al. (1991) fitting to volumetric experimental data during K_0-loading: (a) fitting K / p', (b) fitting p'

K_0-unloading Test SP3

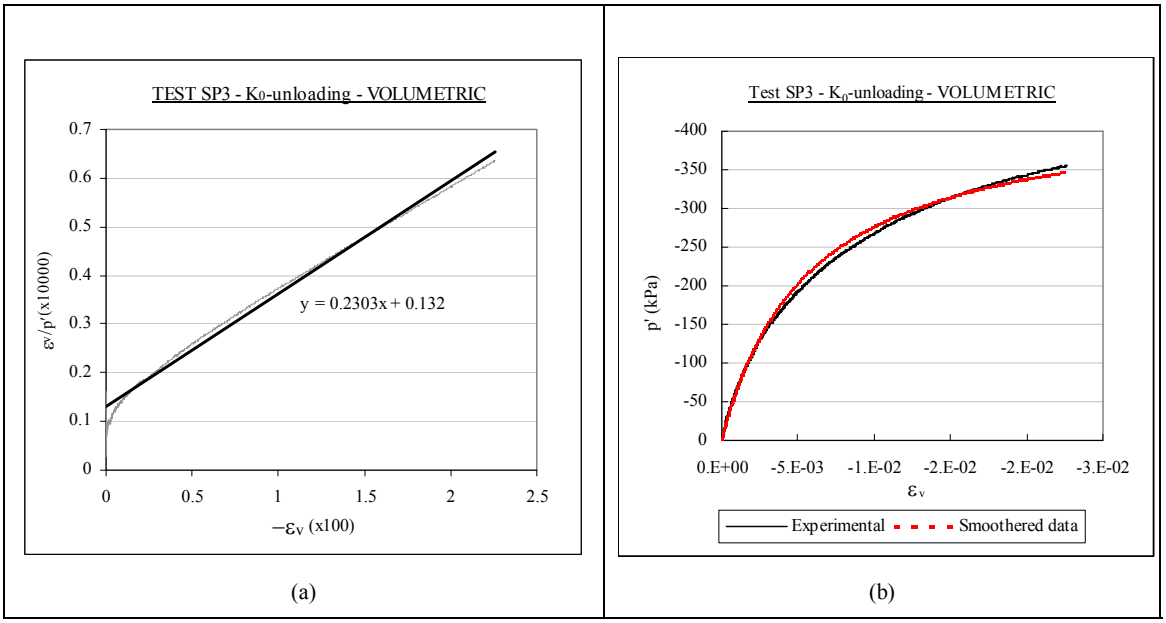

Figure D.94. Test SP3. (a) Chin (1978) method on p'-ε_v data during K_0-unloading; (b) Chin's fitting on p'-ε_v data

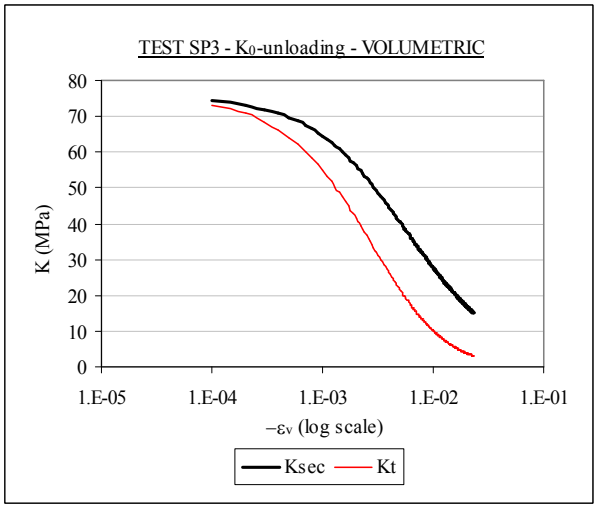

Figure D.95. Test SP3. K_{sec} (and K_t) - ε_v relationship during K_0-unloading

Appendix E: CHAPTER 8 - ADDITIONAL FIGURES

TEST USe5

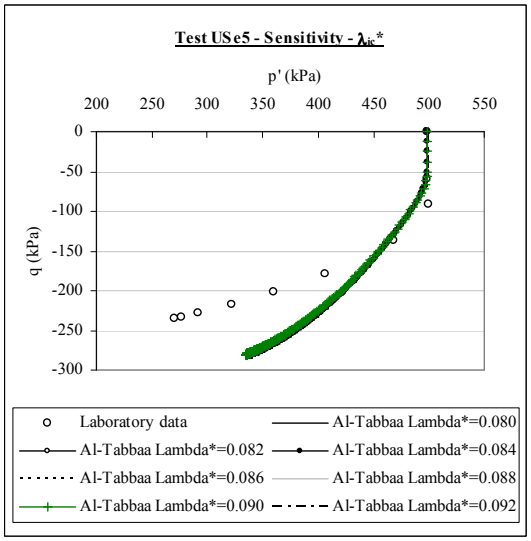

Figure E.1. Sensitivity of the Al-Tabbaa model to λ_{ic}* in terms of the q - p' behaviour during test USe5

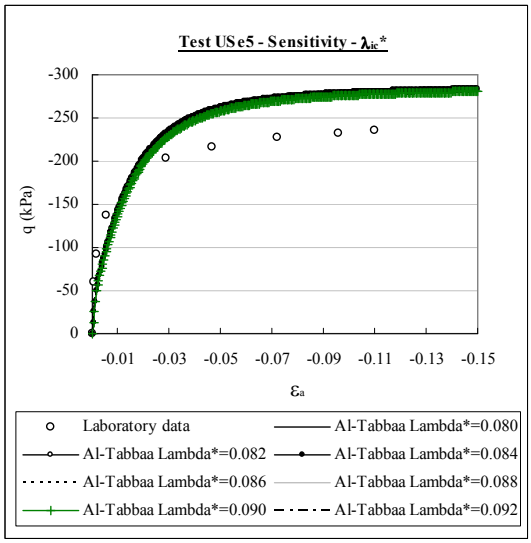

Figure E.2. Sensitivity of the Al-Tabbaa model to λ_{ic}* in terms of the q - ε_a behaviour during test USe5

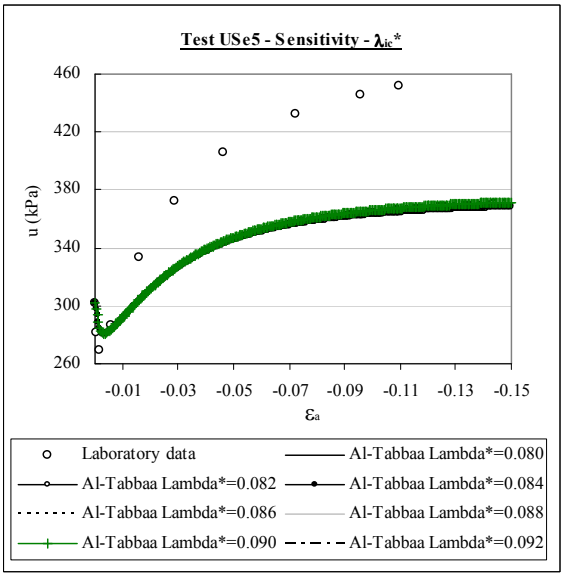

Figure E.3. Sensitivity of the Al-Tabbaa model to λ_c* in terms of the u - ε_a behaviour during test USe5

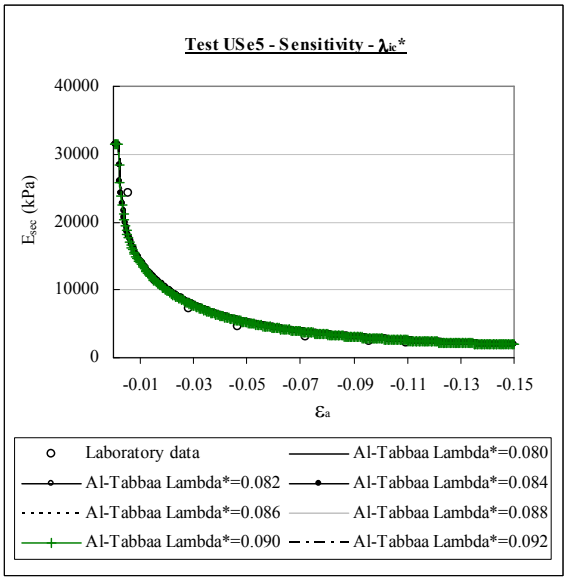

Figure E.4. Sensitivity of the Al-Tabbaa model to λ_{ic}* in terms of the E_{sec} - ε_a behaviour during test USe5

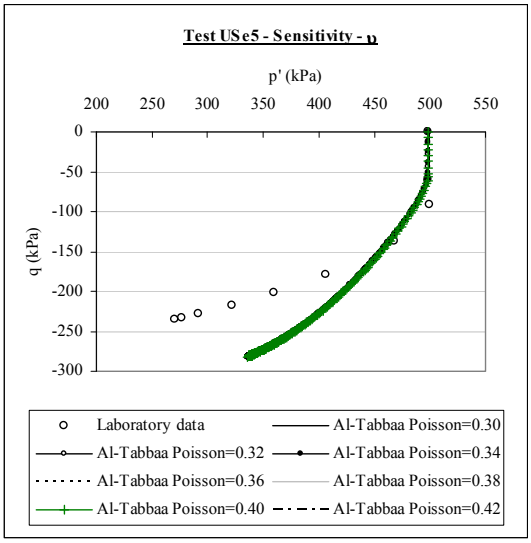

Figure E.5. Sensitivity of the Al-Tabbaa model to υ in terms of the q - p' behaviour during test USe5

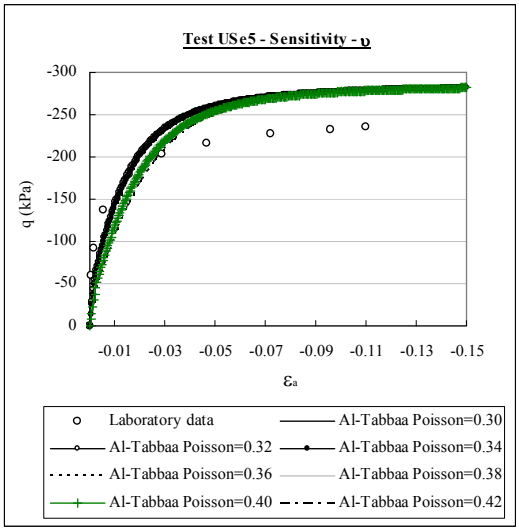

Figure E.6. Sensitivity of the Al-Tabbaa model to υ in terms of the q - ε_a behaviour during test USe5

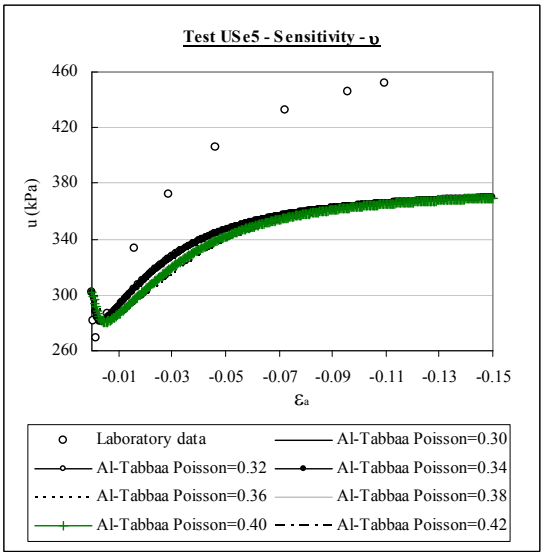

Figure E.7. Sensitivity of the Al-Tabbaa model to υ in terms of the u - ε_a behaviour during test USe5

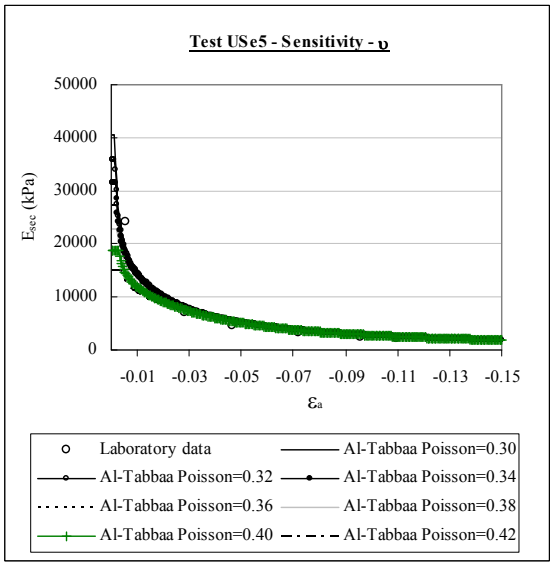

Figure E.8. Sensitivity of the Al-Tabbaa model to υ in terms of the E_{sec} - ε_a behaviour during test USe5

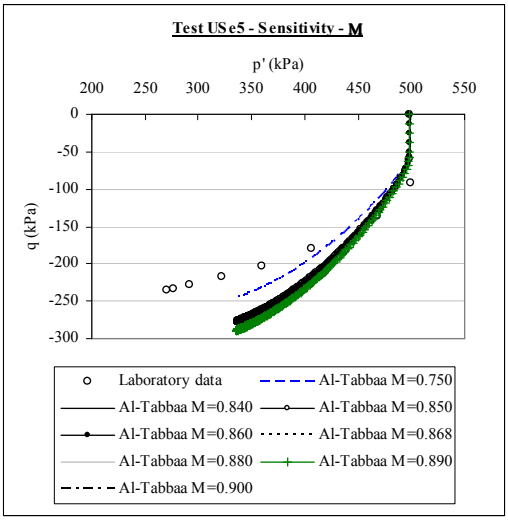

Figure E.9. Sensitivity of the Al-Tabbaa model to *M* in terms of the *q* - *p'* behaviour during test USe5

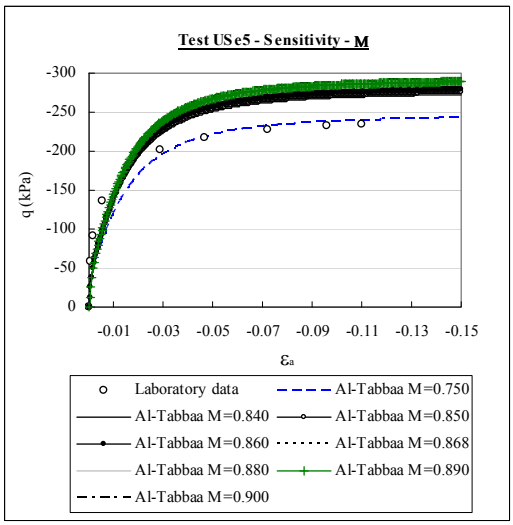

Figure E.10. Sensitivity of the Al-Tabbaa model to *M* in terms of the *q* - ε_a behaviour during test USe5

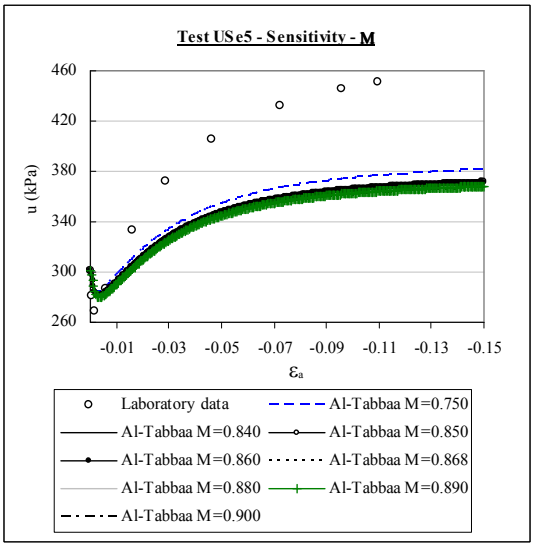

Figure E.11. Sensitivity of the Al-Tabbaa model to *M* in terms of the *u* - ε_a behaviour during test USe5

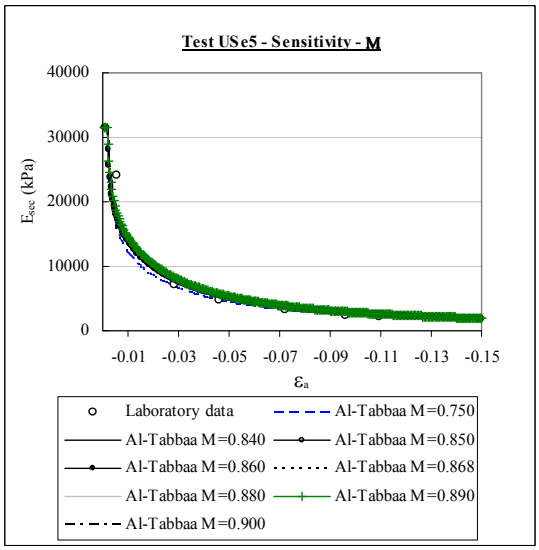

Figure E.12. Sensitivity of the Al-Tabbaa model to *M* in terms of the E_{sec} - ε_a behaviour during test USe5

TEST USc7

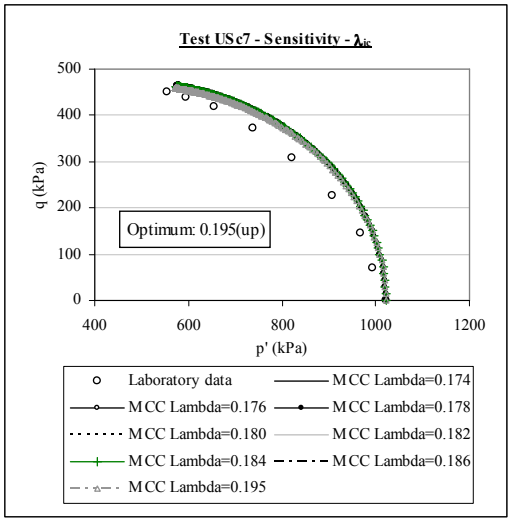

Figure E.13. Sensitivity of the Modified Cam-Clay model to λ_{ic} in terms of the q - p' behaviour during test USc7

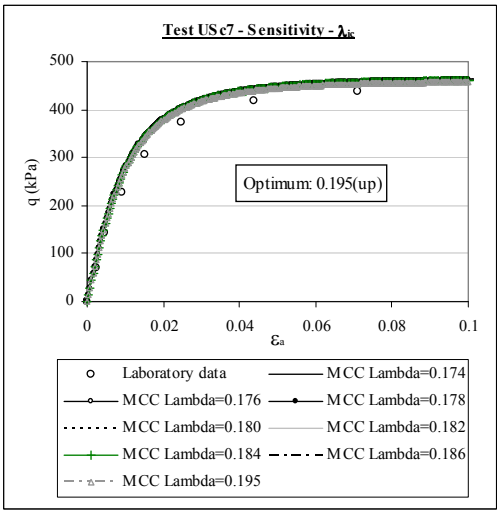

Figure E.14. Sensitivity of the Modified Cam-Clay model to λ_{ic} in terms of the q - ε_a behaviour during test USc7

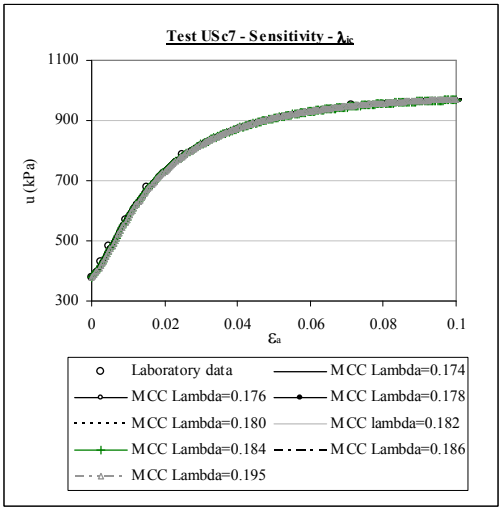

Figure E.15. Sensitivity of the Modified Cam-Clay model to λ_{ic} in terms of the u - ε_a behaviour during test USc7

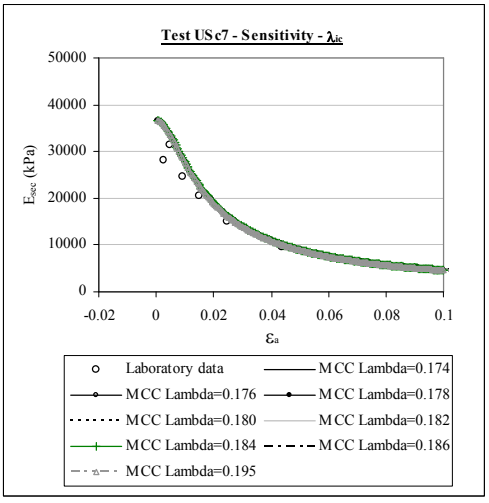

Figure E.16. Sensitivity of the Modified Cam-Clay model to λ_{ic} in terms of the E_{sec} - ε_a behaviour during test USc7

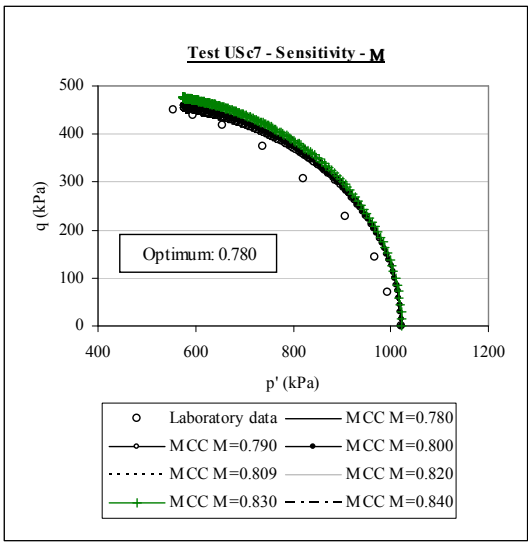

Figure E.17. Sensitivity of the Modified Cam-Clay model to M in terms of the q - p' behaviour during test USc7

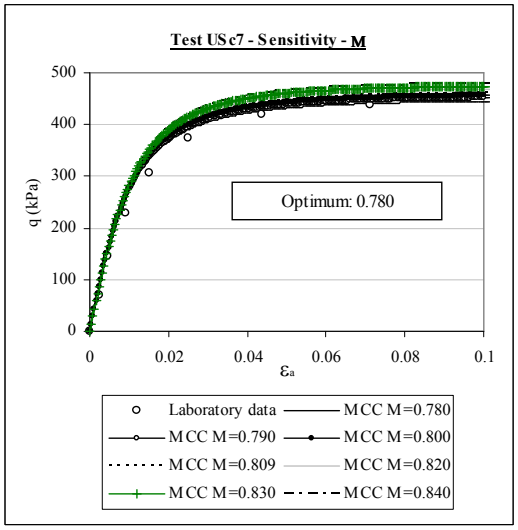

Figure E.18. Sensitivity of the Modified Cam-Clay model to M in terms of the q - ε_a behaviour during test USc7

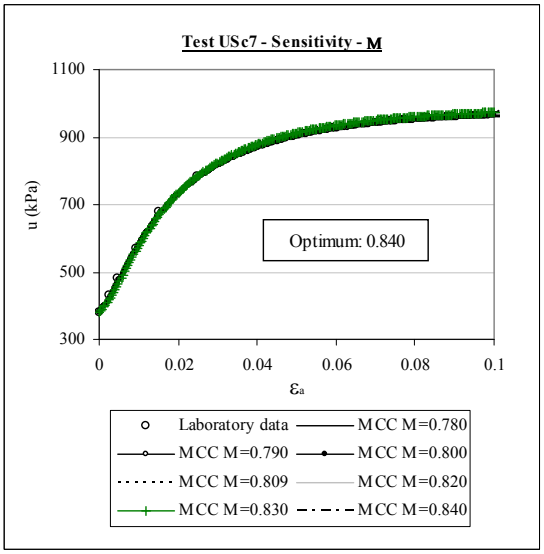

Figure E.19. Sensitivity of the Modified Cam-Clay model to M in terms of the u - ε_a behaviour during test USc7

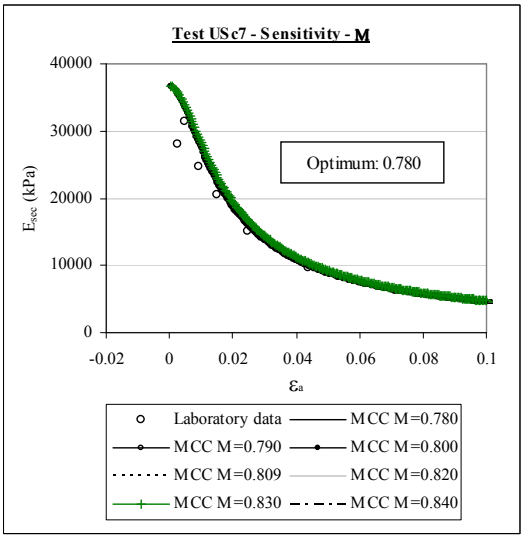

Figure E.20. Sensitivity of the Modified Cam-Clay model to M in terms of the E_{sec} - ε_a behaviour during test USc7

TEST Ko6

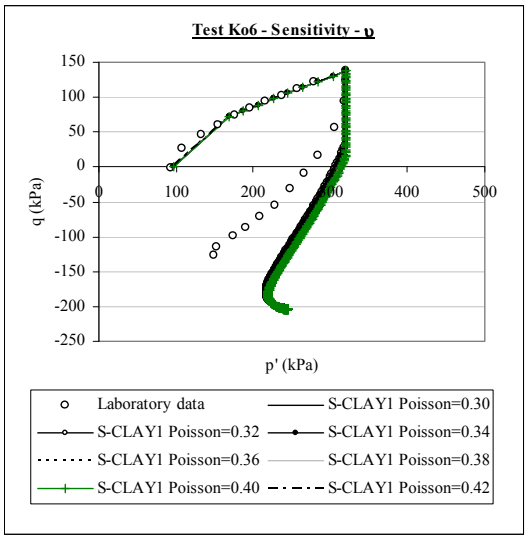

Figure E.21. Sensitivity of the S-CLAY1 model to υ in terms of the q - p' behaviour during test Ko6

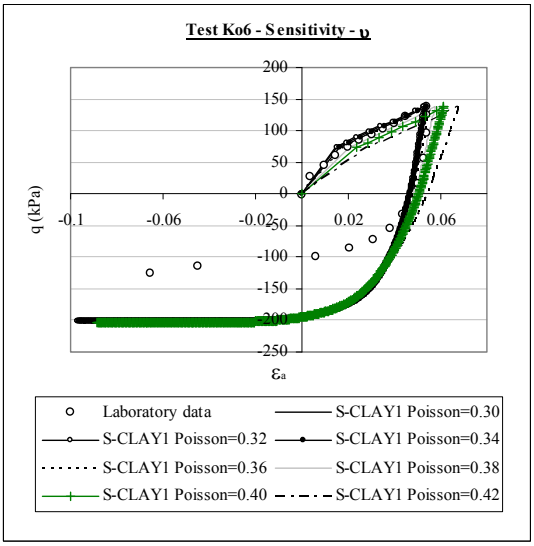

Figure E.22. Sensitivity of the S-CLAY1 model to υ in terms of the q - ε_a behaviour during test Ko6

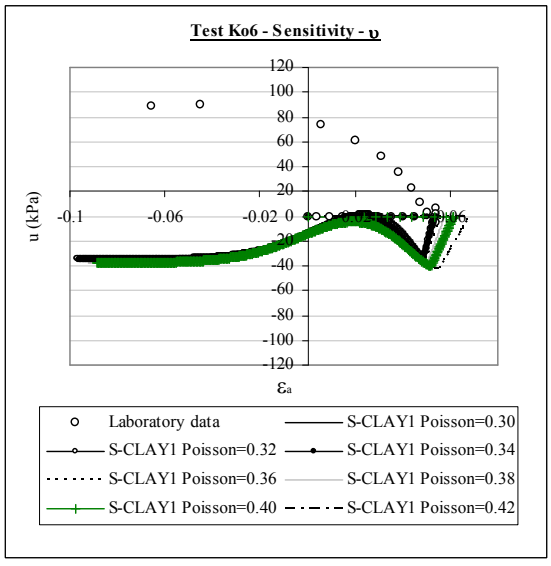

Figure E.23. Sensitivity of the S-CLAY1 model to υ in terms of the u - ε_a behaviour during test Ko6

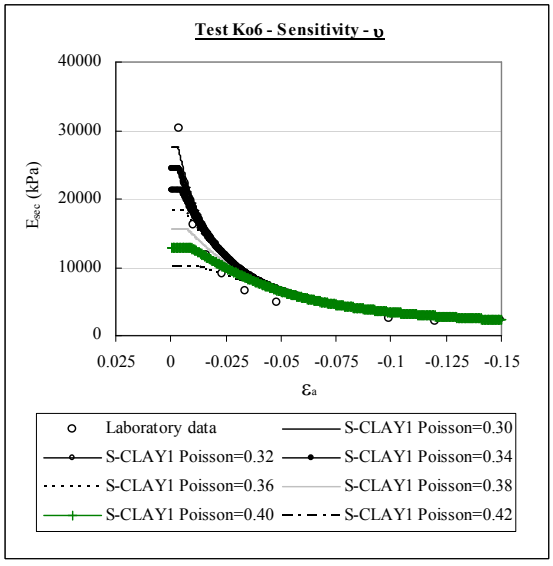

Figure E.24. Sensitivity of the S-CLAY1 model to υ in terms of the E_{sec} - ε_a behaviour during test Ko6

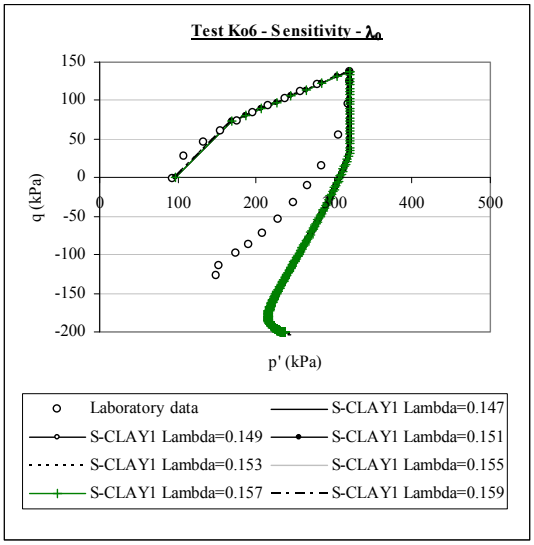

Figure E.25. Sensitivity of the S-CLAY1 model to λ in terms of the q - p' behaviour during test Ko6

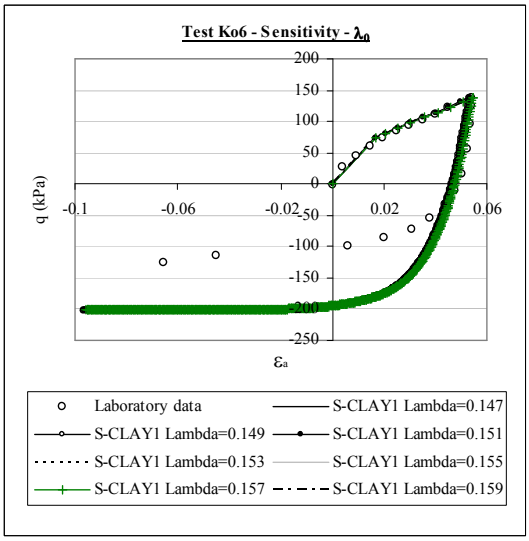

Figure E.26. Sensitivity of the S-CLAY1 model to λ in terms of the q - ε_a behaviour during test Ko6

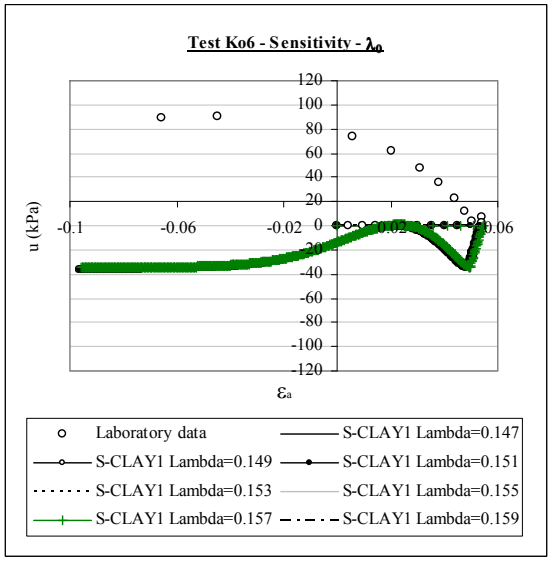

Figure E.27. Sensitivity of the S-CLAY1 model to λ in terms of the u - ε_a behaviour during test Ko6

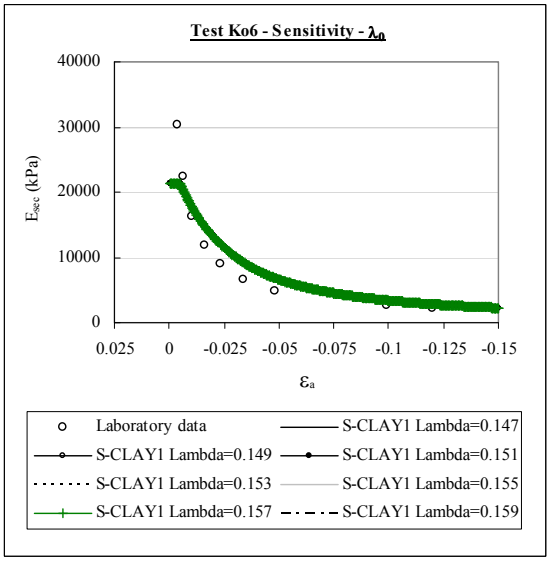

Figure E.28. Sensitivity of the S-CLAY1 model to λ in terms of the E_{sec} - ε_a behaviour during test Ko6

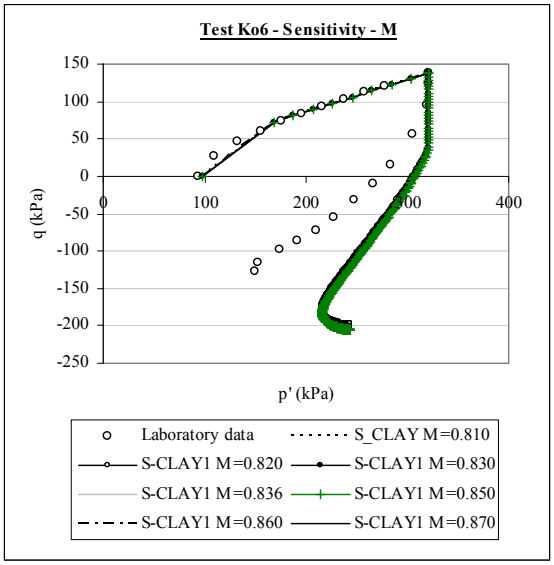

Figure E.29. Sensitivity of the S-CLAY1 model to M in terms of the q - p' behaviour during test Ko6

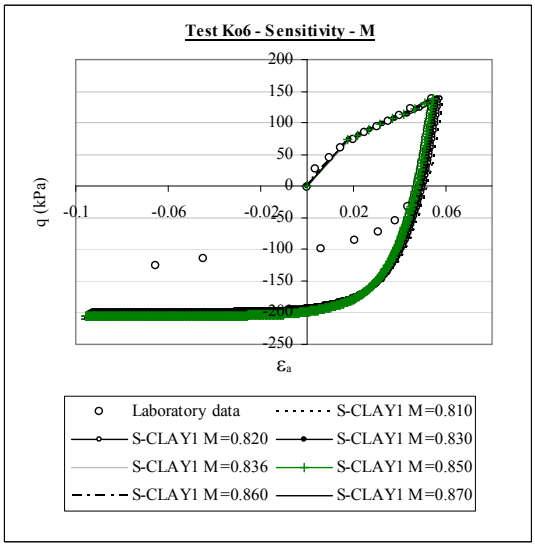

Figure E.30. Sensitivity of the S-CLAY1 model to M in terms of the q - ε_a behaviour during test Ko6

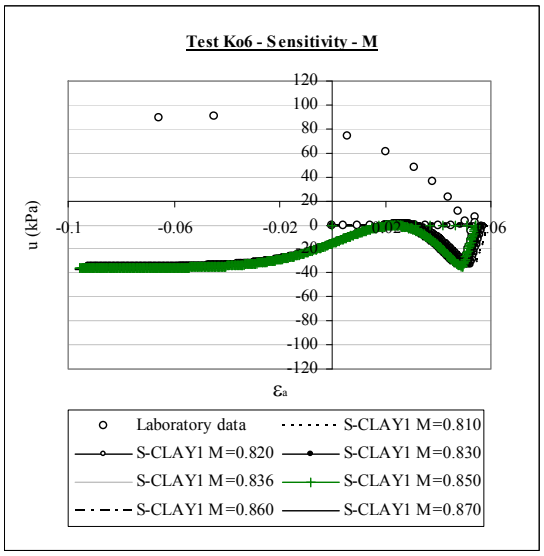

Figure E.31. Sensitivity of the S-CLAY1 model to M in terms of the u - ε_a behaviour during test Ko6

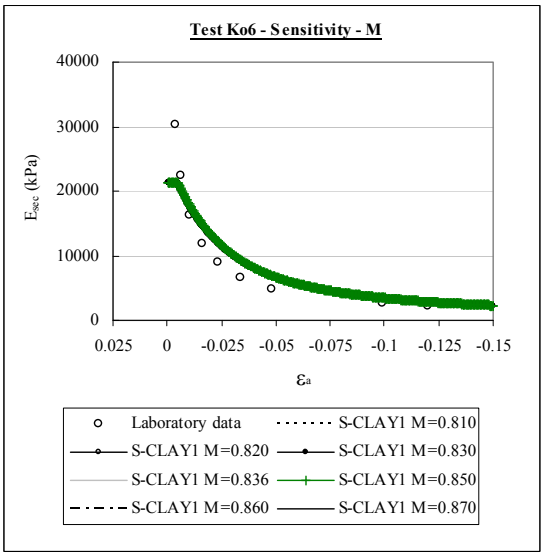

Figure E.32. Sensitivity of the S-CLAY1 model to M in terms of the E_{sec} - ε_a behaviour during test Ko6

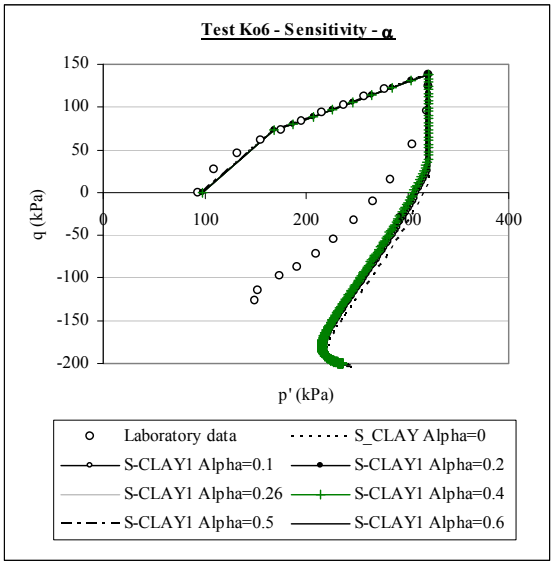

Figure E.33. Sensitivity of the S-CLAY1 model to α in terms of the q - p' behaviour during test Ko6

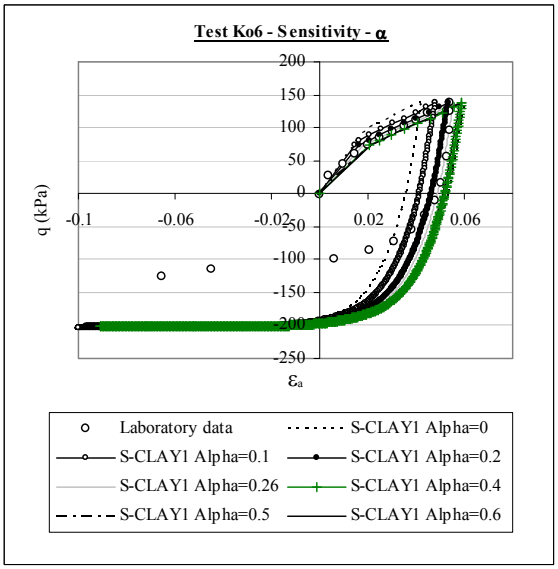

Figure E.34. Sensitivity of the S-CLAY1 model to α in terms of the q - ε_a behaviour during test Ko6

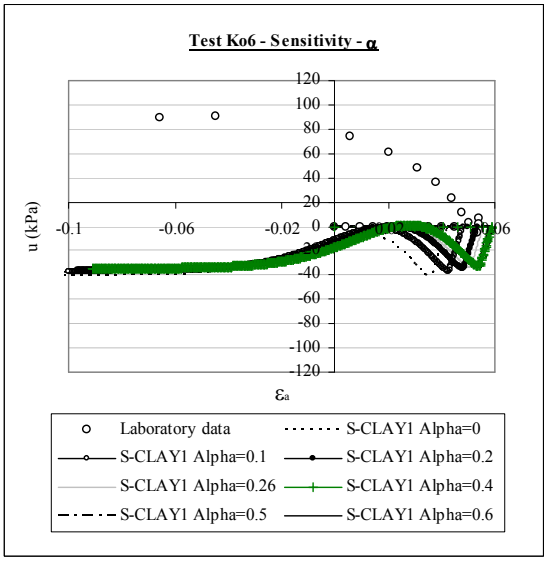

Figure E.35. Sensitivity of the S-CLAY1 model to α in terms of the u - ε_a behaviour during test Ko6

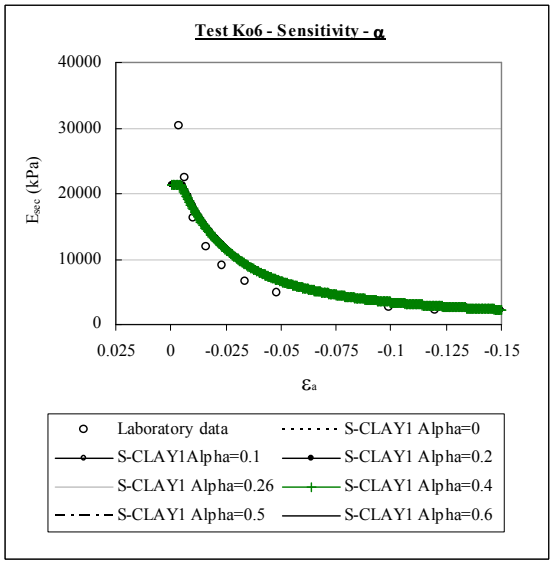

Figure E.36. Sensitivity of the S-CLAY1 model to α in terms of the E_{sec} - ε_a behaviour during test Ko6

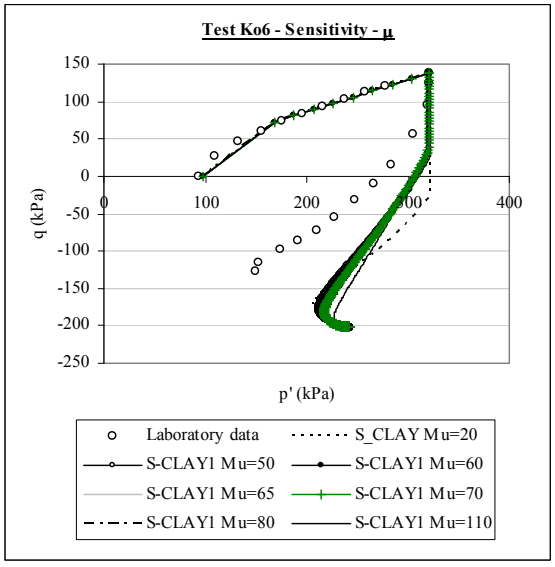

Figure E.37. Sensitivity of the S-CLAY1 model to μ in terms of the q - p' behaviour during test Ko6

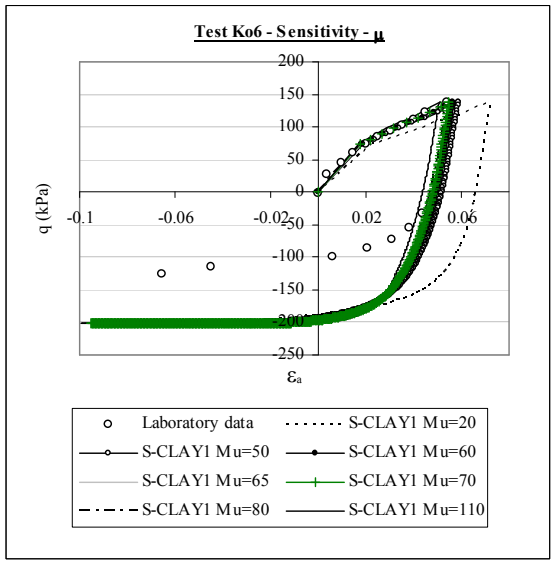

Figure E.38. Sensitivity of the S-CLAY1 model to μ in terms of the q - ε_a behaviour during test Ko6

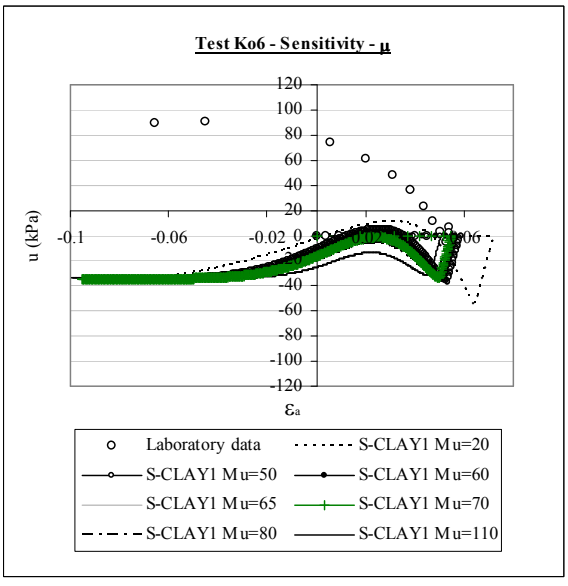

Figure E.39. Sensitivity of the S-CLAY1 model to μ in terms of the u - ε_a behaviour during test Ko6

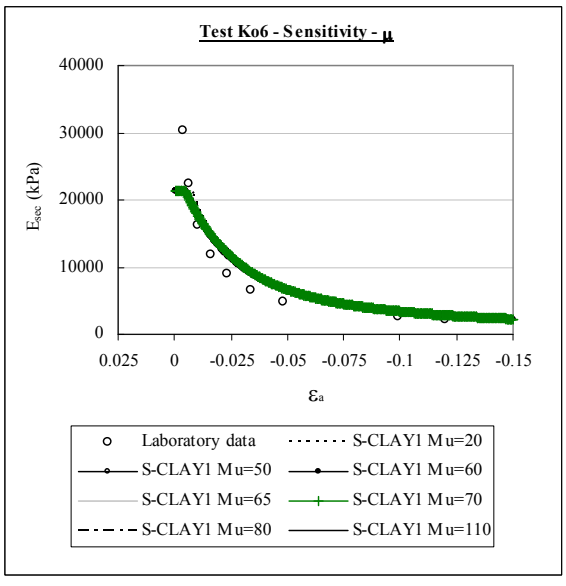

Figure E.40. Sensitivity of the S-CLAY1 model to μ in terms of the E_{sec} - ε_a behaviour during test Ko6

Appendix F: COMPLETE LIST OF LABORATORY EXPERIMENTS

CODE	CHAPTER	TYPE OF TEST / APPLICATION
IN 1.1	5	K_0-consolidation in Consolidation Device A – Study of the sample's properties
IN 1.2	5	K_0-consolidation in Consolidation Device A – Study of the sample's properties
1N 1.3	5	K_0-consolidation in Consolidation Device A – Study of the sample's properties
IN 1.4	5	K_0-consolidation in Consolidation Device A – Study of the sample's properties
IN 1.5	5	K_0-consolidation in Consolidation Device A – Study of the sample's properties
IN 1.6	5	K_0-consolidation in Consolidation Device A – Study of the sample's properties
IN 1.7	5	K_0-consolidation in Consolidation Device A – Study of the sample's properties
IN 1.8	5	K_0-consolidation in Consolidation Device A – Study of the sample's properties
IN 1.9	5	K_0-consolidation in Consolidation Device A – Study of the sample's properties
IN 2.1	5	K_0-consolidation in Consolidation Device A – Study of the sample's properties
IN 2.3	5	K_0-consolidation in Consolidation Device A – Study of the sample's properties
IN 2.4	5	K_0-consolidation in Consolidation Device A – Study of the sample's properties
UU2	5	Unconsolidated Undrained triaxial test – Determination of the soil strength
UU3	5	Unconsolidated Undrained triaxial test – Determination of the soil strength
UU4	5	Unconsolidated Undrained triaxial test – Determination of the soil strength
UU6	5	Unconsolidated Undrained triaxial test – Determination of the soil strength
w1	5	Measurement of the moisture content variation along the samples
w2	5	Measurement of the moisture content variation along the samples
Cuw	5	c_u - w relationship based on the Fall cone test
C1	5	Study of internal structures in the samples using SEM
INWD	5	K_0-consolidation in Device A (adding WD-40 oil) – Evaluation improvement in sample homogeneity
A100-1	5	K_0-consolidation in Device A (larger diameter) – Evaluation improvement in sample homogeneity
A100-2	5	K_0-consolidation in Device A (larger diameter) – Evaluation improvement in sample homogeneity
FP1	5	K_0-consolidation in Device A (flexible piston) – Evaluation improvement in sample homogeneity
FP2	5	K_0-consolidation in Device A (flexible piston) – Evaluation improvement in sample homogeneity
F01	5	Measurement of pore water pressures (and actual vertical stress being applied) during K_0-consolidation
F02	5	Measurement of pore water pressures (and actual vertical stress being applied) during K_0-consolidation
F03	5	Measurement of pore water pressures (and actual vertical stress being applied) during K_0-consolidation
F04	5	Measurement of pore water pressures (and actual vertical stress being applied) during K_0-consolidation
USc2	6	Isotropically consolidated undrained test in compression – Determination of the soil parameters
USc3	6	Isotropically consolidated undrained test in compression – Determination of the soil parameters
USc4	6	Isotropically consolidated undrained test in compression – Determination of the soil parameters
USc5	6	Isotropically consolidated undrained test in compression – Determination of the soil parameters
USc6	6	Isotropically consolidated undrained test in compression – Determination of the soil parameters
USc7	6	Isotropically consolidated undrained test in compression – Determination of the soil parameters
USc8	6	Isotropically consolidated undrained test in compression – Determination of the soil parameters
USc9	6	Isotropically consolidated undrained test in compression – Determination of the soil parameters
USc10	6	Isotropically consolidated undrained test in compression – Determination of the soil parameters
USc11	6	Isotropically consolidated undrained test in compression – Determination of the soil parameters
USe1	6	Isotropically consolidated undrained test in extension – Determination of the soil parameters
USe2	6	Isotropically consolidated undrained test in extension – Determination of the soil parameters
USe3	6	Isotropically consolidated undrained test in extension – Determination of the soil parameters

CODE	CHAPTER	TYPE OF TEST / APPLICATION
USe4	6	Isotropically consolidated undrained test in extension – Determination of the soil parameters
USe5	6	Isotropically consolidated undrained test in extension – Determination of the soil parameters
USe6	6	Isotropically consolidated undrained test in extension – Determination of the soil parameters
DSc1	6	Isotropically consolidated drained test in compression – Determination of the soil parameters
NCL1	6	Isotropic consolidation triaxial test – Determination of the soil parameters
NCL2	6	Isotropic consolidation triaxial test – Determination of the soil parameters
Ko1	6	K_0-consolidation triaxial test – Determination of the soil parameters
Ko2	6	K_0-consolidation triaxial test – Determination of the soil parameters
Ko3	6	K_0-consolidation triaxial test – Determination of the soil parameters
Ko4	6	K_0-consolidation triaxial test plus undrained shearing in compression – Determination of the soil parameters
Ko5	6	K_0-consolidation triaxial test plus undrained shearing in compression – Determination of the soil parameters
Ko6	6	K_0-consolidation triaxial test plus undrained shearing in extension – Determination of the soil parameters
KoAL1	6	Mimic of a K_0-consolidation process in the triaxial using the stress path module
SP1	7	Simulation of a tunnel induced stress path above the crown. Single tunnel. $K_0< 1$. No creep
SP1-c	7	Simulation of a tunnel induced stress path above the crown. Single tunnel. $K_0< 1$. Including creep
SP2	7	Simulation of a tunnel induced stress path at the springline. Twin tunnels. $K_0< 1$. No creep
SP2B	7	Simulation of a tunnel induced stress path at the springline. Twin tunnels. $K_0< 1$. No creep
SP2C	7	Simulation of a tunnel induced stress path at the springline. Twin tunnels. $K_0< 1$. No creep
SP3	7	Simulation of a tunnel induced stress path above the crown. Single tunnel. $K_0> 1$. No creep
SP4	7	Simulation of a tunnel induced stress path at the springline. Twin tunnels. $K_0> 1$. No creep